Agenzia nazionale per le nuove tecnologie,
l'energia e lo sviluppo economico sostenibile

MINISTERO DELLO SVILUPPO ECONOMICO

Ricerca di Sistema elettrico

Raccolta delle principali attività di diffusione

Giovanni Puglisi

Report RdS/PAR2016/272

RACCOLTA DELLE PRINCIPALI ATTIVITÀ DI DIFFUSIONE

G. Puglisi (ENEA)

Settembre 2017

Report Ricerca di Sistema Elettrico

Accordo di Programma Ministero dello Sviluppo Economico - ENEA
Piano Annuale di Realizzazione 2016
Area: Efficienza energetica e risparmio di energia negli usi finali elettrici e interazione con altri vettori energetici
Progetto: D1 - Tecnologie per costruire gli edifici del futuro
Obiettivo: F. Comunicazione e diffusione dei risultati
Responsabile del Progetto: Giovanni Puglisi, ENEA

Indice

1 Introduzione

Il rapporto descrive le attività messe in atto per la comunicazione e diffusione dei risultati prodotti dal progetto D1 “tecnologie per costruire gli edifici del futuro” relativo all’Accordo di Programma MiSE-ENEA, piano annuale di realizzazione 2016.

Tali attività sono state suddivise, per ciascuna linea in cui è diviso il progetto, in:

- pubblicazioni su riviste specializzate o su atti di convegni,
- presentazioni a convegni.

Nei paragrafi successivi si riportano rispettivamente l’elenco delle pubblicazioni, gli articoli integrali e le pe presentazioni ai convegni.

2 ELENCO PUBBLICAZIONI

Di seguito sono riportate le pubblicazioni suddivise per linee.

Linea a

- From natural systems to lighting electronics: designing melanin-inspired electroluminescent materials. V. Criscuolo, P. Manini, C.T. Prontera, A. Pezzella, M.G. Maglione, P. Tassini, C. Minarini. BioEL2017 International Winterschool on Bioelectronics, Kirchberg in Tirol, Austria.
- Controlling of (supra)Molecular Structure of Polymers from Natural Sources to Assess their Electrical Properties. Ri Xu, C.T. Prontera, L.G. Simao Albano, E. Di Mauro, P. Kumar, P. Manini, C. Santato, F. Soavi. MRS spring 2017, Phoenix, USA.
- Melanins in bioelectronics: a survey of the role of these natural pigments from bio-interfaces to (opto)electronic devices. P. Manini, V. Criscuolo, L. Migliaccio, C.T. Prontera, A. Pezzella, O. Crescenzi, M. d’Ischia, S, Parisi, M. Barra, A. Cassinese, P. Maddalena, M.G. Maglione, P. Tassini, C. Minarini. e-MRS spring 2017, Strasbourg, France.
- From Melanins to OLED Devices: Taking Inspiration from the Black Human Pigments for the Design of Innovative Electroluminescent Materials. P. Manini, C. T. Prontera, V. Criscuolo, A. Pezzella, O. Crescenzi, M. Pavone, M. d’Ischia, M. G. Maglione, P. Tassini, C. Minarini. SCI 2017, Paestum (SA), Italy.
- Shedding Light on the Hydratation-Dependent Electrical Conductivity in Melanin Thin Films. Ri Xu, L.G. Simao Albano, E. Di Mauro, S. Zhang, P. Kumar, C. Santato, C.T. Prontera. MRS fall 2016, Boston, USA.
- Advancing the Knowledge of the Structural Properties of the Biocompatible and Biodegradable Electroactive Eumelanin Polymer. D Boisvert, C.T. Prontera, S. Francoeur, A. Badia, C. Santato. MRS spring 2017, Phoenix, USA.
- Designing dopamine-based electroluminescent complexes for innovative melanin-inspired OLED devices. C.T. Prontera, P. Manini, V. Criscuolo, A. Pezzella, O. Crescenzi, M. Pavone, M. d’Ischia, M.G. Maglione, P. Tassini, C. Minarini. ISNSC9 (2017), Napoli, Italy.

- Synthesis and Photo-Physical Properties of Dopamine-Inspired Iridium Complexes for OLED Applications. C.T. Prontera, V. Criscuolo, A. Pezzella, M.G. Maglione, P. Tassini, C. Minarini, M. d'Ischia, P. Manini. SCI 2017, Paestum (SA), Italy.
- G.Zizzo, M.Beccalia, M.Bonomolo, B.Di Pietra, M.G.Ippolito, D.La Cascia, G.Leone, V.Lo Brano, F.Monteleone: A Feasibility Study of Some DSM Enabling Solutions in Small Islands: the Case of Lampedusa – (Journal Energy - September 2017, EGY11563)
- L. Martirano, E. Habib, G. Greco, M. Manganelli, A. Ruvio, B. Di Pietra, A. Pannicelli, S. Piccinelli, G. Puglisi, P. Regina: An example of smart building with a km zero energy performance, (IAS Annual Meeting, October 1-5, 2017, Cincinnati, OH, USA.)
- Bertini, L. Canale, M. Dell'Isola, B. Di Pietra, G. Ficco, G.Puglisi, S. Stoklin: Impatto della contabilizzazione del calore sui consumi energetici in Italia – 17th CIRIAF Congress – Perugia 6-7 Aprile 2017
- M. A. Ancona, L. Branchini, A. De Pascale, F. Melino, B. Di Pietra: Renewable Energy Systems Integration for Efficiency Improvement of a CHP Unit (ASME Turbo Expo Conference - June 26 - 30, 2017, Charlotte, NC USA)

Linea b

- M. Di Somma, B. Yan, N. Bianco, G. Graditi, P. B. Luh, L. Mongibello, V. Naso, Multi-objective design optimization of distributed energy systems through cost and exergy assessments, Applied Energy, Volume 204, 15 October 2017, Pages 1299-1316.
- Di Somma M., Yan B., Bianco N., Luh P.B., Graditi G., Mongibello L., Naso V., Design optimization of a distributed energy system through cost and exergy assessments, Energy Procedia 105 (2017), 2451 – 2459.
- L. Mongibello, G. Graditi, Cold storage for a single-family house in Italy, Energies 2016, 9(12), 1043.
- Luigi Mongibello, Nicola Bianco, Martina Caliano, Giorgio Graditi, A new approach for the dimensioning of an air conditioning system with cold thermal energy storage, Energy Procedia 105 (2017), 4295 – 4304.

Linea c

- Vox Giuliano, Blanco Ileana, Fuina Silvana, Campiotti Carlo Alberto,Scarascia Mugnozza Giacomo , and Schettini Evelia. Evaluation of wall surface temperatures in green facades". Proceedings of the Institution of Civil Engineers - Engineering Sustainability 2017, vol 170:6, 334-344. ISSN 1478-4629; E-ISSN 1751-7680.
- Blanco, I., Scarascia Mugnozza, G., Schettini, E., Puglisi, G., Campiotti, C.A. and Vox, G. (2017). Design of a solar cooling system for greenhouse conditioning in a Mediterranean area. Acta Hortic. 1170, 485-492. DOI: 10.17660/ActaHortic.2017.1170.60. https://doi.org/10.17660/ActaHortic.2017.1170.60 .
- Bibbiani, C., Campiotti, C.A., Schettini, E. and Vox, G. (2017). A sustainable energy for greenhouses heating in Italy: wood biomass. Acta Hortic. 1170, 523-530. DOI: 10.17660/ActaHortic.2017.1170.65. https://doi.org/10.17660/ActaHortic.2017.1170.65 .
- Blanco, I., Schettini, E., Scarascia Mugnozza, G., Campiotti, C.A., Giagnacovo, G. and Vox, G. (2017). Vegetation as a passive system for enhancing building climate control. Acta Hortic. 1170, 555-562. DOI: 10.17660/ActaHortic.2017.1170.69. https://doi.org/10.17660/ActaHortic.2017.1170.69 .
- R. Di Bonito1, D. Biagiotti2,3, G. Giagnacovo2, M. Canditelli4, C.A. Campiotti2, Use of compost as amendment for soilless substrates of plants in green roof installations, Acta Hortic. 1146. ISHS

2016. DOI 10.17660/ActaHortic.2016.1146.19, Proc. III Int. Sym. on Organic Matter Mgt. and Compost Use in Hort.

Linea d

- Buratti, C., Moretti, E., Zinzi, M., High energy-efficient windows with silica aerogel for building refurbishment: Experimental characterization and preliminary simulations in different climate conditions, Buildings, Volume 7, Issue 1, 2017, Article number 8.
- Elisa Moretti, Michele Zinzi, Emiliano Carnielo, Francesca Merli. Advanced Polycarbonate Transparent Systems with Aerogel: Preliminary Characterization of Optical and Thermal Properties,Energy Procedia, Volume 113, May 2017, Pages 9-16.
- Michele Zinzi, Paolo Ruggeri, Fabio Peron, Emiliano Carnielo, Alessandro Righi, Experimental Characterization and Energy Performances of Multiple Glazing Units with Integrated Shading Devices, Energy Procedia, Volume 113, May 2017, Pages 1-8.
- Alessandro Fontia, Gabriele Comodia,*, Stefano Pizzutib, Alessia Arteconic, Lieve Helsend, Low order grey-box models for short-term thermal behavior prediction in buildings, ScienceDirect, Energy Procedia 105 (2017) 2107 – 2112

linea e

- Caldera M., Puglisi G., Zanghirella F., Margiotta F., Ungaro P., Talucci V., Cammarata G. (2017). Proposal of a survey-based methodology for the determination of the energy consumption in the residential sector, International Journal of Heat and Technology, Vol. 35, Sp. 1, pp. S152-S158, DOI: 10.18280/ijht.35Sp0121 (articolo presentato al 2nd AIGE/IIETA International Conference, Genova, 12-13 giugno 2017)

3 Articoli e presentazioni a convegni.

From Melanins to OLED Devices: Taking Inspiration from the Black Human Pigments for the Design of Innovative Electroluminescent Materials.

Paola Manini,[a] *Carmela Tania Prontera*,[a] *Valeria Criscuolo*,[a] *Alessandro Pezzella*,[a] *Orlando Crescenzi*,[a] *Michele Pavone*,[a] *Marco d'Ischia*,[a] *Maria Grazia Maglione*,[b] *Paolo Tassini*,[b] *Carla Minarini*[b]

[a] *Department of Chemical Sciences, University of Naples "Federico II", via Cintia 4, I-80126 Napoli, IT;* [b] *Laboratory of Nanomaterials and Devices, ENEA C. R. Portici, Piazzale E. Fermi, Portici (NA), IT;* paola.manini@unina.it

The growing expansion and impact of OLED devices in our everyday life have stimulated the synthesis of a wide plethora of electroluminescent materials with the aim of improving the efficiency and the life-time of the device as well as of selectively tuning the wavelength of the emitting light.

In the frame of our research activity aimed at exploring the role of melanins, the dark pigments found in mammalian skin, hair and eyes, as soft organic semiconductors in bio-electronic devices (1), we have undertaken a new challenge: to obtain innovative electroluminesct compounds from black melanin pigments.

The strategy of this research activity has been based on the use of melanin precursors, such as 5,6-dihydroxyindole and dopamine, as starting compounds for the synthesis of fluorescent or phosphorescent materials for applications as emitting layer in OLED devices (2).

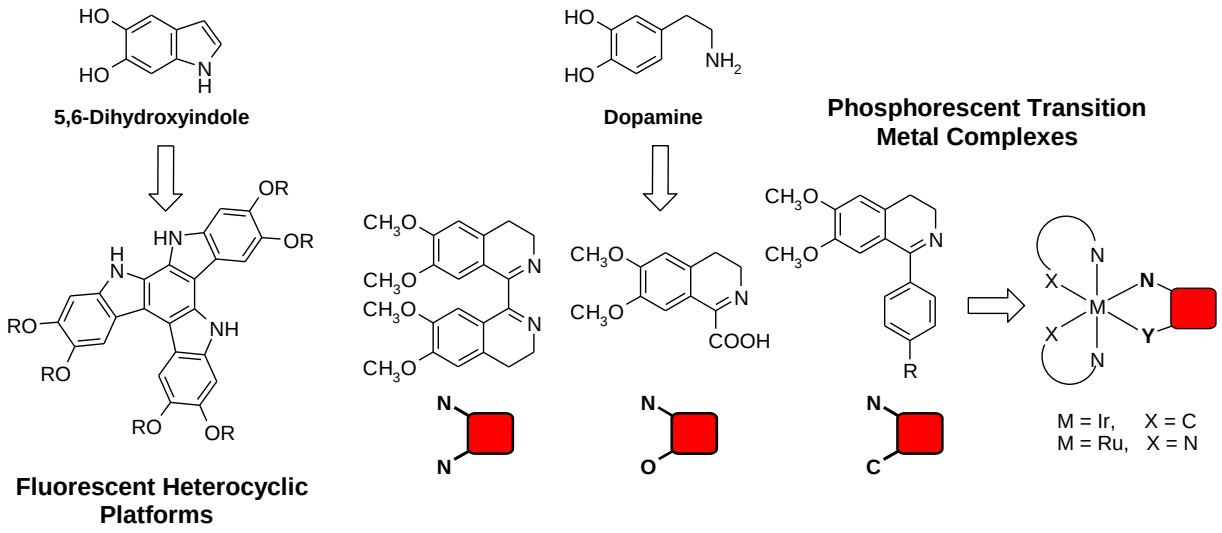

Figure 1

In this communication we will discuss the synthesis of a set melanin-inspired electroluminescent compounds; we will report on their photo-physical and electrical properties; the fabrication and characterization of the corresponding OLED devices will also be presented.

References

(1) Pezzella, A.; Barra, M.; Musto, A.; Navarra, A.; Alfé, M.; Manini, P.; Parisi, S.; Cassinese, A.; Criscuolo, V.; d'Ischia, M. *Mater. Horiz.* **2015**, *2*, 212.

(2) Manini, P.; Criscuolo, V.; Ricciotti, L.; Pezzella, A.; Barra, M.; Cassinese, A.; Crescenzi, O.; Maglione M.G.; Tassini, P.; Minarini, C.; Barone, V.; d'Ischia, M. *ChemPlusChem*, **2015**, *80*, 919.

Shedding Light on the Hydration-Dependent Electrical Conductivity in Melanin Thin Films

Ri Xu [1], Luiz Gustavo Simao Albano [2], Eduardo Di Mauro [1], Shiming Zhang [1], Prajwal Kumar [1], Clara Santato [1], Carmela Tania Prontera [3]

[1] Polytechnique Montreal Montreal Canada
[2] São Paulo State University Bauru Brazil
[3] Deparment of Chemical Sciences Università degli Studi di Napoli Federico II Naples Italy

Eumelanin is a brown-black biopigment present in flora and fauna, exhibiting a number of functional properties, such as metal chelation, free radical scavenging, antioxidant and electronic-ionic hybrid conductive behavior. Like other electronic-ionic hybrid conductive biomolecules, eumelanin has hydration-dependent electrical conduction properties . The possibility to exploit these hydration dependent properties to design novel technologies, e.g. moisture sensors, is the key motivation of the present work.

We report on the behavior of 60 nm-thick films of synthetic eumelanin (Sigma) used as the moisture-sensitive material in planar devices, making use of pairs of photolithographically patterned Pt electrodes, with interelectrode distances at the micrometric scale. We observed changes in the behavior of the electrical current vs time plots, according to different relative humidity (RH) of the atmosphere (ranging from 90% to 50% relative humidity, RH).

In consistency with the hypothesis of a comproportionation equilibrium in eumelanin , which describes the regulation of the distribution of the redox states of the pigment as a function of the humidity conditions, we observe an increase of the electrical current with RH.

In particular, at a sweeping rate of 0.05 mV/s in the interval of 0.05 V – 0.6 V we observe a current of ~ 15 nA at 90% RH and current of 1 nA at 50% RH (interelectrode distance 10 microns and width 4 mm). Only within the range 0.05 V - 0.2 V a linear behavior is observed. Unlike other ionic-electronic hybrid conductive biomolecules, the current exhibits a hysteresis behavior .

Through nano IR investigations, we investigate chemical changes resulting from faraday interfacial processes.

Advancing the Knowledge on the Structural Properties of the Biocompatible and Biodegradable Electroactive Eumelanin Polymer

Dominic Boisvert[1] , Carmela Prontera[2] , Sebastien Francoeur[1] , Antonella Badia[1] , Clara Santato[1]

1 , Polytechnique Montréal, Montreal, Quebec, Canada
2 , University of Naples Federico II, Napoli Italy

Eumelanin is a dark-brown biopigment largely present in animals and plants. This biopolymer results from the polymerization of two monomers (building blocks), namely 5,6-dihydroxyindole (DHI) and 5,6-dihydroxyindole-2- carboxylic acid (DHICA) [1]. Important physicochemical properties of eumelanin include metal chelation, photoprotection (the pigment absorbs in the nearIR – UV region of the spectrum) and mixed ionic-electronic conduction. It also features biocompatibility and biodegradability [2]. Although eumelanin has been studied for a few decades now, the nature of its chromophoric units and the mechanism of charge carrier transport are still largely undiscovered, mainly because of the chemical disorder that characterizes natural eumelanin. Obtaining a good control over the molecular and supramolecular structures of the pigment is therefore imperative to achieve better understanding of those properties, a key to demonstrate eumelanin-based environmentally and human-friendly technologies.

Here we report on the controlled polymerization in films of DHI building blocks spin coated on SiO2 and quartz substrates, observed in situ by Atomic Force Microscopy (AFM). DHI films obtained from methanol solutions of freshly synthesized DHI, were polymerized in ambient conditions (oxidative polymerization). A number of factors likely contribute to establishing the mechanism of polymerization. Besides molecular oxygen, monomer/oligomer aggregates in the methanol suspensions can act as nuclei of the polymerization. Our preliminary results suggest that the physical contact between the AFM tip and the monomers/oligomers plays a role in triggering the polymerization. Once started, the polymerization front develops within a time scale of minutes on a preferential direction, creating elongated, dendritic structures, leading to furrow-like surfaces, separated by a few micrometers. The dendrimers, carefully characterized by AFM, were also investigated by spatially resolved absorption spectroscopy. The large scale, directional and dendritic polymerization can be exploited to obtain chemically controlled eumelanin samples that can be efficiently characterized for their optical and transport properties and, on the long term, exploited in organic electronics devices, such as transistors and solar cells. Further studies on the polymerization in the presence of metallic substrates or metal ions will provide insight on the effect of metal chelation on the polymerization patterns, thus giving more insight for future melanin-based devices.

[1] M. D'Ischia, et. al., "Melanins and melanogenesis: methods, standards, protocols," Pigment Cell & Melanoma Research, vol. 26, no. 5, pp. 616-633, 2013.

[2] C. J. Bettinger, et. al., "Biocompatibility of biodegradable semiconducting melanin films for nerve tissue engineering," Biomaterials, vol. 30, no. 17, pp. 3050-3057, 2009

ISNSC9 9th International Symposium on Nano & Supramolecular Chemistry
4-7th September 2017 – Napoli

Designing dopamine-based electroluminescent complexes for innovative melanin-inspired OLED devices

C.T. Prontera,[a*] P. Manini,[a] V. Criscuolo,[a] A. Pezzella,[a] O. Crescenzi,[a] M. Pavone,[a] M. d'Ischia,[a] M.G. Maglione,[b] P. Tassini,[b] C. Minarini[b]

[a] *Department of Chemical Sciences, University of Naples "Federico II", via Cintia 4, I-80126 Napoli, IT;*
[b] *Laboratory of Nanomaterials and Devices, ENEA C. R. Portici, Piazzale E. Fermi, Portici (NA), IT;*
[*] *carmelatania.prontera@unina.it*

Università degli Studi di Napoli Federico II

ENEA Agenzia nazionale per le nuove tecnologie, l'energia e lo sviluppo economico sostenibile

In the last decades, metal–organic complexes have attracted much attention due to their enormous potential application in optoelectronic devices.
In this work, **dopamine**, the catecholic neurotransmitter and monomer precursor of polydopamine, is used as starting compound for the synthesis of a series of etherocyclic compound to behave as ligands for bio-inspired phosphorescent iridium and ruthenium complexes.

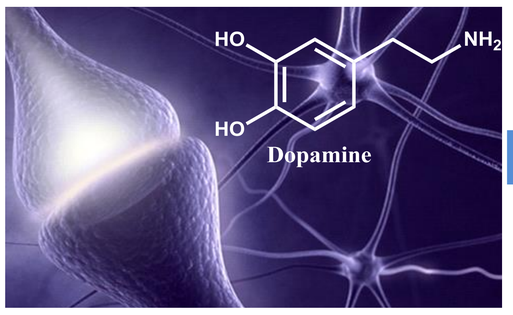

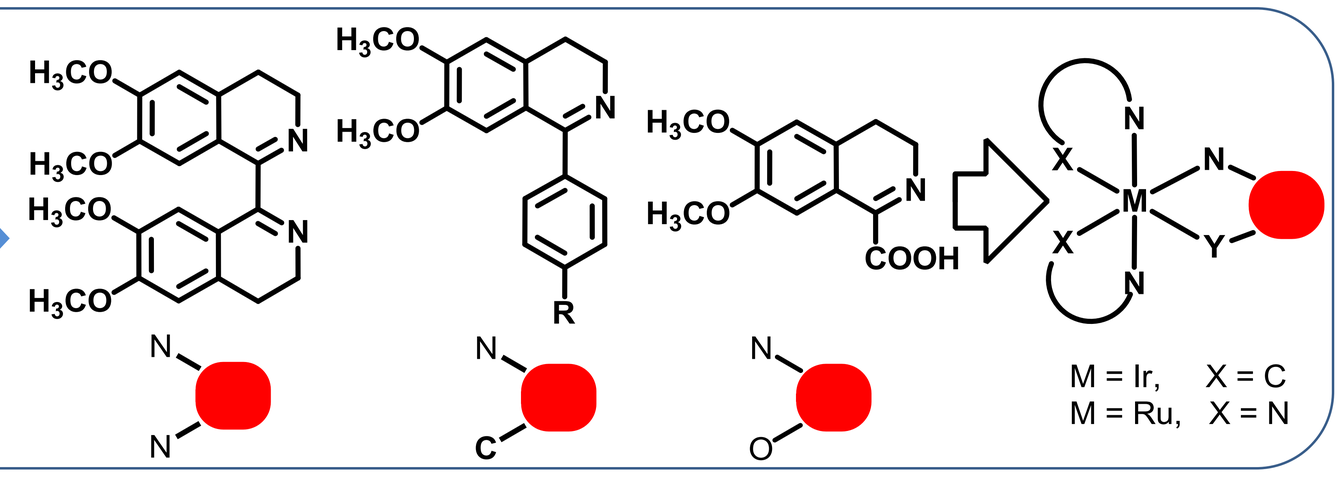

Ligand Synthesis

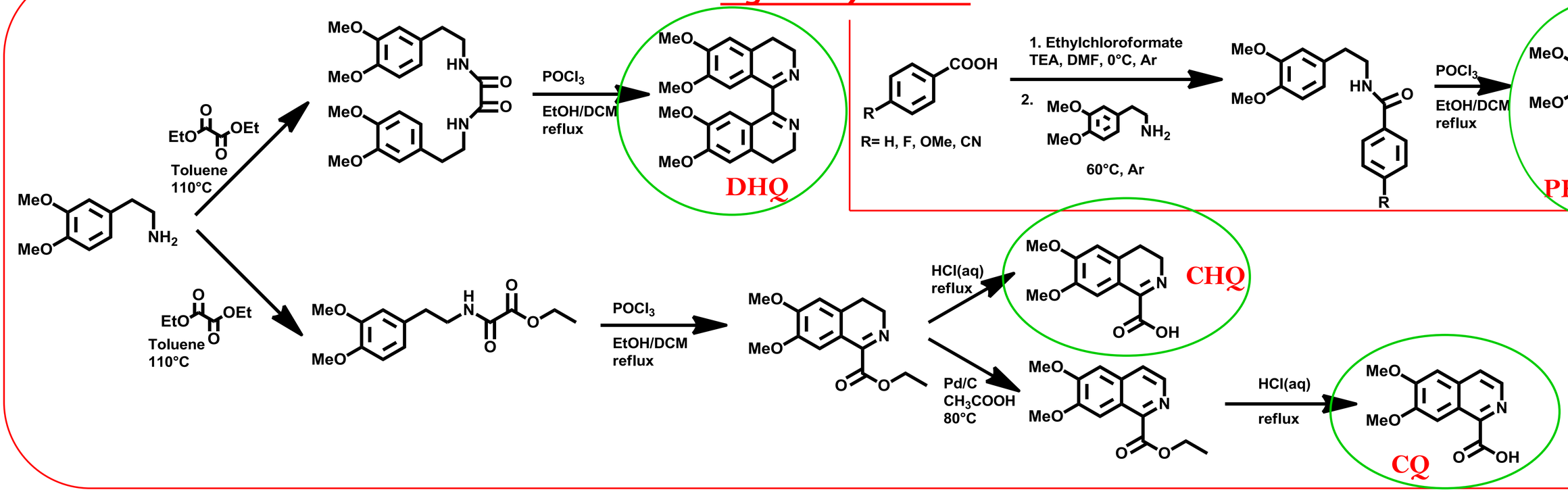

Iridium Complexes

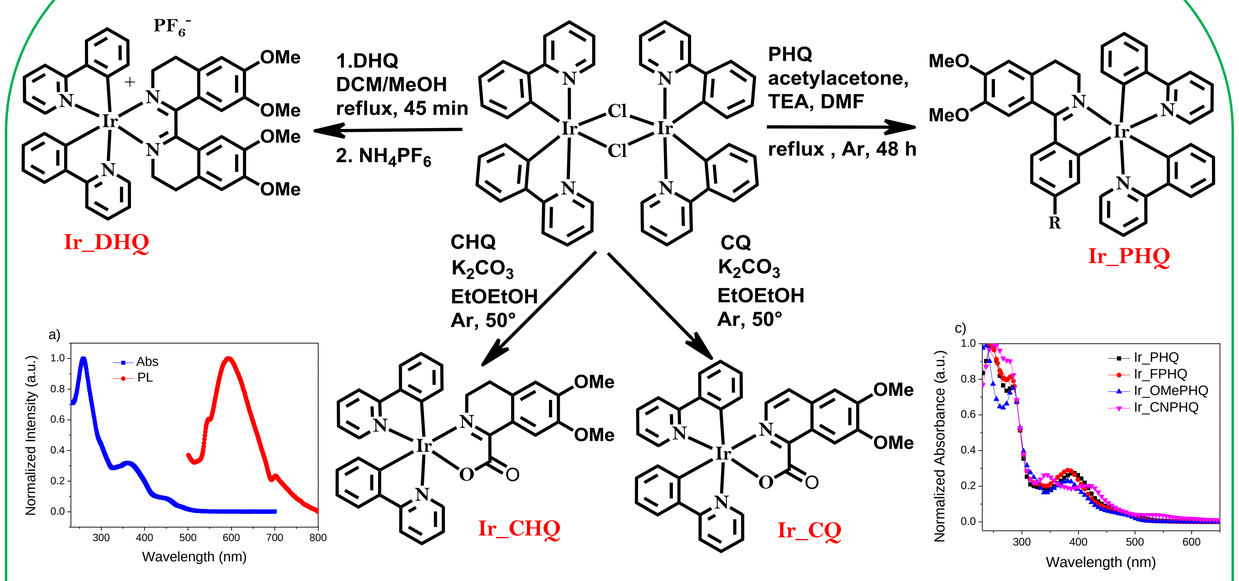

[a] Normalized absorbance and emission spectrum of Ir_DHQPF$_6$;
[b] Normalized absorbance and emission spectrum of Ir_CHQ and Ir_CQ;
[c] Normalized absorbance spectrum of Ir_PHQ complexes series;
[d] Normalized emission spectrum of Ir_PHQ complexes series;
[e] Photo-physical characteristics of iridium complexes ;

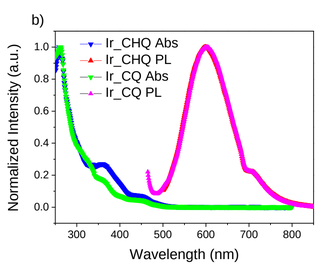

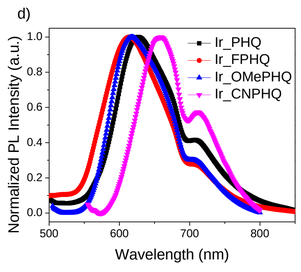

e)

	Ir_PHQ	Ir_FPHQ	Ir_OMePHQ	Ir_CNPHQ	Ir_CHQ	Ir_CQ	Ir_DHQ
Φ (λ_{exc},nm)[1]	0.41 (480)	0.24 (480)	0.21 (490)	0.11 (656)	0.14 (480)	0.36 (450)	0.40 (450)
Φ (λ_{exc},nm)[2]	0.30 (480)	0.70 (480)	0.61 (490)	0.14 (653)	0.25(480)	0.50 (450)	0.38 (450)

[1] determined relatively to fluorescein Φ= 0.9 in a 0.1 M solution of NaOH); [2] determined in oxygen free solutions of DCM

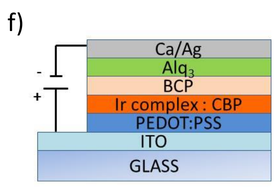

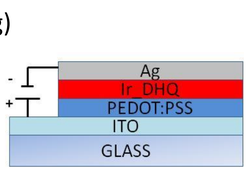

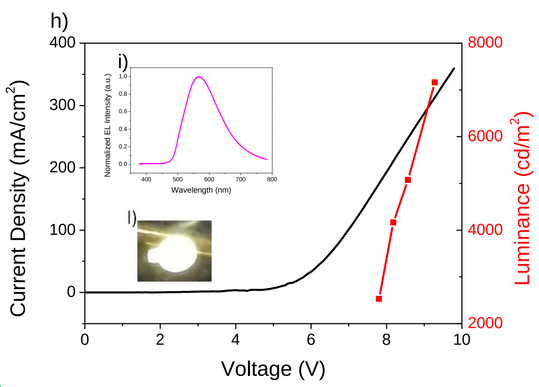

m)

	Lum. Max (cd/m^2)	Eff. max (cd/A)
CBP:Ir_PHQ 2%	527.75@11 V	0.49@9 V
CBP:Ir_FPHQ 6%	764@10 V	0.92@8.5 V
CBP:Ir_OMePHQ 2%	2475.43@14 V	1.78@13 V
CBP:Ir_CNPHQ 2%	469.06@14 V	0.33@10 V
CBP:Ir_CHQ 6%	3031@11.3 V	1.09@8.4 V
CBP:Ir_CQ 12%	7161@9.3 V	3.6@8.2 V
Ir_DHQ (LEEC)	138@23 V	0.07@23 V

[f] OLED device structure; [g] LEEC device structure; [h]IV-EL graph of CBP:Ir_CQ 12% OLED device;
[i] Normalized Electroluminescence spectrum of CBP:Ir_CQ 12% OLED device; [l] OLED picture;
[m] device performances with optimal iridium complexes percentage;

Ruthenium Complexes

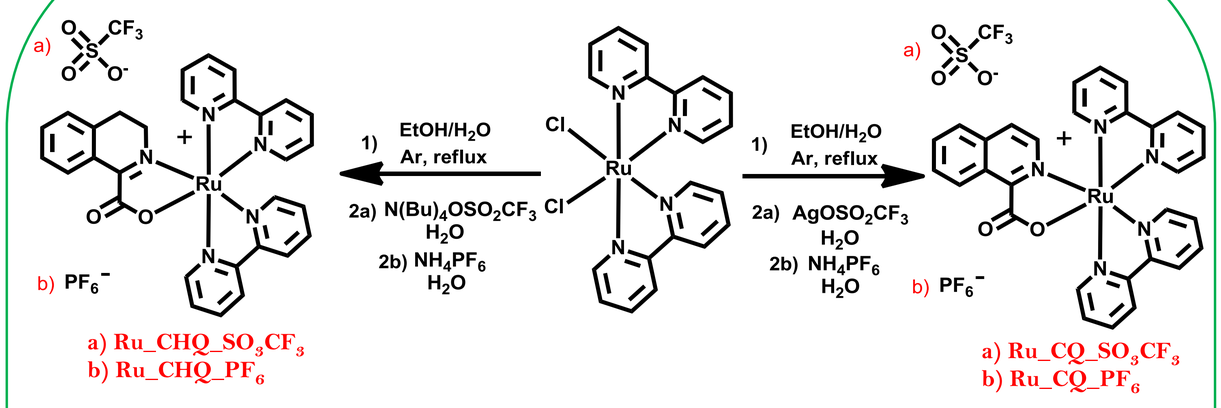

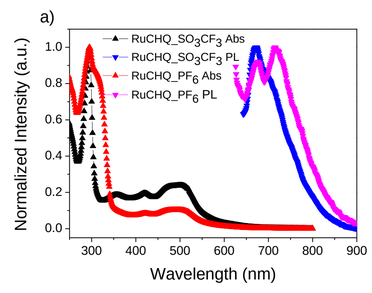

[a] Normalized absorbance and emission spectrum of RuCHQ_SO$_3$CF$_3$ and RuCHQ_PF$_6$;
[b] Normalized absorbance and emission spectrum of RuCQ_SO$_3$CF$_3$ and RuCQ_PF$_6$;
[c] photo-physical characteristics of ruthenium complexes ;

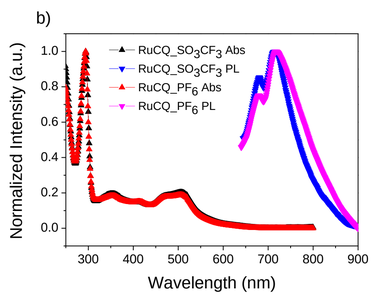

c)

	Ru_CHQ_SO$_3$CF$_3$	Ru_CHQ_PF$_6$	Ru_CQ_SO$_3$CF$_3$	Ru_CQ_PF$_6$
Φ (λ_{exc},nm)[1]	0.015 (500)	0.085 (506)	0.064 (504)	0.061 (606)
Φ (λ_{exc},nm)[2]	0.024 (506)	0.010 (506)	0.089 (504)	0.14 (606)

d)

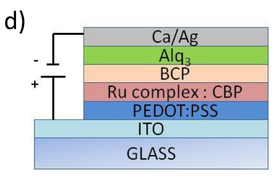

[d] OLED device structure; [e] device performances with optimal ruthenium complexes percentage;

e)

	Lum. Max (cd/m^2)	Eff. max (cd/A)
CBP:RuCHQ_SO$_3$CF$_3$ 8%	311.83@12 V	0.073@12 V
CBP:RuCHQ_PF$_6$ 2%	106.6@10V	0.039@6.2 V
CBP:RuCQ_SO$_3$CF$_3$ 2%	116.5@11.8 V	0.073@9 V
CBP:RuCQ_PF$_6$ 2%	154@12.5 V	0.046@10.5 V

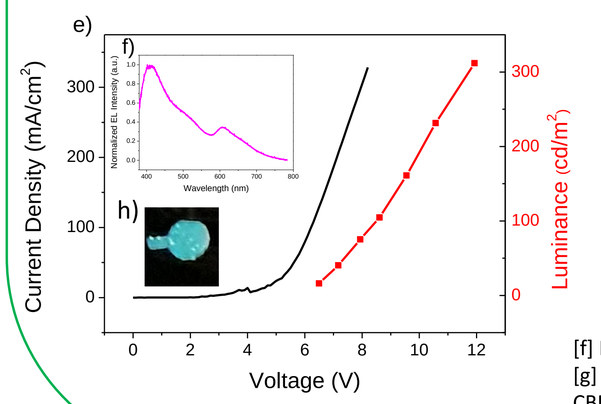

[f] IV-EL graph of CBP:RuCHQ_SO$_3$CF$_3$ 8% OLED device;
[g] Normalized Electroluminescence spectrum of CBP:RuCHQ_SO$_3$CF$_3$ 8% OLED device; [h] OLED picture;

References

[1] Pezzella, A.; Barra, M.; Musto, A.; Navarra, A.; Alfé, M.; Manini, P.; Parisi, S.; Cassinese, A.; Criscuolo, V.; d'Ischia, M. *Mater. Horiz.* **2015**, *2*, 212.

[2] Manini, P.; Criscuolo, V.; Ricciotti, L.; Pezzella, A.; Barra, M.; Cassinese, A.; Crescenzi, O.; Maglione M.G.; Tassini, P.; Minarini, C.; Barone, V.; d'Ischia, M. *ChemPlusChem*, **2015**, *80*, 919.

Synthesis and Photo-Physical Properties of Dopamine-Inspired Iridium Complexes for OLED Applications

Società Chimica Italiana
XXVI Congresso Nazionale della Società Chimica Italiana
10-14 Settembre 2017, Paestum (SA)

C.T. Prontera,[a*] V. Criscuolo,[a] A. Pezzella,[a] M.G. Maglione,[b] P. Tassini,[b] C. Minarini,[b] M. d'Ischia,[a] P. Manini[a]

[a] *Department of Chemical Sciences, University of Naples "Federico II", via Cintia 4, I-80126 Napoli, IT;*
[b] *Laboratory of Nanomaterials and Devices, ENEA C. R. Portici, Piazzale E. Fermi, Portici (NA), IT;*
[*] *carmelatania.prontera@unina.it*

Università degli Studi di Napoli Federico II
Agenzia nazionale per le nuove tecnologie, l'energia e lo sviluppo economico sostenibile

In the last decades, metal–organic complexes have attracted much attention due to their enormous potential application in optoelectronic devices.
In this work **dopamine**, the catecholic neurotransmitter and monomer precursor of neuromelanin and polydopamine, is used as starting compound for the synthesis of a set of heterocyclic compounds with different substituents.
Iridium(III) complexes were obtained with the dopamine-inspired ligands and the effects of the different groups on the optical and electroluminescence characteristics were studied.

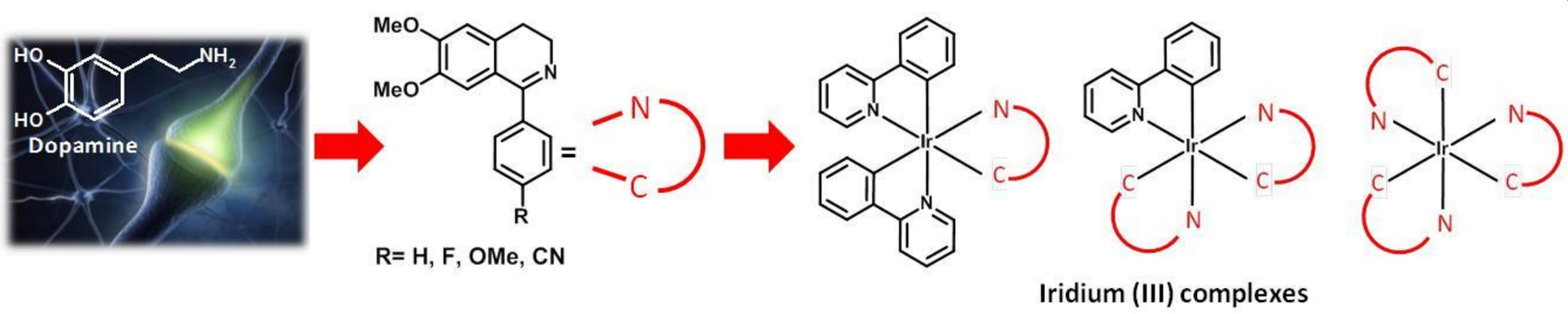

SYNTHESIS

The synthesis of the dopamine-inspired C^N cyclometalating ligands was performed via a Bischler-Napieralski reaction affording a set of 6,7-dimethoxy-3,4-dihydroisoquinolines substituted on the 1 position with phenyl residues, functionalized on the para-position with different groups (PHQs).
The iridium(III) complexes were obtained via the synthetic strategy of Nonoyama involving the intermediate formation of a dinuclear chloro-bridged iridium complex.
The important aspect of this work is that by using an excess of the cyclometalating ligands it was possible to isolate for the first time one-pot a set of three different neutral iridium(III) complexes deriving from the insertion of one, two or three dihydroisoquinoline ligands.

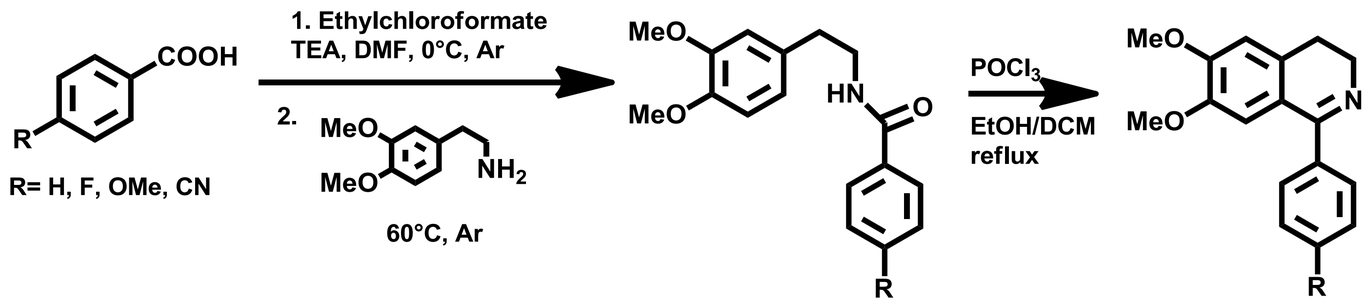

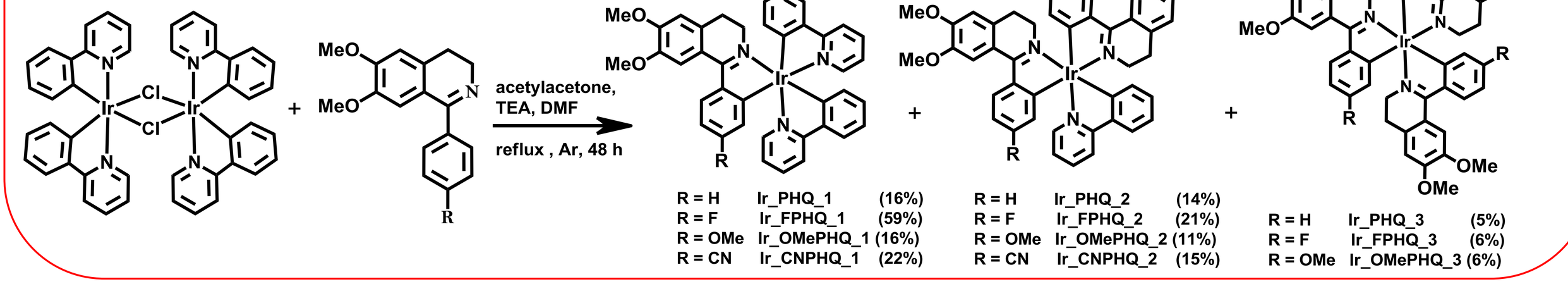

R = H	Ir_PHQ_1	(16%)	
R = F	Ir_FPHQ_1	(59%)	
R = OMe	Ir_OMePHQ_1	(16%)	
R = CN	Ir_CNPHQ_1	(22%)	

R = H	Ir_PHQ_2	(14%)	
R = F	Ir_FPHQ_2	(21%)	
R = OMe	Ir_OMePHQ_2	(11%)	
R = CN	Ir_CNPHQ_2	(15%)	

R = H	Ir_PHQ_3	(5%)
R = F	Ir_FPHQ_3	(6%)
R = OMe	Ir_OMePHQ_3	(6%)

PHOTO-PHYSICAL CHARACTERIZATION

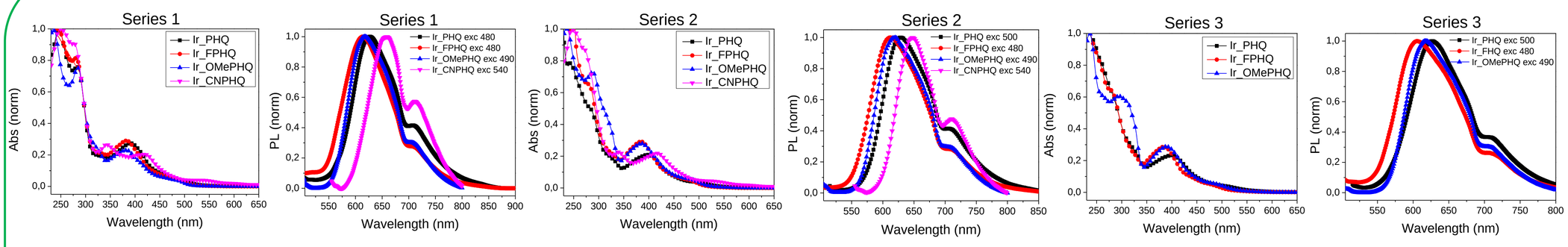

The absorption and emission profiles were influenced by the nature of the group on the phenyl substituent.
All the complexes exhibited a red-orange emission.
The R groups induced shifts of the emission maxima in the order F<OMe<H<CN.
Higher quantum yealds were observed in oxygen depleted solutions.

	Ir_PHQ_1	Ir_FPHQ_1	Ir_OMePHQ_1	Ir_CNPHQ_1	Ir_PHQ_2	Ir_FPHQ_2	Ir_OMePHQ_2	Ir_CNPHQ_2	Ir_PHQ_3	Ir_FPHQ_3	Ir_OMePHQ_3
Φ (λ_{exc},nm)[1]	0.41% (480)	0.24% (480)	0.21% (490)	0.11% (540)	0.14% (500)	0.15 % (480)	0.15% (490)	0.14% (540)	0.18% (500)	0.19% (480)	0.13% (490)
Φ (λ_{exc},nm)[2]	0.30% (480)	0.70% (480)	0.61% (490)	0.14% (540)	0.26% (500)	0.40 % (480)	0.23% (490)	0.15% (540)	0.23% (500)	0.22% (480)	0.19% (490)

[1] determined relatively to fluorescein Φ= 0.9 in a 0.1 M solution of NaOH); [2] determined in oxygen free solutions of DCM

DEVICE CHARACTERISTICS

OLED Devices structure

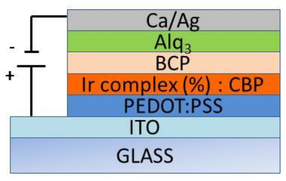

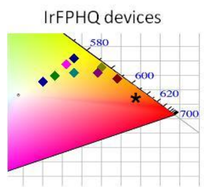

OLED device were fabricated to test the complexes as emitters.
Emitting layer was composed of a blend in which the complexes were used as guests at different percentage within CBP (host).
The emitting layer was realized by solution processing techniques (spin coating).

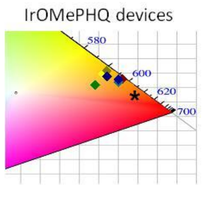

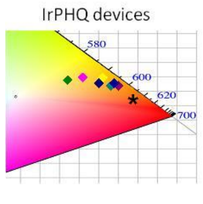

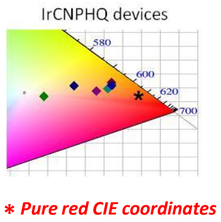

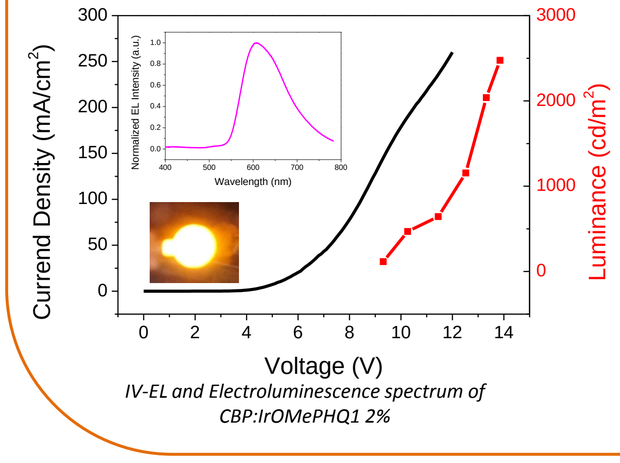

IV-EL and Electroluminescence spectrum of CBP:IrOMePHQ1 2%

** Pure red CIE coordinates*

Device 2%	Lum. Max (cd/m²)	Eff. max (cd/A)	Λ_{max} EL (nm)	Device 6%	Lum. Max (cd/m²)	Eff. max (cd/A)	Λ_{max} EL (nm)	Device 12%	Lum. Max (cd/m²)	Eff. max (cd/A)	Λ_{max} EL (nm)
F1	261.0@10.5V	0.25 @8.3V	600	**F1**	764@10V	0.92@8.5V	605	**F1**	687@13.5V	0.17 @13.5V	605
F2	1092@11V	0.35@11V	585	**F2**	384.9@12.2V	0.55 @10V	605	**F2**	472.2@13V	0.35@11V	605
F3	591.5@10.7V	0.55 @8V	580	**F3**	343@10.7V	0.27 @9.2V	602	**F3**	175@10V	0.07 @10V	602

Device 2%	Lum. Max (cd/m²)	Eff. max (cd/A)	Λ_{max} EL (nm)	Device 6%	Lum. Max (cd/m²)	Eff. max (cd/A)	Λ_{max} EL (nm)	Device 12%	Lum. Max (cd/m²)	Eff. max (cd/A)	Λ_{max} EL (nm)
OMe1	2475.4@14V	1.78 @13V	606	**OMe1**	319.4@10V	0.064 @10V	603	**OMe1**	580.5@12V	0.18 @12V	608
OMe2	1008@13V	0.81 @11V	612	**OMe2**	524.1@13V	0.29 @9V	618	**OMe2**	620.6@13V	0.52 @10V	618
OMe3	583.7@12V	0.34 @9V	615	**OMe3**	745.7@13V	0.24 @11V	616	**OMe3**	425.6@13V	0.18 @11V	619

Device 2%	Lum. Max (cd/m²)	Eff. max (cd/A)	Λ_{max} EL (nm	Device 6%	Lum. Max (cd/m²)	Eff. max (cd/A)	Λ_{max} EL (nm	Device 12%	Lum. Max (cd/m²)	Eff. max (cd/A)	Λ_{max} EL (nm)
H1	527.8@11V	0.49@9V	610	**H1**	718.9@15V	0.92 @10V	610	**H1**	709.3@12V	0.54 @10V	615
H2	682.4 @11V	0.29@10V	620	**H2**	496@15.5V	0.56 @10V	620	**H2**	483.6@12V	0.32 @9V	624
H3	600.6@10V	0.64@7.8V	620	**H3**	435@16V	0.55 @11.5V	625	**H3**	518.7@12V	0.44@10.5V	625

Device 2%	Lum. Max (cd/m²)	Eff. max (cd/A)	Λ_{max} EL (nm	Device 6%	Lum. Max (cd/m²)	Eff. max (cd/A)	Λ_{max} EL (nm	Device 12%	Lum. Max (cd/m²)	Eff. max (cd/A)	Λ_{max} EL (nm)
CN1	469.1@14V	0.33 @10V	628	**CN1**	256.7@13V	0.065 @12V	638	**CN1**	385.6@13V	0.17 @12V	635
CN2	323.5@10V	0.15 @10V	635	**CN2**	159.7@13V	0.051 @11V	639	**CN2**	161.1 @12V	0.056 @12V	640

The best devices in terms of luminance and turn-on voltage resulted those prepared by using a 2% wt of the iridium(III) complexes. The electroluminescence maximum and the CIE coordinates show a red shift as a function of the percentage of the complex used in the device and with the substituent (F → OMe → H → CN).

Ministero dello Sviluppo Economico
relight REsearch for LIGHT

FINANCIAL SUPPORT
- **Program Agreement (Ricerca di Sistema Elettrico) between ENEA and Italian Ministry of Economic Development (MISE);**
- **Italian Project RELIGHT (REsearch for LIGHT);**
- **European Commission (PolyMed project in the FP7-PEOPLE-2013-IRSES frame, r.n. IRSES-GA-2013-612538) .**

From natural systems to lighting electronics: designing melanin-inspired electroluminescent materials

Valeria Criscuolo,[a] Paola Manini,[a] Carmela Tania Prontera,[a] Alessandro Pezzella,[a] Maria Grazia Maglione,[b] Paolo Tassini,[b] Carla Minarini[b]

[a] Department of Chemical Sciences, University of Naples "Federico II" ,Via Cintia 4, I-80126 Napoli, IT

[b] Laboratory of Nanomaterials and Devices, ENEA C. R. Portici, Piazzale E. Fermi 1, I-80055 Portici, IT

valeria.criscuolo@unina.it

The recent advances in the field of organic light emitting diodes (OLEDs) have been focused mainly on the need to combine the main strengths of this technology, that is the versatility (i.e. wide color tuning, ultrathin, flexible and large area devices) and the eco-compatibility (low-energy consumption), with the efficiency and the lifetime of the devices, with the aim of making OLEDs very appealing and competitive with respect to the inorganic LEDs. In the last few years, another issue has been explored in connection with the growing expansion and impact of the green electronic field, that is the challenge of integrating natural or nature-inspired materials within organic electronic devices, and so in OLEDs.

In the frame of a research plan aimed at studying the role of melanins, the dark pigment found in mammalian skin, hair and eyes, in organic electronics,[1] we have recently explored the potentiality of new heterocyclic platforms designed taking inspiration from the mammalian pigments as eco-compatible electroluminescent materials for OLED application. Herein we report on the synthesis of two different types of organic emitters, the fluorescent asymmetrical triazatruxene[2] and the phosphorescent iridium(III) complex (Figure 1). The first one has been obtained starting from 5,6-dihydroxyindole, the eumelanin monomer precursor, and the second one has been prepared by using ligands obtained from dopamine, the catecholic neurotransmitter and monomer precursor of the melanic polydopamine pigment. All the compounds obtained have been subjected to structural characterization and investigation of the photo-physical and electronic properties, also with the support of theoretical calculations. Moreover, a comparative study has been carried out to delineate the role of different kind of functional groups on tuning the wavelength of the emitting light. The most promising compounds have been selected for the fabrication of both fluorescent and phosphorescent OLEDs and of the most advanced light emitting electrochemical cell (LEEC) devices. The performances of the devices is also discussed.

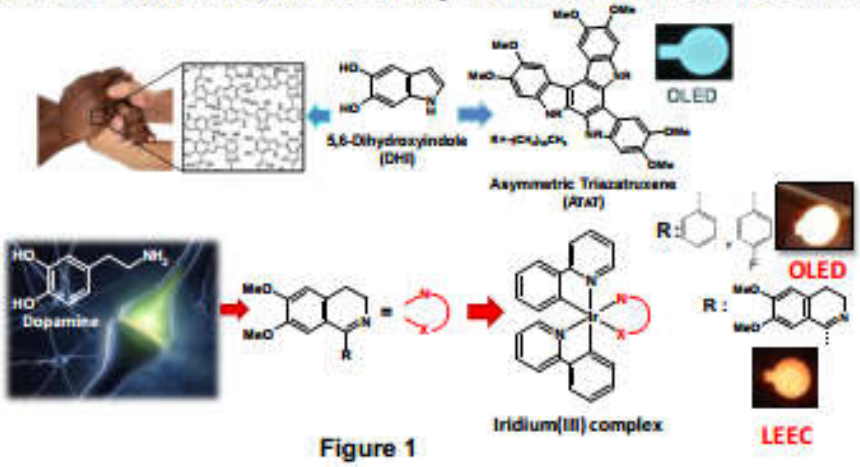

Figure 1

References

1. Pezzella A. *et al. Materials Horizons* **2015**, *2*, 212-220
2. Manini, P. *et al. ChemPlusChem* **2015**, *80*, 898

Controlling the supramolecular structure of polymers from natural sources to assess their electrical properties

Xu Ri, T. Prontera, D. Boisvert, E. Di Mauro, F Soavi, P. Manini, A. Pezzella, C. Santato

clara.santato@polymtl.ca

Département de Génie physique, École Polytechnique de Montréal, Canada
Dipartimento di Chimica, Università di Napoli, Italy
Dipartimento di Chimica, Università di Bologna, Italy

POLYTECHNIQUE MONTRÉAL

Our challenge

Natural materials are relevant for sustainable electronics (abundant, biodegradable) and bioelectronics (biocompatible);
The molecular structure of natural materials can be quite complex;
The effect of the molecular structure on their physicochemical properties has to understood to demonstrate novel technologies.

Controlling the molecular structure of the biopigment eumelanin to properly assess charge transfer and charge carrier transport properties

Strong broad-band UV-vis absorption
Hydration-dependent conductivity
Electrochemically active

Metal ion chelation
Free radical scavenger

Applications at the interface of biological systems and electronics

- Bio-compatible, -degradable, metal ion sensing
- In-vivo sensing and stimulation of biological processes
- Nerve tissue engineering

*J. McGinness et al., *Science* 183 (1974) 853 P. Meredith et al., *Pigment Cell Res.* 19 (2006) 572
M. Ambrico et al., *Adv. Mater.* 23 (2011) 3332 C. J. Bettinger et al., *Biomaterials* 30 (2009) 3050

Introduction: chemistry of eumelanin

Building blocks (monomers):

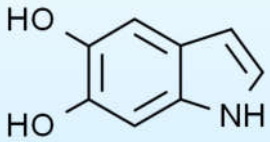

5,6-dihydroxyindole

DHI

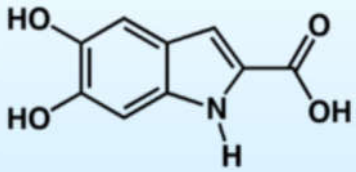

5,6-dihydroxyindole-2-carboxylic acid

DHICA

Monomers synthesis (University of Naples)

DHI synthesis from L-dopa (L-3,4-dihydroxyphenylalanine)

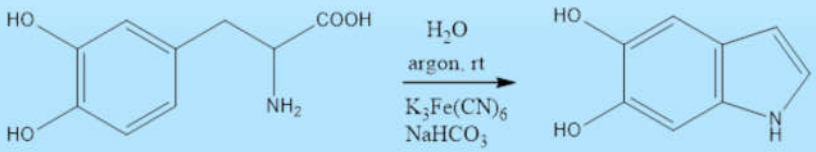

DHICA synthesis from L-dopa

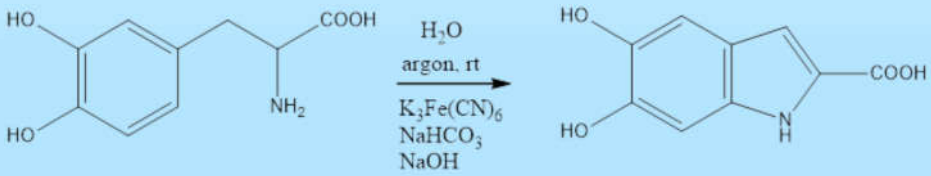

POLYTECHNIQUE MONTRÉAL

The material we selected: the melanin biopigment

Building blocks

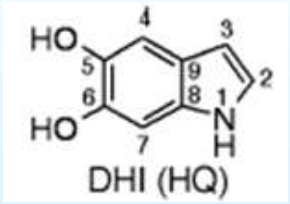

5,6-dihydroxyindole

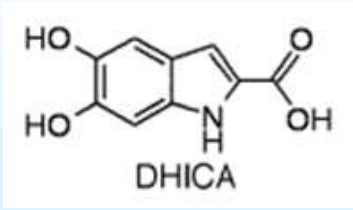

5,6-dihydroxyindole-2-carboxylic acid

+redox forms

Possible macromolecular structures

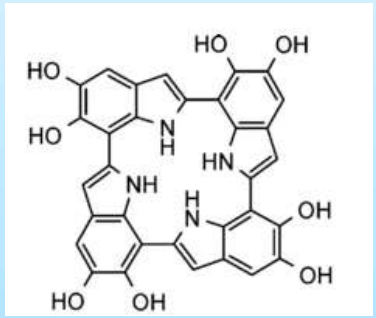

E. Kaxiras, *Phys. Rev. Lett.* 97 (2006) 218102

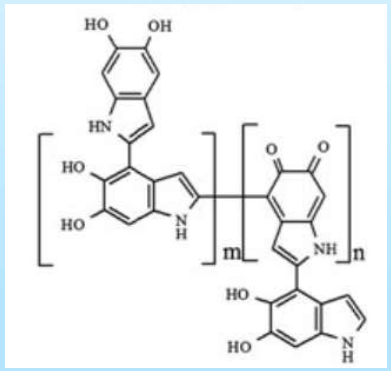

S. Reale et al., *J. Mass Spectrometry* 47 (2012) 49

A. Huijser, *Phys. Chem. Chem. Phys.* 13 (2011) 9119

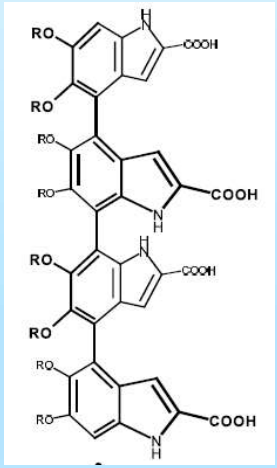

A. Pezzella, *Tetrahedron:Assymetry* 14 (2003) 1133

POLYTECHNIQUE MONTRÉAL

Eumelanin by solid state polymerization of DHI and DHICA building blocks

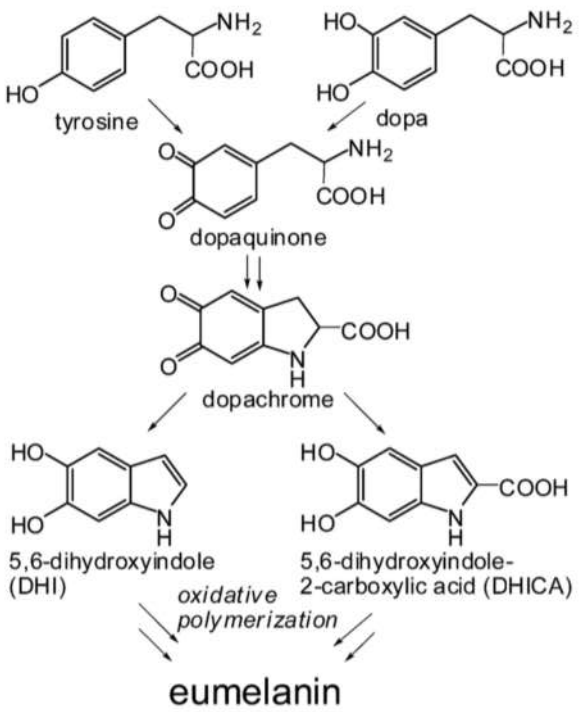

Scheme 1 Schematic view of eumelanin synthesis from tyrosine or dopa. Representative intermediates in the process are highlighted.

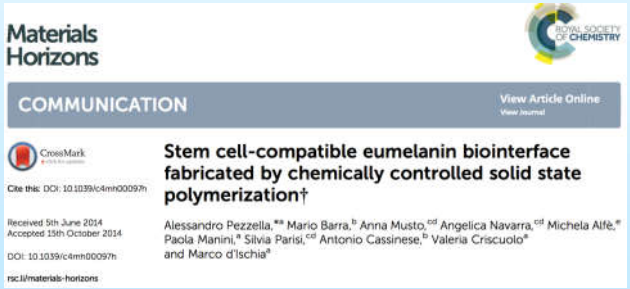

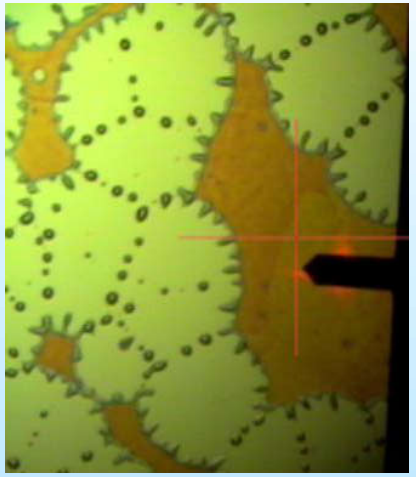

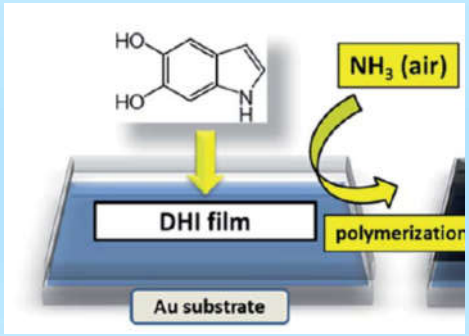

POLYTECHNIQUE MONTRÉAL

Cyclic voltammetry of poly DHI and poly DHICA

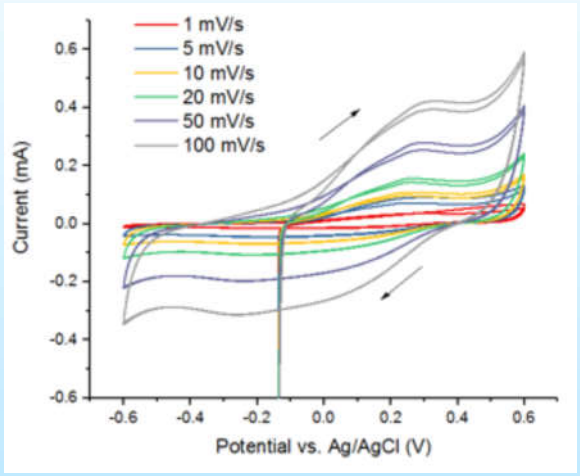

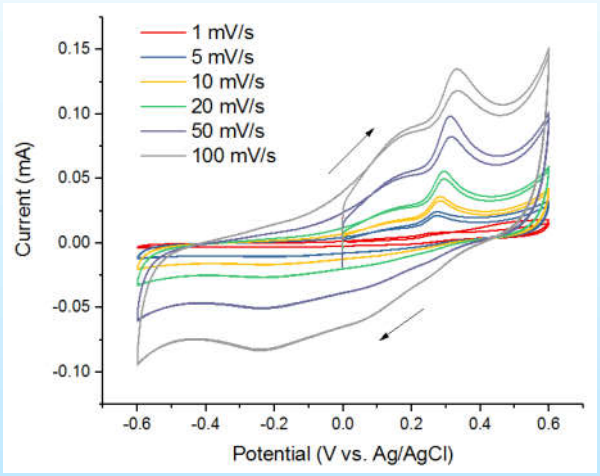

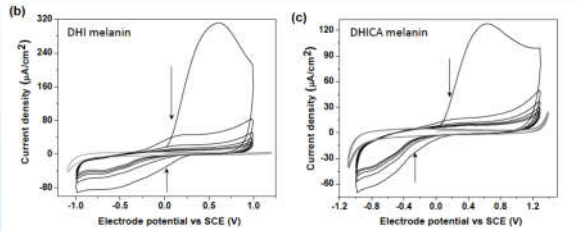

Figure S10: Cyclic voltammetry of *Sigma melanin* (a), *DHI melanin* (b), and *DHICA melanin* films (c) on ITO substrates as working electrode, platinum foil and saturated calomel electrode as the counter and the reference electrodes, respectively. Nitrogen purged PBS buffer (0.01 M) of pH 7.4 is used as the electrolyte and a 50 mV s^{-1} scan rate is maintained. The voltage is cycled from 0 to positive *V* and then to negative. The cyclic voltammogram of ITO without melanin in PBS is represented in gray. Black arrows indicate the decrease in current density as a function of the number of cycles.

DOI: 10.1021/cm502939r
Chem. Mater. 2015, 27, 436−442

Poly DHI and poly DHICA obtained by solid state polymerization on carbon paper

Ammonium acetate buffer (0.25 M) at pH 4.9. Electrode geometric area 0.5 cm^2

Current for polyDHI is 3 times higher than that of polyDHICA, tentatively attributed to a better π-π stacking in polyDHI than polyDHICA.

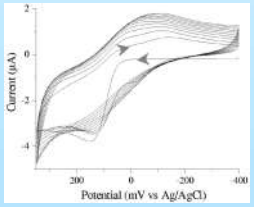

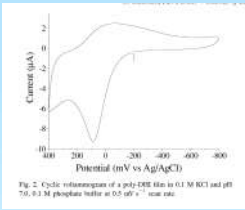

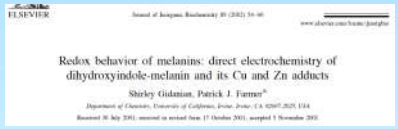
ELSEVIER

Redox behavior of melanins: direct electrochemistry of dihydroxyindole-melanin and its Cu and Zn adducts

Shirley Gidanian, Patrick J. Farmer*

Cyclic voltammetry of poly DHI and poly DHICA

Cyclic voltammograms of polyDHI and polyDHICA on carbon paper electrodes in acetate buffer solutions including different cations (0.25 M) at pH ~4.9 at sweeping rate of 5 mV/s with electrode geometric area of 0.5 cm^2.

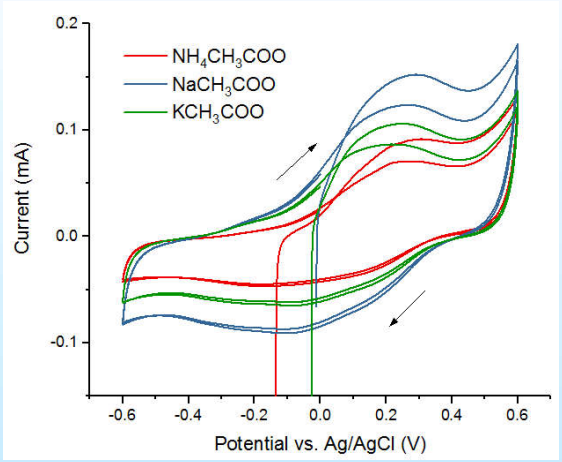

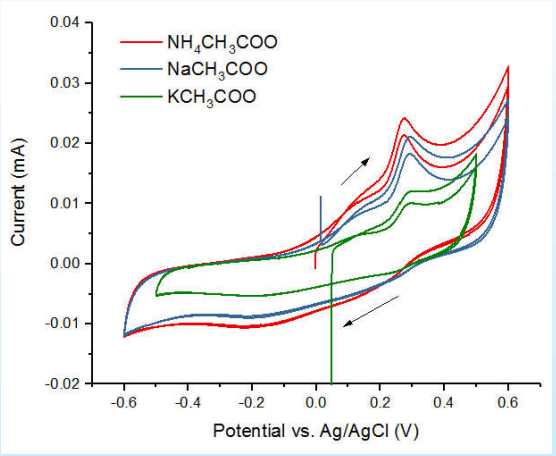

Sigma melanin

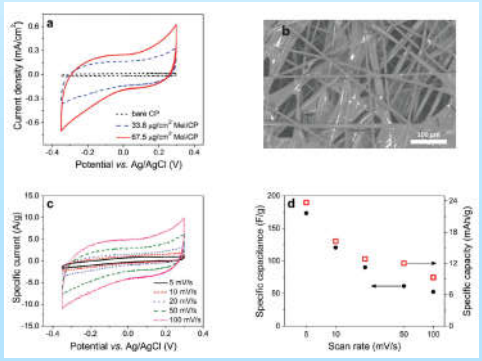

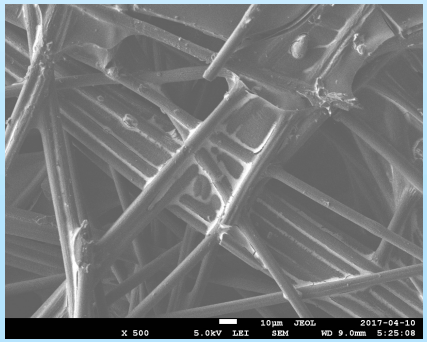

polyDHI, 3 min

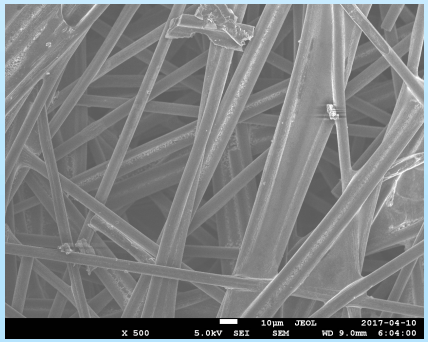

polyDHICA, 60 min

Ongoing study to assess the effect of Cu, Fe ions (biofunctional role eumelanin) Li, Ca and Mg and **the electrode substrate**

Staining 2% uranyl acetate (aq)

POLYTECHNIQUE MONTRÉAL

Thin films of DHI monomers in ambient conditions (O_2)!

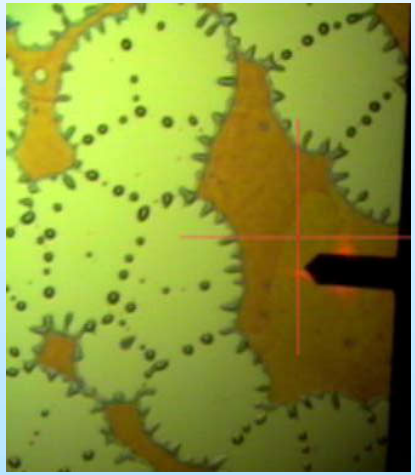

SiO_2 on Si substrate
10 mg/mL DHI monomers in methanol
Measure 1 h after deposition
Spin coated
AFM tip Si (40 N/m) model Acta from Applied Nano inc.

Rq ~ 16 nm

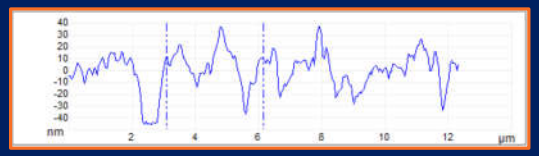

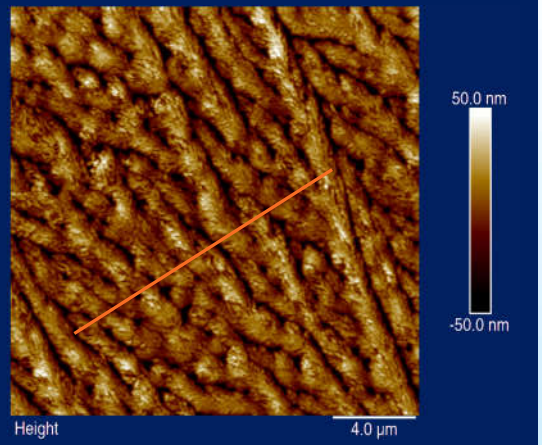

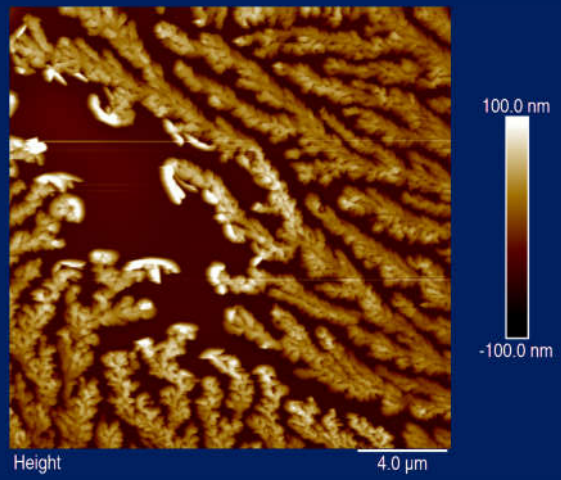

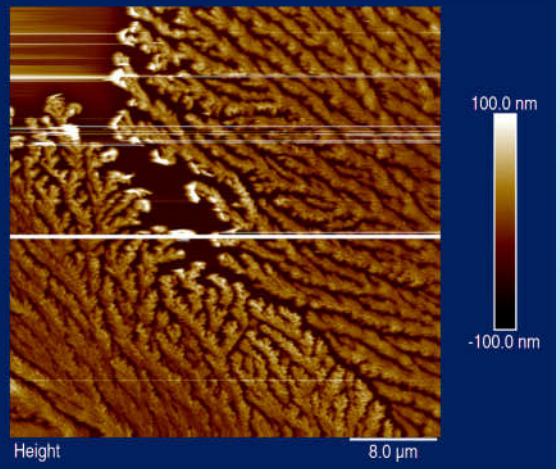

POLYTECHNIQUE MONTRÉAL

Films of DHI monomer in ambient conditions (O_2)!

Polymerization *live* …
4 min between one image and the following one

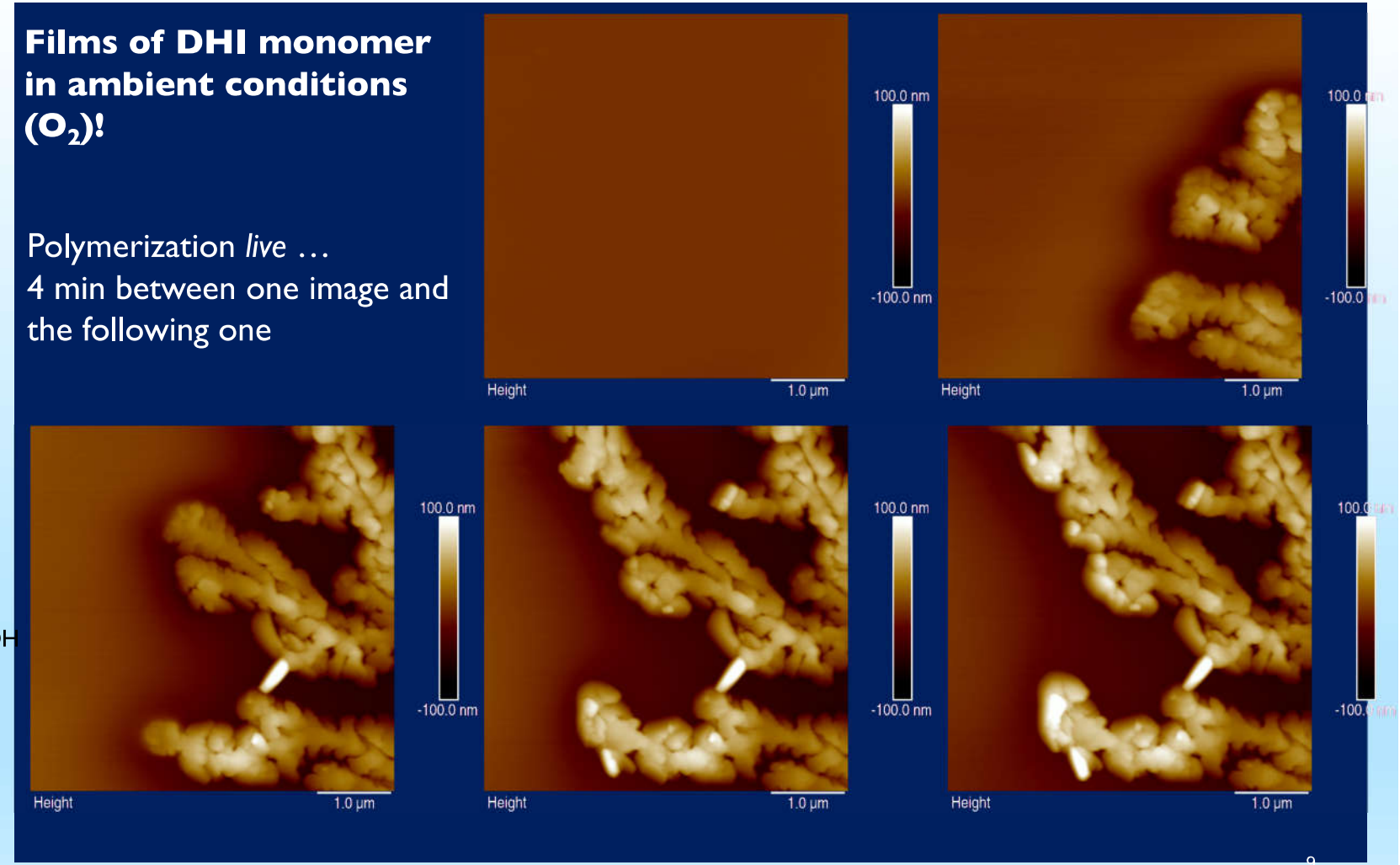

SiO_2 on Si substrate
1 h after deposition
10 mg/mL DHI in CH3OH
Spin coated

POLYTECHNIQUE MONTRÉAL

SEM Images of (poly)DHI on Au

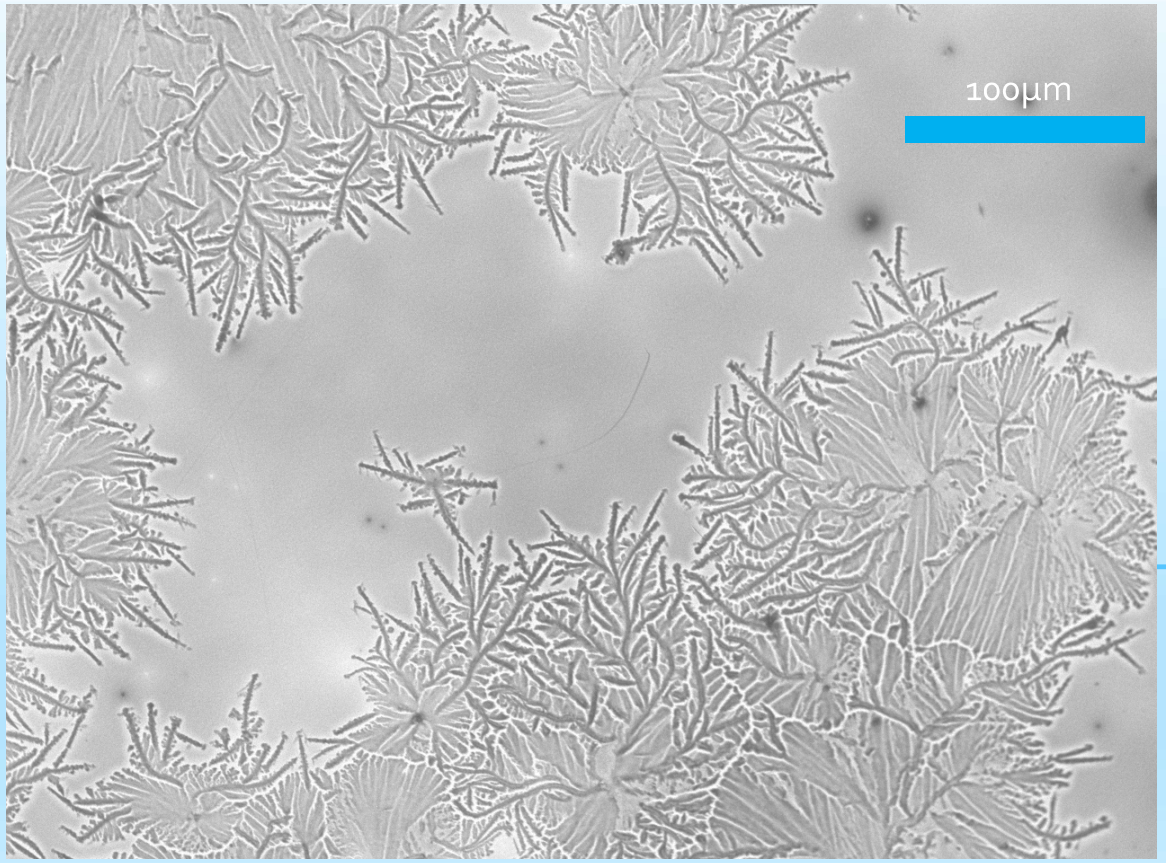

Are these structure polymers (or self assembled structures)?

We are characterizing them by nanoIR and (spatially resolved) optical absorption

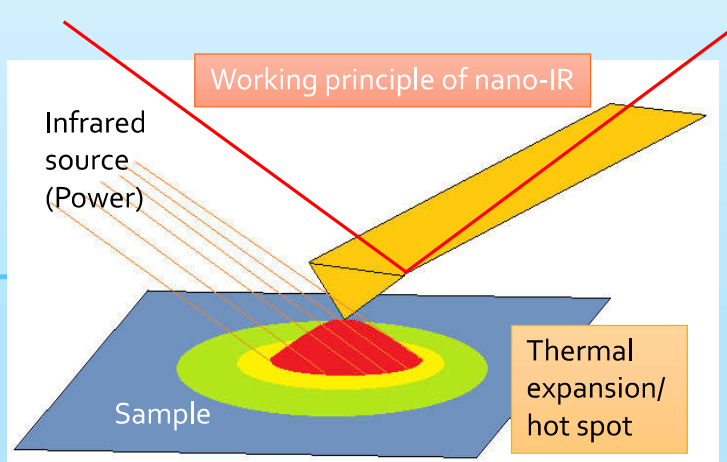

Tip resonates with the thermal expansion to give signal (photothermal resonance)

POLYTECHNIQUE MONTRÉAL

SEM Images of (poly)DHI on Au

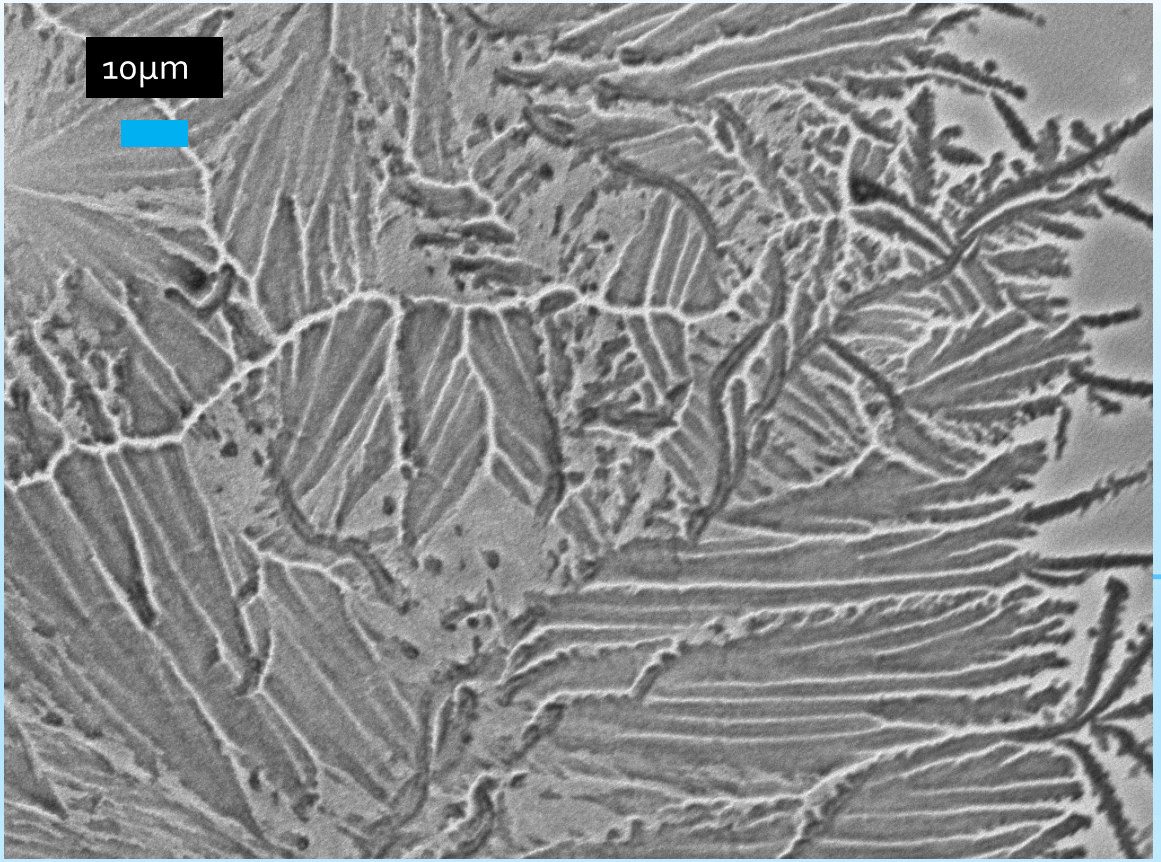

Are these structure polymers (or self assembled structures)?

We are characterizing them by nanoIR and (spatially resolved) optical absorption

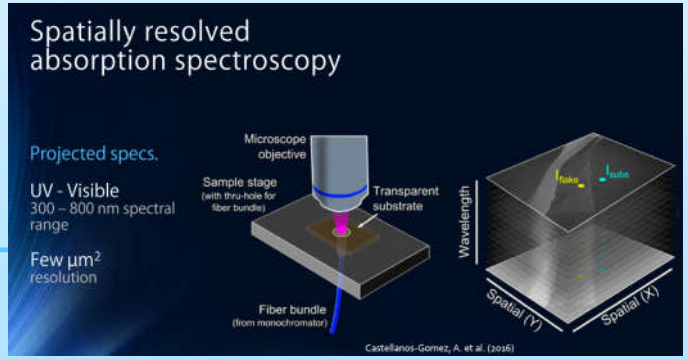

Collaboration Prof Francoeur lab (Polytechnique)

POLYTECHNIQUE MONTRÉAL

SEM Images of (poly)DHI on Au

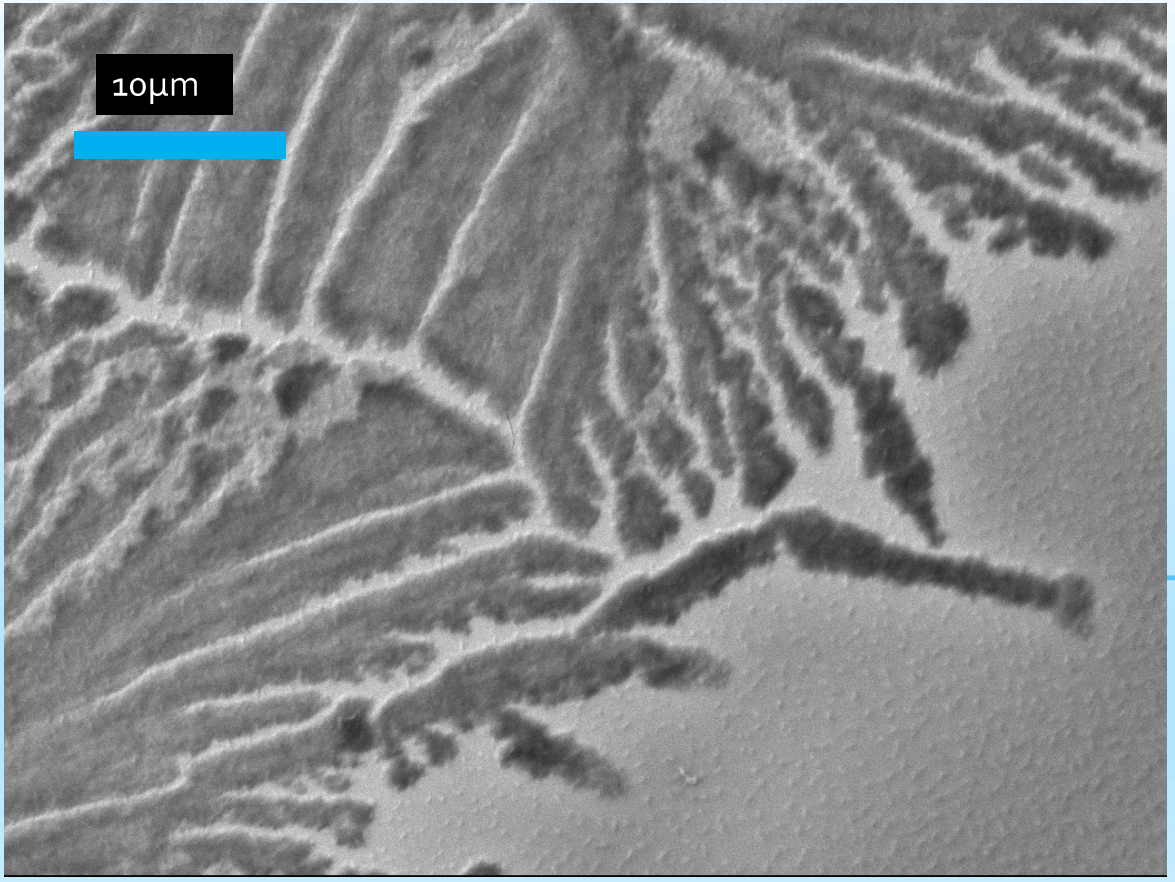

Dendritic structures of poly(DHI) forming on thermally evaporated gold, 30 min after the spin coating of DHI monomers from CH_3OH suspension.

Our structures should contribute to assess the nature of the chromophore in melanin.

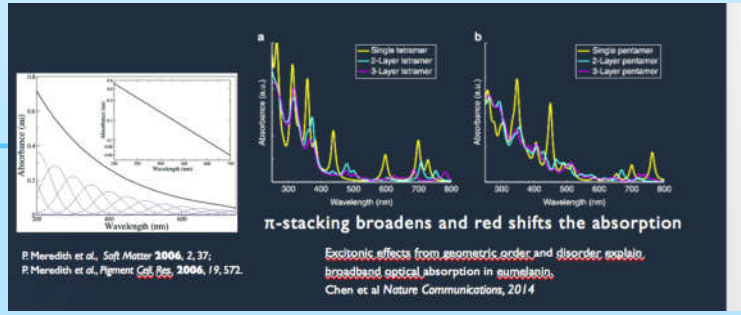

POLYTECHNIQUE MONTRÉAL

SEM images of (poly)DHI on evaporated gold and thermal SiO2 on Si

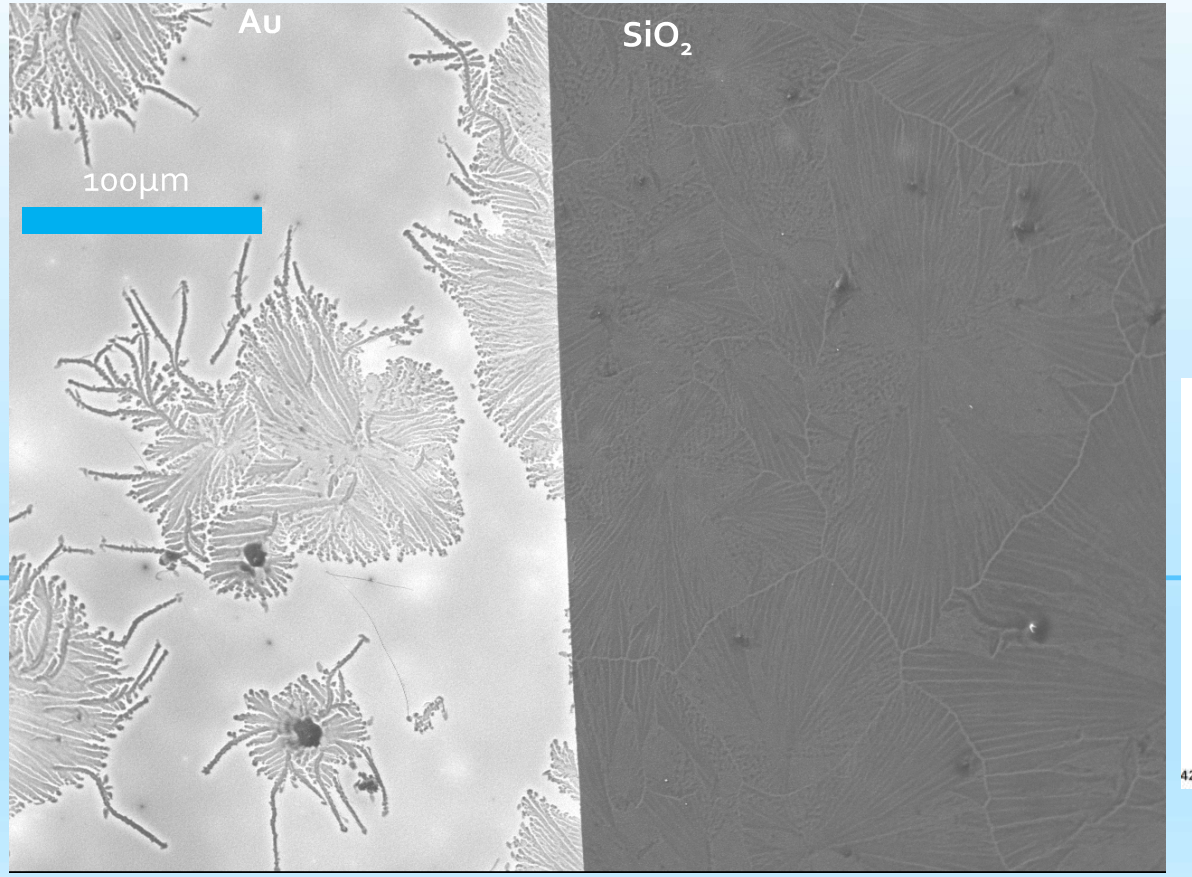

The structures on Au seem to be more branched than on SiO_2.
Full coverage on SiO_2 (better adhesion?)

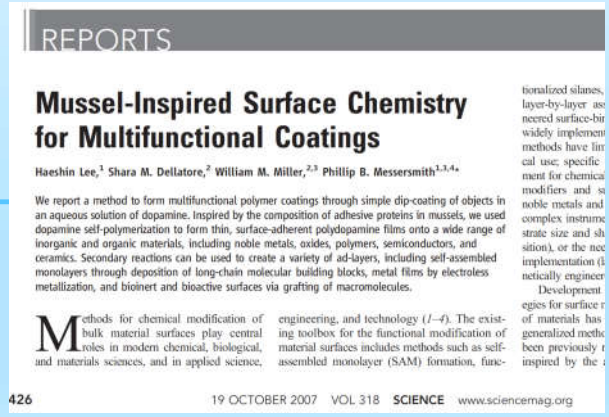

REPORTS

Mussel-Inspired Surface Chemistry for Multifunctional Coatings

Haeshin Lee,[1] Shara M. Dellatore,[2] William M. Miller,[2,3] Phillip B. Messersmith[1,3,4]*

We report a method to form multifunctional polymer coatings through simple dip-coating of objects in an aqueous solution of dopamine. Inspired by the composition of adhesive proteins in mussels, we used dopamine self-polymerization to form thin, surface-adherent polydopamine films onto a wide range of inorganic and organic materials, including noble metals, oxides, polymers, semiconductors, and ceramics. Secondary reactions can be used to create a variety of ad-layers, including self-assembled monolayers through deposition of long-chain molecular building blocks, metal films by electroless metallization, and bioinert and bioactive surfaces via grafting of macromolecules.

Methods for chemical modification of bulk material surfaces play central roles in modern chemical, biological, and materials sciences, and in applied science, engineering, and technology (*1*–*4*). The existing toolbox for the functional modification of material surfaces includes methods such as self-assembled monolayer (SAM) formation, func-

426 19 OCTOBER 2007 VOL 318 SCIENCE www.sciencemag.org

POLYTECHNIQUE MONTRÉAL

CONCLUSIONS, PERSPECTIVES

(Natural materials, chemically heterogeneous and physically disordered)

- To establish extended structure-property-device performance correlation there is a patient systematic *bottom up* type of work to be done THIS IS WHAT WE DID, i.e. we followed the formation of the materials form monomers prior physicochemical characterization
- We are starting to know what are the charge transfer properties of melanin in aqueous media
- We now study the electrical response of melanin forming on pre-patterned substrates

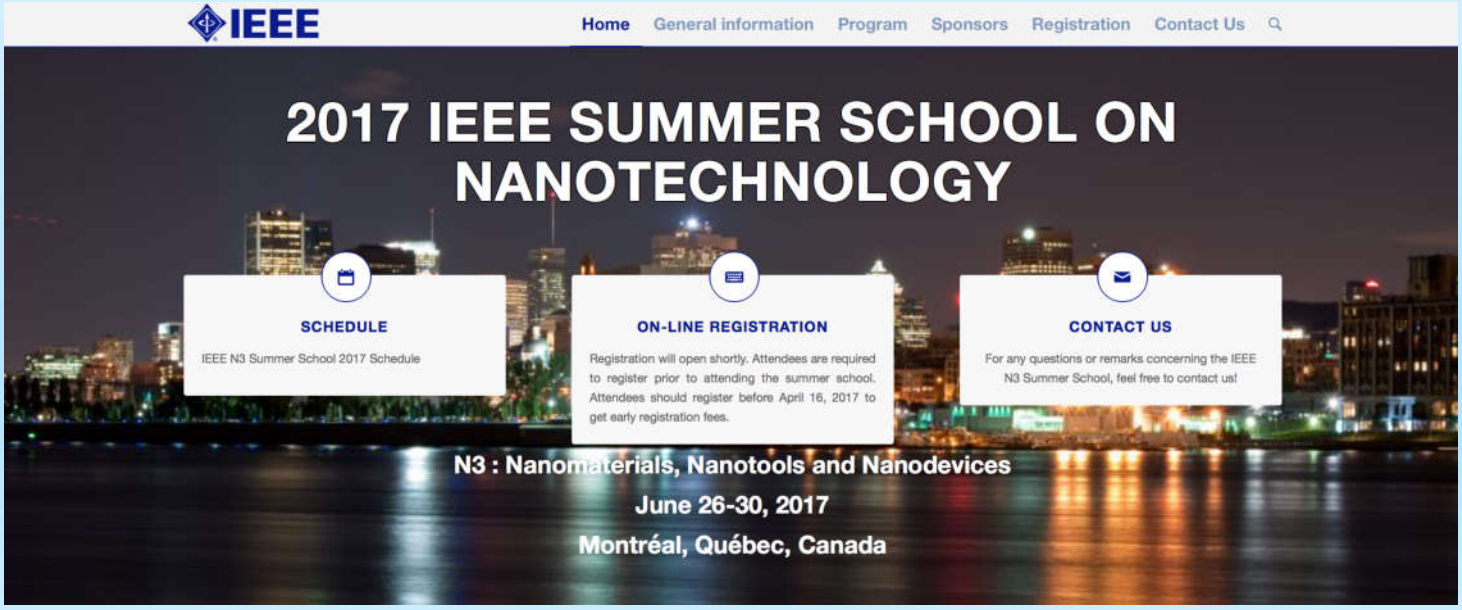

Melanins in bioelectronics: a survey of the role of these natural pigments from bio-interfaces to (opto)electronic devices

Paola Manini,[a] Valeria Criscuolo,[a] Ludovico Migliaccio,[a] Carmela Tania Prontera,[a] Alessandro Pezzella,[a] Orlando Crescenzi,[a] Marco d'Ischia,[a] Silvia Parisi,[b] Mario Barra,[c] Antonio Cassinese,[c] Pasqualino Maddalena,[c] Maria Grazia Maglione,[d] Paolo Tassini,[d] Carla Minarini[d]

[a] Department of Chemical Sciences, University of Naples "Federico II", Napoli, IT
[b] Department of Molecular Medicine and Medical Biotechnology, University of Naples "Federico II", Napoli, IT
[c] CNR-SPIN and Department of Physics, University of Naples Federico II, Napoli, IT
[d] Laboratory of Nanomaterials and Devices, ENEA C. R. Portici, Portici, IT

paola.manini@unina.it

The growing expansion and impact of bioelectronics and the associated challenge of integrating biological or bio-inspired materials within organic electronic devices have thrown new light on the role played by some biologically relevant polymers as soft organic semiconductors. Among these, melanins, the dark pigment found in mammalian skin, hair and eyes, rapidly have gained a prominent position for their bioavailability, biocompatibility and a peculiar set of physical-chemical properties, i.e. broadband absorption in the UV-visible range, intrinsic free radical character, water-dependent hybrid ionic–electronic conductor behavior.[1]
A survey of the recent advances made by our research group in Naples on the possible applications of these natural pigments in bio-electronic devices will be discussed, moving from OPV to OECT devices, up to the design and investigation of melanin-based bio-interfaces for stem cells adhesion, proliferation and differentiation.[2] The design of melanin-inspired functional materials will also be presented with particular attention to the synthesis of new heterocyclic platforms obtained via structural modifications of melanin monomer precursors and their applications as electroluminescent materials in OLED devices.[3]

References

1. d'Ischia, M. *et. al. Angew. Chem. Int. Edit.* **2009**, *48*, 3914-3921.
2. Pezzella, A. *et al. Mater. Horiz.* **2015**, *2*, 212-220.
3. Manini, P. et al. *ChemPlusChem*, **2015**, *80*, 919-927.

Perugia, Italy. April 6-7, 2017

17th CIRIAF National Congress

Sustainable Development, Human Health and Environmental Protection

Impatto della contabilizzazione del calore sui consumi energetici in Italia

I. Bertini[2], L. Canale[1]*, M. Dell'Isola[1], B. Di Pietra[2], G. Ficco[1], G.Puglisi[2], S. Stoklin[1]

[1] Dipartimento di Ingegneria Civile e Meccanica (DICEM), Università di Cassino e del Lazio Meridionale, Via G. Di Biasio 43, 03043 Cassino, Italy

[2] ENEA Agenzia Nazionale per le nuove tecnologie, l'energia e lo sviluppo sostenibile, Unità Tecnica Efficienza Energetica

* Author to whom correspondence should be addressed. E-Mail: l.canale@unicas.it

Abstract: Heat accounting in residential buildings has been identified by the European Union (EU) as one of the main drivers to reduce energy consumption in the residential sector. To this aim, the European Directive 2012/27/EU and the Italian Decree nr. 102/2012 and subsequent modifications set the obligation for apartment and multi-apartment buildings supplied by a common central heating source or by a district heating/cooling network, to install, by December the 31st 2016, sub-metering systems to allow a fair cost allocation through the tenants. In Italy the obligation has been recently extended to June, the 30th, 2017.

In several studies conducted in different EU Member States a very wide range of variability (8-40%) of the expected benefit of heat accounting systems has been found. Unfortunately, specific studies regarding the Italian territory and the Mediterranean climate conditions are still lacking. Nevertheless, due to the large number of buildings virtually subject to the obligation, the potential for energy savings in Italy could be among the highest in Europe. In the present study, after a brief analysis of energetic benefit of common heat accounting systems, the authors evaluate the potential impact of such systems on the energy consumption of the Italian residential building stock. To this end, the Italian residential building stock has been analyzed through both the ISTAT census 2011 and a recent statistical analysis performed by ENEA based on ISTAT data.

Keywords: efficienza energetica, contabilizzazione del calore, termoregolazione.

1. Introduzione

Nel 2012 l'Unione Europea ha formalizzato la sua attenzione verso una maggiore consapevolezza dei consumi energetici delle utenze energivore emanando la Energy Efficiency Directive 2012/27/EU [1]. In particolare, l'articolo 9 stabilisce che il consumatore debba essere incoraggiato a gestire meglio i propri consumi attraverso la contabilizzazione individuale e la fatturazione informativa. Nello stesso articolo si stabilisce l'obbligo per tutti gli Stati Membri di installare, entro il 31 Dicembre 2016 (in Italia recentemente prorogato al 30 Giugno 2017), sistemi di contabilizzazione individuale del calore in tutte quelle utenze del settore residenziale alimentate da una fonte di riscaldamento/raffrescamento centralizzata e/o da teleriscaldamento/teleraffrescamento, a patto che la loro installazione sia efficiente in termini di rapporto costi/benefici.

Celenza et al. (2015) [2] hanno evidenziato che, nei confronti dell'obbligo imposto dalla direttiva, gli Stati Membri hanno adottato strategie politiche variabili: Germania ed Austria, ad esempio, obbligano quasi la totalità degli edifici all'installazione di tali sistemi, mentre Finlandia e Svezia esentano la quasi totalità degli edifici potenzialmente soggetti all'obbligo della direttiva europea, ritenendo in ogni caso svantaggioso il loro rapporto costi/benefici.

Sono pochi i lavori che affermano l'impossibilità di confermare l'esistenza di un reale beneficio. Tra questi, uno studio commissionato al Boverket dallo stato svedese [3], conclude che la contabilizzazione individuale e la fatturazione basata sulla misura della temperatura non è conveniente, richiedendo investimenti infruttuosi per i proprietari. La restante letteratura scientifica europea riguardante la stima dei benefici attesi dall'installazione dei sistemi di contabilzzazione individuale nelle utenze alimentate da impianti centralizzati o da teleriscaldamento, è tuttavia concorde nell'affermare l'esistenza di un beneficio quantificato di fatto in un range di variabilità 8-40%.

Una sintesi degli ultimi 85 anni di letteratura è presentata in un recente lavoro di review bibliografica pubblicato da Felsmann et al. al termine del 2015 [4]. Nello studio si conclude che il risparmio di energia ottenbile in Europa derivante da una fatturazone basata sui reali consumi individuali si attesta in media al 20%. Tale stato dell'arte analizza i risultati di 32 studi, relativi a Stati Membri dai climi continentali (Polonia, Germania, Austria, Svizzera, Russia etc.), di cui soltanto 5 sono basati sulla misura del risparmio effettivo effettuata sulla base dell'osservazione sperimentale degli edifici nelle stagioni di riscaldamento precedente e successiva all'installazione di misuratori di calore.

Analisi sperimentali più recenti confermano i benefici stimati da Felsmann per climi continentali in grandi condomini come conseguenza congiunta della termoregolazione e contabilizzazione. Cholewa et al. [5] hanno inoltre analizzato il consumo di energia di 40 appartamenti in Polonia per oltre 17 stagioni di riscaldamento. Nella metà degli appartamenti investigati è stata sperimentata la ripartizione dei consumi energetici prima e dopo l'installazione di sistemi di termoregolazione e contabilizzazione del calore, mentre l'altra metà ha continuato a dividere collettivamente la spesa. Lo studio ha mostrato un risparmio medio del 26,6%, dovuto sia al controllo termico dell'ambiente interno che alla contabilizzazione del calore. Iordache et al. [6] hanno, invece, analizzato un condominio in Romania di 160 unità abitative nella stagione precedente e successiva all'installazione di valvole termostatiche e ripartitori di calore, osservando una riduzione media dei consumi del 24% (di cui il 15% attribuibile alla termoregolazione e il 9% alla degli utenti).

Per la sola termoregolazione, FIRE ha recentemente condotto per ENEA uno studio sperimentale [7] in nove condomini italiani alimentati da teleriscaldamento nelle fasce climatiche E ed F. Lo studio ha mostrato una riduzione media dei consumi negli ultimi 4 anni grazie ai sistemi di termoregolazione dell'ordine del 10%. In particolare, 6 condomini, dopo una fase iniziale di assestamento, hanno avuto effettive riduzioni, in 1 caso si sono avute riduzioni più limitate mentre in 2 casi i consumi sono rimasti pressochè costanti o addirittura aumentati.

Si deve comunque sottolineare che, a conoscenza degli autori, non esistono campagne sperimentali estensive a lungo termine né studi riguardanti la quantificazione empirica di tale beneficio per climi mediterranei e per i quali risulta difficile estendere i risultati Europei citati a causa delle forti differenze climatiche e ancora della diversa connotazione costruttiva del parco edilizio nazionale.

In questo studio, a valle di un'analisi statistica del patrimonio edilizio italiano, gli autori stimano ed analizzano l'impatto dei sistemi di misura e contabilizzazione sui consumi energetici in Italia in relazione agli adempimenti fissati dalla D.Lgs. 102 e s.m.i. e dalla European Directive 2012/27/EU e presentano i primi risultati di una più estesa campagna sperimentale attualmente in corso.

2. Analisi dei benefici potenzialmente ottenibili e dei possibili fattori di influenza

La variabilità dei benefici potenzialmente ottenibili dalla termoregolazione e contabilizzazione del calore è connessa anche alla diversa impostazione metodologica degli studi (es.: dimensione e composizione del campione, presenza o meno di un gruppo di controllo, durata temporale dell'investigazione e conseguente possibilità di osservare gli effetti di lunga durata e la persistenza dei risparmi energetici nel tempo).

Si può comunque affermare con una certa ragionevolezza, che il beneficio ottenibile, così come i consumi energetici, risulta variabile in funzione di diversi fattori quali:

- *i)* il reddito delle famiglie residenti: in generale la correlazione tra i consumi energetici e le caratteristiche delle famiglie è nota alla letteratura scientifica da tempo [8, 9, 10]. A questo proposito, Cayla et al. [11] hanno dimostrato la dipendenza lineare dal reddito del livello del fattore di servizio per scopi di riscaldamento degli ambienti;
- *ii)* la tipologia di feedback e livello di informazione dell'utente: la consapevolezza e la partecipazione del cliente finale stimolata anche attraverso una più frequente e dettagliata informazione sui consumi può generare fino al 4% ca. sul totale del risparmio [12]; anche la modalità con cui tale informativa viene trasmessa al cliente può avere rilevanza;
- *iii)* il tempo intercorso dall'installazione dei sistemi di termoregolazione e contabilizzazione: in generale il beneficio atteso si realizza pienamente dal secondo anno dall'installazione dei sistemi di contabilizzazione individuale; in un'analisi di Siggelsten [13] si evidenzia in particolare che il risparmio ottenibile al secondo anno è circa doppio rispetto a quello dell'anno immediatamente successivo all'installazione;
- *iv)* il criterio adottato per la ripartizione delle spese in contesti con più unità immobiliari: una prevalenza della quota connessa ai consumi involontari rispetto a quella connessa ai consumi volontari disincentiva il cliente finale ad adottare comportamenti virtuosi di

risparmio energetico. A tal proposito l'Olanda, con uno studio pilota coinvolgente circa 100 unità abitative, ha dimostrato la sostanziale inefficienza della "socializzazione" dei consumi energetici normalmente praticata senza contabilizzazione [14, 15];

v) le condizioni climatiche (i.e. zona climatica): il risparmio energetico atteso dall'utilizzo di sistemi di termoregolazione è influenzato dagli apporti gratuiti e dalle variazioni climatiche giornaliere [5, 6, 7].

Allo scopo di verificare sperimentalmente i benefici attesi in Italia è stata condotta una campagna sperimentale su 15 condomini di cui si riportano i primi risultati sperimentali. In tabella 1 e figura 1 vengono riportati i dati caratteristici dei diversi condomini e il beneficio stimato normalizzato rispetto alle condizioni climatiche annuali. Dai risultati emerge che il beneficio medio è pari a circa 8% al primo anno successivo all'installazione e circa 2% al secondo anno, con una variabilità molto elevata probabilmente dovuta alla diversità delle condizioni climatiche e delle numerose variabili su citate. Per consentire una stima puntuale del beneficio previsto nelle diverse condizioni applicative, è necessario estendere il campione statistico ad un numero più elevato di utenze come previsto dal progetto ENEA-UNICAS attualmente in corso.

Tabella 1 - Beneficio derivante da termoregolazione normalizzato rispetto al dato climatico

Num. alloggi	(PR)	Anno costr.	Consumo PRE [m³/DD]	Consumo dopo il 1° anno [m³/DD]	Consumo dopo il 2° anno [m³/DD]	Beneficio al 1° anno [%]	Beneficio al 2° anno [%]
105	TO	1982	28.949	30.208	30.172	4.4%	-0.1%
48	TO	1999	14.944	15.117		1.2%	
36	TO	1984	10.363	7.879		-24.0%	
21	TO	1983	6.483	5.368		-17.2%	
13	TO	1980	6.433	5.311	5.895	-17.4%	11.0%
24	TO	1961	8.480	7.298	7.038	-13.9%	-3.6%
100	TO	1999	11.306	13.171	12.436	16.5%	-5.6%
100	TO	1999	11.948	13.205	12.947	10.5%	-2.0%
30	TO	1984	8.910	8.125	7.939	-8.8%	-2.3%
40	TO	1981	5.758	6.667	6.525	15.8%	-2.1%
68	TO	1923	22.830	20.188	19.084	-11.6%	-5.5%
58	RM	n/d	26.396	22.470		-14.9%	
36	RM	n/d	10.751	8.633		-19.7%	
21	RM	n/d	14.569	12.036		-17.4%	
54	RM	n/d	25.567	20.905		-18.2%	
		Totale	**213.69**	**196.58**		**-8.0%**	**-2.1%**

Figura 1 - Dipendenza del beneficio dai consumi pre-installazione

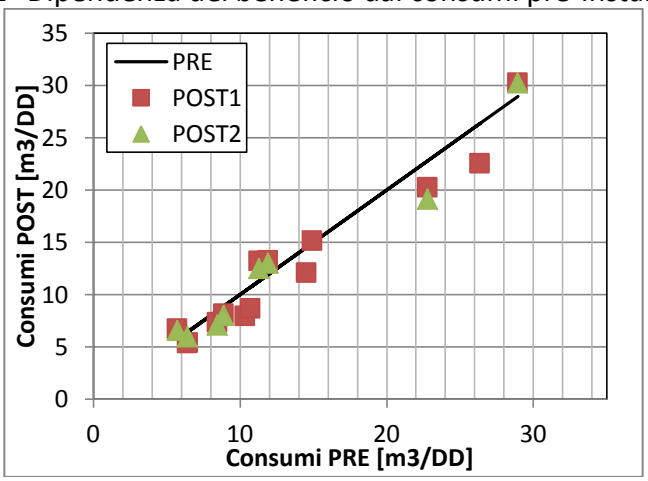

3. Impatto dell'istallazione dei sistemi di contabilizzazione in Italia

Al fine di consentire una stima del beneficio energetico connesso alla contabilizzazione dei consumi di energia termica nel settore residenziale in Italia, è stata effettuata un'analisi dei consumi energetici per riscaldamento connessi al patrimonio edilizio nazionale. Lo studio è basato sull'analisi statistica delle caratteristiche geometriche (i.e. superfici utili, numero piani, numero appartamenti) ed impiantistiche (i.e. riscaldamento centralizzato e autonomo) degli edifici derivanti dall'ultimo censimento ISTAT [16], delle caratteristiche tipologiche e costruttive degli "edifici tipo" (i.e. trasmittanze, rendimenti di impianto etc.) [17, 18], delle modalità di conduzione degli impianti e dei dati climatici regionali [19].

In particolare, nel 2011 in Italia ISTAT ha censito 31,138,278 abitazioni. Di queste, circa il 22% non è abitato, mentre risulta occupato esclusivamente da persone non residenti lo 0.001% degli alloggi, che è ritenuto trascurabile ai fini della presente analisi. ISTAT divide le abitazioni italiane censite nel 2011 in 6 categorie occupazionali e 9 epoche costruttive (con riferimento agli anni 1918, 1945, 1960, 1970, 1980, 1990, 2000, 2005 e successivi).

Con esclusivo riferimento agli alloggi occupati da persone residenti, dai dati in tabella 2 si evince che circa il 64% degli alloggi italiani rientra nella categoria di edificio multifamiliare, mentre la restante quota parte si divide equamente tra le restanti tipologie (mono/bi-familiare). Ai fini della presente analisi è utile osservare che circa il 70% delle abitazioni occupate da persone residenti è stata edificata prima del 1980, ovvero prima che venisse emanato qualsiasi obbligo legislativo relativamente all'efficienza energetica degli edifici (Legge 373 del 1976). Di questi, circa il 45% è rappresentato da edifici multifamiliari.

Tabella 2 - Abitazioni italiane occupate da persone residenti per categoria occupazionale ed epoca costruttiva (elaborazione UNICAS di dati ISTAT)

Categoria occupazionale	Numero di abitazioni nell'edificio	Valori assoluti	Valori percentuali	Pre 1980	1981 - 2000	Post 2001	Tutte le epoche
Monofamiliare	1	4,688,972	19%	14.27%	3.82%	1.39%	19.48%
Bifamiliare	2	3,995,081	17%	12.32%	3.32%	0.96%	16.60%
Multifamiliare	3-4	3,518,114	15%	44.85%	13.28%	5.79%	63.92%
	5-8	3,443,130	14%				
	9-15	3,044,095	13%				
	16 e più	5,375,902	22%				
Totali		24,065,294	100%	71.44%	20.43%	8.13%	100.00%

Per poter tenere conto della variabilità delle condizioni climatiche e della geometria costruttiva degli edifici (i.e. le superfici disperdenti) delle singole regioni italiane, il database ISTAT è stato interrogato su base regionale, al fine di individuare: i) il numero di abitazioni per categoria occupazionale ed epoca costruttiva, ii) il numero medio di piani fuori terra degli edifici per categoria occupazionale, iii) le superfici medie utili delle abitazioni occupate da persone residenti. In fig. 3(a) e 2(b) vengono mostrati i risultati più significativi di tale analisi.

Figura 2. - (a) Distribuzione regionale delle categorie occupazionali (valori assoluti); (b) Incidenza percentuale regionale di edifici per numero di piani (elaborazione UNICAS di dati ISTAT)

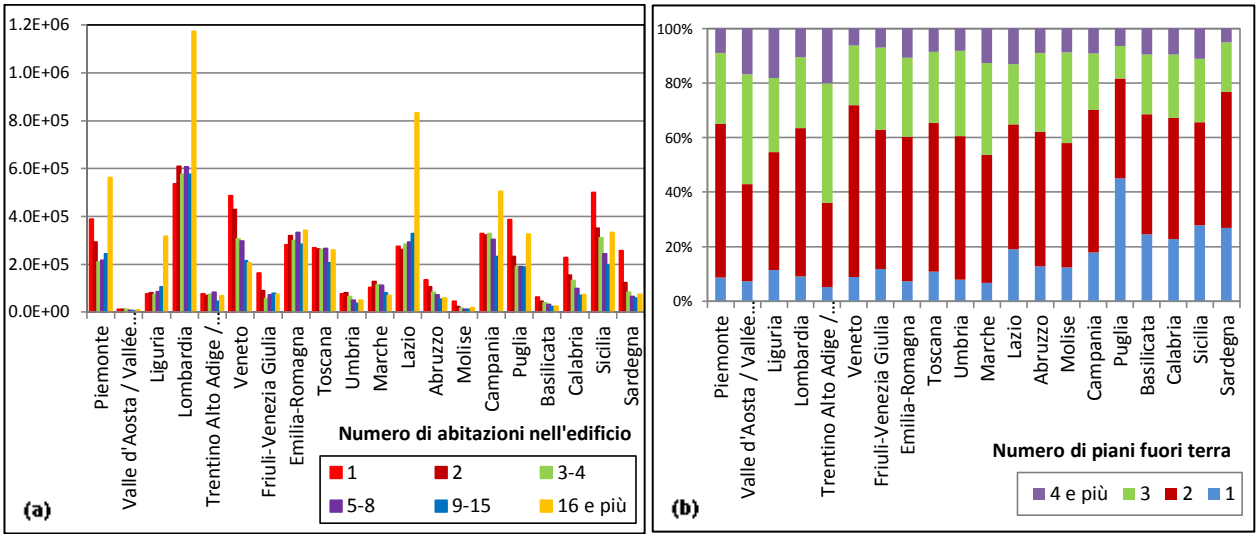

Infine, relativamente alle considerazioni più specificatamente impiantistiche, dai dati ISTAT si evince che circa il 18.75% del totale degli impianti di riscaldamento in abitazioni occupate da persone residenti in Italia è del tipo centralizzato, come mostrato in tabella 3. In figura 3, è inoltre visualizzata la distribuzione percentuale regionale degli impianti centralizzati da cui si evince che circa il 55% del totale di impianti centralizzati nazionale si distribuisce tra sole 3 regioni (Piemonte, Lombardia e Lazio), mentre tale tipologia impiantistica è praticamente trascurabile in 5 regioni (incidenza inferiore all'1%), delle quali solo la Valle d'Aosta situata nel Nord Italia. E' opportuno sottolineare che, nelle stesse regioni nelle quali si registra la percentuale più elevata di impianti centralizzati, si riscontra anche la prevalenza della categoria edilizia multifamiliare a 16 e più abitazioni, ad eccezione della Campania (fig. 2 e 3).

Tabella 3 - Abitazioni occupate da persone residenti per tipo di impianto, valori assoluti e percentuali (elaborazioni UNICAS di dati ISTAT)

Tipologia di impianto che alimenta l'abitazione	Numero impianti [-]	Percentuale impianti [%]
Impianto centralizzato ad uso a più abitazioni	4,871,072	18.75%
Impianto autonomo ad uso alla singola abitazioni	15,717,341	60.51%
Apparecchi singoli fissi per l'intera abitazione	2,137,636	8.23%
Apparecchi singoli fissi per alcune parti dell'abitazione	3,246,891	12.50%
TOT.	**25,972,940**	**100 %**

Figura 3 - Distribuzione regionale delle abitazioni con impianto centralizzato sul totale italiano (elaborazioni UNICAS di dati ISTAT)

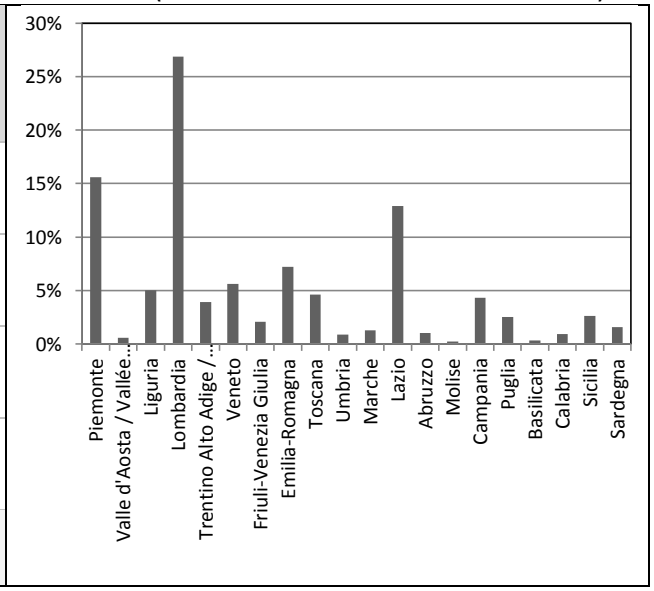

3.1. Definizione degli "edifici tipo" e stima del fabbisogno termico per riscaldamento

I dati ricavati dall'analisi statistica sono stati utili alla definizione della geometria degli edifici tipo (in termini di superfici utili, numero di piani, categoria occupazionale ed epoca costruttiva) utilizzati per caratterizzare su base regionale l'intero parco edilizio residenziale. E' stata in particolare operata la classificazione degli edifici tipo in 54 classi (6 categorie di occupazione per 9 epoche costruttive), poi associate a ciascuna regione assegnando un valore caratteristico, alle seguenti grandezze geometriche e costruttive caratteristiche:

i) numero medio di piani per categoria occupazionale, determinato mediante media pesata numero di piani/numero edifici;

ii) altezza interpiano, ricavato dalla caratterizzazione del parco edilizio nazionale uso ufficio pubblicata da ENEA [18] (variabile in funzione della sola epoca costruttiva, passando da un massimo di 3.4 m, relativo all'epoca costruttiva meno recente, ad un minimo di 2.9 m, relativo all'epoca costruttiva più recente);

iii) superfici disperdenti degli edifici tipo, ipotizzando: i) unico volume riscaldato di forma cubica; ii) rapporto superfici finestrate/ superficie utile dell'abitazione pari all'attuale limite di legge (1/8) per tutte le tipologie ed epoche costruttive; iii) superfici disperdenti orizzontali e verticali (solaio, copertura e pareti opache) divise in parti uguali per tutti gli appartamenti componenti l'edificio;

iv) maggiorazione per ponti termici pari al 10% per tutte le tipologie ed epoche costruttive;

v) trasmittanze tipo delle superfici opache e finestrate differenziate rispetto alle epoche costruttive (figura 4), ricavate sulla base del rapporto TABULA [17], in cui vengono individuate le tipologie costruttive nazionali ed il relativo periodo di maggiore diffusione, per la sola fascia climatica E. Ai fini del presente studio tali tipologie costruttive sono state ritenute rappresentative di tutto il territorio nazionale. Per tenere in considerazione sia gli interventi di retrofit già avvenuti sulle superfici opache e finestrate di tutto il territorio nazionale, che la variabilità climatica delle caratteristiche costruttive dei diversi parchi edilizi regionali, le trasmittanze medie degli edifici antecedenti il 1990 sono state ridotte percentualmente in funzione del dato climatico e delle regioni.

Figura 4 - Trasmittanze medie stimate del patrimonio edilizio nazionale (elaborazione UNICAS di dati TABULA [17])

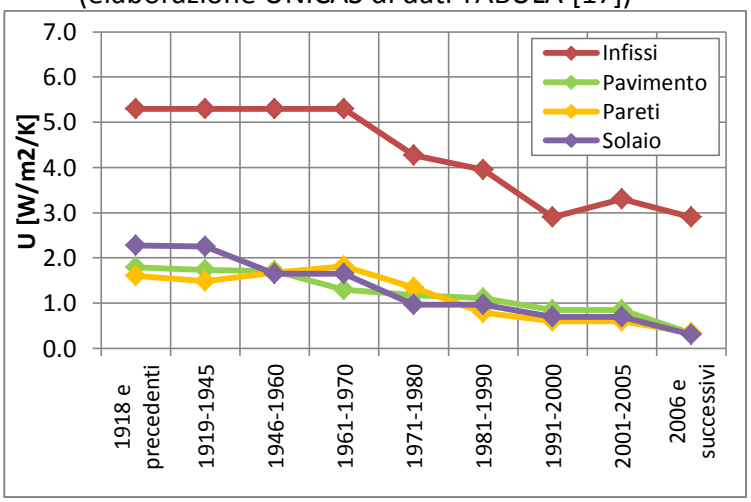

Il calcolo del fabbisogno di energia primaria h24 (Asset Rating) per la climatizzazione invernale italiana è stato effettuato in forma semplificata descritta nell'Allegato 2 del Decreto Ministeriale del 26/06/2009 ed attingendo sia alla normativa tecnica UNI TS 11300 [20] che al rapporto TABULA [17], sotto le seguenti ipotesi semplificative: *i)* apporti gratuiti solari calcolati in maniera forfetaria per un edificio reale di riferimento e variabile in funzione della latitudine; *ii)* rendimenti dei sottosistemi di emissione, distribuzione e regolazione pari a 0.95 indipendentemente dalla categoria edilizia e dall'epoca costruttiva; *iii)* generatore interno fino al 1975, esterno nelle epoche successive; *v)* caldaia standard con bruciatore atmosferico con camino <10 m per le categorie mono/bi-familiare, con camino >10 m per la categoria multifamiliare; *iv)* caldaia a condensazione per gli edifici costruiti dopo il 2006; v) assenza di ambienti non riscaldati nell'edificio; *vi)* fattore di utilizzazione degli apporti gratuiti pari a 0.95.

L'energia primaria nelle effettive condizioni di utilizzo dell'impianto (Operational Rating) è stata quindi determinata, per ciascuna categoria edilizia e ciascuna regione, utilizzando i coefficienti di intermittenza precedentemente stimati da ENEA a valle di un'analisi campionaria che ha coinvolto 20,000 unità abitative del territorio italiano. I coefficienti di intermittenza sono stati resi disponibili su base provinciale, per 6 province rappresentative delle rispettive fasce climatiche del territorio italiano e per singola unità abitativa (monofamiliare, plurifamiliare, appartamento primo piano, appartamento ultimo piano, appartamento piano intermedio). I suddetti coefficienti provinciali sono stati quindi estesi all'intera regione conservando la corrispondenza tra la fascia climatica di appartenenza della provincia ed il dato climatico regionale. Quest'ultimo è fornito, fino all'anno 2009, dal database EUROSTAT liberamente accessibile online [19].

3.2. Impatto della contabilizzazione e termoregolazione

Il consumo per riscaldamento invernale del parco edilizio nazionale ad uso residenziale calcolato dagli autori utilizzando il modello descritto ammonta a 20.37 Mtep. Il dato ottenuto è stato confrontato con quelli dei Piani Energetici ed Ambientali Regionali (PEAR), resi disponibili da ENEA [21], ed i Bilanci Energetici Nazionali (BEN), dal Ministero dello Sviluppo Economico [22], con l'obiettivo di validare il modello di calcolo utilizzato e le sue ipotesi di base. Sfortunatamente, non è a tutt'oggi disponibile un dato certo del consumo residenziale strettamente legato al riscaldamento degli edifici. Infatti nei bilanci energetici, questa voce risulta generalmente accorpata nella macro area "Residenziale", comprendente i consumi energetici derivanti da: riscaldamento e raffrescamento degli edifici, illuminazione ed apparecchiature elettriche domestiche, uso cottura e produzione di acqua calda sanitaria. L'Unione Europea [23] stima che circa il 78% del consumo totale del settore residenziale europeo sia imputabile al solo riscaldamento e raffrescamento degli edifici residenziali. Tale percentuale risulta comunque variabile in funzione delle condizioni climatiche, oscillando tra l'80% per i climi più freddi e il 50% dei climi più caldi. A tal proposito, in tabella 4 dati dei consumi residenziali dei bilanci energetici nazionali EUROSTAT dal 1990 al 2015 [22], sono stati coniugati con quelli di un'analisi condotta da ENEA relativi ai soli consumi per condizionamento degli edifici residenziali dal 2000 al 2013 [24] al fine di individuare una percentuale media riferibile alle condizioni climatiche italiane. Ulteriore problematica deriva dal fatto che i Piani Energetici e Ambientali Regionali (PEAR) sono stati emanati dalle regioni in anni differenti, a partire dal 1998 (regione Liguria)

fino ad arrivare al più recente, datato 2013 (regione Molise). Al fine di consentirne un confronto, tutti i dati sono stati attualizzati rispetto all'anno di riferimento 2017, considerando un incremento percentuale dei consumi per riscaldamento degli edifici dell'1% annuo (tabella 4 (a)). Il confronto tra i consumi calcolati con il modello ed il dato attualizzato è riportato su base regionale e nazionale in tabella 4 (b).

Tab. 4 - (a) Consumi residenziali (BEN) e quota parte per condizionamento dal 1990 al 2015; (b) Confronto tra i consumi per riscaldamento calcolati ed il dato da PEAR attualizzato. (Elaborazioni UNICAS di dati EUROSTAT [20] ed ENEA [25])

(a)

Year	Italian residential sector consumption (EUROSTAT) [Mtep]	Space heating (ENEA) [Mtep]	Share for space heating [%]
1990	26.06		
1995	26.32		
2000	27.59	16.7	60.42 %
2001		17.1	
2002		17.2	
2003		19.7	
2004		19.2	
2005	33.92	21.7	63.88 %
2006		21.1	
2007		20.0	
2008		22.8	
2009		23.3	
2010	35.39	23.9	67.50 %
2011	32.38	20.0	61.77 %
2012	34.35	22.2	64.69 %
2013	34.23	22.2	64.91 %
2014	29.55		
2015	32.49		
Media			**64.02 %**
Incremento % annuo (2000-2013)			**2.56 %**
Incremento % annuo (2003-2013)			**1.15 %**

(b)

	Consumo per riscaldamento calcolato attualizzato [Mtep]	Consumi PEAR attualizzati [Mtep]	Errore percentuale regionale [%]
Sardegna	0.283	0.335	-15.52%
Sicilia	0.599	0.552	8.54%
Calabria	0.267	0.241	10.81%
Basilicata	0.140	0.133	5.35%
Puglia	0.815	0.830	-1.88%
Campania	0.777	0.791	-1.79%
Molise	0.119	0.121	-2.03%
Abruzzo	0.259	0.245	5.49%
Lazio	1.593	1.851	-13.97%
Marche	0.525	0.491	6.85%
Umbria	0.225	0.224	0.63%
Toscana	1.324	1.335	-0.82%
Emilia	1.672	1.485	12.57%
Friuli-Ven.	0.424	0.392	8.28%
Veneto	3.799	3.995	-4.90%
Trentino	0.552	0.529	4.41%
Lombardia	3.805	3.651	4.20%
Liguria	0.685	0.729	-6.05%
Valle d'Ao.	0.101	0.087	16.17%
Piemonte	2.407	2.254	6.77%
	Tot.	**BEN attualizzato**	**Err%**
Italia	20.370	21.212	-3.97%

Dal confronto dei dati di consumo regionali è stato possibile validare il modello proposto. Mentre l'errore medio risulta contenuto entro un margine di circa -4% sul dato nazionale, a livello regionale il consumo per riscaldamento stimato dagli autori presenta scostamenti consistenti ma accettabili (entro un range di circa ± 20%). Si deve comunque considerare che il confronto su base regionale è alterato dalla mancanza di un dato di consumo attuale, nonché dalla variabilità climatica della percentuale uso riscaldamento applicata al consumo uso residenziale PEAR.

Il potenziale impatto dell'installazione dei sistemi di termoregolazione e contabilizzazione del calore in Italia, è stato quindi calcolato "filtrando" i consumi totali regionali rispetto: *i)* alla percentuale totale di impianti centralizzati regionale, *ii)* all'energia primaria dell'abitazione tipo stimata in asset rating (per tener conto dell'obbligo di legge derivante dal D.Lgs. 102/2014 e s.m.i.), *iii)* alla categoria occupazionale dell'abitazione (escluse le monofamiliari).

Il rapporto costi/benefici dell'installazione dei sistemi di termoregolazione e contabilizzazione risulta infatti strettamente connesso al consumo iniziale (i.e. pre-intervento) dell'edificio. Come anche riportato da Celenza et al. [2], esiste infatti un valore minimo di energia primaria per riscaldamento, E_{PH}, al di sotto della quale l'efficacia economica dell'intervento di installazione non è dimostrata. L'Autorità per l'Energia Elettrica ed il Gas e il Sistema Idrico (AEEGSI) nel DCO 252/2016 presenta un'analisi di fattibilità tecnico-economica dell'installazione di contatori individuali di calore in un edificio di 5 appartamenti, il cui risultato porterebbe ad esentare dall'obbligo di installazione di tali sistemi gli edifici aventi E_{PH} inferiore a 80 kWh/m^2/anno e di obbligare tutti gli edifici aventi un valore certificato di E_{PH} desumibile dall'Attestato di Prestazione Energetica (APE) superiore a 155 kWh/m^2/anno. Nello stesso documento, l'AEEGSI individua un livello minimo (10%) e massimo (20%) di beneficio atteso in ambito nazionale.

Tenuto conto di quanto su citato, i consumi associati al beneficio minimo (10%) sono stati decurtati del contributo di tutti gli edifici aventi E_{PH} (in Asset Rating) inferiore a 155 kWh/m^2/anno, quelli associati al beneficio massimo (20%) sono stati decurtati del contributo di tutti gli edifici aventi E_{PH} (in Asset Rating) inferiore a 80 kWh/m^2/anno. Come anche riportato in tabella 5, se tutti gli edifici potenzialmente obbligati installassero i sistemi di contabilizzazione e termoregolazione del calore, ne deriverebbe un beneficio atteso tra 0.247 e 0.839 Mtep/anno.

Tabella 5 - Riepilogo consumi stimati e risparmio potenzialmente ottenibile (dati attualizzati al 2017)

	Appartamenti con impianti centralizzati [%]	Consumo da impianto centralizzato [Mtep]	Consumo da impianti centralizzati (Ep>155 kWh/m^2) [Mtep]	Consumo da impianti centralizzati (Ep>80 kWh/m^2) [Mtep]	Risparmio (beneficio 10%) [Mtep]	Risparmio (beneficio 20%) [Mtep]
Sardegna	11.61%	0.0329	0.0098	0.0226	0.0010	0.0045
Sicilia	6.63%	0.0397	0.0000	0.0231	0.0000	0.0046
Calabria	5.91%	0.0158	0.0000	0.0097	0.0000	0.0019
Basilicata	7.43%	0.0104	0.0045	0.0083	0.0004	0.0017
Puglia	8.04%	0.0655	0.0184	0.0446	0.0018	0.0089
Campania	10.34%	0.0804	0.0040	0.0484	0.0004	0.0097
Molise	8.39%	0.0100	0.0058	0.0087	0.0006	0.0017
Abruzzo	9.53%	0.0246	0.0000	0.0161	0.0000	0.0032
Lazio	27.61%	0.4398	0.1923	0.3998	0.0192	0.0800
Marche	9.97%	0.0523	0.0347	0.0476	0.0035	0.0095
Umbria	11.96%	0.0269	0.0082	0.0215	0.0008	0.0043
Toscana	14.68%	0.1944	0.1179	0.1798	0.0118	0.0360
Emilia	18.82%	0.3147	0.2065	0.2935	0.0206	0.0587
Friuli-Ven.	18.72%	0.0794	0.0047	0.0548	0.0005	0.0110
Veneto	13.99%	0.5317	0.4366	0.5129	0.0437	0.1026
Trentino	45.61%	0.2518	0.1797	0.2457	0.0180	0.0491
Lombardia	31.97%	1.2164	0.5244	1.0820	0.0524	0.2164
Liguria	33.02%	0.2261	0.1396	0.2223	0.0140	0.0445
Valle d'Ao.	47.36%	0.0480	0.0448	0.0477	0.0045	0.0095
Piemonte	39.49%	0.9505	0.5425	0.9078	0.0543	0.1816
Italia				**[Mtep]**	**0.247**	**0.839**
				[%]	**1.21%**	**4.12%**

4. Conclusioni

In questo lavoro sono stati presentati i primi risultati di una campagna sperimentale UNICAS-ENEA attualmente in corso che evidenziano una elevata variabilità del beneficio connesso all'installazione di sistemi di termoregolazione e contabilizzazione del calore negli edifici residenziali forniti da impianti di riscaldamento centralizzati. Sebbene alcuni edifici oggetto di studio abbiano addirittura aumentato i loro consumi, è stato rilevato un risparmio medio degli edifici oggetto di intervento prossimo al 10% al secondo anno successivo all'installazione dei sistemi di contabilizzazione e regolazione. In 7 di 8 casi nei quali era disponibile il dato di consumo al secondo anno successivo all'installazione (compresi anche quelli in cui il consumo dell'edificio è aumentato), si conferma infatti la tendenza ad un'ulteriore diminuzione dei consumi (mediamente 2 punti percentuali in meno rispetto all'anno precedente).

Al fine di valutare il potenziale impatto dell'installazione dei sistemi di contabilizzazione e termoregolazione negli edifici obbligati dal D.Lgs. 102/2014 e s.m.i., è stata condotta un'analisi dei consumi energetici per riscaldamento del settore residenziale italiano attraverso la caratterizzazione del parco edilizio di ciascuna regione del territorio nazionale.

L'analisi mostra che il risparmio complessivo ottenibile su base nazionale attualizzato al 2017 è compreso tra 0.247 e 0.839 Mtep, valori rispettivamente associati ad un beneficio per termoregolazione e contabilizzazione pari al 10 ed al 20%. Inoltre, in corrispondenza di un beneficio medio pari al 10%, per 3 regioni italiane (Abruzzo, Sicilia e Calabria) il risparmio ottenibile sarebbe limitato. E' comunque auspicabile una calibrazione più accurata del modello di calcolo attraverso: *i)* una migliore caratterizzazione delle trasmittanze per ciascuna fascia climatica e/o regione italiana (anche attingendo alle banche dati regionali in corso di costruzione), *ii)* la determinazione del numero di edifici che già hanno installato sistemi di contabilizzazione e termoregolazione, *iii)* il reperimento dei dati di consumo per riscaldamento del parco residenziale italiano e regionale.

Gli autori ritengono che sia comunque necessaria l'estensione della campagna sperimentale attualmente in corso ad un numero consistente di condomini al fine di individuare il beneficio medio applicabile al territorio italiano ed i possibili fattori di influenza.

Riconoscimenti

Il presente lavoro è stato sviluppato nell'ambito delle attività del Progetto ENEA Ricerca di Sistema Elettrico e del Progetto PRIN 2015 "Riqualificazione del Parco Edilizio esistente in ottica NZEB (Nearly Zero Energy Buildings): Costruzione di un network nazionale per la ricerca".

Bibliografia

[1] *Direttiva 2012/27/UE del Parlamento Europeo e del Consiglio del 25 ottobre 2012, sull'efficienza energetica, che modifica le direttive 2009/125/CE e 2010/30/UE e abroga le direttive 2004/8/CE e 2006/32/CE. Gazzetta Ufficiale dell'Unione Europea n. L 31,* 2012.

[2] Celenza, Dell'Isola, Ficco, Greco e Grimaldi, «Economic and technical feasibility of metering and sub-metering systems for heat accounting,» *International Journal of Energy Economics Efficiency,* 2016.

[3] Boverket, «Individual metering and charging in existing buildings,» Boverket, December, 2015.

[4] *Clemens Felsmann, Juliane Schmidt, Tomasz Mróz. Effects of Consumption-Based Billing Depending on the Energy Qualities of Buildings in the EU.,* 2015.

[5] T. Cholewa e A. Siuta-Olcha, «Long term experimental evaluation of the influence of heat cost allocators on energy consumption in a multifamily building,» *Energy and Buildings,* 2015.

[6] F. Iordache e V. Iordache, «Energy Savings in Blocs of Flats Due to Individual Heat Metering,» in *Proceedings of Clima 2007 WellBeing Indoors*, 2007.

[7] E. Biele, D. D. Santo e G. Tomassetti, «Analisi dell'impatto delle valvole termostatiche sui consumi finali degli utenti collegati alle reti di teleriscaldamento dei Comuni montani delle zone climatiche E ed F,» 2014.

[8] O. G. Santin, L. Itard e H. Visscher, «The effect of occupancy and building characteristics on energy use for space and water heating in Dutch residential stock,» *Energy and Buildings,* 2009.

[9] V. CR, *Analysis of the energy requirement for household consumption,* Netherlands Environmental Assessment Agency, 2005.

[10] W. Biesiot e K. Noorman, «Energy requirements of household consumption: a case study of NL,» *Ecological Economics,* Vol. %1 di %2Vol. 28, No. 3, n. ISSN 0921-8009, 1999.

[11] J.-M. Caylaa, N. Maizia e C. Marchandb, «The role of income in energy consumption behaviour: Evidence from French households data,» *Energy Policy,* vol. Volume 39, n. Issue 12, p. 7874–7883, 2011.

[12] S. Andersen, R. K. Andersen e B. W. Olesen, «Influence of heat cost allocation on occupants' control of indoor environment in 56 apartments: Studied with measurements, interviews and questionnaires,» *Building and Environment,* vol. Volume 101, p. 1–8, 2016.

[13] S. S., «Reallocation of heating costs due to heat transfer between adjacent apartments.,» *Energy and Buildings,* vol. 75, p. 256–263, 2014.

[14] E. Edelenbos, *Customer-friendly Individual Heat Metering in the Netherlands,* 2014.

[15] E. Edelenbos e F. Martins, «Cost effectiveness of individual metering/billing,» Concerted Action for the Energy Efficiency Directive, 2014.

[16] ISTAT, «Censimento Popolazione Abitazioni,» 2011. [Online]. Available: http://dati-censimentopopolazione.istat.it/Index.aspx?lang=it.

[17] V. Corrado, I. Ballarini e S. P. Corgnati, «Building Typology Brochure – Italy Fascicolo sulla Tipologia Edilizia Italiana,» Politecnico di Torino – Dipartimento Energia; Gruppo di Ricerca TEBE, Torino, 2014.

[18] F. Margiotta e G. Puglisi, «Caratterizzazione del parco edilizio nazionale Determinazione dell'edificio tipo per uso ufficio,» ENEA, 2009.

[19] «EUROSTAT - Your Key to European statistics,» [Online]. Available: http://ec.europa.eu/eurostat/data/database.

[20] *UNI 11300:2014, Prestazioni energetiche degli edifici,* Milano: Ente Nazionale Italiano di Unificazione.

[21] ENEA, «OSSERVATORIO POLITICHE ENERGETICO-AMBIENTALI,» [Online]. Available: http://enerweb.casaccia.enea.it/enearegioni/UserFiles/Pianienergetici/pianienergetici.htm.

[22] «Ministero dello Sviluppo Economico - Statistiche dell'Energia,» [Online]. Available: http://dgsaie.mise.gov.it/dgerm/ben.asp.

[23] E. Commission, «Communication from the Commission to the European Parliament, the Council, the European Economic and Social Committee and the Committee of the Regions on an EU Strategy for Heating and Cooling,» 2016.

[24] ENEA, «Energy Efficiency trends and policies in ITALY,» 2015.

Proceedings of ASME Turbo Expo 2017
ASME Turbo Expo 2017: Power for Land, Sea and Air
June 26-30, 2017, Charlotte, NC USA

GT2017-64193

Renewable Energy Systems Integration for Efficiency Improvement of a CHP Unit

M. A. Ancona, L. Branchini, A. De Pascale, F. Melino
DIN – Alma Mater Studiorum, Università di Bologna
Viale del Risorgimento 2, 40136 Bologna, Italy

B. Di Pietra
ENEA – Energy Efficiency Technical Unit
Via Anguillarese 301, 00123 Roma, Italy

ABSTRACT

In the next years energy grids are expected to become increasingly complex, due to the integration between traditional generators (operating with fossil fuels, especially natural gas), renewable energy production systems and storage devices. Furthermore, the increase of installed distributed generation systems is posing new issues for the existing grids. The integration involves both electric grids and thermal networks, such as district heating networks. In this scenario, it is fundamental to optimize the production mix and the operation of each system, in order to maximize the renewable energies exploitation, minimize the economic costs (in particular the fossil fuel consumption) and the environmental impact.

The aim of this paper is the analysis of different solutions in terms of energy generators mix, in order to define the optimal configuration for a given network.

With this purpose, in this study a real district heating network served by a combined heat and power unit and four boilers has been considered. The current mode of operation of the selected network has been simulated with an in-house developed software, in order to individuate eventual criticism and/or improvement possibility. On the basis of the obtained results, several scenarios have been developed by considering the addition of thermal or electric energy production systems from renewable energy sources and/or heat pumps.

For a given scenario, a whole year of operation has been simulated with an in-house developed software, called EGO (Energy Grid Optimizer), based on genetic algorithms and able to define the load distribution of a number of energy systems operating into an energy grid, with the aim to minimize the total cost of the energy production. Further considered constraints have been the avoiding of thermal dissipations and the minimization of the electric energy sale to the national grid (in order to increase the grid stability).

The carried out analysis has allowed to evaluate the yearly fuel consumption, the yearly electric energy sold to the network and the yearly electric energy purchased from the network, for each of the developed configurations. In this study the obtained results have been discussed in order to compare the proposed scenarios and to define an optimal solution, which enables to reduce the yearly operation costs of the production plant.

NOMENCLATURE

F	fuel consumption [kWh]
E	electric energy [kWh]
I	solar irradiation [Wh/m^2]
Q	thermal power [kW]
S	surface [m^2]
T	temperature [°C]
V	volume [m^3]

Greek symbols

η	conversion efficiency [-]

Subscripts and Superscripts

i	initial
max	maximum
min	minimum
th	thermal

Acronyms

AB	Auxiliary Boiler
AC	Absorption Chiller
CC	Compression Chiller
CHP	Combined Heat and Power
COP	Coefficient of Performance
DH	District Heating
DHN	District Heating Network
EGO	Energy Grid Optimizer
ES	Energy Storage
HP	Heat Pump
ICE	Internal Combustion Engine
IHENA	Intelligent Heat Energy Network Analysis
LP	Linear Programming
MILP	Mixed Integer Linear Programming
PM	Prime Mover
PV	PhotoVoltaic
RES	Renewable Energy Source
RGe	Renewable Generator-electric energy

Copyright © 2017 by ASME

RGt Renewable Generator-thermal energy
TES Thermal Energy Storage
TSP Thermal Solar Panels

INTRODUCTION

In the last years, energy grids became a central issue for the achievement of the standards imposed by international regulations on environment preservation matter. With this purpose, the integration between renewable energy sources generation and traditional production systems has been promoted for the fulfillment of the users need [1, 2]. The consequent increase in the complexity of the energy networks develops new challenges in energy sector.

Relating to the thermal energy field, District Heating Networks (DHNs) are largely diffused [3], since the elimination of the combustion systems at the final users of thermal energy allows to drastically reduce both pollutant and thermal emissions at the city area. Furthermore, DHNs enable to increase the safety conditions and to eliminate the transportation of fuel to the residential areas.

Often, in order to promote an efficient thermal energy production, DHNs are supplied with the heat produced by means of Combined Heat and Power (CHP) units. For example, in Finland the 80% of the heat distributed through DHN is produced by centralized CHP units [4, 5], while in China about the 62.9% of district heat is produced in cogeneration [6]. In this kind of networks, an energy efficiency improvement and a costs reduction can be reached with an optimal location of the peak boilers, as reported in [7].

For further efficiency improvement, however, the integration of Renewable Energy Sources (RES) in the CHP-DH scenario can be seen as an interesting solution. The intermittent and non-programmable nature of these typology of energy source can be overcome with the introduction of opportune storage systems [8]. In Europe, some instances of integrated thermal grids are present, considering the integration of different technologies – such as heat pumps, solar panels, waste-to-energy systems, CHP, etc. – with renewable sources for the production of thermal energy [9, 10]. As an example, at the Delft University of Technology the 17% of thermal and cooling needs is currently provided by a system which includes CHP units, geothermal systems and aquifer thermal storage [11], allowing an energy saving equal to about the 10%. Particularly, the positive effect of the introduction of heat pumps in district heating networks has been studied and confirmed [12, 13].

The increasing complexity of these energy networks makes of fundamental importance the correct management of the production system operation. The determination of ideal systems set up, as well as the control and operation of the integrated network, is not easy. With this purpose, several optimization algorithms can be applied [14-19]. As an example, an optimization algorithm based on a Mixed Integer Linear Programming (MILP) model has been developed in [20] for the minimization of the annual cost of a CHP-DH network, integrated with a solar thermal plant and supplying industrial users. Furthermore, in [21] the thermal storage size – for a combined cooling, heat and power unit integrated with RES – has been optimized with a TRNSYS unsteady model. Other energy grids management optimization strategies, finally, regard the demand side, as for the Linear Programming (LP) model proposed in [22] for the minimization of the users total energy costs.

The aim of this study consists in the optimization of these complex networks management by means of an in-house developed calculation model based on genetic algorithms [23]. The model allowed both the identification of the typology and of the optimal position for the generation systems to be installed and the definition of the optimal yearly operational profile of each system. In more detail, starting from an existing district heating network supplied by a CHP unit, different scenarios will be proposed, considering the integration of various production system (such as both renewable thermal and electric generators, heat pumps) to be installed at the centralized thermal power station and/or at the final users.

The innovative aspects – in addition to the developed optimization strategies – relate to the improvement in performance and management of an existing network supplying both residential and tertiary users, as well as the consideration of electric energy renewable generators (and not only – as usually in this kind of analysis – thermal energy renewable production systems).

The optimal strategy has been determined for each presented scenario and the optimal configuration has been fixed on the basis of the annual costs.

CALCULATION METHODOLOGY

Reference Case

As starting point for the optimization analysis, an existing District Heating Network (DHN) has been considered. This network is located in the city of Bologna (in the North of Italy) and it is supplied by a thermal power station consisting of an Internal Combustion Engine (ICE), operating as Combined Heat and Power (CHP) unit, and four auxiliary boilers. Relating to the electric production of the CHP unit, it is used to move the pumping station of the plant and – if exceeding the pumps need – it is sold to the national electric grid.

The configuration of the thermal power station is shown in Figure 1, while the technical data of the before-mentioned generation systems are presented in Table 1.

The produced hot water is supplied to the network at 10 bar and 80°C÷90°C, while the pressure drop across all the network's path (supply plus return paths) is about 6 bar.

Table 1 – Generation systems main parameters.

Internal Combustion Engine (CHP Unit)	
Model	Jenbacher JMS 420
Fuel type	Natural gas
Design Electric Power	1415 kW
Design Thermal Power	1492 kW
Design Electric Efficiency	41.9%
Design Thermal Efficiency	44.2%

Auxiliary Boilers (each one)	
Design Thermal Power	2900 kW
Design Thermal Efficiency	80%

Copyright © 2017 by ASME

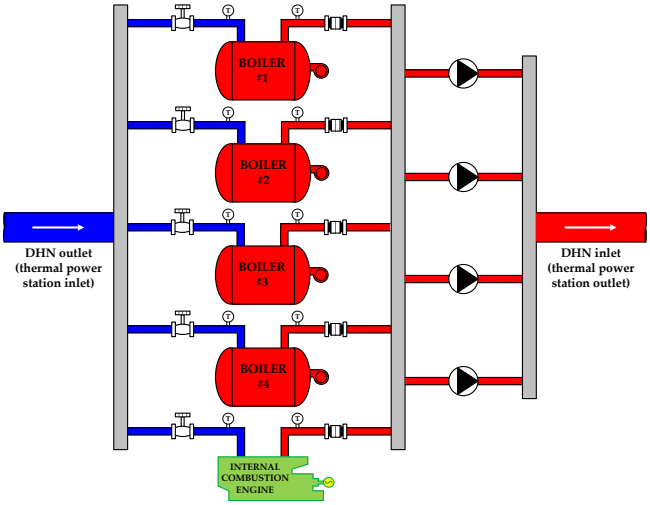

Figure 1 – Configuration of the considered thermal power station.

The considered DHN – presented in Figure 2 – supplies 17 thermal users, composed by 13 residential consumers (for a total of 960 housing units) and four tertiary utilities (two schools, 1 day-hospital building and 1 super-market). The correspondence between identification number and typology of utility is listed in Table 2. Furthermore, the network's length is about 4 km, considering both the supply and the return paths. All the connected utilities are served by the DHN for both space heating and hot water needs, excepting for the super-market where only space heating is needed.

Based on the available measured experimental data, the peaks of thermal need for each utility have been fixed separately for space heating and hot water, as presented respectively in Figure 3 and in Figure 4. The values of the peak thermal needs had then enabled to determine, for each utility, the daily hourly profile of thermal need for space heating and hot water by applying non-dimensional curves available in literature [24]. Obviously, as suggested in [24], different profiles have been considered depending on the considered typology of utility as well as on the thermal need typology, as presented in Appendix.

In particular, two representative days have been considered and set for the further optimization analysis: one winter typical day (space heating and hot water needs) and one summer typical day (only hot water is needed). Then, considering for the utility substations a thermal exchange effectiveness equal to the 99% and for the secondary distribution circuit an efficiency around the 95% (values evaluated through the in-house developed software IHENA), for a typical winter day and for a typical summer day, the real needs which the DHN has to guarantee have been determined.

Thus, as fixed by the Italian framework for the considered location, 183 days a year have been modeled with the winter typical day (so both space heating and hot water are considered) and 182 days with the summer typical one. With these assumptions the hourly thermal need profiles in a whole year have been determined, for space heating and hot water separately and for each utility.

Consequently, the network behavior has been analyzed by applying an in-house developed software named IHENA (Intelligent Heat Energy Network Analysis) [25]: this software – on the basis of the geometry of the network, the utilities thermal needs and the characteristics of the heat source (*i.e.* pressures and temperatures at the outlet and at the return of the thermal power station, as well as the pumping system efficiency) – enables to obtain the thermal power to be produced by the centralized plant, the required electric power for the pumping station and the thermal dissipations through the network.

Once evaluated the hourly thermal power profile to be produced, the operation mode of the centralized station has to be set. With this purpose, an in-house developed software has been applied in order to determine the optimal operation of the generation systems. This software, called EGO (Energy Grid Optimizer) and described in the following paragraph, allowed to define the operation of the thermal station during a year [23]. Thus, the energy fluxes of the plant and the fuel costs for the whole year have been evaluated.

It must be highlighted that this solution, fixed by Authors as Reference Case, is already an optimized solution – in terms of operational management – for the existing network, due to the application of EGO. However, the change in the production plant configuration represents an interesting issue for the further optimization of the CHP-DHN operation and for the minimization of both the auxiliary boilers use and the operational costs.

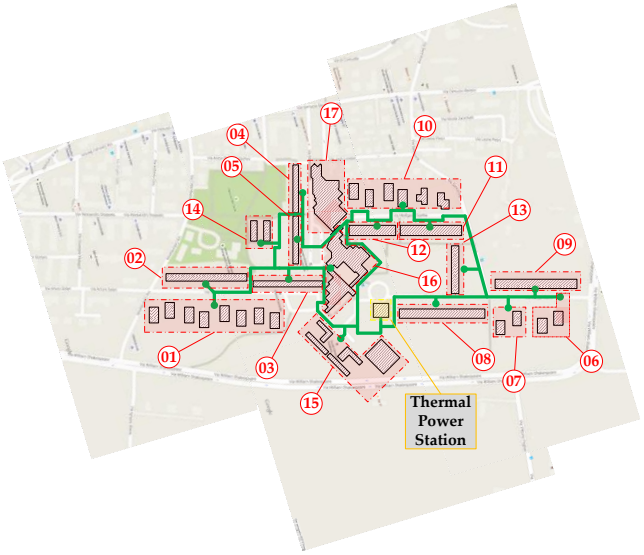

Figure 2 – Schematic of the district heating network set as Reference Case.

Table 2 – Utilities identification numbers and associated typology.

ID	Typology
From #1 to #13	Residential Utility
#14	Infant School
#15	Primary School
#16	Day-Hospital
#17	Supermarket

Copyright © 2017 by ASME

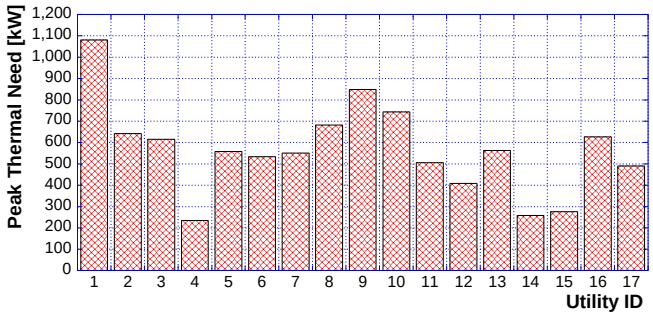

Figure 3 – Peak space heating needs for each utility.

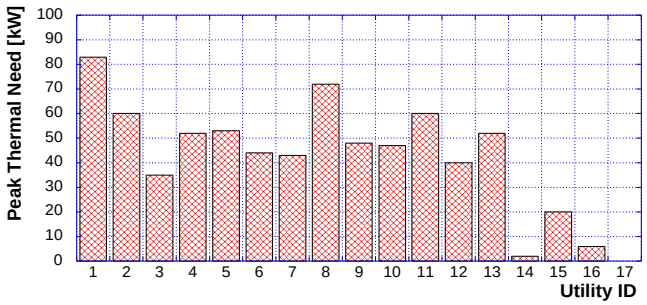

Figure 4 – Peak hot water needs for each utility.

Calculation model – software EGO

In order to develop the load distribution optimization in a smart grid characterized by electrical, thermal, cooling and fuel energy fluxes, a new software has been developed by University of Bologna. The software, named EGO (Energy Grids Optimizer) is able to define the load distribution of a number of energy systems operating into a smart grid with the aim of minimize the total cost of the energy production.

More in details, the realized software can simulate an energy grid, consisting in a (i) arbitrary number of prime movers (PM) even in CHP application, (ii) generators from renewable source (solar thermal panels – RGt – wind turbines and photovoltaic panels – RGe), (iii) energy storage devices – ES (for both electrical and thermal energy), (iv) thermal generators (auxiliary boilers – AB – and heat pumps – HP), (v) cooling machines (compressor – CC – and absorption chillers – AC). The previous generators are used to cover the electrical, thermal and cooling energy load requested by an utility (or a group of utilities); the grid is also connected with the electric grid and the gas distribution network.

The calculation core of the software consists of a genetic algorithm based on the minimization of an objective function which expresses the total cost of energy production.

More in details, the input section requires:

- electrical, thermal and cooling power required by the utilities; further, from Figure 1 it can be noted that it is also possible to define the gas demand (for direct use) for the utilities;
- definition of the number, typology, and main characteristics of:

o prime movers (electrical and thermal design power output, efficiency, off-design behavior, etc.);

o renewable source generators (peak power, performance, etc.);

o heating and cooling systems (size, performance, off-design behavior, etc.):

o electrical and thermal energy storage devices (maximum storable energy);

- the tariff scenario (purchased and sold electrical energy value, cost of the fuel, etc.);
- a series of parameters characteristic of the genetic algorithm (as will be better explained in the following of this paragraph).

Software's output will be the load of each involved energy systems, in order to minimize the total cost of energy furnishing for the utilities.

A detailed description of the algorithm and deeper discussion about the software are presented in [23].

Case studies

With the aim of analyzing the possibility to add different electric and/or thermal generation systems and optimizing the management of the network, various scenarios in terms of considered production systems have been considered:

1. *Case 1*: in addition to the generation systems currently installed, this case considers the installation at the thermal power station of solar thermal panels and of a thermal energy storage system (Figure 5a);
2. *Case 2*: this scenario – in addition to the CHP units and the auxiliary boilers – considers the installation of photovoltaic (PV) panels feeding a heat pump (HP), both the systems installed at the thermal power station. The electric power at the input of the heat pumps can be given by the PV panels (firstly) and by the CHP unit (as second option), while there is no connection between the national electric grid and the HP (Figure 5b);
3. *Case 3*: in the third proposed configuration the photovoltaic panels are installed, along with heat pumps, directly at the utility substations (Figure 5c). It must be highlighted that the installation of PV panels and HPs involves not the totality of the users but only a fraction of them. The choice of the involved utilities is part of the analysis and it has been made with the purpose of unloading the centralized thermal power station, in particular by closing one of the two rings of the network. Moreover, the avoidance of the produced heat dispersion and the minimization of the electric energy introduction into the grid have been maintained for the choice. After this preliminary investigation, the right ring of the network has been fixed for the further analysis, *i.e.* the involved utilities are those with ID #6, #11, #13, #14, #16, #20, #25 and #29.

In order to give an immediate comprehension of the proposed configurations, all the analyzed cases are summarized in Table 3.

Copyright © 2017 by ASME

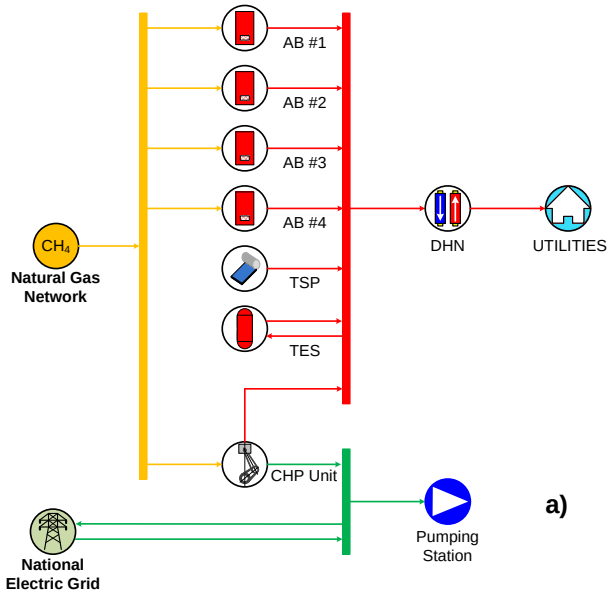

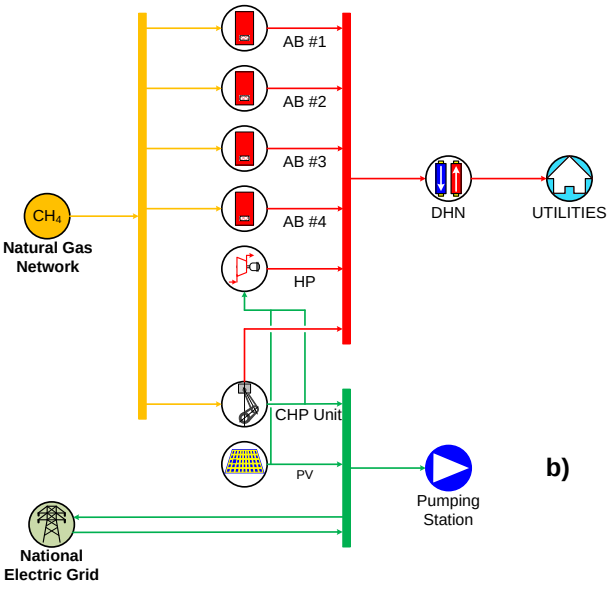

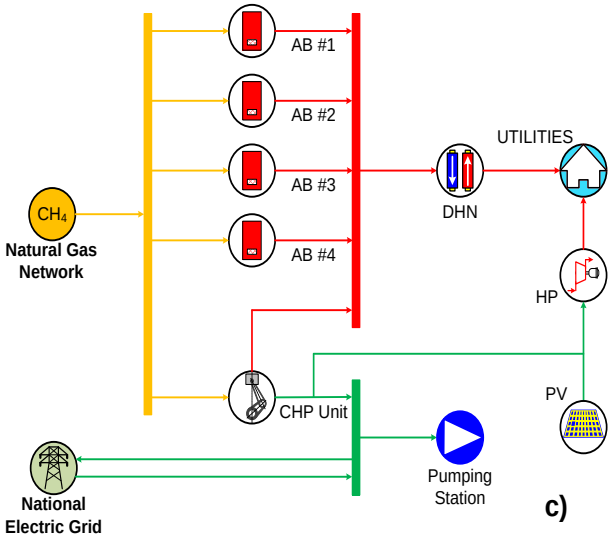

Figure 5 – Case studies configurations: a) Case 1; b) Case 2; c) Case 3.

Table 3 – Summary of the analyzed configurations.

	Ref. Case	Case 1	Case 2	Case 3
ICE	•	•	•	•
Aux. Boilers	•	•	•	•
Thermal Solar Panels		•		
Thermal Energy Storage		•		
PV Panels (centralized)			•	
PV Panels (distributed)				•
HP (centralized)			•	
HP (distributed)				•

Other assumptions

The proposed cases have been simulated with the software EGO in order to evaluate the optimal yearly operational set up. As well as for the Reference Case, the constraint of completely avoiding thermal energy dissipation has been imposed for the operating of the CHP unit.

All the simulations have been carried out considering for the utilities the same thermal needs of the Reference Case. This assumption entails that the hourly profile of the centralized thermal power station production remains the same of the Reference Case, excepting for what regard Case 3. In the last proposed configuration, indeed, the solar PV panels and the heat pumps are placed at the utilities (i.e. distributed generation systems are considered). Thus, in this case the utilities' need is partially covered by the thermal energy produced directly at the utilities themselves, avoiding a part of the thermal dissipations through the DHN.

Moreover, further considerations can be made about the introduction of renewable energy generation systems (thermal od PV panels) as well as of the heat pumps and the thermal storage system. The main characteristics of the introduced systems – listed in Table 4 – have been defined as follows:

- Thermal Solar Panels (TSP) – Case 1: the size of the TSP has been fixed considering the real available surface at the thermal power station. The tilt and the azimuth angles have been chosen on the basis of the optimum for the considered city (latitude 44°30'27"00 N, longitude 11°21'5"04 E).
- Thermal Energy Storage (TES) – Case 1: the volume of the thermal storage tank has been defined as the minimum volume to obtain at the end of the day the complete restitution of the stored energy (*i.e.* every 24 hour the same conditions can be registered for the tank).
- Centralized PV panels – Case 2: similarly to the considerations made for the TSP, the available surface at the thermal power station has been considered to fix the PV size. The produced electric energy is used (i) for the centralized heat pump, (ii) for the pumping station and (iii) only

Copyright © 2017 by ASME

the possible surplus is sold to the national electric grid.

- Centralized Heat Pump – Case 2: the Coefficient Of Performance (COP) has been chosen on the basis of the available literature [26] considering a large-scale HP. The size of the HP, for this case, has been determined with the aim of completely recovering the ICE available heat and contemporarily operating the HP with the electric energy produced by PV panels and ICE, in order to minimize the electric energy exchange with the grid. Thus, the size of the centralized heat pump becomes a result of the optimization analysis.
- Distributed PV panels – Case 3: as explained in the previous section *Case studies*, the first step of the analysis related to Case 3 involved the choice of the utilities to be considered for the distributed generation. Once fixed the involved substations (right ring of the DHN, utilities with ID #6, #11, #13, #14, #16, #20, #25 and #29), the surface of PV panels has been set on the basis of the roof available surfaces faced to South.
- Distributed Heat Pumps – Case 3: in this case, the distributed HPs are supplied by (i) the PV panels production and (ii) the ICE generated electric energy. Obviously, HPs are present only at the utility where also distributed PV panels are installed. the considered COP, as it can be seen in Table 4, is lower than the one for Case 2, due to the lower HP size [26].

Table 4 – Main parameters of the systems considered in the proposed variation scenarios.

Thermal Solar Panels	
Typology	plate
S	300 m²
η	80%
Tilt Angle	30°
Facing	South
Thermal Storage Tank	
V	1 m³
T_{min}	70 °C
T_{max}	130 °C
T_i	70 °C
Solar PV Panels	
S	300 m²
η	10%
Tilt Angle	30°
Facing	South
Centralized Heat Pump	
COP	4
Distributed PV Panels	
η	10%
Tilt Angle	30°
Facing	South
Distributed Heat Pumps	
COP	3

Solar Irradiation

The production obtainable from the solar panels – for both thermal and PV panels – has been evaluated starting from the measured data of solar irradiation profile on a horizontal surface [27] in the city of Bologna. The solar radiation etching on a surface with a tilt angle equal to 30° and facing the South has been calculated, extracting the yearly solar irradiation profile to be applied for the analyzed cases. In Figure 6, the obtained profiles for a typical winter day (*i.e.* January) and for a typical summer day (*i.e.* July) are shown. Different conversion efficiencies have been then considered (as it can be seen in Table 4) for the evaluation of the thermal solar production and for the PV case.

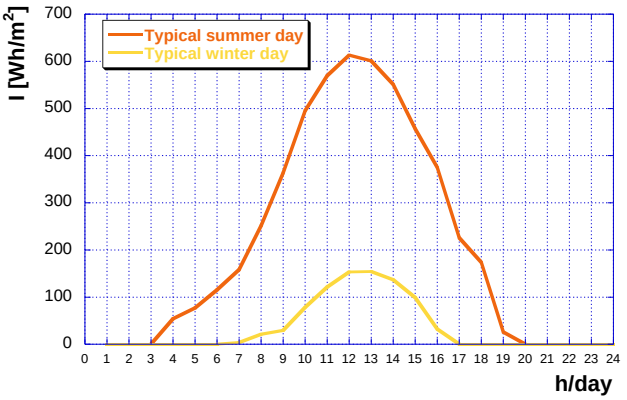

Figure 6 – Incident solar irradiation on a solar panel faced to South and with a tilt angle equal to 30°, for a typical summer day (orange line) and for a typical winter day (yellow line).

RESULTS AND DISCUSSIONS

In Figure 7 the hourly profiles – for typical winter and summer days separately – of the thermal power production in the considered scenarios are shown along with the production mix. In more detail, in the presented figure the centralized thermal production (by means of various generation systems, based on the considered case study) and the distributed thermal generation have been distinguished. All the plotted curves show the same qualitative trend with two peaks of thermal production (at 9 a.m. and 8 p.m. respectively), but different quantitative behavior can be observed. As it can be clearly seen, indeed, the introduction of distributed generation systems (Case 3) allows to considerably unload the centralized thermal power station, both in winter (see Figure 7-g) and summer seasons (see Figure 7-h). The remaining amount of thermal energy for the fulfillment of the utilities' need is guaranteed by the distributed heat pumps (Figures 7-i and 7-j, for winter and summer days respectively).

On the other hand, relating to Reference Case, Case 1 and Case 2, the same trend of production can be seen at the thermal power station (see Figures from 7-a to 7-f). However, as already discussed, this production is guaranteed by a different mix of production systems, that is a result of the optimization analysis depending on the considered case.

Copyright © 2017 by ASME

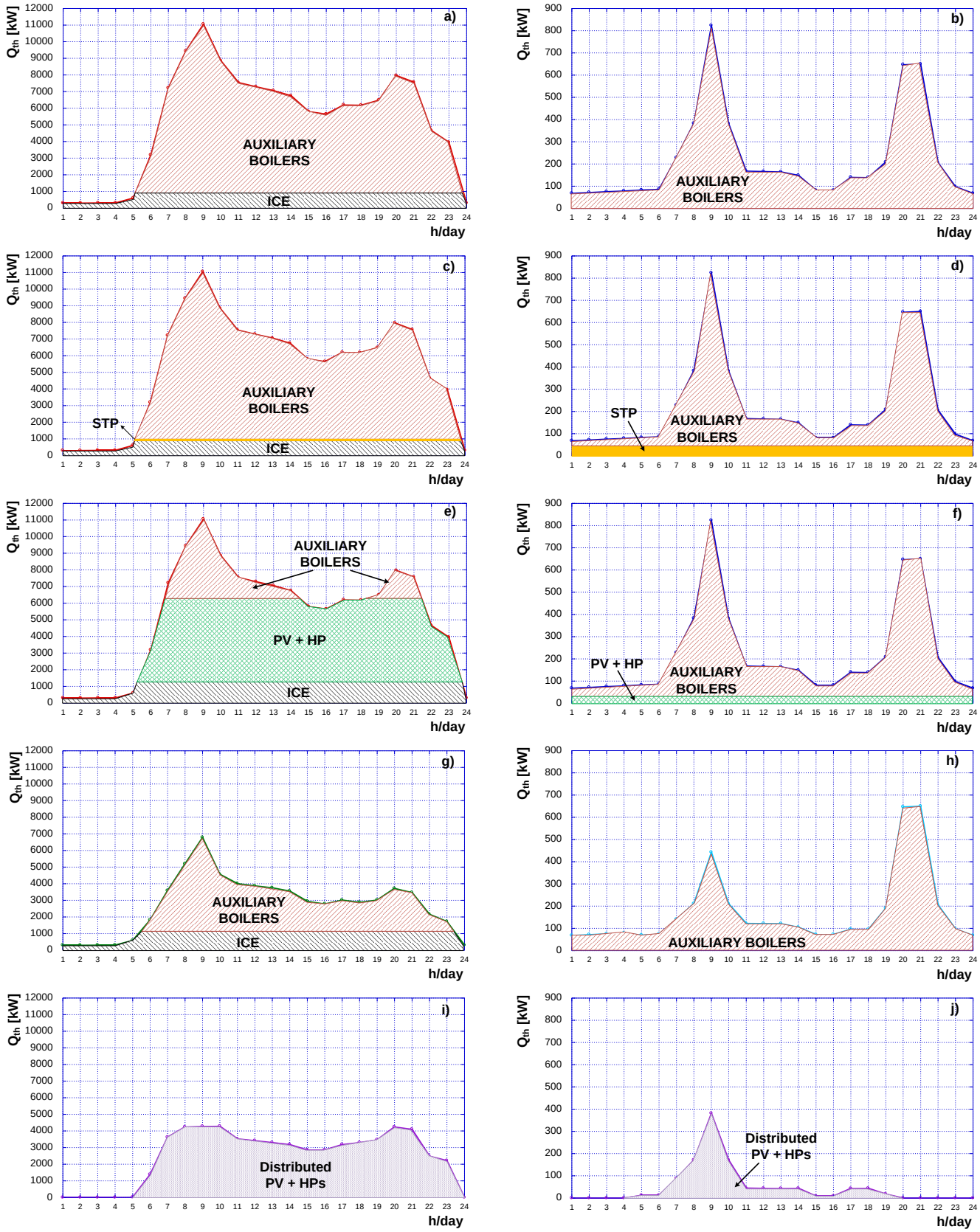

Figure 7 – Thermal production profiles along with the production systems mix for the presented cases: a) Reference Case typical winter day (thermal power station), b) Reference Case typical summer day (thermal power station), c) Case 1 typical winter day (thermal power station), d) Case 1 typical summer day (thermal power station), e) Case 2 typical winter day (thermal power station), f) Case 2 typical summer day (thermal power station), g) Case 3 typical winter day (thermal power station), h) Case 3 typical summer day (thermal power station), i) Case 3 typical winter day (distributed generation units), j) Case 3 typical summer day (distributed generation units).

Copyright © 2017 by ASME

First of all, the optimization of the analyzed configurations, by means of the application of the software EGO, allowed to set the optimal operation profile for the CHP unit. In Figure 8 the results for all the analyzed cases during the typical winter day are presented. Relating to the summer period, instead, the optimal solution identified by the software is the complete shutdown of the internal combustion engine, due to the low thermal needs of the utilities.

As it can be seen from Figure 8, for the Reference Case – Figure 8 a) – and for the Case 1 – Figure 8 b) – the ICE in winter operates from 8 p.m. to 20 p.m. included (when the utilities thermal needs are higher than the ICE capacity) and – when operating – it works always at the rated power. Relating to Case 2, instead, the internal combustion engine operation results extended, working from 6 a.m. to 23 a.m. included, for a total of around 3000 equivalent operating h/year. Furthermore, Figure 8 c) shows that in this case not only the rated power but also the off-design operation of the ICE is considered. This evidence is due to the will of contemporarily avoiding the thermal energy dissipations, operating the heat pump using the CHP unit produced electric energy and minimizing the introduction of electricity into the national electric grid. Further increase in the ICE operational range can be reached with Case 3 – see Figure 8 d) – in which the CHP unit works from 5 a.m. to 23 p.m. included, thanks to the introduction of the distributed generation systems.

Relating to the Reference Case, evidently, only the auxiliary boilers provide in winter for the remaining amount of thermal energy to be produced, once the CHP heat is completely recovered, as well as they provide for the whole production in summer season. For what regard the Case 1, instead, the installed thermal solar panels along with the thermal energy storage contribute to the thermal energy need fulfillment within the auxiliary boilers. This fact entails in the reduction of the auxiliary boilers operation, with consequent benefits in fuel consumption (as better explained in the following of this paragraph). It is also essential to highlight that the thermal solar panels production and the stored thermal energy are completely recovered during the day (and every day/year), thus – as happens for the ICE production – no thermal dissipation occurs. Similarly, in Case 2 and in Case 3, all the electric energy produced from renewable energy source (*i.e.* by means of the PV panels) is used for the thermal energy production through the centralized heat pump (Case 2) or the distributed HPs (Case 3). During winter, the PV-HPs contribute with the auxiliary boilers and the ICE to the thermal energy production, while in summer period only PV-HPs and boilers operate.

Based on the results of the carried out simulations with the software EGO, the evaluation of the yearly fuel consumption, the yearly purchase of electric energy from the grid and the yearly sale of the exceeding electricity to the grid has been made. As a result, the yearly fuel consumption for each of the analyzed cases is shown in the bar graph of Figure 9. As it can be seen, all the elaborated configurations allow to decrease the fuel consumption with respect to the Reference Case (representing the current configuration of the considered CHP-DH network), with a maximum percentage saving equal to about the 57% achieved in Case 2 (fuel consumption decreasing from 35000 MWh to 15000 MWh).

Furthermore, in Figure 10 the yearly purchase of electric energy from the national electric grid is shown for the analyzed cases. As evident considering the CHP unit operation, the same amount of electric energy has to be annually purchased for the Reference Case and Case 1 (equal to 800 MWh/year), while a reduction can be seen for the Case 2 (around the 14%) and for the Case 3 (maximum reduction, equal to about the 30%). The decrease in electricity purchase reached in cases 2 and 3 is clearly due to the installation of the PV panels that – coupled with the heat pumps – enables to obtain the double advantage of fuel consumption and electric energy purchase decrease.

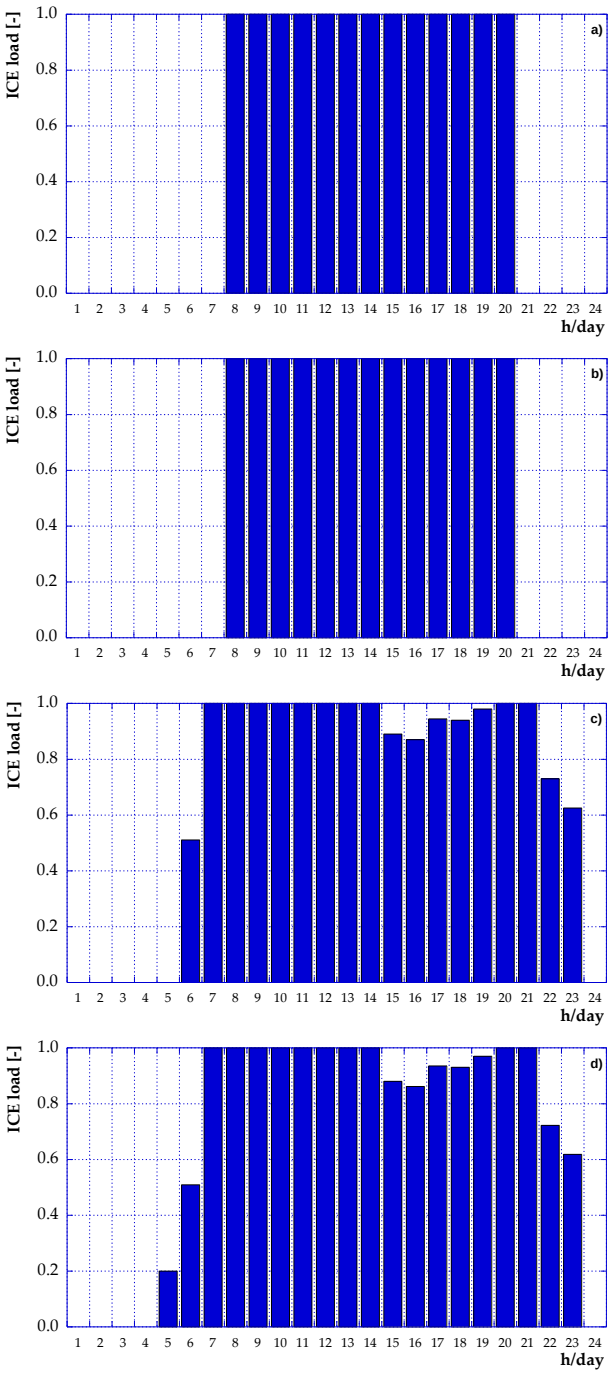

Figure 8 – Daily operation profile of the CHP unit in a typical winter day: a) Reference Case, b) Case 1, c) Case 2 and d) Case 3.

Copyright © 2017 by ASME

Finally, the electric energy annually sold to the national electric grid for each configuration is presented in Figure 11. Relating to Reference Case and Case 1, all the electric energy produced with the ICE is sold to the network excepting for the internal self-consumption of the pumping station (that requires only the 8% of the ICE capacity, thus a high excess of electricity is present).

The introduction of the heat pumps with an optimum management, instead, allows to completely avoid the introduction of electricity into the national grid in Case 2 and to reduce the sale of about the 85% (see Figure 11). This condition is particularly desirable since a higher electric grid stability can be guaranteed.

As a consequence, these results seems to indicate the Case 2 as the best viable solution for the considered CHP-DH network, allowing contemporarily the reduction of the fuel consumption and of the purchase of electric energy, the elimination of the electricity sale and the avoidance of thermal energy dispersion. Generally speaking, the developed analysis indicates that heat pumps coupled with RES generation can be regarded as promising way for complex energy network efficiency improvement, even more when then the production is centralized.

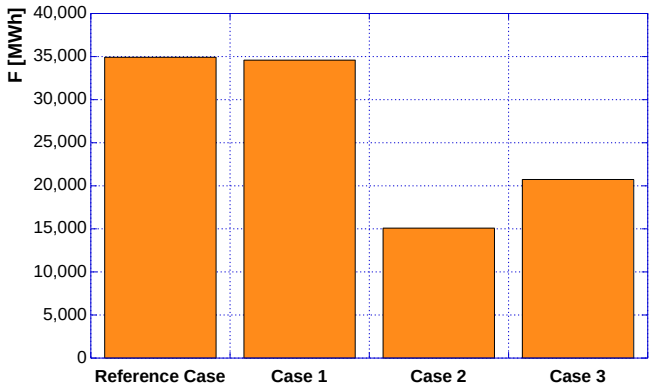

Figure 9 – Yearly fuel consumption (ICE plus auxiliary boilers).

Figure 10 – Electric energy yearly purchased from the national electric grid.

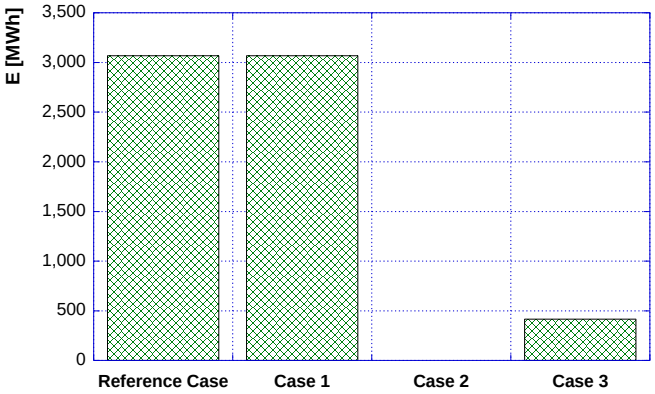

Figure 11 – Electric energy yearly sold to the national electric grid.

CONCLUDING REMARKS

The aim of this paper is the analysis of different solutions in terms of energy generators mix, in order to define the optimal configuration for a given network. Thus, an existing DHN has been considered as starting point for the optimization analysis and three different alternative scenarios (in terms of installed production systems) have been proposed, considering renewable energy generators (both thermal and electric), heat pumps and thermal energy storage and evaluating the possibility to introduce distributed generators to unload the centralized power station.

Firstly, the network behavior has been analyzed by applying an in-house developed software named IHENA (Intelligent Heat Energy Network Analysis) in order to define the annual hourly profile of thermal energy to be produced and guaranteed.

Consequently, the proposed cases have been simulated with the software EGO (Energy Grid Optimizer) in order to evaluate the optimal yearly operational set up. The simulations have been carried out with the purpose of (*i*) minimizing the energy production costs, (*ii*) minimizing the exchange of electric energy with the national electric grid, (*iii*) minimizing the auxiliary boilers use, (*iv*) optimizing the CHP unit operation and (*v*) maximizing the exploitation of renewable energy sources, with a complete avoidance of produced thermal energy dissipations.

The results of the analysis show that all the proposed alternative configurations enable to decrease the fuel consumption with respect to the starting Reference Case, with a maximum percentage saving equal to about the 57% (Case 2) achieved when centralized PV panels and heat pump are considered in addition to the current thermal power station set up (CHP unit and four auxiliary boilers). Furthermore, in this case the electric energy sale to the grid results eliminated and the purchase of electricity reduced (around the 14%). Thus, Case 2 seems to represent the best solution for the considered existing network, considerably reducing the operating costs.

In any case, all the proposed set up allow to improve the CHP-DH network efficiency relating to the current plant configuration performance. Further analysis will investigate the economic aspects linked to the investments required for the current plant modification.

Copyright © 2017 by ASME

REFERENCES

[1] International Energy Agency. Renewable energy medium-term market report 2014 – market analysis and forecast to 2020. Paris, France; 2014.

[2] Directive 2009/28/EC of the European Parliament and of the Council of 23 April 2009 on the promotion of the use of energy from renewable sources and amending and subsequently repealing Directives 2001/77/EC and 2003/30/EC (Text with EEA relevance).

[3] Connolly D, Lund H, Mathiesen BV, Werner S, Möller B, Persson U, et al. Heat roadmap Europe: combining district heating with heat savings to decarbonize the EU energy system. *Energy Policy* 2014;65:475–89.

[4] Statistics Finland. Energy. http://www.stat.fi/til/ene_en.html. 2012 [assessed 17.03.15].

[5] J. Ortiga, J.C. Bruno, A. Coronas, Operational optimisation of a complex trigeneration system connected to a district heating and cooling network. *Appl. Therm. Eng.* 51 (2) (2013) 1536–1542.

[6] H. Wang, W. Yin, E. Abdollahi, R. Lahdelma, W. Jiao. Modelling and optimization of CHP based district heating system with renewable energy production and energy storage. *Applied Energy* 159 (2015) 401–421.

[7] Wang H, Lahdelma R, Wang X, Jiao W, Zhu C, Zou P. Analysis of the location for peak heating in CHP based combined district heating systems. *Applied Thermal Engineering* 87 (2015) 402–411.

[8] A. Arteconi, N.J. Hewitt, F. Polonara, Domestic demand-side management (DSM): role of heat pumps and thermal energy storage (TES) systems. *Appl. Therm. Eng.* 51 (2013) 155–165.

[9] Böttger D, Götz M, Lehr N, Kondziella H, Bruckner T. Potential of the power-to heat technology in district heating grids in Germany. *Energy Proc*. 2014;46:246–53.

[10] Sartor K, Quoilin S, Dewallef P. Simulation and optimization of a CHP biomass plant and district heating network. Appl Energy 2014;130:474–83.

[11] Schmidt RF, Fevrier N, Dumas P. Smart cities and communities, key to innovation integrated solution – smart thermal grids; 2013.

[12] T. Ommen, W.B. Markussen, B. Elmegaard, Heat pumps in combined heat and power systems. *Energy* 76 (2014) 989–1000.

[13] B. Bach, J. Werling, T. Ommen, M. Münster, J.M. Morales, B. Elmegaard, Integration of largescale heat pumps in the district heating systems of Greater Copenhagen. *Energy* 107 (2016) 321–334.

[14] Chicco G, Mancarella P. Matrix modelling of smallscale trigeneration systems and application to operational optimization. *Energy* 34 (2009) 261–73.

[15] Lozano M, Carvalho M, Serra L. Operational strategies and marginal costs in a simple trigeneration systems. *Energy* 34 (2009) 2001–8.

[16] Curti V, von Spakovsky M, Favrat D. An environomic approach for the modeling and optimization of a district heating network based on centralized and decentralized heat pumps, cogeneration and/or gas furnace. Part ii: application. *Int J Therm Sci* 39 (2000) 731–41.

[17] Ren H, Zhou W, Nakagami K, Gao W, Wu Q. Multi-objective optimization for the operation of distributed energy systems considering economic and environmental aspects. *Applied Energy* 87 (2010) 3642–51.

[18] Chinese D. Optimal size and lay-out planning for district heating and cooling networks with distributed generation options. *Int J Energy Sector Manage* 2 (2008) 385–419.

[19] Tveit T, Savola T, Gebremedhin A, Fogelholm C. Multi-period MINLP model for optimising operation and structural changes to CHP plants in district heating networks with long-term thermal storage. *Energy Conversion and Management* 50 (2009) 639–47.

[20] Buoro D, Pinamonti P, Reini M. Optimization of a distributed cogeneration system with solar district heating. *Applied Energy* 124 (2014) 298–308.

[21] Chesi A, Ferrara G, Ferrari L, Magnani S, Tarani F. Influence of the heat storage size on the plant performance in a smart user case study. *Applied Energy* 112 (2013)1454–65.

[22] Ali M, Jokisalo J, Siren K, Lehtonen M. Combining the demand response of direct electric space heating and partial thermal storage using LP optimization. *Electr Power Syst Res* 106 (2014) 160–7.

[23] Ancona MA, Bianchi M, Branchini L, De Pascale A, Melino F, Peretto A. Generation Side Management In Smart Grid. *Proceedings of ASME-ATI-UIT Conference*. Naples, May 17-20th, 2015.

[24] Macchi E, Campanari S, Silva P. La microcogenerazione a gas naturale. 2005, Polipress ISBN: 8873980163.

[25] Ancona MA, Branchini L, De Pascale A, Melino F. Smart District Heating: Distributed Generation Systems' Effects on the Network. *Energy Procedia* 75 (2015) 1208-1213.

[26] Bianchi M, Spina PR, Tomassetti, G, Forni D, Ferrero E. Le tecnologie innovative ed efficienti nei sistemi di generazione in assetto co-trigenerativo e nei sistemi integrati con unità a pompa di calore nelle applicazioni industriali e del terziario. Report RSE/2009/18

[27] http://www.solaritaly.enea.it/

Copyright © 2017 by ASME

APPENDIX

In this section the hourly non-dimensional profiles assumed for the space heating and hot water needs are presented. The typical profiles are shown in Figure A1 and in Figure A2 for residential utilities, in Figure A3 and Figure A4 for school utilities, in Figure A5 and Figure A6 for hospital utilities and in Figure A7 and Figure A8 for super-markets.

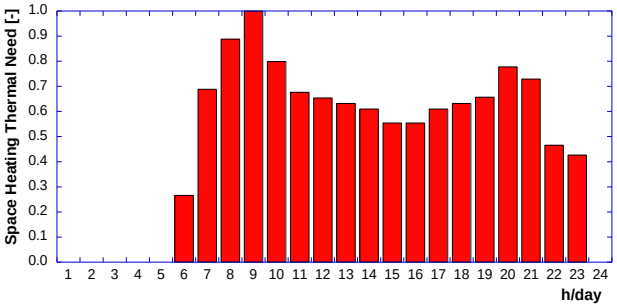

Figure A1 – Space heating non-dimensional thermal need hourly profile for a residential utility.

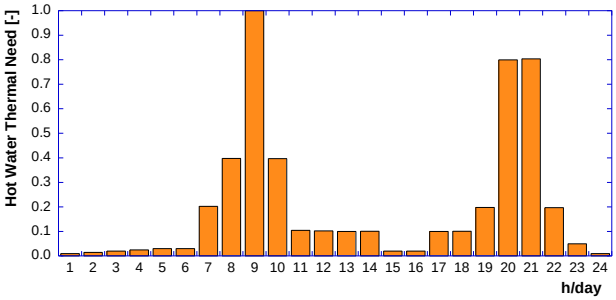

Figure A2 – Hot water non-dimensional thermal need hourly profile for a residential utility.

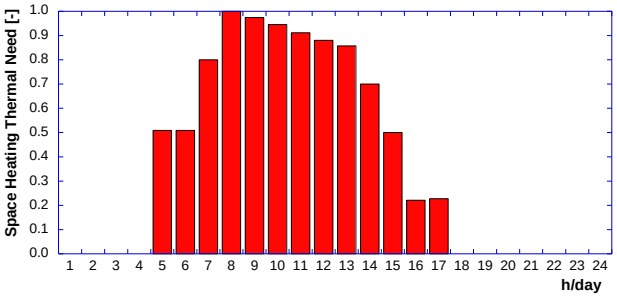

Figure A3 – Space heating non-dimensional thermal need hourly profile for a school.

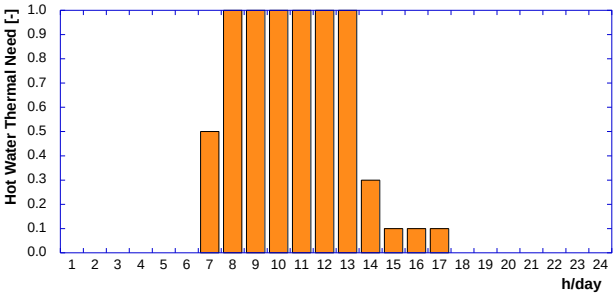

Figure A4 – Hot water non-dimensional thermal need hourly profile for a school.

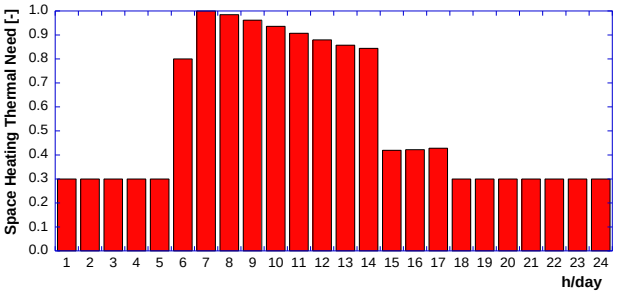

Figure A5 – Space heating non-dimensional thermal need hourly profile for a day-hospital.

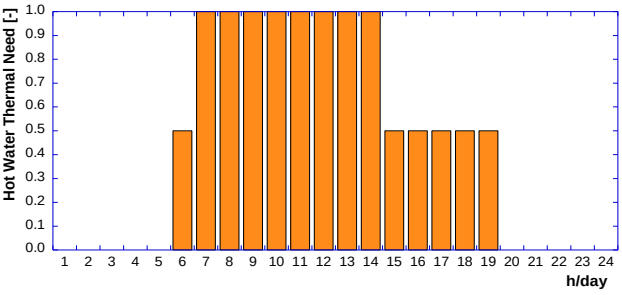

Figure A6 – Hot water non-dimensional thermal need hourly profile for a day-hospital.

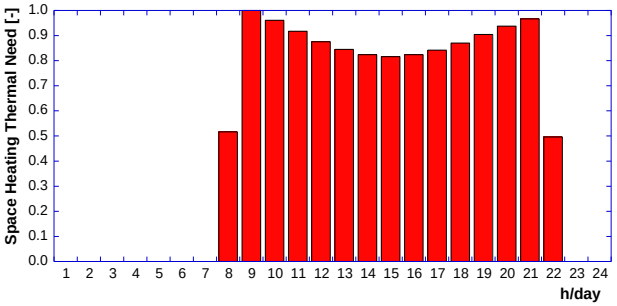

Figure A7 – Space heating non-dimensional thermal need hourly profile for a super market.

Copyright © 2017 by ASME

Energy 140 (2017) 1030–1046

Contents lists available at ScienceDirect

Energy

journal homepage: www.elsevier.com/locate/energy

A feasibility study of some DSM enabling solutions in small islands: The case of Lampedusa

G. Zizzo [a, *], M. Beccali [a], M. Bonomolo [a], B. Di Pietra [b], M.G. Ippolito [a], D. La Cascia [a], G. Leone [a], V. Lo Brano [a], F. Monteleone [b]

[a] DEIM – Department of Energy, Information Engineering and Mathematical Models, Università di Palermo, Palermo, Italy
[b] ENEA – Italian National Agency for New Technologies, Energy and Sustainable Economic Development, Portici, Italy

ARTICLE INFO

Article history:
Received 21 November 2016
Received in revised form
23 August 2017
Accepted 17 September 2017
Available online 18 September 2017

Keywords:
ICT
Small islands
Energy efficiency
BAC
2012/27/EU directive
EN 15232 standard

ABSTRACT

The paper addresses the issue of the transition from a traditional electrical system without automation to a newer active and smart system allowing the possibility of implementing Demand Side Management policies, for little islands not supplied by the main grid. In particular, the paper focuses on two main topics related to the definition of:

- *an effective control, monitoring and communication system as a tool for the full exploitation of the opportunities given by Demand Response policies;*
- *some solutions for the automation of the end-users' electrical installations, in order to offer to the utility flexibility to be used for the improvement of the generation and distribution efficiency.*

After a brief discussion on the international regulatory framework on automation and ICT applications for power systems, the paper presents a feasibility study, based on the characteristics of the island of Lampedusa, of a hierarchical architecture of a suitable control system and of some DSM enabling solutions for residential end-users. The proposed solutions are defined taking into account some main elements:

- *distribution grids in small islands are generally equipped with outdated and hardly automatable devices;*
- *utilities in small islands have reduced budget for new investments;*
- *not less important, the most of the inhabitants has low income and unfamiliarity with automation.*

Therefore, main features of the proposed DSM enabling technologies are low cost and ease of use.

© 2017 Elsevier Ltd. All rights reserved.

1. Introduction

Although small islands not connected to the main power grid have significant availability of Renewable Energy Sources (RESs), at the dawn of their electrification, after World War II, the only way for them to produce electricity was to resort to diesel generators.

It is well-known that the production cost of such generators is very high with respect to other technologies while, on the other hand, the economy of small islands is quasi-totally based on fishing and tourism during summer period [1]. Thanks to the considerable cash inflow from foreign aid, tourism, and remittances from citizens working abroad, many small islands have been able to finance their energy imports [2], whereas in other cases local Governments have established financial subsidies with the purpose of reducing the electricity costs for the inhabitants of the small islands [3–5]. The process is quite different from that occurring in Pacific Small

* Corresponding author.
E-mail address: gaetano.zizzo@unipa.it (G. Zizzo).

https://doi.org/10.1016/j.energy.2017.09.069
0360-5442/© 2017 Elsevier Ltd. All rights reserved.

Nomenclature

AEEGSI	Italian Authority of Electric Energy, Gas and Water Resource
BAC	Building Automation and Control
BAN	Building Area Network
BAT	Building Automation Technology
BEMS	Building Energy Management System
DC	Data Concentrator
DR	Demand Response
DSM	Demand Side Management
DSO	Distribution System Operator
DSS	Decision Support System
EES	Electric Energy Storage
EMC	Electromagnetic Compatibility
EMS	Energy Management System
EPBD	Energy Performance Building Directive
ESWH	Electric Storage Water Heater
EU	European Union
FLEX	Flexible
ICT	Information and Communication Technology
ITU	International Telecommunications Union
LAN	Local Area Network
LC	Local Controller
LV	Low Voltage
MG	Micro-Grid
MGSC	Micro-Grid Supervisory Controller
MV	Medium Voltage
NAN	Neighborhood Area Network
PAN	Personal Area Network
PLC	Power Line Communication
RCU	Room Control Unit
RES	Renewable Energy Sources
SIDS	Small Island Developing States
VAT	Value Added Tax

Island Developing States (SIDS), where donor agencies and international organizations play major roles in funding the exploitation of renewable resources [6,7]. In addition, for many SIDS the electricity production cost from imported fossil fuels is so high and the cost of renewable energy technology has fallen so significantly that transitioning towards renewable energy is likely to produce cost savings [8].

In Italy, because of state subsidies, small islands' electrical utilities had no interest in the promotion of RES-based systems or other technological solutions for improving the generation and distribution efficiency of their plants, until in 2014 the Italian Government started a reform process for abolishing the support mechanism [9–12], obliging small islands' electrical utilities to launch a renovation process in order to enhance the efficiency of their generation and distribution plants.

In this new context, RES exploitation, building energy efficiency, building and grid automation and DSM applications in small islands not connected to the main grid have recently become very topical and urgent issues, on which many research institution are currently discussing. Nevertheless, while many recent scientific papers demonstrate the interest of the scientific community in the promotion of RES-based technologies in small islands all around the world [13–20], few examples of application of DSM actions to this particular Micro-Grids (MGs) are found in literature. On the other side, it is worth to highlight that building automation technologies (BAT) and building energy management systems (BEMS) can play a crucial role in reducing the energy consumption and the dependence on fossil fuel. Indeed, in a realistic scenario, ICT and automation are able to reduce the current energy consumption of 13% by 2035 [21].

The Department of Energy, Information Engineering and Mathematical Models of the University of Palermo (DEIM), in collaboration with the Italian National Agency for New Technologies, Energy and Sustainable Economic Development (ENEA) has faced this issue in the last few years, producing a feasibility study addressing the transition from a “fuel-based” traditional centralized electrical system to a newer active and smart “renewables-based” one. In particular, in some previous works [22–25] the issue of the exploitation of RES-based generators, battery storage systems and switchable capacitor banks for improving the energy efficiency of Mediterranean small islands power system has been faced. This paper focuses on three different topics:

- role that the automation of the end-users' electrical installations have in the improvement of a MGs generation and distribution efficiency;
- definition of an effective and low expensive control architecture for exploiting the opportunities offered by DR policies;
- identification of technologies and replicable solutions for the automation and the integration into a smart micro-grid of a typical house and a typical hotel of a small Mediterranean islands.

With reference to the first topic, it has to be cited a very interesting scientific paper where 105 pilot installations are analyzed and it is shown how ICT can play a potential role in improving the energy performance of buildings by the implementation of effective solutions that take advantage of the energy interactions between all the parts included in a building [26]. Also in Ref. [27], López-González et al., by analyzing more than 9400 energy performance certificates, show how the use of BACS and TBM systems can reduce building energy consumption by up to 26.36%. Finally, in [28–30] is shown the potential of automation and smart metering for reducing CO_2 emissions and energy consumptions.

Moreover, many papers can be found in the most recent literature dealing with DR policies. For example, in Ref. [31] the authors propose a load shedding algorithm able to maximize the power sale and minimize the power surplus for satisfaction of power suppliers, and at the same time maximize end-users satisfaction. In Ref. [32] a multiagent-based distributed load shedding scheme is proposed for restoring frequency in MGs considering both the associated cost and the load flexibility. In Ref. [33] an agent based market model for including DR in the combined operation of MGs is proposed and simulated. In Ref. [34] the author propose a two-stage stochastic framework for day-ahead scheduling of MGs, showing that the coordination of EES systems and DR policies can affect economy of microgrids. Analogously, in Ref. [35] a stochastic programming model is proposed to optimize the performance of smart microgrids in a short term by minimizing operating costs and emissions in presence of renewable sources.

Finally, papers [36] and [37] present two comprehensive reviews of optimal control techniques and load shedding schemes applied to the energy management and control of MGs. As it can be noticed from the example reported above, the most of the papers deals with the definition of load management algorithms and

schemes for smart islanded MGs, taking into account also the frequency and voltage security issue.

On the contrary, few efforts have been done in proposing technological solutions able to overcome the limits imposed by practical, cultural and economical issues. In fact, as highlighted by some recent research papers, the income and education levels, affect the openness towards energy savings and automation and also the preference of particular automation levels [38–41].

The novelty of the present work is to propose a low cost and feasible hierarchical architecture of a load management system for small islands' microgrids and some technological solutions for the automation of electrical installations of residential building, based on the analysis of the actual needs of the inhabitants of Lampedusa and of the actual state of its power generation and distribution system. The work summarizes the results of a technical-economic feasibility study that starts from the data provided by SE.Li.S. SpA, the local electrical utility, surveys of the distribution system and of the buildings of the island, and direct interviews of the inhabitants.

The remainder of the paper is organized as hereafter:

- Section 2 describes the proposed control, monitoring and communication system for islanded MGs and reports some considerations on its practice managing;
- Section 3 reports a technical-economic feasibility study of some replicable solutions for the automation and the integration into a smart micro-grid of a typical house and a typical hotel of small Mediterranean islands. The study is carried out by considering two actual existing building located in Lampedusa. Finally, a proposal of a control algorithm for exploiting the loads flexibility for improving the energy efficiency of the island is described in subsection 3.4;
- Section 4 reports the results of a study aiming at demonstrating the positive effects of automation on the reduction of the overall electricity consumption of the island;
- Section 5 contains the conclusions of the paper.

2. Control and communication system architecture

2.1. Regulatory and technical framework

According to the European Smart Grid Task Force definition, Smart Grids are power systems able to actually integrate the behavior and the actions of all users connected to them, in order to assure an economical and sustainable power system with low energy losses, high quality of the supply and safety for persons [42]. The integration and synchronization of the actions of the various users requests a rapid and effective exchange of information between all the players involved and specific key-nodes of the LV and MV networks, even in presence of significant distances. The information exchange by ICT systems in the power grid involves various areas:

- loads and generators monitoring and control;
- electric energy storage (EES) management;
- voltage and frequency regulation;
- short/long-term scheduling;
- ancillary services;
- grid monitoring;
- state estimation;
- protection against fault effects and fault detection;
- measurement service;
- signals transmission and elaboration.

In the last few years, ICT, smart metering and automation have been the subjects of several initiative from various stakeholders: EU, national governments, industry, utilities and standard committees [43,44].

The European Directive 2009/72/EC [45], concerning common rules for the internal market in electricity, requires EU-Member States to replace at least 80% of electricity meters with smart meters by 2020, in the case of positive cost-benefit analysis. Moreover, EU-Member States must implement intelligent metering systems. Similarly, the European Directive 2009/73/EC [46] recommends that the EU-Member States introduce smart metering systems or smart grids for the natural gas distribution systems, so encouraging an active participation of the end-users to the natural gas market. In addition, the Energy Performance of Buildings Directive 2010/31/EU [47] specifies that EU-Member States have to encourage the introduction of active control systems and intelligent meters in the case of construction or major renovation of buildings. The Energy Efficiency Directive 2012/27/EU [48] supports the implementation of new energy services based on the collection of data from smart meters, Demand Response (DR) services, and dynamic prices. Smart meters for EU Countries must comply with the Measuring Instruments Directive 2004/22/EC [49] and the Recommendation 2012/148/EU [50] reports the minimum functionalities that smart metering systems should provide to the end-users.

One of the most debated standards in the field of automation in buildings is the European Standard EN 15232 [51] that devises terminology, rules and methodologies for estimating the impact of Building Automation and Control (BAC) and Technical Building Management (TBM) systems on the energy performance and the energy use in buildings.

ISO/IEC 14543-3 [52] standard series define the characteristic of the KNX network communication protocol for building automation, including both wired and wireless communications media and independent of the hardware used in the house. ISO/IEC 14543-3 standards have approved CENELEC EN 50090 document as international standard accepted worldwide including China (GB/T 20965 Standard [53]) and US (ANSI/ASHRAE Standard 135 [54]).

IEEE published several guides and standards, delineating valuable and practical indications for Smart Grid interoperability of energy technology and information technology operation with the electric power system, end-use applications, storage systems and loads [55–57]. Among these, one of the most recent is the IEEE Approved Draft Standard for Green Smart Home and Residential Quarter Control Network that provides protocols for measurement and control networks for home and residential quarters so that they can achieve green, smarter functions.

Considering the various tasks in a Smart grid, an effective monitoring, control and telecommunication system for a small island should, first of all, be consistent with the layout of the power network and should include:

- a communication system able to reach the entire territory;
- network components and devices for data exchange with the power system;
- human interfaces, where needed;
- Decision Support Systems (DSS);
- smart meters installed at every monitored and controlled bus;
- sensors and probes for measuring and monitoring specific relevant parameters (voltages, currents and power flows, average and minimum power factors, etc).

One of the most difficult issue to be faced is related to the design of the control system and consists in the management of a very high number of devices and variables. Indeed, in MV and LV distribution networks the buses to be monitored can be thousands. For this reason, the control system should also include calculators

having very great memory space, a great amount of storage during the solution of the problem and very low computational time. Moreover, the designer of the control system must select, among all the measured parameters, those to analyze for every different purpose of the control system. This can be done by dividing the control system into tiers or levels as described in Ref. [58]. The authors of the review paper focalize the attention on the hierarchical control layers of micro-grids and on the functions of the MG Supervisory Controller (MGSC) or MG central controller and of the Local Controllers. The study in Ref. [58] deals with the possibility of increasing the efficiency of the system and also with all the tasks of a micro-grid. The hierarchical architecture here proposed has, certainly, a general application. Therefore, on the basis of the actual trend for micro-grid control, the most suitable structure for the monitoring, control and telecommunication of a small island not connected to the main grid, with only one fuel-based power plant and two different voltage levels, is characterized by a hierarchical structure like the one represented in Fig. 1, with the following three levels:

- 1: Smart Building;
- 2: Smart Micro-Grid;
- 3: Smart Grid.

In the case of Lampedusa, the MV grid is characterized by four 10 kV lines, 39 kiosk and 13 pole-mounted MV/LV substations. About 30 kiosk substations supply residential end-users with an average of about 90 domestic end-user per substation. The most part of the kiosk substations is installed in the town of Lampedusa where about the 85% of the total island's population lives. These data were used for better define the three levels of the control systems.

2.2. Level 1: smart building

Level 1 is related to the single domestic/residential or commercial/industrial building and is characterized by the presence of:

- a Building Management System (BMS), that is the Local Controller that communicates with the other levels;
- one or more smart meters installed within the main switchboards;
- sensors, controlled outlets, dimmers, controlled switches;
- a Building Area Network (BAN).

Level 1 may also include other Local Controller (LC) as Energy Management Systems (EMSs) included in small generating units (Photovoltaic or Wind systems prevalently) or EES systems mounted in or out the buildings.

The major Building Automation systems currently available in the market are distinguished on the basis of their primary domain of functionality: BACnet, KNX, LonWorks, Modbus, etc [59]. The BAN can be both wired and wireless. Fig. 2 synthetizes the most recent technologies for both the types of solutions [43,44].

Wired BAN uses electrical wiring single, multiple twisted pair cables, coaxial cables or optical fiber for connecting the devices and sensors inside the building and sends the data outside the building thanks to an internet connection. Among the various powerline

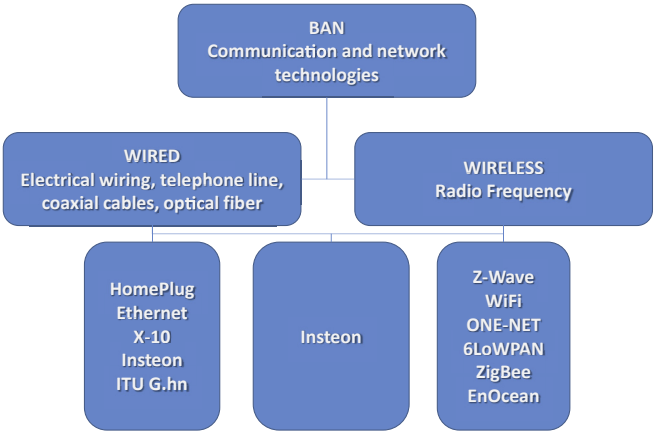

Fig. 2. BAN communications and network technologies [43,44].

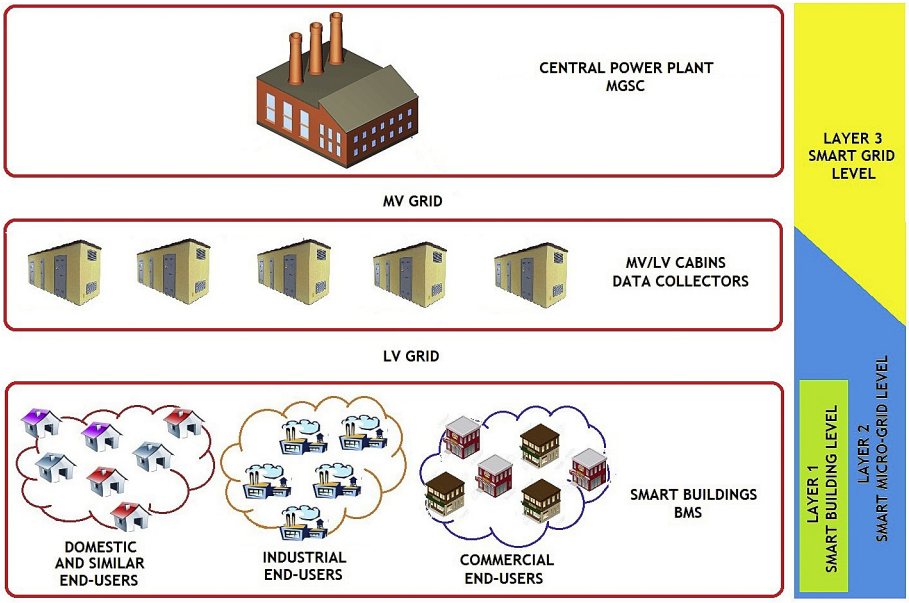

Fig. 1. Monitoring, control and communication system architecture for a small island.

communication (PLC) technologies, the most known are X-10, mainly used for lighting and security sensors, and HomePlug. HomePlug AV and AV2 technology is becoming more and more interesting thanks to the possibility of using house's powerline instead of Ethernet cables and, at the same time, to extend the coverage of a Wi-Fi network [60]. A step forward is done by the Insteon technology, allowing to connect simple and low cost devices using both the house's electrical wiring and Radio Frequency (RF), in a peer-to-peer exchange, without the need of a central controller [61].

In the case of Wireless BAN, the BMS can use the Wi-Fi LAN of the building itself or, a Z-Wave protocol, for communicating with the controlled devices. The Z-Wave protocol is an interoperable, wireless, RF-based communications technology designed specifically for control and monitoring applications and devices in residential and commercial buildings. Z-Wave operates usually at 900 MHz and its action range is about 30 m. The International Telecommunications Union (ITU) has included Z-Wave as an option in the international standard G.9959, devoted to provide guidelines for sub-1-GHz wireless devices [62]. Wireless systems have the potential of being the most used inside buildings. Indeed wireless needs a non-invasive installation process, which eliminates the need to run new cables for connecting the devices and sensors, providing, at the same time, the best performance in terms of self-consumption [63]. Usually the components can be installed in any wall switch box, and can be also easily removed and installed in a new location if the needs of control or monitoring change.

2.3. Level 2: smart micro-grid

Level 2 is related to the LV system between a MV/LV substation and all the supplied buildings.

A data concentrator (DC) is located in every substation and exchanges data and command signals with the BMS/EMS in Level 3 and with the MGSC in the central power plant. Pole-mounted substations are not appropriate for the installation of sensitive devices like the DC; therefore, it is preferable to install DCs only inside kiosk substations. For implementing DR actions and providing ancillary services to the power system, every smart building will send its flexible (FLEX) and not-flexible power profiles to the DC. The DC collects data coming from clusters of homogeneous users in order to create a database of aggregated loads (FLEX, NOFLEX and TOTAL). The substations and the buildings are included in a Neighborhood Area Network (NAN). The communication infrastructure of the NAN can be achieved by adopting several solutions [64]:

- PLC;
- Optical Fiber;
- Wi-Fi or WiMax systems;
- the 4G or the new 5G [65] mobile phone network.

In particular, both PLC and cellular network allows to use the existing networks in small islands, with a relevant reduction of the development and installation costs. PLC, seen from the point of view of the Utility, seems to be the most promising way for having the full control of the transmission medium for Smart Micro-Grid, without depending of a third party company [66]. Nevertheless, in small islands, electric lines and substations' switchboards are usually very old and in poor conditions, and this could increase the noise interference phenomena that can affect PLC technology. Therefore, in some cases, the use of the mobile phone network, generally younger than the electrical one, can be a valid alternative to PLC in small islands, especially in presence of 4G or 5G technology, assuring high performance and data transmission rate. Table 1 reports a summary of the frequency band and limitation of each of the above-listed technologies.

2.4. Level 3: smart grid

Level 3 is related to the MV system between the central power plant and the MV/LV substations. The connection between each substation's DC and the MGSC can be done using optical fiber cables laid in the same ducts used for the passage of MV cable lines. The MGSC receives from the DCs information related to aggregated loads and it has to elaborate a small amount of data. For example, in the case of Lampedusa, where there are almost 4000 end-users and 39 kiosk substations, each substation's DC has to collect the data coming from more or less 100 BMSs and the MGSC has to elaborate the data coming from almost 40 DCs.

3. Feasibility study for the automation and integration of two typical buildings in a smart grid

3.1. The smart house

According to the last statistics [67,68], more than the 80% of the total 2850 houses in Lampedusa are 1–2 floors stone-built buildings hosting only one apartment per floor with an average of four rooms per apartment. The average apartment size is about 110 m^2 and the most widespread energy performance class according to the EPBD is G (typical situation in small island located in the south of Italy). The 71% of the families are composed by 1 up to 3 members and the working-force population (age 20–60) is about the 60% of the total.

Therefore, the feasibility study presented in this section considers a real existing apartment for a typical 3-members family in Lampedusa, with four rooms, as represented in Fig. 3. Table 2 reports the main characteristics of this house.

A data survey done by the DEIM in 2016 shows that domestic end-users in Lampedusa share many common features. Electric Storage Water Heaters (ESWHs) fulfil the domestic hot water needs, sometimes integrated by thermal solar collectors. Air-conditioning systems are used for summer cooling and winter heating. No RES-based electrical generators or electric energy storage systems are present, even if the most suitable RES-based technology to be exploited in the island is photovoltaic, as shown in Ref. [25]. The yearly average electricity consumption of a typical apartment like that in Fig. 3 is 4500 kWh, that is about the 150% of the yearly energy consumption of the average Italian family with two-three persons [69].

The transformation of the apartment into a smart house requires the installations of sensors, components and devices able to:

- receive and send information and command signals;
- control specific electric loads.

In order to define properly the devices to be installed and the DR logics, the daily electricity consumption of the whole apartment and of its ESWH have been monitored for about one year. In particular, the choice of measuring ESWH's electricity consumptions has been driven by a specific query of the same island's inhabitants, that identify the cause of their high energy consumptions with the use of ESWHs. An interesting results of the measurement campaign is that the average evening demand peak of the house occurs at the same time of the average evening demand peak of the ESWH. Interesting reductions of the evening peak could therefore be obtained by load shifting techniques applied to the ESWH and the other energy intensive loads (dishwasher, heat pumps and washing machine).

Table 1
Frequency bands, limitations and advantages of various communication technologies.

Technology	Frequency Band [GHz]	Limitations	Advantages
5G	27, 37, 39	High frequency band fees, still not present in small islands	Very high speed, very high performance
4G	0.8–2.6	High frequency band fees, not present in some small islands	High speed, high performance
PLC	0.001–0.03	Noise sensitivity	Low costs, no need of a third party company
WiMax	2.5, 3.5, 5.8	Not widespread, weather conditions can interrupt the signal, Very power intensive technology	Need of a few number of stations

Fig. 3. Plan of the house.

- reduce the energy consumption of the apartment;
- influence the daily load profile of the apartment according to command signals coming from the DC in the secondary substation, by controlling some flexible (FLEX) loads.

In all the proposed scenarios, the BAC systems operate on the lighting system and on the following flexible loads:

- the heat pump;
- the ESWH;
- the dishwasher;
- the washing machine.

In all the proposed scenarios, the lighting system is controlled by external light and motion detectors, but it is not controllable by the DSO for implementing DR programs. The control of the FLEX loads by the DC, makes the apartment participating to DR programs, contributing in this way to improve the energy efficiency of the island's power system and obtaining, in return to this contribution, an economic benefit thanks to specific agreements with the DSO.

3.1.1. Scenario D.1

The first scenario covers the installation of a BAC system including:

- a control panel with touch screen (BMS or local control unit);

Table 2
Data of the house.

Technological plants	
Service	System
Sanitary Hot Water production	80 L Electric Storage Water Heater – 1.2 kW
Heating/Cooling	Heat Pump - 2.6 kW
Automation	Not present
BAN	WiFi
Appliances and Loads	
Devices	Power [kW]
n.1 Fridge/freezer	0.3
n.1 TV	0.25
n.1 Washing machine	2.5
n.1 Dishwasher	2.2
n.1 Electric oven	2.2
n.1 Microwave oven	0.8
n.1 Fan	0.2
n.1 Electric iron	2.2
n.2 Water system electric pump	0.37
Kitchen lighting system: 4 lamps	0.60
Living room lighting system: 4 lamps	0.60
Bathroom lighting system: 2 lamp	0.36
Bedroom lighting system: 3 lamps	0.47

Starting from this scenario (Scenario D.0: existing not automated house), three possible scenarios are imagined where the proposed BAC systems allow to:

- two actuators for controlling the FLEX loads and the lighting system in the four rooms;
- a webserver for exchanging data with the DC;

- two smart meters for measuring the consumption of the apartment and of the FLEX loads;
- two power supply devices;
- four light and motion detectors (one for each room).

Fig. 4 shows the layout of the proposed system. All the components are inside a wall-mounted electric panel (automation panel) and supplied by the main switchboard of the apartment. In Table 3 all the components to be installed in order to realize scenario D.1 and the related purchase and installation costs are detailed.

The total cost of this solution is about 4340 € and includes the realization of three new electric circuits for the connection of the main switchboard to the automation board:

- the first circuit provides the supply to the devices of the BAC system installed into the automation board;
- the other two circuits supply the lighting system, the air-conditioner, the FLEX loads and what has to be modified in order to include the relay operated activators of the BAC system.

Moreover, starting from the output terminal strips of the actuators, eight new branch lines reach the closer connection boxes where the connection to the existing lines (supplying the controlled lamps and loads) can be accomplished. Finally, the cost includes also the realization of the communication bus for the connection of all the light and motion detectors to the local control unit in order to send to the lighting activator the commands for switching on/off the lamps depending on the outdoor light intensity and on the presence of persons within the rooms.

Scenario D.1 has the advantage of minimizing the length of the communication BUS cables because most of the devices are within the automation board. On the other side, making new branch lines from the automation board to the controlled loads is a very invasive operation that elevates the total cost of this Scenario actions.

3.1.2. Scenario D.2

The second scenario is very similar to the first one, but the local control unit is not included in the BAC system. For configuring such a system, the end-user can access to a webpage using his own laptop, tablet or mobile phone. Scenario D.2 allows to obtain significant economic savings in realizing the BAC system, considering that the local control unit account for 33% of the total cost of the BAC system in Scenario D.1. Moreover, Scenario D.2 represents the configuration the market looks at, being more inclined towards the promotion of the usage of the smart devices already possessed by the end-user than towards the installation of new expensive devices.

The total cost of this solution, represented in Fig. 4, is about 2910 €.

3.1.3. Scenario D.3

In the third scenario, eight contactors are used instead of the two relay operated activators. Differently from the activators, the contactors are installed inside the existing junction boxes in various points of the house in the positions that minimize the carrying out of building works and the modifications to the existing electric lines.

Scenario D.3 needs the installation of only one power supply because the communication BUS no longer requires its dedicated power supply unit given that the control signals to the contactors are sent using a particular switch for electric boards and a router.

Fig. 5 shows the system layout. In Table 4, all the components to be installed in order to realize scenario D.1 and the related purchase and installation costs are detailed.

The total cost of this solution, represented in Fig. 5, is about 3940 €.

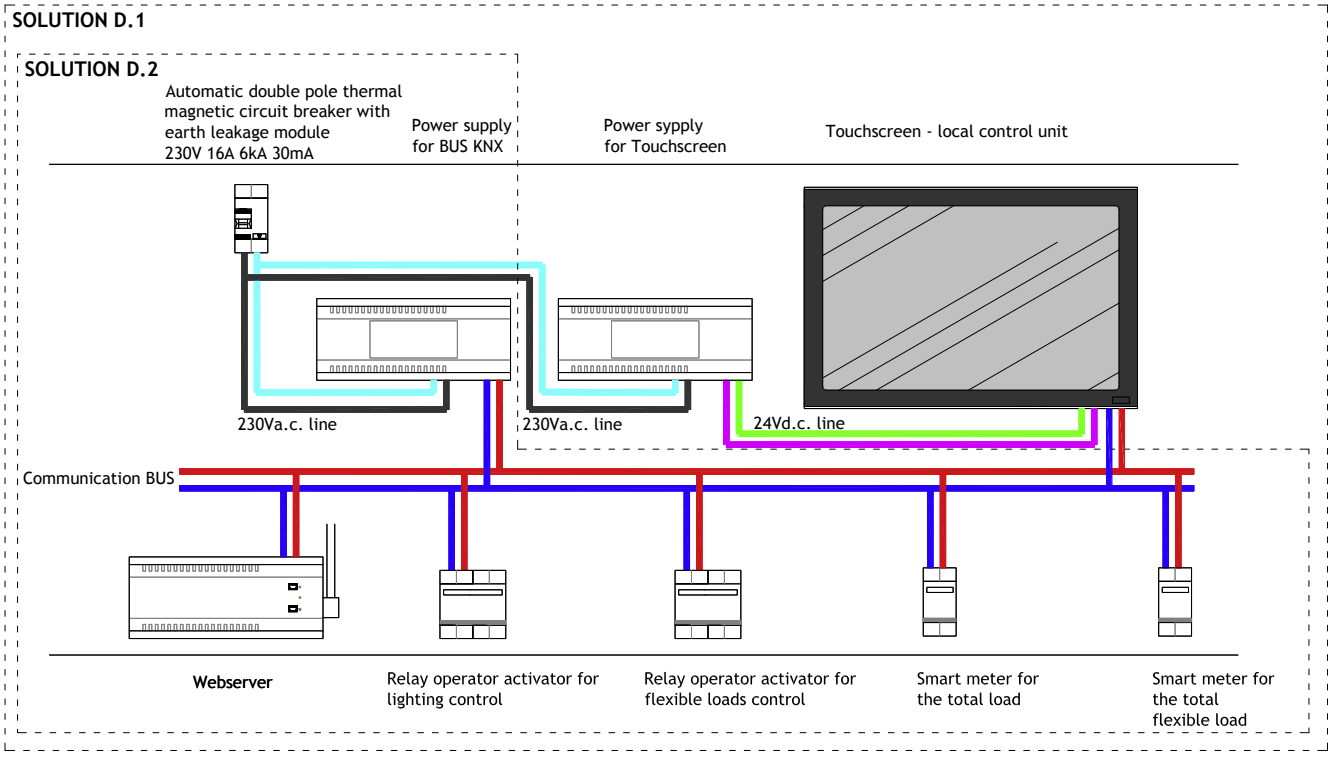

Fig. 4. Scenarios D.1 and D.2: BAC system's layout.

Table 3
Scenario D.1: Purchase and installation costs of the BAC system's components.

Component	Unit price [€]	Quantity	Total price [€]
Power supply	114.45	2	228.90
Digital Smart Meter for single-phase systems	215.95	2	431.90
Webserver	966.00	1	966.00
Local Central Unit/Touch screen	1314.95	1	1314.95
4 Output Relay Operator Activator	265.65	2	531.30
Motion and light sensor	137.90	4	551.60
24 modules resin wall-mounted box for automation board with circuit breakers	163.80	1	163.80
New lines and related works	145.60	1	145.60
TOTAL			4334.05

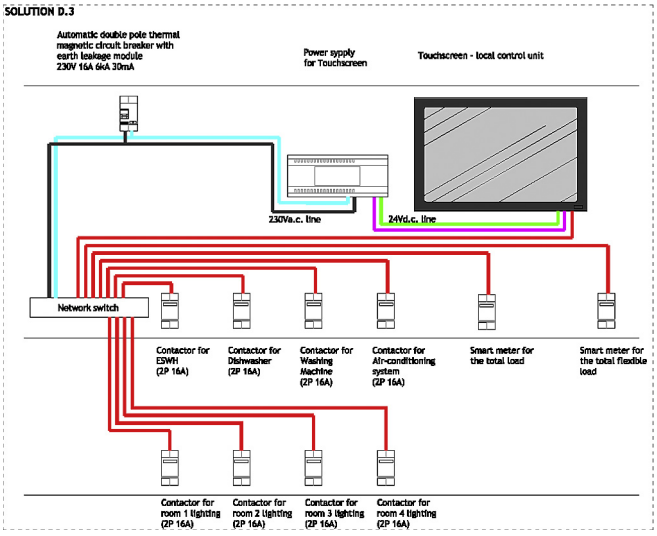

Fig. 5. Scenarios D.3: BAC system's layout.

found, while daily consumption is correlated to the tourist presence in the island. Indeed, the maximum two-monthly consumption occurs in the period July–August, corresponding to the maximum two-monthly value for tourist influx.

The case study considers a hotel located in the Lampedusa city center with 20 rooms and accommodation for 44 guests on two floors. The hotel has a centralized heat pump providing heat and/or air-conditioning and sanitary hot water and is devoid of any BAC or TBM system. The plans of the two floors are reported in Fig. 6. The automation of a hotel for achieving an improvement of the energy performance and for the participation to DR programs is a more complex task with respect to the case of the house.

The major criticism is that the hotel guests request a comfort level adequate to the room price and the hotel star rating. This implies that the load profile flexibility that the hotel can offer to the grid must be limited so as to not create discomfort to the guests.

The DC will send control signals to the hotel BMS only for obtaining ancillary services during emergency operation or for slightly varying the hotel electric profile in specific period of the day. On the other side, the hotel's BAC and TBM system can efficaciously minimize the energy squandering due to an often not

Table 4
Scenario D.3: Purchase and installation costs of the BAC system's components.

Component	Unit price [€]	Quantity	Total price [€]
Power supply	114.45	1	114.45
Digital Smart Meter for single-phase systems	215.95	2	431.90
Smartlink Ethernet	245.00	1	245.00
Local Central Unit/Touch screen	1314.95	1	1314.95
2 poles 25 A contactor	122.50	8	980.00
Motion and light sensor	137.90	4	551.60
24 modules resin wall-mounted box for automation board with circuit breakers	163.80	1	163.80
New lines and related works	131.60	1	131.60
TOTAL			3933.30

3.2. The smart hotel

A survey done by the DEIM in 2016 allowed to collect the basic information for the feasibility study. All the hotels in Lampedusa have been recently refurbished and show similar envelope features: double-glass windows with aluminum (thermal break) or timber frame, reinforced concrete structures with no insulated walls and insulated roofs. The most of the hotels are equipped with a centralized thermal plant for winter heating and domestic hot water production and single-split systems for cooling installed in the rooms. Currently, no RES-based electricity generators are present but about 65% of the hotels owns a thermal solar plant. All the hotels share almost common appliances equipment, and no BAC systems are present.

From the analysis of the energy bills provided by SE.LI.S, an yearly electricity consumption of about 2500 kWh/bed has been

wise behaviour of those guests who have the inclination to not switch off the light leaving the room, use the air-conditioner keeping the windows wide open, reduce/increase the room temperature below/above the set-point value corresponding to the maximum comfort for people and to the maximum efficiency for the building-plant system.

Technical literature reports that the application of BAC and TBM systems to the hotel sector has the potentiality of reduce the energy consumption for lighting, heating/cooling and ventilation for about 5 %–20% depending on the hotel star rating, the performance class of the building and the number of guests per year [70–73]. Taking into account the above-reported considerations, the present case study contemplates two different scenarios.

3.2.1. Scenario H.1

In the first scenario, the TBM system includes a central unit (the

Fig. 6. Plans of the hotel.

BMS of the hotel) hosting a management software and 20 local Room Control Units (RCUs), connected to the BMS by the structured cabling of the hotel itself and using the TCP-IP transmission protocol. The control system design starts from the peculiarities of the chosen hotel and takes into account the following tasks in order to:

- assure ad adequate comfort level to the hotel's guests;
- implement predictive maintenance programs for minimizing the exercise costs;
- minimize the inconveniences due to faults at critical components like the centralized heat pump or the electric pump of the water system;
- measure the electric consumption of the whole hotel, of each room and of the technological plants;
- improve the energy efficiency of the building-plant system.

The block diagram depicted in Fig. 7 shows the connection between a RCU and the local devices and components. The RCU chosen is able to:

- switch off the lighting system (except a courtesy lamp close to the entrance door), if nobody is inside the room;
- detach all the electric outlets (except a courtesy electric outlet for recharging portable devices like laptop or mobile phone and the electric outlet supplying the fridge), if nobody is inside the room;
- open the entrance door by sending a command to the electric-strike lock when the guest's key-card is introduced in the key-card reader;
- send an alarm signal to the personnel at the reception in case of emergency into the room;
- detach the air-conditioner when the entrance room or the windows are wide open;
- inhibit the regulation of the room's temperature outside an established range around the optimal summer or winter design temperature (normally ± 1.5 °C are allowed around the set-point temperature);
- monitor the electric consumption of the loads and the daily load profile of the room.

In order to achieve all the above-listed functions, the original rooms electrical installations have to be modified as depicted in Fig. 8. The local electric board has to be upgraded so as to:

- create a new circuit devoted to supply the RCU;
- create a new circuit for supplying the courtesy lamp, the air-conditioner and the two privileged electric outlets;
- avoid the possibility of supplying the other electric loads after all the guests have left the room.

The total cost calculated for implementing the Scenario H.1 is about 39200 €, including also the cost for programming the BMS, the cost for installing two new 12-outlet network switches for connecting the RCUs to the existing computer network of the hotel and the cost for the expansion of the horizontal cabling (20 new copper UTP cables and RJ45 outlets for connecting the new switches to the RCUs and related PVC trunking system in the corridor). Table 5 reports the costs of the single components.

3.2.2. Scenario H.2

In this scenario, the hotel is devoid of the necessary devices for

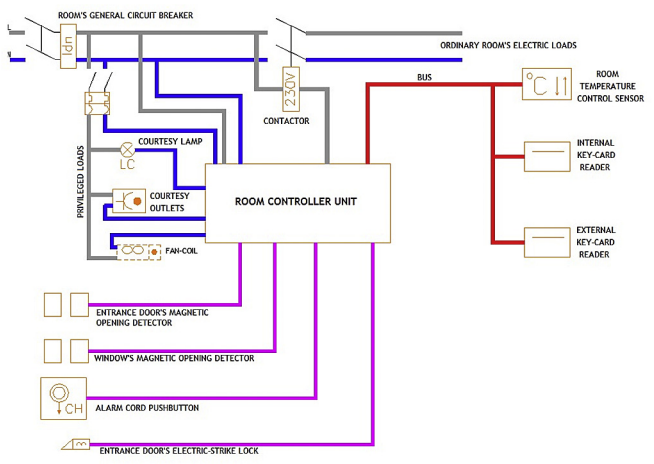

Fig. 7. Connections between a RCU and the local devices and components.

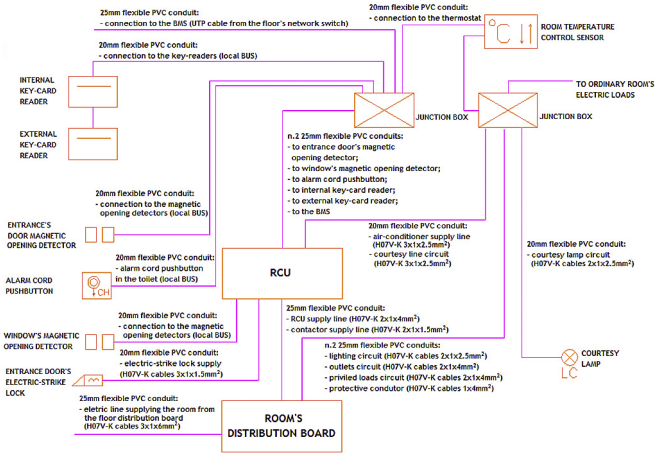

Fig. 8. Junction boxes and conduits for connecting the automation devices to the electrical installation.

Table 5
Scenario H.1: Purchase and installation costs of the BAC system's components.

Component	Unit price [€]	Quantity	Total price [€]
BMS within a 19″ rack, including power supply and management software	6352.50	1	6352.50
RCU	424.55	20	8491.00
Internal key-card reader	150.50	20	301.00
External key-card reader	146.30	20	2926.00
Magnetic opening detector	110.60	40	4424.00
Distribution board	354.20	20	7084.00
12 modules resin wall-mounted box for automation board	34.30	20	686.00
New lines and related works inside 20 rooms	3278.10	1	3278.10
12-outlet network switch including connection	490.00	2	980.00
PVC trunking in the hotel corridor for UTP cables enclosure	700.00	1	700.00
UTP cable from the floor's network switch to the RCU − RJ45 outlet included	63.00	20	1260.00
TOTAL			39191.60

communicating with the DC. There is not a BMS and all the RCUs are stand-alone devices not connected among themselves and to any central controller. The RCUs are able to implement the same functions defined for the first scenario but the total cost is strongly reduced to 28360 € (about 27% less the cost of solution H.1) even thanks to the minor cost of the stand-alone RCUs with respect to those built for being integrated in a computer network.

The very significant limit of this solution is the impossibility of making the hotel part of the smart grid, participating to DR programs. Nevertheless, it will contribute to the overall improvement of the island's power system performance by reducing its own electrical consumption thanks to the actions of the RCUs. Table 6 reports the costs of the single components for the Scenario H.2.

3.3. Summary of the results and discussion

Different solutions have been proposed for the automation, control and monitoring of two typical buildings of a small island, different for the control actions that each can allow to be implemented and for the total costs. It is noteworthy that the ratio between the BMS cost and the number of persons hosted by the building is higher for the house that for the hotel.

Tables 7 and 8 report a synthesis of the comparison of the proposed scenarios for the house and for the hotel, respectively. VAT must be charged to all the costs reported in Tables 7 and 8.

Among the solutions listed in Tables 8 and 9, D.3 and H.1 are chosen. D.3 is indeed the solution that represents the best compromise between reduction of the installation costs and ease of use, being less expensive with respect to D.1 and including the local touchscreen. H.2 has been excluded because, besides less expensive than H.1, does not allow the participation of the hotel to DR programs. Anyway, it is still a valid solution to be suggested to hotel owners that needs to reduce the energy costs of their hotels remaining out from the smart grid. In particular, solution H.2, in the most realistic scenario considering the communication system involving only users located in the urban center of the island, could be applied in hotels located in the north of the island, far from the urban center and from the MGSC.

The proposed technological solutions can be easily integrated in the control and communication system represented in Fig. 1 but are not suitable to be adopted in smart grids with distributed management algorithms.

3.4. Demand response control logic

Considering the control architecture and the technological solutions depicted in the previous sections, it is possible do draw the main step of a suitable algorithm to be implemented in the MGSC in order to achieve an overall efficiency improvement of the generation and distribution system of the island, so as to promote decarbonization.

Firstly, an optimization time interval and a reasonable short operation time step must be established. Considering the natural periodicity of the load profiles, the optimization time interval is set equal to 24 h, while the elaboration time step is assumed equal to 15 min, being the same time interval used by the energy meters for registering the energy consumption of the end-users. If necessary, the operation time step could be reduced to 10 min, according to other experiences of smart grids in the state of the art [74].

For every day, the MGSC taking into account the flexibility offered by the end-users, solve an optimization problem aiming at:

- minimizing the daily energy losses in distribution lines and transformers;
- maximizing the overall generation efficiency of the island;
- minimizing the discomfort for the end-users, due to the exploitation of their flexibility.

The mathematical formulation of the multi-objective optimization problem is not in the aims of this paper and will be presented in a future work. Nonetheless, it is worth to highlight that the second objective depends on the efficiency curves (as function of the generated active power) of the thermal and RES-based generators of the island, while the third objective can be

Table 6
Scenario H.2: Purchase and installation costs of the BAC system's components.

Component	Unit price [€]	Quantity	Total price [€]
Stand-alone RCU	347.20	20	6944.00
Internal key-card reader	150.50	20	3010.00
External key-card reader	146.30	20	2926.00
Magnetic opening detector	110.60	40	4424.00
Distribution board	354.20	20	7084.00
12 modules resin wall-mounted box for automation board	34.30	20	686.00
New lines and related works inside 20 rooms	3278.10	1	3278.10
TOTAL			28352.10

Table 7
Comparison of the scenarios D.1, D.2 and D.3.

Scenario	Cost [€]	Assets	Weak spots
D.1	4340	• Most complete solution • Control from the DSO • Participation to DR programs • A touch screen for a most comfortable local control to the end-user	• High cost • If the only actuator of the system fails, no load control can be achieved • Need of realizing new power lines from the automation board to the controlled loads
D.2	2910	• Most economical solution	• If the only actuator of the system fails, no load control can be achieved • Need of realizing new power lines from the automation board to the controlled loads • No touch screen present. Need of a smartphone or a PC for setting and using the system and for monitoring the loads.
D.3	3940	• Intermediate scenario for cost • Same monitoring and control functions of the first scenario • If suitably installed, contactors avoid the realization of new branch lines	• The communication BUS must be installed also outside the automation board

Table 8
Comparison of the scenarios H.1 and H.2.

Scenario	Cost [€]	Assets	Weak spots
H.1	39200	• Most complete solution • Control from the DSO • Participation to DR programs • The hotel manager can monitor and control the whole building using a management software • A predictive maintenance can be implemented thanks to the monitoring • BAC efficiency class A can be achieved	• High cost • Modifications to the existing computer network of the hotel are requested • Carrying out of expensive building works
H.2	28360	• Most economical solution • No modifications to the existing computer network of the hotel are requested	• The hotel can't take part to DR programs including • The hotel can't of take advantages from the load aggregation • The hotel manager can't monitor and control the energy consumptions and the usage of the hotel • The automation does not support predictive maintenance • BAC efficiency class A can't be achieved

Table 9
System's data.

LV cable	
Type	FG7OR
Conductor cross-section	50 mm^2
Series distributed resistance	0.389 Ω/km
Series distributed reactance	0.0779 Ω/km
Total length of each LV line	120 m
MV/LV Transformer	
Rated power	400 kV AA
Primary rated voltage	10 kV
Secondary rated voltage	0.4 kV
Short-circuit voltage	6%
Rated short-circuit power losses	4600 W
Rated open-circuit power losses	610 W

expressed in various way:

- total number of end-users whose daily load profile is modified following a command from the DSO;
- average or maximum time delay experienced by the end-users in the use of their shiftable loads (washing machine, dish-washer, etc.);
- energy shifted from a time interval to another divided the total energy consumed in one day;
- a combination of the above indicators;
- other indicators.

The solution of the optimization problem is an optimal daily load profile (and the corresponding optimal generation profile) that can be achieved by varying the quota of the total FLEX load at each operation time step.

In Fig. 9 the exchange of data between MGSC, generators (G), DC and BMS is represented.

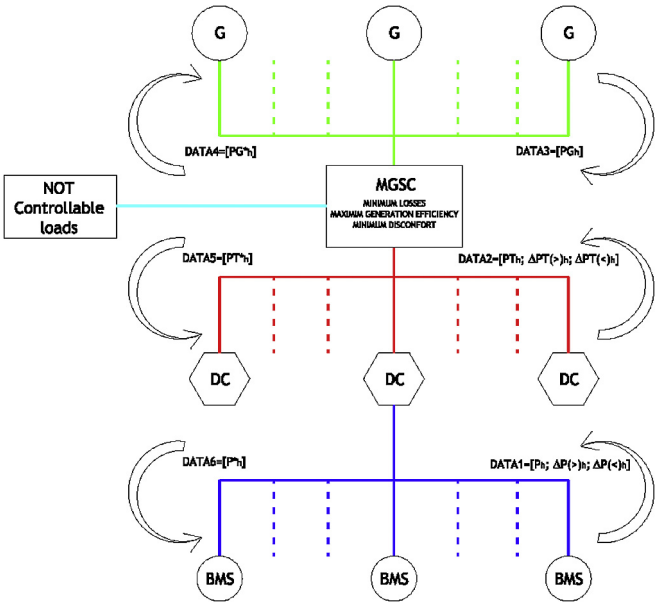

Fig. 9. Information flows in the automated system.

A suitable algorithm for managing such a system can be summarized in the following step.

STEP 1: Every day, the MGSC solves the multi-objective optimization problem starting from the foreseen total load profile and daily FLEX load profile of the island for the next 24 h. This operation can be done at any time but it is suggested to perform between 3:00 and 4:00 in the morning when energy demand is usually flat and the prediction error is the smallest.
STEP 2: The MGSC sends to each dispatchable generator its optimal generation profile for the day, obtained solving the optimization problem taking into account the efficiency curves and technical constraints of the generators. Stops for maintenance and redundancy of some key generators are taken into account, according to the security procedure of the utility.
STEP 3: The MGSC sends to each DC the optimal load profile of the substation desired for the day.
STEP 4: Each DC elaborates the data received by the MGSC and sends to every (or some) of the BMS of the supplied facilities a command for modifying their load profiles.

Nevertheless, being in general the actual operative conditions quite different from the foreseen ones, an on-line correction is needed every 15 min. Therefore, the algorithm needs further steps for updating the solution of the multi-objective optimization problem.

STEP 5: Every 15 min each BMS sends to the DC an information pack (DATA1 in Fig. 9) containing the value of the average power P_h taken from the grid in the hth time interval and the allowed positive/negative variations of the above value ($\Delta P_h(>)$ and $\Delta P_h(<)$) in the same time interval, achievable thanks to specific control actions on the local FLEX loads;
STEP 6: Every 15 min each DC, having collected all the DATA1 information packs from the BMSs, sends to the MGSC an information pack (DATA2 in Fig. 9) containing the value of the average power PT_h flowing through the substation's transformer in the hth time interval and the allowed positive/negative variations of the above value ($\Delta PT_h(>)$ and $\Delta PT_h(<)$) in the same time interval, achievable thanks to specific control actions on the FLEX loads of the supplied facilities;
STEP 7: Every 15 min the MGSC repeats the resolution of the optimization problem using the real data received from the DC and from the generators (DATA3) and sends to each generator a command for modifying its working point (DATA4) and to each DC the desired value of power requested in that time interval (DATA5).
STEP 8: Every 15 min, each DC elaborates the data received by the MGSC and sends to every or some of the BMS of the supplied facilities a command for modifying their electricity consumptions (DATA6).
STEP 9: Every BMS modifies its electricity consumption according to the command signal from the DC.
STEP 10: The procedure is re-initialized from STEP 5 every 15 min and from STEP 1 at 0:00 of the following day.

4. Impact of automation on the electricity consumption of the island

In the present section the positive impact of automation in terms of reduction of the overall electricity consumption of the island is demonstrated. In particular, two cases are examined:

- CASE 1: the BAC system of each house is set for minimizing the daily energy consumption of the end-user, reducing the energy waste;
- CASE 2: the LCU of each house receives a command signal from the DC that impose to maintain the power peak below 2 kW.

In the first case each LCU acts as an independent control system that does not communicate with the DC of the substation supplying the house and is devoted to assure to the end-user the maximum energy saving. In the second case, the end-users are involved in a DR mechanism whose first aim is to provide a benefit for the grid.

4.1. System's data

The example considers the system represented in Fig. 10, comprising one 400 kVA oil-insulated MV/LV distribution transformer supplying five identical LV cable lines and 100 houses (contracted power in the range 3–10 kW). More in detail, each line supplies 20 houses (10 couples of houses indicated with H1, H2, etc.). The characteristics of cables and transformer are listed in Table 9. The houses are supposed identical and equipped with the appliances and devices reported in the previous Table 2. For presenting more clearly the results of the analysis, the presence of other loads different from the residential ones (street lighting, commercial building, etc.) is not considered, being these loads not controlled by the control system.

For simulating the effects of automation on the daily load profile of a generic house, the simulation tool described in Ref. [75] is applied. The software, developed by the University of Palermo and validated on three real pilot installations, is able to evaluate the daily load profile of a typical Italian house starting from the usage probability and the working cycle of each appliance, also in presence of various load control logics and local electricity generation. The appliances' usage probability vary with latitude (daylight, external temperature, number of sunny and rainy days, etc. affects the use of various loads) and with the socio-economic context. Being still in course a research for assessing the usage probability of the most common appliances installed at residential facilities in the island of Lampedusa, the software runs elaborating typical data for

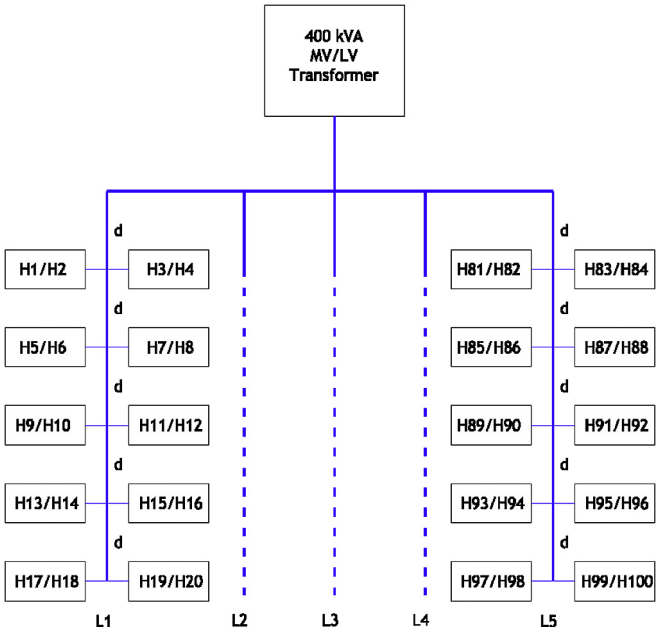

Fig. 10. Simplified scheme of the LV grid supplied by a distribution transformer.

a generic South-Italy cities on the mainland. The load profiles are generated with a time step of 15 min, sufficiently accurate for simulating the behavior of a domestic end-user. Even though the software allows to differentiate the load profiles of typical summer/winter/intermediate seasons and weekdays/holidays, given the aim of the present analysis, only an average daily load profile is considered for each examined case. Similarly, a constant power factor equal to 0.9 is imposed for all the supplied electric loads.

The effects of the BAC system on the electricity consumption in the island are evaluated by calculating the power peak and the energy losses in cables and transformer.

With reference to Fig. 10, yearly energy losses ΔE_{LV} in the LV network are evaluated by the following equation:

$$\Delta E_{LV} = 365 \cdot \sum_{L=1}^{5} \sum_{B=1}^{5} \sum_{dT=1}^{96} \frac{R}{U_r^2} \cdot \left(\frac{P_{L,B,dT}}{0.9} \right)^2 \cdot 0.25 \quad (1)$$

where:

- L, varying from 1 to 5 designate the LV line supplied by the MV/LV transformer;
- B, varying from 1 to 5 designate the branch of a given LV line;
- R is the series resistance of the given branch (in the proposed systems all the lines are identical, therefore R is a constant in the equation);
- U_r is the rated voltage of the LV network;
- dT, varying from 1 to 96, indicates one of the 96 15-min time interval that makes one day;
- $P_{B,L,dT}$ is the active power flowing during the dT-th time interval in the B-th branch of the L-th LV line of the system;
- 0.25 is the duration of a 15-min time interval expressed in hour.

Similarly, the yearly energy losses ΔE_{TR} in the transformer are evaluated by the following equation:

$$\Delta E_{TR} = 365 \cdot \sum_{dT=1}^{96} P_{SC,r} \cdot \left(\frac{P_{LV,dT}}{0.9 \cdot S_r} \right)^2 \cdot 0.25 \quad (2)$$

where:

- $P_{SC,r}$ indicates the rated short-circuit losses of the transformer;
- $P_{LV,dT}$ is the total active power demand of the LV network in the dT-th time interval;
- S_r is the rated power of the transformer.

4.2. Results of the simulations

Figs. 11–13 show the load profiles of 20 of the 100 considered houses:

- without automation;
- in presence of a BAC system set for minimizing the daily energy consumption of each house (CASE 1):
- in presence of a command from the DC imposing to maintain the power peak below 2 kW (CASE 2).

It is worth to notice that in CASE 2 (Fig. 13), power peaks are significantly reduced with respect to the other cases but in some cases can exceed the imposed limit of 2 kW. This is due, on one side, to the presence of power intensive devices such as washing machines, dishwashers and so on, needing in some periods of their working cycles more than 2 kW and, on the other side, to the algorithm implemented in the simulation tool that simulates also the probability that the end-user can force the activation of a given load, even if the DSO sends a switch off command to the LCU. This function has been implemented in order to obtain more realistic load profiles.

In CASE 1, the daily energy consumption of the house is reduced of 1.07 kWh, while in CASE 2 a reduction of 0.42 kWh is achieved. The difference between the two values is due to the different purpose of each implemented algorithm. In CASE 1, the control algorithm is devoted to the minimization of the waste of electricity at the end-user facility, while in CASE 2 the control algorithm tends to reduce the energy peak of the aggregated load to the advantage of the utility.

Table 10 shows a comparison of the power peaks and of the energy losses in transformer and cables for the three examined cases.

Simulations show that in CASE 1, energy losses in the system in Fig. 10 are reduced of 771 kWh/year (−3.8%) with respect to the case without automation. Considering the 30 kiosk substations of the island of Lampedusa and assuming the same characteristics for each of the LV networks supplied by a substation, the reduction of the overall energy losses in all the transformers and LV cables of the island is about 23 MWh/year in CASE 1. To this saving, the overall reduction of the electricity consumption of the 2850 houses of the island must be added, obtaining an overall electricity saving of 1136 MWh/year, equal to 3% of the total yearly electricity consumption of the island (about 37000 MWh/year in 2015).

Analogously, in CASE 2 energy losses in the system in Fig. 10 are reduced of 2649 kWh/year (12%) with respect to the case without automation, and the overall reduction of the energy losses in all the substations is 79.5 MWh/year. Adding to this value the overall reduction of the electricity consumption of the 2850 houses of the island, an yearly electricity saving of about 517 MWh/year, equal to 1.4% of the total yearly electricity consumption of the island, is obtained.

The power peak of the overall load supplied by each transformer in a substation decreases from 255 kW to 234 kW (−8%) in CASE 1 and to 200 kW (−22%) in CASE 2. Fig. 14 reports the aggregated load profile of the 100 houses in the two cases compared with the aggregated load profile of the same end-users in absence of automation. In the figure the modifications produced by the load control algorithm can be easily noticed.

Considering the aggregation of 2850 domestic end-users, in CASE 2, the overall power peak of the island can be reduced of about 530 kW, that is the 6.4% of the summer power peak (8.25 MW in 2015) and the 10.6% of the winter power peak of the island (4.97 MW in 2015). These results contain a certain degree of approximation and will be improved in a future work, considering a more accurate usage probability of domestic appliances and different daily load profiles for each season of the year, and evaluating the energy losses reduction in the MV grid of the island. Nevertheless, the numbers clearly show the potentiality of automation.

4.3. Economic feasibility

To evaluate the economic feasibility of the installation of the designed control and communication system is a quite complicate task and involves issues and themes still debated as the valorization of comfort and of ancillary service provisions. First of all, it is well known that residential automation is still quite expensive and if evaluated considering only energy savings in buildings, BAC systems are in the most of cases not cost-effective. Convenience of these system is currently highest for buildings with energy performance class F or G, therefore, if only based on energy savings considerations, BAC systems should not be installed in highest

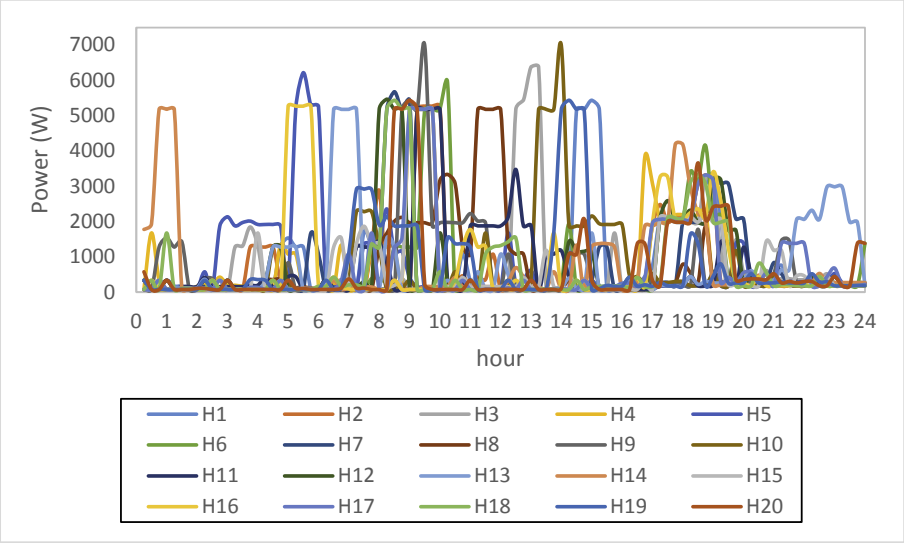

Fig. 11. Load profiles of houses H1-H20 (No automation).

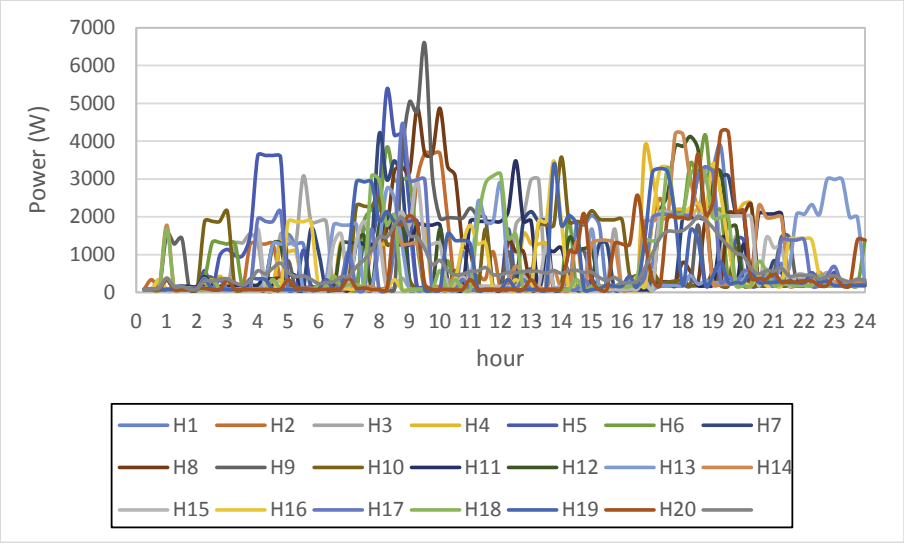

Fig. 12. Load profiles of houses H1-H20 (CASE 1).

performance class buildings. Obviously this is a paradoxical conclusion, given that practical experience demonstrates that BAC systems are prevalently installed in new and highly efficient buildings.

Indeed, two important factors can drive towards the installation of BAC systems independently from energy savings:

- the economic value of comfort;
- public incentives such as VAT reduction, White Certificates and tax deduction (all these mechanism are currently adopted or have been adopted in the last few years in Italy).

As an example, the first factor has been recently discussed in Ref. [76], where comfort co-benefits are estimated by employing the economic-based Contingent Valuation Method. The above-mentioned paper refers to thermal comfort but the method proposed by the authors can be applied to any other aspect of comfort (better indoor lighting, awareness of own consumptions and habits, safety provided by technical alarms, etc.). The increased comfort obtained with automation virtually remunerates the end-user, reducing, consequently, in this way the total purchase and installation cost of the BAC system.

With reference to the second factor, the diffusion of automation in the island community could be encouraged and economically justified by the existing Italian support policies together with the definition of low cost automation solutions, such as those proposed in this paper (D.1-D.3, H.1-H.2). In particular, VAT reduction (from 22% to 10%) and tax deduction (65% of the total cost in 10 years) for building automation are active mechanism in Italy since 2016. Lampedusa Municipality and SE.LI.S. could promote the diffusion of automation culture and the existence of these support policies in the island community.

From the utility's point of view, it is fundamental to consider the current Italian context. As said in the introduction of this paper, the most recent decrees and AEEGSI deliberations oblige small islands' electrical utilities to enhance the efficiency of their generation and

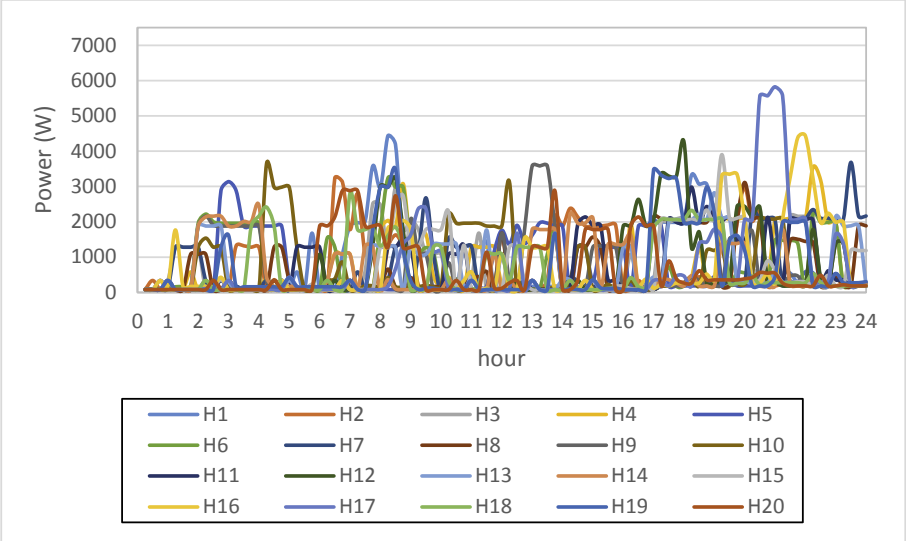

Fig. 13. Load profiles of houses H1-H20 (CASE 2).

Table 10
Comparison of power peak and energy losses with and without automation for a generic substation.

	Power peak at transformer [kVA]	Transformer's energy losses [kWh/year]	LV system's energy losses [kWh/year]	Total energy losses [kWh/year]
Without automation	255	18250	2177	20427
CASE 1	234	17520	1971	19491
CASE 2	200	15700	1683	17383

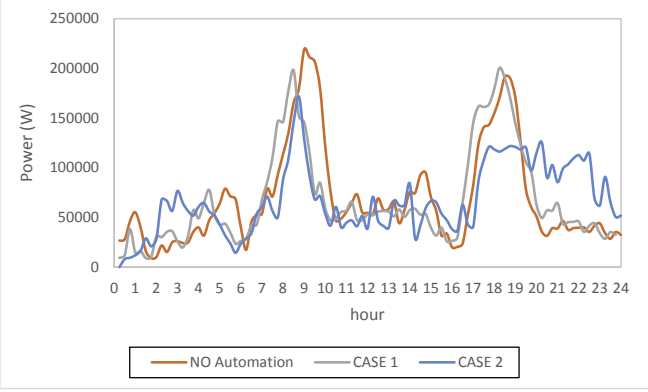

Fig. 14. Aggregated load profile of 100 houses in the three examined situations.

distribution plants by new investments in RESs and automation [12], [77–80]. The proposed architecture of the control and communication system, is able to assure a reduction of the waste of electricity in the island, according to the above national mandatory dispositions and, at the same time, to provide additional services to the utility. Indeed, implementing suitable algorithms, the control and communication system is able to:

- enhance the security of the system during a sudden lack of one of the diesel generator of the island's power plant, by load shifting actions;
- collect data on the user's behavior in order to define customized control logics for specific groups of aggregated end-users;
- promote the diffusion and the participation to DR mechanisms of RES-based generators;
- monitor voltages and currents in grid's nodes and branches reducing the possibilities of faults;
- allow distributed generator and battery storage systems to take part to voltage and frequency regulation, according to the mandatory technical Italian standards CEI 0–16 and CEI 0–21 [81,82];
- improve the voltage profile;
- avoid electricity thefts;
- solve network congestions and maximize the exploitation of RES-based generators.

The economic value of all the above-listed functions and the avoided costs due to their implementation largely justify the cost for the adoption of grid automation.

5. Conclusions and future works

The paper has presented a hierarchical architecture of a suitable control, monitoring and communication system for a little island and has proposed some suitable solutions for the automation of two actual buildings located in the Island of Lampedusa.

Looking at the feasibility study presented on the two case studies, some considerations can be made.

First, a smart micro-grid of a small island can be equated with a Smart City with regard to extension, position and numerousness of loads and generators.

Second, although the concept of ICT for Smart City is instantly associated with the one of economy, looking at the advantages for both the DSO and the end-user (due to the reduction of the electricity need thanks to DR policies ad BAC systems), ICT allows many other applications related to user security and comfort that, for the aim of the present work, the Authors did not consider.

Actually, the design of a Smart Island should cover many other

factors like:

- the energetic independency of the island;
- the development plan of the electric grid;
- the economic development of the area, promoting the rise of new services;
- faults detection, isolation, and recovery;
- grid and generators monitoring for predictive maintenance;
- the capacity of giving an adequate and fast reply to the perturbations in the grid;
- frequency and voltage regulation;
- the quality of the supply;
- the traffic management;
- the tourism development;
- the integration of Electric Vehicles in the grid and the optimization of their recharge;
- the accessibility of the services of the building and of the island by creating suitable human interfaces;
- the availability to the end-users of information related to the offered services.

In order to give effect to all the above-listed possibilities, many other components and devices have to be installed in the buildings in addition to those proposed in the present feasibility study, with a consequent outstanding increment of the total cost of the BAC systems.

Moreover, according to the most recent technical standards, the implementation of additional control actions to those that allow an economic saving for the end-user and the realization of DR programs, could imply a modification of the means of transmission proposed for the communication between the three tiers of the smart grid [55,56].

Finally, with regard to the economic investments for the existing grid upgrading, some solutions for creating a DC inside a secondary substations have been investigated. By examining the devices offered by the main brand in the ICT and automation field, an average cost equal to 8000 € for a DC has been estimated, including the costs for programming and set-up activities. The estimated cost can raise or decrease depending on the functions that the DC can implement.

Finally, for completing the control system ad adequate telecommunication infrastructure must be built. In an existing network, being fundamental to avoid or minimize the excavations for new cable communication lines in the city, the simplest and cheapest way for connecting the DC to the various BMSs is to use a radio wave connection that implies the installation of a base transceiver station at every secondary cabin and at every connected building.

Acknowledgments

The study presented is the result of a collaboration between ENEA (Italian National Agency for New Technologies, Energy and Sustainable Economic Development) and the DEIM (Department of Energy, Information Engineering and Mathematics) of the University of Palermo in the framework of the “Analisi delle tecnologie per la climatizzazione e sistemi ICT applicati agli utenti finali delle isole minori non connesse alla RTN al fine di efficientare il sistema elettrico isolano” (“Electric system efficiency in small islands not interconnected to the main power grid. Analysis of Renewable, Air-conditioning and ICT technologies for end-users”) Italian scientific research project.

References

[1] Nicolosi A, Sapone N, Cortese L, Marcianò C. Fisheries-related tourism in southern Tyrrhenian coastline. Procedia - Soc Behav Sci 2016;223:416–21.
[2] Niles K, Lloyd B. Energy for sustainable development, small island developing states (SIDS) & energy aid: impacts on the energy sector in the Caribbean and Pacific, vol. 17; 2013. p. 521–30.
[3] Gils HC, Simon S. Carbon neutral archipelago – 100% renewable energy supply for the Canary Islands. Appl Energy 2017;188:342–55.
[4] Scobie M. Fossil fuel reform in developing states: the case of Trinidad and Tobago, a petroleum producing small Island developing State. Energy Policy 2017;104:265–73.
[5] Weisser D. On the economics of electricity consumption in small island developing states: a role for renewable energy technologies? Energy Policy 2014;32:127–40.
[6] Keeley AR. Renewable Energy in Pacific Small Island Developing States: the role of international aid and the enabling environment from donor's perspectives. J Clean Prod 2017;147:29–36.
[7] Dornan M, Shah KU. Energy policy, aid, and the development of renewable energy resources in Small Island Developing States. Energy Policy 2016;98:759–67.
[8] Spiegel-Feld D, Rudyk B, Philippidis G. Allocating the economic benefits of renewable energy between stakeholders on Small Island Developing States (SIDS): arguments for a balanced approach. Energy Policy 2016;98:744–8.
[9] Italian Decree 24 June 2014, n. 91, “Disposizioni urgenti per il settore agricolo, la tutela ambientale e l'efficientamento energetico dell'edilizia scolastica e universitaria, il rilancio e lo sviluppo delle imprese, il contenimento dei costi gravanti sulle tariffe elettriche, nonché per la definizione immediata di adempimenti derivanti dalla normativa europea”.
[10] Italian Law 11 August 2014, n. 116, “Conversione in legge, con modificazioni, del decreto-legge 24 giugno 2014, n. 91”.
[11] AEEGSI Deliberation 447/2014/R/EEL, “Avvio di procedimento per l'adozione di provvedimenti dell'Autorità ai fini dell'attuazione della legge 116/2014, in tema di riduzione delle bollette elettriche a favore dei clienti forniti in media e bassa tensione”.
[12] AEEGSI Document 598/2014/R/EEL, “Orientamenti per la riforma delle integrazioni tariffarie per le imprese elettriche minori non interconnesse”.
[13] Rodrigues EMG, Osório GJ, Godina R, Bizuayehu AW, Lujano-Rojas JM, Matiasa JCO, et al. Modelling and sizing of NaS (sodium sulfur) battery energy storage system for extending wind power performance in Crete Island. Energy 2015;90(2):1606–17.
[14] Lau KY, Tan CW, Yatim AHM. Photovoltaic systems for Malaysian islands: effects of interest rates, diesel prices and load sizes. Energy 2015;83:204–16.
[15] Thomas D, Deblecker O, Ioakimidis CS. Optimal design and techno-economic analysis of an autonomous small isolated microgrid aiming at high RES penetration. Energy 2016;116(1):364–79.
[16] Möller B, Sperling K, Nielsen S, Smink C, Kerndrup S. Bernd Möller. Creating consciousness about the opportunities to integrate sustainable energy on islands. Energy 2012;48(1):339–45.
[17] Reyasudin Basir Khan M, Jidin R, Pasupuleti J, Azwa Shaaya S. Optimal combination of solar, wind, micro-hydro and diesel systems based on actual seasonal load profiles for a resort island in the South China Sea. Energy 2015;82:80–97.
[18] Cozzolino R, Tribioli L, Bella G. Power management of a hybrid renewable system for artificial islands: a case study. Energy 2016;106:774–89.
[19] Fazelpour F, Soltani N, Rosen MA. Feasibility of satisfying electrical energy needs with hybrid systems for a medium-size hotel on Kish Island, Iran. Energy 2014;73:856–65.
[20] Rodrigues EMG, Godina R, Santos SF, Bizuayehu AW, Contreras J, Catalão JPS. Energy storage systems supporting increased penetration of renewables in islanded systems. Energy 2014;75:265–80.
[21] Waide P, Ure J, Karagianni N, Smith G, Bordass W. The scope for energy and CO2 savings in the EU through the use of building automation technology. Waide Strategic Efficiency. 2014. p. 1–78. Available at:, http://www.leonardo-energy.org/resources/249.
[22] Cosentino V, Favuzza S, Graditi G, Ippolito MG, Massaro F, Riva Sanseverino E, et al. Smart renewable generation for an islanded system. Technical and economic issues of future scenarios. Energy 2012;39(1):196–204.
[23] Ippolito MG, Di Silvestre ML, Riva Sanseverino E, Zizzo G, Graditi G. Multi-objective optimized management of electrical energy storage systems in an islanded network with renewable energy sources under different design scenarios. Energy 2014;64:648–62.
[24] Riva Sanseverino E, Riva Sanseverino R, Favuzza S, Vaccaro V. Near zero energy islands in the Mediterranean: supporting policies and local obstacles. Energy Policy 2014;66:592–602.
[25] Di Silvestre ML, La Cascia D, Riva Sanseverino E, Zizzo G. Improving the energy efficiency of an islanded distribution network using classical and innovative computation methods. Util Policies 2016;40:58–66.
[26] Morán AJ, Profaizer P, Zapater MH, Valdavida MA, Bribián IZ. Information and Communications Technologies (ICTs) for energy efficiency in buildings: review and analysis of results from EU pilot projects. Energy Build 2016;127:128–37.

[27] López-González LM, López-Ochoa LM, Las-Heras-Casas J, García-Lozano C. Update of energy performance certificates in the residential sector and scenarios that consider the impact of automation, control and management systems: a case study of La Rioja. Appl Energy 2016;178:308–22.
[28] Zhang C, Liu C. The impact of ICT industry on CO_2 emissions: a regional analysis in China. Renew Sustain Energy Rev 2015;44:12–9.
[29] Sekki T, Airaksinen M, Saari A. Effect of energy measures on the values of energy efficiency indicators in Finnish daycare and school buildings. Energy Build 2017;139:124–32.
[30] Ayodele TR, Ogunjuyigbe ASO, Atiba IA. Assessment of the impact of information feedback of prepaid meter on energy consumption of city residential buildings using bottom-up load modeling approach. Sustain Cities Soc 2017;30:171–83.
[31] Choi Y, Lim Y, Hak-Man K. Optimal load shedding for maximizing satisfaction in an islanded microgrid. Energies 2017;10(45):1–13.
[32] Wu X, Jiang P, Lu J. Multiagent-based distributed load shedding for islanded microgrids. Energies 2014;7:6050–62.
[33] Kumar Nunna HSVS, Saklani AM, Sesetti A, Battula S, Doolla S, Srinivasan D. Multi-agent based Demand Response management system for combined operation of smart microgrids. Sustain Energy, Grids Netw 2016;6:25–34.
[34] Geramifar H, Shahabi M, Barforoshi T. Coordination of energy storage systems and DR resources for optimal scheduling of microgrids under uncertainties. IET Renew Power Gener 2017;11(2):378–88.
[35] Aghajani GR, Shayanfar HA, Shayeghi H. Demand side management in a smart micro-grid in the presence of renewable generation and demand response. Energy 2016;126:622–37.
[36] Minchala-Avila LI, Garza-Castanon LE, Vargas-Martınez A, Zhang Y. A review of optimal control techniques applied to the energy management and control of microgrids. Procedia Comput Sci 2015;52:780–7.
[37] Najihah N, Bakara A, Hassana MY, Sulaima MF, Nasird MNM, Khamis A. Microgrid and load shedding scheme during islanded mode: a review. Renew Sustain Energy Rev 2017;71:161–9.
[38] Ahmadi-Karvigh S, Ghahramani A, Becerik-Gerber B, Soibelman L. One size does not fit all:understanding user preferences for building automation systems. Energy Build 2017;145:163–73. http://dx.doi.org/10.1016/j.enbuild.2017.04.015.
[39] Paço A, Lavrador T. Environmental knowledge and attitudes and behaviours towards energy consumption. J Environ Manag 2017;197:384–92.
[40] Hara K, Uwasu M, Kishita Y, Takeda H. Determinant factors of residential consumption and perception of energy conservation: time-series analysis by large-scale questionnaire in Suita, Japan, 87; 2015. p. 240–9.
[41] Good N, Ellis KA, Mancarella P. Review and classification of barriers and enablers of demand response in the smart grid. Renew Sustain Energy Rev 2017;72:57–72.
[42] EU smart grid task force, https://ec.europa.eu/energy/en/topics/markets-and-consumers/smart-grids-and-meters/smart-grids-task-force.
[43] Kailas A, Cecchi V, Mukherjee A. A survey of communications and networking technologies for energy management in buildings and home automation. J. Comput. Net. Commun. 2012;2012:1–12. 932181.
[44] Toschi GM, Campos LB, Cugnasca CE. Home automation networks: a survey. Comput Stand Interfaces 2017;50:42–54.
[45] Directive 2009/72/EC of the European Parliament and of the Council of 13 July 2009 concerning common rules for the internal market in electricity.
[46] Directive 2009/73/EC of the European Parliament and of the Council of 13 July 2009 concerning common rules for the internal market in natural gas and repealing Directive 2003/55/EC (Text with EEA relevance).
[47] Directive 2010/31/EU of the European parliament and of the council of 19 May 2019 on the energy performance of buildings.
[48] Directive 2012/27/EU of the European parliament and of the council of 25 october 2012 on energy efficiency, amending directives 2009/125/EC and 2010/30/EU and repealing directives 2004/8/EC and 2006/32/EC.
[49] Directive 2004/22/EC of the European parliament and of the council of 31 march 2004 on measuring instruments (Text with EEA relevance).
[50] 2012/148/EU: commission Recommendation of 9 March 2012 on preparations for the roll-out of smart metering systems.
[51] European Technical Standard EN 15232. Energy performance of buildings – impact of building automation, control, and building Management. second ed. Brussels: CEN; 2012.
[52] ISO/IEC standard 14543–3 (series), information technology - home Electronic systems (HES) architecture.
[53] Chinese Standard GB/T 20965-2013, Control network HBES technical specification.
[54] ANSI/ASHRAE standard 135-2016, BACnet®–a data communication protocol for building automation and control networks.
[55] IEEE standard 2030.2–2015, IEEE guide for the interoperability of energy storage systems integrated with the electric power infrastructure.
[56] IEEE standard 2030-2011, IEEE guide for smart grid interoperability of energy technology and information technology operation with the electric power system (EPS), end-use applications, and loads.
[57] P1888.4/D1.7, oct 2016, IEEE approved Draft standard for green smart home and residential quarter control network protocol.
[58] Meng L, Riva Sanseverino E, Luna A, Dragicevic T, Vasquez JC, Guerrero JM. Microgrid supervisory controllers and energy management systems: a literature review. Renew Sustain Energy Rev 2016;60:1263–73.
[59] Lilis G, Conus G, Asadi N, Kayal M. Towards the next generation of intelligent building: an assessment study of current automation and future IoT based systems with a proposal for transitional design. Sustain Cities Soc 2017;28:473–81.
[60] HomePlug homepage, Available at: http://www.homeplug.org/explore-homeplug/overview/.
[61] Insteon Whitepaper: the details, version 2.0, Available at: http://cache.insteon.com/documentation/insteon_details.pdf.
[62] International Standard ITU G.9959. Short range narrow-band digital radio-communication transceivers - PHY, MAC, SAR and LLC layer specifications. 2015.
[63] Altmann M, Schlegl P, Volbert K. A low-power wireless system for energy consumption analysis at mains sockets. EURASIP J Embed Syst 2017;8:1–11.
[64] Yan Y, Qian Y, Sharif H, Tipper D. A survey on smart grid communication infrastructures: motivations, requirements and challenges. IEEE Commun Surv Tutorials 2013;15(1) [IEEE].
[65] Gupta A, Jha RK. A survey of 5G network: architecture and emerging technologies. IEEE Access 2015;3:1206–32.
[66] Torsten Berger L, Schwager A, Escudero-Garzás JJ. Power line communications for smart grid applications. J Electr Comput Eng 2013;2013:1–16. 712376.
[67] Istat, population housing census 2011, in http://dati-censimentopopolazione.istat.it/Index.aspx?lang=en cit. 10/10/2016.
[68] ISTAT, L'Italia in 150 anni. Sommario di statistiche storiche 1861-2010, cap 15. Avellino. 2011.
[69] AEEGSI, Indagine conoscitiva sui prezzi finali dell'energia elettrica e del gas naturale, Report 174/2015/I/COM.
[70] Garofalo E, Gargiulo A, Lembo E, Marazzi R, Rondena E, Moneta D, et al. Renewable energy sources' development in small island not interconnected to the main grid (in Italian, orginal title: sviluppo delle Fonti Energetiche Rinnovabili nelle Isole minori non interconnesse). Ricerca sul Sistema Energetico –RSE S.p.A. Technical Report. 2015.
[71] Technical pubblication "Building automation – impact on energy efficiency Application per EN 15232 eu.bac product certification". Siemes.
[72] Hotel Energy Solutions. Analysis on energy use by european hotels: online survey and desk research. Hotel Energy Solutions Project Publications; 2011.
[73] Strategies for C&I demand Response: hotels and motels, at https://bizenergyadvisor.com/members/TAS-RB-7/Research_Brief/DRStrategiesHotelsMotels.
[74] Zanella A, Bui N, Castellani A, Vangelista L, Zorzi M. Internet of things for smart cities. IEEE Internet Things J 2014;1(1):22–32.
[75] Graditi G, Ippolito MG, Lamedica R, Piccolo A, Ruvio A, Santini E, et al. Innovative control logics for a rational utilization of electric loads andair-conditioning systems in a residential building. Energy Build 2015;102:1–17.
[76] Buso T, Dell'Anna F, Becchio C, Bottero MC, Cognati SP. Of comfort and cost: examining indoor comfort conditions and guests' valuations in Italian hotel rooms. Energy Research Social Sci 2017. http://dx.doi.org/10.1016/j.erss.2017.01.006 (in press) Available online 5 February 2017.
[77] Law decree 24/06/2014, n. 91, "Disposizioni urgenti per il settore agricolo, la tutela ambientale e l'efficientamento energetico dell'edilizia scolastica e universitaria, il rilancio e lo sviluppo delle imprese, il contenimento dei costi gravanti sulle tariffe elettriche, nonche' per la definizione immediata di adempimenti derivanti dalla normativa europea".
[78] Deliberation 21/11/2014 AEGGSI 574/2014/R/eel: "Disposizioni relative all'integrazione dei sistemi di accumulo di energia elettrica nel sistema elettrico nazionale".
[79] Deliberation 18/12/2014 AEEGSI 642/2014/R/eel: "Ulteriori disposizioni relative all'installazione e all'utilizzo dei sistemi di accumulo. Disposizioni relative all'applicazione delle Norme CEI 0–16 e CEI 0-21".
[80] Deliberation 16/07/2015 AEEGSI 360/2015/R/eel: "Proroga in merito all'obbligatorietà dei ritardi nell'attivazione di alcune funzioni previste per la generazione distribuita".
[81] CEI Standard 0-16. Reference technical rules for the connection of active and passive consumers to the HV and MV electrical networks of distribution Company. 2014.
[82] CEI Standard 0-21. Reference technical rules for the connection of active and passive users to the LV electrical Utilities. 2014.

An example of smart building with a km zero energy performance

Luigi Martirano, Emanuele Habib, Giacomo Greco, Matteo Manganelli, Alessandro Ruvio
Faculty of Civil and Industrial Engineering
Sapienza University of Rome, Italy
martirano@uniroma1.it

Biagio Di Pietra, Alessandro Pannicelli, Sara Piccinelli, Giovanni Puglisi, Pasquale Regina
Italian National Agency for New Technologies (ENEA)
Rome, Italy
biagio.dipietra@enea.it

***Abstract*—Environmental concerns and European policies push for more energy efficient buildings, towards the goal of Nearly Zero Energy Buildings (nZEBs), buildings with an high efficiency and for which the low amount of energy required for the fixed technical systems (TBS) is covered by energy from renewable sources produced on-site. Innovative technical solutions and social/economic schemes are key elements to this purpose. Results on the simulation of energy performance and control system behavior of a real case are analyzed. The paper shows that the sizing of the local photovoltaic system (PV) based on the yearly energy spent by the TBS allows to obtain the nZEB qualification but it doesn't determine an optimal power behavior. The solution proposed in this work is to arrange a microgrid with a unique point of connection to the grid that includes the local generation systems, the common electric heating system by source grounded heat pumps and the residential units of a part of the buildings. Sizing of on-site power generation from renewable sources, like PV, may be developed based on the energy demand. The microgrid is managed by a common building automation control system (BACS). Control strategies have been analyzed, in order to realize demand-side management (DSM) actions, combining the advantages of thermal inertia, flexible loads, energy pricing and local generation. The DSM strategy operating on the controllable loads and on the electric and thermal storage can reach a "near zero power behavior" so the building can become a "km zero energy building" (KZEB).**

Keywords—Nearly Zero Energy Buildings. Micro grid. Load management. Electric power systems. Thermal energy storage. Photovoltaic systems. Building Management Systems.

I. INTRODUCTION

Developing a strategy to make buildings more efficient and sustainable is a priority in the most recent European energy policies [1]. In particular, "buildings can use automation and controls to serve their occupants better, and to provide flexibility for the electricity system through reducing and shifting demand, and thermal storage" [1].

The introduction of distributed generation owned by the private users and other technologies, like electric energy storage, is changing the characteristics of consumer side of grid.

Actions by the European Union introduce the definitions of the new concepts of *aggregator*, *union*, and *community*. In a traditional definition, the *aggregator* is a virtual aggregation of single users and it is only capable of purchasing energy and reselling it to the users, thus it can only take advantage of energy prices. The *union* is a physical union of single users in a large user, around a common point of connection with the grid, and it can take advantage of new technical solutions (e.g., sharing local power generation or energy storage) to benefit of more convenient economic conditions, not only for energy prices but also other economic components of the electricity bill (network components, green charges, taxes). The *community* is a new solution under construction by European Committees that can be considered a middle way between an aggregator and an union.

An example of aggregator that operates in the energy market is the energy demand aggregator (EDA). In the most accepted way, the EDA collects a large group of energy consumers, even if related to different nodes of the network, and it manages the global energy demand in order to optimize the global economic impact. An advanced way considers the group of energy consumers supplied by the same node of the network. One way used by the EDA is to manage the global electric load by controlling or turning off some of its loads and by managing generation and storage.

As previously investigated by the authors, in the present Italian context there are limitations to the exploitation of distributed generation systems and innovative tariffs [2]. In previous papers the authors demonstrated that in a microgrid management, the control of electric loads and HVAC systems and exploitation of thermal inertia can be useful elements towards more efficient and sustainable buildings [2]-[4].

The aggregations of the users can be profitable both for the cost-effectiveness of DG and for the proper operation of the electricity network itself, increasing power quality. This more relevant whenever transport capacity is lacking, since the coordination of sources and loads inside the aggregation encourages self-consumption, mitigating the upstream grid in terms of power flows, with the consequent deferral of new investments. The economic impact of the aggregation for the users depends on the kind of model accepted (aggregator, union or community) and on the effectiveness of control strategies.

978-1-5090-4894-6/17/$31.00 © 2017 IEEE

Solutions developed for residential and tertiary mixed users, like large buildings, may be further developed in urban perspective. This might be a promising solution for grids with increasing power demand or distributed generation.

II. NEARLY ZERO ENERGY BUILDINGS NZEB

Residential and commercial buildings are strategic for pursuing energy efficiency policies, as identified by the European energy policy. This has lead to the provision of nearly zero energy building (nZEB) performance for all new buildings in Europe, starting from 2020 for privates ones and 2018 for public ones. As a consequence, this requires to install local renewable energy sources (RES), like photovoltaic (PV), in order to balance reach the quantity of energy necessary to classify the building as anZEB. nZEB means a building that has a very high energy performance, as determined in accordance with Annex I of Directive 2010/31/EU [5]. The nearly zero or very low amount of energy required should be covered to a very significant extent by energy from renewable sources, favoring energy from renewable sources produced on-site or nearby.

Starting from a basic performance for new buildings or starting from actual performance for existing buildings, to obtain the nZEB qualification, the designers have to reduce the energy uses by passive measures (envelope insulation and efficient technical systems). The residual energy demand has to be supplied mainly by local generation from RES. The qualification takes care of yearly balance.

The nZEB classification considers:

- the energy spent for the fixed Technical Building Systems (TBS) as heating, ventilation, air conditioned HVAC and domestic hot water DHW. This amount depends on the envelope insulation, the efficiency of the TBS and the building automation control systems (BACS) [6].
- the global annual primary energy amount, not considering the instantaneous power.

This paper shows that in a nZEB, the energy yearly balance (for fixed technical systems) can be equal or close to zero, but the instantaneous electric power may be far from zero with the possibility to determine severe chaotic phenomena. It is possible to have excessive peak and holes in enduser's power profiles with periods in which energy is provided to the grid, that is not economically advantageous due to the strong asymmetry between purchase and resale pricing, as in the latter network components, green charges, taxes are not compensated.

In this framework, the authors investigated Demand Side Management (DSM) strategies operating on the controllable loads, considering not only the fixed systems (HVAC and DHW) but all the electric loads [7]-[9]. The goal is to reach a "near zero power behavior" with optimal exploitation of local RES [10].

Electric loads in a building may be divided into uncontrollable, shiftable and controllable loads. Shiftable (or plannable) loads can be shifted in time (with limitations) without affecting users' comfort, but once they become uncontrollable until the duty cycle ends. Washing machines and dishwashers may be assumed to be plannable and are considered so in this work. Controllable loads can be modified at any operation time (with limitations) exploiting the inertia of the operated system. Heat pumps are the main controllable load in this work. Their operation is assumed to be managed via the central control of local ambient and main system set-point temperatures. All other loads are uncontrollable, i.e., any change in the operation would affect users' comfort.

III. NEW MODELS

The evolution of electric systems for smart buildings and nZEBs regards:

- Technologies
- Regulations, economy and management

The technologies for smart electric systems (BACS- and DMS-compatible) are already available, while innovation is needed regarding the technical and economic regulations, economic agreements, management strategies [11]-[13].

In general, three categories of aggregation can be distinguished [14]:

- Aggregations with "fundamental" or "intrinsic" value, which does not depend on regulation, market awareness or technologies, and is permanent in time;
- Aggregations with "transitory" value, which contribute to a better power system operation but their value can decrease with better regulations, management or technologies;
- Aggregations with "opportunistic" value, which respond to regulation or market "flaws".

The concept of aggregation generates, in general, two different kind of values:

- A "system value"
- A "private value"

With respect to the advancement of regulations and technologies, the three aggregation categories can be associated to the value (value versus regulation/technologies), as shown in Figure 1.

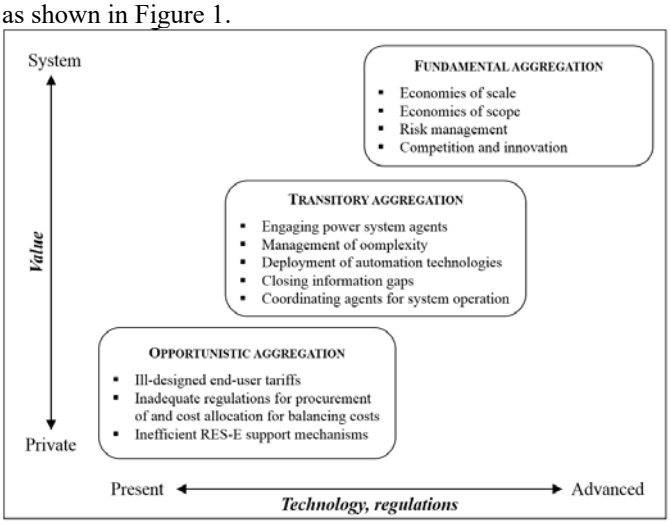

Figure 1. Value of aggregators based on technology and regulatory context. Elaborated from [14]

In the traditional scheme, on one hand, there is a system value, because grid services are provided (e.g., chaotic phenomena

are reduced). On the other hand, there is little or no private value, because the benefits for the users are limited. The energy consumption is only shifted and not reduce, PV is not fully exploited, time slots are not beneficial. The only benefit comes from incentives, in case this activity is supported. In this scheme, only a virtual aggregation is possible, via a virtual power plant (VPP), not a real one. An operation and management entity is needed.

The proposed scheme is based on a microgrid with a single point of connection (POC) to the grid. There is a single billing system for the whole microgrid. The aggregate is regarded as a large consumer, which purchases energy on behalf of all users and subdivides it among them. It is important to note that this entity does not purchase and resell energy but it only fulfills collective energy payments and subdivides them among users. This is similar to the management of other systems in buldings, like water and district heating supply. It may be regarded as an ESCO operating the building.

A significant private value may be achieved, due to the redistribution of supply savings. These savings can be achieved via:

- Economy of scale, i.e., energy can be purchased in bulk at more beneficial tariffs
- Increased RES (PV) self-consumption percent and extent, i.e., net metering applies not only to common areas but also to the aggregate users
- DSM activities, which are economically beneficial in this case
- Dynamic pricing

In the present Italian context, an important barrier is that, in case the energy is billed with respect to the aggregate rather than individual users, quantification of billing components is lost [2]. Present billing components are:

1. Energy and dispatch price
2. Network charges
3. Charges owed to GSE (the company in charge of energy incentive programs) and to the Ministry of Economy and Finances
4. VAT and taxes

While it is acceptable to quantify items 1 and 2 basing on the aggregate consumption (as these items are directly related to energy), this is not acceptable for items 3 and 4, because it would underestimate due charges and taxes. As some charges fund PV support programs, inter alia, PV exploitation would be self-defeating.

Given these two schemes, an intermediate scheme may be further implemented, wherein a dual metering is used: Energy is metered in aggregated form while charges and taxes are quantified individually via single meters.

IV. An Example of a Smart Building with a Km Zero Energy Performance

The reasearch considers a real example of a smart building classified nZEB. It is a complex constitued by two residential/commercial smart buildings in Campobasso, central Italy, made of two towers (A and B) and a common basement used for commercial units and parking [4]. Figure 2 shows a sketch of the building and its utilization. Table I describes the utilization of the building and its main characteristics.

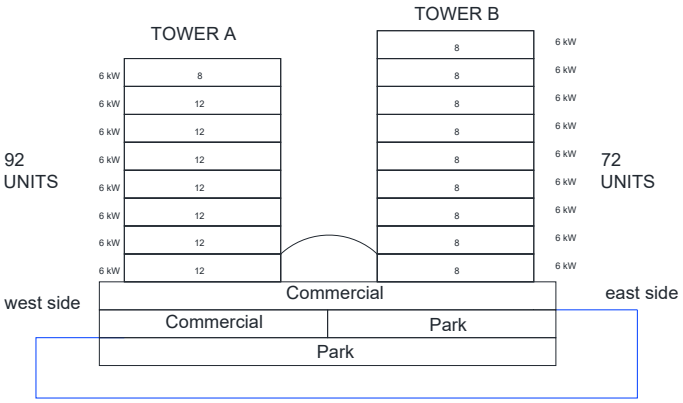

Figure 2. Case study building.

TABLE I
CHARACTERISTICS OF THE BUILDINGS

Area	Type of units	Characteristics
Tower A	Apartments	92 units 50 m^2 each
Tower B	Apartments	72 units 75 m^2 each
Basement	Commercial	2000 m^2 total
Basement	Parking	2000 m^2 total

The complex is classified nZEB as thermal insulation satisfies requirements and the yearly energy consumed by the fixed technical systems is covered by the local PV generation.

Fixed Technical Systems. The building is gas-free and full electric. Power is supplied by an single point of connection with the grid and a private MV/LV substation. Heating and cooling are provided by a common station equipped with three reversible Ground Source Heat Pumps (GSHPs) with a rated electric power of 70 kW each. In dwellings, floor heating systems are used. DHW is centralized. A photovoltaic system (PV) is used as local generation.

Electric loads of Tower A. The private electric microgrid supplies also the residential units of Tower A.

The maximum power of each apartment is 6 kW, mainly due to electric stove.

Electric loads of Tower B. The electric loads of tower B and the commercial units are supplied directly by the public netowrk by independent Point of Connections, one for each unit.

BACS. A central building automation control system (BACS) connected to a central computer operates and manages all the systems by a SCADA software.

At the end, the private microgrid supplies:

- the fixed technical system for all the complex of two towers;
- the common lighting and other common loads
- the single residential units of only tower A.

Table II shows the global load demand of the complex (average-peak demand).

978-1-5090-4894-6/17/$31.00 © 2017 IEEE

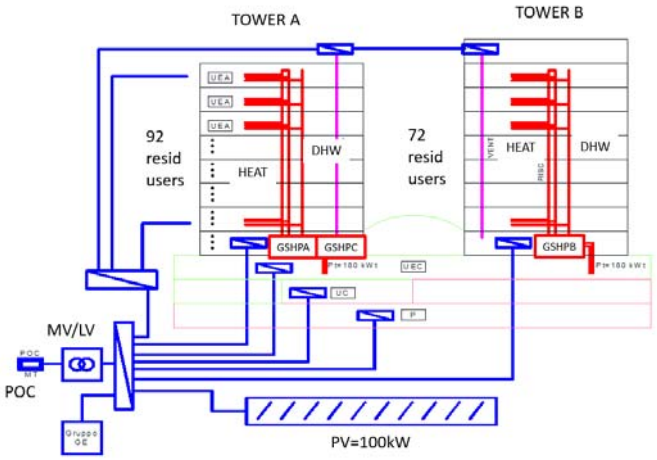

Figure 3. Suggested microgrid.

TABLE II
ELECTRIC POWER DEMAND

Private Microgrid		
	Max (kW)	**Average (kW)**
GSHPs A	70	40
GSHPs B	70	40
GSHPs C	70	40
Fixed Tech.Systems	**210**	**120**
Tower A Units	100	60
Common loads	10	10
Global Microgrid (Union)	**320**	**190**
Public Network		
Tower B	100	60
Commercial	80	50
Global Microgrid (aggregator)	**500**	**300**

According to the regulations, the suggested model was organized in an hybrid system:

- Union for fixed and units tower A (Global power of 190-320 kW)
- Aggregator for the union plus tower B, plus commercial (Global power of 300-500 kW).

Figure 4. Picture of the case study building under construction, with a private MV/LV substation.

A photovoltaic system is installed on top of the tower A, with 100 kW rated power. Figure 3 shows the suggested architecture for the microgrid. Several simulations were done to evaluate both the annual consumptions and the daily profiles. Table III shows a synthesis of the annual energy spent by the building and global energy generated by the PV system.

TABLE III
YEARLY ENERGY SPENT IN THE MICROGRID AND YEARLT ENERGY GENERATED BY THE PV SYSTEM

		kW	**h**	**MWh**
Union	Fixed systems	GSHP A	40	1020	40,8
		GSHP B	40	1020	40,8
		GSHP C	40	1020	40,8
		Total	***120***		***122,4***
		Tower A	60	1425	85,5
		Common	10	3000	30
		Total	***190***		***237,9***
		PV	***100***	***1295***	***129,5***

Table III shows that the energy generated by the PV is sufficient to equalize the energy spent by fixed systems.
The building obtained the qualification of nZEB according to:

1) High level of insulation, with a building to ambient heat transfer coefficient H = 31 W/K
2) High performance of the TBS (floor heating)
3) Ground source heat pumps with high value of the CoP
4) Photovoltaic system of 100 kW and about 130MWh/year
5) Domotic in all the units to better exploit the TBS

Yet preliminary simulation has shown that chaotic phenomena of voltage and power fluctuations, may arise during the day and especially in the summer period.
A second question concerns the economic aspects. The locally generated energy, that is not self consumed and provided to the grid is valued with a low price, lower than the energy generated and self consumed.
In order to solve these problems the authors suggested to operate 2 actions:

i. The electric microgrid with a single point of connection and a private distribution system, including also the residential units of Tower A, has been organized.
ii. The microgrid is managed by the a central Building Energy Management System (BEMS) in order to better exploit the local energy by increasing the self consumption and to optimize the power profile at the point of connection, to take advantage of dynamic supply contracts.

Electric microgrid. In previous papers by the authors [3]-[4], preliminary configurations of the case study were investigated. In this work, the final configuration of the microgrid is considered, as follows (Figure 3):

- Tower A: all loads (GSHPs and residential units)
- Tower B: GSHPs
- Commercial area: GSHPs

The suggested microgrid is composed by:
- a single POC with the DSO at the HV level 300 kW, 20kV 3 wires 50 Hz, and a substation HV/LV with a single 400 kVA transformer (Figure 4);
- a low voltage main switch board (MSB) to supply both the TBS (heating, elevators, etc.) and the units;

978-1-5090-4894-6/17/$31.00 © 2017 IEEE

- a common photovoltaic system (PV) installed on the roof of the building and connected to the MSB;
- a distribution power system from the MSB for all common TBSs;
- a feeder distribution from the MSB supplying each unit of Tower A by an independent feeder in a radial scheme;
- a local panel (ULP) for each unit of the Tower A for the local system.

Figure 5. MV/LV substation with a single 400 kVA transformer.

Concerning electric supplies of users in tower B and commercial areas, they are directly connected to the grid in the final configuration, thus they cannot be controlled and their energy is not included in the microgrid balance. Considering that whole HVAC system (GSHPs of Tower A, B and Commercial) can be controlled, there is a greater possibility to exploit the thermal inertia and the temperature set points, with respect to previous configuration.

Building Energy Management System BEMS. The Tower A is fully wired with an HBES system. Each residential unit of Tower A is supposed to be equipped with a smart dishwashing machine, a smart washing machine, electric cooking devices, a refrigerator, and other usual domestic appliances. The management of the energy systems is organized with a central Building Energy Management System (BEMS) located in the SCADA that manages the whole building as a large user. The goal of the BEMS is to optimize the energy and economic performance of the grid (peak shaving, self-consumption, dynamic price of the energy). The presence of an integrated BACS can transform the individual users (apartments and commercial units) of few kW in a single large user (building) of hundreds kW with the possibility to operate demand side management (DSM) by an user common point of view. The BEMS controls the large load of the HVAC system by exploiting thermal inertia of the tanks as an energy storage, and the inertia of the well-insulated units, by forcing local and central temperature set points according to the actual global net load and the generation. The BEMS controls also the washing smart appliances (dishwashers and washing machines) of the single units, by a user software (APP) connected to the BEMS that permits to shift the starting times. The general aim of BEMS is:

1) to take advantage of the PV self-consumption, as much as possible;
2) to maintain a controlled profile according to the actual cost of the energy by optimizing the energy costs in a dynamic scenario with special contracts;
3) to avoid changes of direction of the power in the POC and to minimize the power.

V. SIMULATIONS

As described previous a paper by the authors, a complete bottom-up model of the systems has been developed [4]. Electric devices are defined by their peak load, duty cycle, and energy demand in a fifteen-minutes period. Their actual load is simulated with a statistical approach simulating the presence and the habits of users. These are used also as input parameters for the heating and cooling model of the building, together with climate data. Heating loads are used to simulate the temperature of the central thermal energy storage and the operation of the heat pumps. Local ambient temperature is PI controlled. Heat pumps operation is on-off controlled in as many steps as the number of compressors of each unit. More details on these models are reported in previous papers from the authors [3]-[4].

In this work 4 different scenarios are simulated:

Scenario 1. Only fixed systems (GSHPs) with PV

Firstly, conventional system use with a microgrid supplying only the GSHPs, and without BEMS, has been simulated.

The model generates a reference single unit residential load profile. The yearly energy spent is evaluate about 123 MWh.

The yeary energy generated by the PV is about 130 MWh.

During the summer months:

- the power injected into the grid can reach values of about 100 kW, the entire amount of the power generated by the PV system, also if the buildings demand is positive.
- The self-consumption ratio of the energy generated by the PV is very low.

Figure 6 shows the monthly energy spent by the TBS (positive 12 bars) and the monthly energy generated by the PV system (negative 12 bars). The black line is the monthly balance. Let's note that during the summer period the black line is negative, so generated energy is more locally consumed energy.

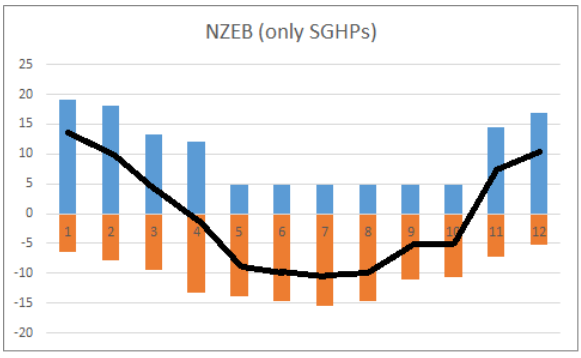

Figure 6. Scenario 1. Monthly energy spent by the TBS (positive values) vs monthly energy generated by the PV system. The black line is the monthly balance.

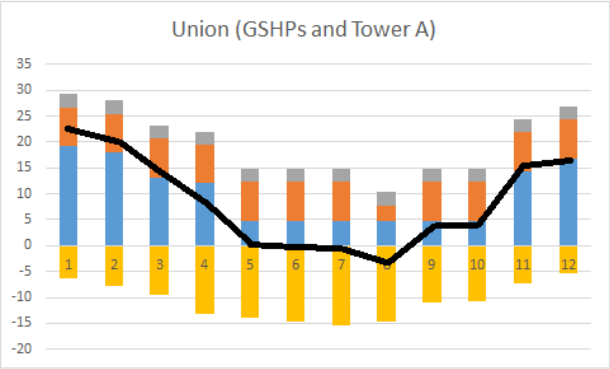

Figure 7. Scenario 2. Monthly energy spent by the microgrid (positive values) vs monthly energy generated by the PV system. The black line is the monthly balance.

Scenario 2. Private Microgrid (GSHPs and Tower A) with PV. In a second scenario the microgrid is simulated with the residential units of Tower A. The suggested model [3]-[4] allows to obtain an aggregation of many dwellings with stochastic occupation and use that is the building load profile at POC. The yearly energy spent is evaluated about 240 MWh. Figure 7 shows the monthly energy spent by the microgrid including Tower A and TBS (positive 12 bars) and the monthly energy generated by the PV system (negative 12 bars). The black line is the monthly balance. Let's note that during the summer period the black line is quite equal to zero and negative only for August. Yet, as there is no control, the mean zero energy demand of the system comes out from averaging periods in which PV generation is much higher than local loads and periods in which the whole load is positive.
In this scenario during the summer months: - the power injected into the grid can reach values of about 50 kW; -the self-consumption ratio of the energy generated by the PV is about 50%. Figure 8 and Figure 9 show an example of daily profile in August and March, respectevely.

Scenario 3. Private Microgrid with PV and BEMS
The microgrid is the same of the Scenario 2 but a suggested DSM operated by the BEMS has been simulated. The scopes of the DSM are:
- minimizing the power peaks;
- maximizing self-consumption of PV electricity;
- controlling the net global demand at the point of connection;
- minimizing the bill in a scenario with a more dynamic cost of the electricity;
- in a future scenario, optimizing the performance of an electric vehicle charging station.

The simulated BEMS controls:
- heating and cooling set-point temperatures,
- refrigerators operation to avoid peaks;
- empty runs of the elevators.
- smart appliances (dishwashers DWs and washing machines WMs) scheduling;

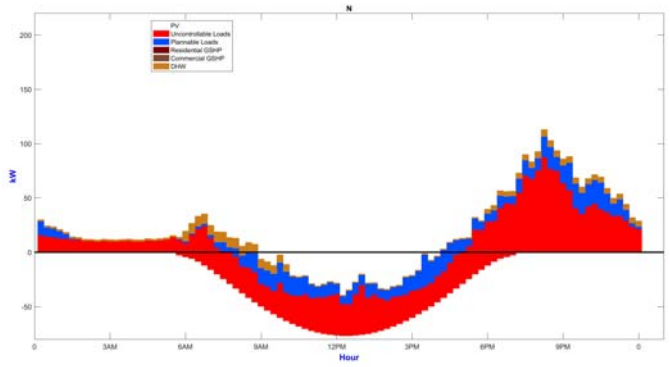

Figure 8. Scenario 2: daily power profile - August day.

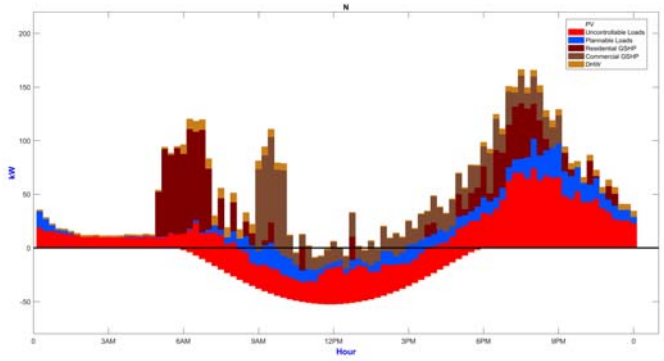

Figure 9. Scenario 2: daily power profile - March day.

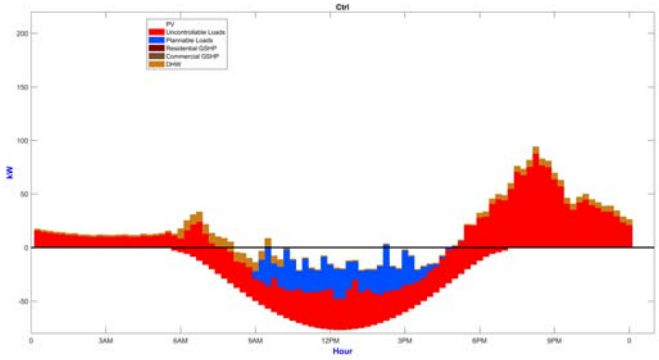

Figure 10. Scenario 3: daily power profile - August day.

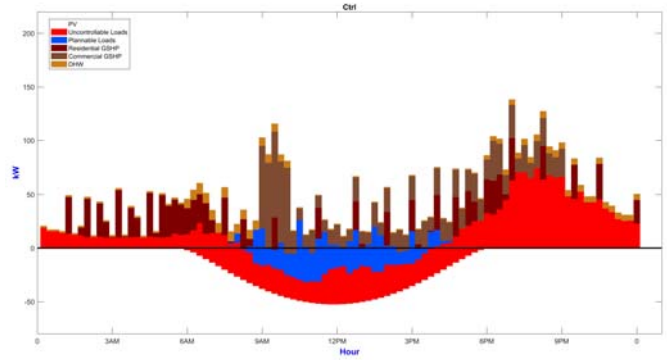

Figure 11. Scenario 3: daily power profile - March day.

The overall rule for the BEMS is to preserve users' comportment, free to use the services and the appliances at will [10]. The HBES is able to control in real time:

- boilers and puffers set-point temperature;
- comfort and economy set-point temperatures of each unit;
- actual ambient set-point temperature T_S of each unit.
- activation of heating and cooling in the commercial unit.

The montly amounts of energy are the same of the scenario 2, but the instantaneous power profile are optimized with a reduction of the peak and an increasing of the self consumption.

Figure 10 and Figure 11 show the power profile of Scenario 3 in the same August day and March day of Figure 8. During the summer, the power injected into the grid is lower than Scenario 2, with a value of about 20 kW. In the March day the power is always positive with a behavior of load.

Scenario 4. Aggregator (GSHPs, Tower A, Tower B and Commercial) with PV and BEMS

The commercial unit load profile is characterized by a high load, during opening hours, and a very low load for the rest of the day (standard shops has been considered as others, like catering and crafts, have much different load profiles that would reduce the general nature of the research). Moreover, there are no shiftable loads as the electricity is used mainly for lighting, apart for HVAC. Notice that the actual combined POC load profile depends on the relative extension of commercial and residential units of Tower B.

Figure 12 shows the monthly energy spent by the whole aggregation (Tower A, Tower B, Commercial and TBS). In this scenario the energy is always positive with load behavior also in August.

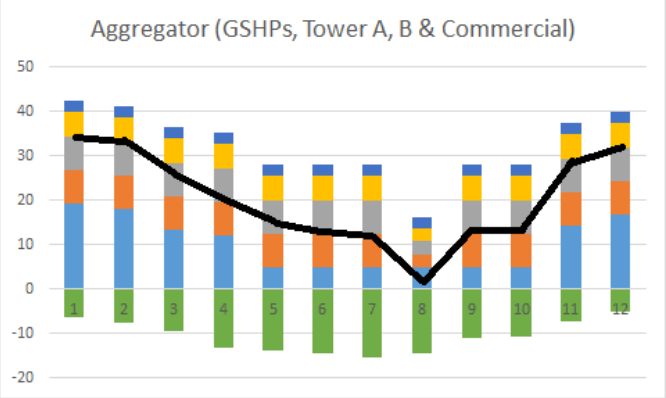

Figure 12. Scenario 4. Monthly energy spent by the whole aggregation (positive values) vs monthly energy generated by the PV system. The black line is the monthly balance.

V – Conclusions

The common and joint energy management of the building both for the thermal and for strictly electric systems allows to obtain several goals, both technical and economic. In the nZEB qualification approach, the PV system of the buildings is sized in order to satisfy the yearly energy spent by the fixed technical systems as heating, ventilation domestic hot water and air conditioned. Considering the yearly power profiles of the microgrid, the simulations demonstrate that in case of a simple microgrid supplying only the fixed systems the economic performance are not optimized. Moreover chaotic phenomena for the power fluctuations may arise. The suggested microgrid approach that includes also the residential units increases the efficiency of the system both technically and economically. The presence of a BEMS is mandatory to reach best results. The goal is to transform the smart building in a km zero energy performance building.

References

[1] European Commission, *An EU strategy on heating and cooling*, Brussels, Belgium, Feb 2016

[2] I. A. Sajjad, M. Manganelli, L. Martirano, R. Napoli, G. Chicco and G. Parise, "Net metering benefits for residential buildings: A case study in Italy," *2015 IEEE 15th International Conference on Environment and Electrical Engineering (EEEIC)*, Rome, 2015, pp. 1647-1652.

[3] L. Martirano *et al*., "Smart micro grids for Nearly Zero Energy Buildings," *2016 IEEE Industry Applications Society Annual Meeting*, Portland, OR, 2016, pp. 1-8.

[4] L. Martirano; E. Habib; G. Parise; G. Greco; M. Manganelli; F. Massarella; L. Parise, "Demand Side Management in Micro-grids for Load Control in Nearly Zero Energy Buildings," in *IEEE Transactions on Industry Applications* , vol.PP, no.99, pp.1-1

[5] Directive 2010/31/EU of the European Parliament and of the Council of 19 May 2010 on the energy performance of buildings.

[6] M.G. Ippolito, E. Riva Sanseverino, and G. Zizzo, "Impact of building automation control systems and technical building management systems on the energy performance class of residential buildings: An Italian case study", Energy and Buildings, Vol. 69 (2014), p. 33-40.

[7] O. Erdinç, A. Taşcıkaraoğlu, N. G. Paterakis, Y. Eren and J. P. S. Catalão, "End-User Comfort Oriented Day-Ahead Planning for Responsive Residential HVAC Demand Aggregation Considering Weather Forecasts," in IEEE Transactions on Smart Grid, vol. 8, no. 1, pp. 362-372, Jan. 2017

[8] A. Prudenzi; A. Silvestri; R. Lamedica; M. C. Falvo; M. Regoli, Residential DSM actions impact prediction through a psychological model of electricity, 2012 IEEE Power and Energy Society General Meeting

[9] B. Hayes; I. Melatti; T. Mancini; M. Prodanovic; E. Tronci, Residential Demand Management Using Individualized Demand Aware Price Policies, IEEE Transactions on Smart Grid, 2017, Vol.8, Issue 3

[10] L. Martirano, E. Habib, G. Parise, G. Greco, M. Cianfrini, M. Manganelli, F. Massarella, L. Parise, Demand side management in mixed residential/commercial buildings with PV on site generation, 2017 IEEE I&CPS, May 8-11, 2017 Niagara Falls (Canada)

[11] Scott Burger, Jose Pablo Chaves-Ávila, Carlos Batlle, Ignacio J. Pérez-Arriaga, "A review of the value of aggregators in electricity systems", Renewable and Sustainable Energy Reviews, Volume 77, September 2017, Pages 395-405.

[12] I. Diaz de Cerio Mendaza, I. G. Szczesny, J. R. Pillai and B. Bak-Jensen, "Demand Response Control in Low Voltage Grids for Technical and Commercial Aggregation Services," in IEEE Trans. on Smart Grid, vol. 7, no. 6, pp. 2771-2780, Nov. 2016.

[13] L. Gkatzikis, I. Koutsopoulos and T. Salonidis, "The Role of Aggregators in Smart Grid Demand Response Markets," in IEEE Journal on Selected Areas in Communications, vol. 31, no. 7, pp. 1247-1257, July 2013.

[14] S. Burger, J. P. Chaves-Ávila, C. Batlle, and I. Perez-Arriaga, "The Value of Aggregators in Electricity Systems." , MIT working paper, 2016.

978-1-5090-4894-6/17/$31.00 © 2017 IEEE

BIOGRAPHIES

Luigi Martirano (StM'98-M02-SM11) received the M.S. and Ph.D. degrees in Electrical Engineering in 1998 and 2003, respectively, from the Sapienza University, Rome Italy. In 2000, he joined the Department of Astronautics, Electrical and Energy Engineering of the Sapienza University of Rome where he's currently an Associate Professor of Electrical Power Systems.

Emanuele Habib received M.S. degree in Mechanical Engineering in 2002 and Ph.D. in Applied Physics in 2007. In 2011, he joined the Department of Astronautics, Electrical and Energy Engineering of the Sapienza University of Rome where he is currently an Assistant Professor of Applied Physics.

Giacomo Greco (StM'14) received the B.D. in 2012 in Automation Engineering and the M.D. in Electrical Engineering in 2016 from the Sapienza University, Rome Italy. He is a PhD student at Sapienza University of Rome.

Matteo Manganelli received his BSc degree cum laude in 2010 and MSc degree cum laude in 2013 in Energy Engineering from Sapienza University of Rome (Italy). Since 2014 he is a PhD student in Electrical Engineering in the same University.

Alessandro Ruvio received his M.Sc. with honours in Electrical Engineering from the University of Rome Sapienza in 2012. He is with Dept. of Electrical Engineering as Assistant research from 2012. He is currently a PhD Student.

Biagio di Pietra has been a Researcher with a permanent contract at Italian National Agency for New Technologies, Energy and Sustainable Economic Development since 2004.

Alessandro Pannicelli has been a Researcher with a permanent contract at Italian National Agency for New Technologies, Energy and Sustainable Economic Development.

Sara Piccinelli has been a Researcher with a permanent contract at Italian National Agency for New Technologies, Energy and Sustainable Economic Development.

Giovanni Puglisi has been a Researcher with a permanent contract at Italian National Agency for New Technologies, Energy and Sustainable Economic Development.

Pasquale Regina has been a Researcher with a permanent contract at Italian National Agency for New Technologies, Energy and Sustainable Economic Development.

978-1-5090-4894-6/17/$31.00 © 2017 IEEE

Available online at www.sciencedirect.com

ScienceDirect

Energy Procedia 105 (2017) 2451 – 2459

Energy Procedia

The 8th International Conference on Applied Energy – ICAE2016

Design optimization of a distributed energy system through cost and exergy assessments

Marialaura Di Somma*[,a], Bing Yan[c], Nicola Bianco[b], Giorgio Graditi[a], Peter B. Luh[c], Luigi Mongibello[a], Vincenzo Naso[b]

[a]*ENEA – Italian National Agency for New Technologies, Energy and Sustainable Economic Development, CR Portici, 80055 Portici, Italy*

[b]*Dipartimento di Ingegneria Industriale (DII), Università degli studi Federico II, P.le Tecchio, Napoli 80125, Italy*

[c]*Department of Electrical and Computer Engineering, University of Connecticut, Storrs, CT 06269, USA*

Abstract

In recent years, Distributed Energy Systems (DESs) have been recognized as a good option for sustainable development of future energy systems. With growing environmental concerns, design optimization of DESs through economic assessments only is not sufficient. To achieve long-run sustainability of energy supply, the key idea of this paper is to investigate exergy assessments in DES design optimization to attain rational use of energy resources while considering energy qualities of supply and demand. By using low-temperature sources for low-quality thermal demand, the waste of high-quality energy can be reduced, and the overall exergy efficiency can be increased. Based on a pre-established superstructure, the aim is to determine numbers and sizes of energy devices in the DES and the corresponding operation strategies. A multi-objective linear problem is formulated to reduce the total annual cost and increase the overall exergy efficiency. The Pareto frontier is found to provide different design options for planners based on economic and sustainability priorities, through minimizing a weighted-sum of the total annual cost and primary exergy input, by using branch-and-cut. Numerical results demonstrate that different optimized DES configurations can be found according to the two objectives. Moreover, results also show that the total annual cost and primary exergy input are reduced by 20% - 30% as compared with conventional energy supply systems.

© 2017 The Authors. Published by Elsevier Ltd. This is an open access article under the CC BY-NC-ND license (http://creativecommons.org/licenses/by-nc-nd/4.0/).

Peer-review under responsibility of the scientific committee of the 8th International Conference on Applied Energy.

Keywords: Distributed Energy System; Design optimization; Annual cost; Exergy efficiency; Multi-objective linear problem.

1. Introduction

In recent years, depletion of fossil energy resources and global warming problems have prompted worldwide awareness about sustainability of energy supply. Distributed Energy Systems (DESs) have been recognized as a good option for sustainable development of future energy systems [1, 2]. A DES may consists of small-scale technologies including renewable ones and storage units, providing electric and thermal energy close to end-users [1]. To achieve the expected potentials of DESs, it is necessary to

* Corresponding author. Tel.: +39 0817723204; fax: +39 0817723344.
E-mail address: marialaura.disomma@enea.it.

1876-6102 © 2017 The Authors. Published by Elsevier Ltd. This is an open access article under the CC BY-NC-ND license (http://creativecommons.org/licenses/by-nc-nd/4.0/).
Peer-review under responsibility of the scientific committee of the 8th International Conference on Applied Energy.
doi:10.1016/j.egypro.2017.03.706

determine the system configuration rationally by selecting the appropriate energy devices, identifying their numbers and sizes, and the corresponding operation strategies, to match energy requirements of a specific end-user [2]. Design optimization of a DES is therefore essential for future energy planning, and inherently involves multiple and conflicting objectives [3, 4]. For instance, the interest of DES developers in achieving a system configuration with lowest costs might conflict with the interest of energy legislations, such as the EU ones, for sustainability concerns on reducing the waste of fossil energy resources and environmental impacts [4, 5]. In such a context, a multi-objective approach helps identify balancing solutions between economic and sustainability priorities to promote participation in the decision-making process and facilitate collective decisions [3].

According to [5], application of exergy principles in energy supply systems can achieve rational use of energy resources by taking into account the different energy quality levels of energy supply and building demand. In the literature, exergy has been linked to sustainability of energy supply since it clearly identifies the efficiency in energy resource use, and the importance of including exergy in energy legislations was discussed [5, 6]. DESs provide a great opportunity to demonstrate the effectiveness of exergy analysis in designing sustainable energy systems since multiple energy resources with different quality levels can be used to satisfy various user demand with different quality levels. By using low exergy sources, e.g., solar thermal or waste heat of power generation, for low-quality thermal demand, the waste of high-quality energy can be reduced, thereby increasing the overall exergy efficiency of DESs.

In previous works, exergy was investigated in DES operation through a multi-objective approach [7, 8]. With fixed DES configurations, optimized operation strategies were established by considering energy costs and exergy efficiency. As regards DES design optimization, most studies focused on minimizing the total annual cost as a crucial objective for DES developers [2, 9 - 13]. Also, before optimizing the design, "superstructures" were pre-established with energy devices chosen among the most commonly used ones in practical DESs. To identify the size of an energy device, several sizes were pre-fixed as possible choices to be selected through binary decision variables [2, 9 - 11]. However, how to select these sizes among the almost infinite possible solutions available in the market is difficult. Conversely, the size of an energy device was a continuous decision variable within the entire available size range, with efficiencies as well as specific capital and operation and maintenance (O&M) costs assumed constant in the entire size range [12, 13], while neglecting their variations with the sizes, which is significant for certain devices.

In this paper, exergy assessments are investigated in DES design optimization through a multi-objective approach. Based on a pre-established superstructure with multiple energy devices, a multi-objective linear problem is formulated to determine numbers and sizes of energy devices with the corresponding operation strategies on the Pareto frontier, thereby providing different design options for planners based on economic and sustainability priorities. In modeling energy devices, the entire size range available in the market as well as the variations of efficiencies, specific capital and O&M costs with sizes are taken into account. The economic objective is formulated as the total annual cost (total annualized investment cost, total annual O&M and energy cost) to be minimized. The exergetic objective is to maximize the overall exergy efficiency of the DES. With given energy demand, the total exergy required to meet the demand is known, and the exergetic objective is formulated as the total annual primary exergy input to be minimized. The Pareto frontier is found by minimizing a weighted sum of the two objectives, by using branch-and-cut. Numerical results show that different optimized DES configurations are found according to the two objectives. The Pareto frontier provides good balancing solutions for planners based on economic and sustainability priorities. The optimized DES configurations allow to reduce the total annual cost and primary exergy input by 20% - 30% as compared with conventional energy supply systems (CESs), where grid power is used for the electricity demand, natural gas boilers for domestic hot water (DHW) and space heating (SH) demand, and electric chillers for space cooling demand (SC).

2. Problem formulation and solution methodology

The DES superstructure consisting of the energy devices considered in the design optimization problem is shown in Fig. 1. Electricity demand and electricity required by heat pumps can be satisfied by grid power and Combined Heat and Power (CHP) systems. SC demand can be satisfied by CHPs, natural gas and biomass boilers through absorption chillers, heat pumps and thermal storage, whereas SH demand by CHPs, natural gas and biomass boilers, and thermal storage. DHW demand can be satisfied by CHPs, natural gas and biomass boilers, solar thermal collectors and thermal storage.

2.1. Decision variables

The decision variables include: existence, numbers, and sizes of energy devices; operation status (on/off) and energy rates provided by energy devices; capacities of thermal storage devices; heat rates input and output to/from thermal storage devices; electricity rate bought from the power grid. Existence and operation status of energy devices are binary. Numbers of energy devices are also determined through binary decision variables to be explained later. All the other decision variables are continuous.

2.2. Economic objective

The economic objective is to minimize the total annual cost of the DES, C_{TOT}, formulated as the sum of the total annualized investment cost, and the total annual O&M and energy costs:

$$C_{TOT} = C_{INV} + C_{O\&M} + C_{FUEL} + C_{PUR}^{GRID}, \tag{1}$$

where C_{INV} is the annualized investment cost of all energy devices of the DES, $C_{O\&M}$ is the total annual O&M cost of all energy devices, C_{FUEL} is the total annual cost of consumed fuels, and C_{PUR}^{GRID} is the annual cost of purchasing electricity from the power grid.

The annualized investment cost of energy devices is obtained through the capital recovery factor [2, 9 - 13], and the annual O&M cost of energy devices depends on the DES operation:

$$C_{INV} = \sum_{i}\sum_{k_i}^{K_i} CRF_i\left(C_{c,i}S_{i,k_i}\right),\ CRF_i = r(1+r)^{N_i}/\left[(1+r)^{N_i}-1\right],\quad C_{O\&M} = \sum_{i}\sum_{k_i}^{K_i}\sum_{d}\sum_{hr} OM_i R_{i,k_i,d,hr} D_t, \tag{2}$$

where CRF_i is the capital recovery factor of technology i; k_i is the energy device associated with technology

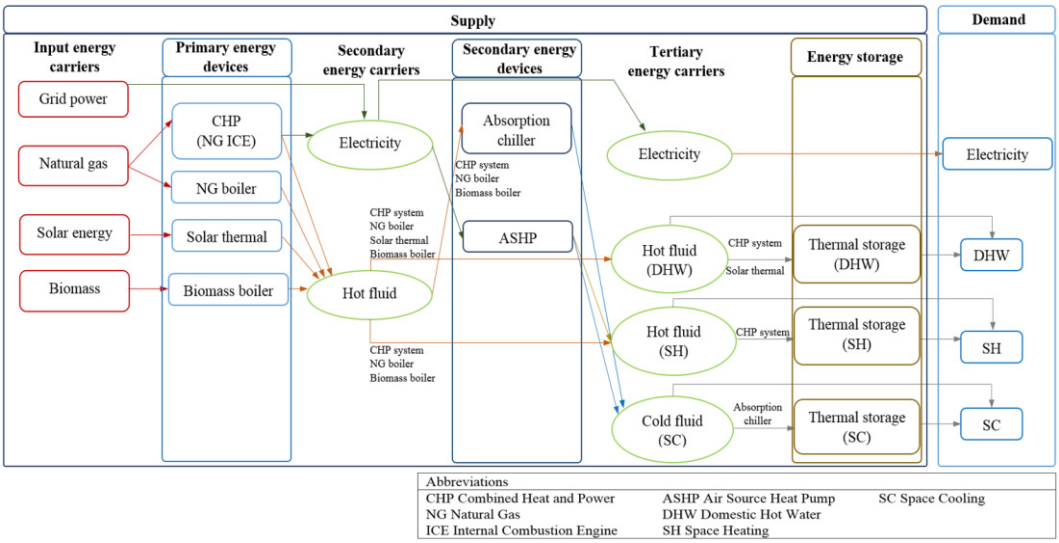

Fig. 1. Superstructure representation of the design optimization problem of the DES.

i, where K_i is its maximum number; S_{i,k_i} is the designed size of device k_i; $C_{c,i}$ is the specific capital cost; r is the interest rate; N_i is the lifetime in years; OM_i is the O&M cost; $R_{i,k_i,d,hr}$ is the energy rate provided by the device k_i at hour hr of day d; and D_t is the time interval length (1 hour).

The total annual costs of the consumed fuels and purchased grid power are formulated as:

$$C_{FUEL}=\sum_i\sum_{k_i}^{K_i}\sum_d\sum_{hr}P_{fuel,i}\left(R_{i,k,d,hr}/\left(\eta_i LHV_{fuel}\right)\right)D_t,\ i\in\left\{NGICE,NGboiler,Bioboiler\right\},\quad C_{PUR}^{GRID}=\sum_d\sum_{hr}P_{e,hr}E_{d,hr}^{GRID}D_t\ , \tag{3}$$

where η_i is the energy efficiency (thermal or electrical); $P_{fuel,i}$ and LHV_{fuel} are the price and lower heat value of the corresponding fuel (i.e., natural gas and biomass fuels), respectively; $P_{e,hr}$ is the time-of-day unit price of electricity from the power grid; and $E_{d,hr}^{GRID}$ is the electricity rate taken from the grid.

2.3. Exergetic objective

The exergetic objective is to maximize the overall exergy efficiency of the DES, as the ratio of the total annual exergy output (exergy required to meet the given user demand), Ex_{out}, to the total annual primary exergy input, Ex_{in}. With given energy demand, the total exergy required to meet the demand is known, and the overall exergy efficiency can be increased by reducing the total primary exergy input. At the supply side, the input energy carriers are grid power, natural gas, biomass and solar energy. Therefore, the exergetic objective is formulated as the total annual primary exergy input to be minimized as:

$$Ex_{in}=\sum_j\sum_d\sum_{hr}Ex_{j,d,hr}D_t\ , \tag{4}$$

where $Ex_{j,d,hr}$ is the exergy rate input to the DES related to the energy carrier j.

Electricity from the power grid is an energy carrier provided by power generation plants, and the exergy input rate to the DES depends on the exergy efficiency of the plants, ε_{gen} [7]:

$$Ex_{e,d,hr}=E_{d,hr}^{GRID}/\varepsilon_{gen},\ \forall d,\forall hr\ , \tag{5}$$

The exergy input rates of natural gas and biomass depend on their specific chemical exergy:

$$\begin{aligned}&Ex_{fuel,d,hr}=\sum_i\sum_{k_i}^{K_i}\sum_{fuel}ex_{fuel}\left(R_{i,k_i,d,hr}/\left(\eta_i LHV_{fuel}\right)\right),\ ex_{fuel}=\varsigma_{fuel}LHV_{fuel},\\&fuel\in\left\{natural\ gas,biomass\right\},\ i\in\left\{NGICE,NGboiler,Bioboiler\right\},\ \forall d,\forall hr\end{aligned}\ , \tag{6}$$

where ex_{fuel} is the specific chemical exergy of the fuel, and ς_{fuel} is the exergy factor [14].

Thermal energy output of solar thermal collectors at the corresponding temperature level is considered as the primary energy source [7]. The exergy input rate to solar thermal collectors, $Ex_{ST,d,hr}$, is defined as:

$$Ex_{ST,d,hr}=R_{ST,d,hr}\left(1-T_{0,d,hr}/T_{coll}^{out}\right),\ \forall d,\forall hr\ , \tag{7}$$

where $T_{0,d,hr}$ and T_{coll}^{out} are the reference temperature (hourly ambient temperature), and the temperature of the heat transfer fluid at the exit of the collector field (assumed constant), respectively.

2.4. Constraints

Three main categories of constraints are established: design constraints, energy balances and operation constraints. As for design constraints, the designed size of the energy device k_i has to be within the minimum and maximum sizes of the related technology $S_i^{\min}$ and $S_i^{\max}$ available in the market:

$$S_i^{\min}x_{i,k_i}\le S_{i,k_i}\le S_i^{\max}x_{i,k_i},\ \forall i,\ k_i\le K_i\ , \tag{8}$$

where x_{i,k_i} is a binary decision variable, which is equal to 1 if the device k_i is implemented in the DES configuration. For the solar collector array, the designed area has to be lower than the available one. In the design optimization problem, the entire size range available in the market as well as the variations of efficiencies, specific capital and O&M costs with sizes are taken into account. These characteristics are

usually piecewise linear functions of the size, which is a continuous decision variable, thereby making the problem nonlinear. To avoid this, the key idea is to divide the entire size range of an energy device into several small ranges, so that these characteristics can be assumed constant in each size range. Consider CHP with a gas-fired internal combustion engine (ICE) as an example. The designed size of CHP in the range l is limited by its minimum and maximum values $S_l^{CHP\min}$ and $S_l^{CHP\max}$ in this range:

$$S_l^{CHP\min} x_{k_{CHP},l}^{CHP} \le S_{k_{CHP},l}^{CHP} \le S_l^{CHP\max} x_{k_{CHP},l}^{CHP},\ \sum_l x_{k_{CHP},l}^{CHP} \le 1,\ \forall l,\ k_{CHP} \le K_{CHP}\ , \tag{9}$$

where $S_{k_{CHP},l}^{CHP}$ and $x_{k_{CHP},l}^{CHP}$ are defined similarly as in Eq (8) in the range l. Also, the summation of binary decision variables $x_{k_{CHP},l}^{CHP}$ over l has to be smaller than or equal to 1, ensuring that at most one range is selected.

To satisfy the given user demand, electricity, DHW, SH and SC energy balances are formulated based on the DES superstructure shown in Fig. 1. As for operation constraints, the energy rate provided by each energy device is limited by its minimum part load and the capacity. Still considering the CHP example, the electricity rate, $R_{k_{CHP},d,hr}$ is limited by its minimum and maximum values $R_{k_{CHP}}^{\min}$ and $R_{k_{CHP}}^{\max}$ if the device is on:

$$R_{k_{CHP}}^{\min} x_{k_{CHP},d,hr} \le R_{k_{CHP},d,hr} \le R_{k_{CHP}}^{\max} x_{k_{CHP},d,hr},\ R_{k_{CHP}}^{\min} = r^{CHP} \sum_l S_{k_{CHP},l}^{CHP},\ R_{k_{CHP}}^{\max} = \sum_l S_{k_{CHP},l}^{CHP},\ k_{CHP} \le K_{CHP},\ \forall d, \forall hr\ , \tag{10}$$

where $x_{k_{CHP},d,hr}$ is the on/off status of CHP, and r^{CHP} is the minimum part load (expressed in percentage of the designed size). The product of one continuous decision variable and one binary decision variable is linearized in a standard way. Beyond ICE, CHPs also involve heat recovery units for thermal purposes. The heat rate recovered by CHPs is subdivided among the heating coils for DHW and SH demand, and absorption chillers for SC as modeled in [7]. CHP ramp-rate constraints are also included to limit power generation between two successive time-steps. The natural gas and biomass boilers can be used to meet DHW and SH demand, and SC through absorption chillers. As regards solar thermal collectors, the heat rate provided is related to the designed area through the hourly solar irradiance and the thermal efficiency. For the operation of thermal storage devices, the amount of energy stored at the beginning of each time interval equals the non-dissipated energy stored at the beginning of the previous time interval (based on the storage loss fraction), plus the net energy flow (heat input rate to the storage minus heat output rate from the storage) [2, 7].

2.5. Optimization method

With the exergetic objective function formulated in Eq. (4) and the economic one formulated in Eq. (1), the problem has two objective functions to be minimized. To solve this multi-objective optimization problem, a single objective function is formulated as a weighted sum of the total annual cost, C_{TOT}, and the total annual primary exergy input, Ex_{in}, to be minimized:

$$F_{obj} = c\omega C_{TOT} + (1-\omega) Ex_{in}\ , \tag{11}$$

where constant c is a scaling factor, chosen such that $c\,C_{TOT}$ and Ex_{in} have the same order of magnitude. The Pareto frontier is found by varying the weight ω in the interval 0 – 1. The solution that minimizes the total annual cost can be found when $\omega = 1$, whereas the one that minimizes the total annual primary exergy input (i.e., maximizes the overall exergy efficiency) when $\omega = 0$. The problem formulated above is linear, and involves both discrete and continuous variables, so this is to be solved by branch-and-cut, which is powerful for mixed-integer linear optimization problems, and easy to code by using commercial solvers.

3. Numerical testing

Numerical testing is presented below, where a hypothetic cluster of 30 buildings located in Torino (Italy) is chosen as the targeted end-user. The method developed in Section 2 is implemented by using IBM ILOG CPLEX Optimization Studio Version 12.6, a popular and powerful solver where branch-and-cut is implemented with flexibility and high-performance.

3.1. Input data

Each building has a surface area of 5000 m^2, and a shape factor S/V of 0.5 m^{-1}. The hourly energy rate demand for electricity, DHW, SH, and SC for four representative days per season are used as input data, based on [15, 16]. To compute the annual energy requirements, the year is assumed to include 90, 92, 91, and 92 days in the cold, cold-mid, hot-mid, and hot seasons, respectively. Table 1 shows the peak and average energy rate demand of the end-user for the four representative season days as well as the annual energy requirements. The average hourly solar irradiance profiles (on a south-oriented and 35° tilted surface) have been assumed for each representative season day [17]. The technical and economic information of energy devices are summarized in Table 2 [18, 19]. The unit price of grid power is assumed as 0.15 €/kWh, and the unit prices of natural gas and biomass (wood pellet) are assumed as 0.477 €/Nm^3, and 120 €/ton, respectively. The exergy efficiency of power generation plants is assumed as 0.40, based on the fossil fuel energy mix for electricity production and on the average efficiency of fossil fuel-fired electricity production in Italy [20]. The exergy factors of natural gas and biomass are assumed as 1.04 and 1.16 [14], respectively. A 5% interest rate is assumed to evaluate the total annualized investment cost.

3.2. Pareto frontier

The optimization problem is solved within few hours with a mixed integer gap lower than 0.15% on a PC with 2.60GHz (2 processors) Intel(R) Xeon(R) E5 CPU and 32G RAM. The Pareto frontier is shown in Fig. 2a. The point marked with *a* is obtained under exergetic optimization ($\omega = 0$), and the point marked with *b* is obtained under economic optimization ($\omega = 1$). The points between these two extreme points are found by subdividing the weight interval into 10 equally-spaced points. Each point on the Pareto frontier corresponds to a different optimized configuration of the DES. Fig. 2b shows the percentages of reduction in the total annual cost and increase in the total annual primary exergy input obtained by varying the weight ω from 0 to 1 with a 0.1 increase.

3.3. Optimized DES configurations

The optimized configurations of the DES (numbers, sizes and total installed capacities of energy devices), and the economic and exergetic performances for points *a* and *b* on the Pareto frontier are shown in Table 3. For the illustration purpose, the point marked with *c* in Fig. 2a (obtained for $\omega = 0.2$) is also selected as an attractive economic/exergetic balancing solution. Under exergetic optimization, the total capacity of CHP is the largest among the three configurations. This highlights its importance for the exergetic objective, due to the possibility of waste heat recovery for thermal purposes, thereby promoting efficient use of the energy resource. As ω increases, the total capacity reduces, reaching the minimum under

Table 1. Peak and average energy rate demand (MW) in the representative season days and annual energy requirements of the building cluster (MWh).

Season	Electricity			DHW			SH			SC		
	Peak	Average	Annual	Peak	Average	Annual	Peak	Average	Annual	Peak	Average	Annual
Cold	0.86	0.52	1114	1.30	0.25	544.3	5.50	2.88	6227	0	0	0
Cold-mid	0.86	0.52	1139	1.30	0.25	556.4	3.22	1.53	3378	0	0	0
Hot-mid	0.86	0.52	1126	1.30	0.25	550.3	0	0	0	0	0	0
Hot	0.86	0.52	1139	1.30	0.25	556.4	0	0	0	4.47	1.47	3235

Table 2. Technical and economic information of energy devices.

Energy device	Size range (kW)	Specific capital cost	O&M costs (€/kWh)	Efficiency		Lifetime
				Electrical	Thermal	
CHP gas-fired ICE	20-5000	1495-840 €/kW	0.020-0.008	0.28-0.41	0.68-0.40	20
NG boiler	10-2000	100 €/kW	0.0014		0.9	15
Biomass boiler	10-2000	400 €/kW	0.0027		0.85	15
Solar Thermal (ST)	-	200 €/m^2	0.0057		0.6	15
Air-source heat pump	10-6000	460 €/kW	0.0025		COP=3.0-3.5	20
Absorption chiller	10-5000	510-230 €/kW	0.0020		COP=0.8	20
Thermal storage	-	20 €/kWh	0.0012		loss fraction=0.05	20

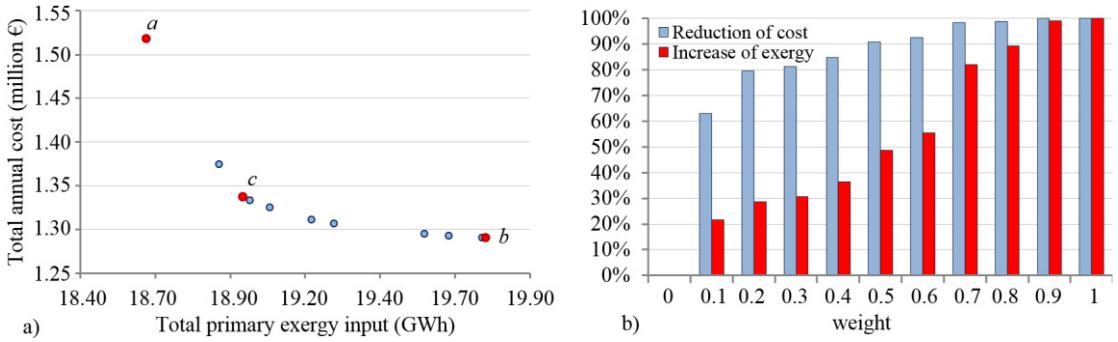

Fig. 2. a) Pareto frontier; b) Percentages of reduction in annual cost and increase in annual primary exergy input for ω varying from 0 to 1 with a 0.1 increase.

economic optimization, due to its high investment cost. Conversely, the total capacity of natural gas boiler is maximum under economic optimization, due to the low investment and O&M costs. The natural gas boiler is not chosen at point *c*, under a higher weight of the exergetic objective, highlighting that natural gas, as high-quality energy, should not be used for low-quality thermal demand. The choice of one natural gas boiler of 345 kW under exergetic optimization is due to the large sizes of the two CHPs, characterized by high minimum part loads, below of which they cannot operate.

The biomass boiler is not chosen in any configuration. Under exergetic optimization, although both wood and natural gas are high-quality energy, the efficiency of the biomass boiler is lower than that of the gas-fired boiler. The biomass boiler is also inconvenient for the economic objective due to the high investment cost. The area of the solar thermal array is maximum and the same for points *a* and *c*, under a higher weight of the exergetic objective, highlighting the convenience of solar thermal for the exergetic objective, due to low exergy of the thermal energy output from the collectors. Also the total capacities of heat pump and absorption chiller reach the maximum under exergetic optimization, highlighting their convenience for the exergetic purpose, due to the high conversion efficiency and the possibility of waste heat recovery for the SC demand, respectively. When ω increases, the total capacities reduce in order to reduce the total annual cost.

The capacity of the DHW thermal storage is maximum and the same for points *a* and *c*, since it is related to the thermal energy provided by the solar thermal plant. The capacity of the SH thermal storage is maximum under exergetic optimization, due to large amount of exhaust gas from CHPs. Conversely, the capacity of the SC thermal storage is minimum and the same for points *a* and *c*, whereas it strongly increases under economic optimization. By increasing the storage capacity, the size of the absorption chiller can be strongly reduced, thereby reducing the total investment costs.

In Table 3, the total annual cost and primary exergy input are also reported for an optimized CES system, where grid power is used for the electricity demand, natural gas boilers for DHW and SH demand, and

Table 3. Optimized solutions resulting from the analysis of the Pareto Frontier.

Optimized solutions		Point *a*	Point *c*	Point *b*	CES
CHP	Number - Sizes - Total (kW_{el})	2 - 1006/2130 - 3136	2 - 453/1103 - 1556	2 - 300/1007 - 1307	
NG boiler	Number – Sizes, Total (kW_{th})	1 - 345 - 345	0	2 - 260/807 – 1067	
Biomass boiler	Number - Sizes - Total (kW_{th})	0	0	0	
Solar Thermal	Area (m^2)	1485	1485	0	
Heat pump	Number - Sizes - Total (kW_{th})	2 - 360/5732 - 6092	2 - 995/2563 - 3558	2 - 402/2466 - 2868	
Absorption chiller	Number - Sizes - Total (kW_{th})	2 - 300/1298 - 1589	1 - 1450 - 1450	1 - 1000 – 1000	
DHW storage	Total capacity (kWh_{th})	2746	2746	2063	
SH storage	Total capacity (kWh_{th})	2268	1382	1450	
SC storage	Total capacity (kWh_{th})	948	948	2406	
Total annual cost (million €)		1.517	1.374	1.290	1.913
Total annual primary exergy input (GWh)		18.620	18.864	19.753	27.641

electric chillers for SC demand (same configurations attained under economic and exergetic optimization). As compared with CES, the total annual cost and primary exergy input of the DES are both reduced by 33% under economic and exergetic optimization. Moreover, as compared with CES, the total annual cost of the DES under exergetic optimization is reduced by 21%, whereas the total annual primary exergy input under the economic optimization is reduced by 28%.

3.4. Operation strategies of optimized DES configurations under economic and exergetic optimization

For each optimized configuration, different operation strategies of energy devices are found. For the illustration purpose, Fig. 3 shows the operation strategies of the DES (electricity and thermal energy provided by energy devices) in the four representative season days at points *a* and *b* of the Pareto frontier for a) electricity, b) DHW and c) SH/SC demand. As shown in Fig. 3a, grid power is generally lower than the electricity provided by CHPs, highlighting that CHP is convenient for both objectives. The contrary occurs in the hot mid-season day under exergetic optimization. In this day, only electricity and DHW demand need to be satisfied, and solar thermal is preferred instead of waste heat from CHPs to meet the demand as shown in Fig. 3b. The integration of the natural gas boiler is due to the large sizes of the CHPs, as discussed earlier. Conversely, waste heat from CHPs is mostly used under economic optimization. In Fig. 3c for SH and SC, heat pumps are mostly used under both exergetic and economic optimization. For SC, the absorption chiller is used more under exergetic optimization than under economic one. Moreover, both Fig.s 3b and c show that to meet the DHW and SH demand, natural gas boilers are more used under economic optimization than under exergetic one.

4. Conclusions

In this paper, exergy assessments are investigated in DES design optimization for sustainable development of energy supply systems. Based on a pre-established superstructure, a multi-objective linear problem is formulated to determine numbers and sizes of energy devices with the corresponding operation strategies through cost and exergy assessments. The Pareto frontier is found through minimizing a weighted sum of the total annual cost and primary exergy input by using branch-and-cut. Numerical results demonstrate that different optimized DES configurations are found according to the two objectives, and the Pareto frontier provides good balancing solutions for planners based on economic and sustainability priorities. The optimized DES configurations allow to reduce the total annual cost and primary exergy input by 20% - 30% as compared with CES. Although there are no exergy requirements (as a methodology or an indicator) yet in current energy legislations, results underline that exergy assessments may allow to meet the main goal of energy legislations in sustainability of energy supply.

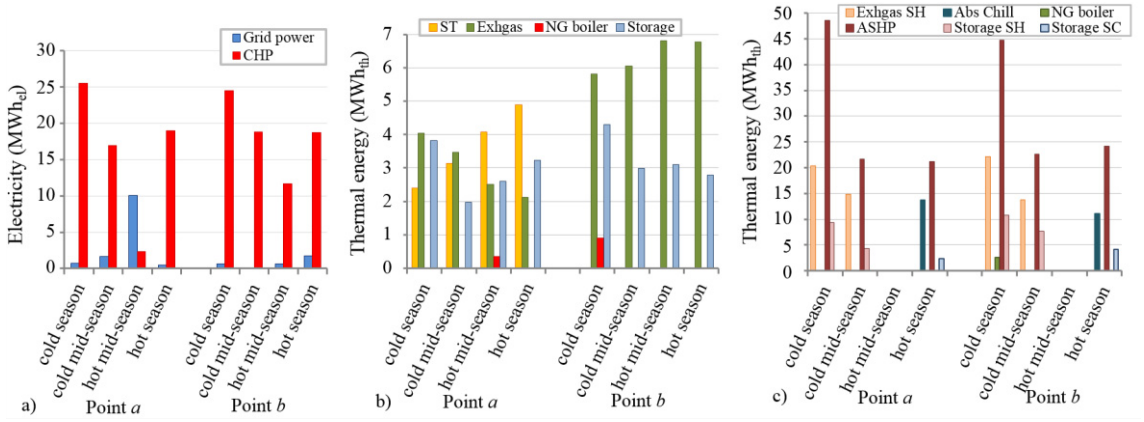

Fig. 3. Operation strategies of the DES in the four season days at points *a* and *b* of the Pareto frontier for a) Electricity, b) DHW, c) SH/SC demand

Acknowledgement

Authors thank ENEA for funding this study within the Italian Research Program *"Ricerca di Sistema Elettrico – PAR 2015*, "Area: Efficienza energetica e risparmio di energia negli usi finali elettrici ed interazione con altri vettori energetici".

References

[1] Kari A, Arto S. Distributed energy generation and sustainable development. *Renew Sustain Energy Rev* 2006;**10**:539–58.

[2] Ren H, Gao W. A MILP model for integrated plan and evaluation of distributed energy systems. *Appl En* 2010;**87**(3):1001-1014.

[3] Ren H, Zhou W, Nakagami KI, Gao W, Wu Q. Multi-objective optimization for the operation of distributed energy systems considering economic and environmental aspects. *Appl En* 2010;**87**(12):3642-3651.

[4] Alarcon-Rodriguez A, Ault G, Galloway G. Multi-objective planning of distributed energy resources: A review of the state-of-the-art. *Renew Sustain Energy Rev* 2010;**14**:1353–66.

[5] ECBCS - Annex 49 - *Low Exergy Systems for High Performance Buildings and Communities*, homepage. Available <http://www.ecbcs.org/annexes/annex49.htm>.

[6] Dincer I, Rosen M. *Exergy-Energy, Environment and Sustainable Development*. 1st Ed., Elsevier Publication, Oxford, UK, (2007).

[7] Di Somma M, Yan B, Bianco N, Luh PB, Graditi G, Mongibello L, Naso V. Operation optimization of a distributed energy system considering energy costs and exergy efficiency. *Energ Convers Manage* 2015;**103**:739-751.

[8] Yan B, Di Somma M, Bianco N, Luh PB, Graditi G, Mongibello L, Naso V. Exergy-based operation optimization of a distributed energy system through the energy-supply chain. *Appl Therm Eng* 2016;**101**:741-751.

[9] Mehleri ED, Sarimveis H, Markatos NC, Papageorgiou LG. A mathematical programming approach for optimal design of distributed energy systems at the neighbourhood level. *Energy* 2012;**44**:396-104.

[10] Hawkes AD, Leach MA. Modelling high level system design and unit commitment for a microgrid. *Appl En* 2009;**86**(7):253-1265.

[11] Omu A, Choudhary R, Boies A. Distributed energy resource system optimisation using mixed integer linear programming. *Energy Policy* 2013:**61**, 249-266.

[12] Zhou Z, Zhang J, Liu P, Li Z, Georgiadis MC, Pistikopoulos EN. A two-stage stochastic programming model for the optimal design of distributed energy systems. *Appl En* 2013;**103**:135-144.

[13] Zhou Z, Liu P, Li Z, Ni W. An engineering approach to the optimal design of distributed energy systems in China. *Appl Therm Eng* 2013;**53**:387-96.

[14] Kotas YJ. *The exergy method for thermal plant analysis*. reprint ed. Malabar, FL: Krieger; 1995.

[15] Mongibello L, Bianco N, Caliano M, Graditi G. Influence of heat dumping on the operation of residential micro-CHP systems. *Appl En* 2015;**160**:206-220.

[16] Barbieri ES, Melino F, Morini M. Influence of the thermal energy storage on the profitability of micro CHP systems for residential building applications. *Appl En* 2012;**97**:714–22.

[17] *ASHRAE International Weather files for Energy Calculations* (IWEC weather files). Users manual and CD-ROM, American Society of Heating, Refrigerating and Air-Conditioning Engineers, Atlanta, GA, USA, 2001.

[18] Darrow, K., Tidball, R., Wang, J., & Hampson, A. 2015. *Catalog of CHP technologies*. Available: https://www.epa.gov/sites/production/files/2015-07/documents/catalog_of_chp_technologies.pdf.

[19] *Technology Data for Energy Plants*. Energinet.dk (2012). Available: http://www.energinet.dk/SiteCollectionDocuments/Danske%20dokumenter/Forskning/Technology_data_for_energy_plants.pdf.

[20] Trudeau N, Francoeur M. *Energy Efficiency indicators for Public Electricity Production from fossil fuels*. OECD/IEA, 2008.

Biography

Marialaura Di Somma received the Ph. D degree in Mechanical Systems Engineering from the Università di Napoli Federico II, Italy, in 2016. She is a research associate at ENEA RC Portici, Italy. Her research interests include design and operation optimization of distributed energy systems through multi-objective criteria.

Applied Energy xxx (2017) xxx–xxx

Contents lists available at ScienceDirect

Applied Energy

journal homepage: www.elsevier.com/locate/apenergy

Multi-objective design optimization of distributed energy systems through cost and exergy assessments ☆

M. Di Somma [a,*], B. Yan [b], N. Bianco [c], G. Graditi [a], P.B. Luh [b], L. Mongibello [a], V. Naso [c]

[a] ENEA, Italian National Agency for New Technologies, Energy and Sustainable Economic Development, CR Portici, 80055 Portici, Italy
[b] Department of Electrical and Computer Engineering, University of Connecticut, Storrs, CT 06269, USA
[c] Dipartimento di Ingegneria Industriale (DII), Università degli studi Federico II, P.le Tecchio, Napoli 80125, Italy

HIGHLIGHTS

- Exergy in design optimization of distributed energy systems (DESs).
- Multi-objective design optimization of DESs through cost and exergy assessments.
- Balancing solutions for planners based on economic and sustainability priorities.
- Cost and primary exergy of DESs reduced by 21–36% as compared with conventional systems.
- Exergy analysis for sustainable development of energy supply systems.

ARTICLE INFO

Article history:
Received 13 January 2017
Received in revised form 6 March 2017
Accepted 22 March 2017
Available online xxxx

Keywords:
Distributed energy system
Design optimization
Multi-objective linear programming
Annual cost
Exergy efficiency

ABSTRACT

In recent years, distributed energy systems (DESs) have been recognized as a promising option for sustainable development of future energy systems, and their application has increased rapidly with supportive policies and financial incentives. With growing concerns on global warming and depletion of fossil fuels, design optimization of DESs through economic assessments for short-run benefits only is not sufficient, while application of exergy principles can improve the efficiency in energy resource use for long-run sustainability of energy supply. The innovation of this paper is to investigate exergy in DES design to attain rational use of energy resources including renewables by considering energy qualities of supply and demand. By using low-temperature sources for low-quality thermal demand, the waste of high-quality energy can be reduced, and the overall exergy efficiency can be increased. The goal of the design optimization problem is to determine types, numbers and sizes of energy devices in DESs to reduce the total annual cost and increase the overall exergy efficiency. Based on a pre-established DES superstructure with multiple energy devices such as combined heat and power and PV, a multi-objective linear problem is formulated. In modeling of energy devices, the novelty is that the entire available size ranges and the variation of their efficiencies, capital and operation and maintenance costs with sizes are considered. The operation of energy devices is modeled based on previous work on DES operation optimization. By minimizing a weighted sum of the total annual cost and primary exergy input, the problem is solved by branch-and-cut. Numerical results show that the Pareto frontier provides good balancing solutions for planners based on economic and sustainability priorities. The total annual cost and primary exergy input of DESs with optimized configurations are reduced by 21–36% as compared with conventional energy supply systems, where grid power is used for the electricity demand, and gas-fired boilers and electric chillers fed by grid power for thermal demand. A sensitivity analysis is also carried out to analyze the influence of energy prices and energy demand variation on the optimized DES configurations.

© 2017 Elsevier Ltd. All rights reserved.

1. Introduction

In recent years, depletion of fossil energy resources and global warming problems have prompted worldwide awareness about sustainability of energy supply. In such context, Distributed Energy Systems (DESs) have been recognized as a promising option for

☆ The short version of the paper was presented at ICAE2016 on Oct 8-11, Beijing, China. This paper is a substantial extension of the short version of the conference paper.

* Corresponding author.
E-mail address: marialaura.disomma@enea.it (M. Di Somma).

http://dx.doi.org/10.1016/j.apenergy.2017.03.105
0306-2619/© 2017 Elsevier Ltd. All rights reserved.

Please cite this article in press as: Di Somma M et al. Multi-objective design optimization of distributed energy systems through cost and exergy assessments. Appl Energy (2017), http://dx.doi.org/10.1016/j.apenergy.2017.03.105

Nomenclature

A	area (m^2)
c	constant in Eq. (34) (kW h/€)
C	cost (€)
C_c	specific capital cost (€/kW) - (€/kW h) - (€/m^2)
$C_{d,hr}$	cooling rate (kW)
COP	coefficient of performance
CRF	capital recovery factor
DR	maximum ramp-down rate (kW)
D_t	length of the time interval (h)
e	minimum part load
$E_{d,hr}$	electricity rate (kW)
ex_{Bio}	specific chemical exergy of biomass (kW h/kg)
ex_{NG}	specific chemical exergy of natural gas (kW h/N m^3)
Ex	exergy (kW h)
$Ex_{d,hr}$	exergy rate (kW)
F_{obj}	objective function
F_q	Carnot factor
G	natural gas volumetric flow rate (N m^3/h)
$H_{d,hr}$	heating rate (kW)
I	total solar irradiance (kW/m^2)
LHV_{Bio}	lower heat value of biomass (kW h/kg)
LHV_{NG}	lower heat value of natural gas (kW h/N m^3)
n_i	total number of energy devices associated with technology i
N	lifetime (years)
OM	O&M cost (€/kW h)
P_{Bio}	biomass price (€/ton)
P_e	electricity price (€/kW h)
P_{NG}	natural gas price (€/N m^3)
r	interest rate
$R_{d,hr}$	energy rate (kW)
S	designed size (kW) – (kW h)
T	temperature (K)
UR	maximum ramp-up rate (kW)
x	binary decision variable

Greek symbols

ε_{gen}	exergy efficiency of electricity generation
ς_{FUEL}	exergy factor of fuel
η	efficiency
φ	storage loss fraction
ψ	overall exergy efficiency
ω	weight in Eq. (34)

Superscript/subscripts

0	reference
Abs	absorption chiller
ASHP	air source heat pump
Bio	biomass
Bioboil	biomass boiler
CHP NGICE	combined heat and power with gas-fired internal combustion engine
CHP NGMTG	combined heat and power with gas-fired micro-turbine
coll	collector
d	day
dem	demand
DHW	domestic hot water
e	electricity
ES	electrical storage
FUEL	fuel
GRID	power grid
hr	hour
i	index of technology
in	input
INV	investment
j	energy carrier
l	range
k_i	energy device associated with technology i
K_i	maximum number of energy devices associated with technology i
max	maximum
min	minimum
NG	natural gas
NGboil	gas-fired boiler
O&M	operation and maintenance
out	output
PV	photovoltaic
req	required
SC	space cooling
SH	space heating
SOLAR	solar
ST	solar thermal
sto	stored
TES	thermal energy storage
th	thermal
TOT	total

Acronyms

CHP	combined heat and power
DES	distributed energy system
MOLP	multi-objective linear programming
O&M	operation and maintenance

sustainable development of future energy systems [1–6]. A DES refers to a multi-input and multi-output energy system, consisting of multiple small-scale technologies, including renewable ones and storage units, providing electric and thermal energy close to end-users [1–8]. Therefore, as compared with conventional energy supply systems, DESs may employ a wide range of technologies, thereby offering the possibility to integrate renewables as well as to recover waste heat from power generation processes for thermal purposes in buildings [2–4]. The application of DESs has increased rapidly in recent years with the supportive government policies and financial incentives [1,3,4,8]. However, to achieve the expected potentials of DESs, it is necessary to determine the system configuration rationally by selecting the appropriate energy devices, and identifying their numbers and sizes, and the corresponding operation strategies, to match energy requirements of a specific end-user [2,9–11]. Design optimization of a DES is therefore essential for future energy planning, and inherently involves multiple and conflicting objectives [12–15]. For instance, the interest of DES developers in achieving a system configuration with lowest costs might conflict with the interest of energy legislations such as the EU ones in increasing sustainability of energy supply, which can be attained by reducing the waste of fossil energy resources and environmental impacts [15,16]. In such a context, a multi-objective approach helps identify balancing solutions to promote participation in the decision-making process and facilitate collective decisions [12].

According to [16], application of exergy principles in building energy supply systems may promote rational use of energy resources, by taking into account the different energy quality levels of energy supply and those of building demand. Electrical and

Please cite this article in press as: Di Somma M et al. Multi-objective design optimization of distributed energy systems through cost and exergy assessments. Appl Energy (2017), http://dx.doi.org/10.1016/j.apenergy.2017.03.105

chemical energy are high-quality energy, whereas low-temperature heat is low-quality energy. In current energy supply systems, energy is commonly supplied as electricity or as fossil energy carriers, whose energy quality is unnecessarily high to meet low-quality thermal demand in buildings, and the First Law of Thermodynamics does not consider the energy quality degradation occurring in such processes. Conversely, based on the Second Law of Thermodynamics, by reducing the supply of high-quality energy for thermal demand in buildings through the usage of low-temperature sources, efficient use of the potential (i.e., quality) of the energy resources is promoted. Since energy resources, and particularly fossil fuels, are limitedly available, better exploiting their potential allows to reduce their waste. In this way, lifetime of fossil fuels can be extended, and the environmental impacts derived from their use can be reduced [16]. In the literature, exergy analysis has been linked to sustainability of energy supply which is essential for the long run, since it clearly identifies the efficiency in energy resource use, by considering their potential; and the importance of including exergy in energy legislations was discussed [16–21]. Exergy was investigated in performance evaluation of single energy supply systems, as cogeneration systems [22–25], renewable energy sources [26,27], various types of heat pumps [28–30], and thermal energy storage [31–33] with the aim to reduce energy quality degradation in designing and managing these systems, thereby improving sustainability of energy supply. DESs provide a great opportunity to demonstrate the effectiveness of exergy analysis in designing more sustainable energy systems since multiple energy resources with different energy quality levels can be used to satisfy user various demand with different quality levels. By using low exergy sources, e.g., solar thermal or waste heat of power generation, for low-quality thermal demand, and high exergy sources for electricity demand, the waste of high-quality energy can be reduced, thereby increasing the overall exergy efficiency of DESs.

In previous work, exergy modeling and optimization were investigated in DES operations through a multi-objective approach [34,35]. Based on fixed DES configurations (types, numbers and sizes of energy devices), optimized operation strategies were established by considering energy costs and exergy efficiency. As for design optimization of DESs, most studies in the literature focused on minimizing the total annual cost (annualized investment costs and annual operating costs of the system) as a crucial objective for DES developers [2,36–42]. Beyond minimizing costs only, design optimization of DESs through multi-objective approach to reduce also environmental impact was analyzed. In [43], a multi-objective linear programming (MOLP) model was established to find the optimal configuration and operation of a DES for an industrial area while reducing the total annual cost and CO_2 emission. The problem was solved by using the compromise programming method. In [44], a MOLP model was developed to optimally design and operate an energy system consisting of buildings equipped with small-size Combined Heat and Power (CHP) plants, with the aim to reduce both annual costs and CO_2 emission. In [45], a general framework was developed to study the application of energy hubs for determining the optimal design and operation of DESs in urban areas according to economic and environmental objectives, and the multi-objective optimization problem was solved by using branch-and-cut. In all the analyzed works, before optimizing the design, "superstructures" were pre-established with energy devices chosen among the most commonly used ones in practical DESs. Moreover, to identify the size of an energy device, several sizes were pre-fixed as possible choices to be selected through binary decision variables [2,36–40,44,45]. However, it is difficult to select the sizes among the almost infinite possible solutions available in the market. Conversely, the size of an energy device was a continuous decision variable within the entire available size range, with efficiencies as well as specific capital and operation and maintenance (O&M) costs assumed constant in the entire size range and their variations with the sizes were not considered [41,42]. The size of an energy device was a continuous decision variable within the entire available size range in [43], with prices and efficiencies approximated as linear functions of the size.

The innovation of this paper is to investigate exergy in DES design optimization through a multi-objective approach to attain rational use of energy resources considering economic and sustainability priorities. A superstructure is pre-established with multiple energy devices, such as CHPs with natural gas-fired internal combustion engines and micro-turbines as prime movers, natural gas and biomass boilers, solar thermal collectors, PV, reversible air-source heat pumps, single-stage absorption chillers, and electrical and thermal energy storage devices. Given user demand includes electricity, domestic hot water, space heating, and space cooling. To take both cost and exergy assessments into account, a MOLP problem is formulated, and the goal is to determine types, numbers and sizes of energy devices in the DES with the corresponding operation strategies on the Pareto frontier, thereby providing different design options for planners based on short- and long-run priorities. In modeling of energy devices, the key novelty is that the entire size ranges available in the market as well as the variations of efficiencies, specific capital and O&M costs with sizes are taken into account, based on a detailed market analysis. These characteristics are usually piecewise linear functions of the device size, which is a continuous decision variable, thereby making the problem nonlinear. To maintain the problem linearity, the key idea is to divide the entire size range of an energy device into several small ranges, so that these characteristics can be assumed constant in each size range. The daily operation of energy devices is modeled based on previous work on operation optimization of DESs [34]. The economic objective is formulated as the total annual cost (total annualized investment cost, total annual O&M and energy cost) to be minimized. The exergetic objective is to maximize the overall exergy efficiency of the DES, defined as the ratio of the total annual exergy required to meet the given energy demand to the total annual primary exergy input to the system. Assuming known the energy demand, the total exergy required to meet the demand is also known. Therefore, the exergetic objective is formulated as the total annual primary exergy input to be minimized. By minimizing a weighted sum of the total annual cost and primary exergy input, the problem is solved by branch-and-cut. The general mathematical formulation established and the optimization method provided could be applicable in real contexts, thereby providing decision support to planners. Given the input data, such as end-user demand, local climate data, energy prices and technical and economic information of the candidate energy devices, the model allows to obtain their optimized combination, and the corresponding operation strategies through cost and exergy assessments. As an illustrative example, the model is implemented for a hypothetic building cluster located in Italy. The optimization is carried out on an hourly basis for four representative season days. Numerical results demonstrate that exergy analysis is a powerful tool for designing more sustainable energy supply systems based on the use of renewables and low-temperature sources for thermal demand in buildings, and that good balancing options for planners are found on the Pareto frontier. Moreover, the total annual cost and primary exergy input of DESs with optimized configurations are significantly reduced, by 21–36% as compared with conventional energy supply systems, where grid power is used for the electricity demand, natural gas boilers for domestic hot water and space heating demand, and electric chillers fed by grid power for space cooling demand. In addition, a sensitivity analysis is carried out to analyze the influence of key parameters such as energy

Please cite this article in press as: Di Somma M et al. Multi-objective design optimization of distributed energy systems through cost and exergy assessments. Appl Energy (2017), http://dx.doi.org/10.1016/j.apenergy.2017.03.105

prices and energy demand variation on the optimized DES configurations and the related economic and exergetic performances.

In the following, Section 2 is on the problem formulation and the optimization method. Numerical testing is presented and discussed in Section 3. Sensitivity analysis is presented in Section 4.

2. Problem formulation and optimization method

The superstructure of the DES under consideration is shown in Fig. 1. The energy devices are chosen among the most commonly used ones in practical DESs.

Electricity demand and electricity required by heat pumps can be satisfied by grid power, by the electricity provided by CHPs with natural gas-fired internal combustion engines and micro-turbines as prime movers, PV, and by the electricity discharged from the electrical storage. It is assumed that all the electricity provided by CHPs and PV is self-consumed, while no extra electricity is sold back to the power grid. Domestic hot water demand can be satisfied by thermal energy provided by CHPs, natural gas and biomass boilers, solar thermal collectors, and by thermal energy discharged from the storage. Space heating demand can be satisfied by thermal energy provided by CHPs, natural gas and biomass boilers, heat pumps, and by thermal energy discharged from the storage. Space cooling demand can be satisfied by thermal energy provided by CHPs, natural gas and biomass boilers through the absorption chillers, heat pumps, and by thermal energy discharged from the storage.

In the following, the decision variables are first introduced in Section 2.1. The economic and exergetic objectives are presented in nd 2.22.3, respectively. The constraints are established in Section 2.4. The optimization method is discussed in Section 2.5.

2.1. Decision variables

In the optimization problem, the decision variables include: existence, numbers, and sizes of energy devices; operation status (on/off) and energy rates provided by energy devices; capacities of electrical and thermal storage devices; electricity and heat rate input and output to/from electrical and thermal storage devices, respectively; and electricity rate bought from the power grid. Existence and operation status of energy devices are binary. Numbers of energy devices are also determined through binary decision variables to be explained later. All the other decision variables are continuous.

2.2. Economic objective

The economic objective is to minimize the total annual cost of the DES, C_{TOT}, formulated as the sum of the total annualized investment cost, and the total annual O&M and energy costs:

$$C_{TOT} = C_{INV} + C_{O\&M} + C_{FUEL} + C_{GRID}, \quad (1)$$

where C_{INV} is the annualized investment cost of all energy devices in the DES; $C_{O\&M}$ is the total annual O&M cost of all energy devices; C_{FUEL} is the total annual cost of consumed fuels; and C_{GRID} is the annual cost of purchasing electricity from the power grid.

The total annualized investment cost of the energy devices is formulated as:

$$C_{INV} = \sum_i \sum_{k_i}^{K_i} CRF_i \left(C_{c,i} S_{i,k_i}\right),$$
$$CRF_i = r(1+r)^{N_i} / \left[(1+r)^{N_i} - 1\right], \quad (2)$$

where CRF_i is the capital recovery factor of technology i; K_i is the maximum number of energy devices associated with technology i, which is assumed to be known; k_i is the energy device associated with technology i; S_{i,k_i} is the designed size of device k_i; $C_{c,i}$ is the specific capital cost; r is the interest rate; and N_i is the lifetime. The size of electrical and thermal energy storage devices represents the capacity expressed in kW h, and the specific capital cost is expressed in €/kW h. The size of the solar thermal collectors is expressed in terms of the total surface of collectors to be installed, and the specific capital cost is expressed in €/m^2.

The total annual O&M cost of energy devices is formulated as:

$$C_{O\&M} = \sum_i \sum_{k_i}^{K_i} \sum_d \sum_{hr} OM_i R_{i,k_i,d,hr} D_t, \quad (3)$$

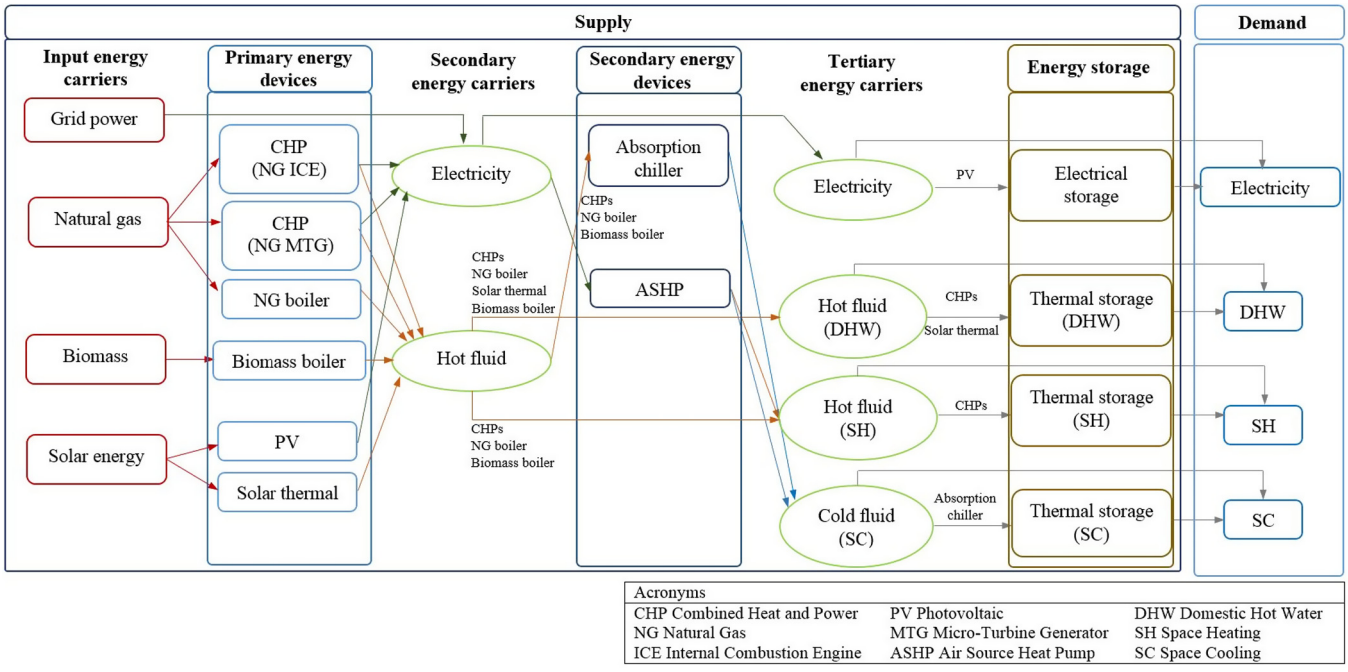

Fig. 1. Superstructure representation of the DES for the design optimization problem.

Please cite this article in press as: Di Somma M et al. Multi-objective design optimization of distributed energy systems through cost and exergy assessments. Appl Energy (2017), http://dx.doi.org/10.1016/j.apenergy.2017.03.105

where OM_i is the O&M cost of the technology i; $R_{i,k_i,d,hr}$ is the energy rate provided by the energy device k_i at hour hr of day d; and D_t is the length of the time interval (1 h). For electrical and thermal storage devices, the O&M costs are based on their capacities.

The total annual cost of the consumed fuels is formulated as:

$$C_{FUEL} = \sum_{i\in\{CHP\,NGICE,\ CHP\,NGMTG,\ NG\,boil\}} \sum_{k_i}^{K_i} \sum_{d} \sum_{hr} P_{NG}\left(R_{i,k_i,d,hr}/(\eta_i LHV_{NG})\right) D_t + \sum_{i\in\{Bioboil\}} \sum_{k_i}^{K_i} \sum_{d} \sum_{hr} P_{Bio}\left(R_{i,k_i,d,hr}/(\eta_i LHV_{Bio})\right) D_t, \quad (4)$$

where η_i is the energy efficiency (thermal or electrical); P_{NG} and P_{Bio} are the price of natural gas and biomass, respectively; and LHV_{NG} and LHV_{Bio} are the lower heat value of natural gas and biomass, respectively.

The annual cost of purchased grid power is formulated as:

$$C_{GRID} = \sum_{d}\sum_{hr} P_{e,hr} E_{GRID,d,hr} D_t, \quad (5)$$

where $P_{e,hr}$ is the time-of-day unit price of electricity from the power grid, and $E_{GRID,d,hr}$ is the electricity rate taken from the grid.

2.3. Exergetic objective

The exergetic objective is to maximize the overall exergy efficiency of the DES, ψ, defined as the ratio of the total annual exergy output, Ex^{out}, to the total annual primary exergy input, Ex_{in} [34,46,47]:

$$\psi = Ex^{out}/Ex_{in}. \quad (6)$$

The total annual exergy output is the total annual exergy required to meet the given user demand in the whole year, formulated as:

$$Ex^{out} = \sum_{dem}\sum_{d}\sum_{hr} Ex^{dem}_{d,hr} D_t, \quad dem \in \{e, DHW, SH, SC\}, \quad (7)$$

where $Ex^{dem}_{d,hr}$ is the total exergy rate required to meet the electricity and thermal demand (domestic hot water, and space heating and cooling). In buildings, energy demands are characterized by different energy quality levels. To meet the electricity demand, the highest quality of energy is needed. The exergy rate required to meet the electricity demand, $Ex^{e}_{d,hr}$, can be evaluated as follows [34,35,48]:

$$Ex^{e}_{d,hr} = E^{e}_{d,hr}, \quad \forall d, \forall hr, \quad (8)$$

where $E^{e}_{d,hr}$ is the electricity demand rate.

As for thermal demand, the energy quality depends on temperature required – the lower the temperature required, the lower the exergy [16,48]. The exergy rate required to meet the demand of domestic hot water can be formulated as:

$$Ex^{DHW}_{d,hr} = H^{DHW}_{d,hr} F^{DHW}_{q,d,hr}, \quad \forall d, \forall hr, \quad (9)$$

where $H^{DHW}_{d,hr}$ is the heat demand rate for domestic hot water, and $F^{DHW}_{q,d,hr}$ is the Carnot factor, formulated as [16,34,35,48]:

$$F^{DHW}_{q,d,hr} = 1 - T_{0,d,hr}/T^{DHW}_{req}, \quad \forall d, \forall hr, \quad (10)$$

which depends on both the temperature required for the domestic hot water, T^{DHW}_{req}, which is assumed to be known based on [49], and the reference temperature, $T_{0,d,hr}$, assumed to be known as the averaged ambient temperature at hour hr of day d [16,34]. The exergy rate required to meet the demand of space heating and cooling can be formulated similarly.

At the supply side, the input energy carriers are grid power, natural gas, biomass, and solar energy. The total annual primary exergy input is formulated as:

$$Ex_{in} = \sum_{j}\sum_{d}\sum_{hr} Ex_{j,d,hr} D_t, \quad j \in \{GRID, FUEL, SOLAR\}, \quad (11)$$

where $Ex_{j,d,hr}$ is the exergy rate input to the DES related to the energy carrier j. As well as for the demand side, also the supply side is characterized by different energy quality levels.

Electricity from the power grid is an energy carrier provided by power generation plants, and the exergy input rate to the DES, $Ex_{GRID,d,hr}$, depends on the exergy efficiency of the plants, ε_{gen} [34,35]:

$$Ex_{GRID,d,hr} = E_{GRID,d,hr}/\varepsilon_{gen}, \quad \forall d, \forall hr, \quad (12)$$

The exergy input rates of fuels (natural gas and biomass) depend on their specific chemical exergy:

$$Ex_{FUEL,d,hr} = \sum_{i\in\{CHP\,NGICE,\ CHP\,NGMTG,\ NGboil\}} \sum_{k_i}^{K_i} ex_{NG}(R_{i,k_i,d,hr}/(\eta_i LHV_{NG})) + \sum_{i\in\{Bioboil\}} \sum_{k_i}^{K_i} ex_{Bio}(R_{i,k_i,d,hr}/(\eta_i LHV_{Bio})),$$
$$ex_{FUEL} = \varsigma_{FUEL} LHV_{FUEL}, \quad FUEL \in \{NG, Bio\}, \forall d, \forall hr, \quad (13)$$

where ex_{FUEL} is the specific chemical exergy of the fuel, and ς_{FUEL} is the exergy factor [50].

As for solar energy, thermal energy output of the solar thermal collectors at the corresponding temperature levels, and electricity output of PV are considered as the primary energy sources [51,52], respectively. The exergy input rate to solar thermal collectors, $Ex_{ST,d,hr}$, is formulated as:

$$Ex_{ST,d,hr} = H_{ST,d,hr}(1 - T_{0,d,hr}/T^{out}_{coll}), \ \forall d, \ \forall hr, \quad (14)$$

where $H_{ST,\,d,\,hr}$ is the heat rate provided by solar thermal collectors, and $T_{0,d,hr}$ and T^{out}_{coll} are the reference temperature, assumed as the averaged ambient temperature at hour h of day d [16,34], and the temperature of the heat transfer fluid at the exit of the collector field (assumed constant), respectively.

The exergy input rate to PV, $Ex_{PV,d,hr}$, is formulated as:

$$Ex_{PV,d,hr} = E_{PV,d,hr}, \quad \forall d, \ \forall hr. \quad (15)$$

where $E_{PV,\,d,\,hr}$ is the electricity rate provided by PV.

Therefore, the exergy rate of solar energy input to the DES is formulated as:

$$Ex_{SOLAR,d,hr} = Ex_{ST,d,hr} + Ex_{PV,d,hr}, \quad \forall d, \forall hr. \quad (16)$$

Since energy demand as well as the temperatures required for the demand of domestic hot water, and space heating and cooling are assumed known, the total exergy required to meet the demand is also known, and the overall exergy efficiency can be increased by reducing the total primary exergy input. Therefore, the exergetic objective is formulated as the total annual primary exergy input to the DES to be minimized as in Eq. (11).

2.4. Constraints

The constraints in the optimization problem include design constraints, energy balances and operation constraints, as discussed below.

Please cite this article in press as: Di Somma M et al. Multi-objective design optimization of distributed energy systems through cost and exergy assessments. Appl Energy (2017), http://dx.doi.org/10.1016/j.apenergy.2017.03.105

2.4.1. Design constraints

The designed size of the energy device k_i has to be within the minimum and maximum sizes of the related technology $S_i^{\min}$ and $S_i^{\max}$ available in the market:

$$S_i^{\min} x_{i,k_i} \leqslant S_{i,k_i} \leqslant S_i^{\max} x_{i,k_i}, \quad k_i \leqslant K_i, \quad n_i = \sum_{k_i}^{K_i} x_{i,k_i}, \quad \forall i, \tag{17}$$

where x_{i,k_i} is a binary decision variable, which is equal to 1 if the device k_i is implemented in the DES configuration; and n_i is the total number of energy devices associated with technology i implemented in the DES configuration. As for solar collector and PV arrays, the total designed area has to be lower than the available one. In the design optimization problem, the entire size range available in the market as well as the variations of efficiencies, specific capital and O&M costs with sizes, are taken into account. These characteristics are usually piecewise linear functions of the size, which is a continuous decision variable, thereby making the problem nonlinear. To avoid this, the key idea is to divide the entire size range of an energy device into several small ranges, so that these characteristics can be assumed constant in each size range. Consider CHP with a natural gas-fired internal combustion engine as an example. The designed size of CHP in range l is limited by its minimum and maximum values $S_{CHP\,NGICE}^{\min,l}$ and $S_{CHP\,NGICE}^{\max,l}$ in this range:

$$S_{CHP\,NGICE}^{\min,l} x_{k_{CHP\,NGICE}}^{l} \leqslant S_{k_{CHP\,NGICE}}^{l} \leqslant S_{CHP\,NGICE}^{\max,l} x_{k_{CHP\,NGICE}}^{l},$$
$$\sum_{l} x_{k_{CHP\,NGICE}}^{l} \leqslant 1, \quad \forall l, k_{CHP\,NGICE} \leqslant K_{CHP\,NGICE}, \tag{18}$$

where $S_{k_{CHP\,NGICE}}^{l}$ and $x_{k_{CHP\,NGICE}}^{l}$ are defined similarly as in Eq. (17) in range l. Also the summation of binary decision variables $x_{k_{CHP\,NGICE}}^{l}$ over l has to be smaller than or equal to 1, ensuring that at most one range can be selected for each energy device associated to each technology.

2.4.2. Energy balances

To satisfy the given user demand, electricity, domestic hot water, and space heating and cooling energy balances are formulated in the following.

For electricity, the sum of the electricity demand and the total electricity required by the reversible air source heat pumps has to be satisfied by the sum of the total electricity provided by CHPs, PV, grid power, and electrical storage:

$$E_{d,hr}^{e} + \sum_{k_{ASHP}} E_{k_{ASHP},d,hr} = E_{PV,d,hr} + \sum_{k_{CHP\,NGICE}} E_{k_{CHP\,NGICE},d,hr} + \sum_{k_{CHP\,NGMTG}} E_{k_{CHP\,NGMTG},d,hr} + E_{GRID,d,hr} + E_{ES,d,hr}^{e,out} - E_{ES,d,hr}^{e,in}, \quad \forall d, hr, \tag{19}$$

where $E_{ES,d,hr}^{e,out}$ and $E_{ES,d,hr}^{e,in}$ are the electricity rates discharged and charged from/to the storage, respectively, which are both continuous decision variables.

For the domestic hot water demand, the demand has to be satisfied by the total thermal energy provided by CHPs, natural gas and biomass boilers, solar thermal collectors, and thermal storage:

$$H_{d,hr}^{DHW} = \sum_{k_{CHP\,NGICE}} H_{k_{CHP\,NGICE},d,hr}^{DHW} + \sum_{k_{CHP\,NGMTG}} H_{k_{CHP\,NGMTG},d,hr}^{DHW} + \sum_{k_{NGboil}} H_{k_{NGboil},d,hr}^{DHW} + \sum_{k_{Bioboil}} H_{k_{Bioboil},d,hr}^{DHW} + H_{ST,d,hr} + H_{TES,d,hr}^{DHW,out} - H_{TES,d,hr}^{DHW,in}, \quad \forall d, hr, \tag{20}$$

where $H_{TES,d,hr}^{DHW,out}$ and $H_{TES,d,hr}^{DHW,in}$ are the heat rates discharged and charged from/to the storage, respectively, which are both continuous decision variables.

The space heating and space cooling energy balances are formulated in a similar way.

2.4.3. Operation constrains

For most of the energy devices included in the DES superstructure, the common constraint is the capacity constraint. The energy rate provided by each energy device is limited by its minimum part load and the capacity, if the device is on. Still considering the CHP with a natural gas-fired internal combustion engine as an example, the electricity rate, $E_{k_{CHP\,NG\,ICE},d,hr}$, is limited by the minimum and maximum rated output $E_{k_{CHP\,NG\,ICE}}^{\min}$ and $E_{k_{CHP\,NG\,ICE}}^{\max}$, if the device is on:

$$E_{k_{CHP\,NG\,ICE}}^{\min} x_{k_{CHP\,NG\,ICE},d,hr} \leqslant E_{k_{CHP\,NG\,ICE},d,hr} \leqslant E_{k_{CHP\,NG\,ICE}}^{\max} x_{k_{CHP\,NG\,ICE},d,hr}, \quad \forall k_{CHP\,NGICE}, \quad \forall d, hr, \tag{21}$$

where $x_{k_{CHP\,NG\,ICE},d,hr}$ is the on/off status of CHP. The minimum part load and the maximum rated output are obtained based on the design capacity of CHP as follows:

$$E_{k_{CHP\,NG\,ICE}}^{\min} = e_{k_{CHP\,NG\,ICE}} \sum_{l} S_{k_{CHP\,NG\,ICE}}^{l}, \quad E_{k_{CHP\,NG\,ICE}}^{\max} = \sum_{l} S_{k_{CHP\,NG\,ICE}}^{l}, \quad \forall k_{CHP\,NG\,ICE}, \tag{22}$$

where $e_{k_{CHP\,NG\,ICE}}$ is the minimum part load expressed in percentage of the designed size. The product of one continuous and one binary decision variables is linearized in a standard way [53].

In the following, the additional constraints of each energy device are presented.

2.4.3.1. CHP systems. Two types of CHPs are involved in the DES superstructure, i.e., CHPs with gas-fired internal combustion engine and with micro-turbines. They consist of prime movers to meet the electricity load, and heat recovery units providing thermal energy to meet the demand of domestic hot water and space heating, and to meet the demand of space cooling through absorption chillers. Operation constraints for CHPs with gas-fired internal combustion engine as prime mover are presented below.

The ramp rate constraint limits the variations in the power generation between two successive time steps to be within the ramp-down, $DR_{k_{CHP\,NGICE}}$, and ramp-up, $UR_{k_{CHP\,NGICE}}$ [34,54]:

$$DR_{k_{CHP\,NGICE}} \leqslant E_{k_{CHPNGICE},d,hr} - E_{k_{CHPNGICE},d,hr-1} \leqslant UR_{k_{CHPNGICE}}, \quad \forall k_{CHP\,NG\,ICE}, \quad \forall d, hr, \tag{23}$$

where the ramp-down and the ramp-up and are expressed in percentage of the designed size.

The volumetric flow rate of natural gas, $G_{k_{CHP\,NGICE},d,hr}$, required by the CHP to provide the electricity rate, $E_{k_{CHP\,NG\,ICE},d,hr}$, is formulated as:

$$G_{k_{CHP\,NGICE},d,hr} = E_{k_{CHP\,NGICE},d,hr} / (\eta_{e,k_{CHP\,NGICE}} LHV_{NG}), \quad \forall k_{CHP\,NGICE}, \quad \forall d, hr. \tag{24}$$

In the above, $\eta_{e,k_{CHP\,NGICE}}$ is the electrical efficiency of the CHP, formulated as:

$$\eta_{e,k_{CHP\,NGICE}} = \sum_{l} x_{k_{CHP\,NGICE}}^{l} \eta_{e,k_{CHP\,NGICE}}^{l}, \quad \forall k_{CHP\,NGICE}, \tag{25}$$

where $\eta_{e,k_{CHP\,NGICE}}^{l}$ is the electrical efficiency of the CHP in the range l.

The heat rate recovered from the CHP, $H_{k_{CHP\,NGICE},d,hr}$, is formulated as:

$$H_{k_{CHP\,NGICE},d,hr} = E_{k_{CHP\,NGICE},d,hr} \eta_{th,k_{CHP\,NGICE}} / \eta_{e,k_{CHP\,NGICE}}, \quad \forall k_{CHP\,NGICE}, \quad \forall d, hr, \tag{26}$$

where $\eta_{th,k_{CHP\,NGICE}}$ is the thermal efficiency of the CHP defined similarly as in Eq. (25).

Please cite this article in press as: Di Somma M et al. Multi-objective design optimization of distributed energy systems through cost and exergy assessments. Appl Energy (2017), http://dx.doi.org/10.1016/j.apenergy.2017.03.105

The heat rate recovered by CHP is subdivided to meet the demand of domestic hot water and space heating, and to meet the demand of space cooling through the absorption chillers:

$$H_{k_{CHP\,NGICE},d,hr} = H^{DHW}_{k_{CHP\,NGICE},d,hr} + H^{SH}_{k_{CHP\,NGICE},d,hr} + H^{SC}_{k_{CHP\,NGICE},d,hr}, \quad \forall k_{CHP\,NGICE}, \quad \forall d, hr. \tag{27}$$

Constraints for CHPs with micro-turbines as prime movers are similar to those formulated above.

2.4.3.2. Boilers. Natural gas and biomass boilers may be involved to meet the demand of domestic hot water, space heating, and to meet the demand of space cooling through absorption chillers. Operation constraints for gas-fired boilers are presented below.

The volumetric flow rate of natural gas, $G_{k_{NGBoil},d,hr}$, required by the gas-fired boiler to provide the heat rate, $H_{k_{NGBoil},d,hr}$, is formulated as:

$$G_{k_{NGBoil},d,hr} = H_{k_{NGBoil},d,hr}/(\eta_{th,k_{NGBoil}} LHV_{NG}), \quad \forall k_{NGBoil}, \quad \forall d, hr, \tag{28}$$

where $\eta_{th,k_{NGBoil}}$ is the thermal efficiency of the boiler defined similarly as in Eq. (25). The heat rate provided by the boiler is subdivided to meet the demand of domestic hot water and space heating, and to meet the demand of space cooling through the absorption chillers:

$$H_{k_{NGBoil},d,hr} = H^{DHW}_{k_{NGBoil},d,hr} + H^{SH}_{k_{NGBoil},d,hr} + H^{SC}_{k_{NGBoil},d,hr}, \quad \forall k_{k_{NGBoil}}, \quad \forall d, hr. \tag{29}$$

Constraints for biomass boilers are similar to those formulated above.

2.4.3.3. Solar energy systems. Solar PV and solar thermal collectors may be involved to meet the electricity load and the domestic hot water demand, respectively.

The electricity rate provided by solar PV, $E_{PV,d,hr}$, is formulated as [36,55]:

$$E_{PV,d,hr} = A_{PV}\eta_{PV} I_{d,hr}, \quad \forall d, hr, \tag{30}$$

where A_{PV} is the total area to be installed, η_{PV} is the electrical efficiency, and $I_{d,hr}$ is the hourly solar irradiance in day d.

The heat rate provided by solar thermal collectors can be expressed in a similar way.

2.4.3.4. Absorption chiller. Absorption chillers may be involved to meet the demand of space cooling, powered by the total thermal energy recovered from CHPs, and provided by natural gas and biomass boilers. The cooling rate provided by the absorption chiller, $C_{k_{Abs},d,hr}$, is expressed as:

$$C_{k_{Abs},d,hr} = \left(\sum_{k_{CHP\,NGICE}} H^{SC}_{k_{CHP\,NGICE},d,hr} + \sum_{k_{CHP\,NGMTG}} H^{SC}_{k_{CHP\,NGMTG},d,hr} + \sum_{k_{NGboil}} H^{SC}_{k_{NGboil},d,hr} + \sum_{k_{Bioboil}} H^{SC}_{k_{Bioboil},d,hr} \right) COP_{k_{Abs}}, \quad \forall k_{Abs}, \quad \forall d, hr, \tag{31}$$

where $COP_{k_{Abs}}$ is the coefficient of performance of the absorption chiller defined similarly as in Eq. (25).

2.4.3.5. Reversible air source heat pump. Reversible air source heat pumps may be involved to meet the space heating and cooling demand in heating and cooling mode, respectively. In the heating mode, the electricity rate required by the air source heat pump, $E^{SH}_{k_{ASHP},d,hr}$, to provide the heat rate, $H^{SH}_{k_{ASHP},d,hr}$, is formulated as:

$$E^{SH}_{k_{ASHP},d,hr} = H^{SH}_{k_{ASHP},d,hr}/COP^{SH}_{k_{ASHP}}, \quad \forall k_{ASHP}, \quad \forall d, hr, \tag{32}$$

where $COP^{SH}_{k_{ASHP}}$ is the coefficient of performance of the heat pump in the hating mode defined similarly as in Eq. (25).

Modeling of cooling mode is similar to that of heating described above.

2.4.3.6. Energy storage devices. For the operation of energy storage devices, the amount of energy stored at the beginning of each time interval equals the non-dissipated energy stored at the beginning of the previous time interval (based on the storage loss fraction), plus the net energy flow (energy input rate to the storage minus energy output rate from the storage) [2,34]. For the electrical energy storage, it can be expressed as:

$$E^{e,sto}_{ES,d,hr} = E^{e,sto}_{ES,d,hr-1}(1 - \varphi_{ES}(D_t)) + (E^{e,in}_{ES,d,hr} - E^{e,out}_{ES,d,hr})D_t, \quad \forall d, hr, \tag{33}$$

where $\varphi_{ES}(D_t)$ is the loss fraction, which takes into account the dissipated energy during the time interval, D_t.

Modeling of thermal storage systems for domestic hot water, and space heating and cooling is similar to that described above.

2.5. Optimization method

With the exergetic objective function formulated in Eq. (11) and the economic one formulated in Eq. (1), the problem has two objective functions to be minimized. To solve this multi-objective optimization problem, a single objective function is formulated as a weighted sum of the total annual cost, C_{TOT}, and the total annual primary exergy input, Ex_{in}, to be minimized:

$$F_{obj} = c\omega C_{TOT} + (1 - \omega)Ex_{in}, \tag{34}$$

where constant c is a scaling factor, chosen such that $c\,C_{TOT}$ and Ex_{in} have the same order of magnitude. The Pareto frontier is found by varying the weight ω in the interval 0–1. The solution that minimizes the total annual cost can be found when $\omega = 1$, whereas the one that minimizes the total annual primary exergy input (i.e., maximizes the overall exergy efficiency) can be found when $\omega = 0$. The problem formulated above is linear, and involves both discrete and continuous variables. Branch-and-cut, which is powerful for mixed-integer linear problems, is therefore used.

3. Numerical testing

The method developed in Section 2 is implemented by using IBM ILOG CPLEX Optimization Studio Version 12.6. A hypothetic cluster of 30 buildings of residential sector located in Turin (Italy) is chosen as the targeted end-user. The optimization is carried out on an hourly basis for a representative day per season to reduce the variables number and the model complexity [2,41,42].

In the following, the input data are described in Section 3.1. The Pareto frontier is presented in Section 3.2. The optimized DESs configurations obtained under the economic and exergetic optimization as well as under two representative trade-off points on the Pareto frontier are compared in Section 3.3. The operation strategies of the energy devices in the optimized DES configurations under the economic and exergetic optimization are presented in Section 3.4.

3.1. Input data

The required input data include energy demand of the building cluster, solar energy availability, prices and exergy factors of primary energy carriers, and technical and economic information of energy devices as presented in the following.

Please cite this article in press as: Di Somma M et al. Multi-objective design optimization of distributed energy systems through cost and exergy assessments. Appl Energy (2017), http://dx.doi.org/10.1016/j.apenergy.2017.03.105

3.1.1. Energy demand of the building cluster

Each building is assumed to have a surface area of 5000 m^2, and a shape factor S/V of 0.5 m^{-1}. The hourly energy rate demand for electricity, domestic hot water, space heating, and space cooling of the building cluster for four representative season days are built based on [56–58], as shown in Fig. 2. To compute the annual energy requirements of the building cluster, the year is assumed to include 90 days in the cold season (December – February), 92 days in the cold mid-season (October 15 – November 30, and March 1 – April 15), 91 days in the hot mid-season (April 15 – May 31, and September 1 – October 15), and 92 days in the hot season (June – August). This assumption is based on the climatic characteristics of the zone, and on the period established by the current Italian law when it is possible to turn on the heating systems in the relative climatic zone (from mid-October to mid-April). Table 1 shows the annual energy requirements of the building cluster.

3.1.2. Solar energy availability

Information about solar energy is taken from the meteorological data in Turin [59]. The hourly solar irradiance on a 35° tilted surface for each representative season day is evaluated as the average of the hourly mean values of the solar irradiance in the corresponding hour of all days in the relative season. The average hourly solar irradiance profiles for the four representative season days are shown in Fig. 3. The maximum available area for installation of solar collector and PV arrays is assumed as 5000 m^2.

3.1.3. Prices and exergy factors of primary energy carriers

Energy prices are chosen according to the Italian market. The unit price of grid power is assumed as 0.15 €/kW h, whereas the unit prices of natural gas and biomass (wood pellet) are assumed as 0.477 €/N m^3, and 120 €/ton, respectively. The exergy efficiency of power generation plants is assumed as 0.40, based on the fossil fuel energy mix for electricity production and on the average efficiency of fossil fuel-fired electricity production in Italy [60,61]. The exergy factors of natural gas and biomass are assumed as 1.04 and 1.16 [50], respectively. In the evaluation of the Carnot factor for the solar exergy input rate (Eq. (14)), the temperature of the heat transfer fluid at the exit of the collector field is assumed constant and equal to 353.15 K.

Table 1
Annual energy requirements of the building cluster (MW h).

Season	Electricity	Domestic hot water	Space heating	Space cooling
Cold	1114	544.3	6227	0
Cold-mid	1139	556.4	3378	0
Hot-mid	1126	550.3	0	0
Hot	1139	556.4	0	3235

3.1.4. Technical and economic information of energy devices

The technical and economic information of energy devices are summarized in Table 2, and they are based on a detailed market analysis [36–38,44,62–69]. For each energy device, Table 2 shows: the minimum and maximum sizes, specific capital costs, O&M costs, efficiencies and lifetime. For CHPs, specific capital costs, O&M costs as well as electrical and thermal efficiencies strongly vary with the sizes. For CHPs with gas-fired internal combustion engine and with micro-turbines, the entire size ranges available in the market are divided into several small ranges, respectively, while the characteristics assumed in each size range are shown in Fig. 4a and b [62,64,68]. Similarly, the capital cost of single-stage absorption chillers is also subject to economies of scale, and the specific capital cost assumed in each size range is shown in Fig. 5 [64,68]. Conversely, O&M costs and efficiencies are assumed constant and equal to the average values in the size range, due to the slight variation of these characteristics with sizes. For

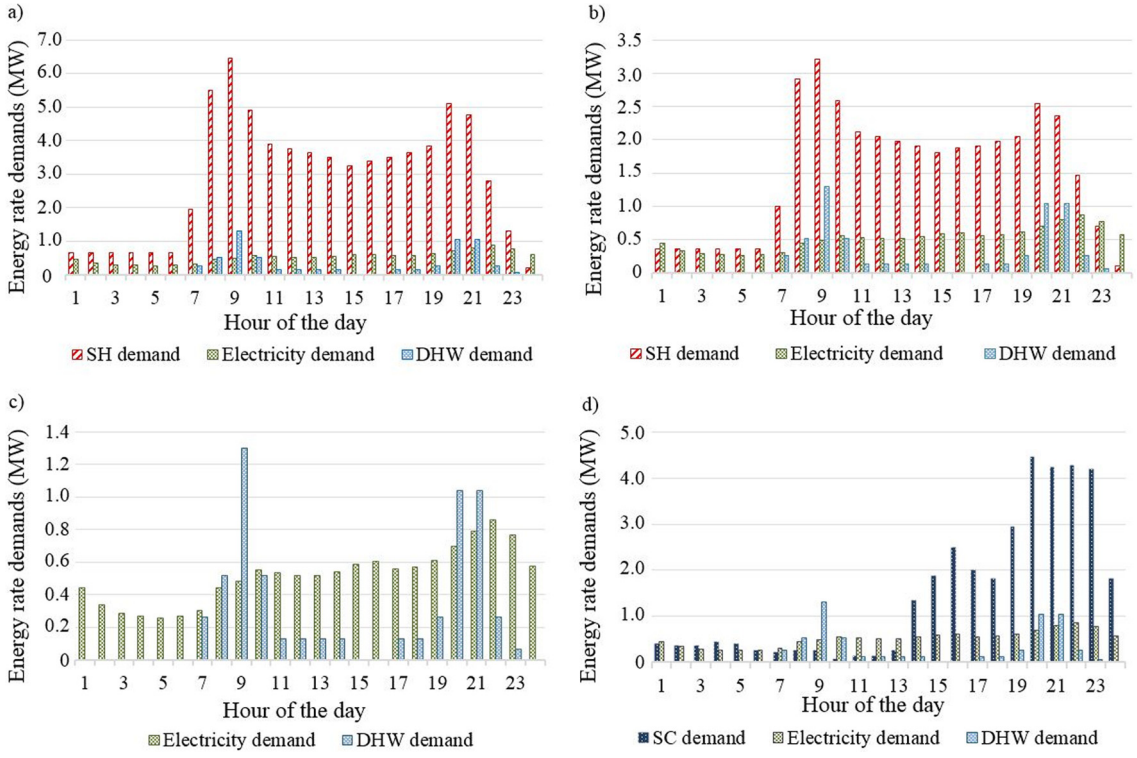

Fig. 2. Hourly mean energy rate demand of the hypothetic building cluster: (a) a representative cold season day; (b) a representative cold mid-season day; (c) a representative hot mid-season day; and (d) a representative hot season day.

Please cite this article in press as: Di Somma M et al. Multi-objective design optimization of distributed energy systems through cost and exergy assessments. Appl Energy (2017), http://dx.doi.org/10.1016/j.apenergy.2017.03.105

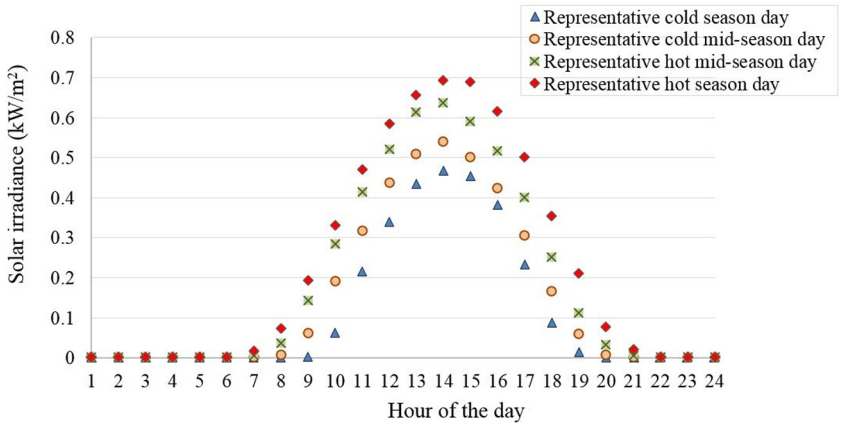

Fig. 3. Average hourly solar irradiance profiles for the four representative season days.

Table 2
Technical and economic information of energy devices.

Energy device	Size range (kW)	Specific capital cost	O&M costs (€/kW h)	Efficiency		Lifetime
				Electrical	Thermal	
CHP NG ICE	20–5000	840–1495 €/kW	0.008–0.023	0.28–0.41	0.40–0.68	20
CHP NG MTG	30–300	1630–2492 €/kW	0.011–0.019	0.26–0.32	0.44–0.52	20
NG boiler	10–2000	100 €/kW	0.0014		0.9	15
Biomass boiler	10–2000	400 €/kW	0.0027		0.85	15
Solar PV	–	2000 €/kW_p	0.010		0.14	30
Solar thermal	–	200 €/m^2	0.0057		0.6	15
Air-source heat pump	10–5000	460 €/kW	0.0025		COP^{SH} = 3.5 COP^{SC} = 3.0	20
Absorption chiller	10–5000	230–510 €/kW	0.0020		COP = 0.8	20
Electrical storage	–	350 €/kW h	0.005	φ_{ES} = 0.25		5
Thermal storage	–	20 €/kW h	0.0012		φ_{TES} = 0.05	20

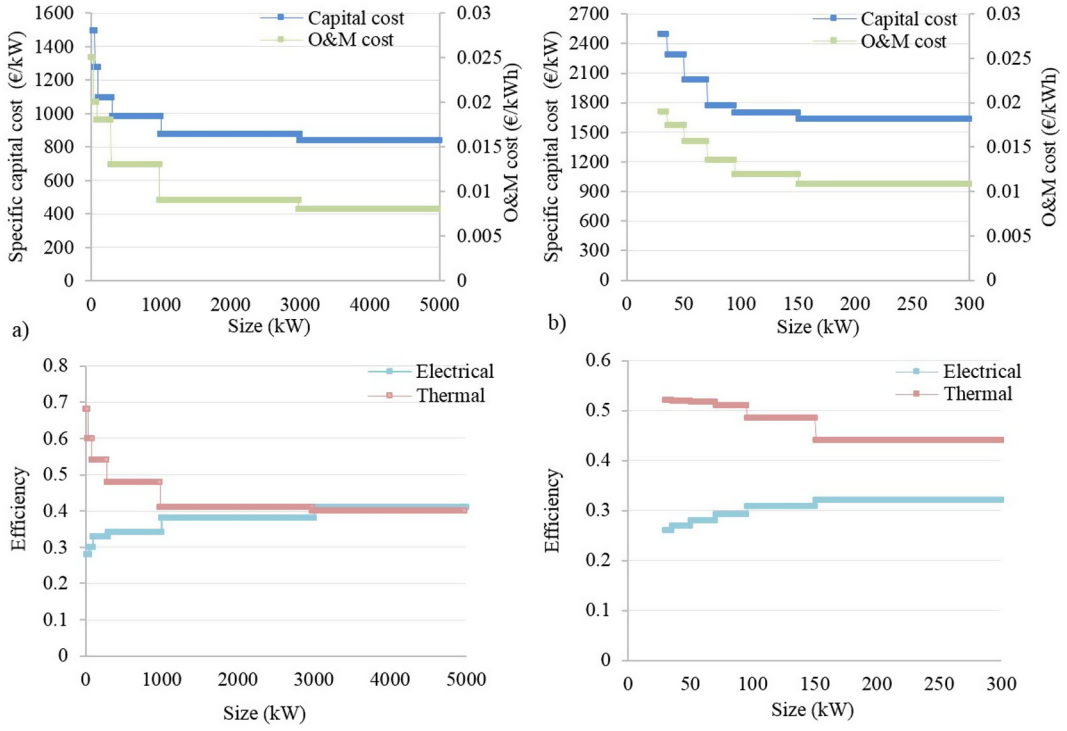

Fig. 4. Specific capitals costs and efficiencies vs. sizes of: (a) CHP with gas-fired internal combustion engine and (b) CHP with gas-fired micro-turbines.

Please cite this article in press as: Di Somma M et al. Multi-objective design optimization of distributed energy systems through cost and exergy assessments. Appl Energy (2017), http://dx.doi.org/10.1016/j.apenergy.2017.03.105

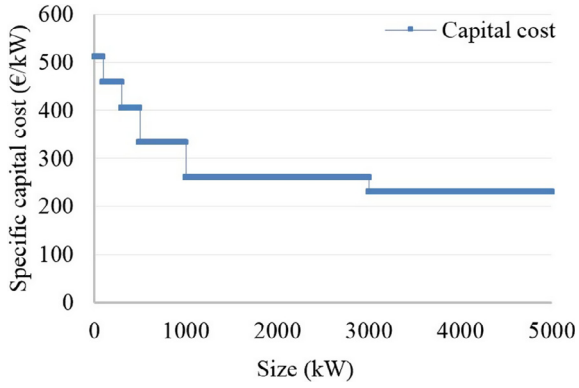

Fig. 5. Specific capital cost vs. size of single-stage absorption chillers.

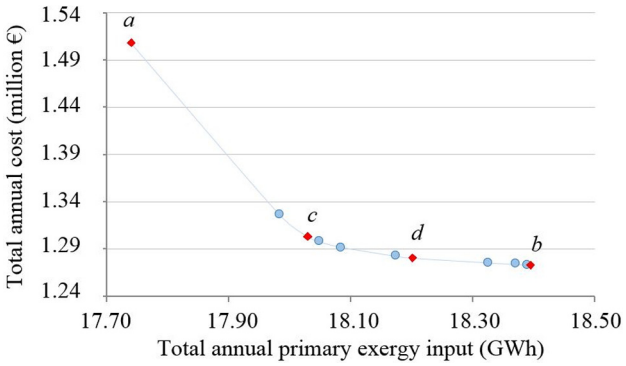

Fig. 6. Pareto frontier.

boilers and air-source heat pumps, the specific capital costs, O&M costs and efficiencies are assumed constant and equal to the average value in the size range considered, due to the slight variation of these characteristics with sizes [63,65–68]. Lead-acid batteries are assumed as electrical storage devices [38]. Moreover, the maximum number of energy devices associated to each technology is assumed as two. To evaluate the total annualized investment cost, the interest rate is assumed as 5%.

3.2. Pareto frontier

For the numerical testing, there are 50,552 constraints; 19,065 binary decision variables; 4,139 other decision variables; and 121,736 non-zero coefficients. The optimization problem can be solved within few hours with a mixed integer gap lower than 0.15% with a PC with 2.60 GHz (2 multi-core processors) Intel(R) Xeon(R) E5 CPU and 32G RAM. The Pareto frontier is shown in Fig. 6. The point marked with *a* is obtained under the exergetic optimization ($\omega = 0$), where the total annual cost is 1.508 MEuro and the total annual primary exergy input is 17.740 GW h. The point marked with *b* is obtained under the economic optimization ($\omega = 1$), where the total annual cost is 1.273 MEuro and the total annual primary exergy input is 18.394 GW h. The points between these two extreme points are found by subdividing the weight interval into 10 equally-spaced points. Each point on the Pareto frontier corresponds to a different optimized configuration of the DES, thereby providing different design options for planners based on short- and long-run priorities.

3.3. Optimized DES configurations

The optimized configurations of the DESs (numbers, sizes and total installed capacities of energy devices), and the economic and exergetic performances for points *a* and *b* on the Pareto frontier are shown in Table 3. For the illustration purpose, the points marked with *c* and *d* in Fig. 6 are chosen to show the optimized configuration of the DES under a higher weight of 0.8 for the exergetic objective ($\omega = 0.2$), and a higher weight of 0.6 for the economic objective ($\omega = 0.6$), respectively.

Under the exergetic optimization, the total capacity of CHPs with gas-fired internal combustion engine is the largest among

Table 3
Optimized solutions at points *a*, *b*, *c* and *d* on the Pareto Frontier.

Optimized solutions		Point *a*	Point *c*	Point *d*	Point *b*
CHP NG ICE	Number	2	2	2	2
	Sizes (MW_{el})	1.122–1.981	0.372–1.190	0.30–1.095	0.30–1.0
	Total (MW_{el})	3.103	1.562	1.395	1.30
CHP NG MTG	Number	2	0	0	0
	Sizes (MW_{el})	0.095–0.270	–	–	–
	Total (MW_{el})	0.365	–	–	–
NG boiler	Number	0	0	1	2
	Sizes (MW_{th})	–	–	0.538	0.261–0.696
	Total (MW_{th})	–	–	0.538	0.957
Biomass boiler	Number	0	0	0	0
	Sizes (MW_{th})	–	–	–	–
	Total (MW_{th})	–	–	–	–
Solar PV	Size (MW_{el})	0.446	0.452	0.485	0.485
	Area (m^2)	4593	4746	5000	5000
Solar thermal	Size (MW_{th})	0.169	0.106	–	–
	Area (m^2)	407	254	–	–
Air-source heat pump	Number	2	2	2	2
	Sizes (MW_{th})	2.120–3.0	0.721–3.0	0.268–2.925	0.269–2.595
	Total (MW_{th})	5.120	3.721	3.193	2.864
Absorption chiller	Number	2	1	1	1
	Sizes (MW_{th})	0.50–0.968	1.265	1.0	1.0
	Total (MW_{th})	1.468	1.265	1.0	1.0
Electrical storage	Total capacity ($MW\ h_{el}$)	0	0	0	0
DHW storage	Total capacity ($MW\ h_{th}$)	1.062	1.670	1.906	2.093
SH storage	Total capacity ($MW\ h_{th}$)	1.60	1.315	1.585	1.425
SC storage	Total capacity ($MW\ h_{th}$)	0.182	0.485	1.233	1.976
Total annual cost (million €)		1.508	1.303	1.280	1.273
Total annual primary exergy input (GW h)		17.740	18.030	18.326	18.394

Please cite this article in press as: Di Somma M et al. Multi-objective design optimization of distributed energy systems through cost and exergy assessments. Appl Energy (2017), http://dx.doi.org/10.1016/j.apenergy.2017.03.105

the four configurations, and similarly for CHPs with gas-fired micro-turbine. This highlights the importance of CHPs for the exergetic objective, due to the possibility of waste heat recovery for thermal purposes, thereby promoting efficient use of the energy resource through a better exploitation of its potential. The large-size CHPs with gas-fired internal combustion engine are selected to satisfy the high electricity loads, whereas the small-size CHPs with micro-turbine are selected to satisfy the low electricity loads. As ω increases, only CHPs with internal combustion engines are selected instead of CHPs with micro-turbines, due to their higher total energy efficiency and lower investment and O&M costs. The chosen CHPs are one small and one large in order to cover most of the electricity load until their minimum part loads. However, the total capacity of CHPs with internal combustion engines reduces, reaching the minimum under the economic optimization, mostly due to the high investment cost. Conversely, the total capacity of natural gas boilers reaches the maximum under the economic optimization, due to the low investment and O&M costs, whereas they are not selected under the exergetic optimization and under a higher weight of the exergetic objective (at point *c*). This result clearly indicates that natural gas, as a high-quality energy resource, should not be used for low-quality thermal demand.

Biomass boilers are not selected in any configuration. The absence of biomass boilers under the exergetic optimization clearly shows that exergy analysis is a powerful tool for designing more sustainable energy supply systems, showing that biomass as a high-quality renewable energy resource, should not be used for low quality thermal demand. Biomass could be used instead for meeting high exergy demand such as for electricity generation, with a better exploitation of the potential of the fuel. In DES design optimization, minimization of not only fossil but also renewable exergy input promotes efficient use of all energy resources, while highlighting that even renewable energy sources need to be used efficiently based on their potential. This result agrees with those presented in [34], where in the operation optimization of a DES, biomass boilers were not used under the exergetic optimization, but they were used under the energy cost minimization due to the low price of biomass. Moreover, this result also agrees with those presented in [16], where different energy systems (i.e., gas-fired boiler, biomass boiler, ground-source heat pump, and waste district heat) were compared through exergy analysis to meet thermal demand in buildings. It was shown that exergy input of the biomass boilers is the largest among the four options, since biomass, although renewable, is a high-quality energy resource, thereby resulting to be not convenient to meet low-quality thermal demand. As for DES design optimization, also under the economic optimization, biomass boilers are not selected due to the high investment cost.

As for solar energy systems, the entire available area is occupied in all the optimized configurations. Under the economic optimization, the entire area is occupied by PV arrays, highlighting the convenience of this technology for the economic objective, especially thanks to the current low costs. The size of PV arrays decreases as ω decreases, reaching the minimum under the exergetic optimization, since the available area is also occupied by solar thermal collectors, whose area is equal to 0 under the economic optimization, and reaches the maximum under the exergetic optimization. This result highlights the convenience of solar thermal for the exergetic purpose, due to the low exergy related to the thermal energy output from the collectors, used to meet the low-quality thermal demand.

The total capacities of air-source heat pumps and absorption chillers increase as ω decreases, reaching the maximum under the exergetic optimization, highlighting their convenience for the exergetic purpose, due to the high conversion efficiency and the possibility of waste heat recovery for space cooling demand, respectively. When ω increases, their total capacities reduce, thereby reducing the total annual cost. Electrical storage (i.e., lead–acid battery) is never selected. The high investment cost makes this technology not competitive. Therefore, it is not selected under the economic optimization. Under the exergetic optimization, electrical storage is not selected mostly due to the high storage loss fraction. As for thermal storage for space cooling demand, the capacity strongly increases as the weight for the economic objective increases, reaching the maximum under the economic optimization. This result clearly shows the economic convenience of the thermal storage for the space cooling demand, whose capacity is strongly related to the sizing of absorption chillers. With larger storage capacity, smaller size of absorption chillers are needed, and the total investment cost reduces.

The capacity of thermal storage for domestic hot water demand is maximum under the economic optimization. The capacity of thermal storage for space heating demand slightly changes with the weight and is maximum under the exergetic optimization. Differently from the thermal storage for space cooling, whose capacity is strongly related to the sizing of absorption chillers, the capacities of thermal storage for domestic hot water and space heating demand mostly depend on the amount of exhaust gas recovered by CHPs, and therefore depend on the operation strategies of multiple energy devices to be discussed later.

The total annual cost and primary exergy input are also investigated for a conventional energy supply system, where grid power is used for the electricity demand, gas-fired boilers for domestic hot water and space heating demand, and electric chillers fed by grid power for space cooling demand. The total annual cost is equal to 1.914 MEuro, and the total annual primary exergy input is equal to 27.641 GW h. Fig. 7 shows the reduction in total annual cost and primary exergy input of the DES configurations at points *a*, *b*, *c* and *d* on the Pareto frontier, as compared with the conventional energy supply system. The maximum reduction in total annual cost, equal to 33.5%, is attained under the economic optimization, whereas the reduction in the total annual primary exergy input is the minimum one, equal to 33.5%. Conversely, the maximum reduction in total annual primary exergy input, equal to 35.8%, is attained under the exergetic optimization, whereas the reduction in total annual cost is the minimum one, equal to 21.2%. Therefore, in all the optimized DES configurations, strong reduction in total annual cost and primary exergy input is attained as compared with the conventional energy supply system.

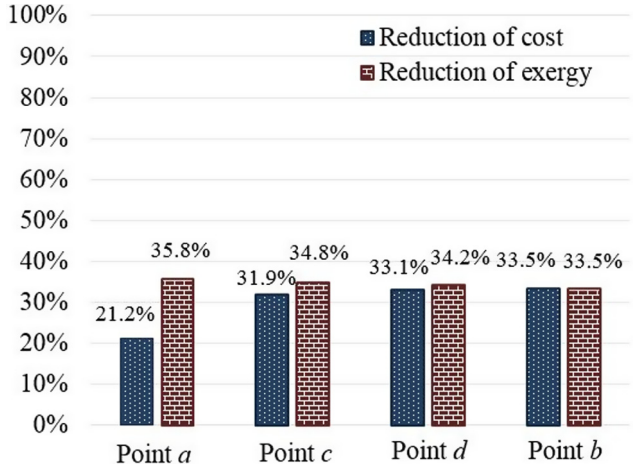

Fig. 7. Reduction in total annual cost and primary exergy input of the optimized DES configurations at points *a*, *b*, *c* and *d* on the Pareto frontier, as compared with the conventional energy supply system.

Please cite this article in press as: Di Somma M et al. Multi-objective design optimization of distributed energy systems through cost and exergy assessments. Appl Energy (2017), http://dx.doi.org/10.1016/j.apenergy.2017.03.105

3.4. Operation strategies of energy devices in the optimized DES configurations under economic and exergetic optimization

For different optimized DES configurations, different operation strategies of energy devices are found. For the illustration purpose, the operation strategies of the energy devices in the optimized DES configurations obtained under the exergetic and economic optimization in the four representative season days are compared in Fig. 8.

Fig. 8a for electricity, shows the total grid power, and the total electricity provided by CHPs and PV to meet the load as the sum of the total demand and the total electricity required by air-source heat pumps in the four representative season days. Under both exergetic and economic optimization, electricity from power grid is generally lower than the electricity provided by CHPs, highlighting that CHP is convenient for both objectives. Moreover, CHPs with micro-turbines are used only under the exergetic optimization, since they are not selected under the economic optimization as presented in the previous subsection, and the electricity provided is smaller than that provided by CHPs with internal combustion engines, coherently with the larger size of the latter CHPs. In the hot mid-season day, the total electricity provided by CHPs is lower than in the other days under both the exergetic and economic optimization, since only electricity and domestic hot water demand need to be satisfied in this day. In this day, under the exergetic optimization, the electricity from power grid is larger than in the other days, and it is also larger than the total electricity provided by CHPs, due to the contribution of solar thermal to meet the domestic hot water demand, as shown in Fig. 8b. It can be also noted that the electricity provided by PV is slightly larger under the economic optimization than under the exergetic one, coherently with the larger size of PV attained under the economic optimization as discussed in the previous subsection.

Fig. 8b for domestic hot water demand shows the total thermal energy provided by CHPs, gas-fired boilers, solar thermal collectors, as well as the total thermal energy input and output to/from the storage to meet the total demand in the four representative season days. Under the economic optimization, the thermal energy from exhaust gas is larger than under the exergetic one. This is due to the fact that, in absence of solar thermal, a larger amount of exhaust gas is used to meet the demand as compared to the exergetic optimization. Natural gas boilers are only used under the economic optimization, since they are not selected under the exergetic optimization as presented in the previous subsection. As for thermal storage, it is generally more used under the economic optimization than under the exergetic one, due to the larger amount of exhaust gas, which also explains the larger capacity required under the economic optimization.

Fig. 8c for space heating and cooling demand shows the total thermal energy provided by CHPs, gas-fired boilers, air-source heat pumps, absorption chillers as well as the total thermal energy input and output to/from the storage systems to meet the total

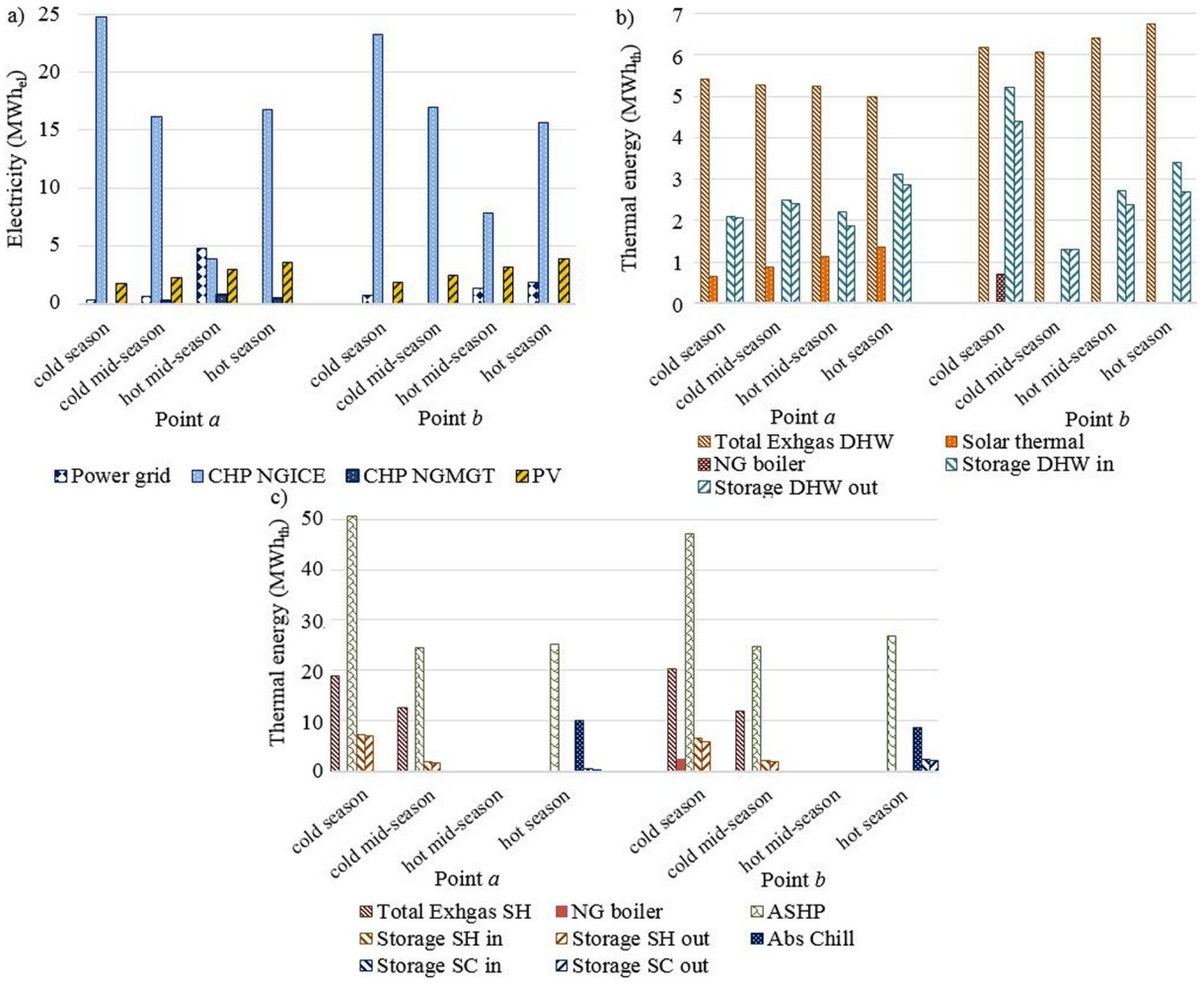

Fig. 8. Operation strategies of optimized DES configurations at points *a* and *b* in the four season days for (a) electricity; (b) domestic hot water; and (c) space heating and cooling.

Please cite this article in press as: Di Somma M et al. Multi-objective design optimization of distributed energy systems through cost and exergy assessments. Appl Energy (2017), http://dx.doi.org/10.1016/j.apenergy.2017.03.105

demands in the four representative season days. For space heating, heat pumps are mostly used to meet the demand under both exergetic and economic optimization, highlighting that this technology is convenient for both the objectives. Heat pumps are generally more used under the exergetic optimization than under the economic one. Similarly to the case of domestic hot water demand, natural gas boilers are only used under the economic optimization. As for thermal storage, the slightly larger capacity required under the exergetic optimization than under the economic one is due to the fact that with a larger usage of heat pumps to meet the demand, a larger amount of exhaust gas is dispatched to charge the storage, as compared with what occurs under the economic optimization. For space cooling demand, similar to space heating demand, heat pumps are mostly used to meet the demand under both exergetic and economic optimization. The thermal energy provided by the absorption chillers is larger under the exergetic optimization than under the economic one, coherently with the larger size attained under the exergetic optimization as presented in the previous subsection. As for thermal storage, it is much more used under the economic optimization than under the exergetic one, in accordance to the larger capacity required under the economic optimization.

4. Sensitivity analysis

A sensitivity analysis is carried out to investigate the influence of key parameters such as energy prices and energy demand scale on the optimized DES configurations and the related economic and exergetic performances. In the following, the results of the sensitivity analysis on energy prices and energy demand scale are presented and discussed in s 4.1 and 4.2, respectively.

4.1. Energy price sensitivity

The operation strategies of energy devices strongly depend on energy prices, which in turn affect their combination and sizes in the DES configurations attained by the optimization model. With the increasing consumption of energy resources, energy prices are expected to increase in next years. In the multi-objective optimization problem, the effect of the energy price increase is maximum under the economic optimization, while no effects are under the exergetic optimization. Results of the economic optimization carried out by considering the increase of electricity and natural gas price are presented and discussed in the following. As for biomass, the effect of the price increase is not investigated, since even with the current price, biomass boilers are not selected under the economic optimization.

4.1.1. Electricity price sensitivity under the economic optimization

The results obtained for electricity price increases of 25% until 100% of the current value are compared in Fig. 9. Fig. 9a shows the increase in the total annual cost and primary exergy input as compared with those obtained with the current electricity price. It can be noted that the economic performance are more affected by the electricity price increase than the exergetic ones. However, the effect of electricity price increase on the economic performance is not that significant: when the electricity price is twice of the current one, the increase in the total annual cost is less than 2%. This is due to the fact that, even with the current electricity price, electricity from the power grid is much less than that provided by CHPs as discussed in the previous section.

For the illustration purpose, the total installed capacities of energy devices in the optimized DES configurations obtained with 50% and 100% electricity price increase and those obtained with the current electricity price are compared in Fig. 9b. As the electricity price increases, the total installed capacity of CHP with gas-fired internal combustion engine increases, since CHPs become more convenient. Similar to the current electricity price, also with higher electricity prices, CHPs with gas- fired micro-turbine are not chosen, due to the high investment costs. When electricity price increases, the size of PV systems reduces, due to the larger capacity of CHPs used to meet the electricity load. Solar thermal is not selected as occurs with the current electricity price. The total capacity of air-source heat pumps and gas-fired boilers remains almost unchanged. However, the total capacity of heat pumps reaches the maximum when the electricity price is twice of the current one due to their high conversion efficiencies, whereas the contrary occurs for gas-fired boilers. With larger usage of heat pumps, boilers are less used to meet the space heating demand. Biomass boilers are not selected due to the high investment costs. As for absorption chillers, the total capacity reaches the maximum when the electricity price is twice of the current one, mainly due to the larger usage of CHPs and consequent larger amount of exhaust gas used for the space cooling demand. This latter also explains the significant increase of the capacity of storage for the space cooling demand occurring when the electricity price increases.

The effect of electricity price increase on the exergetic performances is negligible. However, the small increase in the total annual primary exergy input occurring for higher electricity prices is due to the reduction in the usage of PV systems and the consequent larger usage of natural gas in CHPs to meet the electricity load. This result highlights the importance of PV systems for the exergetic purpose, since the usage of electricity from PV systems to meet high-quality electricity demand results to be better than burning natural gas.

4.1.2. Natural gas price sensitivity under the economic optimization

For natural gas price increases of 25% until 100% of the current value, the results are compared in Fig. 10. Fig. 10a shows the increase in the total annual cost and primary exergy input as compared with those obtained with the current natural gas price. It can be noted that the natural gas price increase has larger effects on both the economic and exergetic performances than electricity price increase: when the natural gas price is twice of the current one, the increase in the total annual cost and primary exergy input are equal to 22.6% and 33.5%, respectively. With the current price, natural gas is the most used primary energy carrier, since it is used to feed both CHPs and gas-fired boilers, which are much used under the economic optimization, as discussed in the previous section. Therefore, the effect of natural gas increase on the economic and exergetic performances becomes significant.

The total installed capacities of energy devices in the optimized DES configurations obtained with 50% and 100% natural gas price increase and those obtained with the current natural gas price are compared in Fig. 10b. As the natural gas price increases, the total installed capacity of CHP with gas-fired internal combustion engine dramatically reduces, reaching the minimum when the gas price is twice of the current one, whereas CHPs with gas-fired micro-turbine are not selected as occurs with the current natural gas price. The total installed capacity of gas-fired boilers reduces as the gas price increases, even though the reduction of the total capacity is not such significant as that of CHPs. This is because when natural gas price increases, grid power becomes much more convenient than CHPs to meet the electricity load, due to the high investment costs. The increase of natural gas price has a lower impact on the installed capacity of gas-fired boilers. Although the gas price increase, gas-fired boilers have low investment costs, and they are still convenient for the economic objective. When natural gas price increases, biomass boilers become more convenient than gas-fired boilers, and they are selected in the optimized DESs configurations, although their investment

Please cite this article in press as: Di Somma M et al. Multi-objective design optimization of distributed energy systems through cost and exergy assessments. Appl Energy (2017), http://dx.doi.org/10.1016/j.apenergy.2017.03.105

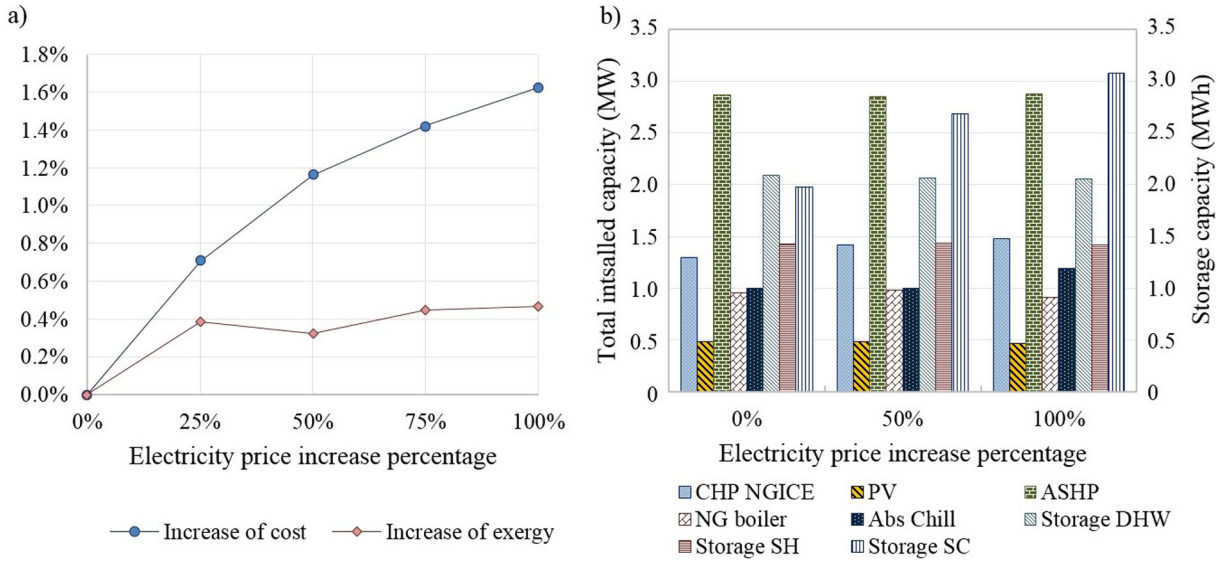

Fig. 9. (a) Economic and exergetic performance of optimized DES configurations under the economic optimization for electricity price increases of 25% until 100% of the current value. (b) Total installed capacity of energy devices for various electricity price increases.

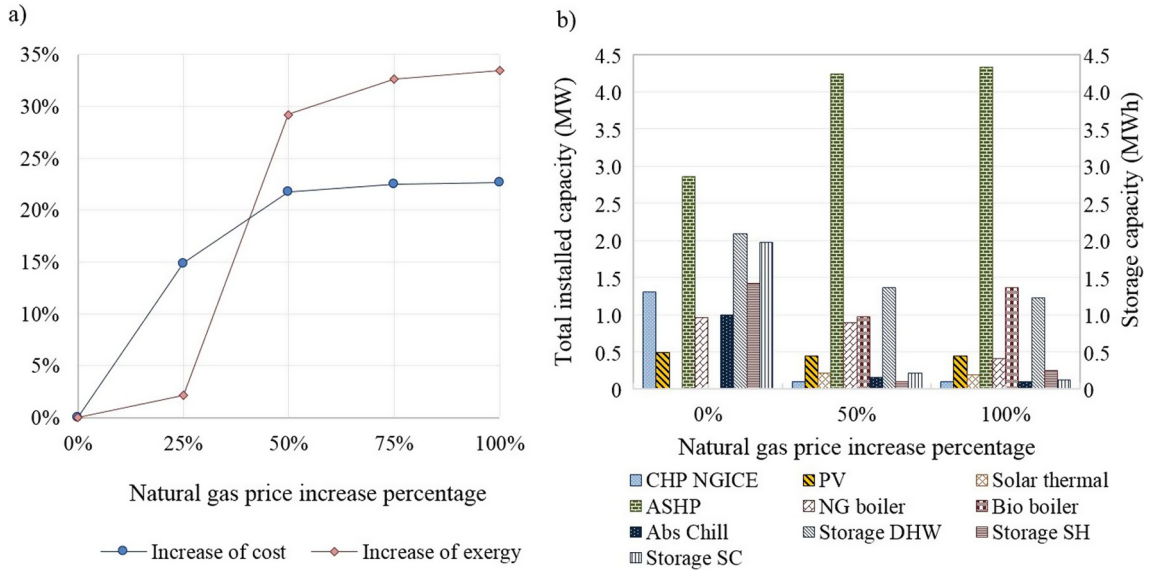

Fig. 10. (a) Economic and exergetic performance of optimized DES configurations under the economic optimization for natural gas price increases of 25% until 100% of the current value. (b) Total installed capacity of energy devices for various natural gas price increases.

costs are higher. For higher natural gas prices, the size of PV systems reduces, since the available area for installation of solar systems is also occupied by solar thermal collectors used to meet the demand of domestic hot water. As for air-source heat pumps, their installed capacity significantly increases when natural gas price increases, due to the strong reduction of exhaust gas from CHPs to meet the demand of space heating and cooling. This latter also explains the significant reduction of the total installed capacity of absorption chillers and of the required capacity of the storage for space cooling demand. The reduction of exhaust gas from CHPs under higher natural gas prices also explains the reduced required capacities of storage for domestic hot water and space heating demands. Similar to the current natural gas price, electrical storage is not selected due to the high investment costs.

The strong reduction in the usage of CHPs is one of the most important factors influencing the strong increase in the total annual primary exergy input occurring for natural gas price increases higher than 25% of the current value. This result underlines the importance of waste heat recovery from CHPs for the exergetic perspective, since, in absence of exhaust gas, other combustion-based energy devices are used to meet the thermal demand, thereby increasing the waste of high-quality energy. Another important factor influencing the increase in the total annual primary exergy is the usage of biomass boilers used to meet the thermal demand. As discussed earlier, biomass is a high-quality renewable energy resource, and it should not be used to meet low-quality thermal demand.

4.2. Energy demand scale sensitivity

The types, number and sizes of energy devices in the DES configurations strongly depend on energy demand, which is one of the uncertainty factors at the demand side. In the multi-objective optimization problem, the effect of energy demand variation is

Please cite this article in press as: Di Somma M et al. Multi-objective design optimization of distributed energy systems through cost and exergy assessments. Appl Energy (2017), http://dx.doi.org/10.1016/j.apenergy.2017.03.105

observable at all the points of the Pareto frontier. For the illustration purpose, the effect of energy demand variation (both electricity and thermal) is investigated under the economic and exergetic optimization in the following.

4.2.1. Energy demand scale sensitivity under the economic optimization

The results obtained under the economic optimization for energy demand decrease and increase of 25% until 50% of the current one, respectively, are compared in Fig. 11. According to Fig. 11a, both the total annual cost and primary exergy input vary almost linearly with the energy demand variation. For energy demand increase of 50% of the current one, the increase in total annual cost and primary exergy input reaches the maximum, equal to 50.0% and 53.5%, respectively. For energy demand decrease of 50% of the current value, the reduction in total annual cost and primary exergy input reaches the maximum, equal to 48.8% and 50.4%, respectively.

For the illustration purpose, the total installed capacities of energy devices in the optimized DES configurations obtained with 50% energy demand decrease and 50% energy demand increase are compared with those obtained with the current energy demand in Fig. 11b. As the energy demand increases, the total installed capacities of most of the energy devices increase. The size of PV systems remains unchanged, occupying the entire available area. CHPs with gas-fired micro-turbine are not selected in the optimized DES configurations, as occurs with the current energy demand. As for thermal storage, the total capacities increase as the energy demand increases, due to the larger amount of exhaust gas from CHPs dispatched to the storage devices. Similar to the current energy demand, the electrical storage is not selected due to the high investment costs. The increase in the total annual primary exergy input is mostly due to the larger usage of grid power to meet the electricity load, and the larger usage of gas-fired boilers to meet the thermal demand.

As the energy demand decreases, the total installed capacities of most of the energy devices decrease. Differently to the case of energy demand increase, the size of PV systems also decreases, and solar thermal is selected for the demand of domestic hot water. The area occupied by solar energy systems is equal to 3464 m^2, lower than the available one. As for thermal storage, the total capacities reduce as the energy demand reduces, due to the lower amount of exhaust gas from CHPs dispatched to the storage devices. The decrease in the total annual primary exergy input is mostly due to the lower usage of grid power to meet the electricity load, and the lower usage of gas-fired boilers to meet the thermal demand.

Under the economic optimization, CHPs with gas-fired internal combustion engine, gas-fired boilers and air-source heat pumps are the energy devices which are most influenced by the energy demand variation. When the energy demand is 50% higher than the current one, the total capacities of CHPs, boilers and heat pumps increase by 53.8%, 69.4%, and 55.9%, as compared to those obtained with the current energy demand, respectively. Conversely, when the energy demand is 50% lower than the current one, their total capacities decrease by 53.8%, 58.9%, and 54.7%, respectively. The variation of energy demand has also noticeable effects on the capacities of storage for domestic hot water and space cooling demand. When the energy demand is 50% higher than the current one, the capacities of storage for domestic hot water and space cooling increase by 56.7% and 86.7%, respectively, whereas for energy demand decrease of 50% than the current one, they reduce by 65.4% and 19.3%, respectively.

4.2.2. Energy demand scale sensitivity under the exergetic optimization

The results obtained under the exergetic optimization for energy demand decrease and increase of 25% until 50% of the current one, respectively, are compared in Fig. 12. Fig. 12a shows the reduction/increase in the total annual cost and primary exergy input as compared with those obtained with the current energy demand. Similar to what occurs under the economic optimization, both the total annual cost and primary exergy input vary almost linearly with the energy demand variation. For energy demand increase of 50% of the current one, the increase in total annual cost and primary exergy input reaches the maximum, equal to 42.5% and 51.2%, respectively. For energy demand decrease of 50% of the current value, the reduction in total annual cost and primary exergy input reaches the maximum, equal to 43.0% and 51.7%, respectively.

The total installed capacities of energy devices in the optimized DES configurations obtained with 50% energy demand decrease

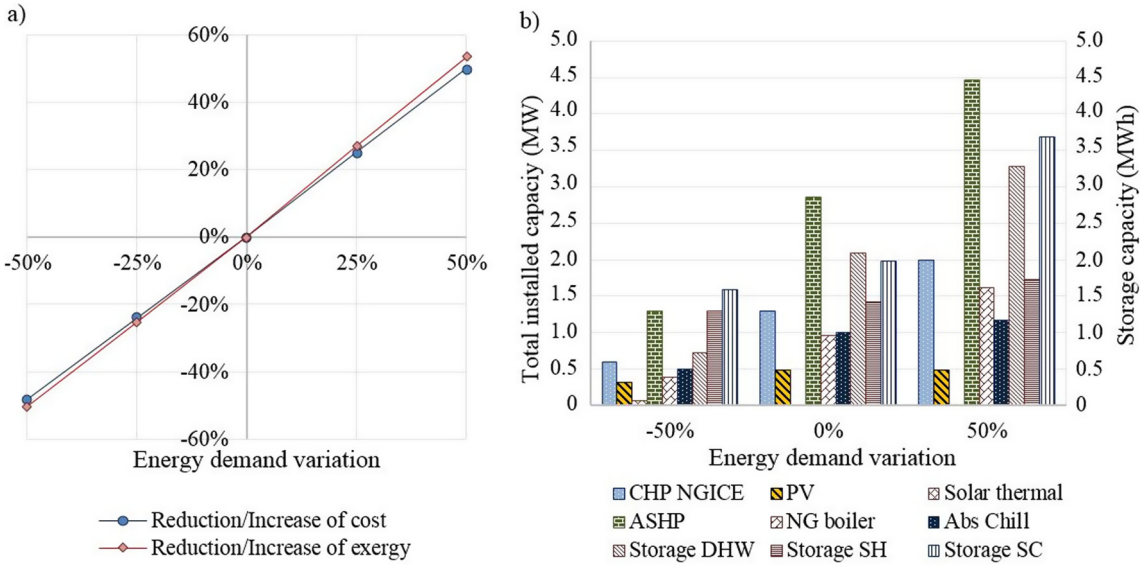

Fig. 11. (a) Economic and exergetic performance of optimized DES configurations under the economic optimization for energy demand decrease and increase of 25% until 50% of the current one, respectively. (b) Total installed capacity of energy devices for various energy demand decreases/increases.

Please cite this article in press as: Di Somma M et al. Multi-objective design optimization of distributed energy systems through cost and exergy assessments. Appl Energy (2017), http://dx.doi.org/10.1016/j.apenergy.2017.03.105

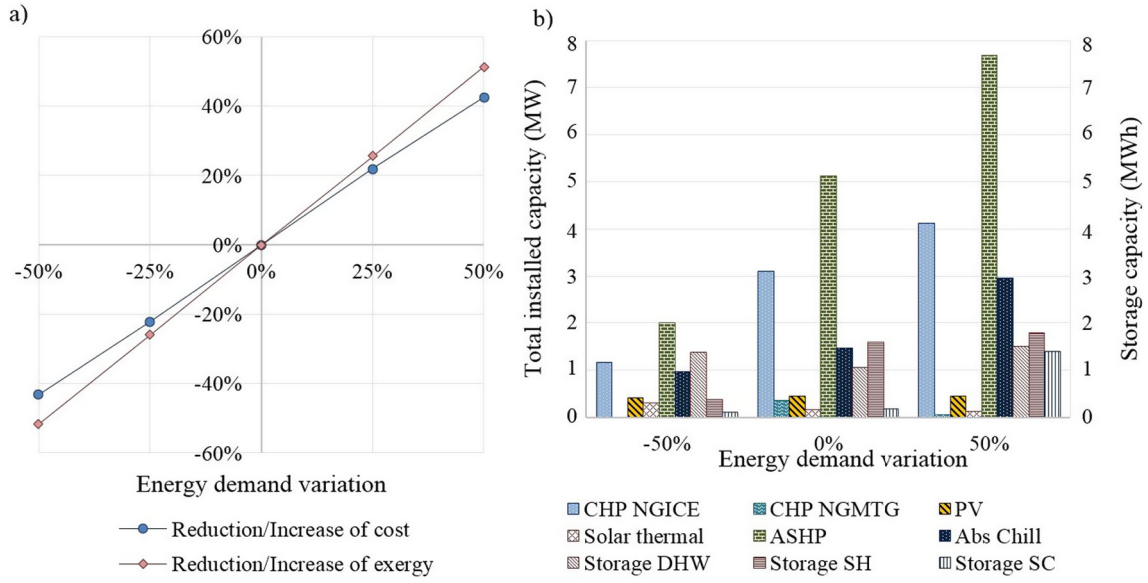

Fig. 12. (a) Economic and exergetic performance of optimized DES configurations under the exergetic optimization for energy demand decrease and increase of 25% until 50% of the current one, respectively. (b) Total installed capacity of energy devices for various energy demand decreases/increases.

and 50% energy demand increase are compared with those obtained with the current energy demand in Fig. 12b. As the energy demand increases, the total installed capacities of most of the energy devices increase. The opposite occurs for CHPs with gas-fired micro-turbine. The choice of only one CHP with gas-fired micro-turbine of 53 kW is related to the sizes of CHPs with gas-fired internal combustion engines, which are equal to 1.152 MW and 2.978 MW, instead of 1.122 MW and 1.981 MW attained with the current energy demand. Although the total capacity increases by 33.1% as compared to that obtained with the current energy demand, the size of the smaller CHP only increases by 2.7%. Therefore, these two CHPs, with the increase of electricity demand and the electricity required by heat pumps, can satisfy most of the total electricity load until their minimum part loads. The size of solar thermal also reduces as the energy demand increases, due the increase of the PV size, which occupy a larger area. As for thermal storage, the total capacities increase as the energy demand increases, due to the larger amount of exhaust gas from CHPs dispatched to the storage devices. The increase in the total annual cost is mostly due to larger investment costs related to the larger sizes of CHPs, air-source heat pumps and absorption chillers.

As the energy demand decreases, the total installed capacities of most of the energy devices decrease. For energy demand decrease of 50% than the current one, CHPs with gas-fired micro-turbine are not selected. This is related to the sizes of CHPs with gas-fired internal combustion engines, which are equal to 0.227 MW and 0.937 MW. The size of the smaller CHP decreases by 79.8% as compared to the smaller one in the current case. Therefore, the two CHPs can satisfy most of the total electricity load until their minimum part loads. Differently from the case of energy demand increase, the size of PV systems decreases, whereas the size of solar thermal increases. However, in all the optimized DES configurations, the entire available area for solar energy systems is occupied. As the energy demand decreases, the total capacities of storage for space heating and cooling reduce, due to the lower amount of exhaust gas from CHPs dispatched to the storage devices. As for thermal storage for domestic hot water, the total capacity increases, due to the larger amount of thermal energy from solar thermal dispatched to the storage. The reduction in the total annual cost is mostly due to lower investment costs related to the lower sizes of CHPs, air-source heat pumps and absorption chillers.

Under the exergetic optimization, CHPs with gas-fired internal combustion engine and with micro-turbine, air-source heat pumps, and absorption chillers are the energy devices which are most influenced by the energy demand variation. When the energy demand is 50% higher than the current one, the total capacities of CHPs with gas-fired internal combustion engine, heat pumps, and absorption chillers increase by 33.1%, 50.0%, and 100.0%, as compared to the those attained with the current energy demand, respectively. The total capacity of CHPs with micro-turbine reduces by 85.5%. Conversely, when the energy demand is 50% lower than the current one, their total capacities decrease by 62.5%, 60.7%, and 34.3%, respectively, and CHPs with micro-turbine are not selected. The variation of energy demand has also noticeable effects on the size of solar thermal, which reduces by 21.6% for energy demand increase of 50%, and increases by 82.1% for energy demand decrease of 50%. Remarkable effects of energy demand variation can be also noted on the capacities of storage for space heating and cooling demand.

5. Conclusions

In this paper, exergy is investigated in design optimization of distributed energy systems (DESs) for sustainable development of energy supply systems through multi-objective approach for not neglecting the crucial economic factor. Based on a pre-established DES superstructure with multiple energy devices such as combined heat and power and PV, a multi-objective linear programming problem is formulated to determine types, numbers and sizes of energy devices in the DES with the corresponding operation strategies in order to reduce the total annual cost and increase the overall exergy efficiency. In modeling of energy devices, the entire size ranges available in the market as well as the variations of efficiencies, specific capital and operation and maintenance costs with sizes are taken into account. The Pareto frontier is found by minimizing a weighted sum of the total annual cost and primary exergy input. The problem is solved by branch-and-cut. The

Please cite this article in press as: Di Somma M et al. Multi-objective design optimization of distributed energy systems through cost and exergy assessments. Appl Energy (2017), http://dx.doi.org/10.1016/j.apenergy.2017.03.105

models and methods provided can be applied in real contexts. Given the needed input data, the model allows to obtain the optimized combination of the candidate energy devices and the corresponding operation strategies through cost and exergy assessments, thereby providing decision support to planners.

Numerical results demonstrate that exergy analysis is a powerful tool for designing more sustainable energy supply systems based on the use of renewables and low-temperature sources for thermal demand in buildings, and on a better exploitation of the high potential of fossil fuels. Moreover, the Pareto frontier provides good balancing solutions for planners based on economic and sustainability priorities. It is found that, through proper design optimization, DESs can offer a good investment opportunity when compared with conventional energy supply systems, through rational use of energy resources. The total annual cost and primary exergy input of DESs with optimized configurations are significantly reduced as compared with a conventional energy supply system, where grid power is used for the electricity demand, gas-fired boilers for domestic hot water and space heating demand, and electric chillers fed by grid power for space cooling demand. As compared with the conventional case, the maximum reduction in the total annual cost and primary exergy input are equal to 33.5% and 35.8%, respectively. Also in the other points of the Pareto frontier, a strong reduction in total annual cost and primary exergy input is attained. In addition, a sensitivity analysis is carried out to analyze the influence of key parameters, such as energy prices and energy demand variation on the optimized DES configurations and the related economic and exergetic performances. It is found that natural gas price increase has larger effects than the electricity price increase on the optimized DES configurations and economic and exergetic performances, whereas the effects of energy demand variation are noticeable under both the economic and the exergetic optimization. The results found in this work clearly indicate that, among the candidate energy devices, combined heat and power systems with gas-fired internal combustion engine are the best options for both reduction of cost and primary exergy input, whereas solar energy systems are important for the exergetic purpose.

Although there are no exergy requirements as a methodology or an indicator yet in current energy legislations, results underline that exergy assessments may allow to meet the main goal of energy legislations in improving sustainability of energy supply. Minimization of not only fossil but also renewable exergy input promotes an efficient energy resource use through the reduction of the waste of high-quality energy, by avoiding burning processes and substituting them by low-temperature sources for thermal demand in buildings.

References

[1] Kari A, Arto S. Distributed energy generation and sustainable development. Renew Sustain Energy Rev 2006;10:539–58.
[2] Ren H, Gao W. A MILP model for integrated plan and evaluation of distributed energy systems. Appl Energy 2010;87(3):1001–14.
[3] Akorede MF, Hizam H, Poresmaeil E. Distributed energy resources and benefits to the environment. Renew Sustain Energy Rev 2010;14:724–34.
[4] Pepermans G, Driesen J, Haesoldoncklx D, Belmans R, D'haeseleer W. Distributed generation: definition, benefits and issues. Energy Policy 2005;33:787–98.
[5] Söderman J, Pettersson F. Structural and operational optimisation of distributed energy systems. Appl Therm Eng 2006;26:1400–8.
[6] Bayod-Rujula AA. Future development of the electricity systems with distributed generation. Energy 2009;34(3):377–83.
[7] Huang J, Jiang C, Xu R. A review on distributed energy resources and microgrid. Renew Sustain Energy Rev 2008;12(9):2472–83.
[8] Han J, Ouyang L, Xu Y, Zeng R, Kang S, Zhang G. Current status of distributed energy system in China. Renew Sustain Energy Rev 2016;55:288–97.
[9] Chinese D, Meneghetti A. Optimisation models for decision support in the development of biomass-based industrial district-heating networks in Italy. Appl Energy 2005;82(3):228–54.
[10] Manfren M, Caputo P, Costa G. Paradigm shift in urban energy systems through distributed generation: methods and models. Appl Energy 2011;88(4):1032–48.
[11] Ruan Y, Liu Q, Zhou W, Firestone R, Gao W, Watanabe T. Optimal option of distributed generation technologies for various commercial buildings. Appl Energy 2009;86(9):1641–53.
[12] Ren H, Zhou W, Nakagami KI, Gao W, Wu Q. Multi-objective optimization for the operation of distributed energy systems considering economic and environmental aspects. Appl Energy 2010;87(12):3642–51.
[13] Pohekar SD, Ramachandran M. Application of multi-criteria decision making to sustainable energy planning—a review. Renew Sustain Energy Rev 2004;8(4):365–81.
[14] Wang JJ, Jing YY, Zhang CF, Zhao JH. Review on multi-criteria decision analysis aid in sustainable energy decision-making. Renew Sustain Energy Rev 2009;13(9):2263–78.
[15] Alarcon-Rodriguez A, Ault G, Galloway G. Multi-objective planning of distributed energy resources: a review of the state-of-the-art. Renew Sustain Energy Rev 2010;14:1353–66.
[16] ECBCS – Annex 49 – Low Exergy Systems for High Performance Buildings and Communities, homepage. Available <http://www.ecbcs.org/annexes/annex49.htm>.
[17] Dincer I, Rosen MA. Energy, environment and sustainable development. Appl Energy 1999;64(1):427–40.
[18] Dincer I, Rosen MA. Exergy-energy, environment and sustainable development. 1st ed. Oxford, UK: Elsevier Publication; 2007.
[19] Dincer I, Rosen MA. Exergy: energy, environment and sustainable development. Newnes; 2012.
[20] Wall G, Gong M. On exergy and sustainable development—part 1: conditions and concepts. Exergy Int J 2001;1(3):128–45.
[21] Rosen MA, Dincer I, Kanoglu M. Role of exergy in increasing efficiency and sustainability and reducing environmental impact. Energy Policy 2008;36(1):128–37.
[22] Bilgen E. Exergetic and engineering analyses of gas turbine based cogeneration systems. Energy 2000;25(12):1215–29.
[23] Gonçalves P, Angrisani G, Rosselli C, Gaspar AR, Da Silva MG. Comparative energy and exergy performance assessments of a microcogenerator unit in different electricity mix scenarios. Energy Convers Manage 2013;73:195–206.
[24] Feidt M, Costea M. Energy and exergy analysis and optimization of combined heat and power systems. Comparison of various systems. Energies 2012;5:3701–22.
[25] Barelli L, Bidini G, Gallorini F, Ottaviano A. An energetic–exergetic analysis of a residential CHP system based on PEM fuel cell. Appl Energy 2011;88(12):4334–42.
[26] Hepbasli A. A key review on exergetic analysis and assessment of renewable energy resources for a sustainable future. Renew Sustain Energy Rev 2008;12(3):593–661.
[27] Kalogirou SA, Karellas S, Badescu V, Braimakis K. Exergy analysis on solar thermal systems: a better understanding of their sustainability. Renewable Energy 2016;85:1328–33.
[28] Hepbasli A, Akdemir O. Energy and exergy analysis of a ground source (geothermal) heat pump system. Energy Convers Manage 2004;45(5):737–53.
[29] Tsaros TL, Gaggioli RA, Domanski PA. Exergy analysis of heat pumps. ASHRAE Trans 1987;93(2):1781–93.
[30] Crawford RR. An experimental laboratory investigation of second law analysis of a vapor-compression heat pump. ASHRAE Trans 1988;94(2):1491–504.
[31] Bjurström H, Carlsson B. An exergy analysis of sensible and latent heat storage. J Heat Recov Syst 1985;5(3):233–50.
[32] Dincer I. On thermal energy storage systems and applications in buildings. Energy Build 2002;34(4):377–88.
[33] Koca A, Oztop HF, Koyun T, Varol Y. Energy and exergy analysis of a latent heat storage system with phase change material for a solar collector. Renewable Energy 2008;33(4):567–74.
[34] Di Somma M, Yan B, Bianco N, Luh PB, Graditi G, Mongibello L, et al. Operation optimization of a distributed energy system considering energy costs and exergy efficiency. Energy Convers Manage 2015;103:739–51.
[35] Yan B, Di Somma M, Bianco N, Luh PB, Graditi G, Mongibello L, et al. Exergy-based operation optimization of a distributed energy system through the energy-supply chain. Appl Therm Eng 2016;101:741–51.
[36] Mehleri ED, Sarimveis H, Markatos NC, Papageorgiou LG. A mathematical programming approach for optimal design of distributed energy systems at the neighbourhood level. Energy 2012;44:396–1104.
[37] Mehleri ED, Sarimveis H, Markatos NC, Papageorgiou LG. Optimal design and operation of distributed energy systems: application to Greek residential sector. Renewable Energy 2013;51:331–42.
[38] Hawkes AD, Leach MA. Modelling high level system design and unit commitment for a microgrid. Appl Energy 2009;86(7):253–1265.
[39] Omu A, Choudhary R, Boies A. Distributed energy resource system optimisation using mixed integer linear programming. Energy Policy 2013;61:249–66.
[40] Wouters C, Fraga ES, James AM, Polykarpou EM. Mixed-integer optimisation based approach for design and operation of distributed energy systems. In: Power engineering conference (AUPEC), 2014 Australasian Universities IEEE. p. 1–6.
[41] Zhou Z, Zhang J, Liu P, Li Z, Georgiadis MC, Pistikopoulos EN. A two-stage stochastic programming model for the optimal design of distributed energy systems. Appl Energy 2013;103:135–44.

Please cite this article in press as: Di Somma M et al. Multi-objective design optimization of distributed energy systems through cost and exergy assessments. Appl Energy (2017), http://dx.doi.org/10.1016/j.apenergy.2017.03.105

[42] Zhou Z, Liu P, Li Z, Ni W. An engineering approach to the optimal design of distributed energy systems in China. Appl Therm Eng 2013;53:387–96.
[43] Buoro D, Casisi M, De Nardi A, Pinamonti P, Reini M. Multicriteria optimization of a distributed energy supply system for an industrial area. Energy 2013;58:128–37.
[44] Bracco S, Dentici G, Siri S. Economic and environmental optimization model for the design and the operation of a combined heat and power distributed generation system in an urban area. Energy 2013;55:1014–24.
[45] Maroufmashat A, Sattari S, Roshandel R, Fowler M, Elkamel A. Multi-objective optimization for design and operation of distributed energy systems through the multi-energy hub network approach. Ind Eng Chem Res 2016;55 (33):8950–66.
[46] Ramirez-Elizondo LM, Paap GC, Ammerlaan R, Negenborn RR, Toonssen R. On the energy, exergy and cost optimization of multi-energy-carrier power systems. Int J Exergy 2013;13:364–85.
[47] Krause T, Kienzle F, Art S, Andersson G. Maximizing exergy efficiency in multicarrier energy systems. In: Proceedings of IEEE power and energy society general meeting; Minneapolis, USA; 2010 June 25–29.
[48] Lu H, Alanne K, Martinac I. Energy quality management for building clusters and districts (BCDs) though multi-objective optimization. Energy Convers Manage 2014;79:525–33.
[49] ANSI/ASHRAE Standard 55. Thermal environmental conditions for human occupancy; 2013. <http://www.techstreet.com/products/1868610>.
[50] Kotas YJ. The exergy method for thermal plant analysis. reprint ed. Malabar, FL: Krieger; 1995.
[51] Torìo H, Angelotti A, Schmidt D. Exergy analysis of renewable energy-based climatisation systems for buildings: a critical view. Energy Build 2009;41:248–71.
[52] Torìo H, Schmidt D. Framework for analysis of solar energy systems in the built environment from an exergy perspective. Renew Energy 2010;35:2689–97.
[53] Available online: <http://www.ibm.com/developerworks/forums/thread.jspa?threadID=368044>.
[54] Aiying R, Risto L. An effective heuristic for combined heat-and-power production planning with power ramp constraints. Appl Energy 2007;84:307–25.
[55] Weber C, Shah N. Optimisation based design of a district energy system for an eco-town in the United Kingdom. Energy 2011;36(2):1292–308.
[56] Mongibello L, Bianco N, Caliano M, Graditi G. Influence of heat dumping on the operation of residential micro-CHP systems. Appl Energy 2015;160:206–20.
[57] Barbieri ES, Melino F, Morini M. Influence of the thermal energy storage on the profitability of micro CHP systems for residential building applications. Appl Energy 2012;97:714–22.
[58] Bianchi M, De Pascale A, Spina PR. Guidelines for residential micro-CHP systems design. Appl Energy 2012;97:673–85.
[59] ASHRAE International Weather files for Energy Calculations (IWEC weather files). Users manual and CD-ROM, American Society of Heating, Refrigerating and Air-Conditioning Engineers, Atlanta, GA, USA; 2001.
[60] Deloitte. European Energy Market reform – Country Profile: Italy. Available online: <https://www2.deloitte.com/content/dam/Deloitte/global/Documents/Energy-and-Resources/gx-er-market-reform-italy.pdf>.
[61] Trudeau N, Francoeur M. Energy Efficiency indicators for Public Electricity Production from fossil fuels. OECD/IEA; 2008.
[62] Darrow K, Tidball R, Wang J, Hampson A. Catalog of CHP technologies; 2015. Available: <https://www.epa.gov/sites/production/files/2015-07/documents/catalog_of_chp_technologies.pdf>.
[63] Technology Data for Energy Plants. Energinet.dk; 2012. Available: <https://www.energinet.dk/SiteCollectionDocuments/Danske%20dokumenter/Forskning/Technology_data_for_energy_plants.pdf>.
[64] Goldstein L, Hedman B, Knowles D, Freedman SI, Woods R, Schweizer T. Gas-fired distributed energy resource technology characterizations. National Renewable Energy Laboratory; 2003, NREL/TP-620-34783. Available: <http://www.nrel.gov/docs/fy04osti/34783.pdf> <http://www.nrel.gov/docs/fy04osti/34783.pdf>.
[65] Technology Roadmap: Energy-efficient Buildings: Heating and Cooling Equipment. OECD/IEA; 2011. Available: <https://www.iea.org/publications/freepublications/publication/buildings_roadmap.pdf>.
[66] Research on cost and performance of heating and cooling technologies. Final Report. Department of Energy and Climate Change; 2013. Available: <https://www.gov.uk/government/uploads/system/uploads/attachment_data/file/204275/Research_on_the_costs_and_performance_of_heating_and_cooling_technologies__Sweett_Group_.pdf>.
[67] Heat Pumps: Technology Brief. IEA-ETSAP and IRENA; 2013. Available: <https://www.irena.org/DocumentDownloads/Publications/IRENA-ETSAP%20Tech%20Brief%20E12%20Heat%20Pumps.pdf>.
[68] Combined Heat and Power: Policy Analysis and 2011 – 2030 Market Assessment. ICF International, Inc; 2012. Available: <http://www.energy.ca.gov/2012publications/CEC-200-2012-002/CEC-200-2012-002.pdf>.
[69] Thermal Energy Storage: Technology Brief. IEA-ETSAP and IRENA; 2013. Available: <https://www.irena.org/DocumentDownloads/Publications/IRENA-ETSAP%20Tech%20Brief%20E17%20Thermal%20Energy%20Storage.pdf>.

Please cite this article in press as: Di Somma M et al. Multi-objective design optimization of distributed energy systems through cost and exergy assessments. Appl Energy (2017), http://dx.doi.org/10.1016/j.apenergy.2017.03.105

Available online at www.sciencedirect.com

ScienceDirect

Energy Procedia 105 (2017) 4295 – 4304

Energy Procedia

The 8th International Conference on Applied Energy – ICAE2016

A new approach for the dimensioning of an air conditioning system with cold thermal energy storage

Luigi Mongibello[a,*], Nicola Bianco[b], Martina Caliano[b], Giorgio Graditi[a]

[a]*ENEA Italian National Agency for New Technologies, Energy and Sustainable Economic Development - Portici RC, 80055 Portici (NA), Italy*

[b]*Dipartimento di Ingegneria Industriale (DII) – Università degli Studi Federico II, 80125 Napoli, Italy*

Abstract

In this work, a new approach for the design of air conditioning systems with cold thermal energy storage is described and tested, considering the case study represented by a vapor-compression chiller, coupled with a chilled water storage system, producing cooling for a small multi-apartment building situated in Italy. In the present approach, at the aim of limiting shut-downs and start-ups of the chiller, which involve inefficiencies during transients, and can lead to a drastic reduction of the equipment lifetime, the nominal power of the chiller, and the amount of cooling to be stored are first estimated in a pre-design phase. Successively, the outputs of the pre-design are used to fix the size of the cold storage tank, and to set up the numerical simulation of the cold thermal energy storage system. Finally, the results of the numerical simulation of the cold storage system are used to evaluate the effective size of the chiller. Both the pre-design and the numerical simulations of the cold storage systems have been done by means of home-made numerical tool realized with Simulink.

In the paper, the specifications relative to the operational strategy are explored, and the analytical models used for the numerical simulation of the cold storage system relative to the Italian case study are reported in detail. Finally, the results of the pre-design, and of the cold storage system simulations relative to the case study are presented and discussed. The results relative to the Italian case study demonstrates the effectiveness of the present approach in limiting the number of shut-downs and start-ups of the chiller.

The present approach can represent a useful tool for the economic optimization of the design of air conditioning systems.

© 2017 The Authors. Published by Elsevier Ltd. This is an open access article under the CC BY-NC-ND license (http://creativecommons.org/licenses/by-nc-nd/4.0/).

Peer-review under responsibility of the scientific committee of the 8th International Conference on Applied Energy.

Keywords: cold storage ; chilled water ; partial storage strategy ; numerical simulation

* Corresponding author. Tel.: +39-081-7723584; fax: +39-081-7723345.
E-mail address: luigi.mongibello@enea.it.

1876-6102 © 2017 The Authors. Published by Elsevier Ltd. This is an open access article under the CC BY-NC-ND license (http://creativecommons.org/licenses/by-nc-nd/4.0/).

Peer-review under responsibility of the scientific committee of the 8th International Conference on Applied Energy.
doi:10.1016/j.egypro.2017.03.900

1. Introduction

Cold thermal energy storage (CTES) in HVAC&R systems can allow to shift the electric demand/electric rate fully or partially from on-peak hours to off-peak ones. This generally implies a reduction of the operating costs and of the equipment ones, since thermal energy storage allows to reduce the equipment size, and to have longer operating hours of compressors and pumps, and chillers and cooling towers at full load at lower outdoor temperatures during nighttime. Nevertheless, in general the use of thermal energy storage systems also presents some drawbacks, which essentially are the high initial costs, complicated operation, maintenance and control, and high encumbrance [1,2]. For a generic application, the design of such a system is strongly interconnected with the operation strategy, that can follow a full storage or a partial storage approach, depending essentially on the user demand, the electricity tariffs, and the equipment efficiencies and costs.

The effectiveness of cold storage in obtaining a profitable peak load shifting for refrigeration systems has been demonstrated by a number of works. Many control strategies and several storage materials have been tested to the purpose, with chilled water and ice being the most used cold storage materials. Lin et al. [3] conducted a thermo-economic analysis of an air conditioning system with chilled water storage, in which part of the chilled water back from the user is mixed to the chilled water supplied to the user, and analyzed the thermodynamic performance influence on cost saving. Yan et al. [4] optimized the design of an air conditioning system based on the use of a seasonal heat pipe-based ice storage system. Following their approach, during winter the seasonal ice storage system collects cold energy from ambient low-temperature air. In summer, ice cold energy is extracted for air conditioning, and the melted ice is used as storage medium for chilled water storage. Soler et al. [5] analyzed the performance of a cooling network composed of eight chillers with different capacities and coefficients of performance, and a storage system, at the aim of maximizing chillers operating efficiency, and minimizing the number of shut-downs and start-ups. Meyer and Emery [6] optimized from the economical point of view the operation of an air conditioning system composed of two chillers, one designated for ice storage charging, the other for direct cooling, an air-handling unit, a cooling tower, and water pumps. Habeebullah [7] investigated the economic feasibility of retrofitting an ice thermal energy storage system for an air conditioning system, considering both full storage and partial storage approach.

In the last years, great attention has been also addressed to phase change materials (PCMs) different from ice, which have the potential to considerably lower the size of the storage, and consequently its encumbrance that represents one of the main limits of such systems [8-10].

In this work, a new approach for the dimensioning of air conditioning systems with cold thermal energy storage is described and tested, considering the case study represented by a vapor-compression chiller coupled with a chilled water cold storage system producing cooling for a small multi-apartment building situated in Italy.

In the first part of the paper, the specifications relative to the operational strategy adopted, and to the analytical models used for the numerical simulation of the cold storage system are discussed. Successively, the user thermal and electricity demand for air-conditioning in the summer season are reported. Finally, the results of the pre-design, and of the cold storage system simulations relative to the case study are presented and discussed.

2. Operation strategy and simulation model

2.1. Operation strategy and pre-design

Considering, for example, an air conditioning system based on an electric chiller and without cold storage, for a generic user and for a fixed set-point of the internal ambient temperature, generally the chiller operation cannot be continuous during the hours characterized by a refrigeration load that is lower than the minimum chiller thermal power. Indeed, in those hours, the controller of the air conditioning system would switch off the system each time the user internal ambient temperature reaches the predetermined set-point.

In the present approach for the dimensioning of an air conditioning system with cold thermal energy storage, in order to limit the number of shut-downs and start-ups of the chiller, the nominal power of the chiller, and the amount of cooling to be stored are calculated, in a pre-design phase, applying the following operation constraints: during its operation, the chiller has to work at constant power; the chiller cannot feed the cold storage system only, that, in other words, means that cooling can be accumulated only when the chiller has to feed the user; the ratio between the cooling power transferred to the user and the chiller power has to be higher than or equal to a predetermined minimum value, otherwise the chiller is shut down. Successively, the outputs of the pre-design are used to fix the size of the cold storage tank, and to set up the numerical simulation of the cold thermal energy storage system. Finally, the numerical results are used to evaluate the effective size of the chiller.

2.2. Chilled water storage tank model

One-dimensional analytical models have been used in order to simulate the cold water storage tank and the coiled tube heat exchanger [11]. Fig. 1 shows a sketch of the close vertical cylindrical tank with a single immersed serpentine considered in the present study.

The internal water volume is divided into isothermal nodes representing water layers of equal volume. The energy balance for each node is written as:

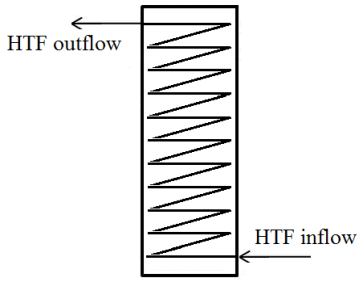

Fig. 1. Sketch of the cold water storage tank

$$\rho_w V_w c_{p_w} \frac{dT_w}{dt} = \frac{(T_{HTF} - T_w)}{R_{coil}} + Q_{cond} - \frac{(T_w - T_{amb})}{R_{tank}} \quad (1)$$

where Q_{cond} represents the conductive heat exchange with adjacent layers. The thermal resistance relative to each layer of the storage wall has been evaluated as:

$$R_{tank} = R_{conv\_int} + R_{cond} + R_{conv\_ext} \quad (2)$$

where

$$R_{conv\_int} = \frac{1}{\bar{h}_{int\_tank} A_{int\_tank}} \tag{3}$$

The mean convective heat transfer coefficient relative to the inner tank wall in equation (3) is evaluated using the Nusselt number correlation for free convection relative to vertical flat plate [12].

The conductive thermal resistance relative to the tank wall has been evaluated as:

$$R_{cond} = \frac{ln\left(\frac{r_{out\_tank}}{r_{in\_tank}}\right)}{2\pi k_{ins} \Delta_{layer}} \tag{4}$$

It has been assumed that the tank thickness is equal to the insulation thickness (0.1m, expanded polyurethane), namely that the conductive thermal resistance relative to the tank steel wall is negligible.

The convective thermal resistance relative to the external tank wall has been evaluated as:

$$R_{conv\_ext} = \frac{1}{\bar{h}_{ext\_tank} A_{ext\_tank}} \tag{5}$$

For each time-step and for each node, the energy balance equations system composed of equation (1) written for all nodes is solved using the implicit Euler method. The empirical reversion-elimination algorithm [13,14] has been adopted in order to include the effects of natural convection heat transfer between the water layers at different heights on the thermal stratification inside the tank.

A transient one-dimensional model has been adopted for the evaluation of the temperature field of the heat transfer fluid (HTF) flowing through the immersed coil heat exchanger.

Also the heat exchanger has been divided in isothermal nodes representing tube sections having the same volume. For each node, the energy balance equation is given by:

$$\rho_{HTF} V_{nod} c_{p_{HTF}} \frac{dT_{HTF}}{dt} = \frac{\left(T_{tank} - T_{HTF}\right)}{R_{coil}} + \rho_{HTF} \dot{V}_{HTF} c_{p\,HTF} \left(T_{HTF\_in} - T_{HTF\_out}\right) \tag{6}$$

The thermal resistance between the HTF in the coil heat exchanger and the water in the cold storage tank is given by:

$$R_{coil} = R_{conv\_int} + R_{conv\_ext} + R_{cond} \tag{7}$$

where

$$R_{conv\_int} = \frac{1}{\bar{h}_{int\_coil} A_{int\_coil}} \tag{8}$$

The mean internal convective heat transfer coefficient in equation (8) is evaluated using the Gnielinski's correlation for coiled tube heat exchanger [15] for the Nusselt number calculation.

The external convective thermal resistance has been evaluated as:

$$R_{conv\_ext} = \frac{1}{\bar{h}_{ext\_coil} A_{ext\_coil}} \tag{9}$$

The mean external convective heat transfer coefficient in equation (9) is evaluated using the Morgan's correlation for natural convection for horizontal cylinders [16] for the evaluation of the Nusselt number.

The conductive thermal resistance of the coil has been neglected, because its order of magnitude is much lower than the internal and external convective thermal resistances.

For each time-step and for each node, equation (6) is solved using the implicit Euler method.

The coupling between the cold water tank balance equations system and the one relative to the serpentine has been dealt with an iterative approach.

3. Case study

In the analysed application, the user is represented by a small multi-apartment building, characterized by a total surface area equal to 800 m^2 and an envelope shape factor of 0.5 m^{-1}, and situated in the Italian climatic zone E. The yearly thermal energy demand and the daily thermal and electrical load profiles for the air conditioning in the warm season have been evaluated as in reference [17]. In particular, it has been considered that the air conditioning in the warm season is realized by means of an electrical vapour-compression chiller with a hydronic loop, the yearly thermal energy demand is 21 kWh/m^2/yr, and that the daily thermal and electrical load profiles are the same for all the operation days. Fig. 2 shows the hourly averaged thermal and electrical load profiles for refrigeration relative to the user for the standard day considered.

The electrical load profile has been evaluated considering the EER of the chiller depending on the ambient temperature. Fig. 3 shows the variation of the EER as a function of the hourly averaged ambient temperature. In this figure, the temperature profile and the EER one are normalized using the maximum average temperature equal to 28°C, and the maximum value of EER equal to 3, respectively. Thus, with reference to the Fig. 2, and without considering a cold storage integrated into the refrigeration system, for the present user it is necessary a chiller of 7.9 kW of nominal electric power in order to fulfill the request for air conditioning in the summer season.

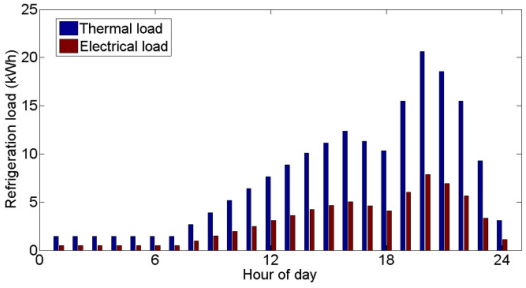

Fig. 2. Refrigeration load of the user

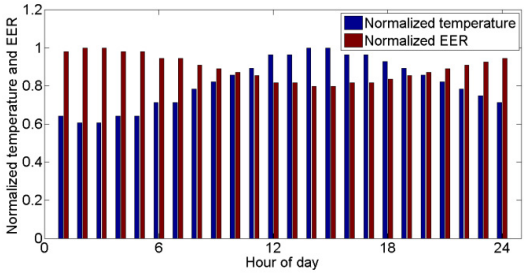

Fig. 3. Non-dimensional temperature and EER profiles

4. Results

4.1. Pre-design and operation strategy implementation

Fig. 4 shows the thermal and electrical powers of the chiller through the day, resulting from the pre-design relative to the considered case study, obtained by fixing the minimum ratio between the cooling power to the user and the chiller power to 0.5, while Fig. 5 shows on the same graph the resulting chiller thermal power and the refrigeration loads. It can be noticed the peak-shaving effect due to the cold storage. Fig. 6 shows, for each hour of the day, the minutes of continuous operation of the chiller. It can be noticed that the present operation strategy involves only 10 shut-downs and start-ups a day, However, it can be also seen that a large part of the chiller production still remains concentrated in the on-peak hours.

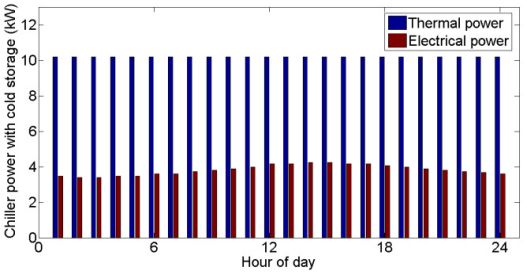

Fig. 4. Chiller power with cold storage

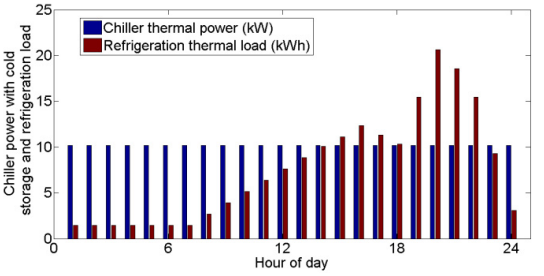

Fig. 5. Chiller thermal power and refrigeration loads

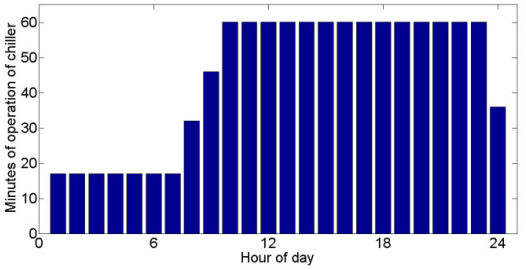

Fig. 6. Minutes of operation of the chiller

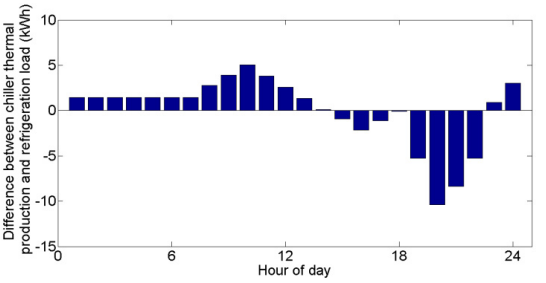

Fig. 7. Difference between the chiller thermal production and the refrigeration loads

Fig. 7 shows, for each hour of the day, the difference between the chiller thermal production and the refrigeration load. Thus, with the adopted approach, the resulting chiller thermal power for the refrigeration system with cold storage is constant and equal to 10.2 kW, with a maximum absorbed electric power of 4.2 kW, that is about the half of the maximum electric power that is needed in the case without the cold storage. The resulting amount of cooling to be stored is 33.6 kWh, that is about the 18% of the user daily total request.

The implementation of the above operation strategy, as well as the numerical simulation of cold storage system, has been performed by means of a home-made tool realized in Simulink. To the purpose, with reference with the simplified layout of the refrigeration system shown in Fig. 8, it has been assumed that the HTF exits the chiller at a constant temperature $T_{c,out}$=7.0°C, and at a constant flowrate of 0.4 kg/s.

Owing to the assumption of constant chiller thermal power, the expected temperature of the HTF at the inflow section of the chiller is equal to $T_{c,in}$=13.1°C. The operation constraint of fixing the minimum ratio between the cooling power to the user and the chiller power to 0.5 is equivalent to fixing the minimum ratio between the mass flow rate through the user and the mass flow rate through the chiller to 0.5.

During chiller operation, the mass flow rate of HTF through the user is controlled by means of valve V1 so that the temperature at the user exit, i.e. at point A, is equal to $T_{c,in}$. In case the valve V1 is partially open, the HTF passing through V1 goes to the cold storage tank charging it. A further control is applied by means of valve V2 in order to maintain the temperature at point B equal to $T_{c,in}$. In this case the valve V3 is fully open while valve V4 is fully close.

Otherwise, in case valve V1 is fully close, which implies that all HTF from the chiller goes to the user and that the HTF exits the user at a temperature that is higher than $T_{c,in}$, the cold storage tank is discharged.

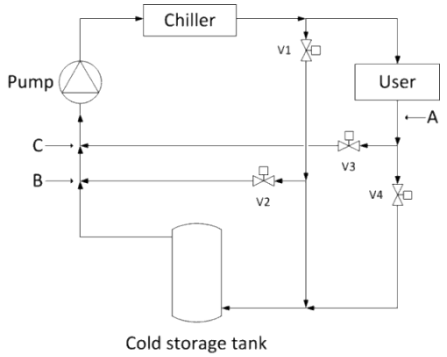

Fig. 8. Layout of the refrigeration system

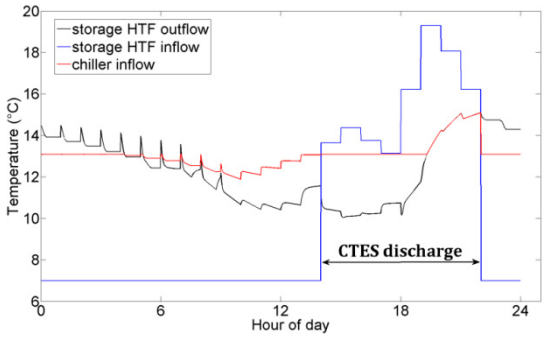

Fig. 9. HTF temperature profiles at the tank heat exchanger inflow and outflow sections, and at the chiller inflow section

In this case, a control is applied by means of valve V3 in order to maintain the HTF temperature at point C equal to $T_{c,in}$, and valve V2 is fully closed.

4.2. Cold storage tank numerical simulation

The size of the water tank is calculated by using the value of the cooling to be stored coming from the pre-design, i.e. 33.6 kWh, and the difference between the HTF inflow and outflow temperatures relative to the chiller, namely 13.1°C and 7°C, respectively. The resulting water volume is equal to about 4.8 m^3. Finally, a commercial cylindrical tank with a capacitance of 4 m^3 has been used for the simulations. The tank height from its bottom surface is equal to 2.55 m (not including insulation), and the entire external surface of the tank is insulated by means of a 0.1 m layer of rigid expanded polyurethane. The tank is provided with a single 1" serpentine with a heat exchange surface of 12 m^2, and the tank capacitance does not include the volume occupied by the serpentine. The inflow section of the serpentine is placed at 5 cm from the tank bottom surface, while the outflow one at 5 cm from the tank top surface. The results of the numerical simulation presented in this section refer to a spatial discretization of the tank realized using 50 nodes, while the serpentine discretization has been made so that its nodes represent the serpentine portions included in the tank layers relative to the tank nodes. A time-step of 60 s has been adopted. Independency of results from the spatial discretization and time-step has been assured.

At each time-step, the HTF mass flow rate flowing through the tank heat exchanger, and the HTF temperature at the inflow section of the heat exchanger are evaluated according to the operation strategy

reported in section 4.1. The main outputs of the numerical simulation are the temperatures at the tank and serpentine nodes.

The following results refer to periodic conditions, obtained starting from an initial temperature of the tank water and of the HTF in the serpentine equal to 13.1°C.

Fig. 9 shows the temporal evolution of the HTF temperature at the serpentine outflow during the day, the one relative to the HTF temperature at the serpentine inflow, and the resulting temporal evolution of the HTF temperature at the chiller inflow, while Fig 10 shows the HTF mass flow rate through the serpentine and through the user.

In Fig. 9, it can be noticed that, from h=5 to the end of the storage charging phase, the HTF temperature at the chiller inflow is lower than the nominal chiller inflow temperature, i.e. 13.1°C. This is because, in that time interval, the HTF temperature at the serpentine outflow is lower than 13.1°C, implying that the chiller has to work at a lower power in that period in order to maintain the HTF temperature at its outflow constant and equal to 7°C.

It can be also noticed that, at the end of the discharging phase, the HTF temperature at the serpentine outflow, and the one at the chiller inflow are higher than 13.1°C. In this case, the chiller has to work consuming a higher electrical power than the one evaluated in the pre-design, up to 6.1 kW, in order to keep the outflow temperature constant and equal to 7°C, implying that the chiller operating at a constant absorbed electric power of 4.2 kW, together with the considered commercial size of the cold storage tank, is not capable to fulfill continuously the user request.

The above consideration are evident if Fig 11, showing the cold energy taken and released from the storage during the day evaluated in the pre-feasibility analysis, and the ones resulting from the numerical simulations, is analyzed. In fact, it can be seen that, at the end of the charging phase, the storage system accumulates less cold than the one resulting from the pre-feasibility analysis. Moreover, it can be seen that at the end of the discharging phase, the cold released by the storage system is much lower than the one evaluated in the pre-feasibility analysis. This results are essentially due to chosen tank size, to the storage degradation due to the cold energy losses through the tank external walls, and to the degradation of the temperature stratification inside the tank. Figure 12 and 13 show the evolution of the water temperature profile in the tank during the charging phase and the discharging one, respectively.

Thus, considering the operation strategy and the size of the cold storage system adopted in this study, in the case with cold storage it is necessary to have a chiller, provided with an inverter, characterized by a maximum absorbed electric power of 6.1 kW, that, however, is well below the one relative to the case without the cold storage, namely 8 kW. Table 1 shows the storage tank and chiller sizes obtained by varying the minimum ratio between the cooling power transferred to the user and the chiller power.

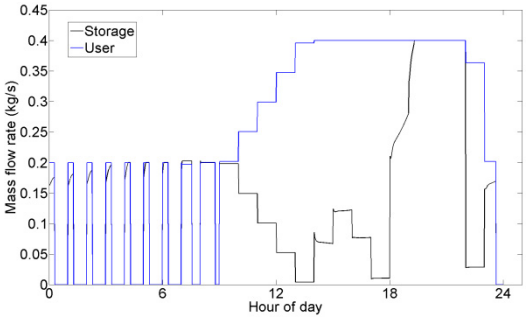

Fig. 10. HTF mass flow rate through the tank heat exchanger and the user

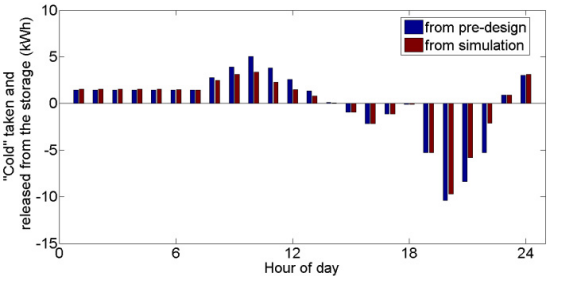

Fig. 11. Cooling energy taken and released from the cold water tank

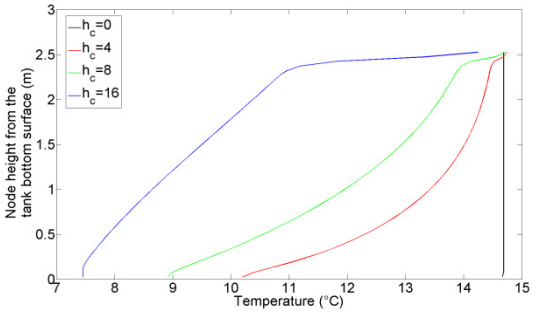

Fig. 12. Temperature profiles in the cold water tank during the charging phase (h_c=0 refers to the beginning of the phase)

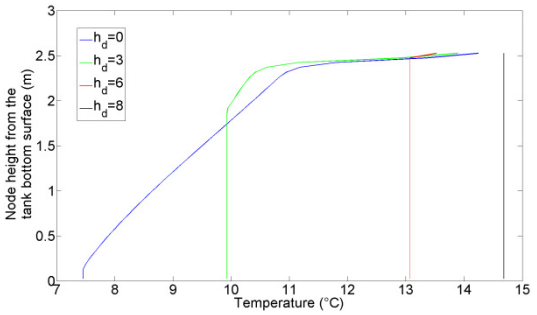

Fig. 13. Temperature profiles in the cold water tank during the discharging phase (h_d=0 refers to the beginning of the phase)

Table 1. Main results by varying the minimum ratio between the cooling power transferred to the user and the chiller power

Minimum ratio between the cooling power transferred to the user and the chiller power	Storage capacity (pre-design) (kWh)	Storage volume (pre-design) (m^3)	Storage volume (simulation) (m^3)	Chiller powers (pre-design) (kW_t , kW_e)	Chiller power (simulation) (kW_t , kW_e)
0	59.9	11.4	8.0	(7.6 , 3.2)	(11.5 , 4.8)
0.25	51.84	8.85	8.0	(8.3 , 3.5)	(11.4 , 4.7)
0.5	33.60	4.80	4.0	(10.2 , 4.2)	(13.5 , 5.6)
0.75	23.35	2.85	2.0	(11.8 , 4.9)	(15.1 , 6.3)
1	0	0	-	(20.6 , 7.9)	-

5. Conclusion

In this work, a new approach for the design of air conditioning systems with cold thermal energy storage is described and tested, considering the case study represented by a vapor-compression chiller, coupled with a chilled water storage system, producing cooling for a small multi-apartment building situated in Italy.

The specifications relative to the operational strategy have been reported, and the characteristics of the analytical models used for the numerical simulation of the cold storage system relative to the Italian case study have been shown as well. The results relative to the Italian case study have demonstrated the effectiveness of the present approach in limiting the number of shut-downs and start-ups of the chiller.

References

[1] Silvetti B, MacCracken M. Thermal storage and deregulation. *ASHRAE Journal*, 1998;**4**:55–59.
[2] Wang SK. *Handbook of air conditioning and refrigeration*. 2nd ed. New York: McGraw-Hill; 2001.
[3] Lin H, Li XH, Cheng PS, Xu BG. Thermoeconomic evaluation of air conditioning system with chilled water storage. *Energy Conversion and Management*, 2014;**85**: 328–32.
[4] Yan C, Shi W, Li X, Zhao Y. Optimal design and application of a compound cold storage system combining seasonal ice storage and chilled water storage. *Applied Energy*, 2016;**171**:1–11.
[5] Soler MS, Sabaté CC, Santiago VB, Jabbari F. Optimizing performance of a bank of chillers with thermal energy storage. *Applied Energy*, 2016;**172**:275–85.
[6] Kintner-Meyer M, Emery A. Optimal control of an HVAC system using cold storage and building thermal capacitance. *Energy and Buildings*, 1995;**23**(1):19–31.
[7] Habeebullah BA. Economic feasibility of thermal energy storage systems. *Energy and Buildings*, 2007;**39:**355–63.
[8] Sun Y, Wang S, Xiao F Gao D. Peak load shifting using different cold thermal energy storage facilities in commercial buildings: A review. *Energy Conversion and Management*, 2013;**71**:101–14.
[9] Navidbakhsh M, Shirazi A, Sanaye S. Four E analysis and multi-objective optimization of an ice storage system incorporating PCM as the partial cold storage for air-conditioning applications. *Applied Thermal Engineering*, 2013;**58**(1-2): 30–41.
[10] Oró E, Depoorter V, Plugradt NSJ. Overview of direct air free cooling and thermal energy storage potential energy savings in data centres. *Applied Thermal Engineering*, 2015;**85**:100–110.

[11] Mongibello L, Bianco N, Caliano M, de Luca A, Graditi G. Transient analysis of a solar domestic hot water system using two different solvers. Energy Procedia, 2015;**81**:89-99.
[12] Bejan A, Kraus AD. *Heat Transfer Handbook*, Hoboken: John Wiley & Sons Inc. 2003.
[13] Mather DW, Hollands KGT, Wright JL. Single- and Multi-Tank energy storage for solar heating systems: Fundamentals. *Solar Energy* 2002;**73**:3-13.
[14] Newton BJ, Schmid M, Mitchell JW, Beckman WA. Storage tank models. *Proceedings of ASME/JSME/JSES International Solar Energy Conference* 1995, Maui, Hawaii.
[15] Gnielinski Y. Heat transfer and pressure drop in helically coiled tubes. *8th International Heat Transfer Conference* 1986;6:2847–54.
[16] Morgan VT. The overall convective heat transfer from smooth circular cylinders. *Adv. Heat Transfer* 1975;11:199-264.
[17] Mongibello L, Bianco N, Caliano M, Graditi G. Influence of heat dumping on the operation of residential micro-CHP system. *Applied Energy*, 2015;**160**:206–20.

Acknowledgement

This work was funded within the Italian Research Program “Ricerca di Sistema Elettrico – PAR 2015, Area: Efficienza energetica e risparmio di energia negli usi finali elettrici ed interazione con altri vettori energetici”.

Biography

Luigi Mongibello, PhD. He graduated in aerospace engineering at the University of Naples “Federico II” (Italy) in 2002, where he completed, in 2005, a doctorate in aerospace engineering with a thesis on actuators for flow control. His research activities are focused on the experimentation, simulation, and optimization of components and systems for solar collectors, CSP and DES plants, and on the thermal design of PV, BIPV and CPV systems.

energies

MDPI

Article

Cold Storage for a Single-Family House in Italy

Luigi Mongibello * and Giorgio Graditi

ENEA—Italian National Agency for New Technologies, Energy and Sustainable Economic Development, Portici Research Center-Piazzale E. Fermi, 1, 80055 Portici (NA), Italy; giorgio.graditi@enea.it
* Correspondence: luigi.mongibello@enea.it; Tel.: +39-081-7723584

Academic Editor: Francesco Asdrubali
Received: 13 September 2016; Accepted: 6 December 2016; Published: 12 December 2016

Abstract: This work deals with the operation, modeling, simulation, and cost evaluation of two different cold storage systems for a single-family house in Italy, that differ from one another on the cold storage material. The two materials used to perform the numerical simulations of the cold storage systems are represented by cold water and a phase change material (PCM), and the numerical simulations have been realized by means of numerical codes written in Matlab environment. The main finding of the present work is represented by the fact that, for the considered user characteristics, and under the Italian electricity tariff policy, the use of a proper designed cold storage system characterized by an effective operation strategy could represent a viable solution from an economical point of view.

Keywords: cold storage; cold water; PCM; simulation; single-family house; economic analysis

1. Introduction

The adoption of thermal energy storage in air conditioning systems permits the shifting of the electric demand/electric rate fully or partially from on-peak hours to off-peak ones. This generally implies a reduction of the operating costs and of the equipment ones, since thermal energy storage allows reduction of the equipment size, and to have longer operating hours of compressors and pumps, and chillers and cooling towers at full load at lower outdoor temperatures during night-time. Nevertheless, in general, the use of thermal energy storage systems also presents some drawbacks, which essentially are the high initial costs; complicated operation, maintenance, and control; and high encumbrance [1,2].

The effectiveness of cold storage in obtaining a profitable peak load shifting for refrigeration systems has been demonstrated by a number of works. Many control strategies and several storage materials have been tested to the purpose, with chilled water and ice being the most used cold storage materials. Lin et al. [3] conducted a thermo-economic analysis of an air conditioning system with chilled water storage, in which part of the chilled water back from the user is mixed with the chilled water supplied to the user, and analyzed the thermodynamic performance influence on cost savings. Yan et al. [4] optimized the design of an air conditioning system based on the use of a seasonal heat pipe-based ice storage system. Following their approach, during winter the seasonal ice storage system collects 'cold energy' from ambient low-temperature air. In summer, ice cold is extracted for air conditioning, and the melted ice is used as storage medium for chilled water storage. Soler et al. [5] analyzed the performance of a cooling network composed of eight chillers with different capacities and coefficients of performance, and a storage system, with the aim of maximizing chiller operating efficiency and minimizing the number of shut-downs and start-ups. Meyer and Emery [6] economically optimized the operation of an air conditioning system composed of two chillers, one designated for ice storage charging, the other for direct cooling, an air-handling unit, a cooling tower, and water pumps.

Habeebullah [7] investigated the economic feasibility of retrofitting an ice thermal energy storage system for an air conditioning system, considering both full storage and partial storage approaches.

In the last years, great attention has been also addressed to phase change materials (PCMs) different from ice, which have the potential to considerably lower the size of the storage, and consequently its encumbrance that represents one of the main limits of such systems [8–10].

This work relies on a novel approach for the design of refrigeration systems with cold storage for single-family houses in Italy. This approach consists of two stages: the first one, that in the following is referred to as pre-design, relies on the implementation of an original operation strategy for the refrigeration system based on partial storage, and aims to perform the dimensioning of the cold storage system and a first dimensioning of the chiller; in the second one, the results of the pre-design are used to set up the numerical simulation of the cold storage system, whose results are used to fix the final size of the chiller.

The above design approach has been applied in order to characterize two different cold storage systems for a single-family house in Italy, that differ from one another on the cold storage material. In particular, the operation, modeling, simulation, and cost evaluation of the two storage systems are presented in this work. The two materials used to perform the numerical simulations of the cold storage systems are represented by cold water and a phase change material (PCM), and the numerical simulations have been realized by means of numerical codes written in Matlab environment.

In the first part of the paper, the characteristics of the user thermal and electricity demand for air-conditioning in the summer season are described. Successively, the specifications of the operation strategy adopted, and of the analytical models used for the numerical simulations, are explained in detail. Finally, the results of pre-design, of simulations, and of an economic analysis are presented and discussed.

2. Case Study

In the present study, the user is represented by a single-family house, characterized by a surface area equal to 200 m^2 and an envelope shape factor of 0.9 m^{-1}, and situated in the Italian climatic zone E. The yearly thermal energy demand and the daily thermal and electrical load profiles for the air conditioning in the warm season have been evaluated as in reference [11]. In particular, it has been considered that the air conditioning in the warm season is limited to the months of June, July, and August, and that is realized by means of an electrical vapor compression chiller with a hydronic loop. The yearly thermal energy demand has been fixed to 21 kWh/m^2/year, and the same daily thermal and electrical load profiles have been used for all the operation days. Figure 1 shows the hourly averaged thermal and electrical load profiles for refrigeration of the considered user for the standard day considered. The electrical load profile has been evaluated considering the energy efficiency ratio (EER) of the chiller depending on the ambient temperature. Figure 2 shows the variation of the EER as a function of the hourly averaged ambient temperature. The temperature profile and the EER one have been normalized using the maximum average temperature equal to 28 °C, and the maximum value of EER equal to 3, respectively.

Thus, with reference to the Figure 1, and without considering a cold storage integrated into the refrigeration system, for the present user it is necessary to have a chiller of at least 2 kW of nominal electrical power, corresponding to the maximum electrical load, in order to fulfill the request for air conditioning in the summer season.

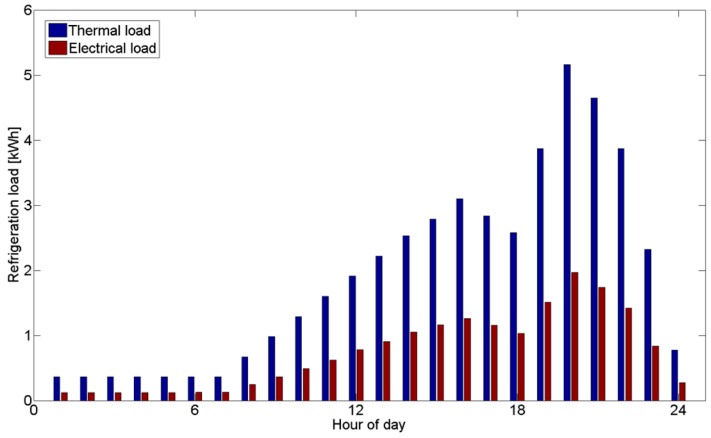

Figure 1. Refrigeration loads of the user.

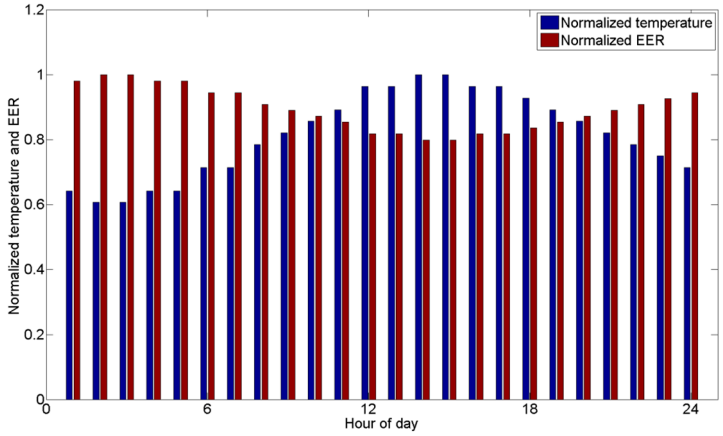

Figure 2. Non-dimensional temperature and EER profiles.

3. Operation Strategy and Methodologies of Analysis

With the aim of performing a reasonable integration and dimensioning of a cold storage system into the hydronic loop of the refrigeration system for the single-family house under study, a qualitative preliminary analysis has been done in order to evaluate what could be the most convenient approach between full storage and partial storage. The above analysis has been done taking into consideration that the Italian scenario concerning the electricity tariff allows private consumers to benefit from a reduced price of the electricity when it is used during night-time at off-peak hours. Nevertheless, it has emerged that partial storage is likely more convenient than full storage, mainly because the difference between the tariffs in on-peak hours and off-peak ones is not so high. Moreover, full storage would require a much larger tank for the cold storage, and it would also require a chiller with nominal power not much lower than the one in the case without storage. For the above reasons, the partial storage approach could be preferable and has been adopted in this study.

3.1. Operation Strategy and Pre-Design

3.1.1. Assumptions and Pre-Design

Considering the refrigeration loads reported in Figure 1, it is clear that, without cold storage, and for a fixed set-point of the user internal ambient temperature, the chiller operation cannot be continuous during the hours characterized by a refrigeration load that is lower than the minimum chiller thermal power. In those hours, the controller of the refrigeration system would implement several shut-downs of the chiller, that generally affects the chiller lifetime negatively. Indeed, the

controller would switch off the chiller each time the user internal ambient temperature has reached the predetermined set-point. Taking into account the above considerations, in the present study the amount of cold to be stored, and the nominal power of the chiller, in the case with cold storage, have been initially calculated by considering the following assumptions:

1. during its operation, the chiller has to work at constant power, constant mass flow rate, and constant outflow temperature $T_{c,out}$;
2. the ratio between the cooling power transferred to the user and the chiller power has to be higher than or equal to a predetermined minimum value, otherwise the chiller is shut down;
3. the chiller cannot feed the cold storage system only, that, in other words, means that the cold can be accumulated only when the chiller has to feed the user.

Clearly, assumption 1 implies that also the inflow temperature of the chiller $T_{c,in}$ is constant.

The above assumptions allow to uniquely identify the size of the chiller and the total amount of cold to be stored for the considered user. Later in the paper, it will be shown that this operational approach involves a relatively low size of the cold storage tank, a considerable reduction of the chiller power with respect to the case without the cold storage, and also that the chiller operates continuously for great part of the day. The results of the pre-design are then used to fix the size of the cold storage tank, and to set up the numerical simulation of the cold thermal energy storage system. Finally, the numerical results are used to evaluate the effective size of the chiller.

3.1.2. Operation of the Refrigeration System with Cold Storage

Figure 3 shows a schematic of the layout of the refrigeration system adopted for the implementation of the operational approach described in the previous section.

During chiller operation, the mass flow rate of the heat transfer fluid (HTF) through the user is controlled by means of valve V1 so that the temperature at the user exit—i.e., at point A—is equal to $T_{c,in}$. In case the valve V1 is partially open, the HTF passing through V1 goes to the cold storage tank charging it. A further control is applied by means of valve V2 in order to maintain the temperature at point B equal to $T_{c,in}$. In this case the valve V3 is fully open while valve V4 is fully close.

Otherwise, in case valve V1 is fully close, which implies that all HTF from the chiller goes to the user and that the HTF exits the user at a temperature that is higher than $T_{c,in}$, the cold storage tank is discharged. In this case, a control is applied by means of valve V3 in order to maintain the HTF temperature at point C equal to $T_{c,in}$, and also V2 is fully closed.

Assumptions 1 and 2 of the operational approach imply that the mass flow rate of HTF flowing through the user has to be higher than or equal to a minimum value, fixed equal to half the nominal HTF mass flow rate through the chiller, otherwise the chiller is shut down.

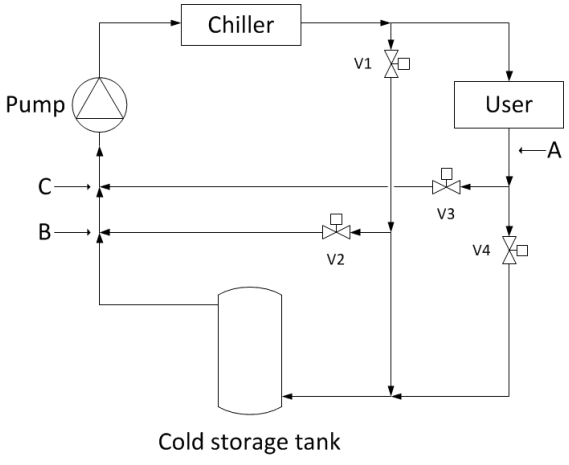

Figure 3. Layout of the refrigeration system.

3.2. Cold Water Storage Tank Model

1D analytical models have been used in order to simulate the cold water storage tank and the coiled tube heat exchanger [12]. Figure 4 shows a sketch of the close vertical cylindrical tank with a single immersed serpentine considered in the present study. This cold water storage tank configuration, in which the HTF is separated from the water in the tank, permits the use of HTFs different from water, and consequently allows HTF temperatures at the chiller outflow ($T_{c,out}$) even slightly higher than 0 °C, as for example 1 °C or 2 °C. Indeed, in such cases it would be not possible to use water as HTF since water could freeze inside the chiller, and a mixture of water and antifreeze should be used.

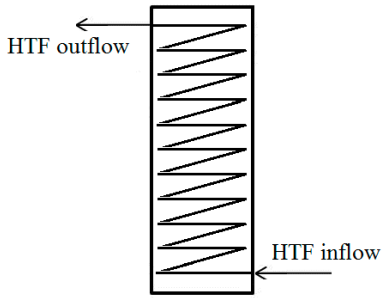

Figure 4. Sketch of the cold water storage tank.

The internal water volume is divided into isothermal nodes representing water layers of equal volume. The energy balance for each node is written as:

$$\rho_w V_w c_{p_w} \frac{dT_w}{dt} = \frac{(T_{\mathrm{HTF}} - T_w)}{R_{coil}} + Q_{cond} - \frac{(T_w - T_{amb})}{R_{tank}} \quad (1)$$

where Q_{cond} represents the conductive heat exchange with adjacent layers. The thermal resistance relative to each layer of the storage wall has been evaluated as:

$$R_{tank} = R_{conv\_int} + R_{cond} + R_{conv\_ext} \quad (2)$$

where

$$R_{conv\_int} = \frac{1}{\bar{h}_{int\_tank} A_{int\_tank}} \quad (3)$$

The mean convective heat transfer coefficient relative to the inner tank wall in Equation (3) is evaluated using the Nusselt number correlation for free convection relative to a vertical flat plate [13].

The conductive thermal resistance relative to the tank wall has been evaluated as:

$$R_{cond} = \frac{\ln\left(\frac{r_{out\_tank}}{r_{in\_tank}}\right)}{2\pi k_{ins} \Delta_{layer}} \quad (4)$$

It has been assumed that the tank thickness is equal to the insulation thickness (0.1 m, expanded polyurethane), namely that the conductive thermal resistance of the tank steel wall is negligible.

The convective thermal resistance relative to the external tank wall has been evaluated as:

$$R_{conv\_ext} = \frac{1}{\bar{h}_{ext\_tank} A_{ext\_tank}} \quad (5)$$

For each time-step and for each node, the energy balance equations system composed of Equation (1) written for all nodes is solved using the implicit Euler method. The empirical reversion-elimination algorithm [14,15] has been adopted in order to include the effects of natural convection heat transfer between the water layers at different heights on the thermal stratification inside the tank.

A transient one-dimensional model has been adopted for the evaluation of the temperature field of the HTF flowing through the immersed coil heat exchanger. The HTF considered is water.

Also, the heat exchanger has been divided in isothermal nodes representing tube sections having the same volume. For each node, the energy balance equation is given by:

$$\rho_{\mathrm{HTF}} V_{nod} c_{p_{\mathrm{HTF}}} \frac{dT_{\mathrm{HTF}}}{dt} = \frac{(T_{tank} - T_{\mathrm{HTF}})}{R_{coil}} + \rho_{\mathrm{HTF}} \dot{V}_{\mathrm{HTF}} c_{p\mathrm{HTF}} (T_{\mathrm{HTF\_in}} - T_{\mathrm{HTF\_out}}) \quad (6)$$

The thermal resistance between the HTF in the coil heat exchanger and the water in the cold storage tank is given by:

$$R_{coil} = R_{conv\_int} + R_{conv\_ext} + R_{cond} \quad (7)$$

where

$$R_{conv\_int} = \frac{1}{\bar{h}_{int\_coil} A_{int\_coil}} \quad (8)$$

The mean internal convective heat transfer coefficient in Equation (8) is evaluated using the Gnielinski's correlation for coiled tube heat exchanger [16] for the Nusselt number calculation.

The external convective thermal resistance has been evaluated as:

$$R_{conv\_ext} = \frac{1}{\bar{h}_{ext\_coil} A_{ext\_coil}} \quad (9)$$

The mean external convective heat transfer coefficient in Equation (9) is evaluated using the Morgan's correlation for natural convection for horizontal cylinders [17] for the Nusselt number.

The conductive thermal resistance of the coil has been neglected, because its order of magnitude is much lower than the internal and external convective thermal resistances.

For each time-step and for each node, Equation (6) is solved using the implicit Euler method.

The coupling between the cold water tank balance equations system and the one relative to the serpentine has been dealt with an iterative approach.

3.3. PCM Storage Tank Model

Figure 5 shows a schematic of the cylindrical cold storage tank with a PCM as storage material considered in this study. The inflow and outflow plenums for the HTF are connected by uniformly distributed straight parallel 1/4" pipes passing through the PCM material placed in the central body of the tank, and composing the heat exchanger.

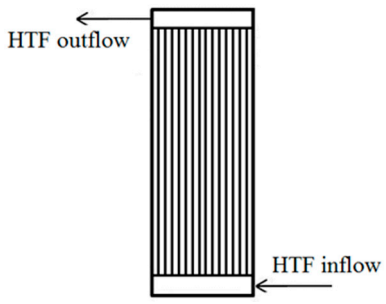

Figure 5. Schematic of the cold storage tank with PCM.

Table 1 reports the main thermo-physical characteristics of the organic PCM considered in the present study. Also in this case, the HTF flowing through the heat exchanger is water.

Table 1. Characteristics of the PCM.

Property	Value
Density	900 kg/m^3
Thermal conductivity	0.2 W/m/K
Latent heat of fusion	18×10^4 J/kg
Melting temperature	13 °C

It has been supposed that the charging and discharging processes are isothermal and realized at the PCM solidification/melting temperature, namely that the cold is stored only as latent heat. Thus, the volume of PCM that is necessary to store a certain amount of cold E_c is given by:

$$V_{\mathrm{PCM}} = \frac{E_c}{LH_{\mathrm{PCM}}\rho_{\mathrm{PCM}}} \tag{10}$$

where LH_{PCM} and ρ_{PCM} are the PCM latent heat of fusion and density, respectively.

The size of the heat exchanger has been evaluated by means of the ε-NTU method [13], implemented on an hourly basis. This method is typically employed for the thermal design of standard heat exchangers, and it has been recently adopted by Tay et al. [18] and Mongibello et al. [19] for latent heat thermal energy storage systems. Therefore, for each pipe of the heat exchanger, the thermal power exchanged between the HTF to the PCM is given by:

$$\dot{Q} = \varepsilon \dot{m} c_{p,\mathrm{HTF}} \Delta T \tag{11}$$

where ΔT represents the difference between the HTF temperature at the inlet section of the pipe and the PCM melting temperature, $\dot{m}$ is the mass flow rate of the HTF through the pipe, and ε represents the heat exchanger efficiency, given by:

$$\varepsilon = 1 - e^{(NTU)} \tag{12}$$

The number of transfer units NTU is calculated using the following expression:

$$NTU = \frac{1}{R_{\mathrm{tot}} \dot{m} c_{p,\mathrm{HTF}}} \tag{13}$$

The overall thermal resistance is given by:

$$R_{\mathrm{tot}} = R_{\mathrm{HTF}} + R_{\mathrm{wall}} + R_{\mathrm{PCM}} \tag{14}$$

where the thermal resistance relative to the heat transfer between the pipe external surface and the PCM is calculated as:

$$R_{\mathrm{PCM}} = \frac{1}{C(\delta) k_{\mathrm{PCM}}} \tag{15}$$

In Equation (15), the parameter $C(\delta)$ refers to the conduction between the pipe external surface and the phase change front supposed concentric to the pipe, and it is a function of the parameter δ representing the ratio between the liquefied portion of the PCM total volume and the PCM total volume. Accordingly, being the phase change front variable with time during the charging phase, the heat exchanger efficiency ε results to be time dependent. Thus, for each operation hour, the average value of the efficiency can be used in Equation (11), that becomes:

$$\dot{Q} = \bar{\varepsilon} \dot{m} c_{p,\mathrm{HTF}} \Delta T \tag{16}$$

For given values of the mass flow rate, of the minutes of operation of the chiller, of the temperature of the HTF entering the storage tank, and of cold to be accumulated at each operation hour, and for a fixed reasonable volume of PCM filling up the storage tank and a fixed aspect ratio of the tank, the number of pipes of the heat exchanger can be evaluated by means of the iterative procedure prescribing the following steps:

1. Fix an initial tentative value for the number of pipes;
2. Divide the total PCM volume in its initial state by the number of pipes in order to evaluate the volume of PCM surrounding each pipe, that is supposed concentric to the pipe;
3. Knowing the cold to be stored or released and the minutes of operation at each hour, evaluate the thermal power to be exchanged at each hour, and evaluate for each hour the fraction of the PCM volume surrounding the pipes that undergoes solidification or melting using Equation (10);
4. Knowing the fraction of PCM that has undergone phase change, determine for each hour the average efficiency of the heat exchanger using Equations (12)–(15);
5. For each hour, calculate the thermal power exchanged by means Equation (16);
6. For each hour, compare the value of thermal power calculated at Step 5 with the one calculated at Step 3. If the maximum of the absolute values of the differences between thermal power values is lower than a certain tolerance, then stop the procedure and accept the number of pipes. Otherwise, increase or reduce the number of pipes as a function of the above differences and return to Step 2.

Finally, once dimensioned the heat exchanger, the energy balance at the heat exchanger pipes permits the calculation of the HTF temperature at the storage tank exit.

The initial tentative value of the number of pipes has to be low enough to avoid the occurrence of conditions in which the cold can be only stored by sensible energy. Indeed, the present model cannot be applied when only sensible energy storage is expected, as for example in the case charging is done when the entire PCM volume is already in the solid phase, or, equivalently, when the discharging is done when the entire PCM volume is already in the liquid one.

A similar procedure can be implemented to evaluate the total PCM volume for a fixed aspect ratio of the tank. In this case, a reasonable number of pipes is fixed, and the total PCM volume is varied in order to match the exchanged thermal power values. Similarly, in this case the initial tentative value of total PCM volume has to be high enough to avoid that the occurrence of conditions in which the cold can be only stored by sensible energy.

4. Results

4.1. Pre-Design

Figure 6 shows the thermal and electrical powers of the chiller through the day, while Figure 7 shows on the same graph the chiller thermal power and the refrigeration loads, resulting from the pre-design. Thus, with the adopted operational approach, the chiller thermal power for the refrigeration system with cold storage resulting from the pre-design is equal to 2.55 kW, with a maximum absorbed electric power of 1.05 kW, that is about the half of the maximum electric power that is needed in the case without the cold storage. Furthermore, it can be noticed the peak-shaving effect due to the cold storage. Figure 8 shows, for each hour of the day, the minutes of operation of the chiller resulting from the pre-design. It can be noticed that, owing to the adopted operational approach, the chiller operation is continuous over a great part of the day, and that the chiller production still remains concentrated in the on-peak hours.

Figure 9 shows, for each hour of the day, the difference between the chiller thermal production and the refrigeration load. The total amount of cold to be stored resulting from the pre-design is 8.4 kWh, that is about the 18% of the user daily total request.

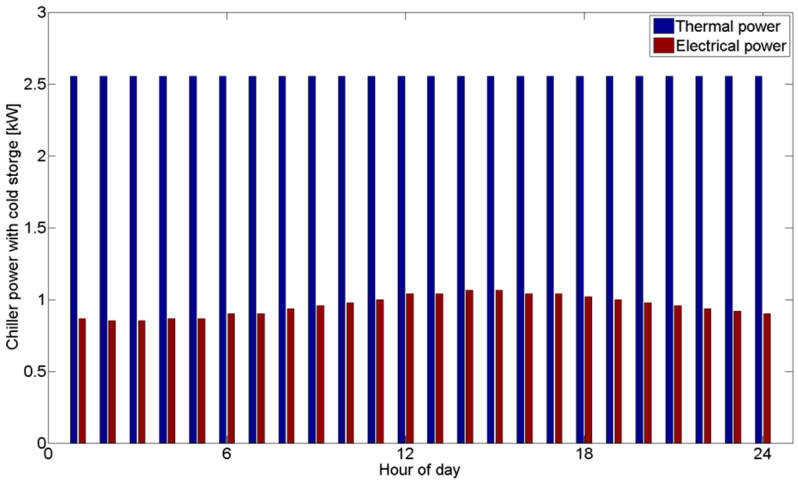

Figure 6. Chiller power with cold storage.

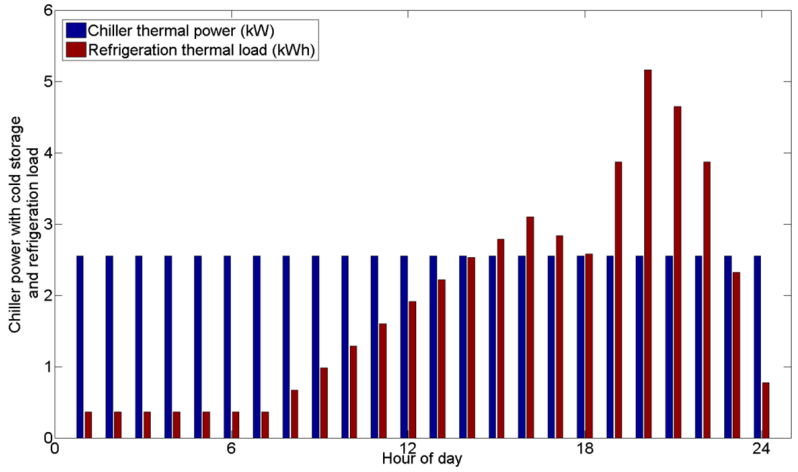

Figure 7. Chiller thermal power and refrigeration loads.

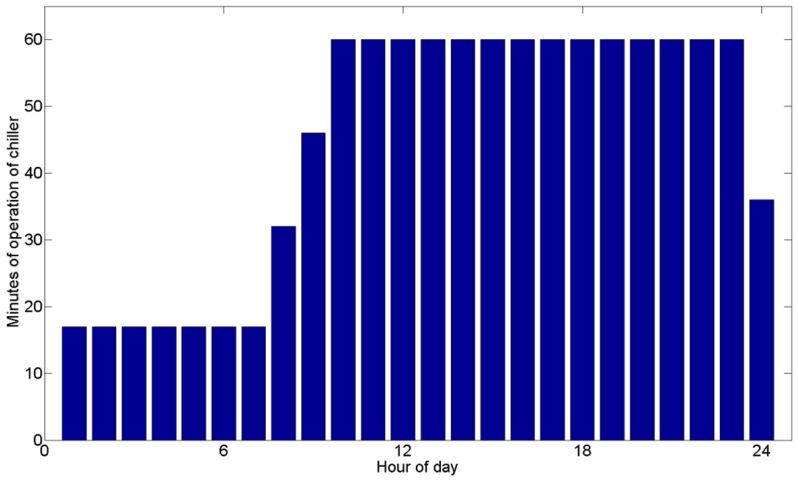

Figure 8. Minutes of operation of the chiller.

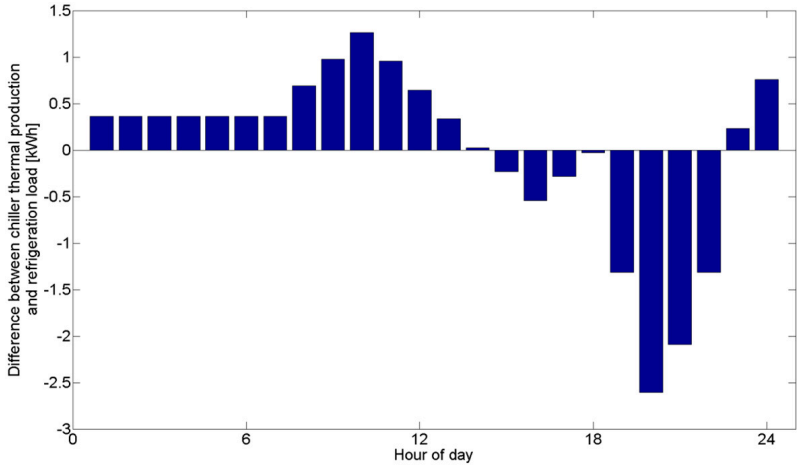

Figure 9. Difference between the chiller thermal production and the refrigeration loads.

4.2. Cold Water Storage Tank

The numerical simulation of the cold water storage tank has been done assuming that the HTF exits the chiller at a constant temperature $T_{c,out}$ = 7.0 °C, and at a constant total mass flowrate of 0.1 kg/s. The assumption of constant chiller thermal power implies that the expected temperature of the HTF at the inflow section of the chiller is equal to $T_{c,in}$ = 13.1 °C.

The volume of the cold water storage tank has been calculated by using the difference between the HTF temperatures at the chiller inflow and outflow sections, namely 13.1 °C and 7 °C, respectively. It is given by:

$$V_{w,\mathrm{tot}} = \frac{SC}{\rho_w c_{p_w}(T_{c,in} - T_{c,out})} \tag{17}$$

where SC represents the maximum storage capacity resulting from the pre-design, i.e., 8.4 kWh (30.27 MJ). The resulting water volume is equal to about 1200 L. Finally, a commercial cylindrical tank with a capacitance of 1000 L has been used for the simulations. The tank height from its bottom surface is equal to 2 m (not including insulation), and the entire external surface of the tank is insulated by means of a 0.1 m layer of rigid expanded polyurethane. The tank is provided with a single 1" serpentine with a heat exchange surface of 8 m^2, and the tank capacitance does not include the volume occupied by the serpentine. The inflow section of the serpentine is placed at 5 cm from the tank bottom surface, while the outflow one at 5 cm from the tank top surface. The results of the numerical simulation presented in this section refer to a spatial discretization of the tank realized using 50 nodes, while the serpentine discretization has been made so that its nodes represent the serpentine portions included in the tank layers relative to the tank nodes, and a time-step of 60 s has been adopted. Independence of results from the spatial discretization and time-step has been assured.

The main outputs of the Matlab code are the temperatures at the tank and serpentine nodes. At each time-step, the HTF mass flow rate flowing through the tank heat exchanger, and the HTF temperature at the inflow section of the heat exchanger have been evaluated according to the operation strategy reported in Section 3.1. At each hour, the chiller is active, and the mass flow rate is different from zero, only during the corresponding minutes of operation of the chiller reported in Figure 8. Finally, the following results refer to periodic conditions, obtained starting from an initial temperature of the tank water and of the HTF in the serpentine equal to 13.1 °C.

Figure 10 shows the temporal evolution of the HTF temperature at the serpentine outflow during the day, of the HTF temperature at the serpentine inflow, and the resulting temporal evolution of the HTF temperature at the chiller inflow, while Figure 11 shows the HTF mass flow rate through the serpentine and through the user. With reference to Figure 10, it can be noticed that, around h = 12, the HTF temperature at the chiller inflow is slightly lower than the expected value of $T_{c,in}$, i.e., 13.1 °C.

This is because, in that time interval, the HTF temperature at the serpentine outflow is lower than 13.1 °C, implying that the chiller has to work at a lower power in that period in order to maintain the HTF temperature at its outflow constant and equal to 7 °C.

It can be also noticed that, at the end of the discharging phase, the HTF temperature at the serpentine outflow and the one at the chiller inflow are higher than 13.1 °C. In this case, the chiller has to work consuming a higher electrical power, i.e., 1.3 kW, in order to keep the outflow temperature constant and equal to 7 °C, meaning that a chiller operating at a constant absorbed electric power of 1.05 kW together with the considered cold storage tank is not capable of fulfilling the user request.

The above considerations are evident if Figure 12, showing the cold taken and released from the storage during the day evaluated in the pre-design, and the ones resulting from the numerical simulations, is analyzed. In fact, it can be seen that, at 11, 12, and 13 h, from the simulation it has emerged that the storage system accumulates less cold than the one resulting from the pre-design. Moreover, it can be seen that at the end of the discharging phase, the cold released by the storage system is much lower than the one evaluated in the pre-design. The reasons explaining the above results are represented by the storage degradation due to the losses through the tank external walls, and to the degradation of the temperature stratification inside the tank. Figures 13 and 14 show the evolution of the water temperature profile in the tank during the charging phase and the discharging one, respectively.

Thus, considering the operation strategy and the size of the cold storage system adopted in this study, in the case with cold storage it is necessary to have a chiller, provided with an inverter, characterized by a maximum absorbed electric power of 1.3 kW, that, however, is much lower than the one in the case without cold storage, namely 2 kW.

From the economic point of view, the chiller and storage tank costs have been evaluated on the basis of real prices in the Italian market. The market price of vapor compression chillers with hydronic loop clearly depends on the chiller size, with the minimum size present in the market equal to 2 kWe at a cost that can be assumed equal to 2500 €. The chiller size in the case with cold storage, i.e., 1.3 kWe, is lower than the above minimum available size in commerce, so its cost has been extrapolated considering an average unitary cost of such chillers in the range from 2 to 10 kWe equal to 800 €/kWe. Hence, as the difference between the chiller absorbed power in the two cases is equal to 700 W, the cost difference is 560 €. Relatively to the storage system cost, considering that it is a closed system not used to store domestic water, its cost can be assumed equal to 1000 €. All the other investment costs have been considered equal in the two different cases.

As concerns the electricity consumption, it is practically the same in the two cases, and this is explained considering that, in the case with cold storage, the consumption surplus due to the higher power needed at the end of the discharging phase is compensated by the higher electricity consumption during night-time at a higher EER. Moreover, in the case without cold storage, it would be necessary to have an available maximum electric power higher than 3 kW in order to avoid power outages during on-peak hours. This would involve an annual fixed cost of 150 €, that is avoided in the case with cold storage.

So, for the present application, the installation of a hydronic vapor compression chiller with cold storage would involve an investment cost that is 440 € higher than the one in the case without cold storage. Nevertheless, due to the avoided annual fixed cost of 150 €, in the case with cold storage the higher investment cost would be returned in less than four years if an interest rate of 5% is applied.

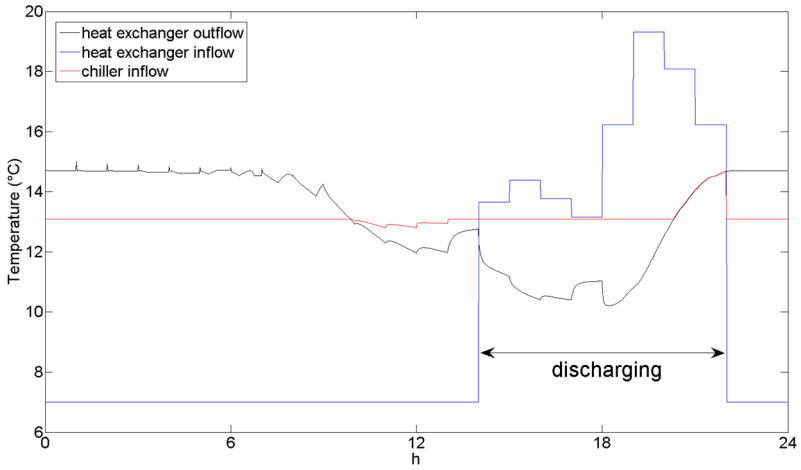

Figure 10. HTF temperature profiles at the water tank heat exchanger inflow and outflow sections, and at the chiller inflow section.

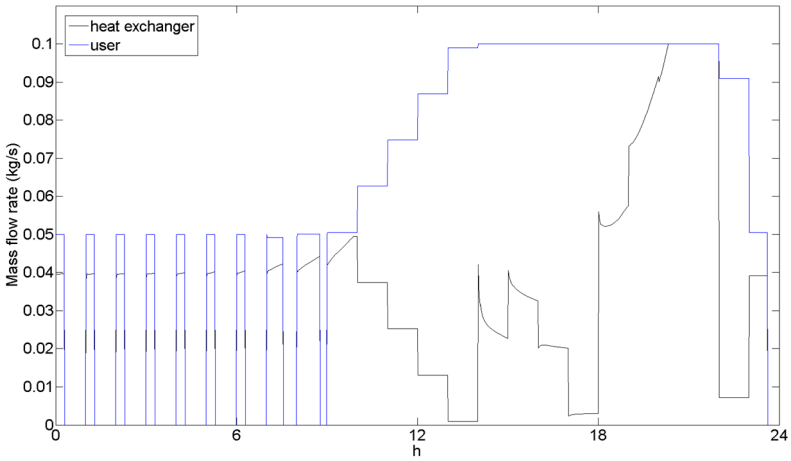

Figure 11. HTF mass flow rate through the water tank heat exchanger and the user.

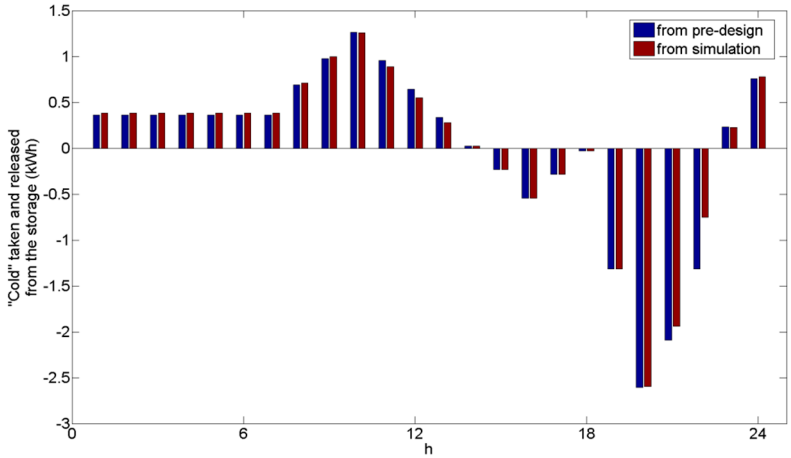

Figure 12. "Cold" taken and released from the cold water tank.

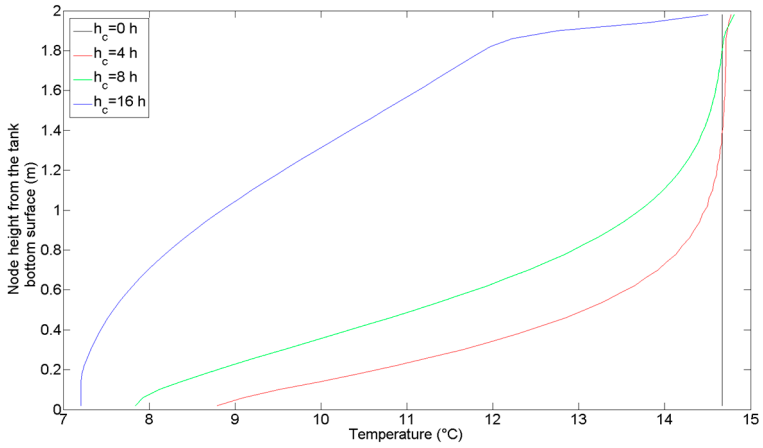

Figure 13. Temperature profiles in the cold water tank during the charging phase (h_c = 0 h refers to the beginning of the phase).

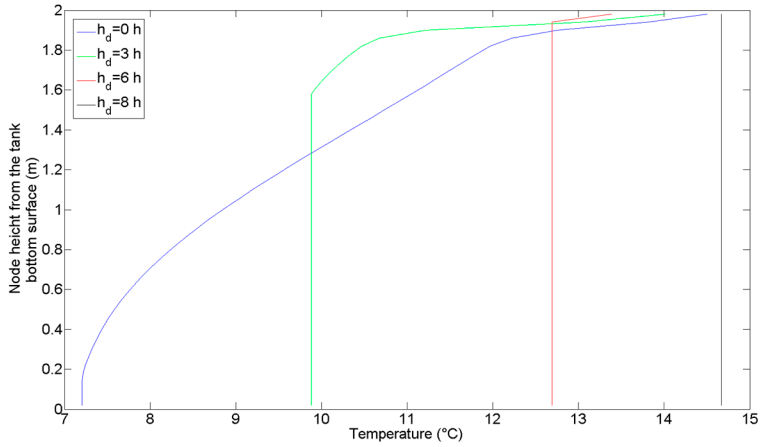

Figure 14. Temperature profiles in the cold water tank during the discharging phase (h_d = 0 h refers to the beginning of the phase).

4.3. PCM Storage Tank

Also in this case, it is assumed that the HTF exits the chiller at a constant temperature $T_{c,out}$ = 7.0 °C, and at a constant total mass flowrate of 0.1 kg/s, and the evaluation of the HTF mass flow rate flowing through the tank heat exchanger and of the HTF temperature at the inflow section of the heat exchanger has been made according to the operation strategy reported in Section 3.1.

The volume of the PCM storage tank has been calculated by means of Equation (10), considering the total amount of cold to be stored equal to the value resulting from the pre-design. The resulting tank volume is 190 L including about 170 kg of PCM. The size of the heat exchanger, considered composed of uniformly distributed straight parallel 1/4" pipes, has been calculated following the iterative procedure described in Section 3.3. In particular, the total heat exchange surface has been calculating by fixing the tank aspect ratio at 4, the initial tentative value equal to 2 m^2, and a stop condition prescribing that the iterations stop when the maximum normalized difference between the thermal power values from the pre-design and the ones calculated using the model described in Section 3.3 is lower than 1%. The resulting total heat exchange surface is 3.8 m^2.

Figure 15 shows the temporal evolution of the HTF temperatures at the pipes inflow and outflow, and the resulting temporal evolution of the HTF temperature at the chiller inflow, while Figure 16 shows the HTF total mass flow rate through the heat exchanger pipes and through the user. It can be seen in Figure 16 that the two profiles are superimposed for 0–9 h in the charging phase, and for 15–22 h

during the discharging phase, namely over the entire discharging phase. This last finding indicates that, during discharge, the entire HTF mass flow rate is sent to the cold storage for pre-cooling, and is consistent with the fact that the HTF temperature at the chiller inflow coincide with the one at the heat exchanger outflow over the entire discharging phase, as shown in Figure 15. Figure 15 also shows that the HTF temperature at the chiller inflow is always equal to about 13.1 °C, that is the value of $T_{c,in}$ from the pre-design, implying that the chiller practically works at constant power during both charging and discharging. Thus, in this case, the chiller operating at a constant absorbed electric power of 1.05 kW—i.e., the absorbed power resulting from the pre-design—together with the considered PCM storage tank are able to fulfill the user request. This result is confirmed by Figure 17, showing that the profile of the cold taken and released from the storage during the day evaluated by means of the PCM storage tank model is practically the same as the one resulting from the pre-design.

However, as regards the economic aspects, the estimated cost of the PCM (8 €/kg) and the one of the non-standard tank (around 500 €) make this solution impractical from the economic point of view. In this case, about the same payback period as in the case with cold water storage can be obtained with a target cost for the PCM of 3 €/kg.

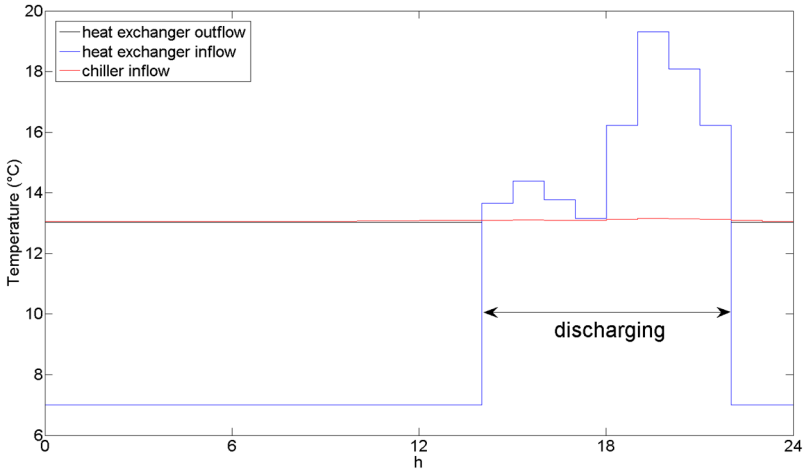

Figure 15. HTF temperature profiles at the PCM tank heat exchanger inflow and outflow sections, and at the chiller inflow section.

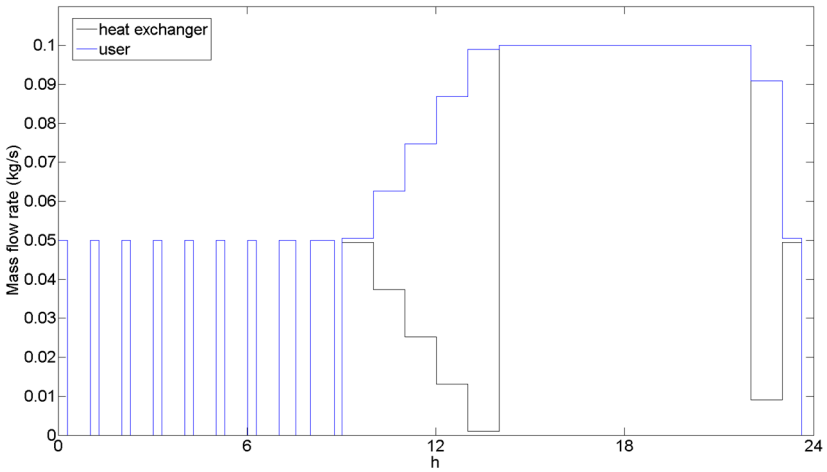

Figure 16. HTF mass flow rate through the PCM tank heat exchanger and the user.

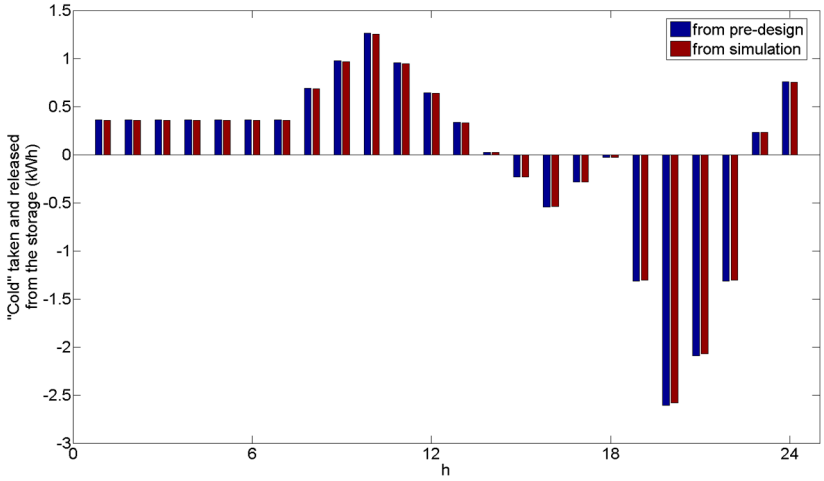

Figure 17. "Cold" taken and released from the PCM tank.

5. Conclusions

In this work, the operation, modeling, simulation, and cost evaluation of two different cold storage systems for a single-family house in Italy, that differ from one another on the cold storage material, have been addressed. The two materials used to perform the numerical simulations of the cold storage systems are represented by cold water and a phase change material, and the numerical simulations have been realized by means of numerical codes written in Matlab environment.

Results have shown that, for the considered user characteristics, a cold water storage system characterized by an effective operation strategy could represent a viable solution from the economical point of view.

Future studies may regard the dimensioning of a storage system integrated into the fluidic system of a reversible vapor compression heat pump, that can be also used to store heat during the cold season.

Author Contributions: Both authors conceived the work. Luigi Mongibello selected the models and realized the numerical codes for the simulations. Both authors analyzed the data resulting from the numerical simulations. The paper was written by Luigi Mongibello, and revised by both authors.

Conflicts of Interest: The authors declare no conflict of interest.

References

1. Silvetti, B.; MacCracken, M. Thermal storage and deregulation. *ASHRAE J.* **1998**, *4*, 55–59.
2. Wang, S.K. *Handbook of Air Conditioning and Refrigeration*, 2nd ed.; McGraw-Hill: New York, NY, USA, 2001.
3. Lin, H.; Li, X.H.; Cheng, P.S.; Xu, B.G. Thermoeconomic evaluation of air conditioning system with chilled water storage. *Energy Convers. Manag.* **2014**, *85*, 328–332. [CrossRef]
4. Yan, C.; Shi, W.; Li, X.; Zhao, Y. Optimal design and application of a compound cold storage system combining seasonal ice storage and chilled water storage. *Appl. Energy* **2016**, *171*, 1–11. [CrossRef]
5. Soler, M.S.; Sabaté, C.C.; Santiago, V.B.; Jabbari, F. Optimizing performance of a bank of chillers with thermal energy storage. *Appl. Energy* **2016**, *172*, 275–285. [CrossRef]
6. Kintner-Meyer, M.; Emery, A. Optimal control of an HVAC system using cold storage and building thermal capacitance. *Energy Build.* **1995**, *23*, 19–31. [CrossRef]
7. Habeebullah, B.A. Economic feasibility of thermal energy storage systems. *Energy Build.* **2007**, *39*, 355–363. [CrossRef]
8. Sun, Y.; Wang, S.; Xiao, F.; Gao, D. Peak load shifting using different cold thermal energy storage facilities in commercial buildings: A review. *Energy Convers. Manag.* **2013**, *71*, 101–114. [CrossRef]
9. Navidbakhsh, M.; Shirazi, A.; Sanaye, S. Four E analysis and multi-objective optimization of an ice storage system incorporating PCM as the partial cold storage for air-conditioning applications. *Appl. Therm. Eng.* **2013**, *58*, 30–41. [CrossRef]

10. Oró, E.; Depoorter, V.; Plugradt, N.S.J. Overview of direct air free cooling and thermal energy storage potential energy savings in data centres. *Appl. Therm. Eng.* **2015**, *85*, 100–110. [CrossRef]
11. Mongibello, L.; Bianco, N.; Caliano, M.; Graditi, G. Influence of heat dumping on the operation of residential micro-CHP system. *Appl. Energy* **2015**, *160*, 206–220. [CrossRef]
12. Mongibello, L.; Bianco, N.; Caliano, M.; de Luca, A.; Graditi, G. Transient analysis of a solar domestic hot water system using two different solvers. *Energy Procedia* **2015**, *81*, 89–99. [CrossRef]
13. Bejan, A.; Kraus, A.D. *Heat Transfer Handbook*; John Wiley & Sons Inc.: Hoboken, NJ, USA, 2003.
14. Mather, D.W.; Hollands, K.G.T.; Wright, J.L. Single- and Multi-Tank energy storage for solar heating systems: Fundamentals. *Sol. Energy* **2002**, *73*, 3–13. [CrossRef]
15. Newton, B.J.; Schmid, M.; Mitchell, J.W.; Beckman, W.A. Storage tank models. In Proceedings of the ASME/JSME/JSES International Solar Energy Conference, Maui, HI, USA, 19–24 March 1995.
16. Gnielinski, Y. Heat transfer and pressure drop in helically coiled tubes. In Proceedings of the 8th International Heat Transfer Conference, San Francisco, CA, USA, 17–22 August 1986; Volume 6, pp. 2847–2854.
17. Morgan, V.T. The overall convective heat transfer from smooth circular cylinders. *Adv. Heat Transf.* **1975**, *11*, 199–264.
18. Tay, N.H.S.; Belusko, M.; Bruno, F. An effectiveness-NTU technique for characterising tube-in-tank phase change thermal energy storage systems. *Appl. Energy* **2012**, *91*, 309–319. [CrossRef]
19. Mongibello, L.; Capezzuto, M.; Graditi, G. Technical and cost analyses of two different heat storage systems for residential micro-CHP plants. *Appl. Therm. Eng.* **2014**, *71*, 636–642. [CrossRef]

© 2016 by the authors; licensee MDPI, Basel, Switzerland. This article is an open access article distributed under the terms and conditions of the Creative Commons Attribution (CC-BY) license (http://creativecommons.org/licenses/by/4.0/).

Engineering Sustainability

Evaluation of wall surface temperatures in green facades
Vox, Blanco, Fuina *et al.*

ice | proceedings

Proceedings of the Institution of Civil Engineers
Engineering Sustainability
http://dx.doi.org/10.1680/jensu.16.00019
Paper 1600019
Received 11/03/2016 Accepted 22/07/2016
Keywords: buildings, structures & design/sustainability/urban regeneration

ICE Publishing: All rights reserved

ice Institution of Civil Engineers publishing

Evaluation of wall surface temperatures in green facades

Giuliano Vox MSc
Professor, Department of Agricultural and Environmental Science Disaat, University of Bari, Bari, Italy

Ileana Blanco PhD
Researcher, Department of Agricultural and Environmental Science Disaat, University of Bari, Bari, Italy

Silvana Fuina MSc
PhD Student, Department of Agricultural and Environmental Science Disaat, University of Bari, Bari, Italy

Carlo Alberto Campiotti PhD
Research Manager, Technical Unit for Energy Efficiency and Agriculture Unit, Enea – Italian National Agency for New Technologies, Energy and Sustainable Economic Development, Rome, Italy

Giacomo Scarascia Mugnozza MSc
Professor, Department of Agricultural and Environmental Science Disaat, University of Bari, Bari, Italy

Evelia Schettini PhD
Professor, Department of Agricultural and Environmental Science Disaat, University of Bari, Bari, Italy (corresponding author: evelia.schettini@uniba.it)

Green walls can be used to control the building microclimate as passive systems for energy saving. Three vertical walls were built at the University of Bari (Italy). The first wall was covered with *Pandorea jasminoides* variegated and the second with *Rhyncospermum jasminoides*; the third wall was kept uncovered as a control. High-definition infrared images were recorded, and several climatic parameters concerning the walls and the ambient conditions were collected during the experimental test. The daylight temperatures observed on the shielded walls during warm days were lower than the respective temperatures of the uncovered wall by up to 9·0°C; the nighttime temperatures observed during cold days were higher than the respective temperatures of the control wall by up to 6·0°C. The effective thermal resistance of the plants was calculated, using experimental data for a whole year; it ranged from 0·07 to 3·61 m^2 K/W.

Notation

C	heat capacity, J/(kg K)
Q	heat flux, W/m^2
R	thermal resistance, (m^2 K)/W
T	temperature (K)
λ	thermal conductivity, W/(m K)
Subscripts	
bw	bare wall
ext	external
int	internal
plant	plant layer
s	surface
vw	vegetated wall

1. Introduction

The presence of urban green infrastructures (UGIs), such as urban forests, street trees, parks, turf grass, private gardens, green roofs and green walls, plays an important role in contributing to a broad range of ecosystem services. In cities or metropolitan areas, UGIs contribute to the mitigation of the urban heat island (UHI) effect – that is, a hotter urban area compared with the surrounding rural areas, with differences of air temperature of about 5–6°C (Berdahl and Bretz, 1997; Bretz and Akbari, 1997; Bretz *et al*., 1998; Gentle *et al*., 2011; Gladis and Schumann, 2011; Jo *et al*., 2010; Joudi *et al*., 2013; Kanechi *et al*., 2014; Karlessi *et al*., 2011; Li *et al*., 2013, 2015; Prado and Ferreira, 2005; Rowe, 2011; Synnefa *et al*., 2006; Uemoto *et al*., 2010; Zinzi *et al*., 2012). UGIs also reduce the ambient temperatures, improve human thermal comfort and decrease energy loads on buildings (Cameron *et al*., 2014; Campiotti *et al*., 2013; Fernandez-Cañero *et al*., 2013; Köhler and Poll, 2010; Norton *et al*., 2015; Pérez *et al*., 2014; Rowe, 2011). An UHI causes an increase in the use of air-conditioning systems and, consequently, an excessive energy consumption, a rise in air pollution and greenhouse gases' concentration in the atmosphere, poor levels of comfort outdoors and possible threats to human health (Jaffal *et al*., 2012; Kalkstein and Davis, 1989; Karlessi *et al*., 2011; Petralli *et al*., 2006). The main factors contributing to the UHI phenomenon are: the use of non-reflective and water-resistant materials for building external surfaces; dense urbanisation geometry characterised by wide surfaces that can absorb incident and reflected solar radiation, contributing to radiation trapping and to wind speed reduction in the emerging urban canyons; and anthropogenic heat emitted from activities such as those of industrial processes, heating and cooling systems and motorised vehicular traffic (Ryu and Baik, 2012; Santamouris, 2012; Vox *et al*., 2016).

Green roofs and green walls, as UGIs, are living vegetated horizontal and vertical layers positioned on the external envelope of the buildings aimed at energy consumption reduction for air conditioning in summer and thermal insulation increment in winter (Berardi *et al*., 2014; Fernandez-Cañero *et al*., 2013; Santamouris, 2012; Schettini *et al*., 2015, 2016).

Green vertical systems can be employed as a passive sustainable technology for mitigating the UHI effect and also for enhancing the energy efficiency of buildings, in particular in dense urban areas, where buildings with a high wall-to-roof ratio offer large surface areas available for retrofitting (Cheng *et al*., 2010; Raji *et al*.,

Offprint provided courtesy of www.icevirtuallibrary.com
Author copy for personal use, not for distribution

2015). The cooling effect of greenery systems is obtained by intercepting and absorbing solar radiation; the resulting reduction in the buildings' solar heat gain implies less energy consumption for air cooling in summer. The evapotranspirative effect, generated from the plants and the substrate on their surroundings, leads to a cooler ambient temperature and consequently to reduction in the cooling load of the buildings (Raji *et al*., 2015; Sunakorn and Yimprayoon, 2011; Wong *et al*., 2010). The vegetation and the substrate layer can influence the thermal performance of the buildings in winter, acting as an insulation against wind, depending on the climate of the region and on the characteristics of the greenery system used (Berardi *et al*., 2014; Cheng *et al*., 2010; Fernandez-Cañero *et al*., 2013; Jim and He, 2011; Köhler and Poll, 2010; Pérez *et al*., 2011; Perini *et al*., 2011; Vox *et al*., 2015).

The Mediterranean regions, characterised by hot and dry climates, are areas where greenery systems can produce benefits, due to the shading effect and to the high evapotranspiration rate of plants (Castleton *et al*., 2010; Raji *et al*., 2015). It is important to use vegetation characterised by low irrigation requirements in order to be suitable for the exposure conditions and for the specific weather conditions. Europe and North America are reported as the regions where green roofs can be profitably applied, requiring low maintenance (Castleton *et al*., 2010; Refahi and Talkhabi, 2015).

In the literature, experimental results on green walls relate to investigations of not more than 2 weeks during summertime, rather than the whole year, and simulation models often were not validated with real data (Hunter *et al*., 2014; Pérez *et al*., 2014; Raji *et al*., 2015). Few studies report the evaluation of the effects of green wall systems on energy savings, useful to define suitable plant species and options in regions characterised by the Mediterranean climate. When studying the potential of green facades for energy savings, one of the most relevant parameters for comparison could be the registered abatement of the temperature of the building's external wall surface during daytime as an effect generated by the green layer (Pérez *et al*., 2014); actually, the building's external wall surface is the most commonly evaluated parameter (Hunter *et al*., 2014).

The aim of this paper is to examine the effects of two different climbing evergreen plants used as green vertical passive systems on building walls during a whole year. The field test was carried out at the University of Bari (Italy) in order to overcome the lack of literature on experimental data for a longer period in the Mediterranean region. Several climatic parameters concerning the walls and the ambient conditions were analysed for estimating the variations in the walls' surface temperature equipped with the greenery systems. The effective thermal resistance of the green layer was evaluated as a useful tool for models in order to estimate internal climate and energy fluxes.

2. Materials and methods

The field test was carried out from June 2014 to March 2016 at the experimental farm of the University of Bari in Valenzano (Bari, Italy), at a latitude of 41° 05′ N and a longitude of 16° 53′ E and an altitude of 85 m above sea level. Three identical walls were made as a prototype of a commonly used vertical building closure in Mediterranean civil construction. The walls facing south were built using perforated bricks joined with mortar; they were characterised by a width of 1·00 m, a height of 1·55 m and a thickness of 0·22 m. The bricks have a thickness of 0·20 m, a height of 0·25 m and a length of 0·25 m, a thermal conductivity λ (Uni, 2012) equal to 0·282 W/(m K), an average density of the masonry work (including plaster) equal to 695 kg/m^3 and a specific heat capacity C equal to 840 J/(kg K).

The structures including the walls were insulated on the back side, setting up a sealed structure in order to better evaluate the influence of the vegetation layer on the wall; the insulating structure was made of sheets of expanded polystyrene, having a thickness of 30 mm and a thermal conductivity of 0·037 W/(m K). In order to reduce the effect of the incident solar radiation on the sealed structure, a shading net was positioned onto the structures.

Two different evergreen climbing plants were chosen as greenery vertical systems components (Figure 1): one wall was covered with *Pandorea jasminoides* variegated and the second with *Rhyncospermum jasminoides*; a third wall was kept uncovered as a control. A plant-supporting structure made of an iron net was placed at a distance of 15 cm from the vertical wall. The plants were transplanted on 18 June 2014. The plants were irrigated with the drip method.

The experimental data were collected by means of a meteorological station consisting of a data logger (CR10X, Campbell, Logan, UT, USA) and several sensors for measuring different climatic parameters. The data were measured at a frequency of 60 s, averaged every 15 min and stored in the data logger. The solar radiation normal to the walls was measured using a pyranometer (model 8-48, Eppley Laboratory, Newport, RI, USA) in the wavelength range of 0·3–3·0 μm. The external air

Figure 1. The experimental structures: the wall covered with *R. jasminoides* (right), the wall with *P. jasminoides* variegated (middle) and the uncovered control wall (left)

Offprint provided courtesy of www.icevirtuallibrary.com
Author copy for personal use, not for distribution

temperature was measured by using a Hygroclip-S3 sensor (Rotronic, Zurich, Switzerland); it was adequately shielded from solar radiation. The temperature of the external plaster surfaces exposed to the solar radiation (Figure 2) was measured using thermistors (Tecno.El S.r.l., Rome, Italy).

Statistical analyses were carried out with the CoStat software (CoHort Software, Monterey, CA, USA). One-way analysis of variance at a 95% probability level was carried out in order to compare mean temperature values; Duncan's test was applied at a significance level equal to 0·05.

High-definition infrared images of the walls were recorded using a thermal infrared camera (model B660, Flir Systems, Burlington, ON, Canada) in order to analyse the surface temperatures both of the plant leaves and of the walls. The measurements were carried out setting an average value of emissivity equal to 0·95 for both *P. jasminoides* variegated and *R. jasminoides*; the emissivity value was set to 0·96 for the white plaster of the uncovered wall.

The effective thermal resistance of the plant layer (R_{plant}) is a metric for accounting the reductions in conductive heat transfer through the wall, in terms of additional resistance, as an effect of the vegetation layer (Susorova *et al*., 2013). The overall thermal resistance of the vegetated wall (R_{vw}) is the sum of R_{plant} and of the thermal resistance of the bare wall (R_{bw}). The heat fluxes through the bare (Q_{bw}) and green walls (Q_{vw}) were calculated by

$$1.\quad Q_{bw} = \frac{T_{ext,s,bw} - T_{int,s,bw}}{R_{bw}}$$

$$2.\quad Q_{vw} = \frac{T_{ext,s,vw} - T_{int,s,vw}}{R_{bw}}$$

Figure 2. Sensor for the measurement of the surface temperature of the external plaster

where $T_{ext,s,bw}$ and $T_{int,s,bw}$ are the external and internal surface temperatures of the bare wall (control), respectively, R_{bw} is the thermal resistance of the bricks and plaster (0·73 m^2 K/W), and $T_{ext,s,vw}$ and $T_{int,s,vw}$ are the external and internal surface temperatures of the vegetated walls, respectively (Susorova *et al*., 2013). In the steady-state hypothesis, R_{vw} and R_{plant} were estimated using the following equations

$$3.\quad R_{vw} = R_{bw}\frac{Q_{bw}}{Q_{vw}}$$

$$4.\quad R_{plant} = R_{vw} - R_{bw}$$

R_{plant} was calculated for two cases: conditioned and unconditioned spaces. The difference between the external and internal surface temperatures of the wall, in the case of conditioned space, was calculated by setting the internal air temperature at 24°C during the warm months and at 20°C during the cold months; the internal air temperature of the space was assumed equal to the internal surface temperature. In unconditioned space, the measured values were used for $T_{ext,s}$ and $T_{int,s}$.

3. Results and discussion

Data were collected at the experimental field from April 2015 to March 2016, during which the values of the external air temperature ranged from 1·7 to 41·4°C.

The greenery systems affected the wall surface temperatures mainly in the warm period, as shown by the thermal images of the walls' surfaces and of the plants recorded in the field (Figures 3 and 4). Figure 3 shows the temperatures measured on 1 April 2015. The temperature of the leaves was influenced by the different exposure to the solar radiation; on the whole, the leaves recorded an average temperature of 26·1°C, and the temperature of the plaster behind the plant was 22·2°C, while the average temperature of the uncovered wall was 23·7°C. Figure 4 shows the temperatures measured on 7 July 2015. The average temperature of the plants was 26·9°C, and the temperature of the covered plaster was 26·9°C, while the average temperature of the uncovered wall was 29·0°C.

Figure 5 shows the temperatures of the external surface of the green walls and of the control wall, the external air temperature and the solar radiation normal to the surface on a summer day of July (8 July 2015), which was characterised by a maximum external air temperature equal to 40·7°C. The selected day was part of a heat wave event (Meehl and Tebaldi, 2004); the decrease in the air temperature around noon was related to an upward variation in the north wind speed. In the daytime the presence of the vegetation layer mitigated the temperature of the external plaster of the walls, in comparison with the temperature of the control wall. On 8 July 2015, maximum temperature decreases of 4·2 and 4·7°C were recorded for the walls protected with

Offprint provided courtesy of www.icevirtuallibrary.com
Author copy for personal use, not for distribution

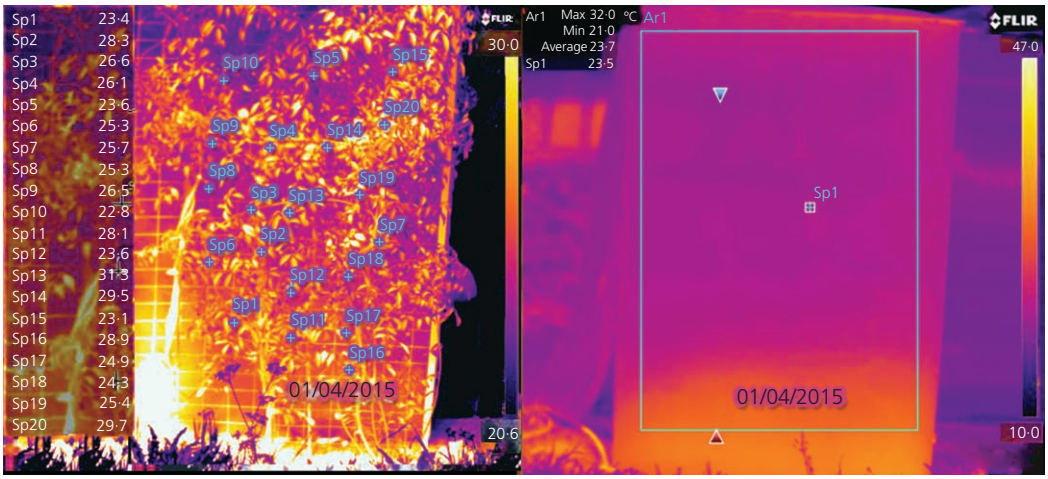

Figure 3. Thermal image of the control wall and of the green facade with *P. jasminoides* variegated, recorded on 1 April 2015 at 1.15 p.m.

R. jasminoides and *P. jasminoides* variegated, respectively; these were due to the plant shading effect and the evapotranspiration rate (Raji *et al*., 2015).

The maximum reduction in temperature between the uncovered wall and the covered ones was equal to 9·0°C and was recorded on 31 August 2015 at 1.00 p.m. for the wall protected with *P. jasminoides* variegated. During non-heat-wave summer days, the maximum temperature decrease on the walls was about 4°C.

Pérez *et al*. (2014) reported the following reduction in the external building surface temperature: from 1·7 to 13°C in warm, temperate climate regions and from 7·9 to 16°C in snow climate regions in the case of a wall covered with traditional green facades during summertime. Susorova *et al.* (2014) reported an average decrease in the facade surface temperatures due to the presence of vegetation on the facade from 1·0 to 9·0°C during summer on the external surface. Chen *et al*. (2013) reported for a living wall system in a hot and humid climate a reduction in the exterior wall temperature by a maximum of 20·8°C and in the interior wall temperature by 7·7°C.

The mitigation of the wall surface temperature due to the plants was observed throughout the year; the monthly average values of the maximum daily temperatures shows that in the daytime the application of the greenery systems allowed the external surface temperature of the green walls to be maintained at values lower than those of the control wall; no significant difference was pointed out between the two plants (Table 1). The differences between the average values of the maximum daily temperatures recorded for the control and for the walls covered with the plants ranged between 1·6 and 5·0°C, the higher differences being recorded from July to September.

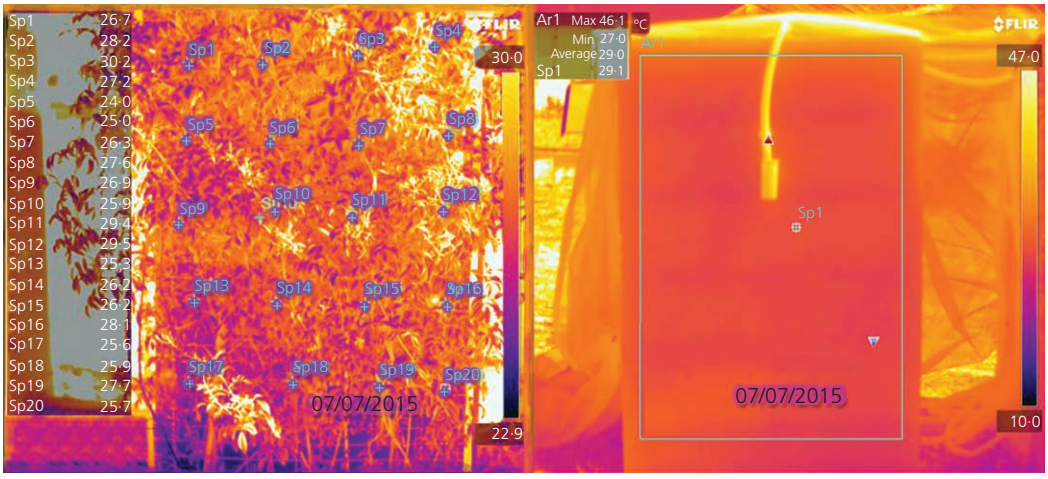

Figure 4. Thermal image of the control wall and of the green facade with *P. jasminoides*, recorded on 7 July 2015 at 9.30 a.m.

Offprint provided courtesy of www.icevirtuallibrary.com
Author copy for personal use, not for distribution

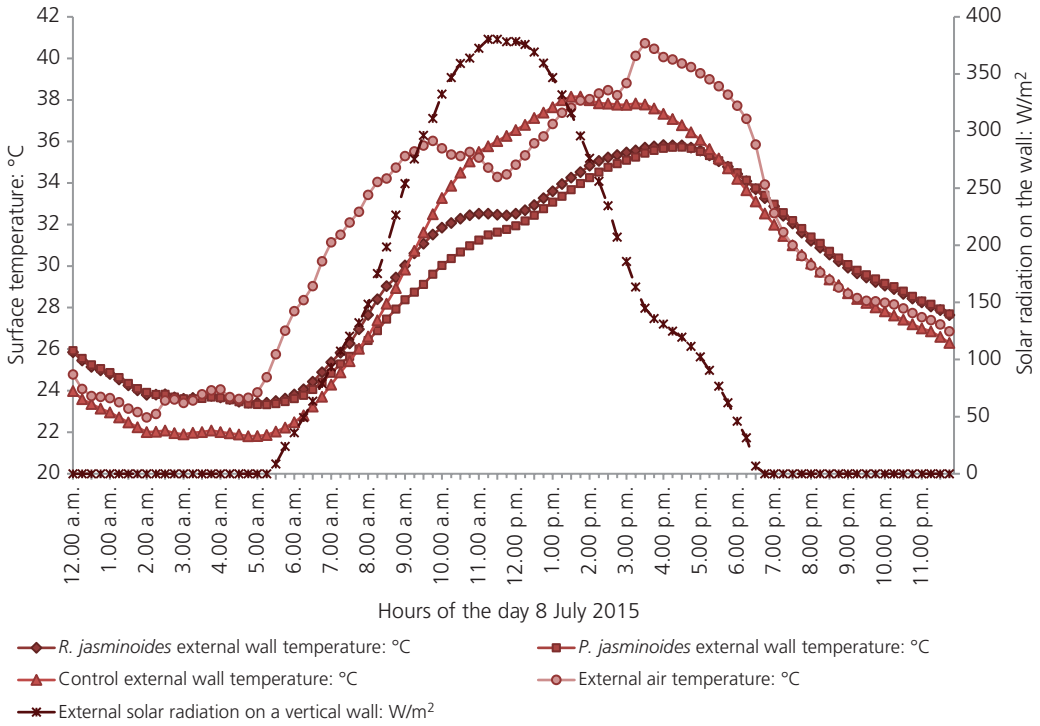

Figure 5. Surface temperatures of the external plaster exposed to solar radiation (external wall) of the three walls, external air temperature and solar radiation normal to the walls (secondary axis); data recorded on 8 July 2015

	April 2015	May 2015	June 2015	July 2015	August 2015	September 2015	October 2015	November 2015	December 2015	January 2016	February 2016	March 2016
	Average maximum daily temperature: °C											
R. jasminoides external wall	19·3^{a}	24·3^{b}	27·2^{b}	32·6^{c}	30·6^{c}	27·4^{b}	20·7^{b}	17·1^{b}	14·5^{c}	13·2^{b}	15·7^{c}	14·2^{b}
P. jasminoides variegated external wall	19·4^{a}	25·2^{b}	28·1^{b}	32·9^{c}	30·6^{c}	27·7^{b}	21·2^{b}	17·2^{b}	14·8^{bc}	13·2^{b}	16·0^{bc}	15·2^{b}
Control external wall	21·0^{a}	27·1^{a}	30·8^{a}	37·1^{a}	35·6^{a}	32·2^{a}	24·2^{a}	20·5^{a}	18·1^{a}	15·9^{a}	18·8^{a}	17·2^{a}
External air	21·3^{a}	27·7^{a}	30·5^{a}	35·8^{b}	33·8^{b}	30·6^{a}	23·6^{a}	19·1^{ab}	15·9^{b}	14·7^{ab}	17·6^{ab}	17·1^{a}
	Monthly cumulative solar radiation normal to the wall: MJ/m^{2}											
	330·2	291·5	269·5	304·1	343·9	356·9	320·8	320·8	331·1	289·2	298·1	275·7

Means in the same column with different superscript letters are significantly different ($P < 0{\cdot}05$)

Table 1. Average values of the maximum daily external air temperature and surface temperature of the external plaster of the three walls exposed to solar radiation and cumulative solar radiation normal to the wall, April 2015–March 2016

Offprint provided courtesy of www.icevirtuallibrary.com
Author copy for personal use, not for distribution

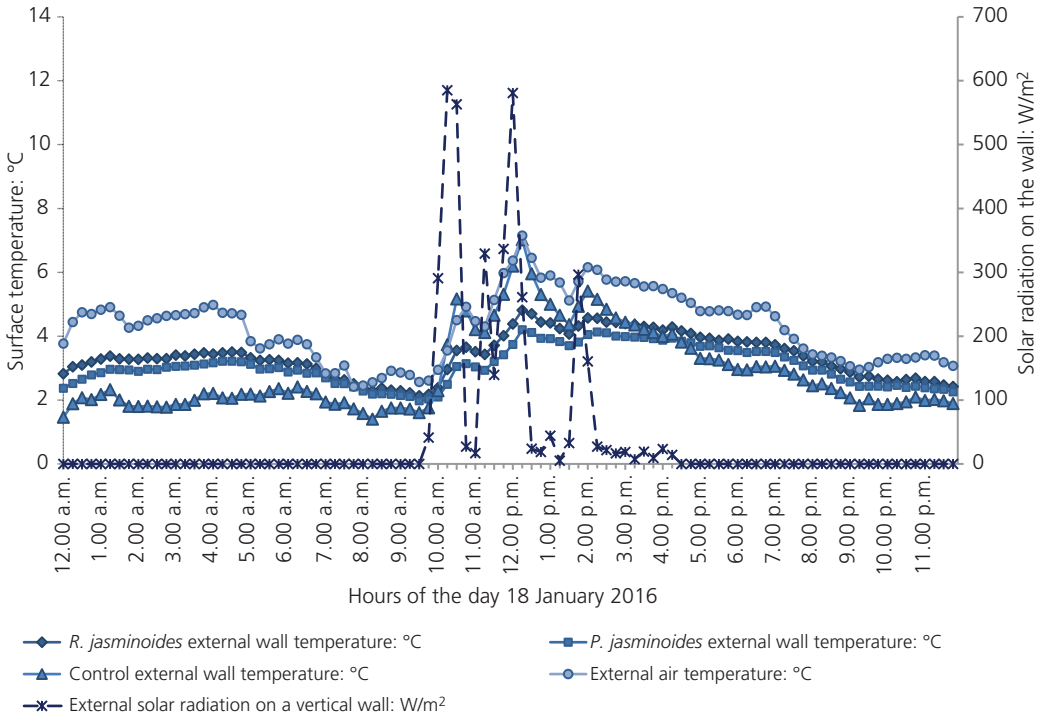

Figure 6. Surface temperatures of the external plaster exposed to solar radiation (external wall) of the three walls, external air temperature and solar radiation normal to the walls (secondary axis); data recorded on 18 January 2016

	April 2015	May 2015	June 2015	July 2015	August 2015	September 2015	October 2015	November 2015	December 2015	January 2016	February 2016	March 2016
						Average minimum daily temperature: °C						
R. jasminoides external wall	9·7^{a}	15·3^{a}	18·2^{a}	22·6^{a}	22·3^{a}	18·6^{a}	14·3^{a}	9·7^{a}	7·2^{a}	6·4^{a}	8·8^{a}	7·7^{a}
P. jasminoides variegated external wall	9·8^{a}	15·2^{a}	18·3^{a}	22·2^{a}	22·0^{ab}	18·3^{a}	14·2^{a}	9·7^{a}	7·1^{a}	6·3^{a}	8·8^{a}	7·8^{a}
Control external wall	8·4^{a}	13·8^{b}	16·8^{b}	21·1^{b}	21·1^{b}	17·4^{a}	13·1^{a}	8·2^{b}	5·6^{b}	4·8^{a}	7·3^{a}	6·5^{b}
External air	9·8^{a}	15·3^{a}	18·4^{a}	22·5^{a}	22·4^{a}	18·9^{a}	14·7^{a}	10·0^{a}	7·1^{a}	6·3^{a}	8·1^{a}	7·4^{ab}
						Monthly cumulative solar radiation normal to the wall: MJ/m^{2}						
	330·2	291·5	269·5	304·1	343·9	356·9	320·8	320·8	331·1	289·2	298·1	275·7

Means in the same column with different superscript letters are significantly different ($P < 0·05$)

Table 2. Average values of the minimum daily external air temperature and surface temperature of the external plaster of the three walls exposed to solar radiation and cumulative solar radiation normal to the wall, April 2015–March 2016

Offprint provided courtesy of www.icevirtuallibrary.com
Author copy for personal use, not for distribution

Figure 6 shows the temperatures of the wall external surface and of the external air, and the solar radiation normal to the wall on a winter's day in January (18 January 2016), which was cold and cloudy, as evidenced by the decreases in the walls' surface temperatures in the daytime, due to the presence of clouds. This day, part of a cold wave event, was characterised by a minimum external air temperature equal to 2·4°C; at nighttime the vegetation layer increased the insulation performance of the walls.

The highest increase in temperature of the external covered surface in comparison with the control, equal to 6·0°C, was recorded during a cold wave on 1 November 2015 at 4.15 a.m. for *P. jasminoides* variegated; in contrast, during non-cold-wave winter days, the maximum temperature increase on the walls was about 1·5°C.

The monthly average values of the minimum daily temperatures showed that at nighttime the application of the greenery systems kept the external surface temperature of the green walls at values higher than those of the control wall throughout the year; no significant temperature difference was recorded between the surfaces covered with the two plants. The differences between the lowest mean temperatures recorded for the wall shielded with plants and the control ranged from 0·9 to 1·6°C (Table 2). The minimum surface temperature of the external plaster protected with the two green walls closely followed the daily minimum external air temperature.

The evaluation of the effect of the green walls in the different seasons is shown in Tables 3 and 4.

The differences between the highest temperatures recorded for the control and for the walls covered with the plants ranged between 1·9 and 4·6°C; the maximum difference was recorded in summer and the minimum in spring (Table 3).

The differences between the lowest temperatures recorded for the wall shielded with plants and the control varied in the range of 1·0–1·5°C; the minimum difference was recorded in summer, and the maximum difference was recorded in winter (Table 4).

	Average maximum daily temperature: °C			
	Spring 21/03/2015–20/06/2015	Summer 21/06/2015–20/09/2015	Autumn 21/09/2015–20/12/2015	Winter 21/12/2015–20/03/2016
R. jasminoides external wall	22·4[b]	30·6[c]	18·4[c]	14·1[b]
P. jasminoides variegated external wall	23·1[b]	30·7[c]	18·7[c]	14·4[b]
Control external wall	25·0[a]	35·2[a]	22·0[a]	17·0[a]
External air	25·3[a]	33·8[b]	20·7[b]	16·0[a]

Means in the same column with different superscript letters are significantly different ($P < 0·05$)

Table 3. Seasonal data of the average maximum values of the daily external air temperature and of the surface temperature of the walls' external plaster from spring 2015 to winter 2015–2016

	Average minimum daily temperature: °C			
	Spring 21/03/2015–20/06/2015	Summer 21/06/2015–20/09/2015	Autumn 21/09/2015–20/12/2015	Winter 21/12/2015–20/03/2016
R. jasminoides external wall	13·5[a]	21·5[a]	11·3[a]	7·3[a]
P. jasminoides variegated external wall	13·5[a]	21·2[a]	11·3[a]	7·3[a]
Control external wall	12·1[b]	20·1[b]	9·9[b]	5·8[b]
External air	13·6[a]	21·6[a]	11·6[a]	7·0[a]

Means in the same column with different superscript letters are significantly different ($P < 0·05$)

Table 4. Seasonal data of the average minimum values of the daily external air temperature and of the surface temperature of the walls' external plaster from spring 2015 to winter 2015–2016

Offprint provided courtesy of www.icevirtuallibrary.com
Author copy for personal use, not for distribution

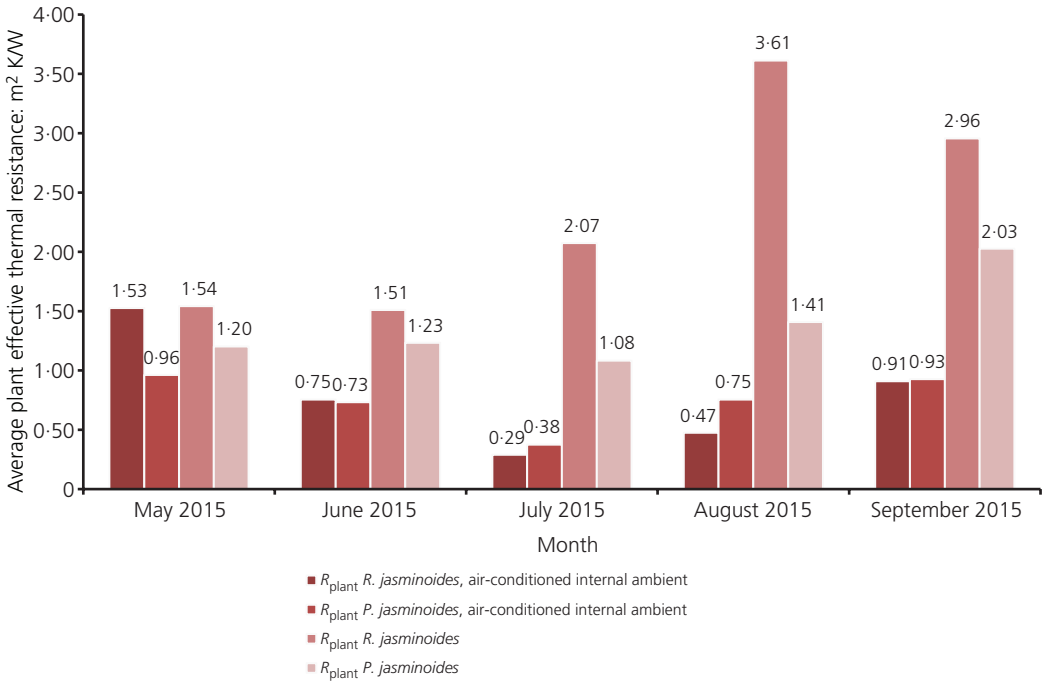

Figure 7. Average monthly effective thermal resistance of the plant layer in daytime during the warm months

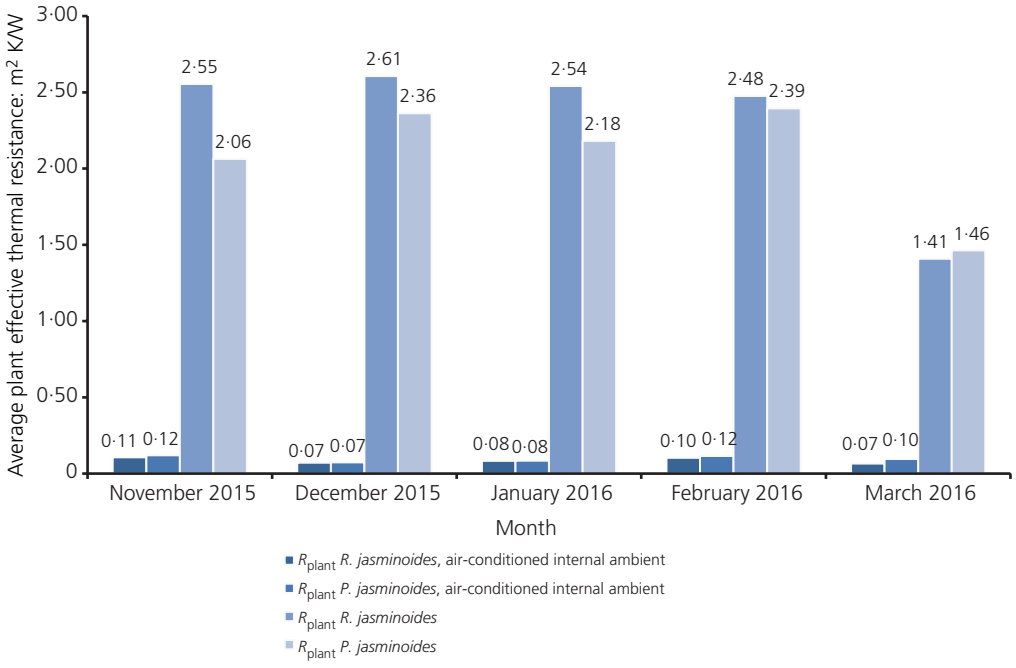

Figure 8. Average monthly effective thermal resistance of the plant layer at nighttime during the cold months

Offprint provided courtesy of www.icevirtuallibrary.com
Author copy for personal use, not for distribution

Figures 7 and 8 show the effective thermal resistance of the plant layer (R_{plant}) calculated both for the air-conditioned and for the non-air-conditioned ambient. In this study, the authors considered warm months the ones characterised by an average external air temperature higher than 20°C – that is, from May to September 2015 – and cold months those having an average external air temperature lower than 15°C – that is, from November 2015 to March 2016. R_{plant} was not evaluated in April and October 2015 because these months were characterised by fluctuating temperatures and by heat flux direction that was not well defined.

During the daytime of the warm months (May to September), when the heat flux was from outside to inside the closed space, R_{plant} ranged from 0·29 to 1·53 m^2 K/W for the conditioned space and from 1·08 to 3·61 m^2 K/W for the unconditioned space (Figure 7). In July and August, a more remarkable increase in the R_{plant} average value emerged for *R. jasminoides*, compared to *P. jasminoides* variegated, for the non-air-conditioned ambient. The fluctuations were higher due to the lower difference in temperature recorded on the two sides of the wall, in comparison with the conditioned case. The increase in the resistance could be attributed to the higher relative humidity and to the lower temperature of the air in the gap between plant and wall (data not shown), due to the different evapotranspiration rates of the two plants.

In the cold months (November to March) at nighttime, with the heat flux from inside to outside, R_{plant} ranged from 0·07 to 0·12 m^2 K/W for the conditioned space and from 1·41 to 2·61 m^2 K/W in case of the unconditioned space (Figure 8).

Susorova *et al*. (2013) found R_{plant} values ranging from 0·0 to 0·71 m^2 K/W; Kontoleon and Eumorfopoulou (2010) estimated that the thermal resistance of a 25-cm-wide plant foliage is almost 0·5 m^2 K/W.

4. Conclusions

Green walls can represent a sustainable solution for construction of new buildings and for retrofitting of existing buildings, in order to reduce the energy demands of the buildings' cooling systems, to mitigate the UHI and to improve the thermal energy performance of buildings.

The application of the green vertical walls to mitigate solar radiation effects on the buildings' external surfaces during warm periods led to lowering of the external surface daylight temperatures by up to 9·0°C in comparison with the wall not covered with plants. During cold periods, the green walls kept the external surface nighttime temperatures up to about 6·0°C above the surface temperature of the control wall.

Future research should be addressed to evaluate throughout the year if and to what extent the resulting decrease in the summer cooling load counterbalances the increase in the winter heating load, if present.

Anyway, the presence of the green layer provides the benefit of decreasing the exposure of building envelope to direct solar radiation and to large temperature fluctuations, which can cause its early deterioration.

The value of the plant effective thermal resistance calculated in the present research, using experimental data for a whole year, provides a useful contribution to the scientific literature that is focused on modelling the thermal behaviour of green walls.

Acknowledgements

The present work has been carried out under the 'Piano triennale 2012–2014 per la Ricerca di Sistema Elettrico Nazionale, progetto C.2 "Sviluppo di modelli per la realizzazione di interventi di efficienza energetica sul patrimonio immobiliare pubblico", Piano Annuale di Realizzazione (PAR) 2013', funded by the Italian Ministry of Economic Development.

The data processing and the editorial work were shared, within the competencies of the research groups, equivalently among the authors.

REFERENCES

Berardi U, Ghaffarianhoseini AH and Ghaffarian Hoseini A (2014) State-of-the-art analysis of the environmental benefits of green roofs. *Applied Energy* **115**: 411–428, http://dx.doi.org/10.1016/j.apenergy.2013.10.047.

Berdahl P and Bretz SE (1997) Preliminary survey of the solar reflectance of cool roofing materials. *Energy and Buildings* **25(2)**: 149–158, http://dx.doi.org/10.1016/S0378-7788(96)01004-3.

Bretz SE and Akbari H (1997) Long-term performance of high-albedo roof coatings. *Energy and Buildings* **25(2)**: 159–167, http://dx.doi.org/10.1016/S0378-7788(96)01005-5.

Bretz SE, Akbari H and Rosenfels A (1998) Practical issues for using solar-reflective materials to mitigate urban heat islands. *Atmospheric Environment* **32(1)**: 95–101, http://dx.doi.org/10.1016/S1352-2310(97)00182-9.

Cameron RWF, Taylor JE and Emmett MR (2014) What's 'cool' in the world of green façades? How plant choice influences the cooling properties of green walls. *Building and Environment* **73**: 198–207, http://dx.doi.org/10.1016/j.buildenv.2013.12.005.

Campiotti CA, Schettini E, Alonzo G *et al.* (2013) Building green covering for a sustainable use of energy. *Journal of Agricultural Engineering* **44**: 253–256, http://dx.doi.org/10.4081/jae.2013.(s1):e50.

Castleton HF, Stovin V, Beck SBM and Davison JB (2010) Green roofs: building energy savings and the potential of retrofit. *Energy and Buildings* **42(10)**: 1582–1591, http://dx.doi.org/10.1016/j.enbuild.2010.05.004.

Chen Q, Li B and Liu X (2013) An experimental evaluation of the living wall system in hot and humid climate. *Energy and Buildings* **61**: 298–307, http://dx.doi.org/10.1016/j.enbuild.2013.02.030.

Cheng CY, Cheung KKS and Chu LM (2010) Thermal performance of a vegetated cladding system on facade walls. *Building and*

Offprint provided courtesy of www.icevirtuallibrary.com
Author copy for personal use, not for distribution

Environment **45(8)**: 1779–1787, http://dx.doi.org/10.1016/j.buildenv.2010.02.005.

Fernandez-Cañero R, Emilsson T, Fernandez-Barba C and Herrera Machuca MA (2013) Green roof systems: a study of public attitudes and preferences in southern Spain. *Journal of Environmental Management* **128**: 106–115, http://dx.doi.org/10.1016/j.jenvman.2013.04.052.

Gentle AR, Aguilar JLC and Smith GB (2011) Optimized cool roofs: integrating albedo and thermal emittance with *R*-value. *Solar Energy Materials and Solar Cells* **95(12)**: 3207–3215, http://dx.doi.org/10.1016/j.solmat.2011.07.018.

Gladis F and Schumann R (2011) Influence of material properties and photocatalysis on phototropic growth in multi-year roof weathering. *International Biodeterioration & Biodegradation* **65(1)**: 36–44, http://dx.doi.org/10.1016/j.ibiod.2010.05.014.

Hunter AM, Williams NSG, Rayner JP *et al.* (2014) Quantifying the thermal performance of green façades: a critical review. *Ecological Engineering* **63**: 102–113, http://dx.doi.org/10.1016/j.ecoleng.2013.12.021.

Jaffal I, Ouldboukhitine SE and Belarbi R (2012) A comprehensive study of the impact of green roofs on building energy performance. *Renewable Energy* **43**: 157–164, http://dx.doi.org/10.1016/j.renene.2011.12.004.

Jim CY and He H (2011) Estimating heat flux transmission of vertical greenery ecosystem. *Ecological Engineering* **37(8)**: 1112–1122, http://dx.doi.org/10.1016/j.ecoleng.2011.02.005.

Jo JH, Carlson JD, Golden JS and Bryan H (2010) An integrated empirical and modeling methodology for analyzing solar reflective roof technologies on commercial buildings. *Building and Environment* **45(2)**: 453–460, http://dx.doi.org/10.1016/j.buildenv.2009.07.001.

Joudi A, Svedung H, Cehlin M and Rönnelid M (2013) Reflective coatings for interior and exterior of buildings and improving thermal performance. *Applied Energy* **103**: 562–570, http://dx.doi.org/10.1016/j.apenergy.2012.10.019.

Kalkstein LS and Davis RE (1989) Weather and human mortality: an evaluation of demographic and interregional responses in the United States. *Annals of the Association of American Geographers* **79(1)**: 44–64, http://dx.doi.org/10.1111/j.1467-8306.1989.tb00249.x.

Kanechi M, Fujiwara S, Shintani N and Uno Y (2014) Performance of herbaceous *Evolvulus pilosus* on urban green roof in relation to substrate and irrigation. *Urban Forestry & Urban Greening* **13(1)**: 184–191, http://dx.doi.org/10.1016/j.ufug.2013.08.003.

Karlessi T, Santamouris M, Synnefa A *et al.* (2011) Development and testing of PCM doped cool colored coatings to mitigate urban heat island and cool buildings. *Building and Environment* **46(3)**: 570–576, http://dx.doi.org/10.1016/j.buildenv.2010.09.003.

Köhler M and Poll PH (2010) Long-term performance of selected old Berlin greenroofs in comparison to younger extensive greenroofs in Berlin. *Ecological Engineering* **36(5)**: 722–729, http://dx.doi.org/10.1016/j.ecoleng.2009.12.019.

Kontoleon KJ and Eumorfopoulou EA (2010) The effect of the orientation and proportion of a plant-covered wall layer on the thermal performance of a building zone. *Building and Environment* **45(5)**: 1287–1303, http://dx.doi.org/10.1016/j.buildenv.2009.11.013.

Li H, Harvey J and Kendall A (2013) Field measurement of albedo for different land cover materials and effects on thermal performance. *Building and Environment* **59**: 536–546, http://dx.doi.org/10.1016/j.buildenv.2012.10.014.

Li D, Sun T, Liu M *et al.* (2015) Contrasting responses of urban and rural surface energy budgets to heat waves explain synergies between urban heat islands and heat waves. *Environmental Research Letters* **10(5)**: 054009, http://dx.doi.org/10.1088/1748-9326/10/5/054009.

Meehl GA and Tebaldi C (2004) More intense, more frequent and longer lasting heat waves in the 21st century. *Science* **305(5686)**: 994–997, http://dx.doi.org/10.1126/science.1098704.

Norton BA, Coutts AM, Livesley SJ *et al.* (2015) Planning for cooler cities: a framework to prioritise green infrastructure to mitigate high temperatures in urban landscapes. *Landscape and Urban Planning* **134**: 127–138, http://dx.doi.org/10.1016/j.landurbplan.2014.10.018.

Pérez G, Rincón L, Vila A, González JM and Cabeza LF (2011) Green vertical systems for buildings as passive systems for energy savings. *Applied Energy* **88(12)**: 4854–4859, http://dx.doi.org/10.1016/j.apenergy.2011.06.032.

Pérez G, Coma J, Martorell I and Cabeza LF (2014) Vertical Greenery Systems (VGS) for energy saving in buildings: a review. *Renewable and Sustainable Energy Reviews* **39**: 139–165, http://dx.doi.org/10.1016/j.rser.2014.07.055.

Perini K, Ottelé M, Fraaij ALA, Haas EM and Raiteri R (2011) Vertical greening systems and the effect on air flow and temperature on the building envelope. *Building and Environment* **46(11)**: 2287–2294, http://dx.doi.org/10.1016/j.buildenv.2011.05.009.

Petralli M, Prokopp A, Morabito M *et al.* (2006) Ruolo delle aree verdi nella mitigazione dell'isola di calore urbana: uno studio nella città di Firenze. *Rivista Italiana di Agrometeorologia* **1**: 51–58 (in Italian).

Prado RTA and Ferreira FL (2005) Measurement of albedo and analysis of its influence the surface temperature of building roof materials. *Energy and Buildings* **37(4)**: 295–300, http://dx.doi.org/10.1016/j.enbuild.2004.03.009.

Raji B, Tenpierik MJ and Van Den Dobbelsteen A (2015) The impact of greening systems on building energy performance: a literature review. *Renewable and Sustainable Energy Reviews* **45**: 610–623, http://dx.doi.org/10.1016/j.rser.2015.02.011.

Refahi AH and Talkhabi H (2015) Investigating the effective factors on the reduction of energy consumption in residential buildings with green roofs. *Renewable Energy* **80**: 595–603, http://dx.doi.org/10.1016/j.renene.2015.02.030.

Rowe DB (2011) Green roofs as a means of pollution abatement. *Environmental Pollution* **159(8–9)**: 2100–2110, http://dx.doi.org/10.1016/j.envpol.2010.10.029.

Offprint provided courtesy of www.icevirtuallibrary.com
Author copy for personal use, not for distribution

Ryu YH and Baik JJ (2012) Quantitative analysis of factors contributing to urban heat island intensity. *Journal of Applied Meteorology and Climatology* **51**: 842–854, http://dx.doi.org/10.1175/JAMC-D-11-098.1.

Santamouris M (2012) Cooling the cities – a review of reflective and green roof mitigation technologies to fight heat island and improve comfort in urban environments. *Solar Energy* **103**: 682–703, http://dx.doi.org/10.1016/j.solener.2012.07.003.

Schettini E, Blanco I, Scarascia Mugnozza G, Campiotti CA and Vox G (2015) Contribution of green walls to building microclimate control. *Proceedings of the 2nd International Symposium on Agricultural Engineering (ISAE 2015), Belgrade, Serbia*, pp. V-53–V-60 (257–264).

Schettini E, Blanco I, Campiotti CA *et al.* (2016) Green control of microclimate in buildings. *Agriculture and Agricultural Science Procedia* **8**: 576–582, http://dx.doi.org/10.1016/j.aaspro.2016.02.078.

Sunakorn P and Yimprayoon C (2011) Thermal performance of biofacade with natural ventilation in the tropical climate. *Procedia Engineering* **21**: 34–41, http://dx.doi.org/10.1016/j.proeng.2011.11.1984.

Susorova I, Angulo M, Bahrami P and Stephens B (2013) A model of vegetated exterior facades for evaluation of wall thermal performance. *Building and Environment* **67**: 1–13, http://dx.doi.org/10.1016/j.buildenv.2013.04.027.

Susorova I, Azimi P and Stephens B (2014) The effects of climbing vegetation on the local microclimate, thermal performance, and air infiltration of four building facade orientations. *Building and Environment* **76**: 113–124, http://dx.doi.org/10.1016/j.buildenv.2014.03.011.

Synnefa A, Santamouris M and Livada I (2006) A study of the thermal performance of reflective coatings for the urban environment. *Solar Energy* **80(8)**: 968–981, http://dx.doi.org/10.1016/j.solener.2005.08.005.

Uemoto KL, Sato NMN and John VM (2010) Estimating thermal performance of cool colored paints. *Energy and Buildings* **42(1)**: 17–22, http://dx.doi.org/10.1016/j.enbuild.2009.07.026.

Uni (Ente Nazionale Italiano di Unificazione) (2012) UNI EN 1745: Masonry and masonry products – methods for determining thermal properties. Uni, Milan, Italy.

Vox G, Blanco I, Campiotti CA, Giagnacovo G and Schettini E (2015) Vertical green systems for buildings climate control. *Proceedings of the 43rd International Symposium – Actual Tasks on Agricultural Engineering, Sveučilište u Zagrebu, Agronomski fakultet, Zavod za mehanizaciju poljoprivrede*. Opatija, Croatia, pp. 723–732.

Vox G, Maneta A and Schettini E (2016) Evaluation of the radiometric properties of roofing materials for livestock buildings and their effect on the surface temperature. *Biosystems Engineering* **144**: 26–37, http://dx.doi.org/10.1016/j.biosystemseng.2016.01.016.

Wong NH, Kwang Tan AY, Chen Y *et al.* (2010) Thermal evaluation of vertical greenery systems for building walls. *Building and Environment* **45(3)**: 663–672, http://dx.doi.org/10.1016/j.buildenv.2009.08.005.

Zinzi M, Carnielo E and Agnoli S (2012) Characterization and assessment of cool coloured solar protection devices for Mediterranean residential buildings application. *Energy and Buildings* **50**: 111–119, http://dx.doi.org/10.1016/j.enbuild.2012.03.031.

HOW CAN YOU CONTRIBUTE?

To discuss this paper, please email up to 500 words to the editor at journals@ice.org.uk. Your contribution will be forwarded to the author(s) for a reply and, if considered appropriate by the editorial board, it will be published as discussion in a future issue of the journal.

Proceedings journals rely entirely on contributions from the civil engineering profession (and allied disciplines). Information about how to submit your paper online is available at www.icevirtuallibrary.com/page/authors, where you will also find detailed author guidelines.

Vegetation as a passive system for enhancing building climate control

I. Blanco[1], E. Schettini[1,a], G. Scarascia Mugnozza[1], C.A. Campiotti[2], G. Giagnacovo[2] and G. Vox[1]

[1]Department of Agricultural and Environmental Science, University of Bari, Via Amendola 165/a, 70126 Bari, Italy; [2]ENEA - Italian National Agency for New Technologies, Energy and Sustainable Economic Development, Technical Unit Energy Efficiency, Via Anguillarese, 301, 00123 Rome, Italy.

Abstract

Building indoor air temperature depends on several different parameters related to the climate of the region, the building itself and its use. The main parameters influencing the microclimate are: external air temperature and relative humidity, incident solar radiation, long wave radiation exchange between the building surfaces and its surroundings, incidence and speed of the wind, air exchanges, physical and thermal properties of the building's envelope materials, design variables such as building dimensions and orientation, presence of artificial light, electrical equipment. A sustainable technology for improving the energy efficiency of buildings and to mitigate urban heat island is the use of green roofs and walls. The green technology can allow the physical shading of the building and promote evapotranspiration in summer and increase the thermal insulation in winter. An experimental test was carried out at the University of Bari (Italy). Three vertical walls, made with perforated bricks, were tested: two were covered with plants (one with *Pandorea jasminoides* variegated, the second with *Rhyncospermum jasminoides*) while the third wall was kept uncovered and used as control. A system composed by a data logger and sensors was used to measure and record the following parameters: temperature of the wall surface under solar radiation and of the surface on the other side of the wall, solar radiation falling on the wall, and external air temperature. The use of the green walls during cold months allowed increasing the thermal insulation performance of the walls by keeping the external surface temperature in nighttime hours up to about 2.8°C over the surface temperature of the wall not covered with plants.

Keywords: urban agriculture, air-conditioning, energy savings, green walls, microclimate, urban heat island

INTRODUCTION

The presence of urban green infrastructures (UGI) in a city can improve urban climate and reduce the variations of the urban air temperature, surface temperature and surface maxima temperature, especially in the Mediterranean climatic area (Norton et al., 2015; Pérez et al., 2014; Tan et al., 2014; Vox et al., 2015). UGI includes public and private green open spaces, planned and unplanned, such as remaining native vegetation, parks, private gardens, street trees, sporting fields, golf courses, and so on, and more engineered options such as greenery systems in a building (Norton et al., 2015; Raji et al., 2015). The choice on what kind of UGI to apply is influenced by the climate of the region, the characteristics of the plant and soil, the water availability but also by community norms and cultural values (Norton et al., 2015).

The greenery systems in a building can be classified in: green roof, green wall, green balcony, sky garden and indoor sky garden (Raji et al., 2015). The performance of each greenery system is related to the characteristics of the building (roof and wall construction materials, insulation level, dimension, building indoor usage, wall orientation), of the climate conditions (air temperature, air relative humidity, solar radiation, wind velocity and

[a]E-mail: evelia.schettini@uniba.it

direction) and of the plants used. Vegetation type, plant position, plant height, coverage ratio, leaf area index (LAI), foliage (orientation, dimension, thickness and density), radiometric characteristics of the leaves (emissivity, reflectivity, absorptance and transmissivity), plant's biological processes (photosynthesis, respiration and transpiration), and the growing medium (thickness, water content and density, substrate thermal properties) will affect the thermal effect of the vegetation (Raji et al., 2015; Gagliano et al., 2015).

Greenery systems are passive systems for energy savings in buildings due to the following effects: shading, cooling, insulation and wind barrier effect (Pérez et al., 2014). The shading effect is linked to the solar radiation interception provided by plants; the cooling effect is related to the water evapotranspiration process from plants and substrates; the insulation effect takes place due to the insulation capacity of the different layers composing the greenery system such as the substrate layer, the plants, the air in the plant layer, and so on; the effect of the wind on the facades and on energy losses is influenced by plants and support structures (Pérez et al., 2014).

Green roof on a flat or sloped rooftop includes different supportive layers: plants, growing media, filter, drainage, root barrier, insulation layer, waterproofing membrane on the top of the roof (Raji et al., 2015). Green roofs can be extensive, intensive and semi-intensive roofs in accordance with the thickness of the layer of the growing medium (extensive green roofs are characterized by a thickness of the growing media less of 15-20 cm, the intensive green roofs up to 20 cm, the semi-intensive green roofs less of 25 cm), the kind of ground covering plant (sedum, herbs and grasses for extensive green roofs, grass-herbs and shrubs for semi-intensive green roofs, and trees and shrubs for intensive green roofs), irrigation, maintenance and costs (from high for intensive green roofs to low for extensive green roofs) (Raji et al., 2015; Pérez et al., 2014).

Among the green roofs, an innovative cool-green roof was developed by Pisello et al. (2015) using Helichrysum Italicum plants that have white or light-colored leaves or flowers in summer, characterized by high short-wave solar reflectance, and seasonal deciduous leaves in winter. The cool-green roof, due to the periodical leaves development, is a reflective surface in spring and summer while an absorbing surface in winter (Pisello et al., 2015).

Green wall systems are classified into green façades and living walls: the former is characterized by plants, rooted in the ground or in pots at different heights of the façade, that climb directly on the façade of the building or on a structural support (such as wire, mesh, trellis) located to a small distance to the wall; living walls are composed of pre-cultivated panels, modules, or planted bags, that are fixed to a wall or free-standing frame (Raji et al., 2015; Pérez et al., 2014). The presence of a gap between the building façade and the green wall (generally from 3 cm to 15 cm) acts as a thermal buffer, improving its thermal insulation impact on building (Raji et al., 2015; Pérez et al., 2014).

Balconies with plants, through evapotranspiration, shading effect and wind control, can limit their action as a thermal bridge between the indoor and outdoor environment (Raji et al., 2015). The presence of plants on a balcony can reduce the wall surface temperature and the indoor air temperature with an abatement of the cooling demand in summer and an increasing of the heating demand in winter (Raji et al., 2015).

Sky gardens can be designed for high-rise buildings as open green space on a structure on top of the roof and on the sky bridge, i.e. on an external structure that is not directly connected with the building, and on intermediate floors (Raji et al., 2015). Indoor sky gardens, i.e. indoor spaces characterized by a height more than one-storey and by potted plants, have benefits for indoor thermal comfort and indoor air quality (Raji et al., 2015).

Greening the walls of a building in an urban area has potentially more effect than greening roofs because the surface area of the walls of a tall building can be about 20 times the area of the roof (Pérez et al., 2014).

The use of vegetated horizontal and vertical systems is a sustainable technology for improving the energy efficiency of buildings in cities by reducing the energy consumption for air conditioning in summer and increasing the thermal insulation in winter (Cheng et al., 2010; Jim and Tsang, 2011; Köhler and Poll, 2010; Perini et al., 2011; Pérez et al., 2011;

Santamouris, 2012). In literature there are more data concerning the summer period rather than the whole year (Pérez et al., 2014). In summer the efficacy of greenery systems in terms of energy savings is achieved for all the climatic areas of the world, while in winter the vegetated systems could produce negative effects in terms of increased energy consumptions for heating (Pérez et al., 2014; Raji et al., 2015). Pérez et al. (2014) reported the following reduction ranges of the external surface temperature: 1.7-13°C in warm temperate climate region and 7.9-16°C in snow climate region in the case of a wall covered with green facades during summertime; 11-20°C in summer and 5-16°C in autumn in warm temperate climate region in the case of a green wall. Susorova et al. (2014) reported an average decrease of the surface temperatures due to the presence of vegetation on the façade of about 1-9°C during summer.

More knowledge about benefits and characteristics of greenery systems is needed and more research has to be undertaken into plant species suitable for the areas with high levels of solar radiation, such as the Mediterranean regions.

The aim of this research was to investigate the effective influences of two different climbing plants for green vertical passive systems on a building wall during winter time. An experimental test was carried out at the University of Bari during different seasons, and surface temperatures and climatic data were evaluated in order to estimate the wall surface temperatures of the walls with vertical greenery systems.

MATERIALS AND METHODS

An experimental test was carried out at the experimental farm of the University of Bari in Valenzano (Bari), Italy, having latitude 41°05'N, longitude 16°53'E, altitude 85 m a.s.l. A prototype of a building vertical wall was made in scale with perforated bricks joined with mortar. This wall is commonly used as a system of vertical closure for civil construction in the Mediterranean area. Each brick (20 cm thick, 25 cm height and 25 cm length) was characterized by thermal characteristics such as: thermal conductivity λ (following UNI EN 1745: 2012) equal to 0.282 W m^{-1} K^{-1}; average weight of the masonry work (including plaster) equal to 695 kg m^{-3}; specific heat capacity C equal to 840 J kg^{-1} K^{-1}.

Three south oriented walls were made, each having a width of 1.00 m, a height equal to 1.55 m and a thickness of 0.20 m. In order to allow the correct evaluation of the influence of the plants on the effects of incident solar radiation, the backside of each vertical wall was insulated by means of a sealed structure. The sealed structure was made of sheets of expanded polystyrene, characterized by a thickness of 30 mm and a thermal conductivity equal to 0.037 W m^{-2} K^{-1}. A blue shading net was positioned onto the structure to reduce the effect of the incident solar radiation.

Two vertical walls were covered with vigorous evergreen climbing plants, one with *Pandorea jasminoides* variegated, the second with *Rhyncospermum jasminoides*, while the third wall was kept uncovered and used as control. The plants were transplanted on June 18, 2014. The day after the transplant, in order to provide a better support for the climbing plants, a net has been placed between the plant and the wall; each net was placed about 15 cm far from the vertical wall (Figure 1).

The drip irrigation method was used for all the plants and fertilization with N:P:K 12:12:12 was performed.

The experimental field was equipped with a meteorological station consisting of a data logger (CR10X, Campbell, Logan, USA) and sensors for measuring several climatic parameters. The parameters measured were: the external air temperature, the solar radiation incident on the vertical surface, the speed and wind direction, the surface temperature of the wall on the inner side, the surface temperature of the external plaster exposed to the solar radiation, and the indoor air temperature inside the sealed volume behind each wall. The data, measured with a frequency of 60 s, were averaged every 15 min and stored in the data logger.

Figure 1. The three walls at the experimental field of the University of Bari; the right wall is covered with *Rhyncospermum jasminoides*, the central wall with *Pandorea jasminoides* variegated and the left wall is the uncovered control.

The surface temperature of the wall on the inner side, the surface temperature of the external plaster exposed to solar radiation, and the indoor temperature inside the sealed volume behind each wall were measured using thermistors (Tecno.el s.r.l. Formello, Rome, Italy) (Figure 2).

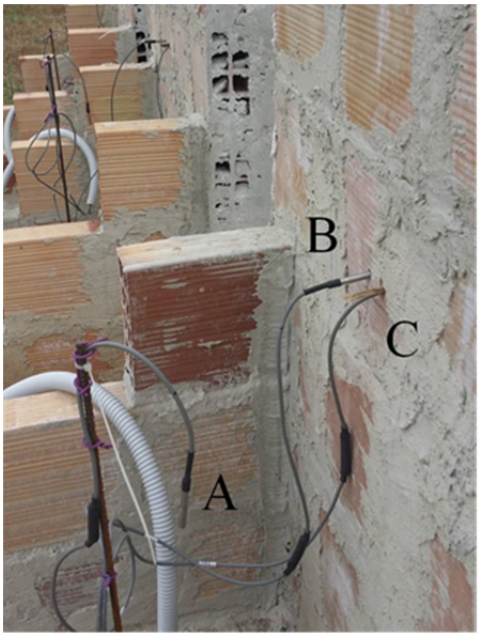

Figure 2. Location of the temperature sensors before the application of the plaster: (A) sensor for the indoor temperature inside the volume behind each wall, (B) sensor for the surface temperature of the wall on the inner side, and (C) sensor for the surface temperature of the external plaster exposed to the solar radiation.

The solar radiation incident on the vertical surface was measured by a pyranometer (model 8-48, Eppley Laboratory, Newport, RI, USA) in the wavelength range 0.3-3 mm. External air temperature was measured during the test by using an Hygroclip-S3 sensor (Rotronic, Zurich, Switzerland), which was shielded from solar radiation. The speed and direction of the wind were measured by a Young Wind Sentry 03002 sensor (Wind Sentry Data Sheet 03002, RM Young Company 1999): the wind speed by an anemometer with small rotating vanes that produce a sinusoidal signal whose frequency is proportional to the wind speed; the wind direction by a potentiometer wind vane whose resistance is a function of the orientation vane. The measuring ranges are 0-50 m s^{-1} for the wind speed and 0-360 ° for the wind direction.

RESULTS AND DISCUSSION

Figure 3 shows the average values of the minimum daily external air temperature and surface temperature of the external plaster of the three walls exposed to solar radiation during winter of 2014-2015. The greenery systems allowed keeping the external surface temperature of the green walls at values higher than the control wall in the night-time of coldest periods (Figure 3).

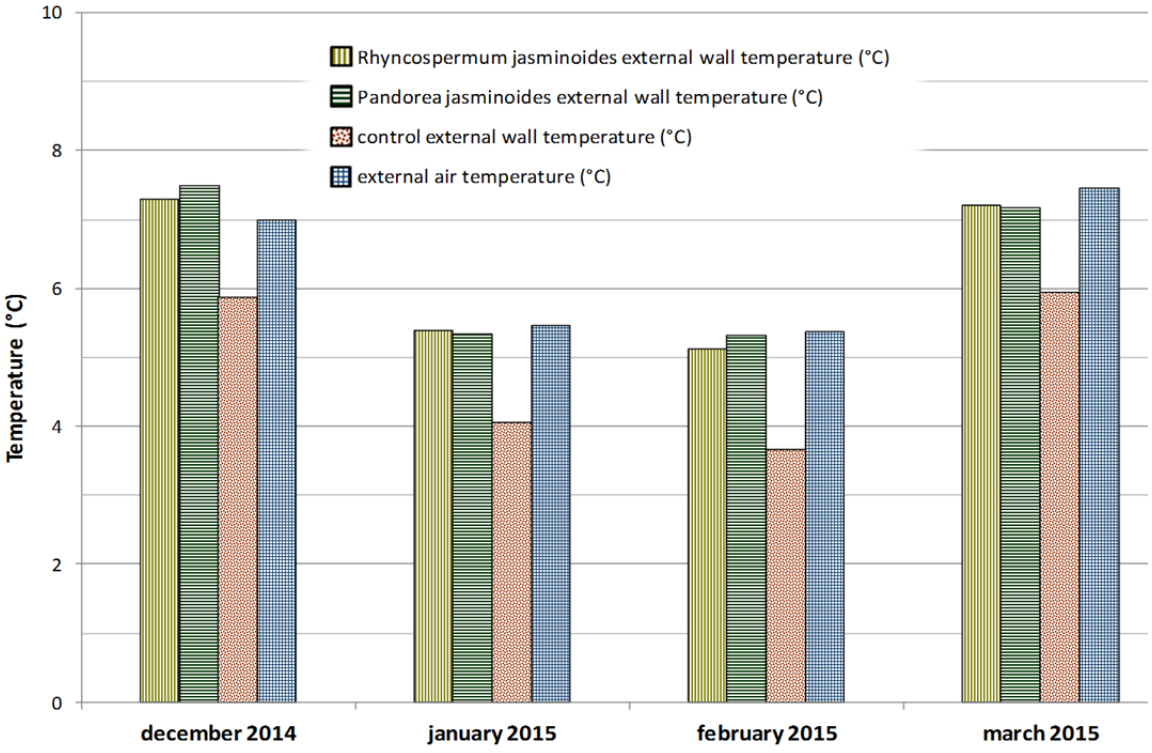

Figure 3. Average values of the minimum daily external air temperature and surface temperature of the external plaster of the three walls exposed to solar radiation from December 2014 to February 2015.

In the examined period, the average values of the minimum surface temperature of the wall not covered with plants were always lower than the temperatures recorded in the same hours for the vertical walls covered with *Rhyncospermum jasminoides* and *Pandorea jasminoides* variegated. There were no significant differences between the performances of the two species. In wintertime the presence of vegetation increases the thermal insulation of the wall. The differences between the lower temperatures recorded for the control and for the wall covered with plants ranged from 2.4 to 2.8°C (Figure 4).

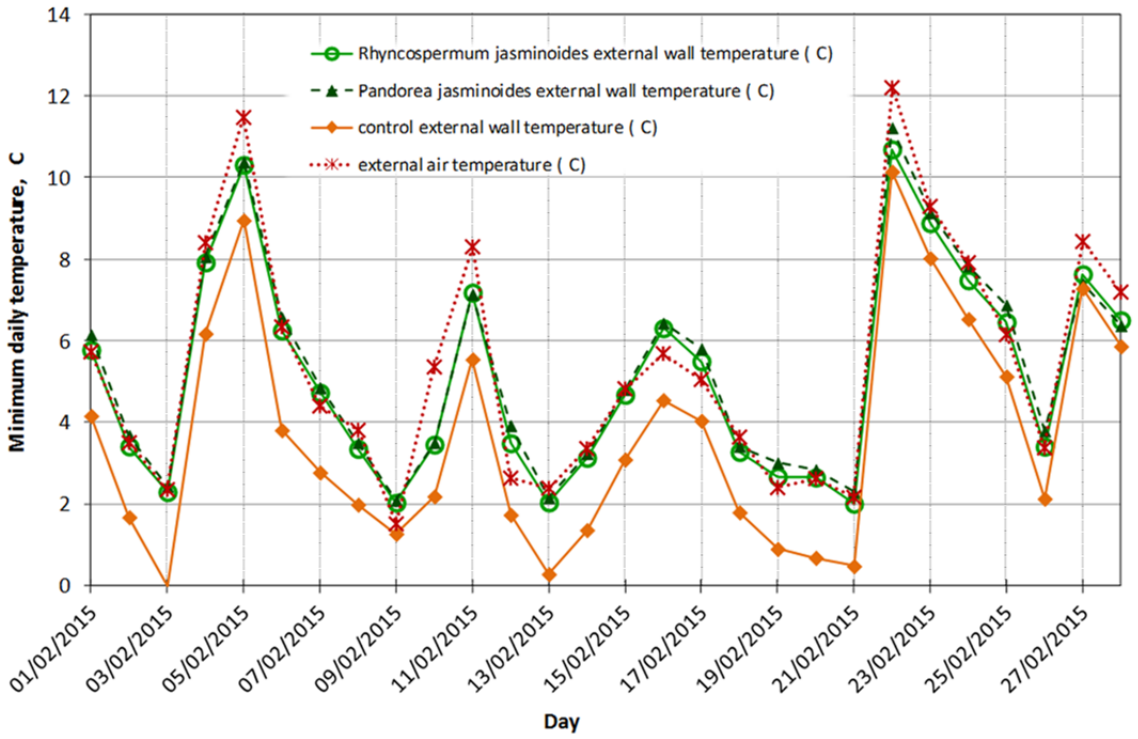

Figure 4. Daily minimum surface temperature of the external plaster of the three walls exposed to solar radiation during February 2015.

CONCLUSION

The experimental test was conducted on vegetated vertical systems applied on south oriented walls during winter 2014-2015 in South Italy. The use of the green walls during cold months allowed increasing the thermal insulation performance of the walls by keeping the external surface temperature in nighttime hours up to about 2.8°C over the surface temperature of the wall not covered with plants.

The study is in progress in order to analyze the data concerning a whole year. Further experimental data are needed regarding the impact of a different orientation of the green vertical systems in the Mediterranean area and throughout the whole year.

Green roofs and vertical greenery popularity is growing because of their high potential to be used as a sustainable solution for enhancing the thermal performance of building envelopes and for reducing energy consumption in the sector of residential and rural constructions in the Mediterranean area. Like other forms of urban green infrastructures, they offer many ecosystem services like the mitigation of the urban heat island effect, the creation of natural habitats for improving urban biodiversity, noise attenuation, improved air quality and aesthetical impact of constructed areas. Moreover the greening technology offers the additional benefits of reducing the energy consumption for air conditioning in summer and increasing the thermal insulation in winter.

ACKNOWLEDGEMENTS

The contribution to programming and executing this research must be equally shared, within the competencies of the research groups, between the authors. The present work has been carried out under the “Piano triennale 2012-2014 per la Ricerca di Sistema Elettrico Nazionale, progetto C.2 ‘Sviluppo di modelli per la realizzazione di interventi di efficienza energetica sul patrimonio immobiliare pubblico’, Piano Annuale di Realizzazione (PAR) 2013”, funded by the Italian Ministry of Economic Development.

Literature cited

Cheng, C.Y., Cheung, K.K.S., and Chu, L.M. (2010). Thermal performance of a vegetated cladding system on facade walls. Build. Environ. *45* (*8*), 1779–1787 http://dx.doi.org/10.1016/j.buildenv.2010.02.005.

Gagliano, A., Detommaso, M., Nocera, F., and Evola, G. (2015). A multi-criteria methodology for comparing the energy and environmental behavior of cool, green and traditional roofs. Build. Environ. *90*, 71–81 http://dx.doi.org/10.1016/j.buildenv.2015.02.043.

Jim, C.Y., and Tsang, S.W. (2011). Biophysical properties and thermal performance of an intensive green roof. Build. Environ. *46* (*6*), 1263–1274 http://dx.doi.org/10.1016/j.buildenv.2010.12.013.

Köhler, M., and Poll, P.H. (2010). Long-term performance of selected old Berlin greenroofs in comparison to younger extensive greenroofs in Berlin. Ecol. Eng. *36* (*5*), 722–729 http://dx.doi.org/10.1016/j.ecoleng.2009.12.019.

Norton, B.A., Coutts, A.M., Livesley, S.J., Harris, R.J., Hunter, A.M., and Williams, N.S.G. (2015). Planning for cooler cities: A framework to prioritise green infrastructure to mitigate high temperatures in urban landscapes. Landsc. Urban Plan. *134*, 127–138 http://dx.doi.org/10.1016/j.landurbplan.2014.10.018.

Pérez, G., Rincón, L., Vila, A., González, J.M., and Cabeza, L.F. (2011). Green vertical systems for buildings as passive systems for energy savings. Appl. Energy *88* (*12*), 4854–4859 http://dx.doi.org/10.1016/j.apenergy.2011.06.032.

Pérez, G., Coma, J., Martorell, I., and Cabeza, L.F. (2014). Vertical Greenery Systems (VGS) for energy saving in buildings: A review. Renew. Sustain. Energy Rev. *39*, 139–165 http://dx.doi.org/10.1016/j.rser.2014.07.055.

Perini, K., Ottelé, M., Fraaij, A.L.A., Haas, E.M., and Raiteri, R. (2011). Vertical greening systems and the effect on air flow and temperature on the building envelope. Build. Environ. *46* (*11*), 2287–2294 http://dx.doi.org/10.1016/j.buildenv.2011.05.009.

Pisello, A.L., Piselli, C., and Cotana, F. (2015). Thermal-physics and Energy performance o fan innovative green roof system: the cool-green roof. Sol. Energy *116*, 337–356 http://dx.doi.org/10.1016/j.solener.2015.03.049.

Raji, B., Tenpierik, M.J., and van den Dobbelsteen, A. (2015). The impact of greening systems on building energy performance: A literature review. Renew. Sustain. Energy Rev. *45*, 610–623 http://dx.doi.org/10.1016/j.rser.2015.02.011.

Santamouris, M. (2012). Cooling the cities – A review of reflective and green roof mitigation technologies to fight heat island and improve comfort in urban environments. Sol. Energy *110*, 682–703.

Susorova, I., Azimi, P., and Stephens, B. (2014). The effects of climbing vegetation on the local microclimate, thermal performance, and air infiltration of four building facade orientations. Build. Environ. *76*, 113–124 http://dx.doi.org/10.1016/j.buildenv.2014.03.011.

Tan, C.L., Wong, N.H., and Jusuf, S.K. (2014). Effects of vertical greenery on mean radiant temperature in the tropical urban environment. Landsc. Urban Plan. *127*, 52–64 http://dx.doi.org/10.1016/j.landurbplan.2014.04.005.

Vox, G., Blanco, I., Campiotti, C.A., Giagnacovo, G., and Schettini, E. (2015). Vertical green systems for buildings climate control. Actual Tasks on Agricultural Engineering. Paper presented at: 43rd International Symposium on Agricultural Engineering (Opatija, Croatia) http://atae.agr.hr.

Design of a solar cooling system for greenhouse conditioning in a Mediterranean area

I. Blanco[1], G. Scarascia Mugnozza[1], E. Schettini[1,a], G. Puglisi[2], C.A. Campiotti[2] and G. Vox[1]

[1]Department of Agricultural and Environmental Science DISAAT, University of Bari, via Amendola 165/A, 70126 Bari, Italy; [2]ENEA - Italian National Agency for New Technologies, Energy and Sustainable Economic Development, Technical Unit Energy Efficiency, Via Anguillarese, 301, 00123 Rome, Italy.

Abstract

Monitoring and controlling environmental parameters inside a greenhouse are required to reach high yields and low environmental impacts. Ventilation, shading, evaporative cooling and refrigeration are methods of controlling air temperature and relative humidity in Mediterranean greenhouses. Nevertheless ventilation and shading are often not sufficient to remove the excess heat, refrigeration is generally expensive and evaporative cooling is based on the exploitation of high quality water, a resource to be preserved in the Mediterranean areas. In order to enhance the sustainability levels of the greenhouse sector, renewable energy sources can be exploited with the application of solar absorption systems for greenhouse cooling in areas with high outdoor temperatures. These systems take advantage of the simultaneity between the solar energy availability and the greenhouse cooling demand allowing the reduction of conventional electricity. This paper presents the simulation and optimization of a solar cooling system designed for a Mediterranean greenhouse, having a surface of 300 m^2, using 68 m^2 of evacuated tube solar collectors, a LiBr absorption unit with a cooling capacity of 17.6 kW and a pilot distribution system providing the cooling power for the volume surrounding the crop. The simulation study, predicting the performance of the unit, was based on the experimental data collected at the experimental centre of the University of Bari, Southern Italy. The results of the simulation indicated that the system is seasonally in phase with the climatic data; the delivered yearly cooling capacity for the greenhouse was 113 GJ, the required solar energy 157 GJ and the available solar energy on the 68 m^2 capturing surface, with a slope of 30°, was 265 GJ. The simulation can be used as a forecasting tool of the effects of the changes on the parameters of the system before applying them on the greenhouse system.

Keywords: absorption unit, evacuated tube solar collectors, climate control, renewable energy sources

INTRODUCTION

The optimized climatic management of the greenhouse environment leads to suitable growing condition for the cultivations, safety working conditions and energy savings (Von Zabeltitz, 1999; Vox et al., 2010). Heating and cooling systems based on the use of fossil fuels have a strong influence on the cost and environmental sustainability of greenhouse cultivation; renewable energy is an important resource for the energetic and environmental retrofitting of the rural industry. In the Mediterranean region the intense solar radiation induces the overheating of the indoor air and often the overcoming of the critical temperature values for different types of crops. During the spring-summer period different cooling systems are used in order to remove the thermal overload to obtain balanced environmental parameters of the greenhouses. The natural and artificial ventilation is the cheapest and simplest method for cooling greenhouse, even though during hottest periods it does not remove sufficiently the surplus energy. The refrigeration method is too expensive in terms of installation and operation costs, due to the large quantity of heat to be removed

[a]E-mail: evelia.schettini@uniba.it

Acta Hortic. 1170. ISHS 2017. DOI 10.17660/ActaHortic.2017.1170.60
Proc. Int. Symp. on New Tech. and Mgt. for Greenhouses – GreenSys2015
Eds.: F.J. Baptista, J.F. Meneses and L.L. Silva

from the greenhouse internal ambient (Vox et al., 2010; Davies, 2005; Kumar et al., 2009).

The fan-pad and fog systems, known as evaporative cooling methods, efficiently control the internal air temperature in warm regions, requiring minimum power consumption. Nevertheless they work best when evaporative cooling is maximum, which occurs in hot and semi-arid climate (Ahmed et al., 2011; Kumar et al., 2009); however they mainly rely on the use of fossil fuels and require large quantity of high quality water. Alternative cooling methods are based on the exploitation of earth ground or of the underground aquifer water since they maintain a constant year round temperature that in warm periods can be profitably used for greenhouse cooling; the underground energy is then used in ground heat exchangers or horizontal earth tube systems (Mongkon et al., 2014). The application of these composite systems for greenhouse cooling has been widely researched; it involves favourable energy savings as compared to other conventional cooling systems (Ghosal and Tiwari, 2006; Ghosal et al., 2004; Sharan, 2009; Ozgener and Ozgener, 2010; Yildiz et al., 2012). Earth to air heat exchanger systems perform better in regions where the heating and cooling demands are similar in order to avoid long-term changes in ground temperature (Li et al., 2013).

The solar-powered cooling systems use part of the available solar energy in air-conditioning applications; they could be a promising option even in the greenhouse sector to reduce the electricity consumption in regions with abundant solar energy and long daily sunny hours (El-Sharkawy et al., 2014; Al-Alili et al., 2012; Ghaddar et al., 1997; Chidambaram et al., 2011). Solar cooling systems can be classified in solar collector-based thermally driven systems, solar photovoltaic-based electrical cooling systems, and solar combined power and cooling systems (Chidambaram et al., 2011; Hwang et al., 2008; Sarbu and Sebarchievici, 2013). The solar thermal cooling systems mainly consist of solar thermal collectors to convert solar radiation into heat, a heat storage tank storing heat all day long, a cooling machine generating chilled water, a cold distribution system, a cooling tower to reject waste heat to the atmosphere; the solar energy is employed to produce thermal energy for cooling through the thermochemical or thermophysical processes in thermally driven cooling machines (Hwang et al., 2008; Sharma et al., 2011; Sarbu and Sebarchievici, 2013; Ghafoor and Munir, 2015). Among the solar collector-based thermally driven systems, the absorption cycle cooling system operates with some liquid materials able to absorb liquid through an exothermic reaction and to desorb steam through an endothermic reaction (Kalkan et al., 2012; Allouhi et al., 2015). The system typically consists of an absorber, a desorber, a pump, an expansion valve, a generator, a regenerator, an evaporator, a storage tank and a heater. The absorbent solution is diluted with the refrigerant in the absorber generating an absorbent/refrigerant solution; in the generator the solution is pumped to a higher pressure and heated. In the desorber, the refrigerant is separated from the solution by means of the desorption process by adding heat. Then the refrigerant vapor is liquefied in the condenser, expanded through the expansion device, and evaporated in the evaporator in order to be again absorbed in the absorbent solution (Hwang et al., 2008; Kalkan et al., 2012). The cooling effect is obtained by the evaporation of the refrigerant (water) in the evaporator at very low pressure. The hot water storage tank store the excess heat provided by the solar collectors; hot water stored is later used when it is necessary. Solar cooling systems can be particularly interesting for remote areas applications where conventional cooling is difficult and where there is abundant solar energy.

This paper presents the results of a research on the application of a solar absorption cooling system to a Mediterranean greenhouse at the experimental farm of the University of Bari where the integration of renewable energy sources for greenhouse heating and climate control has been widely investigated (Russo et al., 2014; Vox et al., 2008, 2014; Blanco et al., 2014, 2015). The present study aims to maximize the solar energy use in the summer season for air conditioning of the greenhouse, exploiting the coincidence between the period of the greenhouse cooling peak demand and that of greatest abundance of solar energy. The solar collector surface related to the greenhouse cultivated area, the cooling capacity and the energy consumption of the cooling system were assessed; then a dynamic simulation model of the pilot solar cooling plant was developed.

MATERIALS AND METHODS

The experimental greenhouse is located in Valenzano (Bari, Italy; latitude 41°05'N, longitude 16°53'E); it is an arched roof type covered with plastic film, made of tubular galvanized steel, south-north oriented. The greenhouse has a covered area of 300 m^2 (30 m in length, 10 m in width), it is 4.45 m high along the ridge and 2.45 m along the gutters (Figure 1). The covering film is an ethylene-vinyl acetate copolymer film (EVA), having a thickness of 200 μm and a solar total transmissivity coefficient of about 85-90% in the wavelength range 300-3,000 nm. The base and the warheads (south and north-facing greenhouse surface) are polycarbonate (PC) sheets. The cultivation of the plants takes place in plastic pots (1.00×0.40×0.40 m) with a growing substrate made of a mixture of soil and peat. The greenhouse is equipped with four electrical fans on the north-facing greenhouse surface, two air inlet louvers on the south-facing greenhouse surface, two vents on the greenhouse ridge and two on the east and west sides respectively, an electronically controlled horizontal shading net (placed inside the greenhouse). The designed cooling system task is to keep the greenhouse inside air temperature not above 30°C in order to allow crop cultivation during warm months.

The simulation model was developed in Matlab Simulink. This allows the modeling of a dynamic system by drawing a block diagram on the screen, specifying the setting parameters and interconnecting multiple blocks in order to model even more complete and complex systems. In this approach the blocks represent differential equations or difference whose independent variable is time. The built solar cooling plant was modeled by creating the different several components (i.e. solar collectors, accumulation, absorption chiller, etc.) on the basis of physical equations related to their operation (Puglisi et al., 2015) and connecting them. The model processes the variables according to the sequential modular approach so that the output data of a component are used as input to the next component. To start the simulation, the user must specify a time step, a start time, a final time and an integration method. Signal values are updated during the simulation at each time step between the initial and the final step.

RESULTS AND DISCUSSION

The system was designed based on the climatic data (external air temperature, external air relative humidity, solar radiation) measured at the experimental farm of the University of Bari. The system consists mainly of an evacuated tube solar thermal collector field providing heat to an absorption chiller that produces cooled water. The cooling distributing system consists of pipes, positioned at the crop level, through which the cooled water circulates lowering the plant temperature (Figure 1). The design of the cooling system permitted to evaluate the cooling energy demand necessary to guarantee suitable growing conditions for the crop. It was supposed a plant configuration with a distribution system in which the cooling power is not provided for the entire volume of the greenhouse, but only for the air volume surrounding the crop, in order to reduce the energy consumption for cooling demand in the greenhouse and to reduce the visual impact of the large capturing surface required for the solar collectors.

The cooling capacity was calculated through the heat balance equation:

$$Q_C = I_r \cdot \tau_{cp} \cdot (1-\rho) \cdot S - U \cdot S \cdot \Delta T \quad (1)$$

where I_r is the incident solar radiation, assumed equal to 900 W m^{-2}; τ_{cp} is the covering transmissivity, assumed equal to 0,85; ρ is the reflectance of the soil and of the shading net, assumed equal to 0.5; S is the covered area that must be cooled; U is the global heat transfer coefficient of the greenhouse, assumed equal to 10 W m^{-2} $°C^{-1}$; ΔT is the temperature values difference between the inside and outside temperature of the greenhouse, equal to 1°C. The area to be cooled was assumed equal to 40 m^2, considering only the growing area. The cooling energy demand that the solar cooling system must supply was 14.9 kW.

Figure 1. The inside of the experimental greenhouse and the cooling distributing system.

The designed solution was determined considering the equipment available on the market; the system (Figure 2), set up during 2015 at the experimental farm, consists of:

- Evacuated tube collectors, facing south with a 30° tilt angle, for a total area of 68 m^2;
- A water-fired single effect absorption chiller using a combination of water/lithium bromide as fluid for absorption cooling, having a cooling capacity of 17.6 kW with a heat input of 25.1 kW, an electrical consumption of 1.45 kW, a $COP_{thermal}$ of 0.70 with a supply/return cooling water of 7/12.5°C, nominally requiring an in/out temperature from the solar array of 88/83°C;
- A cooling tower with a heat rejection of 42.7 kW and an inlet/outlet cooling water temperature of 35/31°C;
- An hot water storage tank with a global capacity of 2 m^3;
- A cool water storage tank with a global capacity of 0.5 m^3.

Figure 2. The experimental solar cooling plant.

The designed system is in phase with the available solar radiation at the same moment during the working period; furthermore a simulation based on the climatic data collected at the experimental farm during 2013 showed that the designed system is in phase on a seasonal basis (Figure 3): the available solar energy, calculated for a capturing surface of 68 m^2 with a slope of 30°, was 265 GJ, the yearly solar energy required by the solar cooling plant was 157 GJ and the yearly cooling capacity produced by the system for the greenhouse was 113 GJ.

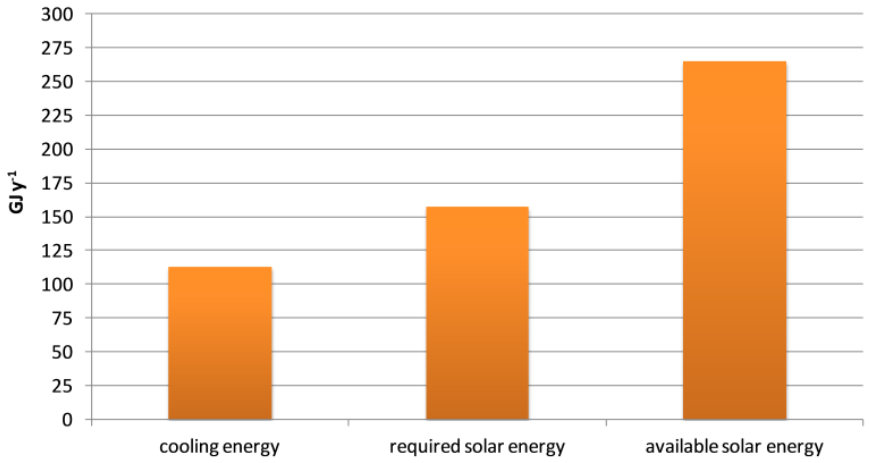

Figure 3. Predicted yearly cooling energy demand, predicted required solar energy and the effective available solar energy during 2013.

Figure 4 shows the trend of the cooling demand of the greenhouse and of the cooling power produced by the absorption chiller, calculated every 15 mins. with the Simulink simulation, for the period 01/04-30/09. The data show as the modelled solar cooling system is able to supply the greenhouse cooling demand: the cooling power produced by absorber chiller is always higher than that required. The simulation results also confirm that the designed system is well balanced from an energetic point of view because the temperature data values related to the cold storage tank vary in the range 7-12°C corresponding to the work conditions of outlet water produced by absorption chiller.

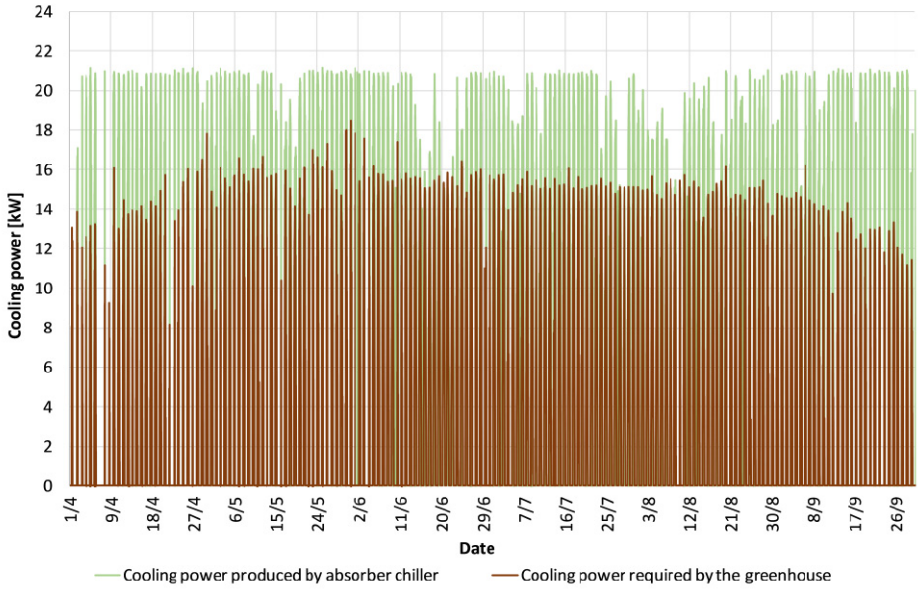

Figure 4. Simulink simulation of the cooling power required by the greenhouse and of the cooling power generated by the absorber chiller, 01/04-30/09.

The present research was carried out in order to preliminarily assess the cooling potential of such systems in the greenhouse sector. The effectiveness of the localized cooling energy distributing system on the crop will be evaluated by means of the experimental data that will be afterwards collected in the field.

CONCLUSIONS

The application of a solar cooling system to greenhouses could be an interesting alternative solution for reducing the electricity consumption in regions with abundant solar energy; nevertheless a careful design must be developed due to the delay between the onset of solar radiation and the cooling demand of the greenhouse. A solution with a localised cooling system was analysed; the effective efficiency of this method is going to be proven experimentally. The simulations performed confirm that the designed system was able to satisfy the cooling power required. The developed dynamic model can be used as a functional tool for the validation of the system correct design and for generate different management scenarios in order to maximize the primary energy savings.

ACKNOWLEDGEMENTS

The research was carried out under the project "Diffusion of Cooling and Refreshing Technologies using the Solar Energy Resource in the Adriatic Regions (Adriacold)", funded by the European Commission in the frame of IPA Adriatic Cross Border Cooperation Programme.

The authors shared programming and editorial work equivalently within the areas of their expertise.

Literature cited

Ahmed, E.M., Abaas, O., Ahmed, M., and Ismail, M.R. (2011). Performance evaluation of three different types of local evaporative cooling pads in greenhouses in Sudan. Saudi J Biol Sci *18* (*1*), 45–51. PubMed http://dx.doi.org/10.1016/j.sjbs.2010.09.005

Al-Alili, A., Islam, M.D., Kubo, I., Hwang, Y., and Radermacher, R. (2012). Modeling of a solar powered absorption cycle for Abu Dhabi. Appl. Energy *93*, 160–167 http://dx.doi.org/10.1016/j.apenergy.2010.11.034.

Allouhi, A., Kousksou, T., Jamil, A., Bruel, P., Mourad, Y., and Zeraouli, Y. (2015). Solar driven cooling systems: an updated review. Renew. Sustain. Energy Rev. *44*, 159–181 http://dx.doi.org/10.1016/j.rser.2014.12.014.

Blanco, I., Pascuzzi, S., Anifantis, A.S., and Scarascia Mugnozza, G. (2014). Study of a pilot photovoltaic-electrolyzer-fuel cell power system for a geothermal heat pump heated greenhouse and evaluation of the electrolyzer efficiency and operational mode. J. Agricult. Engineer. *45* (*3*), 111–118 http://dx.doi.org/10.4081/jae.2014.238.

Blanco, I., Schettini, E., Scarascia Mugnozza, G., Puglisi, G., Campiotti, C.A., Giagnacovo, G., and Vox, G. (2015). Thermal solar collectors and absorption system applied to greenhouse cooling. Actual tasks on agricultural engineering. Paper presented at: 43rd International Symposium on Agricultural Engineering (Opatija, Croatia) http://atae.agr.hr.

Chidambaram, L.A., Ramana, A.S., Kamaraj, G., and Velraj, R. (2011). Review of solar cooling methods and thermal storage options. Renew. Sustain. Energy Rev. *15* (*6*), 3220–3228 http://dx.doi.org/10.1016/j.rser.2011.04.018.

Davies, P.A. (2005). A solar cooling system for greenhouse food production in hot climates. Sol. Energy *79* (*6*), 661–668 http://dx.doi.org/10.1016/j.solener.2005.02.001.

El-Sharkawy, I.I., AbdelMeguid, H., and Saha, B.B. (2014). Potential application of solar powered adsorption cooling systems in the Middle East. Appl. Energy *126*, 235–245 http://dx.doi.org/10.1016/j.apenergy.2014.03.092.

Ghaddar, N.K., Shihab, M., and Bdeir, F. (1997). Modeling and simulation of solar absorption system performance in Beirut. Renew. Energy *10* (*4*), 539–558 http://dx.doi.org/10.1016/S0960-1481(96)00039-0.

Ghafoor, A., and Munir, A. (2015). Worldwide overview of solar thermal cooling technologies. Renew. Sustain. Energy Rev. *43*, 763–774 http://dx.doi.org/10.1016/j.rser.2014.11.073.

Ghosal, M.K., and Tiwari, G.N. (2006). Modeling and parametric studies for thermal performance of an earth to air heat exchanger integrated with a greenhouse. Energy Convers. Manage. *47* (*13–14*), 1779–1798 http://dx.doi.org/10.1016/j.enconman.2005.10.001.

Ghosal, M.K., Tiwari, G.N., and Srivastava, N.S.L. (2004). Thermal modelling of a greenhouse with an integrated earth to air heat exchanger: an experimental validation. Energy Build. *36* (*3*), 219–227 http://dx.doi.org/10.1016/j.enbuild.2003.10.006.

Hwang, Y., Radermacher, R., Al Alili, A., and Kubo, I. (2008). Review of solar cooling technologies. HVAC & R Res. *14* (*3*), 507–528 http://dx.doi.org/10.1080/10789669.2008.10391022.

Kalkan, N., Young, E.A., and Celiktas, A. (2012). Solar thermal air conditioning technology reducing the footprint of solar thermal air conditioning. Renew. Sustain. Energy Rev. *16* (*8*), 6352–6383 http://dx.doi.org/10.1016/j.rser.2012.07.014.

Kumar, K.S., Tiwari, K.N., and Jha, M.K. (2009). Design and technology for greenhouse cooling in tropical and subtropical regions: A review. Energy Build. *41* (*12*), 1269–1275 http://dx.doi.org/10.1016/j.enbuild.2009.08.003.

Li, H., Nagano, K., Lai, Y., Shibata, K., and Fujii, H. (2013). Evaluating the performance of a large borehole ground source heat pump for greenhouses in northern Japan. Energy *63*, 387–399 http://dx.doi.org/10.1016/j.energy.2013.09.009.

Mongkon, S., Thepa, S., Namprakai, P., and Pratinthong, N. (2014). Cooling performance assessment of horizontal earth tube system and effect on planting in tropical greenhouse. Energy Convers. Manage. *78*, 225–236 http://dx.doi.org/10.1016/j.enconman.2013.10.076.

Ozgener, L., and Ozgener, O. (2010). An experimental study of the exergetic performance of an underground air tunnel system for greenhouse cooling. Renew. Energy *35* (*12*), 2804–2811 http://dx.doi.org/10.1016/j.renene.2010.04.038.

Puglisi, G., Morosinotto, G., and Emmi, G. (2015). Development of an advanced simulation model for solar cooling plants. Energy Procedia *70*, 495–503 http://dx.doi.org/10.1016/j.egypro.2015.02.153.

Russo, G., Anifantis, A.S., Verdiani, G., and Scarascia Mugnozza, G. (2014). Environmental analysis of geothermal heat pump and LPG greenhouse heating systems. Biosyst. Eng. *127*, 11–23 http://dx.doi.org/10.1016/j.biosystemseng.2014.08.002.

Sarbu, I., and Sebarchievici, C. (2013). Review of solar refrigeration and cooling systems. Energy Build. *67*, 286–297 http://dx.doi.org/10.1016/j.enbuild.2013.08.022.

Sharan, G. (2009). Controlled environment agriculture in semi-arid north-west India. Ann. Arid Zone *48* (*2*), 95–102.

Sharma, V.K., Marano, D., Anyanwu, C.N., Okonkwo, G.I., Ibeto, C.N., and Eze, I.S. (2011). Solar cooling a potential option for energy saving and abatement of greenhouse gas emissions in Africa. Singapore. J. Sci. Res. *1*, 1–12.

Von Zabeltitz, C. (1999). Greenhouse structures. In Greenhouse Ecosystems, Ecosystems of the World, Vol 20, G. Stanhill, and H. Zvi Enoch, eds. (Amsterdam: Elsevier), p.17–69.

Vox, G., Schettini, E., Lisi Cervone, A., and Anifantis, A.S. (2008). Solar thermal collectors for greenhouse heating. Acta Hortic. *801*, 787–794 http://dx.doi.org/10.17660/ActaHortic.2008.801.92.

Vox, G., Teitel, M., Pardossi, A., Minuto, A., Tinivella, F., and Schettini, E. (2010). Chapter 1: Sustainable Greenhouse Systems. In Sustainable Agriculture: Technology, Planning and Management, A. Salazar, and I. Rios, eds. (NY USA: Nova Science Publishers, Inc.), p.1–79.

Vox, G., Blanco, I., Scarascia Mugnozza, G., Schettini, E., Bibbiani, C., Viola, C., and Campiotti, C.A. (2014). Solar absorption cooling system for greenhouse climate control: technical evaluation. Acta Hortic. *1037*, 533–538 http://dx.doi.org/10.17660/ActaHortic.2014.1037.66.

Yildiz, A., Ozgener, O., and Ozgener, L. (2012). Energetic performance analysis of a solar photovoltaic cell (PV) assisted closed loop earth-to-air heat exchanger for solar greenhouse cooling: an experimental study for low energy architecture in Aegean Region. Renew. Energy *44*, 281–287 http://dx.doi.org/10.1016/j.renene.2012.01.091.

A sustainable energy for greenhouses heating in Italy: wood biomass

C. Bibbiani[1,a], C.A. Campiotti[2], E. Schettini[3] and G. Vox[3]

[1]University of Pisa, Pisa, Italy; [2]ENEA - Italian National Agency for New Technologies, Energy and Sustainable Economic Development - Technical Unit Energy Efficiency - Agriculture Unit, Rome, Italy; [3]Dept. of Agricultural and Environmental Science DISAAT, University of Bari, Bari, Italy.

Abstract

More than 0.7 million ton of oil equivalent is the total requirement for thermal energy in the Italian greenhouse vegetable industry, derived mostly from fossil fuels, which corresponds to 2 Mt CO_2 emissions. The technology of wood biomass system is a good candidate for heating greenhouses, since this resource is considered as 'greenhouse gas' (GHG) neutral when converted to heat, excluding the GHG generation during harvesting, transportation, and pre-processing of raw materials. Besides, the CO_2 enrichment in greenhouses from the exhaust gas of a biomass heating system can bring benefits for greenhouse production, along with optimal management strategies to reduce fuel consumption. Unfortunately, CO_2 enrichment from the exhaust gas of biomass boilers is still challenging and expensive, considering that wood biomass boilers generate a higher volume of particulate matters (PM) and ash emissions than other fossil fuels. However, wet scrubbers and other recent flue gas conditioning devices could help to reduce costs and make this process more feasible. In the Italian peninsula, the power energy load for greenhouses heating was estimated to be between 30 and 175 W m^{-2}, while the thermal energy consumption varies between 21 to 546 kWh m^{-2} $year^{-1}$ according with internal air temperature and climatic zones. In general, the total cost of a heating system with boiler, loading system, accumulator, control system and safety, installation, and heat delivering can vary from a maximum of 1400 € kW^{-1} for systems with power up to 100 kW, 600-800 € kW^{-1} for power over 100 kW, to a minimum of 400 € kW^{-1} for systems with power over 1000 kW. Thus, a techno-economic assessment is highly recommended to ascertain the economic feasibility of wood biomass boilers for the greenhouse industry, as related to the economic incentives by the National Decree of 28 December 2012, so-called "White Certifies".

Keywords: wood biomass, greenhouses heating system, CO_2 enrichment

INTRODUCTION

The agro-food industry is the leading manufacturing sector in Europe, in terms of turnover, value added, employment and number of companies. In Europe, its turnover was around 950 billion Euros in 2010 and it employed nearly four million people. In general, the agro-food industry is composed by transformation companies, using products from agriculture (primary production) to supply the agro-food industry. As general figure, the Italian added gross value of the agro-food system, in its wider meaning of agriculture and food industry, has reached in 2011 a global economic value of 250 billions €, which correspondents to about 16% of the added gross value of Italian economic in 2010. About 12.9 million ha is agricultural land in Italy. According to Campiotti et al. (2011), the national agri-food system amounted to a total final energy consumption of 16.43 million tonne of oil equivalent (Mtoe) (Table 1).

[a]E-mail: carlo.bibbiani@unipi.it

Table 1. Agriculture and energy consumption of productive sectors in Italy.

Productive sectors in the agro-food system	Energy consumption (Mtoe)[a]
Direct consumption (irrigation, processing land, air heating, utilities)	3.03
Food industry	2.90
Indirect consumption (phytosanitary, fertilizers, plastics), transport, preparation, storage, distribution, storage, sales	10.50
Total	**16.43**

[a]1 toe = 41.868 GJ.

GREENHOUSE ENERGY CONSUMPTION IN EUROPE

The EU greenhouse farming sector is facing a trend that responds to the changing consumer demands in a society where the safety of the environment is a growing concern, i.e. with regard to high fossil energy-demand, energy consumption, environmental impacts, and carbon dioxide (CO_2) emissions. Greenhouses are used to control or modify the many environmental factors affecting plant growth, mainly temperature and relative humidity, rain, wind, hail and snow. As a general statement, the most important climatic factors which influence the quality of the indoor microclimate are the quality of solar radiation and the temperature. Solar radiation is the main source of photosynthetic energy for plant growth and production. On the other hand, temperature is the most critical climatic factor for the greenhouse functionality. Therefore, the greenhouse design must follow regulations related to the local climate as well as the greenhouse heating technologies in order to maintain an optimal microclimate, especially as solar radiation and temperature, for the cultivated plants. Thus, the covering materials with their mechanical and radiometric properties determine the transmittance and the good insulation performance.

The greenhouse sector, with about 150,000 ha of covered surface in Europe, represents one of the most intensive energy sectors in the agro-food industry. In South Europe, about 5÷6 kg yr^{-1} m^{-2} fossil fuel are required for keeping the inside air at around 15÷20°C; on the other side, in Central-North Europe, from 60 to 80 kg yr^{-1} m^{-2} heating oil are required for maintaining optimal air temperature inside the greenhouse area. Estimation made in Spain, Italy, The Netherlands and Greece reported for these countries a greenhouse fossil energy consumption of about 4 Mtoe, corresponding to 11.3 Mt CO_2 emissions, and a total yearly economy value in products and structures in the range of 12.5 billions € (Table 2).

Table 2. Greenhouse agriculture in Europe.

Country	Greenhouse surface (ha)	Economic turnover (billions €)	Heating (MWh_{th})[1]	Electricity (MWh_{el})[2]
Italy	30,000	3	8,432,500	112,866
The Netherlands	10,311	6.8-7.7	29,510,800	3,723,000
Spain	43,964	1.5	989,627	33,623
Greece	5,646	0.5	87,644	1,700
Total	89,921	About 12.50	39,020,500	3,871,189
			3.35 Mtoe	0.77 Mtoe
			9.4 $MtCO_2$	2.1 $MtCO_2$[3]

[1]1 MWh_{th} = 0.0860 toe; 'th' stands for 'thermal'.

[2]1 MWh_{el} = 0.201 toe; 'el' stands for 'electric'.

[3]1 toe = 2.81 t CO_2 emissions.

More in details, the Italian greenhouse is characterized with not less than 6,000 ha as permanent greenhouse structures, and equipped with fossil acclimatization systems, which accounts for a total energy consumption of about 0.74 Mtoe, predominantly coming from fossil fuel (Table 3). The greenhouses are widespread all over the Italian peninsula with a

greater concentration (about 60% of the total) in southern regions, where most of the greenhouses consist of low-cost structures covered with plastic films. They are usually provided with simple heating systems, while greenhouse acclimatization is mainly used in the northern areas of Italy, with most of the greenhouse structures covered with glass.

Table 3. Electrical and thermal energy consumption in greenhouse sector in Italy.

Country	Greenhouse[1] surface (ha)	Heating[2] (toe)	Electricity[3] (toe)
Italy	6,000	706,786	24,830

[1]Plastic-greenhouses and glass-greenhouses.

[2]Yearly energy consumption.

[3]Yearly electricity demand of greenhouse systems (ventilation, opening, pumping).

Within the direct energy inputs of Italian agriculture, the greenhouse agriculture is one of the most intensive sub-sector in terms of direct energy consumption, mostly due to greenhouse acclimatization showing 0.72 Mtoe for fuel for greenhouses heating, respect to a total fuel consumption of 1.84 Mtoe.

Recently, in Italy, which is one of the European countries most vulnerable to the impacts of high energy cost, the renewable energies come along as the most promising energy resource for application in greenhouse acclimatization to face the present concern on fuel costs, that has posed a serious threat to the viability of the agricultural companies in the field of greenhouse productions. Particularly, the photovoltaic and the solid biomass for heating and cooling purposes have attracted a lot of attention in substitution of conventional fuels, since it is general conviction that the increasing of oil energy price is a trend which doubtless will continue for the coming years in Europe, and this will increase risks and lower profit for agricultural companies and growers. Nevertheless, biomass energy production (such as energy crops) can compete with food production for agricultural land and raw materials, as the recent experience in Italy brought to light when a large number of biogas plants were built during the last 5 years, or in early 2007 when the demand for maize increased due to ethanol production in the USA (Mathiesen et al., 2011). However, the carbon balance should be carefully evaluated. Besides, there is some concern over their usage in residential heating due to the emissions of various pollutants, such as polycyclic aromatic hydrocarbons, NOx, CO, SOx, and particulate matter (PM).

CLASSIFICATION OF BIOMASS SOURCES

The classification of solid biofuels is based on their origin and source. The fuel production chain of fuels shall be unambiguously traceable back over the whole chain. Both EN 14961 (2010) and EN 15234 (2010) have been divided into 6 parts, where part 1 gives the general requirements, and parts 2-6 are specific for fuels to be used by relatively small-scale users and non-industrial applications. In the standards, the limit is drawn at boilers with a capacity of 500 kW. All boilers above that size are considered 'industrial', those under that limit are 'non-industrial'.

Taking into account the energy content, Table 4 shows the Net calorific value (CV) or Lower Heating Value (LHV) (this means that the latent heat of vaporization of the water vapour created by combustion is not recovered by condensation).

The solid biofuels are divided into the following sub-categories (EN 14961-1, 2010):

- woody biomass;
- herbaceous biomass;
- fruit biomass;
- blends and mixtures.

The purpose of classification is to allow the possibility to differentiate and specify raw material based on origin with as much detail as needed.

Table 4. Greenhouse agriculture in Europe. Source: http://www.biomassenergycentre.org.uk.

Fuel	Net calorific value (CV) by mass (GJ t^{-1})	Net calorific value (CV) by mass (kWh kg^{-1})	Bulk density (kg m^{-3})	Energy density by volume (MJ m^{-3})
Biomass Fuel				
Wood chips (30% MC)	12.5	3.5	250	3,100
Log wood (stacked - air dry: 20% MC)	14.7	4.1	350-500	5,200-7,400
Wood (solid - oven dry)	19	5.3	400-600	7,600-11,400
Wood pellets and wood briquettes	17	4.8	650	11,000
Miscanthus (bale - 25% MC)	13	3.6	140-180	1,800-2,300
Fossil fuels				
House coal	27-31	7.5-8.6	850	23,000-26,000
Anthracite	33	9.2	1,100	36,300
Heating oil	42.5	11.8	845	36,000
Natural gas (NTP)	38.1	10.6	0.9	35.2
LPG	46.3	12.9	510	23,600

BIOMASS HEATING SYSTEMS

Biomass with low moisture content, provided in its raw form or processed as pellets, chips, briquettes, etc., can be converted in both heat and CO_2 to a greenhouse via combustion or other thermo-chemical processes such as gasification or pyrolysis (McKendry, 2002).

Several different types of biomass boilers can be supplied with wood chips, pellets, or briquettes: their sizes range from small (10÷20 kW), to medium (50 kW and above), and to power-station (100 MW and more).

Biomass fuel is fed to the grate mechanically where it undergoes the four-stage combustion process to produce energy:

- Warming and drying temperature T< 150°C;
- Pyrolysis 150< T<500°C;
- Gasification 500< T<800°C;
- Combustion of gases 800< T<1600°C.

The biomass boilers systems should provide a drying of the first load of fuel on the grate and then the heating towards the spontaneous ignition temperature of 400°C, accomplished by automatic ignition systems, most notably hot air.

Warming and drying requires hot combustion chamber above and around where the fuel enters the grate. Thus, boilers contain some refractory material, and the greater this quantity of refractory walls, the less responsive the boiler to changes in heat demand, the longer the time taken to reach ignition temperature and the greater the residual heat that will need to be dissipated when the boiler is switched off. To prevent the formation of slag on the grate, the combustible gases (mainly CO and H_2) are burned some distance away from the grate at a high temperature, while maintaining the temperature range on the grate itself.

Incomplete gasification and oxidation can occur, and black smoke can be produced, if for some reasons wet fuel is not dried sufficiently by the boiler. Moreover, the tars released during the 'Pyrolysis stage' will gradually coat the heat exchanger surfaces resulting in reduced heat exchange efficiency and the eventual failure of the boiler (Palmer et al., 2011).

Automatic feed burner main types are:

- Stoker burner boilers;
- Stoker boiler using an underfed combustion system.

Both boilers can burn wood pellets and wood chips up to 30% moisture content (MC). For wood chip with a MC of between 30 and 50%, moving grate boilers, also known as stepped grate or inclined grate boilers, have been designed.

Since the last decade, the gasification technology has been gaining a great importance when coupled with syngas combustion for heat and power, due to its high efficiency; moreover, it makes the thermo-chemical conversion of biomass cleaner and easier to control, compared to direct combustion of solid fuels (Reed and Das, 1988; Quaak et al., 1999; Whitt et al., 2008; Caputo et al., 2005; Dion et al., 2013).

Biomass boilers are not normally sized to meet the peak heat load but rather to provide a large percentage of the heat requirement, thus needing a buffer vessel: heat produced by the boiler that exceeds the immediate heat requirement of the greenhouse is stored to meet subsequent heating requirements.

Biomass consumption as fuel for greenhouse heating is related to both the greenhouse surface and the specific energy needs of crops. Considering a thermal power of the greenhouse surface to be heated equivalent to 100 W m^{-2}, a conversion yield of 85%, biomass producing 3.9 kWh kg^{-1}, the annual average biomass consumption is about 45÷90 kg m^{-2} with 1,500÷3,000 running hours.

The capacity of the heat store places a limit on the amount of heat that can be stored. The size of heat store, tipically 15÷20×10^{-3} m^3 per unit greenhouse area, depends on the control strategies and on the CO_2 enrichment in the greenhouse, if any (Chalabi et al., 2002; Nederhoff, 2004).

CLEAN CO_2 ENRICHMENT

The enrichment of greenhouse air with CO_2 leads to better plant growth, shorter cropping times, and higher quality. Therefore, low-cost CO_2 sources may result in the most profitable choice for crop growth in greenhouses, combining control of ventilation and CO_2 enrichment.

Carbon dioxide gas for enrichment can be derived either from pure gas and the combustion gases from a hydrocarbon fuel such as low sulphur paraffin, propane, butane or natural gas, or from the combustion of biomass fuel. In Canada, the fuel cost for providing heat and CO_2 represents about 28% of the operating cost of a greenhouse, and in the recent past years, a detailed economic study has been completed by Caputo et al. (2005) on utilizing wood residue for producing electricity using combustion in comparison with gasification technologies in Europe. The optimal CO_2 concentration for growth and yield seems to be 700÷900 vpm (volume parts per million). The CO_2 concentration should be kept to at least the outside level, but CO_2 enrichment is not a current practice in mild climates up to now (von Zabeltitz, 2011).

A number of studies have been carried out to determine the most economically profitable CO_2 enrichment strategy for greenhouse using CO_2 from the exhaust gases of natural gas boilers (Houter et al., 1989; Nederhoff, 1990; Rijsdijk and Houter, 1993; Ioslovich et al., 1995; Aikman et al., 1997; Stanghellini et al., 2008, 2009). The EUPHOROS project, within the 7th Framework Programme of RTD, dealt with the efficient use of inputs in protected horticulture, and investigated the optimum ventilation, thermal storage and CO_2 management for different climates and available sustainable energy sources, giving valuable information on costs and technologies (Baeza et al., 2007).

Exhaust gases from gas burners can be led directly into the greenhouse. Gas will be burned, and the CO_2 is blown with the circulating air into the greenhouse. Special control systems are necessary, and care must be taken to avoid carbon monoxide production. Thus, it seems convenient to mix the exhaust gas with fresh air (von Zabeltitz, 2011), in order to condense water vapour, dilute the concentrations of the emissions, and permit distribution in the greenhouse. The current world prices of bottled or piped CO_2 are between 0.1 and 0.2 € kg^{-1}, which is comparable to the cost of producing carbon dioxide by burning gas.

If the flue gas contains high level of NOx, a catalytic process, based on urea as a reactant to remove the pollutant, has been described by Lugt et al. (1996). The return on investment and the pay out time were estimated to be 700% and 0.5 year, respectively, for large power stations.

On the contrary, biomass combustion is not as clean as natural gas combustion. While it produces CO_2 and water vapour as well, it also leads to higher emissions of NOx, SOx, CO,

Particulate Matter, and VOCs.

In terms of enrichment applications, combustion of dry and clean wood biomass can produce two times more useful CO_2 than natural gas for the same energy unit (Chau et al., 2009). Exact flue gas composition depends on furnace technology and efficiency: a comprehensive review of exhaust gas composition and toxicity, and of CO_2 recovery methods from the exhaust gas of biomass heating systems for safe enrichment in greenhouses, has been carried on by Dion et al. (2011).

Most of the pollutants mentioned previously are due to incomplete combustion. VOCs and large organic pollutants can be significantly reduced controlling residence time, temperature and turbulence (Reed and Das, 1988). Scrubbing system with particular catalysts can transform nitrogen oxides NOx and sulphur oxides SOx found in exhaust gases into valuable byproducts, but the economical feasibility and the overall sustainability of developed methods should be assessed. Cyclones, scrubbers, electrostatic precipitators (ESP) and fabric filters can typically stop PM, up to aerodynamic diameter size as large as 0.1 μm, but care should be taken to control PM concentrations, as well (Dion et al., 2011). Membrane based CO_2 separation process seems to be the most promising technology due to its energy-saving, space-saving and ease for scale up, as reviewed by Yang et al. (2008), but currently no applications to CO_2 enrichment in greenhouses have been reported due to the still high cost.

ECONOMIC ASSESSMENT

A techno-economic assessment, combining the technical and economical parameters which could affect the economics of a project, is highly recommended before taking the final decision (Chau et al., 2009).

From this point of view, in Italy the National Decree 28 December 2012 introduced large economic incentives, called “White Certifies”, in order to shift boilers to wood biomass types, if addressed to greenhouses heating. The technical Datasheet n. 40E – Installation of wood biomass boilers in the greenhouse industry – sets up some requirements of the whole system to be installed.

Boilers must comply with standards EN 303-05 (2012), EN 12809 (2001), and Italian UNI 10683 (2005), dealing with technical parameters and maximum power (500 kW), and:

- efficiency not less than 85%;
- emission standards, as required in class 5, EN 303-05 (2012).

Biomass must fulfill the quality classes provided by EN standards, in particular:

- wood pellets: class A1/A2, EN 14961-2 (2010);
- wood briquettes: class A1/A2 and B, EN 14961-3 (2010);
- wood chips: class A1/A2 and B, EN 14961-4 (2010).

The cost of the boiler varies considerably, in relation to the technological level of the boiler itself. In Italy, the cost of a modern wood chips/pellets boiler is about 100÷250 € kW^{-1}, depending on its size. Other devices complete the system: loading system, accumulator, control system and safety, installation, heat delivering, etc. In practice, the total cost (including building works) is several times more than the one above.

In general, the total cost can be considered in the order of 800÷1400 € kW^{-1} for systems of lesser power (up to approximately 80÷100 kW), in the order of 600÷800 € kW^{-1} for boilers of greater power (over 100 kW, but less than 1000 kW), and in the order of 400÷600 € kW^{-1} for boilers of greater power (over 1000 kW).

The economic incentives called “White Certifies” cover only a part of the above mentioned costs, thus needing a thorough economic assessment to tell whether it is profitable or not. In fact, incentives provided in the time span of 5 years may vary between 5 and 100 € kW^{-1}, related to the area of the greenhouse floor surface, and in relation to cladding materials, shape ratio of the greenhouse, and to 6 climatic zones as defined by the degree-day method.

As the power energy load was estimated to be between 30 W m^{-2} (in southern regions) and more than 175 W m^{-2} (in northern regions), the overall cost for the biomass heating system, calculated as average from the above-mentioned costs, may vary considerably

between ~20 € m^{-2} (30 W m^{-2} × 700 € kW^{-1}) and 125 € m^{-2} (175 W m^{-2} × 700 € kW^{-1}), thus resulting in most cases higher than the incentives themselves.

A vast variety of cases may be found dealing with the replacement of already existing boilers, thus taking into account only the costs for boilers, loading system, and installation: in such cases, the profitability is likely to be fulfilled. In North Italy, the price for wood chips and wood pellets are 0.032 and 0.06 € kWh^{-1}, respectively. Compared to heating oil price, they result in 2÷3 times lower price, making greenhouses management more profitable.

CONCLUSIONS

The present work deals with wood biomass systems for space heating of the greenhouses. In Italy, the average overall cost for the biomass heating system was estimated to be between 20 € m^{-2} (in southern regions) and 125 € m^{-2} (in northern regions). Besides a techno-economic analysis of wood biomass boiler systems, it is worth noting that the flue gas contains a large amount of CO_2, and that this resource can be exploited to increase the production. Since some decades ago, carbon dioxide enrichment has been established in northern Europe greenhouses, recycling the exhaust gas coming from gas heating systems, due to benefits brought to plant production: anyway it needs optimal management strategies to reduce fuel consumption.

Unfortunately, biomass boilers generate a higher volume of NOx, SOx, VOCs, particulate matters (PM), and ash emissions than other fossil fuels, thus making CO_2 enrichment still challenging and expensive. Recently, some flue gas conditioning devices proved themselves able to reduce costs, but economic feasibility is still far to be achieved.

All this standing, in relation to the economic incentives by the Italian National Decree of 28 December 2012, it is worth converting boilers to wood biomass boilers, as the price for wood chips and wood pellets ensures more than twice a reduction with respect to the heating oil price.

ACKNOWLEDGEMENTS

The data processing and the editorial work must be shared, within the competencies of the research groups, equivalently among the authors.

Literature cited

Aikman, D.P., Lynn, J.R., Chalabi, Z.S., and Bailey, B.J. (1997). CO2 optimisation in the glasshouse tomato. Acta Hortic. *443*, 137–145 http://dx.doi.org/10.17660/ActaHortic.1997.443.17.

Baeza, E.J., López, J.C., Fernández, M.D., Meca Abad, D.M., Magán, J.J., González, M., Montero, J.I., Anton, A., Stanghellini, C., and Kempkes, F.L.K. (2007). EUPHOROS, Deliverable n.14. DSS for optimum ventilation, thermal storage & CO_2 management for different climates & available sustainable energy sources. http://www.wageningenur.nl/en/Research-Results/Projects-and-programmes/Euphoros-1/Reports.htm

Biomass Energy Centre. http://www.biomassenergycentre.org.uk.

Campiotti C.A., Viola C., Scoccianti M., Giagnacovo G., Lucerti G., and Alonzo G. (2011). Le filiere del sistema agricolo per l'energia e l'efficienza energetica. RT/2011/11/ENEA.

Caputo, A., Palumbo, M., Pelagagge, P., and Scacchia, F. (2005). Economics of biomass energy utilization in combustion and gasification plants: effects of logistic variables. Biomass Bioenergy *28* (*1*), 35–51 http://dx.doi.org/10.1016/j.biombioe.2004.04.009.

Chalabi, Z.S., Biro, A., Bailey, B.J., Aikman, D.P., and Cockshull, K. (2002). Optimal control strategies for carbon dioxide enrichment in glasshouse tomato crops, Part II: use of carbon dioxide from the exhaust gases of natural gas "red boilers. Biosyst. Eng. *81* (*4*), 421–431 http://dx.doi.org/10.1006/bioe.2001.0039.

Chau, J., Sowlati, T., Sokhansanj, S., Preto, F., Melin, S., and Bi, X. (2009). Techno-economic analysis of wood biomass boilers for the greenhouse industry. Appl. Energy *86* (*3*), 364–371 http://dx.doi.org/10.1016/j.apenergy.2008.05.010.

Dion, L.M., Lefsrud, M., and Orsat, V. (2011). Review of CO2 recovery methods from the exhaust gas of biomass heating systems for safe enrichment in greenhouses. Biomass Bioenergy *35* (*8*), 3422–3432 http://dx.doi.org/10.1016/j.biombioe.2011.06.013.

Dion, L., Lefsrud, M., Orsat, V., and Cimon, C. (2013). Biomass gasification and syngas combustion for greenhouse

CO_2 enrichment. BioResources *8* (*2*), 1520–1538 http://dx.doi.org/10.15376/biores.8.2.1520-1538.

EN14961:2010. Solid Biofuels - Fuel specifications and classes, parts 1-6.

EN15234:2010. Solid Biofuels - Fuel quality assurance, parts 1-6.

EN 12809:2001. Residential independent boilers fired by solid fuel — Nominal heat output up to 50 kW — Requirements and test methods. EUPHOROS Project. http://www.wageningenur.nl/en/Research-Results/Projects-and-programmes/Euphoros-1.htm

EN 303-05:2012. Heating boilers. Part 5: Heating boilers for solid fuels, manually and automatically stoked, nominal heat output of up to 500 kW — Terminology, requirements, testing and marking.

Houter, G., Gijzen, H., Nederhoff, E.M., and Vermeulen, P.C.M. (1989). Simulation of CO_2 consumption in greenhouses. Acta Hortic. *248*, 315–332 http://dx.doi.org/10.17660/ActaHortic.1989.248.38.

Ioslovich, I., Seginer, I., Gutman, P.O., and Borshchevsky, M. (1995). Sub-optimal CO_2 enrichment of greenhouses. J. Agric. Eng. Res. *60* (*2*), 117–136 http://dx.doi.org/10.1006/jaer.1995.1006.

Lugt, P.M., de Niet, A., Bouwman, W.H., Bosma, J.C.N., and van den Bleek, C.M. (1996). Catalytic removal of NOx from total energy installation flue-gases for carbon dioxide fertilization in greenhouses. Catal. Today *29* (*1-4*), 127–131 http://dx.doi.org/10.1016/0920-5861(95)00291-X.

Mathiesen, B.V., Lund, H., and Karlsson, K. (2011). 100% renewable energy systems, climate mitigation and economic growth. Appl. Energy *88* (*2*), 488–501 http://dx.doi.org/10.1016/j.apenergy.2010.03.001.

McKendry, P. (2002). Energy production from biomass (Part 2): conversion technologies. Bioresour. Technol. *83* (*1*), 47–54. PubMed http://dx.doi.org/10.1016/S0960-8524(01)00119-5

Nederhoff, E.M. (1990). Technical aspects, management and control of CO2 enrichment in greenhouses. Acta Hortic. *268*, 127–138 http://dx.doi.org/10.17660/ActaHortic.1990.268.11.

Nederhoff E.M. (2004). 'Open' and 'closed' buffer systems for heat storage (New Zealand Grower: Horticulture New Zealand), pp.41.

Palmer, D., Tubby, I., Hogan, G., and Rolls, W. (2011). Biomass Heating: a Guide to Medium Scale Wood Chip and Wood Pellet Systems (Farnham: Biomass Energy Centre, Forest Research).

Quaak, P., Knoef, H., and Stassen, H.E. (1999). Energy from Biomass. A Review of Combustion and Gasification Technologies (Washington, D.C.: World Bank).

Reed, T.B., and Das, A. (1988). Handbook of Biomass Downdraft Gasifier Engine Systems (Golden, CO: Solar Technical Information Program, Solar Energy Research Institute).

Rijsdijk, A.A., and Houter, G. (1993). Validation of a model for energy consumption, CO2 consumption and crop production (ECP-model). Acta Hortic. *328*, 125–131 http://dx.doi.org/10.17660/ActaHortic.1993.328.9.

Stanghellini, C., Incrocci, L., Gázquez, J.C., and Dimauro, B. (2008). Carbon dioxide concentration in Mediterranean greenhouses: how much lost production? Acta Hortic. *801* (*2*), 1541–1550 http://dx.doi.org/10.17660/ActaHortic.2008.801.190.

Stanghellini, C., Kempkes, F.L.K., and Incrocci, L. (2009). Carbon dioxide fertilization in mediterranean greenhouses: when and how is it economical? Acta Hortic. *807*, 135–142 http://dx.doi.org/10.17660/ActaHortic.2009.807.16.

UNI 10683:2005. Generatori di calore alimentati a legna o da altri biocombustibili solidi. Requisiti di installazione.

von Zabeltitz, C. (2011). Integrated Greenhouse Systems for Mild Climates (Berlin, Heidelberg, Germany: Springer-Verlag), pp.363.

Whitt, K.J., Zhang, H.R., and Eddings, E.G. (2008). Emissions from syngas combustion. Combust. Sci. Technol. *180* (*6*), 1117–1136 http://dx.doi.org/10.1080/00102200801963326.

Yang, H., Xu, Z., Fan, M., Gupta, R., Slimane, R.B., Bland, A.E., and Wright, I. (2008). Progress in carbon dioxide separation and capture: a review. J Environ Sci (China) *20* (*1*), 14–27. PubMed http://dx.doi.org/10.1016/S1001-0742(08)60002-9

Use of compost as amendment for soilless substrates of plants in green roof installations

R. Di Bonito[1], D. Biagiotti[2,3], G. Giagnacovo[2], M. Canditelli[4], C.A. Campiotti[2]

[1]UTAGRI, ENEA, Roma, Italy; [2]UTEE, ENEA, Roma, Italy; [3]Dafne, University of Studies of Tuscia, VT, Italy; [4]UTAMB, ENEA, Roma, Italy.

Abstract

The effect of amendment with compost obtained from food waste in soilless substrate was evaluated with respect to the growth of *Sedum reflexum*, *Sedum palmieri*, *Sedum acre*, *Sedum spurium* and *Sempervivum tectorum* under conditions simulating a green roof in central Italy. Plants were grown in a mix of soilless media developed for green roofs with 5 and 10% v/v amendment and a starter dose of fertilizer. The 5% amendment produced a significant increase of fresh and dry weight on *Sedum reflexum* plants growing in pots after 15 weeks. A long-term experiment was conducted in containers with 10% compost and the five species transplanted together with a fixed pattern. After 139 days, the compost amendment produced a significant increase on surface coverage for *Sedum reflexum*, *Sedum palmieri* and *Sempervivum tectorum*. The evaluation on day 251, at the end of the winter season, showed a reduced growth rate in the control, while the compost treatment produced significant increases for the *Sedum* species. The increase in plant weight was significant for *Sedum palmieri*, *Sedum acre* and *Sempervivum tectorum*. The N content at day 251 was higher in plants with compost, suggesting a compensation of the nutrient depletion and cold damage during the winter.

Keywords: *Crassulaceae*, *Sedum* sp., *Sempervivum tectorum*, organic amendment, greenery

INTRODUCTION

The installation of green roofs and green facades on urban buildings has valuable environmental benefits such as mitigation of the temperature, improvement of the air quality, preservation of biodiversity and regulation of storm-water. The installations and the materials for green roofs are regulated at the local level by specific rules, as reported in Germany by the Landscaping and Landscape Development Research Society e.V. - FLL (FLL, 2008). Extensive green roofs have shallow depth (3-15 cm) and the vegetation is obtained by a blend of different species of perennial stonecrops, selected for prostrate growth, succulent leaves able to store water, and the ability to survive under the seasonal variation (Monterusso et al., 2005). In the Mediterranean regions, the selection of native ecotypes adapted to dry and hot summers could improve the success of green roofs (Giagnacovo et al., 2014). The substrates of green roofs are made of lightweight materials with low density, water-holding capacity and resistance to environmental factors. The most common lightweight materials are expanded shale, lapilli, perlite, pumice and crushed bricks with the addition of peat as organic matter. The use of compost obtained from different sources as amendment in soilless media has been tested in horticulture (Restrepo et al., 2013; DeKalb et al., 2014) and could be a source of organic matter in green roof substrates (Olszewski et al., 2010; Ondoño et al., 2014). In this work, we have tested the effect of amendment with compost obtained from food waste in soilless substrate for the growth of five species of *Crassulaceae* under conditions simulating a green roof in central Italy.

MATERIALS AND METHODS

Plants and substrates

The study was conducted on the species *Sedum acre*, *Sedum reflexum*, *Sedum spurium*

Acta Hortic. 1146. ISHS 2016. DOI 10.17660/ActaHortic.2016.1146.19
Proc. III Int. Sym. on Organic Matter Mgt. and Compost Use in Hort.
Eds.: M. Cayuela et al.

and *Sempervivum* sp., natives of the Mediterranean regions, and *Sedum palmieri*, which originated from Mexico but is widespread in Italy and Mediterranean regions. *Sedum acre* and *Sedum reflexum* were obtained from a local nursery (Albani and Ruggieri s.s.a., Civitavecchia, RM, Italy), *Sedum palmieri* and *Sempervivum* sp. were collected in central Italy and propagated at ENEA Casaccia, Roma, Italy, and *Sedum spurium* was obtained from the Botanical Garden of the University of Tuscia, Viterbo, Italy. The plants were vegetatively propagated in the spring starting from cuttings of 3 cm length, and after 6 weeks were used for transplant in the experiments. The substrate used for the propagation and all the experiments was a mix 1:1 of commercial products (Perlite Italiana srl, Corsico, MI, Italy): Agrilit 3™ (expanded perlite with particle size of 2-5 mm, pH 6-7) and Agriterram TVS™ containing lapilli, pumice, zeolite and 10% peat, with particle size of 1-10 mm and pH 6-7. Agriterram TVS™ contained a slow-release fertilizer 16N-24P-12K at the dose of about 1.0 kg m^{-3} that was the only fertilization applied to the experiments. The compost was obtained from food waste (about 500 kg) of a local cafeteria, mixed with 13.7% residual wood chips and bark, and composted at the Laboratory UTAMB-Rif ENEA, using a community pilot plant provided by CRTEC s.r.l., (Potenza, Italy). The characterization of the compost is reported in Table 1. The heavy metals Cr, Hg, Ni, Cd and Pb presented concentrations much lower of the limits admitted from the Italian regulations (D.lgs 7/2013) and were not reported.

Table 1. Characterization of the compost used in this study.

pH	7.40
Electrical conductivity (mS cm^{-1})	69.300
Total organic carbon (%)	44.2
N (%)	2.6
NH_4-N (%wt.)	0.07
NO_3-N (%)	0.001
K (%)	1.6
P (%)	1.0
Ca (%)	1.13
Mg (%)	0.14
Fe (%)	0.14
Mn (mg kg^{-1})	154.8
Cu (mg kg^{-1})	13.9
Zn (mg kg^{-1})	180.8

Experiments

In the first experiment, the plantlets were transplanted in 1 L pots of 10 cm height (one each), filled with growing media amended with compost at 5 and 10%, v/v. In order to keep constant the ratio of the inorganic fertilizer, a volume equal to the compost was subtracted from the Agrilit 3 and the resulting mix was 50% Agriterram, 50% Agrilit 3 plus compost. The experiment included a control and six replicates for each treatment. The transplant was carried out on 5 August 2014 and the pots were randomly placed on a sunny terrace on the third floor of a building in Roma. The plants were uniformly irrigated with a sprinkler every other day until mid-September, and in the following period, rainfall was the only source of irrigation. The aerial part of the plants was harvested after 15 weeks for the evaluations.

The second experiment was conducted on two platforms of 1.5×3.5 m each, made of a wooden frame containing (from the bottom) a rigid support made of modules Drainroof, (Geoplast, Grantorto, PD, Italy), a filter fabric and the growing medium. The support presented hills of 6 cm height and allowed water retention and drainage. The growing medium had a depth of 6 cm and the compost was uniformly mixed with the lightweight materials at 10% as previously described. Each platform was ideally divided into squares

with sides of 50 cm and five plants of different species were planted in each one. The plants were equally distributed along the diagonals with one in the center and the same pattern was replicated in all the squares, in both the control and the compost platforms. The experiment started on 4 July 2014 and the containers were irrigated with a sprinkler twice per week until mid-September when the rainfall became the only source of water. The surface coverage of each plant was periodically evaluated by the intersect grid method, posing a grid with squares of 1 cm on the surface of plants and measuring the number of intersections. The aerial part of plants was harvested after 251 days for the evaluation of the fresh and dry weight and the nutrient content. The plants were oven dried for 4 days at 65°C and ground. The four replicates of each treatment were combined for the analyses and total nitrogen was evaluated by the Kjeldahl method using a Buchi 426 and the Distiller Buchi K355. Analyses of phosphorus, potassium, magnesium and calcium were obtained using the ICP-MS Agilent 7700. Statistical differences among the means of weight and surface coverage were evaluated by ANOVA and independent *t*-test, using SPSS 15.0 software.

RESULTS

The 5% compost amendment produced a significant increase in fresh and dry weight of the aerial part of *Sedum acre* in pots after 15 weeks as reported in Figure 1.

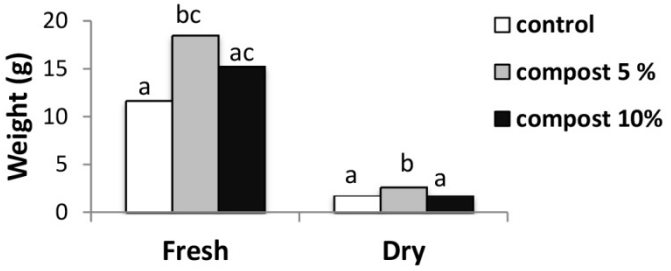

Figure 1. Fresh and dry weight of *Sedum acre* plants after 15 weeks from transplant in pots. Differences among means with different letters are significant (P=0.05, Waller-Duncan test).

In the experiment in platforms, the surface coverage per plant for each of the five species was recorded at days 46, 139 and 251 on four squares and the results are reported in Figure 2. At day 139, the compost amendment produced a significant increase in surface coverage in *Sedum reflexum*, *Sedum palmieri* and *Sempervivum tectorum.* The third observation was taken at the end of the winter season and reported a slower growth rate for *Sedum reflexum* and *Sedum acre*, with a decline of surface coverage for the other species, as a result of depletion of the initial nutrients and the effect of the cold damage. Compost amendment produced a significant increase in all the *Sedum* species, reducing the winter decline observed in *Sedum acre* and *Sedum spurium*. The increase in fresh weight was significant with compost for *Sedum palmieri* and *Sedum acre*, while *Sedum acre* and *Sempervivum tectorum* presented higher dry weights (Figure 3). In succulent species able to store water in the leaves, the increase in fresh weight is also a valuable character related to the survival of plants under dry conditions. The analysis of the plant macronutrient reported in Table 2 shows an increase in the total nitrogen content after compost amendment for all the species and increase in all the elements for *Sempervivum tectorum.*

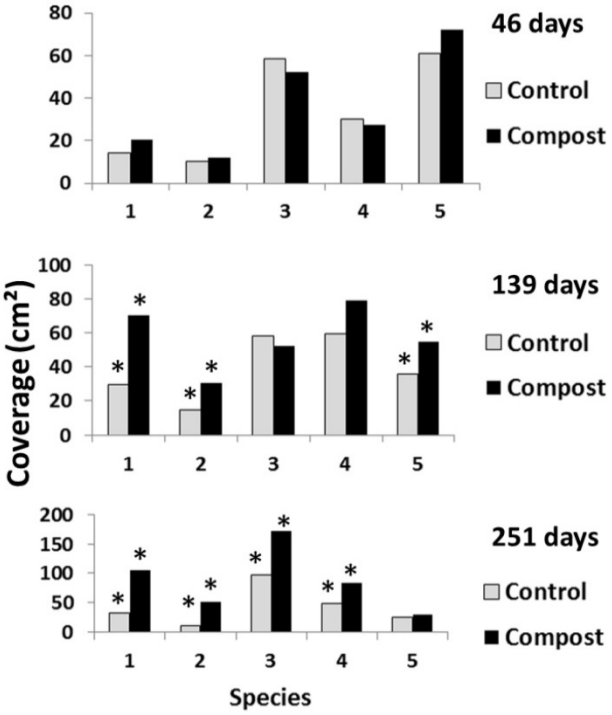

Figure 2. Average surface coverage per plant on five species evaluated at three time points after the transplant. Species: 1, *Sedum reflexum*; 2, *Sedum palmieri*; 3, *Sedum acre*; 4, *Sedum spurium*; 5, *Sempervivum tectorum.* Asterisks denote means are significantly different (P=0.05, independent *t*-test).

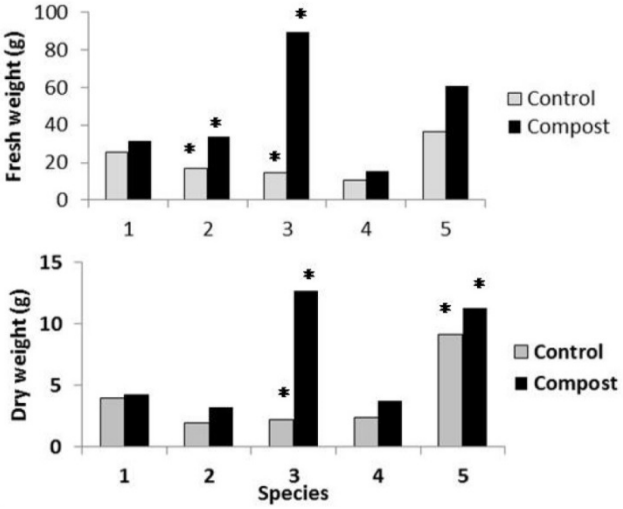

Figure 3. Fresh and dry weight of plants after 251 days. Species: 1, *Sedum reflexum*; 2, *Sedum palmieri*; 3, *Sedum acre*; 4, *Sedum spurium*; 5, *Sempervivum tectorum.* Asterisks denote means are significantly different (P=0.05, independent *t*-test).

Table 2. Accumulation of nutrients (% dry weight) in plants after 251 days.

Nutrient	*Sedum*				*Sempervivum tectorum*
	S. reflexum	*S. palmieri*	*S. acre*	*S. spurium*	
N					
Control	0.56	0.42	0.45	0.64	0.25
Compost	0.87	0.53	0.50	0.87	0.36
P					
Control	0.17	0.20	0.24	0.25	0.18
Compost	0.35	0.29	0.22	0.35	0.30
K					
Control	0.61	1.05	0.56	1.10	0.62
Compost	0.60	1.30	0.39	0.77	0.93
Mg					
Control	0.29	0.41	0.23	0.27	0.53
Compost	0.33	0.41	0.22	0.34	0.68
Ca					
Control	1.68	3.22	1.43	0.93	4.23
Compost	2.96	3.50	1.33	1.49	5.10

CONCLUSIONS

The amendment of 10% compost from food waste on a soilless substrate for green roofs produced a positive effect on the growth of five species of *Crassulaceae* under the climatic conditions of central Italy. However, this effect was more significant for the *Sedum* species after 251 days and resulted in a reduction of the winter decline observed in some cases. The results agree with a previous report where an increase in plant biomass was observed on *Sedum reflexum* (Biagiotti et al., 2014). The negative effect of the 10% compost amendment compared to the 5% at 15 weeks indicated a possible initial inhibitory effect and the need of modulation of the dose amendment in relation to the length of cultivation. The use of compost is already reported as a sustainable source of organic matter in soilless media for horticulture (Raviv, 2014) and this work suggests its potential use in substrates for green roofs in Mediterranean areas.

ACKNOWLEDGMENTS

The work was supported by the project RDS: Eco-green roof & vertical greenery systems Accordo di Programma ENEA-Ministry of the Economic Development of Italy, 2012-14. We thank Dr. Fabio Vitali, head of the laboratory UTAGRI-INN, ENEA, and Dr. Maurizio Coronidi, head of the laboratory UTAMB-RIF, ENEA, for support of this research.

Literature cited

Biagiotti, D., Giagnacovo, G., Di Bonito, R., and Campiotti, C.A. (2014). Evaluation of plant species and soilless substrates for Mediterranean sustainable green roof installations. Paper presented at: 11th International Phytotechnologies Conference (Heraklion, Crete, Greece: Grafima Publishing).

DeKalb, C.D., Kahn, B.A., Dunn, B.L., Payton, M.E., and Barker, A.V. (2014). Substitution of a soilless medium with yard waste compost for basil transplant production. HortTechnology *24*, 668–675.

FLL. (2008). Guideline for the Planning, Construction, and Maintenance of Green Roofing (Bonn, Germany: Landscaping and Landscape Development Research Society E.V. - FLL).

Giagnacovo, G., Biagiotti, D., Di Bonito, R., Mascioli, C., and Campiotti, C.A. (2014). Selezione di ecotipi spontanei di Crassulaceae per la realizzazione di tetti verdi in ambiente mediterraneo. Paper presented at: X Convegno Nazionale sulla Biodiversità, 3-5 Sept 2014 (Roma, Italy: CRA-Centro di Ricerca per lo Studio delle Relazioni tra Pianta e Suolo).

Monterusso, M.A., Rowe, D.B., and Rugh, C.L. (2005). Establishment and persistence of *Sedum* spp. and native taxa for green roof applications. HortScience *40*, 391–396.

Olszewski, M.W., Holmes, M.H., and Young, C.A. (2010). Assessment of physical properties and stonecrop growth in green roof substrates amended with compost and hydrogel. HortTechology *20*, 438–444.

Ondoño, S., Bastida, F., and Moreno, J.L. (2014). Microbiological and biochemical properties of artificial substrates: A preliminary study of its application as Technosols or as a basis in Green Roof Systems. Ecol. Eng. *70*, 189–199 http://dx.doi.org/10.1016/j.ecoleng.2014.05.003.

Raviv, M. (2014). Compost in growing media: feedstock, composting methods and potential applications. Acta Hortic. *1018*, 513–523 http://dx.doi.org/10.17660/ActaHortic.2014.1018.56.

Restrepo, A.P., Medina, E., Pérez-Espinosa, A., Agulló, E., Bustamante, M.A., Mininni, C., Bernal, M.P., and Moral, R. (2013). Substitution of peat in horticultural seedlings: suitability of digestate-derived compost from cattle manure and maize silage co-digestion. Commun. Soil Sci. Plant Anal. *44* (*1-4*), 668–677 http://dx.doi.org/10.1080/00103624.2013.748004.

Available online at www.sciencedirect.com

ScienceDirect

Energy Procedia 113 (2017) 1 – 8

Energy Procedia

International Scientific Conference "Environmental and Climate Technologies", CONECT 2016, 12–14 October 2016, Riga, Latvia

Experimental characterization and energy performances of multiple glazing units with integrated shading devices

Michele Zinzi[a]*, Paolo Ruggeri[b], Fabio Peron[b], Emiliano Carnielo[c], Alessandro Righi[b]

[a]*ENEA, Via Anguillarese 301, Rome 00123, Italy*
[b]*IUAV Universityof Venice, Santa Croce 191, Venezia 30135, Italy*
[c]*University of Roma Tre, Via Ostiense 159, Roma 00154, Italy*

Abstract

Modern architecture is characterized by the use of large glazed surfaces. New technologies ensure thermal insulation by multiple glazing units so that, maintaining good solar gains, highly glazed buildings can achieve good energy performance during the heating season. More complicated is the management of the energy performance during the cooling season due to high permeability to solar radiation. External shading devices are a suitable solution but they are often neglected for functional and aesthetic reasons. Solar protection devices can be, however, introduced in the air gap of multiple glazing units, providing solar protection without interfering with the building envelope. Solar and thermal properties of several solution of glazing units with in-gap shading devices were measured with advanced experimental set-up, to be compared with conventional systems. Numerical analyses were also performed to estimate the impact of this technology on the energy performance of office buildings.

© 2017 The Authors. Published by Elsevier Ltd. This is an open access article under the CC BY-NC-ND license (http://creativecommons.org/licenses/by-nc-nd/4.0/).

Peer-review under responsibility of the scientific committee of the International Scientific Conference "Environmental and Climate Technologies".

Keywords: shading devices; solar properties measurements; U-value measurements; energy performance of buildings

* Corresponding author: Tel.: +39 06 30486256; fax: +39 06 30483930.
E-mail address: michele.zinzi@enea.it

1876-6102 © 2017 The Authors. Published by Elsevier Ltd. This is an open access article under the CC BY-NC-ND license (http://creativecommons.org/licenses/by-nc-nd/4.0/).
Peer-review under responsibility of the scientific committee of the International Scientific Conference "Environmental and Climate Technologies".
doi:10.1016/j.egypro.2017.04.002

1. Introduction

The building sector account for more than 40 % of the energy consumption in Europe and has a significant impact on the achievement of the environmental and energy targets, at national and European level [1, 2]. According to the relevant EU Directive [3], the energy performances of building should be addressed to the whole relevant energy services, while efforts were focused on the space heating systems until few years ago.

One of the key elements for improving the energy efficiency towards the near zero energy building are the solar shading systems. They enable adjustment of the properties of windows and facades to the weather conditions and the need of the occupant providing a good impact on comfort and energy consumption [4, 5]. Despite this they are still under-utilized for functional and aesthetic reasons. Solar protection devices can be, however, introduced in the air gap of multiple glazing units, providing solar protection without interfering with the building envelope [6].

In this context objective of this study is an assessment of the potentialities of double glazing units with shading devices in gap to improve the energy performances of commercial buildings, respect to un-shaded glazing units or with internal shading devices. This aspect is worth of investigation, because modern architecture makes large use of glazed facades with no external solar protections. The intrinsic properties of glass make such building vulnerable during the heating and cooling seasons.

Solar and thermal properties of several solution of glazing units with in-gap shading devices were measured with advanced experimental set-up, to be compared with conventional systems. Moreover numerical analyses were performed to estimate the impact of this technology on the energy performance of office buildings.

2. Methods and samples

Shading systems integrated in the gap of multiple glass units (MGU) can improve the thermal response of transparent building envelope basically in two way: 1) it increases the thermal resistance of the systems, thus increases its insulation power; 2) it lowers the solar gains through the MGU, with increased solar control performance respect to the MGU without shading or with the latter mounted inside.

A relevant issue is the fact that actual standards can be applied on a limited amount of shading materials and products [7, 8], with the consequence that few data about the impact of such products on the energy performance of buildings are available. In order to quantify the energy savings of such solutions, three phases were identified:

1) Optical and thermal experimental characterization of the selected materials;
2) Solar factor calculation starting from measured quantities;
3) Assessment of the energy performances of building equipped with different glazing technologies.

Even if the market of this technology is still limited due to several restraints, many technological solutions are available. Three different double glazing units (DGU), with shading in gap, were analyzed in this study. No spectral data were provided for the single glasses and blinds. Main properties are following described:

- DGU_A. The composition is the following: external 6 mm laminated glass; 27 mm 90 % argon and 10 % air gap; internal 6 mm low-emissivity (0.03) laminated glass. The DGU has a low-emissivity blackout roller blind in gap;
- DGU_B. The composition is the following: external 6 mm laminated glass; 27 mm 90 % argon and 10 % air gap; internal 6 mm low-emissivity (0.03) laminated glass. The DGU has a honeycomb roller blind in gap. The test was carried out also inverting the layer sequence, i.e. the internal glass was moved to the external side;
- DGU_C. The composition is the following: external 6 mm low-emissivity (0.03) laminated glass; 27 mm 90 % argon and 10 % air gap; internal 6 mm laminated glass. In this case the low-e coated glass was placed as external layer, to test its performance as solar filter unit. The DGU has pleated low-emissivity venetian blinds in gap. The lamellae are low-e coated on the convex side.

No spectral data were provided for the single glasses and blinds. Several configurations were tested for the optical characterisation, details about the test configurations are provided in the Results section.

3. Experimental

3.1. Optical

The optical characterization of the selected samples was carried out using a built-in spectrophotometers with large diameter integrating sphere, needed to accurately characterize geometrically complex and scattering glazing units, full description can be found in [9]. The experimental facility consists of the following relevant parts:

- Two light sources were used: a 300 W xenon arc lamp and a tungsten halogen lamp, with adjustable power, ranging from 250 up to 1000 W. The size of the collimated beam can be modulated through a system of lenses and diaphragms according to the measurement requirements. The light beam diameter was set to 60 mm so that all the radiation transmitted by the sample enters into the integrating sphere;
- The light source in transmittance is placed on a rotating holder, so that it is possible to set the angle of the incident radiation and perform off-normal measurements (typically from 0° to 60° incidence angle);
- The spectrophotometer is coupled to an integrating sphere with a 75 cm diameter. The sphere has the internal surface made of Spectralon, a material with reflectivity greater than 95 % in the whole solar range (300–2500 nm). The can be adjusted to perform transmittance, reflectance and absorptance measurements;
- The detection system consists of three array spectrometers and three detectors to explore different spectral bands: NMOS for the 250–1000 nm range (dispersion 1.4 nm/pixel); InGaAs for the 900–1700 nm range (dispersion 3.125 nm/pixel); ExtInGaAs for the 1600–2500 nm range (dispersion 3.52 nm/pixel).

Since the measurement procedure is of the single beam type and the samples are mounted outside the sphere, the transmittance and reflectance measurements are corrected with the auxiliary port method. The instrument error is estimated to be 0.02 for the different measurement modes. Measurements were performed between 380 and 2300 nm, covering 97 % of the whole solar spectrum.

3.2. Thermal

The thermal transmittance of the selected samples is calculated starting from thermal resistance and conductance measured with a hot plate with guard ring experimental facility. The hot plate is designed to perform measurements in the double sample mode, according to the procedures defined in [10] and in the single sample mode, by means of a thermal compensator replacing one of the two sample. The sequence of layers in the single sample mode is shown in Fig. 1(a). Standard sample must be 80 x 80 centimeters, samples with thickness up to 12 centimeters can be tested. Samples with size smaller than 80 x 80 cm can also be tested with a practical lower limit given by the plate guard ring (50 x 50 cm). In case off standard size samples are to be tested, ad-hoc adjustments of the test configuration need to be taken.

The test is carried out in single sample method measuring the following quantities: the hot plate power, the temperature of the chiller, the surface temperature on the cold and hot sides in five different spots for each side. More over controls are made to check that not thermal flux takes place to the guard ring and between the hot plate and the thermal compensator. Measurement scans are run every 3 minutes and measurements are taken every 30 minutes, averaging the last 10 scans. To ensure a high stability level, the test is considered accomplished when the variation of the measured thermal resistance is lower than 0.3 % for three successive measurements. The final U-value error is estimated in 0.03 W/m^2K.

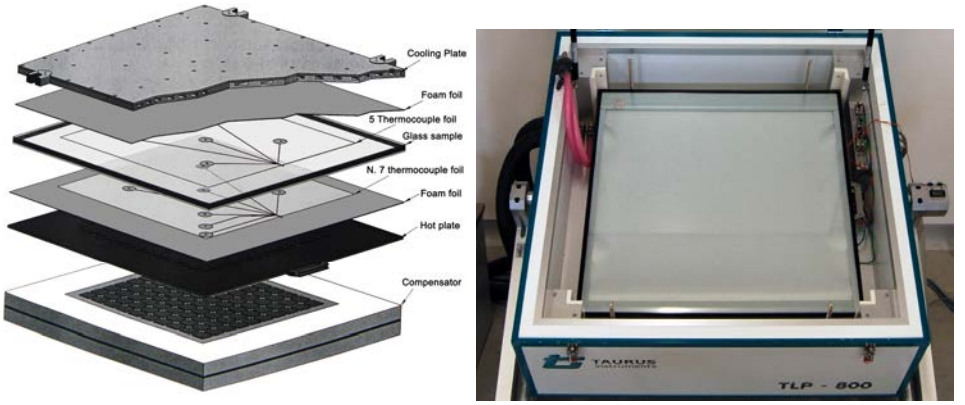

(a) (b)

Fig. 1. Sequence of layers during measurements (a) and view of the experimental facility (b).

4. Calculation

4.1. Estimation of the solar factor of the tested glazing unit

In order to estimate the solar factor g of glazing samples of which the optical and thermal parameters are experimentally tested, we looked for a relationship between the absorbance values αe (given by $\alpha_e=1-\tau_e-\rho_e$) the value of the thermal transmittance U_g and the secondary heat transfer factor qi. It was therefore carried out a regression of the analytical values obtained by simulation using the software *Winshelter V3.0* [11] that implements the methods described in the standard UNI EN 13363-2 [12] in reference conditions. The method can be applied on the product typology this paper deals with, in particular: multiple glazing units with shading devices integrated in the glazing gap. Other glazing configurations are not taken into account for the limitation of the experimental facilities.

To optimize the number of simulations a series of double-glazing systems similar to the ones used in the experimentation were chosen: double-glazing systems with low-emissivity coating in position 3, a 27 mm gap filled with argon 90 %. Between the two glass plates are installed the shading devices. The simulations were carried out maintaining the features of the first glass pane (clear glass 6 mm thick), the cavity size and the percentage of argon.

The optical characteristics of the second plate are chosen from the *Winshelter* database; the fabric and the venetian blinds parameters are also obtained from the same database with three different color gradations (light, medium and dark). The regression equations are obtained with two different methods: the first performs a linear regression from α_e and q_i/U_g ratio values; the second equation is obtained from a second order polynomial regression from α_e, U_g and qi. The two equations are respectively listed below, where the absorbance values are expressed in percentage. In the first case the relative coefficients of determination $R^2 = 0.94$, in the second $R^2 = 0.98$.

$$q_i = (0.31 \cdot \alpha_e - 2.46) \cdot U_g \tag{1}$$

$$q_i = -14.37 + 37.79 \cdot U_g - 0.1487 \cdot \alpha_e - 22.49 \cdot U_g^2 + 0.3889\ \mathrm{Ug} \cdot \alpha_e + 0.0005267 \cdot \alpha_e^2 \tag{2}$$

4.2. Energy performance of a commercial building

In order to evaluate the variation of the energy performance of buildings after the application of glazing units with integrated shading devices, a numerical model of an office building has been set up. The energy behavior has been analyzed in different configurations using Energy Plus software with Design Builder GUI [13]. The energy simulations focus on a typical floor of an office building with a total area of 900 m^2 divided into 800 m^2 of office space and 100 m^2 in service and core zonas. The plane has a height of 3.2 m. The building is located in Rome. In the building plane

90 people work from Monday to Friday from 09.00 to 13.00 and from 15.00 to 19.00. The heating temperature for the office is 20 °C and 18 °C for service zone. The core zone area with services has no conditioning both in summer and winter. In summer all local, with the exception of the core zone, has a temperature of 26 °C. In the offices are present electronic equipment with an overall load equal to 3 W/m^2. The infiltration rate is equal to 0.3 h^{-1}. The entire complex is heated and cooled with a heat pump with a COP of 3.00. The lighting has a power of 4.5 W/m^2. The normative reference for all previous data are the Italian standard UNI TS 11300 [14, 15]. The optical thermal and energetic characteristics of the transparent enclosures are the ones measured on DGU_A and DGU_C samples installed in a frame with a thermal transmittance equal to 1.8 W/m^{2}K. The simulations were performed with a value of thermal transmittance of the opaque envelope elements equal to 0.25 W/m^{2}K and two rates of WWR (Windows to Wall Ratio), homogeneous in all orientations: 50 % and 100 %.

5. Results

5.1. Optical

The spectral transmittance and reflectance curves of the measured samples are plotted in Fig. 2 and Fig. 3 respectively, Table 1 presents the broadband values of transmittance and reflectance both in the solar and visible spectrum. Values are calculated starting from the spectral values according to reference spectra given in [14]. Samples were measured considering two configurations: Blind up and down. Moreover sample DGU_C with blind down was tested with convexity of lamellae towards indoor and outdoor. By observing Fig. 2, the shading systems cut almost to zero the transmittance being 0.02 and 0.05 the measured maximum values for DGU_A and DGU_C respectively. DGU_B is characterized by a total shading device so, in the blind down configuration, the transmittance is equal to 0. The spectral response of DGU_B with blind up was not presented since it is equal to sample DGU_C being the two samples characterized by the same external and internal glass components. It is worthy to notice the spectral behavior in reflectance reported in Fig. 3. The blind down configuration increases the reflectance values in the visible band and tends to decrease them in the near infrared region. As expected the sensibly high spectral values (up to 0.7) in the near infrared band, as inferred from the trends of the not-shaded configurations, denote low-emissivity properties of the internal glass components.

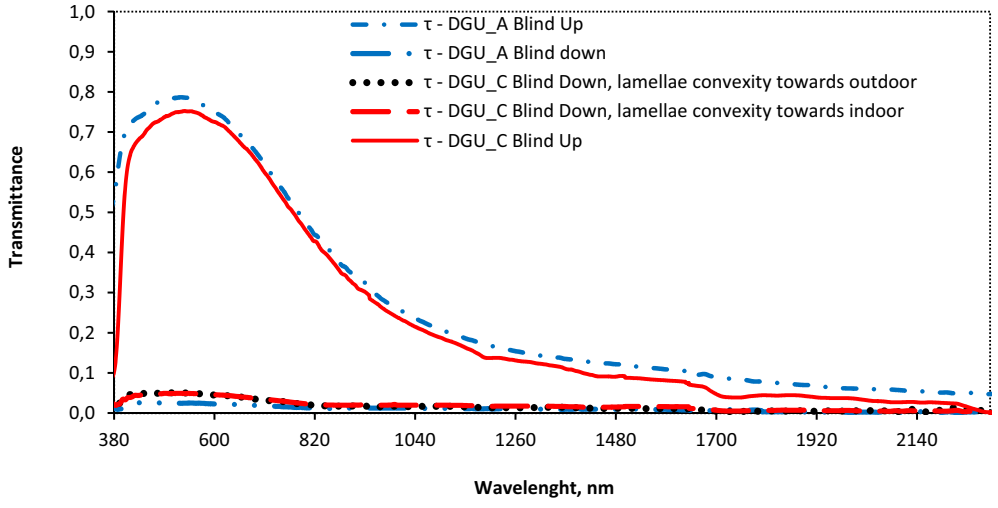

Fig. 2. Spectral transmittance of the selected samples.

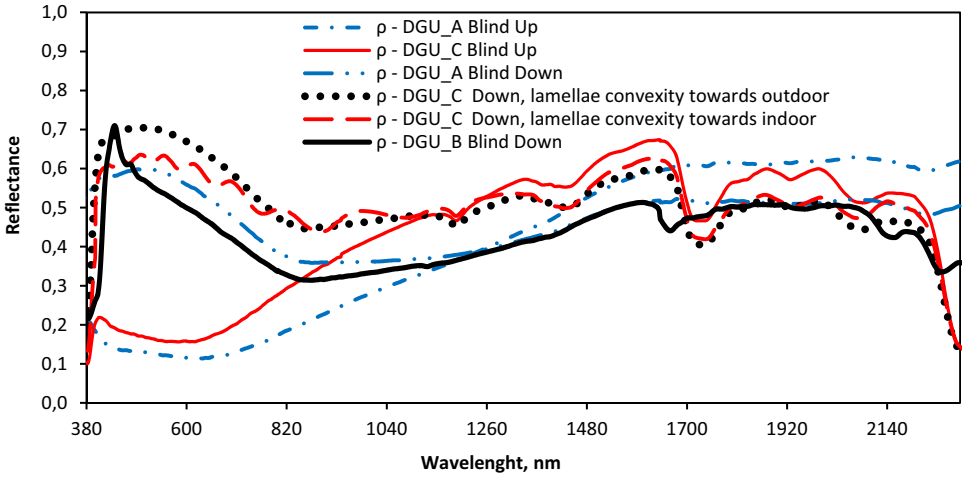

Fig. 3. Spectral reflectance of the selected samples.

Table 1. Broadband transmittance and reflectance values of the selected samples.

	τ_v	ρ_v	τ_e	ρ_e
DGU_A Blind up	0.77	0.12	0.51	0.22
DGU_A Blind down	0.02	0.58	0.02	0.48
DGU_B Blind down	0.00	0.53	0.00	0.44
DGU_C Blind up	0.74	0.16	0.46	0.28
DGU_C Blind down, lamellae convexity to outdoor	0.05	0.69	0.03	0.55
DGU_C Blind down, lamellae convexity to indoor	0.05	0.62	0.03	0.52

5.2. Thermal

The measurement results are presented in Table 2. As inferred the temperature difference and the mean temperature are in the range indicated in the relevant standard, respectively ± 0.5 K and ± 0.5 °C, or present slightly higher variations, considered negligible for this test purposes. The same relevant standard was used to calculate the U-values, applying the surface thermal resistance values for according to the sample lying position. The Table 2 reports the results achieved for all the sample configurations, which are explained in a dedicated column.

Table 2. Thermal measurement results.

Sample	Zone	Mean temperature, °C	Temperature difference, K	U-value , W/m^{2}K
DGU_A	Blind up	14.6	10.0	1.2
DGU_A	Blind down	14.6	10.0	0.83
DGU_B	Blind up	13.9	10.0	1.2
DGU_B	Blind down, low-e glass internal	14.9	10.4	1.1
DGU_B	Blind down, low-e glass internal	15.0	10.1	1.1
DGU_C	Blind up	15.5	9.60	1.2
DGU_C	Blind down, lamellae convexity to outdoor	14.5	9.40	1.1
DGU_C	Blind down, lamellae convexity to indoor	15.6	10.4	1.2

It can be observed the strong impact of the roller blind on the DGU_A, with 0.4 W/m^{2}K reduction of U-value, respect the glazing system only. The convertina blind has a moderate impact on the insulation performance, since the U-value is reduced by 0.4 W/m^{2}K for both configurations. The same improvement is achieved for the lamellae systems with the low emissivity convexity towards the indoor side for sample C; on the contrary now significant effect is measured for outdoor oriented convexity of the lamellae.

5.3. Solar factor

The solar factor of the samples is calculated with Eq. (1) and Eq. (2) from the results of the experimental campaign on the test samples as described in paragraph 5.1 and 5.2. In Table 3 are reported the values of thermal transmittance, U_g and absorbance α_e, the secondary heat transfer factor q_i and g obtained from $g= q_i+\tau_e$.

The g values of the samples A and C with blind up condition is estimate from the optical properties obtained combining two glass plates matching as close as possible the optical values obtained experimental. They are respectively 61 % and 51 %.

Table 3. Values of q_i and g.

Sample	Zone	U value, W/m²K	α_e, %	q_i (eq.1), %	g (eq.1), %	q_i (eq.2), %	g (eq.2), %
DGU_A	Blind down	0.8	50	11	13	12	13
DGU_B	Blind down	1.1	56	17	17	17	17
DGU_C	Blind down, lamellae convexity to outdoor	1.1	42	11	14	12	15
DGU_C	Blind down, lamellae convexity to indoor	1.2	44	13	16	14	17

5.4. Energy performances

The energy performances of the offices building after the application of glazing units with integrated shading devices, are summarized in Table 4. Heating and cooling loads have been evaluated in five case-study applying to glazing units integrated shading devices: DGU_A blind up and down, DGU_C blind up, blind down lamellae convexity to outdoor and blind down lamellae convexity to indoor. For all configurations has been adopted two WWR (Windows to Wall Ratio), homogeneous for all orientations: 50 % and 100 %. The total energy performances improve in all cases with blind down as a consequence of the limitation of cooling loads. Correspondingly there is a relative high increasing of heating loads but have limited influence on the total energy demand as a consequence of good thermal insulation level of walls and glazing. The bigger WWR gives up an augment of the cooling loads in the order of 50 % without blind and around 20–25 % with blind down. As inferred in figure 4 the decrease in total thermal loads, both for DGU_A and DGU_C, are around 40–50 % with WWR 50 % and around 50–60 % with WWR 100 %. The convexity orientation of the lamellae in DGU_C have a little impact on energy demand around 3–5 %.

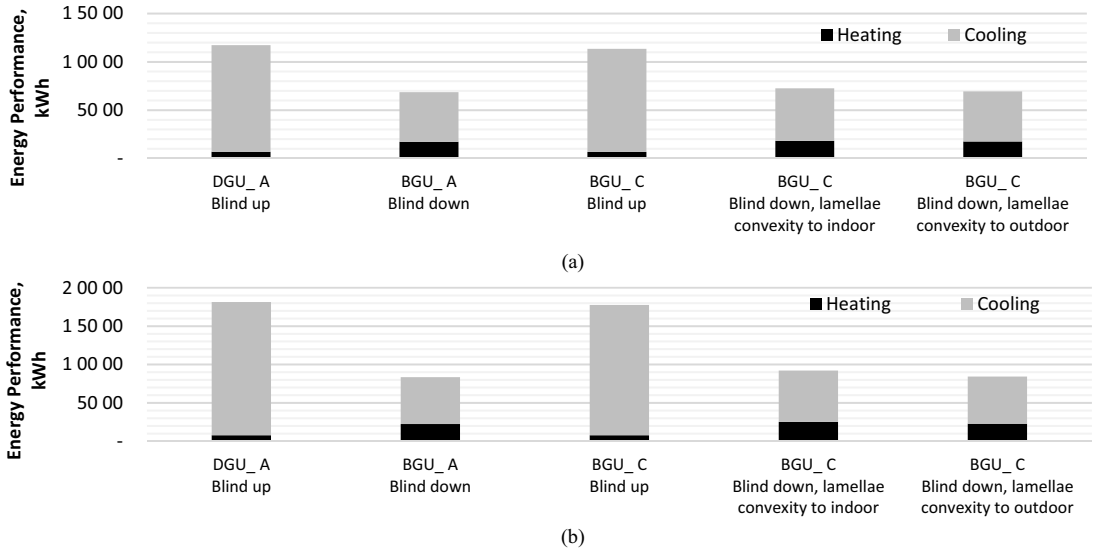

Fig. 4. (a) Energy performances with WWR to 50 %; (b) Energy performances with WWR to 100 %.

Table 4. Energy performance.

WWR Windows to Wall Ratio, %		DGU_A Blind up, kWh	DGU_A Blind down, kWh	DGU_C Blind up, kWh	DGU_C Blind down, lamellae convexity to outdoor, kWh	DGU_C Blind down, lamellae convexity to indoor, kWh
50	Heating	688	1.719	661	1.807	1.755
	Cooling	11.032	5.138	10.682	5.447	5.184
	Total	11.719	6.857	11.344	7.255	6.939
100	Heating	779	2.254	787	2.525	2.285
	Cooling	17.343	6.095	16.975	6.686	6.151
	Total	18.122	8.349	17.761	9.211	8.436

6. Conclusions

In this study three different double glazing units (DGU), with shading in gap, were analysed. The aim was to set up a methodology able to estimate the solar factor and secondary heat transfer factor qi starting from the optical and thermal parameters quite easily experimentally obtained (absorbance and thermal transmittance). Two relationships between the absorbance and thermal transmittance and secondary heat transfer factor q_i .and g factor are obtained by regression. The potentialities of these systems to improve the energy performances of commercial building are demonstrate a high impact in terms of primary energy use. The total energy performances improve in all cases with blind down as a consequence of the limitation of cooling loads, the relative increase of heating loads but have limited influence on the total energy demand as a consequence of good thermal insulation level of walls and glazing.

Acknowledgements

Authors warmly acknowledge Luca Papaiz for his technical support and Pellini S.p.A. for sample preparation.

References

[1] BPIE – Buildings Performance Institute Europe. Europe's buildings under the microscope. Brussels; 2011.
[2] IPCC. Climate Change 2014, Mitigation of Climate Change, Working Group III Technical Support Unit. Cambridge University Press; 2014.
[3] 2002/91/EC, the EP and the EC Directive on Energy performance building directive (EPDB) and EU Directive 2010/31/EC (EPDB recast). Brussels; 2002.
[4] Bellia L, Marino C, Minichiello F, Pedace A. An Overview on Solar Shading Systems for Buildings. Energy Procedia 2014;62:309–317.
[5] Dubois M. Solar Shading and Building Energy Use - A Literature Review, Report TABK—97/3049. Lund Institute of Technology; 1997.
[6] Sharda A, Kumar S. Heat transfer through Glazing Systems with Inter-Pane Shading Devices: A Review. Energy Technology & Policy 2014:1:23–34.
[7] EN 13363-2:2005. Solar protection devices combined with glazing – Calculation of total solar energy transmittance and light transmittance - Part 2: Detailed calculation method. European Committee for Standardization; 2005.
[8] ISO 15099:2003, Thermal performance of windows, doors and shading devices – Detailed calculations.
[9] Maccari A, Montecchi M, Treppo F, Zinzi M. CATRAM: an apparatus for the optical characterization of advanced transparent materials. Applied Optics 1998;37(22):5156-5161.
[10] EN 674:2011, Glass in building - Determination of thermal transmittance (U-value) – Guarded hot plate method. BSI Standards Publication; 2011.
[11] Winshelter. WINdows and SHading Energy Lighting and Thermal Evaluation Routine; ENEA. Available: http://www.pit.enea.it/
[12] EN 13363-2:2006. Solar protection devices combined with glazing. Calculation of total solar energy transmittance and light transmittance. Detailed calculation method. European Committee for Standardization; 2006.
[13] EnergyPlus™. Engineering Reference, The Reference to EnergyPlus Calculations; 2014.
[14] UNI TS 11300-1: 2014. Prestazioni energetiche degli edifici. Determinazione del fabbisogno di energia dell'edificio per la climatizzazione estiva ed invernale; 2014.
[15] UNI TS 11300-2: 2014. Prestazioni energetiche degli edifici. Determinazione del fabbisogno di energia dell'edificio per la climatizzazione estiva ed invernale; 2014.

Available online at www.sciencedirect.com

ScienceDirect

Energy Procedia 113 (2017) 9 – 16

Energy Procedia

International Scientific Conference "Environmental and Climate Technologies", CONECT 2016, 12–14 October 2016, Riga, Latvia

Advanced polycarbonate transparent systems with aerogel: preliminary characterization of optical and thermal properties

Elisa Moretti[a], Michele Zinzi[b]*, Emiliano Carnielo[c], Francesca Merli[a]

[a]*University of Perugia, Department of Engineering, Via G. Duranti 93, 06125 Perugia, Italy*
[b]*ENEA Casaccia Research Centre, Via Anguillarese 301, 00123 Rome, Italy*
[c]*University of Roma Tre, Department of Engineering, Via della Vasca Navale 79/81, 00146 Rome, Italy*

Abstract

The market penetration of polycarbonate (PC) multi-sheets panels for building applications is increasing due to intrinsic properties of the material: high transparency, reduced weight if compared to glass and competitive costs. The presence of air gaps within the panel assures good thermal insulation; however, to further improve the thermal properties of the component, the air gaps can be filled by granular silica aerogel. These materials are also characterized by high scattering optical properties, so that the incident radiation can be diffused in the built environment, preventing from glare. This paper deals with the characterization of several configurations of PC systems, differing in thickness and geometry. Thermal transmittance measurements were carried out using a guarded hot plate apparatus, according to EN 674:2011. Spectral transmittance and reflectance measurements were carried out by means of a large integrating sphere apparatus, broad-band light and solar quantities were then calculated. A valid data set of product specification is thus provided. The investigated polycarbonate systems could be a valid solution in place of classic windows for non-residential buildings, enhance the thermal insulation and the light control of the building envelope, thus providing improved comfort conditions for occupants.

© 2017 The Authors. Published by Elsevier Ltd. This is an open access article under the CC BY-NC-ND license (http://creativecommons.org/licenses/by-nc-nd/4.0/).

Peer-review under responsibility of the scientific committee of the International Scientific Conference "Environmental and Climate Technologies".

Keywords: optical properties; thermal properties; aerogel; glazing systems; building integration

* Corresponding author: Tel.: +39-06-304862565; fax: +39-06-30483930.
E-mail address: michele.zinzi@enea.it

1876-6102 © 2017 The Authors. Published by Elsevier Ltd. This is an open access article under the CC BY-NC-ND license (http://creativecommons.org/licenses/by-nc-nd/4.0/).
Peer-review under responsibility of the scientific committee of the International Scientific Conference "Environmental and Climate Technologies".
doi:10.1016/j.egypro.2017.04.003

1. Introduction

Buildings account for more than 40 % of the energy consumption in Europe and current legislation is oriented towards the introduction of restrictive energy efficiency standards for building envelope components, with focus on thermal insulation properties in temperate climates as Europe and North America [1, 2]. Transparent elements have a significant role in building performance in terms of energy demand, thermal comfort, and daylighting: most of the total energy losses (up to 60 %) can depend on the windows especially in highly glazed buildings such as non-residential buildings, and they can strictly affect the cooling loads [3, 4]. In this context, in order to encourage refurbishment of existing buildings towards Nearly Zero Energy Buildings (NZEB), innovative and advanced materials and solutions have been appearing in the building and construction industry, also including nanomaterials, such silica aerogels [5–7].

In the paper, co-extruded polycarbonate panels with aerogel in interspace are investigated as an advanced glazing solution for non-residential buildings, considering different thickness of aerogel layers. Optical properties were measured using a large sphere apparatus, because conventional spectrophotometers cannot measure optical properties of such samples due to of the geometry and structural complexities, as well as for scattering phenomena in non-regular and diffusing materials. Thermal transmittance (U-value) was measured using the guarded hot plate method, also considering different inclinations (horizontal and vertical), because the investigated solutions are also suitable as roof solutions in buildings, due to their lightness. Moreover, in order to highlight the effect of aerogel in the multi-sheet PC panels, the same experimental campaign was carried out on the samples without aerogel, considering the PC system only. Finally, in order to evaluate the potential spread of these solutions in the fenestration market, their performance was compared to conventional glazing solutions.

2. Objective and Methods

Polycarbonate is an important class of polymers which is widely reflected in architectural applications. It is moldable material, durable, lightweight, fireproof and unbreakable. Moreover, one of its best properties is high impact resistance, which can be more than 200 times greater than tempered glass. Polycarbonate panels are efficient solution for non-residential buildings because they are weather resistant and UV protected.

Polycarbonate sheets could be used as fenestration systems, continuous windows, shed, roofs, walls and indoor partitions: they can be as clear as glass, translucent or completely opaque, depending on the specific use. A lot of products with different cell geometric characteristics, colors, thicknesses and kind of application are available in the market: this solution could represent a possible and cheaper option for non-residential building instead of standard glazing facades [8].

A good thermal insulation is ensured by the presence of air gaps inside the panel; however, in order to improve the thermal properties of the component, the air gaps can be filled by granular silica aerogel (Fig. 1). The aerogel used in fenestration products is an amorphous form of synthetic silica structured by nano-sized pores. About 95 % of its volume is occupied by air, making aerogel the world's lightest solid material. The low solid content and extremely small pore size make it very effective against conduction and convection of heat. In addition to high thermal insulation capacity, aerogel ensures good light transmission and good acoustic performance [9–11].

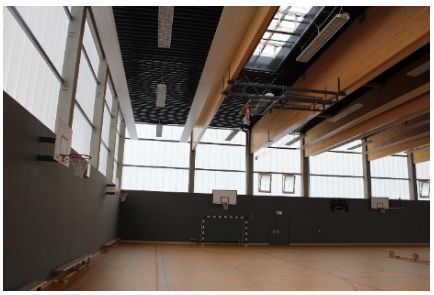

Fig. 1. Example of a building with granular aerogel filled PC panels.

In this paper three types of multiwall polycarbonate panels were investigated considering different thickness and geometry. They consist of three walls, two external layers (about 1 mm thickness) and an internal one (0.5 mm thickness), with a double chamber filled of aerogel (particles size about 0.7–3 mm). These samples are investigated for assessing thermal and optical properties, with and without aerogel. For the thermal measurement, only two types of samples are considerate (16 and 40 mm thickness) because they have appropriate dimension (80 x 80 cm) for instrument measurement. For this reason, a frame of insulating material has been applied to PC 40/3 (50 x 50 cm), so from reaching requests test size.

The standard polycarbonate width is 2100 mm and maximum length is 7000 mm, so they need to be installed in building thanks to male-female joints.

Table 1 shows the main characteristics of the examined samples.

Table 1. Features of polycarbonate panels.

Sample	Thickness, mm	Scheme panel	Sample dimensions, cm	Picture
PC 16/3	16	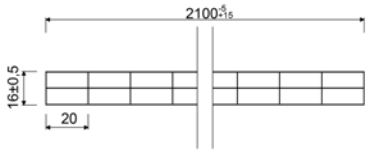	1 sample 30 x 30 1 sample 80 x 80	
PC 25/3	25	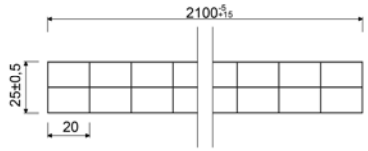	30 x 30	
PC 40/3	40	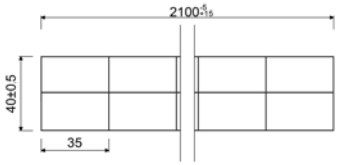	50 x 50	

3. Experimental

3.1. Optical

The optical characterization of the selected samples was carried out using a built-in spectrophotometer with large diameter integrating sphere, needed to accurately characterize geometrically complex and scattering glazing units; full description can be found in [12]. The experimental facility consists of the following relevant parts:

- The light source is a tungsten halogen lamp with adjustable power, ranging from 250 up to 1000 W. The size of the collimated beam can be modulated through a system of lenses and diaphragms according to the measurement requirements. The light beam diameter was set to 60 mm so that all the radiation transmitted by the sample enters into the integrating sphere;
- The light source in transmittance is placed on a rotating holder, so that it is possible to set the angle of the incident radiation and perform off-normal measurements (typically from 0° to 60° incidence angle);
- The spectrophotometer is coupled to an integrating sphere with a 75 cm diameter. The sphere has the external shell made of aluminum and an internal surface made of Spectralon, a white material with reflectivity greater than 95 % in the whole solar range (300–2500 nm). The layout of the facility can be adjusted to perform transmittance, reflectance and absorptance measurements;

- The detection system consists of three array spectrometers and three detectors to explore different spectral bands: NMOS for the 250–1000 nm range (dispersion 1.4 nm/pixel); InGaAs for the 900–1700 nm range (dispersion 3.125 nm/pixel); ExtInGaAs for the 1600–2500 nm range (dispersion 3.52 nm/pixel).

Fig. 2 shows the experimental facility in the transmittance and reflectance measurement modes. Since the measurement procedure is of the single beam type and the samples are mounted outside the sphere, the transmittance and reflectance measurements are corrected with the auxiliary port method [8, 12]. The measurement procedures are:

- Transmittance mode. The transmittance is measured as the ratio of the energy transmitted by the specimen mounted on the sample port on the energy directly entering the sphere; see Fig. 2. The measurements are performed at normal incidence;
- Reflectance mode. The radiation enters the sphere through a port facing the sample port and hits the sample with an 8 deg. angle of incidence. The reflectance is measured as the ratio of the energy reflected by the specimen mounted on the sample port and the energy entering and hitting the sphere wall directly. Only the near-normal incidence reflectance is carried out.

The instrument error is estimated to be 0.02 for the different measurement modes.

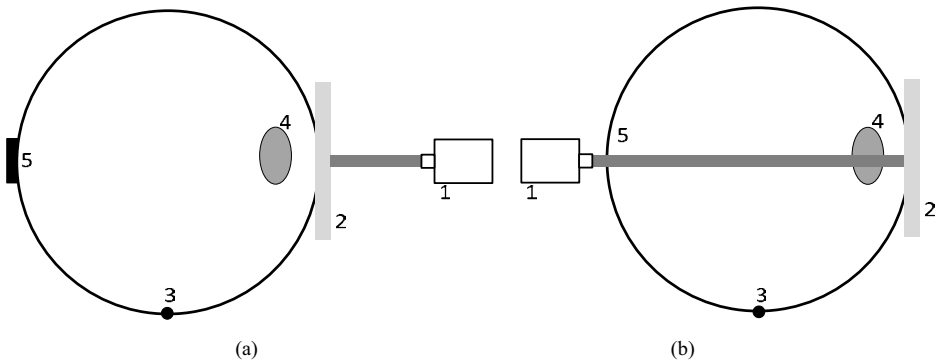

Fig. 2. Optical bench apparatus in transmittance (a) and reflectance (b) modes. Main parts: 1–light source; 2–sample port (transmittance port) with holder; 3–opticfibre connected to the detection system; 4–auxiliary port; 5–reflectance port.

3.2. Thermal

The thermal transmittance of the selected samples is calculated starting from thermal resistance and conductance measured with a hot plate with guard ring experimental facility. The hot plate is designed to perform measurements in the double sample mode, according to the procedures defined in [13], and in the single sample mode, by means of a thermal compensator replacing one of the two sample. The sequence of layers in the single sample mode is shown in Fig. 3(a), a view of the facility with an aerogel filled PC sample mounted on can be observed on the right. Standard sample must be 80 x 80 cm, samples with thickness up to 12 cm can be tested. Samples with size smaller than 80 x 80 cm can also be tested with a practical lower limit given by the plate guard ring (50 x 50 cm). In case of standard size samples are to be tested, ad-hoc adjustments of the test configuration need to be taken.

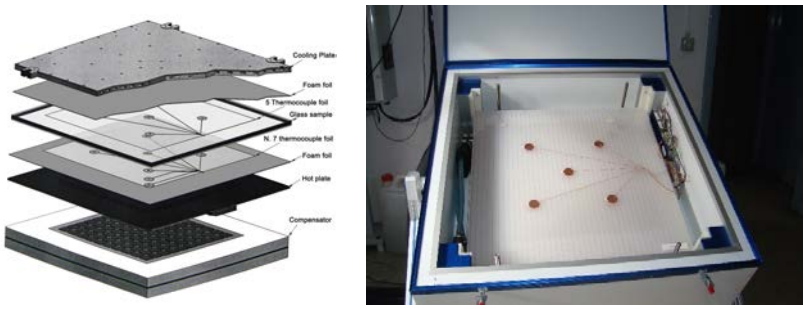

(a) (b)

Fig. 3. Sequence of layers during measurements (a) and view of the experimental facility (b).

The test is carried out measuring: the hot plate power, the temperature of the chiller, the surface temperature on the cold and hot sides in five different spots for each side. More over controls are made to check that not thermal flux takes place to the guard ring and between the hot plate and the thermal compensator. Measurement scans are run every 3 minutes and measurements are taken every 30 minutes, averaging the last 10 scans. To ensure a high stability level, the test is considered accomplished when the variation of the measured thermal resistance is lower than 0.3 % for three successive measurements. The final U-value error is estimated in 0.03 W/m^2K.

4. Results

4.1. Optical

The spectral transmittance and reflectance curves of the three samples are plotted in Fig. 4 and Fig. 5 respectively. They were measured in a spectral band confined within 400 and 2300 nm, covering the 96 % of the solar spectrum. Table 2 reports the broadband values calculated for transmittance, reflectance and absorptance in the visible and solar spectrum according to the standard reference ISO 9050 [14, 15].

By observing figure 4 the three polycarbonate panels show an almost superimposed transmittance trend in the whole investigated spectrum regardless the sample thickness. In fact, as shown in Table 2, the transmittance difference are confined within 0.02, in broadband terms, for the empty samples both in visible and solar range. When panels air gaps are filled with granular silica aerogel transmittance values progressively decrease as a function of thickness. By comparing empty and aerogel filled samples it is interesting to note a modification of the spectral response shape in the band ranging between 400 and 700 nm.

Moreover the aerogel sensibly affects the reflectance spectrum between 400 and 1400 nm increasing the reflectance properties, as inferred in Fig. 5. The maximum difference in broadband values (Table 2) between empty and aerogel filled samples reaches 0.20 in the visible range and 0.14 in the solar range.

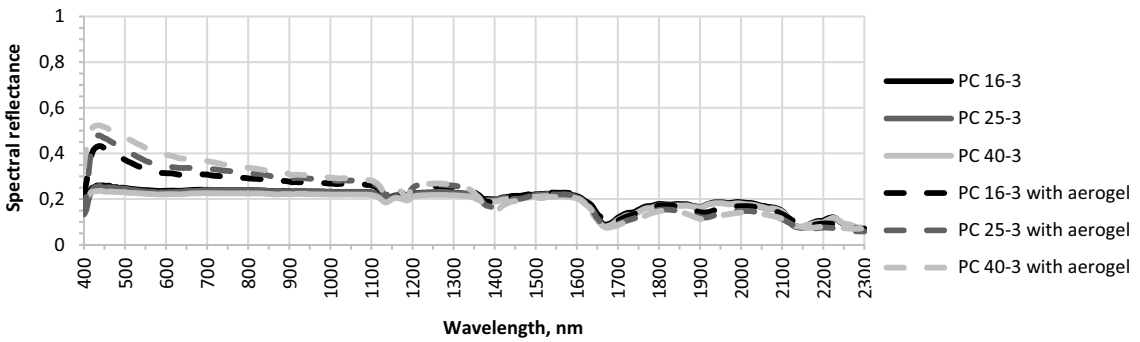

Fig. 4. Spectral transmittance of the selected samples: normal incidence.

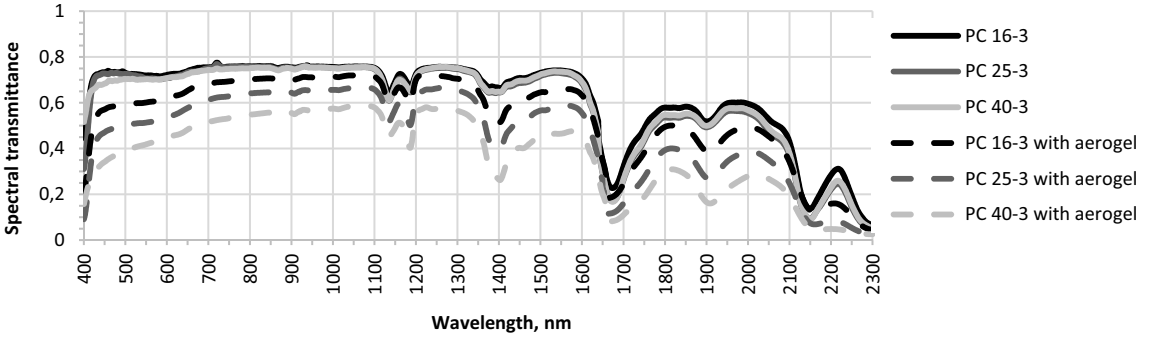

Fig. 5. Spectral reflectance of the selected samples.

Table 2. Light and solar direct transmittance and reflectance.

Sample	Light transmittance, τ_v	Solar transmittance, τ_e	Light reflectance, ρ_v	Solar reflectance, ρ_e	Light absorptance, α_v	Solar absorptance, α_e
PC 16/3	0.72	0.70	0.24	0.23	0.04	0.07
PC 16/3 with aerogel	0.61	0.61	0.33	0.29	0.06	0.10
PC 25/3	0.71	0.68	0.23	0.22	0.06	0.11
PC 25/3 with aerogel	0.52	0.53	0.37	0.31	0.11	0.16
PC 40/3	0.70	0.68	0.22	0.21	0.08	0.11
PC 40/3 with aerogel	0.42	0.44	0.42	0.35	0.16	0.21

4.2. Thermal

The measurement results are presented in Table 3. As inferred the temperature difference and the mean temperature are in the range indicated in the relevant standard [13], respectively ± 0.5 K and ± 0.5 °C. The same relevant standard was used to calculate the U-values, applying the surface thermal resistance values for according to the sample lying position. It can be observed that the thermal resistance for horizontal and vertical position is the same in case of the aerogel filled components, which implies a thermal transfer mainly by conduction in the gap. To be noted that the same behavior can be observed for the 16 mm sample, while, as expected, for the 40 mm sample the horizontal position leads a lower thermal resistance respect to that achieved with the sample in vertical. Concerning the impact of the aerogel on the insulation performances of transparent polycarbonate, it can be observed that U-value is reduced by about 45 % and 70 % for, respectively, the 16 and 40 mm samples.

Table 3. Thermal measurement results.

Sample	Mean temperature, °C	Temperature difference, K	Thermal resistance, m^2K/W	U value, W/m^2K
PC 16/3 aerogel horizontal	9.9	15.1	0.59	1.4
PC 16/3 aerogel vertical	9.9	15.0	0.59	1.3
PC 16/3 without aerogel horizontal	10.0	14.9	0.26	2.5
PC 16/3 without aerogel vertical	10.0	14.8	0.25	2.4
PC 40/3 aerogel horizontal	9.8	15.4	1.58	0.6
PC 40/3 aerogel vertical	9.9	15.4	1.58	0.6
PC 40/3 without aerogel horizontal	10.3	15.0	0.31	2.2
PC 40/3 without aerogel vertical	9.9	14.7	0.37	1.9

5. Discussion

In order to evaluate the potential of polycarbonate panels in the fenestration market, the investigated solutions were compared to conventional solutions for glazing units, as multilayer glass systems (double or triple glazing) with gas filling: optical properties (light τ_v and solar transmittance τ_e) are plotted versus the thermal transmittance (U) (Fig. 6).

The PC systems data come from the experimental campaign (relating to sample PC 25/3, U value from the manufacturer was used for the comparison), whereas the ones related to glazing system solutions result from the literature [16]. The light transmittance of all PC systems is lower than glazing units, especially when aerogel thickness increases. However, they are adequate for highly glazed buildings and, due to high scattering optical properties, they can produce comfortable visual comfort conditions in buildings, diffusing the light and reducing the bright zones near the window area: glare problems are limited and, simultaneously, the uniformity of illumination level distribution could be increased. In general, the solar transmittance of PC panels are ever higher than the glass units ones (about 40 %), allowing a heating energy demand reduction thanks to high solar heat gains, especially in coldest climates.

When highly energy-efficient windows are needed (U < 1 W/m^{2}K), PC systems with translucent granular aerogels could reach 0.6 W/m^{2}K for a 40 mm thickness only; the value is of the same order of magnitude of a triple glazing window with two low-e layers argon filled, but innovative PC systems could be easier applied in commercial buildings (roofs or walls), because of the lightness (the weight is lower than 5 kg/m^2, whereas conventional triple glazing have a weight in the 30–40 kg/m^2 range, depending on the glass layers). However, at same time, the reduction in light transmission is acceptable (about 30 %).

Finally, as consequence of the results reported in Table 3, roof applications are suitable, because the U-values are not influenced by the inclination to the vertical, such as in the gas-filled glazing systems which have a worse behavior when used as roofs instead of vertical panels.

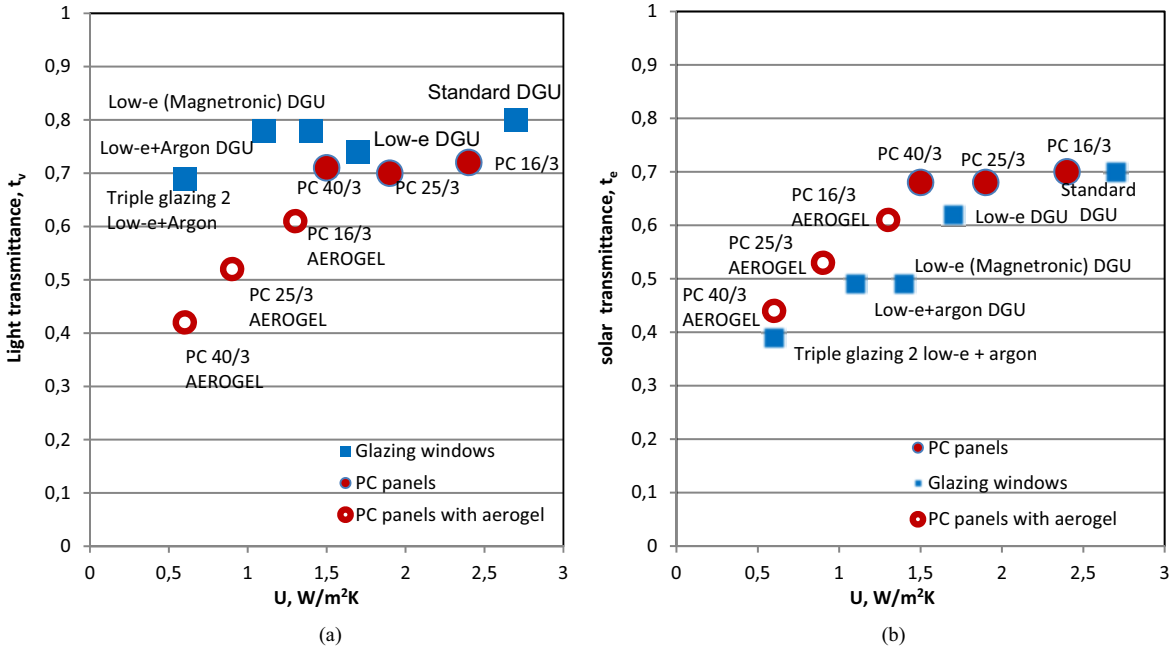

Fig. 6. Comparison between PC systems (with air gap and aerogel filled) and conventional glazing systems: light transmittance (τ_v) versus U-value (a) and direct solar transmittance (τ_e) versus U-value (b).

6. Conclusions

Polycarbonate (PC) multi-sheets panels have been spreading in the market due to high transparency, good thermal performance, reduced weight if compared to glass, and competitive costs. To further improve the thermal properties of these solutions, the air gaps can be filled by translucent granular silica aerogel, a low density nano-structured porous material with very low thermal conductivity (about 0.018–0.020 W/mK at room temperature).

Three aerogel-filled PC systems, differing in thickness (from 16 to 40 mm), were investigated and optical and thermal performance were analyzed with to a large sphere apparatus and a guarded hot-plate facility. Experimental results showed very good thermal behaviour of all the investigated PC panels: U-values vary in the 0.6 (for 40 mm thickness only) – 1.4 (16 mm thickness) W/m^2K range. Due to aerogel, the convection in the gap between PC layers is removed (thermal performance is independent of the inclination) and the thermal transmittance is reduced by about 45 and 70 % for, respectively, the 16 and 40 mm samples, when compared to empty PC panels. Simultaneously, the reduction in light transmittance, which increases with aerogel thickness, is acceptable and it is in the 15–40 % range. Compared to conventional glazing windows, PC systems have a lower light transmittance (about −30 % for higher thickness of aerogel) together with a higher solar transmittance (about + 40 %), considering a glazing with similar thickness and comparable U-value; nevertheless the light is diffused, avoiding glare problems and improving visual comfort. The investigated solutions could be a valid solution in place of conventional glazing windows in non-residential buildings: they contribute to reduce energy consumption without substantially reducing the light transmission and at the same time they are characterized by an easier application, because of extreme lightness.

A critical issue to assess the benefits of aerogel-filled PC systems on the energy performance of buildings is the assessment of the solar factor, which takes into account the direct solar transmission and the secondary heat transfer. A further step of the research here presented is the implementation of a calculation method able to estimate the solar factor from measured solar transmittance and absorptance, as well the thermal resistance values.

Finally, due to their good functional features, innovative aerogel-filled polycarbonate panels are very attractive for applications in non-residential buildings as walls, roofs, sheds, and continuous windows, even if they need to be more cost effective in order to compete with the conventional solutions.

Acknowledgements

The authors wish to thank RODA – E.M.B. Products AG (Emmerich, Germany: https://www.roda.de/products/daylight-technology/lumira-aerogel/info/) for the precious information on the investigated solutions and for supplying the samples.

References

[1] 2010/21/EU, EU directive on Energy performance of buildings (EPBD2). Available: http://eur-lex.europa.eu/LexUriServ/LexUriServ.do?uri=OJ:L:2010:065:0027:0030:EN:PDF
[2] EC (European Commission); 2007. Available: http://www.ec.europa.eu/comm/energy_transport/atlas/html/buildings.html
[3] Jelle BP, Hynd A, Gustavsen A, Arasteh D, Goudey H, Hart R. Fenestration of today and tomorrow: A state-of-the-art review and future research opportunities. Sol Energ Mat Sol C 2012;96:1–28.
[4] Krawczyk DA. Analysis of energy consumption for heating in residential house in Poland. Energy Procedia 2016;95:216–222.
[5] Buratti C, Moretti E. Experimental performance evaluation of aerogel glazing systems. Appl Energ 2012;97:430–437.
[6] Ihara T, Gao T, Grynning S, Jelle BP, Gustavsen A. Aerogel granulate glazing facades and their application potential from an energy saving perspective. Appl Energ 2015;142:179–191.
[7] Buratti C, Moretti E, Belloni E. Nanogel windows for energy building efficiency. In: Pacheco Torgal F, Buratti C, Kalaiselvam S, Granqvist CG, Ivanov V, editors. Nano and biotech based materials for energy building efficiency. Switzerland: Springer International Publishing; 2016.
[8] Moretti E, Zinzi M, Belloni E. Polycarbonate panels for buildings: experimental investigation of thermal and optical performance. Energy Buildings 2014;70:23–35.
[9] Buratti C, Moretti E. Lighting and energetic characteristics of transparent insulating materials: experimental data and calculation. Indoor Built Environ 2011;20:400–411.
[10] Buratti C, Moretti E. Silica nanogel for energy-efficient windows. In: Pacheco-Torgal F, Diamanti MV, Nazari A and Granqvist CG, editors. Nanotechnology in eco-efficient construction. Cambridge: Woodhead Publishing Limited; 2013.
[11] Buratti C, Moretti E. Nanogel windows. In: Pacheco Torgal F, Mistretta M, Kaklauskas A, Granqvist CG, Cabeza LF, editors. Nearly zero energy building refurbishment. London: Springer-Verlag; 2013.
[12] Maccari A, Montecchi M, Treppo F, Zinzi M. CATRAM: an apparatus for the optical characterization of advanced transparent materials. Appl Optics 1998;37:5156–5161.
[13] UNI EN 674. Glass in building - Determination of thermal transmittance (U value) - Guarded hot plate method; 2011.
[14] EN ISO 9050:2003, Glass in building-determination of light transmittance, solar direct transmittance, total solar energy transmittance, ultraviolet transmittance and related glazing factors.
[15] UNI EN 410. Glass in building – Determination of luminous and solar characteristics of glazing; 2011.
[16] AGC Glass Europe. Available: http://www.yourglass.com/configurator/tp/it/toolbox/configurator/main.html

buildings

MDPI

Article

High Energy-Efficient Windows with Silica Aerogel for Building Refurbishment: Experimental Characterization and Preliminary Simulations in Different Climate Conditions

Cinzia Buratti [1], Elisa Moretti [1,*] and Michele Zinzi [2]

[1] Department of Engineering, University of Perugia, Via G. Duranti 67, 06125 Perugia, Italy; cinzia.buratti@unipg.it

[2] ENEA Casaccia Research Centre, Via Anguillarese 301, 00123 Rome, Italy; michele.zinzi@enea.it

* Correspondence: elisa.moretti@unipg.it; Tel.: +39-075-5853694

Academic Editor: Gianpiero Evola

Received: 29 November 2016; Accepted: 10 January 2017; Published: 16 January 2017

Abstract: The paper deals with the potential of high energy-efficient windows with granular silica aerogel for energy saving in building refurbishment. Different glazing systems were investigated considering two kinds of granular silica aerogel and different glass layers. Thermal transmittance and optical properties of the samples were measured and used in building simulations. The aerogel impact on heat transfer is remarkable, allowing a thermal transmittance of 1.0–1.1 W/(m^2·K) with granular aerogel in interspace only 15 mm in thickness. A 63% reduction in U-value was achieved when compared to the corresponding conventional windows, together with a significant reduction (30%) in light transmittance. When assembled with a low-e glass, the U-value reduction was lower (31%), but a moderate reduction in light transmittance (about 10%) was observed for larger granules. Energy simulations for a case study in different climate conditions (hot, moderate, and cold) showed a reduction in energy demand both for heating and cooling for silica aerogel glazing systems, when compared to the conventional ones. The new glazings are a suitable solution for building refurbishment, thanks to low U-values and total solar transmittance, also in warm climate conditions.

Keywords: high energy-efficient windows; nanogel windows; silica aerogel; building refurbishment; Nearly Zero Energy Buildings (NZEBs); energy saving in buildings

1. Introduction

Glass façades have an important role in buildings in terms of energy demand, thermal comfort, and daylighting: the main total energy losses (up to 60%) can depend on the windows, especially in highly glazed buildings. In order to speed up refurbishment of existing buildings towards Nearly Zero Energy Buildings (NZEBs), innovative glazing systems have been spread in the market and might be suitable in places of conventional glazing windows, especially in cold climates [1–3]. Aerogel windows seem to have the largest potential for improving the thermal performance and daylighting in glazing systems, because of very low thermal conductivity (about 0.020 W/m·K for translucent granular aerogel at room temperature) and density (about 80 kg/m^3), together with good optical transparency and acoustic insulation [4–9].

Opaque silica aerogel-based materials, such as flexible blankets and aerogel-based plasters and concrete, have recently appeared on the market [10,11]. Silica aerogels, both in monolithic and granular translucent form, can be used in high-insulated nanogel windows: transparent monolithic panes were developed 20–30 years ago, but their application in glazing systems has still not penetrated the market, and few prototypes have been manufactured for research purposes [12,13]; for these reasons,

building applications have focused on glazing systems with granular aerogels [14–17]. Different translucent daylighting systems with granular aerogel have been emerging in the market. The most popular systems are multiwall polycarbonate panels for skylights, roofs, walls, structural panels for continuous façades, and finally insulated glass units. Many of these innovative solutions can be found in schools, commercial and industrial buildings, airports, etc., especially in the US and in Northern Europe [4,6,7,18]. The main application has been focusing on roof solutions [7,8], where an outside view is usually not essential or where they can also be integrated at façade spandrels [14].

Thermal and optical properties of granular aerogel glazing systems are significantly affected by aerogel layer thickness and particle size: a significant reduction in U-value is observed by incorporating the aerogel granules into the cavity of double glazings (58% and 63%) [19–21]. When the aerogel layer thickness increases to 60 mm, a U-value of 0.3 W/(m^2·K) can be achieved [16,22]. When compared to conventional glazings, the ones with granular aerogel also have significant benefits when used for roof solutions, because U-values are not dependent on the tilted angle to the vertical plane, for example, in gas-filled glazings [8,22].

The paper deals with the potential of highly energy-efficient windows with silica aerogel for energy saving in order to create Nearly Zero Energy Buildings (NZEBs) or as a strategy in building refurbishment; in order to evaluate the potential spread of these solutions in the fenestration market, their performance was compared to conventional glazing solutions. The experimental characterization of double glazing units (DGUs) with aerogel in interspace is carried out by considering different kinds of silica granular aerogel and glass layers. Solar and light transmittance of aerogel windows are investigated by means of advanced instrumentation, able to measure the optical properties of diffusing and scattering materials. In this work, a large integrating sphere apparatus, designed for complex transparent and translucent systems, was used. Thermal transmittance (U-value) of DGUs is measured using a Heat Flux Meter in steady-state conditions. Then, the energy performance of aerogel windows is discussed thanks to a case study: energy demand of a non-residential building is calculated by means of Energy Plus software by using experimental data as input data and considering different climate conditions (cold, moderate, and hot climates). The results are finally compared in order to evaluate the benefits of using innovative systems with aerogel instead of conventional solutions.

2. Materials and Methods

2.1. The Investigated Samples

Two prototypes of aerogel glazing units were assembled by incorporating aerogel granules into the air space of the corresponding double glazing units, in order to investigate their optical and thermal properties and to carry out numerical simulations on energy performance based on experimental data.

The double-glazing units with aerogel in interspace (Figure 1b) were used to realize two prototypes of windows (an aluminum frame window, Type 1 [20], and a wood frame window, Type 2) with two mobile shutters. The two windows were compared to conventional solutions with the same frame and glass, but with an air gap (Figure 1a).

Aerogel in granular form was put in a gap 15 mm thick, while external and internal layers are float glass 4 mm in thickness. Window Type 1 was assembled with two conventional clear float glass layers, whereas Window Type 2 has a low-e and solar control coating on the inner side of the external glass. During the assembly process, the glazing system was subject to mechanical vibration in order to ensure a compact packing of aerogel granules between the glass layers. Two kinds of silica aerogel granules were considered: type "A" for the window frame Type 1 and type "B" for the other window. Type "B" is the most recent aerogel, characterized by larger granules, allowing enhanced daylighting properties, as shown in Figure 2. Table 1 shows the main characteristics of the DGU samples.

(**a**) (**b**)

Figure 1. Wood frame window prototype Type 2 (**a**) with conventional double glazing units (DGUs) and (**b**) with aerogel in the interspace between glass layers.

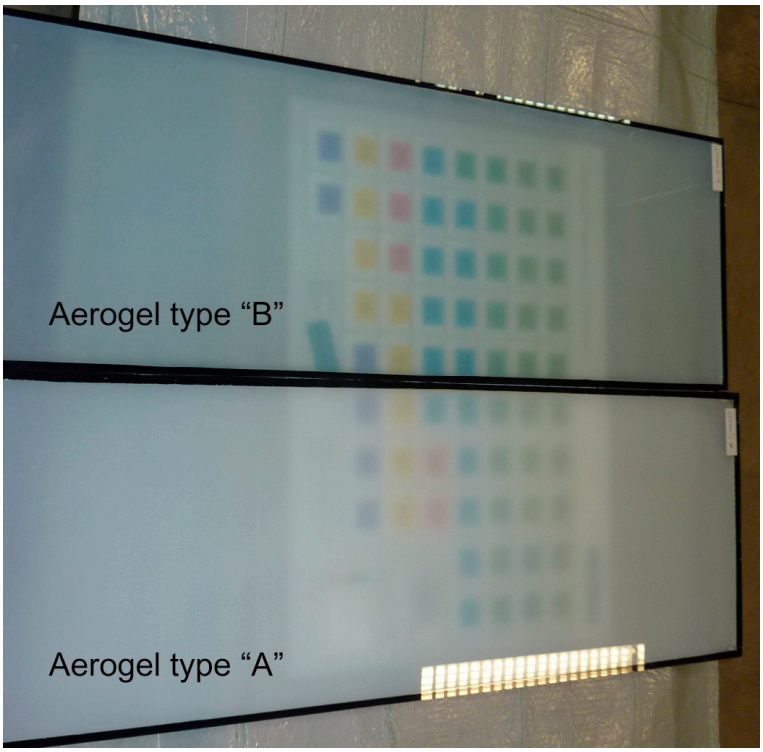

Figure 2. Glazing units with aerogel: LOW-E DGU AEROGEL with aerogel type “B” (at the **top**) and DGU-AEROGEL with aerogel type “A” (at the **bottom**).

Table 1. The investigated glazing systems: conventional DGU and DGU with aerogel.

Name	External Layer	Interspace	Internal Layer	Window Frame
DGU	Float clear glass (4 mm)	Air (15 mm)	Float clear glass (4 mm)	Type 1 aluminum
DGU-AEROGEL	Float clear glass (4 mm)	Granular aerogel type "A" (15 mm)	Float clear glass (4 mm)	
LOW-E DGU	Solar control and low-e glass (4 mm)	Air (15 mm)	Float clear glass (4 mm)	Type 2 wood
LOW-E DGU-AEROGEL	Solar control and low-e glass (4 mm)	Granular aerogel type "B" (15 mm)	Float clear glass (4 mm)	

2.2. Experimental Campaign

The optical characterization of all the samples was carried out by means of a built-in spectrophotometer with a large-diameter integrating sphere (75 cm diameter, with an internal surface made of Spectralon, SphereOptics GmbH, Herrsching, Germany), needed to accurately characterize geometrically complex and scattering transparent materials; a full description can be found in the literature [23,24]. The layout of the facility can be adjusted to perform transmittance, reflectance, and absorptance measurements, using a single beam measurement procedure (Figure 3). The near-normal incidence transmittance and reflectance were measured in the 350–2000 nm range, covering about 97% of the solar spectrum.

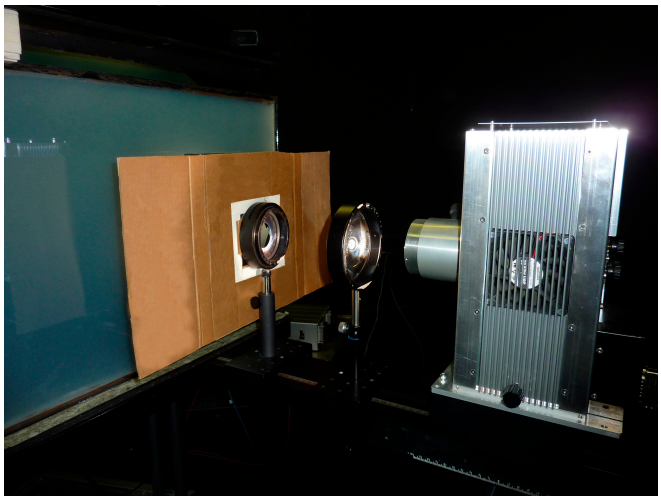

Figure 3. Optical measurements for a glazing unit with aerogel.

The thermal transmittance of the window prototypes was measured according to UNI EN ISO 12567-1 [25]: during the measurements, three thermofluximeters were fixed on the glazing system, in order to evaluate the U-value of the glazing only in steady-state conditions [20].

2.3. Simulations

The energy performance of the innovative glazing systems proposed in the present paper was investigated by EnergyPlus^{TM} software (Version 8.4, U.S. Department of Energy's (DOE), Washington DC, USA) [26–28]. Many simulations with different configurations and settings were performed considering a typical office building built in the 1990s as a reference (Figure 4). The external dimensions are 80 m $\times$ 20 m $\times$ 10 m, and large strip windows (window-to-wall ratio about 50%) are in the East and West walls. The mid-floor of the building was chosen for the study so that just the façades are exposed to the external environment conditions (weather, sun, wind, etc.), whereas the roof and the floor exchange heat with zones at the same temperature. Moreover, the ground temperature has no effect on the performance of the chosen zone. The internal loads (people, lighting, and equipment) were defined as reported in Table 2. The lights are fully dimmable in order to ensure energy savings: artificial light is automatically reduced and switched off when the illuminance level is equal to 500 lux. The heating and cooling system operating periods are set according to the climatic zone, considering an indoor air temperature of 20 °C and 26 °C, respectively. The office occupancy was set from 8:00 to 18:00, five days a week.

The influence of aerogel glazings on building energy performance was evaluated in terms of heating, cooling, and lighting energy demands, taking into account different climatic conditions. The simulations were run for three different cities: Rome (Italy), characterized by hot climate, Paris (France), with a moderate climate, and Ottawa (Canada) with a cold climate (Figure 5).

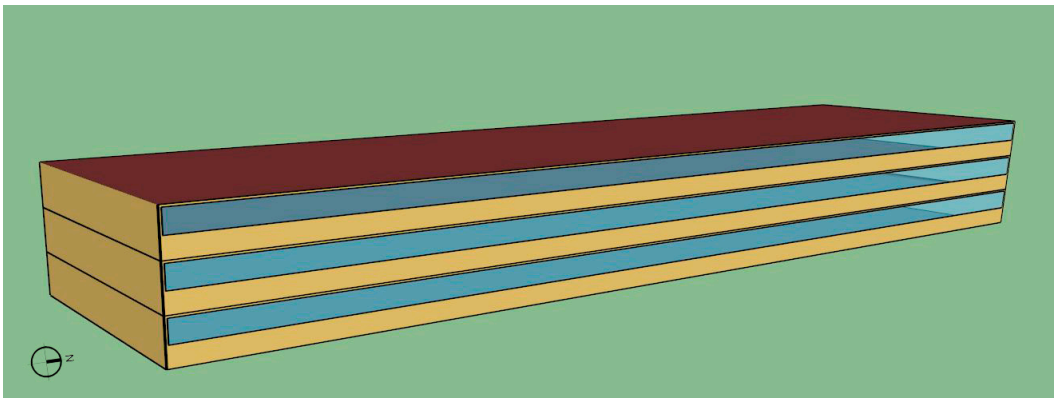

Figure 4. The reference office building for energy simulations.

Table 2. Simulation hypotheses.

Internal Loads	Values	Schedule
Lighting	7 W/m^2 (500 lux, fully dimmable)	8:00–18:00 five days a week
People	0.05 persons/m^2	
Equipment	7 W/m^2	
Operating Periods of Heating and Cooling System and schedule		
City	**Heating (20 °C)**	**Cooling (26 °C)**	**Schedule**
Rome	1 November–15 April	16 April–14 October	7:00–19:00 five days a week
Paris	15 October–30 April	1 May–14 October	
Ottawa	15 October–30 April	1 May–14 October	

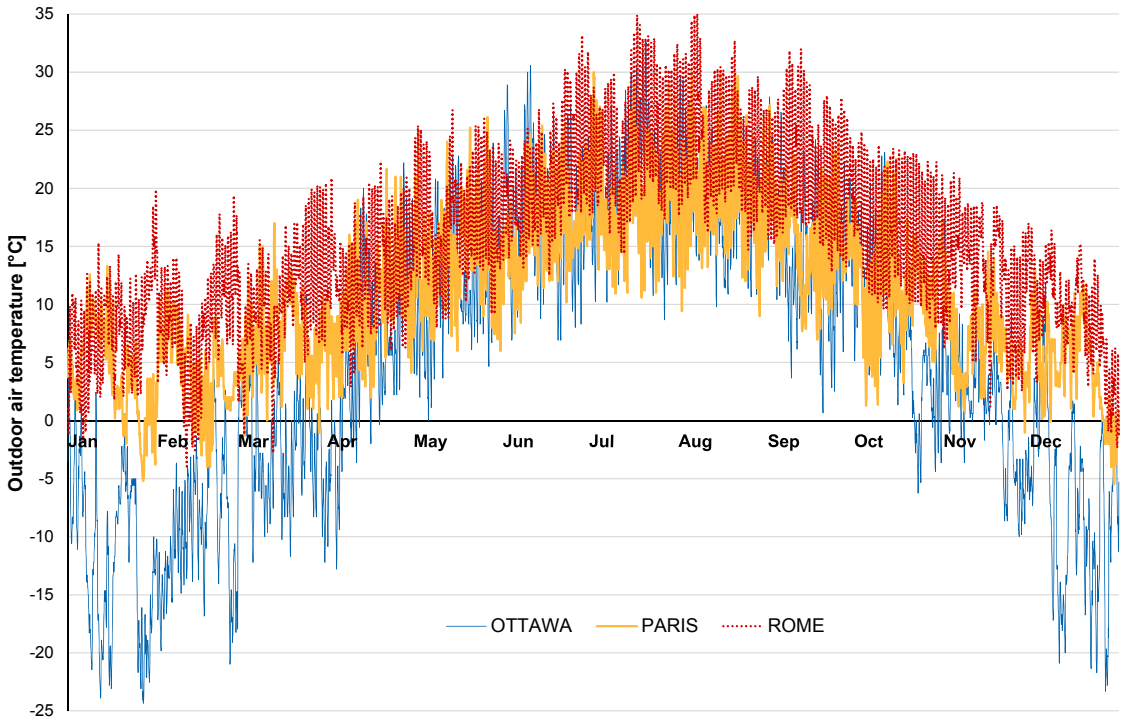

Figure 5. Outdoor air temperature for the investigated cities.

3. Results and Discussion

3.1. Optical and Thermal Performance

The spectral transmittance and reflectance of all the samples are reported in Figures 6 and 7, respectively. By comparing empty and aerogel filled glazings, it is interesting to note a modification of the spectral response shape, especially in the visible range, and typical selective absorption peaks are shown in the spectral transmittance values (at about 1400 nm, 1700 nm, and 1900 nm) [20]. As known, part of the radiation is diffused and scattered when transmitted through the material [19–22,29]. Data about the assembled sample with float glasses and aerogel show a significant impact on the granules: the reduction is more evident in the visible range, whereas the transmittance diminishes by about 0.1 in the IR range. The transmission of the samples LOW-E DGU and LOW-E DGU-AEROGEL in the near infrared range is very low due to solar control and low-e coating, and the influence of aerogel granules is negligible. Moreover, the reduction in the visible range due to the granular aerogel is very low and equal to about 0.1.

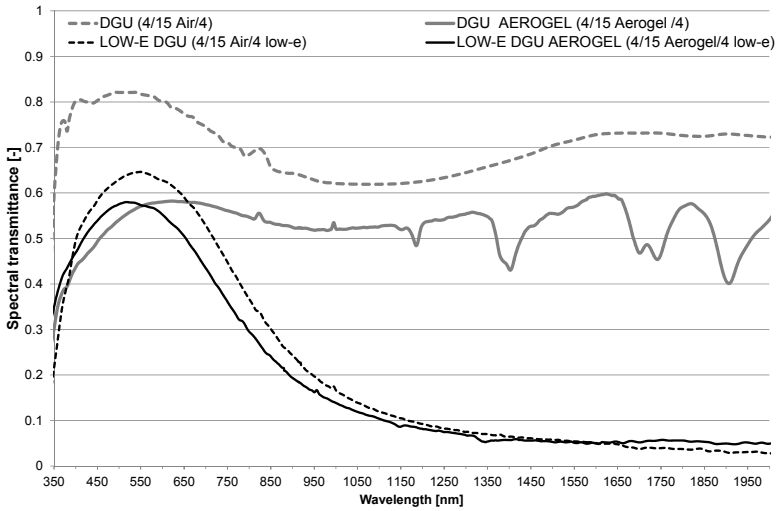

Figure 6. Spectral transmittance at normal incidence.

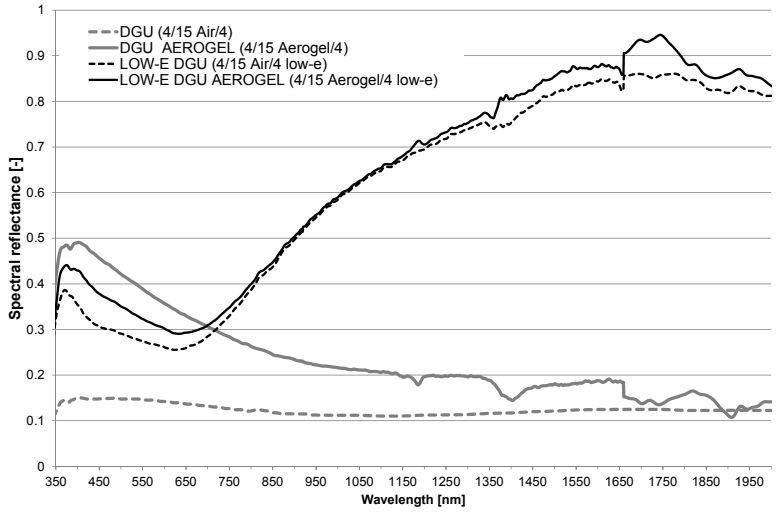

Figure 7. Spectral reflectance at normal incidence.

The aerogel significantly also influences the reflectance spectrum (Figure 7), especially in the visible range, where the values increased up to 0.45–0.5. As expected, the reflectance trend is strictly

linked to the glass layer type: for the samples with solar control and low-e coating, the reflectance is very high in the NIR range, up to about 0.9 at 1750 nm.

In Table 3, the broadband values calculated for transmittance and reflectance in the visible and solar spectrum are reported, according to the standard reference EN 410 [30] and the U-value of the only glazing calculated by data measured with the thermofluximeters [20].

Table 3. Lighting, solar, and thermal performance of the samples.

Acronym	Light Transmittance τ_v	Light Reflectance ρ_v	Direct Solar Transmittance τ_e	Solar Reflectance ρ_e	Total Solar Transmittance g	U–value ($W/m^2 \cdot K$)
DGU	0.82	0.15	0.76	0.14	0.80	2.7
DGU-AEROGEL	0.57	0.38	0.53	0.31	0.57	1.0
LOW-E DGU	0.63	0.27	0.39	0.43	0.41	1.6
LOW-E DGU-AEROGEL	0.57	0.32	0.35	0.46	0.36	1.1

The contribution of the innovative glazing system on thermal properties is remarkable: the thermal transmittance is 1.0–1.1 $W/(m^2 \cdot K)$ for the aerogel glazing systems, in good agreement with literature data [7–9,14,19,31]. The U-value of the glazing depends on the thermal resistivity of each glass layer and on the gas (convective heat transfer) and radiation conductance in the interspace, where the radiation heat transfer is strictly related to the emissivity of the inner side of the glasses: with a low-e coating (the emissivity is about 0.1) and air (or argon) in the interspace, a significant reduction in the radiation conductance can be observed; the U-value of LOW-E DGU is in fact 1.6 $W/(m^2 \cdot K)$ instead of 2.7 $W/(m^2 \cdot K)$. The aerogel in the interspace between the glass layers has a dual impact on thermal conductance: the convective heat transfer within the cavity becomes negligible, as reported in the literature [18,22], and the radiative heat transfer is limited due to the transmittance of the aerogel in the infrared spectral range, which is very low [8], except in the 3500–5000 nm range. For this reason, the low-e coating does not influence the overall heat transfer in the window when aerogel is placed in the interspace between the glass layers (Table 3). Therefore, the thermal conductivity of silica aerogel granules is the main responsible for the glazing U-value, and the particle size has an impact on thermal performance of the glazing, as shown in the literature [14,16,31]. In particular, small granules allow a better performance than the larger ones: for instance, the thermal conductivity varies in the 19–21 mW/mK range at 10 °C, when the average particle size increases [31]. For these reasons, the measured U-value of DGU-AEROGEL is lower than the value of the glazing with the low-e coating and larger granules of aerogel in the interspace.

The reduction of the U-value due to the aerogel in the interspace with respect to DGU and LOW-E DGU samples is about 63% and 31%, respectively. The corresponding reduction in light transmittance (τ_v) is about 30% and 10%, respectively, due to the improved daylighting performance of granules type "B".

Finally, the total solar transmittance or solar factor (g) was estimated using the methodology suggested by the EN 410, based on the thermal properties of the samples and on the spectral reflectance and transmittance of the glazing and of the glass layers [32] (Table 3). For both windows, the presence of granules reduces the solar factor (12–39% reduction) due to the lower transmittance in the NIR range, reaching a value of 0.36 for the glazing with the solar control low-e glass (LOW-E DGU AEROGEL).

3.2. Energy Performance

The influence of aerogel glazings on building energy performance was evaluated in terms of heating, cooling, and lighting energy demands, expressed in kWh/m^2: ideal energy loads were calculated by the software to meet the zone loads, without considering any equipment for heating, ventilation, and air conditioning in the simulations (Figure 8).

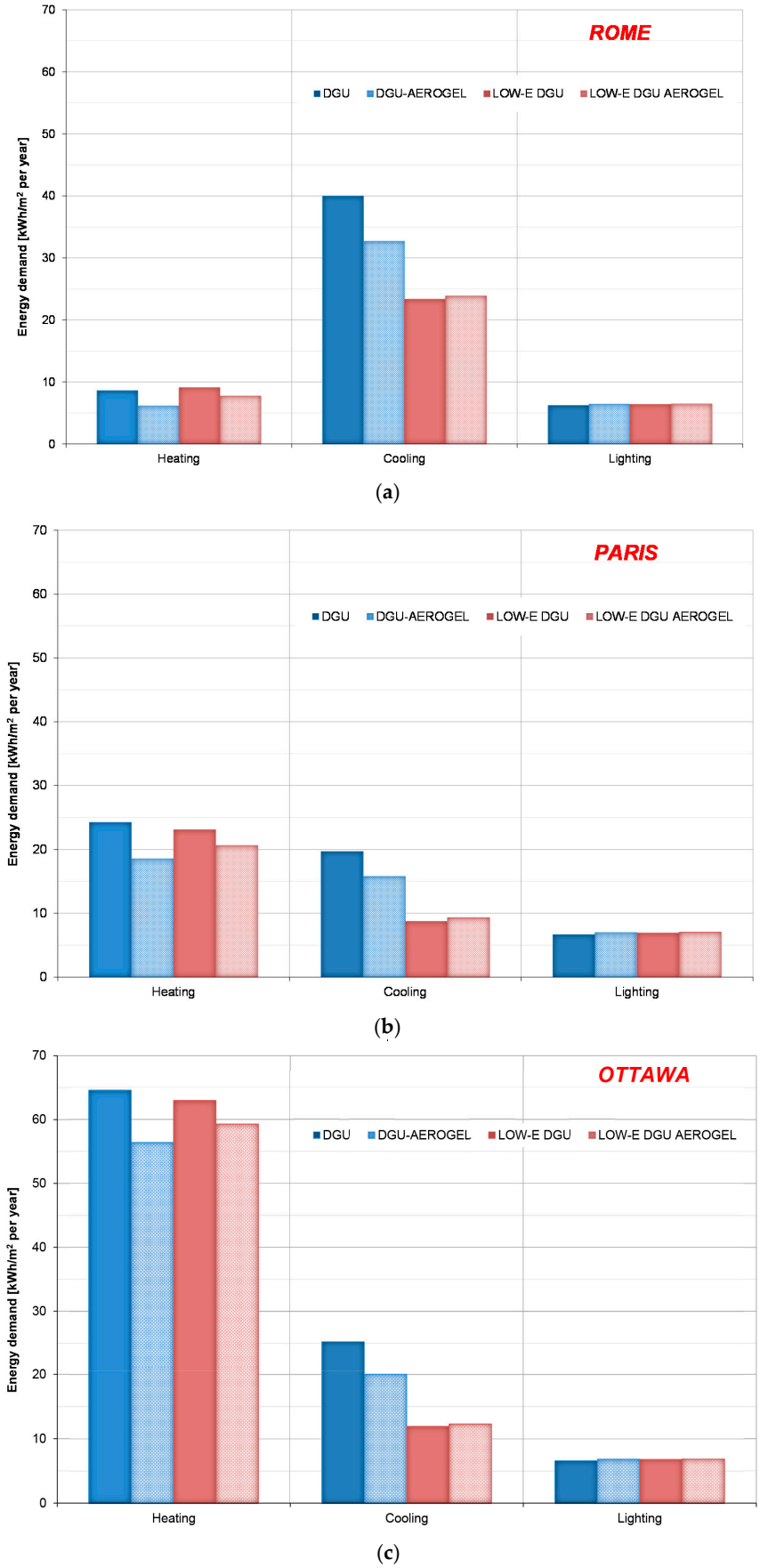

Figure 8. Heating, cooling, and lighting energy demand for the investigated glazings in Rome (**a**); Paris (**b**); and Ottawa (**c**).

Glazings with granular aerogel in interspace (DGU-AEROGEL) result in the most efficient systems for heating in all climate conditions: the reduction in energy demand is 13% for Ottawa, 24% for Paris, and 29% for Rome, when compared to the conventional glazing. The reduction is consistent with U- and g-values of the windows: in Ottawa (Figure 8c), with higher solar radiation, especially in the wintertime, the solar factor reduction diminishes the heat gain from the aerogel window, penalizing the overall result. For the same reasons, glazings with low-e coating have the worst behavior than the other solutions due to the lower g-value.

The annual cooling energy demand for DGU-AEROGEL decreases by a percentage from about 18% (Rome) to 21% (Ottawa) with respect to DGU. As expected, the energy demand for cooling is minimum for the glazing systems with low-e coating (LOW-E DGU and LOW-E DGU AEROGEL), due to the significant reduction in solar factor (i.e., 0.36–0.41): when compared to DGU, the reduction is in a range from 40% (Rome) to 56% (Ottawa). However, when the aerogel window is assembled with low-e glass, the benefits of the translucent material in the interspace are negligible, and the energy demands for cooling are quite similar.

In general, for building refurbishment, granular aerogel glazing systems could be considered a good solution in terms of annual energy demand reduction with respect to conventional double glazings, especially in warm climates. The results are in agreement with literature data [33,34]: Huang and Niu evaluated the influence of translucent aerogel glazing systems on the energy performance in humid subtropical cooling-dominant climates (Hong Kong). With respect to the reference case (conventional double glazing), aerogel glazing systems reduce the total annual space cooling load by around 4%, and the annual cooling load reduction was almost the same as the one achieved by low-e glazing, showing that silica aerogel glazings might be a suitable solution, also in cooling-dominated climates.

Finally, the energy demands for artificial lights are quite similar for all windows: the daylight illuminance on the working plane is higher than the recommended value (500 lux) for a large amount of time during the year, also for glazing systems with aerogel, due to the high window-to-wall ratio for the investigated building, and the increase in energy demand for the aerogel solution is negligible.

4. Conclusions

Different design options for windows have a large impact on the energy efficiency in highly glazed buildings: low thermal transmittance values can be crucial to ensure acceptable heating demand and low energy use; at the same time, the solar transmittance should be thoroughly evaluated, especially in warm climates. Among innovative glazing solutions, windows with granular aerogel in interspace seem to be the most promising, because of very low thermal transmittance, good daylight transmittance, and a remarkable light weight, and some translucent glazing systems are spreading in the market [7,8,18,34].

Two innovative glazing systems with silica granular aerogel in interspace were manufactured and investigated for building refurbishment by means of a thermal and lighting experimental campaign and energy simulations. Two types of granular silica aerogel (15 mm thickness with different particle sizes) and different glass layers (conventional float glass and solar control low-e glass) were considered, and the results were compared in order to evaluate the benefits of using innovative systems with aerogel in place of conventional solutions.

The aerogel impact on thermal properties is remarkable: the thermal transmittance is 1.0–1.1 W/(m^2·K), lower than a glazing with low-e coating and a similar total thickness. With respect to the corresponding conventional windows, a 63% reduction in U-value was achieved for windows with clear float glasses, whereas, when assembled with a low-e glass, the reduction was lower (31%). Optical measurements with a large sphere apparatus allowed for an accurate optical characterization of the samples, which diffuse and scatter the light. When compared to conventional windows with the same external and internal glass layers, a very modest reduction in light transmittance (about 10%) was observed for large granules, whereas the reduction is significant (30%) for the small granules;

however, the τ_v value is suitable for daylighting (it is equal to 0.55). For both windows, the presence of granules reduces the solar factor (12–39% reduction), due to the lower transmittance in the NIR range.

The results of the preliminary energy simulations for this case study showed that the new aerogel glazing systems are a suitable solution for building refurbishment, thanks to low U-values and solar transmittance, also in warm climate conditions. Moreover, they allow for significant daylighting illuminance in buildings, improving visual comfort due to light diffusing, and could have energy demands for lights very similar to those of conventional solutions, especially in buildings with a high window-to-wall surface ratio. In general, translucent systems such as granular aerogel filled systems allow light to propagate uniformly within rooms, thus minimizing daylight problems, such as high contrast zones, and preventing glare, as shown in the literature [14,15,29]. Future studies should focus on the impact of aerogel systems on indoor visual comfort and on energy consumption for artificial lights in buildings.

Acknowledgments: The authors wish to thank Francesco Cristarella Orestano and Elisa Belloni for their valuable help during the experimental campaign and Francesca Merli for her precious collaboration during data elaboration.

Author Contributions: The work presented in this paper is a collaborative development by all of the authors.

Conflicts of Interest: The authors declare no conflict of interest.

References

1. Jelle, B.P.; Hynd, A.; Gustavsen, A.; Arasteh, D.; Goudey, H.; Hart, R. Fenestration of today and tomorrow: A state-of-the-art review and future research opportunities. *Sol. Energy Mater. Sol. Cell* **2012**, *96*, 1–28. [CrossRef]
2. Ihara, T.; Gustavsen, A.; Jelle, B.P. Effect of facade components on energy efficiency in office buildings. *Appl. Energy* **2015**, *158*, 422–432. [CrossRef]
3. Mohammadpourkarbasi, H.; Sharples, S. The Eco-Refurbishment of a 19th Century Terraced House: Energy and Cost Performance for Current and Future UK Climates. *Buildings* **2013**, *3*, 220–244. [CrossRef]
4. Koebel, M.; Rigacci, A.; Achard, P. Aerogel-based thermal superinsulation: An overview. *J. Sol-Gel Sci. Technol.* **2012**, *63*, 315–339. [CrossRef]
5. Cuce, E.; Cuce, P.M.; Wood, C.J.; Riffat, S.B. Toward aerogel based thermal superinsulation in buildings: A comprehensive review. *Renew. Sustain. Energy Rev.* **2014**, *34*, 273–299. [CrossRef]
6. Baetens, R.; Jelle, B.P.; Gustavsen, A. Aerogel insulation for building applications: A state-of-the-art review. *Energy Build.* **2011**, *43*, 761–769. [CrossRef]
7. Buratti, C.; Moretti, E. Silica nanogel for energy-efficient windows. In *Nanotechnology in Eco-Efficient Construction*; Pacheco Torgal, F., Diamanti, M.V., Nazari, A., Granqvist, C.G., Eds.; Woodhead Publishing Limited: Cambridge, UK, 2013; pp. 207–235.
8. Buratti, C.; Moretti, E. Nanogel windows. In *Nearly Zero Energy Building Refurbishment*; Pacheco Torgal, F., Mistretta, M., Kaklauskas, A., Granqvist, C.G., Cabeza, L.F., Eds.; Springer: Londra, UK, 2013; pp. 555–582.
9. Cotana, F.; Pisello, A.L.; Moretti, E.; Buratti, C. Multipurpose characterization of glazing systems with silica aerogel: In-field experimental analysis of thermal-energy, lighting and acoustic performance. *Build. Environ.* **2014**, *81*, 92–102. [CrossRef]
10. Buratti, C.; Moretti, E.; Belloni, E.; Agosti, F. Development of innovative aerogel based plasters: Preliminary thermal and acoustic performance evaluation. *Sustainability* **2014**, *6*, 5839–5852. [CrossRef]
11. Buratti, C.; Moretti, E.; Belloni, E. Aerogel plasters for energy building efficiency. In *Nano and Biotech Based Materials for Energy Building Efficiency*; Pacheco Torgal, F., Buratti, C., Kalaiselvam, S., Granqvist, C.G., Ivanov, V., Eds.; Springer International Publishing AG: Basel, Switzerland, 2016; pp. 17–40.
12. Berardi, U. The development of a monolithic aerogel glazed window for an energy retrofitting project. *Appl. Energy* **2015**, *154*, 603–615. [CrossRef]
13. Bhuiya, M.M.H.; Anderson, A.M.; Carroll, M.K.; Bruno, B.A.; Ventrella, J.L.; Silberman, B.; Keramati, B. Preparation of Monolithic Silica Aerogel for Fenestration Applications: Scaling up, Reducing Cycle Time, and Improving Performance. *Ind. Eng. Chem. Res.* **2016**, *55*, 6971–6981. [CrossRef]
14. Ihara, T.; Gao, T.; Grynning, S.; Jelle, B.P.; Gustavsen, A. Aerogel granulate glazing facades and their application potential from an energy saving perspective. *Appl. Energy* **2015**, *142*, 179–191. [CrossRef]

15. Gao, T.; Ihara, T.; Grynning, S.; Jelle, B.P.; Gunnarshaug Lien, A. Perspective of aerogel glazings in energy efficient buildings. *Build. Environ.* **2016**, *95*, 405–413. [CrossRef]
16. Gao, T.; Jelle, B.P.; Ihara, T.; Gustavsen, A. Insulating glazing units with silica aerogel granules: The impact of particle size. *Appl. Energy* **2014**, *128*, 27–34. [CrossRef]
17. Garnier, C.; Muneer, T.; McCauley, L. Super insulated aerogel windows: Impact on daylighting and thermal performance. *Build. Environ.* **2015**, *94*, 231–238. [CrossRef]
18. Moretti, E.; Zinzi, M.; Carnielo, E.; Merli, F. Advanced polycarbonate transparent systems with aerogel: Preliminary characterization of optical and thermal properties. *Energy Procedia* **2016**, in press.
19. Buratti, C.; Moretti, E. Lighting and energetic characteristics of transparent insulating materials: Experimental data and calculation. *Indoor Built Environ.* **2011**, *20*, 400–411. [CrossRef]
20. Buratti, C.; Moretti, E. Experimental performance evaluation of aerogel glazing systems. *Appl. Energy* **2012**, *97*, 430–437. [CrossRef]
21. Buratti, C.; Moretti, E. Glazing systems with silica aerogel for energy savings in buildings. *Appl. Energy* **2012**, *98*, 396–403. [CrossRef]
22. Ihara, T.; Grynning, S.; Gao, T.; Gustavsen, A.; Jelle, B.P. Impact of convection on thermal performance of aerogel granulate glazing systems. *Energy Build.* **2015**, *88*, 165–173. [CrossRef]
23. Moretti, E.; Zinzi, M.; Belloni, E. Polycarbonate panels for buildings: Experimental investigation of thermal and optical performance. *Energy Build.* **2014**, *70*, 23–35. [CrossRef]
24. Maccari, A.; Montecchi, M.; Treppo, F.; Zinzi, M. CATRAM: An apparatus for the optical characterization of advanced transparent materials. *Appl. Opt.* **1998**, *37*, 5156–5161. [CrossRef] [PubMed]
25. CEN. EN 12567-1. *Thermal Performance of Windows and Doors. Determination of Thermal Transmittance by the Hot-Box Method. Complete Windows and Doors*; International Organization for Standardization (ISO): Geneva, Switzerland, 2010.
26. Moretti, E.; Belloni, E. Evaluation of energy, thermal, and daylighting performance of solar control films for a case study in moderate climate. *Build. Environ.* **2015**, *94*, 183–195. [CrossRef]
27. Buratti, C.; Moretti, E.; Belloni, E.; Cotana, F. Unsteady simulation of energy performance and thermal comfort in non-residential buildings. *Build. Environ.* **2013**, *59*, 482–491. [CrossRef]
28. Mujeebu, M.A.; Ashraf, N.; Alsuwayigh, A. Energy performance and economic viability of nano aerogel glazing and nano vacuum insulation panel in multi-story office building. *Energy* **2016**, *113*, 949–956. [CrossRef]
29. Huang, Y.; Niu, J. Energy and visual performance of the silica aerogel glazing system in commercial buildings of Hong Kong. *Constr. Build. Mater.* **2015**, *94*, 57–72. [CrossRef]
30. EN 410. *Glass in Building—Determination of Luminous and Solar Characteristics of Glazing*; Europeen Committte for standardization (CEN): Brussels, Belgium, 2011.
31. Moretti, E.; Merli, F.; Cuce, E.; Buratti, C. Thermal and acoustic properties of aerogels: Preliminary investigation of the influence of granule size. *Energy Procedia* **2016**, in press.
32. AGC Glass Europe. Available online: http://www.yourglass.com/configurator/tp/it/toolbox/configurator/main.html (accessed on 9 November 2016).
33. Huang, Y.; Niu, J. Application of super-insulating translucent silica aerogel glazing system on commercial building envelope of humid subtropical climates: Impact on space cooling load. *Energy* **2015**, *83*, 316–325. [CrossRef]
34. Buratti, C.; Moretti, E.; Belloni, E. Nanogel windows for energy building efficiency. In *Nano and Biotech Based Materials for Energy Building Efficiency*; Pacheco Torgal, F., Buratti, C., Kalaiselvam, S., Granqvist, C.G., Ivanov, V., Eds.; Springer International Publishing AG: Basel, Switzerland, 2016; pp. 41–69.

© 2017 by the authors; licensee MDPI, Basel, Switzerland. This article is an open access article distributed under the terms and conditions of the Creative Commons Attribution (CC-BY) license (http://creativecommons.org/licenses/by/4.0/).

Available online at www.sciencedirect.com

ScienceDirect

Energy Procedia 105 (2017) 2107 – 2112

Energy Procedia

The 8th International Conference on Applied Energy – ICAE2016

Low order grey-box models for short-term thermal behavior prediction in buildings

Alessandro Fonti[a], Gabriele Comodi[a,*], Stefano Pizzuti[b], Alessia Arteconi[c], Lieve Helsen[d]

[a]*Università Politecnica delle Marche, via Brecce Bianche 1, Ancona, 60131, Italy*
[b]*ENEA, via Anguillarese 301, Rome, 00123, Italy*
[c]*Università eCampus, via Isimbardi 10, Novendrate (CO), 22060, Italy*
[d]*KU Leuven, Celestijnenlaan 300 - bus 2421, Leuven, 3001, Belgium*

Abstract

Low order grey-box models are suitable to be used in predictive controls. In real buildings in which the measured quantities are few the reliability of these models is crucial for the control performance. In this paper an identification procedure is analyzed to investigate the accuracy of different order grey-box models for short-term thermal behavior prediction in a real building, part of a living smart district. The building has a low number of zones and a single indoor temperature measuring point. The models are identified on the data acquired in 31 days during the winter 2015. The second order model shows the best performance with a root-mean-square error (RMSE) less than 0.5°C for a prediction horizon of 1-hour and a RMSE less than 1°C for a prediction horizon of 3-hours.

© 2017 The Authors. Published by Elsevier Ltd. This is an open access article under the CC BY-NC-ND license (http://creativecommons.org/licenses/by-nc-nd/4.0/).
Peer-review under responsibility of the scientific committee of the 8th International Conference on Applied Energy.

Keywords: Grey-box modeling; Reduced order models; Building energy modeling

1. Introduction

Model Predictive Control (MPC) has shown good results for achieving higher energy efficiency in buildings [1]. Such control strategy necessarily needs thermal building models [1] and the reliability of these models is crucial for the control performance [2]. Reduced order grey-box models are particularly suitable in predictive control as they combine building physics and model structure knowledge typical of the white-box approach with the parameter estimation through measured data of a black-box approach [3].

In this work an identification procedure is performed to investigate the accuracy of low order models for short-term thermal behavior prediction in a real building with a low number of zones and a single indoor temperature measuring point. The lumped element models analyzed are derived directly from Reynders et

* Corresponding author. Tel.: +39-071-220-4761; fax: +39-071-220-4770.
E-mail address: g.comodi@univpm.it.

1876-6102 © 2017 The Authors. Published by Elsevier Ltd. This is an open access article under the CC BY-NC-ND license (http://creativecommons.org/licenses/by-nc-nd/4.0/).
Peer-review under responsibility of the scientific committee of the 8th International Conference on Applied Energy.
doi:10.1016/j.egypro.2017.03.592

al. [4], that proposed different reduced-order models, identified on simulation data obtained using Modelica IDEAS library [5]. Parameters of different order models are here identified using Matlab through measures of: indoor and outdoor air temperature, thermal and electrical load power and global horizontal irradiance. Indeed, the main contribution of the present study is the use in the identification process of data acquired in a real and living building rather than simulated data, as often done in literature. This helps to highlight practical issues, otherwise neglected, arising from the identification process in real applications.

2. Methods

A smart building that belongs to a living smart district has been considered as case study. Data obtained from sensors installed in the building are used to train and validate three grey-box models of increasing order. Different identification parameters have been analyzed to select the model that shows the best performance.

2.1. The Smart Village and the F70 building

The *Smart Village* is a small smart district located within the ENEA Research Centre in Rome and comprises 8 single floor buildings (progressively numbered F66÷F73) together with the thermal plant (F85). The buildings are intended for office use and are connected each other and to the common thermal plant by a heating-cooling thermal network.

Fig.1a presents an overview of the Smart Village. For every building there is a remotely controlled three-port valve which allows to control the thermal fluid flow rate. The thermal plant outlet temperature and flow rate are fixed. Each office in the building is heated by a fancoil equipped with a hysteresis thermostat and there are no fancoils in the corridors. For every building measures of corridor temperature, global thermal power, difference between inlet and outlet supply water temperature, active and reactive electric power are available.

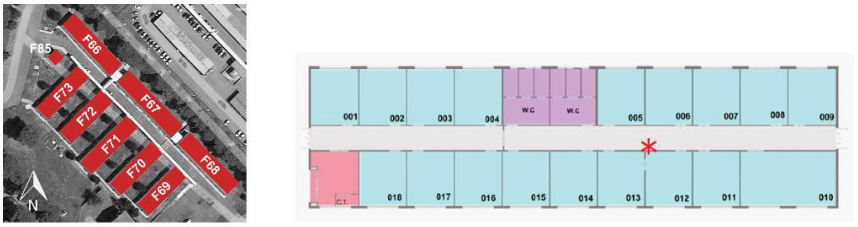

(a) (b)

Fig.1. The Smart Village (a) and the F70 plan (b). The F70 has a floor area of 363 m^2.

The identification process carried out in this study focuses on the building F70. Fig.1b shows the F70 plan and the red asterisk indicates the position of the only temperature measuring point in the corridor. It has been assumed as hypothesis that the temperature detected along the corridor is closely related to the temperatures of the adjacent zones. This aspect will be further analyzed in the following sections.

2.2. Lumped element models

Resistance–capacitance (RC) lumped element models for representing the building are here analyzed. Fig. 2 shows the three considered models and reports the parameters and the input-output quantities. It reports also the equations of the 2nd order model which is the best identified model as shown in the results.

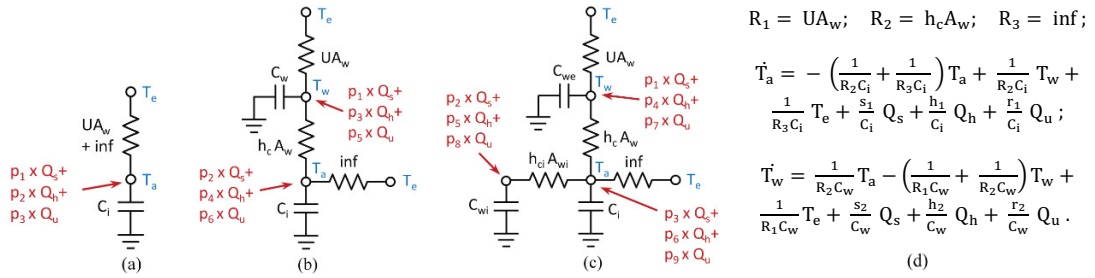

Fig. 2. Low order RC building models: (a) first order, (b) second order, (c) third order. Second order model equations (d).

In the first order model (Fig. 2a) the entire thermal mass of the building is lumped to a single capacity and no distinction has been made between the structural mass and the indoor air mass. The 2nd order model (Fig. 2b) takes into account this difference by including a second capacity. The 3rd order model (Fig. 2c) instead, has 3 different capacities for the envelope (C_{we}), the internal walls (C_{wi}) and the indoor air (C_i) [4].

For these models the inputs are: the outdoor air temperature (T_e), solar gains (Q_s), internal gains (Q_u) and heating gains (Q_h). The observation variable is the indoor air temperature (T_a). The indoor air temperature is obtained by the sensor installed in the corridor, the heating gains are measured through the thermal power meter and the outdoor temperature measures are retrieved by the weather station. As proposed in Reynders et. al. [4], the building electrical power is used as an alternative input for the effective user gains and the global horizontal irradiance from the weather station is used as an alternative to the effective solar gains which are difficult to obtain. For all model orders the solar gains, internal gains and heating gains are distributed over the capacities. The distribution coefficients are assumed to be constant and are identified as part of the parameter identification process.

The models in Fig. 2 are parametrized and so can be treated as grey-box models. A grey-box model consists of a set of continuous stochastic differential equations formulated in a state space form together with an output equation as follow [4,6] :

$$dX(t) = A(\theta)X(t) + B(\theta)U(t) + \sigma(\theta)d\omega \quad (1)$$

$$Y(t) = C(\theta)X(t) + D(\theta)U(t) + \varepsilon \quad (2)$$

$X(t)$ is the state vector of the dynamic system. $U(t)$ is a vector containing the measured inputs of the system and ω is a Wiener process. The measured output of the system $Y(t)$ is given as a function of the states $X(t)$ and the inputs $U(t)$. ε is the measurement error. The parameters θ are estimated using Matlab.

2.3. Identification process and data

The data used for the system identification process are retrieved from the Smart Village centralized database. Such database collects the sensor measurements coming from all the cluster buildings and the thermal plant with a fixed sample time of 900s. Measured data have been available since September 2014. Useful data for the identification are selected considering periods in which there were no data outliers and no missing data. From such selection two useful datasets are obtained: *Train-set* from 19 January 2015 to 7 February 2015 (20 days) and *Test-set* from 8 January 2015 to 18 January 2015 (11 days). Train-set has been used as training dataset while Test-set has been used as validation and test dataset in order to validate the identified models and to investigate a possible model overfitting.

The parameter identification procedure has been conducted using the *greyest* function in Matlab. This function leads to the maximum likelihood estimates and uses three different algorithms as search method

for the iterative parameter estimation: the Gauss-Newton direction, the Levenberg-Marquardt and the steepest descent gradient search method. At each iteration *greyest* chooses the search method to obtain the highest reduction in error.

After identification, the models have been validated and tested by the following parameters:

- the root-mean-square errors (RMSE-values) at 1 step;
- the RMSE-values 1 hour-ahead and 3 hours-ahead;
- the final prediction errors (FPE);
- the level of fit (FIT);
- the auto-correlation of the residuals.

The 1-step prediction errors correspond to the residuals obtained by the method that is used to estimate the parameters and thus indicate the goodness of fit. In addition, the RMSE-values for 1-hour and 3-hours ahead predictions on the Train-set and Test-set are useful to evaluate possible model overfitting and to quantify the uncertainty that can be expected in MPC applications. The FPE-values are Akaike's final prediction errors and measure model quality as well. According to Akaike's theory, the most accurate model has the smallest FPE [7]. FIT-values are the percent normalized root mean square errors and thus these summarize in percentage the model goodness of fit (similarly to RMSE). Finally, the level of the auto-correlation in the residuals shows if the model explains well the dynamics contained in the dataset and if some dynamics of the real process cannot be taken into account by the low order analyzed model.

3. Results

In this section the results of the system identification process are discussed. Table 1 presents the identification parameters values calculated on both training and test datasets and for each model order.
The minimum value of the RMSE for the 1-step prediction on Train-set is obtained in the second and third order models. Thus increasing the model complexity beyond the second order does not produce a significant improvement in accuracy. Also analyzing the values of the same parameter calculated on the Test-set, the minimum value is reached with the second order model. Therefore the RMSE behavior indicates clearly overfitting for the third order model. Overfitting is also confirmed by the values of the FPE parameter which reaches the minimum for each dataset in the second order model. The second order model is therefore the best choice in terms of accuracy and complexity, although it can be noticed that even the simple first order model presents an accuracy not so much lower.

Table 1. Identification parameters calculated on both training and test datasets and for each model order. The values highlighted are the best values obtained. The second order model shows the best performance.

Dataset	Training Dataset			Test Dataset		
Model Order	First	Second	Third	First	Second	Third
RMSE 1 step (°C)	0.154	0.148	0.148	0.137	0.136	0.148
RMSE 1 hour (°C)	0.491	0.442	0.468	0.417	0.417	0.418
RMSE 3 hours (°C)	1.116	0.896	1.132	0.905	0.885	0.932
FPE (10^3)	23.92	22.33	22.47	-	-	-
FIT 1 step (%)	94.24	94.46	94.46	94.31	94.38	94.37

In the following, the second order model prediction capabilities are analyzed. Fig. 3 presents a comparison between the measured indoor temperature and the same quantity predicted by the model with a prediction horizon of 1-hour (a) and 3-hours (b) on the Test-set.

The model performance is good for the 1-hour ahead prediction with a RMSE less than 0.5°C for both the datasets and pretty good in case of longer horizon with a RMSE close to 1°C. FIT-values are also

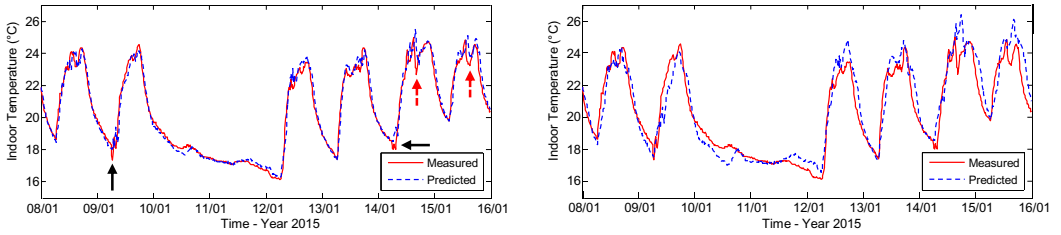

(a) (b)

Fig. 3. Measured (red solid line) and predicted (blue dotted line) indoor temperature profiles by the identified second order model on a part of the Test-set. 1-hour ahead prediction (a); 3-hour ahead prediction (b).

adequate since they are higher than 94% in all cases. The worst correspondence occurs during the weekends, when the thermal power is zero, and during working hours when there are temperature peaks.

Looking at Table 1, it is possible to observe a slightly better performance of all the models on the Test-set rather than on the Train-set. In a grey-box model this can happen when there are behaviors of the real process or approximations in the measurement system not taken into account in the model.

In the present identification process different reasons causing such effect can be recognized:

- Not predicted windows and doors opened manually by users (bad-behaviors)
- Sample time too wide for the thermal power measures
- Single point of temperature measurement may not be sufficiently representative of the adjacent zones temperatures.

In Fig. 3 indoor temperature rapid changes are indicated through black (solid) arrows and red (dotted) arrows. The rapid changes indicated by the black arrows occur at the early morning and are due to windows and doors opening by the cleaning service. The ones indicated through red arrows are due to the same bad-behavior by users. The sample time of 900s for the thermal power may be too wide in a building equipped with fancoils. Indeed, if fancoil switching times are too fast, related measures may be affected by a major aliasing. In this case part of the thermal power dynamic is lost and this cannot be taken into account by the identified models. Moreover, a single measuring point in the corridor for the indoor temperature may not be sufficient to describe the offices thermal behavior. Further proper measures would be needed to verify if this assumption was adequate for the performed analysis. However, the lack of a wide set of sensors in real applications can frequently occur and it represents a typical practical issue to be faced during process identification in reality. Finally, Fig. 4 shows the auto-correlation of residuals for all order models calculated with a lag of 25. Dotted lines indicate a 99% limit of confidence. The autocorrelation levels in the second and third order models are closer to the confidence limit, meaning that these models describe better the building dynamics in the dataset. The autocorrelation plots for the second and third order models are pretty good. The points out of the confidence limits in these cases are related to the behaviors not represented by the models, as discussed above.

4. Conclusion and future work

In this work three lumped element grey-box models of first, second and third order have been identified and validated on measured data coming from a living building, part of a smart district. The identification process of the unknown parameters has been conducted through Matlab. The analyzed error indices point out the best accuracy of the second order model. The RMSE values are less than 0.5°C for 1-hour prediction and close to 1°C for 3-hour prediction. The second order model can be used therefore in MPC applications in which it is sufficient to have a so short-term predictive horizon and accuracy. The residual autocorrelation analysis shows that the second order model describes pretty well the building dynamics but underlines also

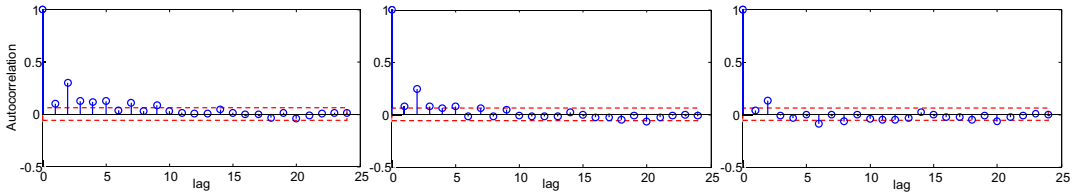

Fig. 4. Residual autocorrelation with a lag of 25 on the Train-set. (a) First order, (b) Second order, (a) Third order model.

that there are behaviors and approximations that the model cannot take into account. User bad-behaviors, measured signal aliasing and low correlation between the measured temperature and the temperatures of the represented thermal zones can make the identification difficult and even give a poor result in terms of accuracy. In order to obtain longer prediction horizon (i.e. 1-day ahead) with a good accuracy, future works will be targeted to deeply analyze and describe these sources of error. In particular, 1) it shall be evaluated the possibility of introducing new measuring points and utilize the average of these values as a reference temperature; 2) the measure sample time shall be reduced properly; 3) user bad-behaviors should be modelled and predicted. Finally the application of the studied grey-box model in an real MPC is foreseen.

Acknowledgements

The data used in this study were kindly provided by the Italian National Agency for New Technologies, Energy and Sustainable Economic Development, Casaccia Research Centre, Rome.

References

[1] Maasoumy M, Razmara M, Shahbakhti M, and Vincentelli AS. Handling model uncertainty in model predictive control for energy efficient buildings. *Energy Build* 2014;**77**:377–92.

[2] Prívara S, Cigler J, Váňa Z, Oldewurtel F, Sagerschnig C, Žáčeková E. Building modeling as a crucial part for building predictive control. *Energy Build* 2013;**56**:8–22.

[3] De Coninck R, Magnusson F, Åkesson J, and Helsen L. Toolbox for development and validation of grey-box building models for forecasting and control. *J. Build. Perform. Simul.* 2015;**July**:1–16.

[4] Reynders G, Diriken J, Saelens D. Quality of grey-box models and identified parameters as function of the accuracy of input and observation signals. *Energy Build* 2014;**82**:263–74

[5] De Coninck R, Magnusson F, Åkesson J, Helsen L. Grey-Box Building Models for Model Order Reduction and Control. *10th Int Model Conf* 2014;657–66.

[6] Madsen H. *Time Series Analysis*. Boca Raton (Florida): Chapman & Hall/CRC; 2007.

[7] Keesman KJ. *System Identification*. 1st ed. London: Springer-Verlag; 2011.

Biography

Alessandro Fonti received the M.S. degree in electronic and automation engineering in 2010 and the Ph.D. degree in industrial engineering in 2016 from Università Politecnica delle Marche, Italy. Currently, he is a postdoctoral research fellow in the department of industrial engineering and mathematical sciences at Università Politecnica delle Marche.

INTERNATIONAL JOURNAL OF HEAT AND TECHNOLOGY

ISSN: 0392-8764
Vol. 34, No. 3, September 2016, pp. 491-497
DOI: 10.18280/ijht.340320
Licensed under CC BY-NC 4.0
A publication of IIETA
http://www.iieta.org/Journals/IJHT

A Methodology for the Generation of Energy Consumption Profiles in the Residential Sector

Giovanni Puglisi [1*], Fabio Zanghirella [1], Paola Ungaro [2] and Giuliano Cammarata [3]

[*1] ENEA (Italian National Agency for New Technologies, Energy and Sustainable Economic Development), via Anguillarese 301, 00123 Roma, Italy
[2] ISTAT (Italian National Institute of Statistics), Viale Oceano Pacifico 171, 00144, Roma, Italy
[3] Università degli Studi di Catania, p.zza Università, 2, 95125 Catania, Italy

Email: giovanni.puglisi@enea.it

ABSTRACT

The residential sector has been achieved in the last years more and more importance in the total energy consumption scenario by stimulating the research for solutions to promote energy efficiency and to raise awareness on energy consumption by end user.
The profile of an end-users energy consumption assumes a central role in finding solutions to reduce energy demand and increase the efficiency in the production of the same energy.
European regulations impose an obligation on Member States to provide annually data on energy consumption of households for end use and energy product. Data will be provided for Italy basing on data collected by ISTAT Survey on energy consumption in the residential sector, appropriately processed by ENEA and ISTAT.
In this paper it is presented a methodology that allowed to define a series of dwelling types, representative of the entire national sample, as a function of building, family and environmental characteristics. These dwellings, through the application of a dynamic simulation model, allowed the generation of monthly energy consumption profiles (for heating, cooling and domestic heat water) for each cluster of dwelling types and the evaluation of the energy consumption distribution of the residential sector for end use and energy product.

Keywords: Energy consumption, Residential sector, Dwelling types, Energy efficiency, Energy demand.

1. INTRODUCTION

The European and national policies, aimed at containing the energy product consumption and at promoting the diffusion of renewable sources, have stimulated the search for ways to reduce the energy demand and to boost the efficiency in energy production. In particular, for the residential sector, the knowledge of the consumption habits of the families is of vital importance for achieving the goals set by the various European directives, as well as for raising awareness on energy consumption and for stimulating rational behaviors on energy use by end-users.

The regulation (EC) No 1099/2008 of the European Parliament and of the Council of 22 October 2008 on energy statistics, and the amending Commission Regulation (EU) No 431/2014 of 24 April 2014 on energy statistics, as regards the implementation of annual statistics on energy consumption in households, impose an obligation on Member States to provide annual data on energy consumption of households for final destination and energy source. In this framework, ISTAT in collaboration with ENEA and MiSE (Italian Ministry of Economic Development) carried out the survey on households energy consumption [1, 2], as part of the Italian National Statistics Plan. The survey was conducted in 2013 for the first time in Italy, on a representative sample of 20,000 households at regional level and made it possible to obtain information on characteristics, consumption habits, types of plant and energy costs of Italian households, specified by energy product (primary energy sources and energy carriers) and end-use (heating, cooling, domestic hot water, cooking, lighting and electrical equipment).

This paper describes the methodology used to estimate the energy consumption for heating and the creation of monthly load profiles for residential dwellings. For the sake of simplicity we have chosen to present the results for the Veneto Region and heating systems fueled by natural gas; the calculation method remains the same for other energy products and for the entire Italian national territory.

Furthermore, this methodology will be used in the activity ENEA-ISTAT to estimate the energy consumption of households for the years between two replications of the ISTAT survey, starting from the ISTAT 2016 survey that will be used to deliver the first data to Eurostat.

2. METHODOLOGY

The presented methodology is based on the processing of the provided statistical data from the ISTAT 2013 survey on households energy consumption, and on the identification of dwelling-type classes representative of the entire Italian residential building stock.

The information provided by the ISTAT 2013 survey and used for the methodology are mainly:

- dwelling characteristics (type of dwelling, year of build, floor surface, opaque envelope type, transparent envelope type, main exposure of the external walls);
- characteristics of heating, cooling and DHW systems (number, energy products, systems type –centralized, individual or single device-, emission and temperature control system, frequency of use and daily hours of use);
- frequency of use of the systems;
- energy cost by energy product.

The classification of the dwellings was chosen as a function of:

- period of build: before 1950, 1950-1969, 1970-1989, from 1990;
- type of dwelling: single family house, multi-family house, ground floor apartment, middle floor apartment and top floor apartment.

Table 1 summarizes the 20 identified dwelling-type classes (DTC).

Table 1. Dwelling-type classes

	Before 1950	1950-1969	1970-1989	From 1990
Single fam. House	DTC1	DTC6	DTC11	DTC16
Multi-fam. House	DTC2	DTC7	DTC12	DTC17
Ground fl. apt.	DTC3	DTC8	DTC13	DTC18
Middle fl. apt.	DTC4	DTC9	DTC14	DTC19
Top fl. apt.	DTC5	DTC10	DTC15	DTC20

The evaluation of the energy product consumption for heating has been carried out in different stages, as exemplified in Figure 1:

a. determination of the thermal energy demand, in continuous heating mode, of the dwelling-type [kWhy] by means of a dynamic simulation software; the simulations were performed assuming a continuous heating mode (heating system on 24 hours a day), because the survey answers do not allow to determine an hourly power profile; the simulation results also provide the time profile of the heating demand of each dwelling-type;
b. calculation of the reduction factor for intermittent heating as a function of the average number of daily hours during which the heating system is switched on, based on the answers of the survey;
c. assumption of the efficiency of the different types of plant for each dwelling-type, and estimation of the heating consumptions per floor area [kWh/m^{2}y];
d. estimation of the total annual energy product consumption for heating for each class (m^3, kg, l, etc.) for a certain energy product, obtained by multiplying the consumption per area by the total area of the dwellings, that use that specific energy product for heating, that fall in each dwelling-type class.

The decision to estimate the thermal energy demand for all the dwelling-types by means of a dynamic simulation of the dwelling, and then calculate the energy product consumption by multiplying the heating demand calculated in continuous mode by the reduction factor for intermittent heating and by the average total efficiency of the heating system was related to the information provided by survey about the type and the characteristics of the heating systems. Clearly, the information provided by the survey can not have a level of detail sufficient to estimate a management profile of the heating systems, which is instead essential to perform a dynamic simulation of the building-plant system.

Since the energy performances of buildings are strongly influenced by climatic conditions, the same dwelling-type was simulated in each climate zone. For each climatic zone in which the country is divided, the input weather data (temperature, radiation and humidity) adopted for the simulations were those of the chief town whose degree days are "barycentric" with respect to the degree days interval of the climatic zone.

3. DEFINITION OF THE DWELLING-TYPE CLASSES

Each dwelling-type class is characterized by thermo-physical and dimensional parameters, determined on the basis of both the information gathered from the ISTAT survey results, appropriately processed, and the input data required by the simulation model. Below, the main properties that define each dwelling-type class, are listed and described.

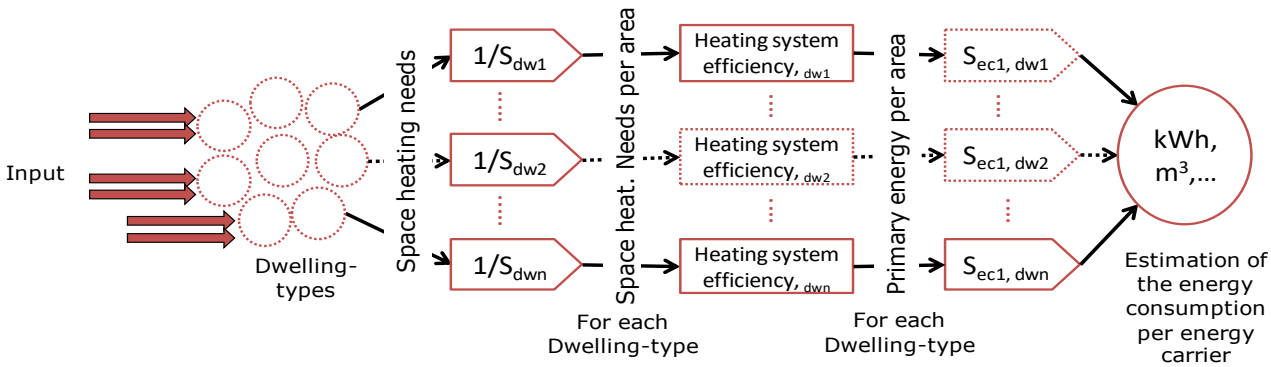

Figure 1. Methodology scheme, for space heating and for a single energy product

- Thermal transmittance of the opaque envelope: for each period of build a specific structure was deduced for the exterior walls, the floor and the ceiling. The corresponding thermal transmittance was determined, using data from the Italian standard UNI/TR 11552:2014. Table 2 summarizes the adopted values.

Table 2. Thermal transmittance of the opaque envelope by period of build [kW/m^{2}K]

	Before 1950	1950-1969	1970-1989	From 1990
Walls	1.093	1.065	0.675	0.456
Floor	0.781	0.781	0.850	0.442
Roof	1.376	1.376	0.777	0.441

- Thermal transmittance of the transparent envelope: the survey provided as possible answers two types of glass (single, double) and three types of frame (wood, metal, PVC): for these types the average transmittance values were calculated according to the Italian standard UNI/TR 11552: 2014 [3]; the equivalent transmittance of the glass and of the frame for each dwelling-type, was determined weighting the thermal transmittances corresponding to the answers of the survey on their incidence on the total number of dwellings that fall in the class; since the transparent surface is not an information inferable from the survey, a transparent surface equal to 1/8 of the floor surface was assumed to calculate the transmittance of the window. Table 3 summarizes the obtained values.

Table 3. Thermal trasmittance of the trasparent envelope by period of build and type of dwelling [kW/m^{2}K]

	Before 1950	1950-1969	1970-1989	From 1990
S. F. House	3.320	3.490	3.280	2.450
Multi-fam. House	3.010	3.230	2.950	2.400
Apartments	3.240	3.530	3.400	2.560

- Floor surface: since the survey answers are provided for 10 m^2 surface intervals, the floor area of the dwelling-type is calculated as the average of the central values of the surface intervals weighted on the frequency of the answers for each surface interval (Table 4).

Table 4. Dwelling-types' heated floor surfaces [m^2].

	Before 1950	1950-1969	1970-1989	From 1990
S. F. House	121.5	115.0	119.9	130.3
Multi-f. House	122.0	103.7	115.9	122.6
Gr. Fl. Apt.	86.3	92.4	82.1	83.1
Mid. Fl. Apt.	90.8	83.6	89.1	92.8
Top Fl. Apt	98.5	89.6	93.4	90.8

- Exposure: the survey provides information about two main exposures (without specifying the prevailing one) of the external walls of the dwelling. Analyzing the frequency of all possible answers and the combinations between them it was assumed that the multi-family dwellings have two possible types of exposure: two opposite sides or three adjacent sides exposed to the outside; for apartments the types of exposure are three: one single side, two opposite sides and two adjacent sides exposed to the outside; for the single family house all the 4 sides are considered exposed to the outside. Table 5 summarizes all the 34 considered types of exposure, corresponding to the simulations to be performed for each period of build. The weight of each type of exposure is proportional to the number of dwellings that fall in it; Table 6 summarizes the weight of the identified types of exposure and of their consequent simulations.

Table 5. Dwelling walls' main exposures and consequent simulations.

	S1	S2	S3	S4	S5	S6	S7	S8	S9	S10
SFH	all	-	-	-	-	-	-	-	-	-
MFH	N+S	E+W	N+E+S	-	-	-	-	-	-	
GFApt	N	E	S	W	N+S	E+W	N+E	N+W	E+S	S+W
MFApt	N	E	S	W	N+S	E+W	N+E	N+W	E+S	S+W
TFApt	N	E	S	W	N+S	E+W	N+E	N+W	E+S	S+W

Table 6. Weight of each identified type of exposure and consequent simulation.

	S1	S2	S3	S4	S5	S6	S7	S8	S9	S10
SFH	100.0%	-	-	-	-	-	-	-	-	-
MFH	44.1%	23.9%	32.0%	-	-	-	-	-	-	-
GFApt	14.2%	11.7%	12.6%	4.9%	10.5%	10.8%	7.6%	7.6%	12.4%	7.9%
MFApt	14.2%	11.7%	12.6%	4.9%	10.5%	10.8%	7.6%	7.6%	12.4%	7.9%
TFApt	14.2%	11.7%	12.6%	4.9%	10.5%	10.8%	7.6%	7.6%	12.4%	7.9%

- Heat losing surfaces: the vertical heat losing surfaces are determined in accordance with the previously identified types of exposure, considering a square shaped floor and assuming the height of the walls for each type of dwelling; the total window surface, assumed to be equal to 1/8 of the floor surface, is divided equally among the walls exposed to the outside. For both the single and the multi-family house, the floor and the ceiling are considered heat losing surfaces. As far as the apartments are concerned, the middle floor apartment has no horizontal heat losses, the ground floor has heat losses through the floor and the top floor apartment has heat losses through the ceiling.

4. THE SIMULATION MODEL

Since the aim of the work is the determination of both the energy consumption and the thermal load profiles, we chose to use a dynamic simulation model, made by the University of Catania, based on the equivalent resistance-capacitance model proposed in the European standard EN ISO 13790 [4].

Dynamic models for the evaluation of energy consumption in buildings are developed taking into account the variability of both the external climatic conditions of the internal loads. In general, the calculation of the heat load in summer is done with dynamic methods that take into account the thermal capacity and the thermal transients of the buildings.

The European standard EN ISO 13790 proposes an electro-thermal dynamic model simplified with five thermal

conductance and a heat capacity, called 5R1C, shown in Figure 2.

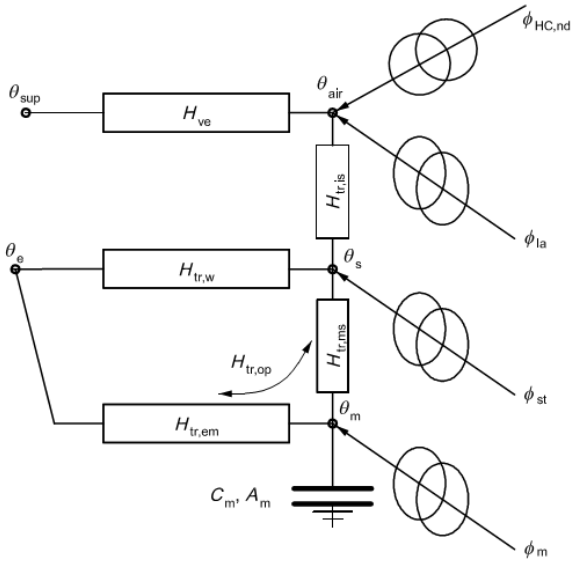

Figure 2. 5R1C Model Scheme

The nodes in the model scheme represent the ventilation (θ_{sup}), the outdoor air (θ_e), the envelope mass (θ_m), the envelope indoor surface (θ_s) and the indoor air (θ_{air}) temperatures. The heat transfer coefficients are: the ventilation heat transfer coefficient (H_{ve}), the transmission heat transfer coefficient for windows ($H_{tr,w}$), the emissive transmission heat transfer coefficient for the opaque envelope towards the envelope mass ($H_{tr,em}$), the conductive transmission heat transfer coefficient for the opaque envelope towards the envelope indoor surface ($H_{tr,ms}$), the coupling conductance between the envelope indoor surface and the indoor air ($H_{tr,is}$). The heat flows are: heat flow rate from internal and solar sources towards the envelope mass (Φ_m), heat flow rate from internal and solar sources towards the envelope indoor surface (Φ_{st}), heat flow rate from internal sources towards indoor air (Φ_{ia}), heating or cooling needs ($\Phi_{HC,nd}$).

The EN ISO 13790 standard defines uniquely the heat transfer coefficients and proposes a mode of solution refers to the monthly average daily conditions and monthly average daily time conditions.

The direct solution, set the temperature and the thermal conductance, allow the calculation of the net flux exchanged, $\Phi_{HC,nd}$, under changing climatic conditions. This solution involves the solution of a differential equation related to the heat balance to Φ_m node:

$$C\frac{dT_m}{dt}+\left(H_{tr,em}+H_{tr,ms}-H_{tr,ms}\frac{H_{tr,ms}}{H_{tr,w}+H_{tr,ms}+H_{si}}\right)T_m =$$

$$=\Phi_m+H_{tr,em}T_e+H_{tr,ms}\frac{\Phi_{si}+H_{tr,w}T_e+H_{si}T_{air}}{H_{tr,w}+H_{tr,ms}+H_{si}}$$

For the net flow we have:

$$\Phi_{HC,nd}=H_{ve}\left(T_{air}-T_{\sup}\right)+H_{si}\left(T_{air}-T_{si}\right)-\Phi_{air}$$

The recursive solution based on Heun method is:

$$T_m\left(t_{n+1}\right)=\left(1-\lambda\frac{T}{2}\right)T_m\left(t_n\right)+\frac{T}{2}\left(-\lambda T_m\left(t_n\right)+g\left(t_n\right)\right)+\frac{T}{2}g\left(t_{n+1}\right)$$

where:

$$\lambda=\frac{H_{tr,em}+H_{tr,ms}-H_{tr,ms}\dfrac{H_{tr,ms}}{H_{t,w}+H_{tr,ms}+H_{si}}}{C}$$

$$g=\frac{\Phi_m+H_{tr,em}T_e+H_{tr,ms}\dfrac{\Phi_{si}+H_{tr,w}T_e+H_{si}T_{air}}{H_{tr,w}+H_{tr,ms}+H_{si}}}{C}$$

The calculation thus prepared is sufficient and can be quickly implemented on Excel spreadsheet.

The input data required for the model are:

- thermal transmittance of the component, W / (m².K).
- participation factor (required by UN EN 13790)
- total surface of each element m².
- solar absorption factor for opaque walls and global solar transmittance for transparent surfaces;
- shading factor (as per UNI EN 13790).
- total building height, m;
- number of air changes per hour in the absence of VMC;
- air flow temperature of ventilation in the case of controlled mechanical ventilation;
- ambient temperature that you want to have during the night attenuation.
- specific flow to the sky;
- reference temperature for plant regulation (set equal to 20 °C in winter and 26 °C in summer);
- total atmospheric pressure for the town considered;
- humidity of the ventilation;
- latent heat intensity for internal sources.

An important feature of the method is the ability to customize the input vectors as a function of weather data, the real profiles for plants and internal gains.

As output, the model provides for each day (representative of the month) a time profile of the latent load, the total load required, the attenuation coefficient, the indoor air temperature and the inner surface of the walls.

5. ESTIMATION OF THE ENERGY PRODUCT CONSUMPTION

The consumption of primary energy from the thermal energy demand is determined according to the following parameters:

- number of hours of daily usage of the plant for each dwelling-type, calculated as the average of the answers and divided into climatic zones;
- reduction factor, $a_{H,red}$,for intermittent heating;
- average overall efficiency of the heating plant.

The $a_{H,red}$ coefficient takes into account that the plants do not run for all day, the solar and inner gains and the building time constant and are calculated according to the formula proposed in the UNI TS 11300-1 / 2014 [5]:

$$a_{H,red}=1-b_{H,red}\left(\tau_{H,O}/t\right)g_H(1-f_{H,hr})$$

The overall performance of thermal plants is calculated as the product of the efficiencies of the subsystems in which is divided, namely the generation, distribution, control and emission.

The efficiency of each subsystem is determined as a weighted average for the plant surface of each type of dwelling inferred from the survey responses, to which a value as indicated in the UNI TS 11300-2 / 2014 [6] was assigned.

The efficiency of the generation subsystem is dependent on the primary source used, while other subsystems are independent. In the case of single or portable heating systems, it was assigned to each type a single overall efficiency.

The types of considered subsystems, are:

- emission: radiators, fan coils and radiant panels;
- control: on-off and thermostatic valves;
- distribution: before and after 1990 with different efficiency values for single and multi-family house, ground floor autonomous apartments, middle and top floor autonomous apartments, last and centralized apartments.

For the generation subsystem supplied by natural gas, it was considered the boiler for centralized and autonomous systems and stoves for those individuals.

Table 7 shows the values of the overall efficiency calculated:

Table 7. Global efficiency of natural gas heating systems, for each dwelling-type class [-]

	Before 1950	1950-1969	1970-1989	From 1990
S. F. House	0.767	0.765	0.767	0.768
Multi-f. House	0.766	0.767	0.769	0.761
Gr. Fl. Apt.	0.794	0.788	0.792	0.771
Mid. Fl. Apt.	0.788	0.795	0.797	0.773
Top Fl. Apt	-	0.794	0.798	0.785

6. RESULTS, DISCUSSION AND FUTURE WORK

The first result, which is also the most important for the many activities in which it can be used, is the classification of the whole Italian residential housing stock in 20 classes of dwelling-types, determined as previously described.

6.1 Thermal load

For each dwelling-type, the profiles of the indoor air temperature, of the thermal energy demand (assuming a continuous heating mode) and of the thermal load (that is the dwelling energy demand with a power profile for a total number of hours equal to the maximum allowed), were obtained.

Figure 3,
Figure 4 and
Figure 5 show an example of the available hourly profiles for the dwelling-type class “top floor apartment”, period of build “before 1950”, in the case of controlled mechanical ventilation.

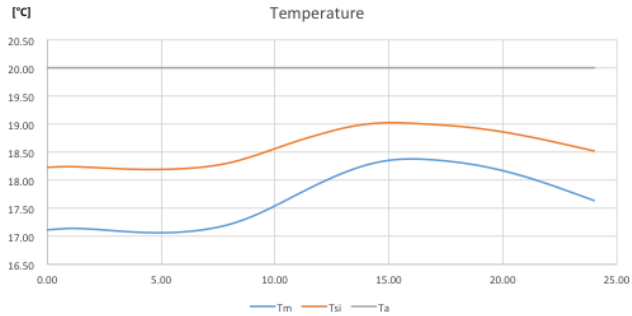

Figure 3. Indoor temperature hourly profile, continuous heating mode [°C]

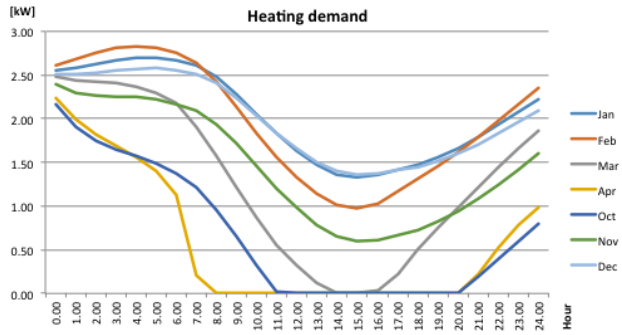

Figure 4. Heating demand hourly profile of the average day for each month, continuous heating mode [kW]

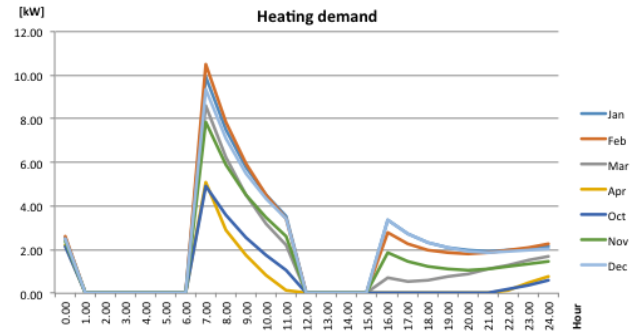

Figure 5. Thermal load hourly profile of the average day for each month, intermittent heating mode [kW]

Figure 5 clearly shows how the presence of a power profile highlights a different distribution of the thermal output required by the heating system, providing much more detailed information closer to a real trend.

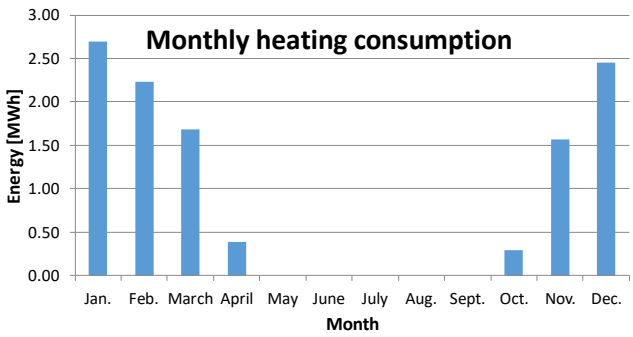

Figure 6. Monthly heating consumption profile [MWh]

In

Figure 6 an example of a monthly consumption of thermal energy for heating profile is plotted: it is referred to a single simulation run of the 34 possible for each period of build and for each climatic zone.

6.2 Energy product consumption

Starting from the results of the 34 simulations performed for each period of build (Table 5), it is possible to obtain the thermal energy consumption of each dwelling-type, as the average weighted on the table of weights (Table 6) multiplied by its corresponding reduction factor for intermittent heating, $a_{H,red}$ (Table 8).

Table 8. Reduction factor for intermittent heating ($a_{H,red}$) corresponding to each simulation, period of build "before 1950", climatic zone E [-]

	S1	S2	S3	S4	S5	S6	S7	S8	S9	S10
SFH	0.70	-	-	-	-	-	-	-	-	-
MFH	0.83	0.81	0.82	-	-	-	-	-	-	-
GFApt	0.80	0.74	0.77	0.78	0.77	0.73	0.75	0.77	0.73	0.75
MFApt	0.71	0.62	0.66	0.67	0.72	0.68	0.70	0.73	0.67	0.70
TFApt	0.73	0.64	0.68	0.69	0.70	0.66	0.68	0.71	0.66	0.69

Since four periods of build have been identified, for each climatic zone 136 simulations are performed, and their results, weighted on Table 6 and multiplied by their corresponding reduction factors for intermittent heating, allow the calculation of the thermal energy consumption of the 20 identified dwelling-types, as shown in Table 9.

Table 9. Heating consumption for each dwelling-type, climatic zone E [kWhy]

	Before 1950	1950-1969	1970-1989	From 1990
S. F. House	19342	18232	17957	18500
Multi-f. House	24138	21245	22979	23325
Gr. Fl. Apt.	9947	11287	9802	9704
Mid. Fl. Apt.	5832	5678	5966	6018
Top Fl. Apt	11154	9669	10774	10174

Dividing the heating consumption table of the dwelling-types (Table 9) by the table of the dwelling-types' heated floor surfaces (Table 4), the heating consumption per area for each dwelling-type class, for the considered climatic zone, is obtained (Table 10).

Table 10. Heating consumption per area for each dwelling-type class, climatic zone E [kWh/m^{2}y].

	Before 1950	1950-1969	1970-1989	From 1990
S. F. House	159.20	158.54	149.77	141.99
Multi-f. House	197.85	204.88	198.27	190.26
Gr. Fl. Apt.	115.27	122.16	119.39	116.78
Mid. Fl. Apt.	64.24	67.93	66.96	64.86
Top Fl. Apt	113.24	107.92	115.35	112.05

The procedure described above is then applied for all climatic zones, and a table similar to Table 10 is obtained for each climatic zone.

For each dwelling-type class, is then possible to calculate the weight of each climatic zone by considering the share of floor surface of the class, falling in each zone: in the case of the Veneto Region, for instance, the single family house class is distributed between zone E (91.5 % of the heated floor surface) and zone F (8.5 % of the heated floor surface).

This distribution is then summarized for each climatic zone, as shown in Table 11 for the climatic zone E.

Table 11. % of floor surfaces of the building-type classes falling in the climatic zone E [-]

	Before 1950	1950-1969	1970-1989	From 1990
S. F. House	91.5%	95.6%	94.7%	96.6%
Multi-f. House	94.6%	93.4%	95.6%	97.2%
Gr. Fl. Apt.	100.0%	97.2%	94.5%	94.3%
Mid. Fl. Apt.	96.6%	95.6%	98.6%	100.0%
Top Fl. Apt	100.0%	95.9%	76.4%	75.8%

Weighting the simulation results of each climatic zone by the percentage of floor falling in the zone itself, the heating consumption per area for each dwelling-type class is calculated. The results for the Veneto Region are summarized in Table 12.

Table 12. Heating consumption per area for each dwelling-type class [kWh/m^{2}y]

	Before 1950	1950-1969	1970-1989	From 1990
S. F. House	145.69	151.58	141.69	137.22
Multif. House	187.27	191.28	189.62	184.93
Gr. Fl. Apt.	115.27	118.75	112.82	110.14
Mid. Fl. Apt.	62.03	64.92	66.01	64.86
Top Fl. Apt	113.24	103.47	88.18	84.99

Multiplying the heating consumption per area by the total area of the dwellings, that use a specific energy product for heating (in the present example: natural gas), that fall in each dwelling-type class (Table 13) and dividing by the respective system's global efficiency (Table 7), it is possible to assess the total energy product consumption for heating of each dwelling-type class for the specific energy product, as shown in Table 14.

Table 13. Total floor surface of each dwelling-type class, using Natural gas as energy product for heating [m^2]

	Before 1950	1950-1969	1970-1989	From 1990
S. F. House	5135	7785	11520	5665
Multi-f. House	1915	4950	6370	7865
Gr. Fl. Apt.	3340	7330	7375	3960
Mid. Fl. Apt.	720	3135	3400	2500
Top Fl. Apt	0	225	525	690

The sum of the elements of Table 14, reporting the total annual consumption of the dwelling-type classes for the considered energy product provides the overall annual energy product consumption for heating of the residential building

stock for the considered energy product which, in the case of the Veneto Region and of natural gas, is approx. 15,014 MWh.

Table 14. Total annual energy product consumption for heating of each dwelling-type class, natural gas [MWhy]

	Before 1950	1950-1969	1970-1989	From 1990
S. F. House	975.3	1542.9	2129.3	1011.5
Multi-f. House	468.3	1234.0	1570.6	1910.9
Gr. Fl. Apt.	484.9	1105.2	1050.0	565.4
Mid. Fl. Apt.	56.7	255.9	281.5	209.8
Top Fl. Apt	0.00	29.31	58.03	74.69

The project activity is still in progress. The present step, in progress, is the comparison between the consumption data calculated with the presented methodology and those estimated by the ISTAT survey, the final results of the comparison will be published later.

7. CONCLUSIONS

The above presented methodology has enabled, by means of processing the data on energy consumption of Italian families provided by the ISTAT survey and with the aid of a dynamic simulation model, the realization of a tool able to estimate the energy consumption and to create the thermal load profiles of the representative dwellings of the Italian residential sector.

In particular the methodology allowed to group the entire national sample in 20 cluster of type dwellings, as a function of building (dimensions, equipment, energy characteristics, etc.), family (number of occupants, consumption habits, etc.) and environmental (region, climatic zone, etc.) characteristics.

The methodology is able to estimate energy consumptions distinguished for end use (heating, cooling and domestic hot water) and energy product.

The aim of the work is to increase knowledge of consumer habits of end user to outline a real scenery of the buildings consumption useful to address the choice of the most efficient technological solutions and to provide guidance on the policy actions of support for the dissemination of the most promising technologies.

REFERENCES

[1] Istat, (2014, Dec. 15). “I consumi energetici delle famiglie”, Statistiche Report, (In Italian). [Online]. Available: http://www.istat.it/it/archivio/142173.

[2] P. Ungaro, I. Bertini, (2014), “I modelli per la stima dei consumi energetici per finalità d'uso e fonte”. [Online]. Available: http://www.istat.it/it/archivio/141193.

[3] Abaco delle strutture costituenti l'involucro opaco degli edifici - Parametri termo fisici, UNI/TR 11552:2014 Standard, 2014.

[4] Energy performance of buildings - Calculation of energy use for space heating and cooling, EN ISO 13790:2008 Standard, 2008.

[5] Prestazioni energetiche degli edifici. Parte 1: Determinazione del fabbisogno di energia termica dell’edificio per la climatizzazione estiva ed invernale. UNI/TS 11300-1:2014.

[6] Prestazioni energetiche degli edifici. Parte 2: Determinazione del fabbisogno di energia primaria e dei rendimenti per la climatizzazione invernale, per la produzione di acqua calda sanitaria, per la ventilazione e per l'illuminazione in edifici non residenziali. UNI/TS 11300-2:2014.

INTERNATIONAL JOURNAL OF HEAT AND TECHNOLOGY

ISSN: 0392-8764
Vol. 34, No. 1, March, 2016, pp.
DOI:

A publication of IIETA

International Information and Engineering Technology Association
Advancing the World of Information and Engineering

http://www.iieta.org/Journals/IJHT

A methodology for the generation of energy consumption profiles in the residential sector

Giovanni Puglisi[1*], Fabio Zanghirella[1], Paola Ungaro[2], Giuliano Cammarata[3]

[*1] ENEA (Italian National Agency for New Technologies, Energy and Sustainable Economic Development), via Anguillarese 301, 00123 Roma, Italy
[2] ISTAT (Italian National Institute of Statistics), Viale Oceano Pacifico 171, 00144, Roma, Italy
[3] Università degli Studi di Catania, p.zza Università, 2, 95125 Catania, Italy

Email: giovanni.puglisi@enea.it

ABSTRACT

The residential sector has been achieved in the last years more and more importance in the total energy consumption scenario by stimulating the research for solutions to promote energy efficiency and to raise awareness on energy consumption by end users.
The profile of a end-users energy consumption assumes a central role in finding solutions to reduce energy demand and increase the efficiency in the production of the same energy.
European regulations impose an obligation on Member States to provide annually data on energy consumption of households for end use and energy product. Data will be provided for Italy basing on data collected by ISTAT Survey on energy consumption in the residential sector, appropriately processed by ENEA and ISTAT.
In this paper it is presented a methodology that allowed to define a series of dwelling types, representative of the entire national sample, as a function of building, family and environmental characteristics. These dwellings, through the application of a dynamic simulation model, allowed the generation of monthly energy consumption profiles (for heating, cooling and domestic heat water) for each cluster of dwelling types and the evaluation of the energy consumption distribution of the residential sector for end use and energy product.

Keywords: energy consumption, residential sector, dwelling types, energy efficiency, end use, energy demand, energy product, dynamic simulation.

1. INTRODUCTION

The European and national policies aimed at containing the energy product consumption and at promoting the diffusion of renewable sources, have stimulated the search for ways to reduce the energy demand and to boost the efficiency in energy production. In particular, for the residential sector, the knowledge of the consumption habits of the families is of vital importance for achieving the goals set by the various European directives, as well as for raising awareness on energy consumption and for stimulating rational behaviors on energy use by end-users.

The regulation (EC) No 1099/2008 of the European Parliament and of the Council of 22 October 2008 on energy statistics, and the amending Commission Regulation (EU) No 431/2014 of 24 April 2014 on energy statistics, as regards the implementation of annual statistics on energy consumption in households, impose an obligation on Member States to provide annual data on energy consumption of households for final destination and energy source. In this framework ISTAT in collaboration with ENEA and MiSE (Italian Ministry of Economic Development) carried out the survey on households energy consumption [1,2], as part of the Italian National Statistics Plan. The survey was conducted in 2013 for the first time in Italy, on a representative sample of 20'000 households at regional level and made it possible to obtain information on characteristics, consumption habits, types of plant and energy costs of Italian households, specified by energy product (primary energy sources and energy carriers) and end-use (heating, cooling, domestic hot water, cooking, lighting and electrical equipment).

This paper describes the methodology used to estimate the energy consumption for heating and the creation of monthly load profiles for residential dwellings. For the sake of simplicity we have chosen to present the results for the Veneto Region and heating systems fueled by natural gas; the calculation method remains the same for other energy products and for the entire Italian national territory.

Furthermore, this methodology will be used in the activity ENEA-ISTAT to estimate the energy consumption of households for the years between two replications of the

ISTAT survey, starting from the ISTAT 2016 survey that will be used to deliver the first data to Eurostat.

2. METHODOLOGY

The presented methodology is based on the processing of the provided statistical data from the ISTAT 2013 survey on households energy consumption, and on the identification of dwelling-type classes representative of the entire Italian residential building stock.

The information provided by the ISTAT 2013 survey and used for the methodology are mainly:

- dwelling characteristics (type of dwelling, year of build, floor surface, opaque envelope type, transparent envelope type, main exposure of the external walls);
- characteristics of heating, cooling and DHW systems (number, energy products, systems type –centralized, individual or single device-, emission and temperature control system, frequency of use and daily hours of use);
- frequency of use of the systems;
- energy cost by energy product.

The classification of the dwellings was chosen as a function of:

- period of build: before 1950, 1950-1969, 1970-1989, from 1990;
- type of dwelling: single family house, multi-family house, ground floor apartment, middle floor apartment and top floor apartment.

Table 1 summarizes the 20 identified dwelling-type classes (DTC).

Table 1 – Dwelling-type classes.

	Before 1950	1950-1969	1970-1989	From 1990
Single fam. House	DTC1	DTC6	DTC11	DTC16
Multi-fam. House	DTC2	DTC7	DTC12	DTC17
Ground fl. apt.	DTC3	DTC8	DTC13	DTC18
Middle fl. apt.	DTC4	DTC9	DTC14	DTC19
Top fl. apt.	DTC5	DTC10	DTC15	DTC20

The evaluation of the energy product consumption for heating has been carried out in different stages, as exemplified in Figure 1:

a. determination of the thermal energy demand, in continuous heating mode, of the dwelling-type [kWhy] by means of a dynamic simulation software; the simulations were performed assuming a continuous heating mode (heating system on 24 hours a day), because the survey answers do not allow to determine an hourly power profile; the simulation results also provide the time profile of the heating demand of each dwelling-type;
b. calculation of the reduction factor for intermittent heating as a function of the average number of daily hours during which the heating system is switched on, based on the answers of the survey;
c. assumption of the efficiency of the different types of plant for each dwelling-type, and estimation of the heating consumptions per floor area [kWh/m^{2}y];
d. estimation of the total annual energy product consumption for heating for each class (m^3, kg, l, etc.) for a certain energy product, obtained by multiplying the consumption per area by the total area of the dwellings, that use that specific energy product for heating, that fall in each dwelling-type class.

The decision to estimate the thermal energy demand for all the dwelling-types by means of a dynamic simulation of the dwelling, and then calculate the energy product consumption by multiplying the heating demand calculated in continuous mode by the reduction factor for intermittent heating and by the average total efficiency of the heating system was related to the information provided by survey about the type and the characteristics of the heating systems. Clearly, the information provided by the survey can't have a detail level sufficient to estimate a management profile of the heating systems, which is instead essential to perform a dynamic simulation of the building-plant system.

Since the energy performances of buildings are strongly influenced by climatic conditions, the same dwelling-type was simulated in each climate zone. For each climatic zone in which the country is divided, the input weather data (temperature, radiation and humidity) adopted for the simulations were those of the chief town whose degree days are "barycentric" with respect to the degree days interval of the climatic zone.

3. DEFINITION OF THE DWELLING-TYPE CLASSES

Each dwelling-type class is characterized by thermo-physical and dimensional parameters, determined on the basis of the information gathered from the ISTAT survey results, appropriately processed, and of the input data required by the simulation model. Below the main properties that define each dwelling-type class are listed and described.

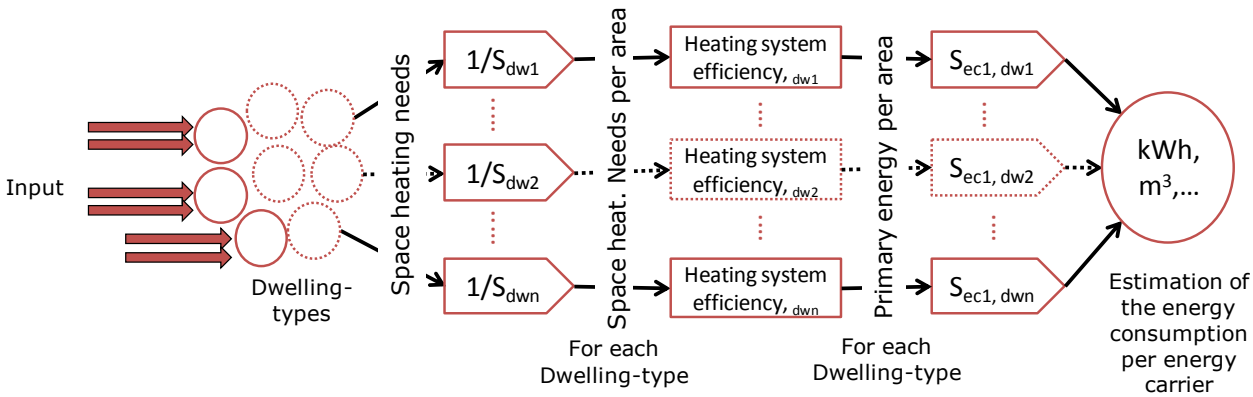

Figure 1 - Methodology scheme, for space heating and for a single energy product.

- Thermal transmittance of the opaque envelope: for each period of build a specific structure was deduced for the exterior walls, the floor and the ceiling, the corresponding thermal transmittance was determined, using data from the Italian standard UNI/TR 11552:2014. Table 2 summarizes the adopted values.

Table 2 – Thermal transmittance of the opaque envelope by period of build [kW/m^{2}K].

	Before 1950	1950-1969	1970-1989	From 1990
Walls	1.093	1.065	0.675	0.456
Floor	0.781	0.781	0.850	0.442
Roof	1.376	1.376	0.777	0.441

- Thermal transmittance of the transparent envelope: the survey provided as possible answers two types of glass (single, double) and three types of frame (wood, metal, PVC): for these types the average transmittance values were calculated according to the Italian standard UNI/TR 11552: 2014 [3]; the equivalent transmittance of the glass and of the frame for each dwelling-type, was determined weighting the thermal transmittances corresponding to the answers of the survey on their incidence on the total number of dwellings that fall in the class; since the transparent surface is not an information inferable from the survey, a transparent surface equal to 1/8 of the floor surface was assumed to calculate the transmittance of the window. Table 3 summarizes the obtained values.

Table 3 – Thermal trasmittance of the trasparent envelope by period of build and type of dwelling [kW/m^{2}K].

	Before 1950	1950-1969	1970-1989	From 1990
S. F. House	3.320	3.490	3.280	2.450
Multi-fam. House	3.010	3.230	2.950	2.400
Apartments	3.240	3.530	3.400	2.560

- Floor surface: since the survey answers are provided for 10 m^2 surface intervals, the floor area of the dwelling-type is calculated as the average of the central values of the surface intervals weighted on the frequency of the answers for each surface interval (Table 4).

Table 4 – Dwelling-types' heated floor surfaces [m^2].

	Before 1950	1950-1969	1970-1989	From 1990
S. F. House	121.5	115.0	119.9	130.3
Multi-f. House	122.0	103.7	115.9	122.6
Gr. Fl. Apt.	86.3	92.4	82.1	83.1
Mid. Fl. Apt.	90.8	83.6	89.1	92.8
Top Fl. Apt	98.5	89.6	93.4	90.8

- Exposure: the survey provides information about two main exposures (without specifying the prevailing one) of the external walls of the dwelling. Analyzing the frequency of all possible answers and the combinations between them it was assumed that the multi-family dwellings have two possible types of exposure: two opposite sides or three adjacent sides exposed to the outside; for apartments the types of exposure are three: one single side, two opposite sides and two adjacent sides exposed to the outside; for the single family house all the 4 sides are considered exposed to the outside. Table 5 summarizes all the 34 considered types of exposure, corresponding to the simulations to be performed for each period of build. The weight of each type of exposure is proportional to the number of dwellings that fall in it; Table 6 summarizes the weight of the identified types of exposure and of their consequent simulations.

Table 5 - Dwelling walls' main exposures and consequent simulations.

	S1	S2	S3	S4	S5	S6	S7	S8	S9	S10
SFH	all	-	-	-	-	-	-	-	-	-
MFH	N+S	E+W	N+E+S	-	-	-	-	-	-	-
GFApt	N	E	S	W	N+S	E+W	N+E	N+W	E+S	S+W
MFApt	N	E	S	W	N+S	E+W	N+E	N+W	E+S	S+W
TFApt	N	E	S	W	N+S	E+W	N+E	N+W	E+S	S+W

Table 6 – Weight of each identified type of exposure and consequent simulation.

	S1	S2	S3	S4	S5	S6	S7	S8	S9	S10
SFH	100.0%	-	-	-	-	-	-	-	-	-
MFH	44.1%	23.9%	32.0%	-	-	-	-	-	-	-
GFApt	14.2%	11.7%	12.6%	4.9%	10.5%	10.8%	7.6%	7.6%	12.4%	7.9%
MFApt	14.2%	11.7%	12.6%	4.9%	10.5%	10.8%	7.6%	7.6%	12.4%	7.9%
TFApt	14.2%	11.7%	12.6%	4.9%	10.5%	10.8%	7.6%	7.6%	12.4%	7.9%

- Heat losing surfaces: the vertical heat losing surfaces are determined in accordance with the previously identified types of exposure, considering a square shaped floor and assuming the height of the walls for each type of dwelling; the total window surface, assumed to be equal to 1/8 of the floor surface, is divided equally among the walls exposed to the outside. For both the single and the multi-family house, the floor and the ceiling are considered heat losing surfaces. As far as the apartments are concerned, the middle floor apartment has no horizontal heat losses, the ground floor has heat losses through the floor and the top floor apartment has heat losses through the ceiling.

4. THE SIMULATION MODEL

Since the aim of the work is the determination of both the energy consumption and the thermal load profiles, we chose to use a dynamic simulation model, made by the University of Catania, based on the equivalent resistance-capacitance model proposed in the european standard EN ISO 13790 [4].

Dynamic models for the evaluation of energy consumption in buildings are developed taking into account the variability of both the external climatic conditions of the internal loads. In general, the calculation of the heat load in summer is done with dynamic methods that take into account the thermal capacity and the thermal transients of the buildings

The european standard EN ISO 13790 proposes an electro-thermal dynamic model simplified with five thermal

conductance and a heat capacity, called 5R1C, shown in Figure 2.

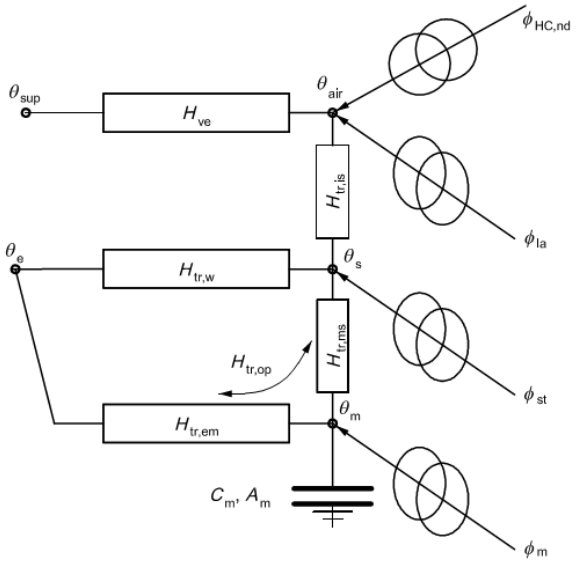

Figure 2 - 5R1C Model Scheme.

The nodes in the model scheme represent the ventilation (θ_{sup}), the outdoor air (θ_e), the envelope mass (θ_m), the envelope indoor surface (θ_s) and the indoor air (θ_{air}) temperatures. The heat transfer coefficients are: the ventilation heat transfer coefficient (H_{ve}), the transmission heat transfer coefficient for windows ($H_{tr,w}$), the emissive transmission heat transfer coefficient for the opaque envelope towards the envelope mass ($H_{tr,em}$), the conductive transmission heat transfer coefficient for the opaque envelope towards the envelope indoor surface ($H_{tr,ms}$), the coupling conductance between the envelope indoor surface and the indoor air ($H_{tr,is}$). The heat flows are: heat flow rate from internal and solar sources towards the envelope mass (Φ_m), heat flow rate from internal and solar sources towards the envelope indoor surface (Φ_{st}), heat flow rate from internal sources towards indoor air (Φ_{ia}), heating or cooling needs ($\Phi_{HC,nd}$).

The EN ISO 13790 standard defines uniquely the heat transfer coefficients and proposes a mode of solution refers to the monthly average daily conditions and monthly average daily time conditions.

The direct solution results in the calculation, set the temperature and the thermal conductance, the net flux exchanged, $\Phi_{HC,nd}$, under changing climatic conditions. This solution involves the solution of a differential equation related to the heat balance to Φ_m node:

$$C\frac{dT_m}{dt}+\left(H_{tr,em}+H_{tr,ms}-H_{tr,ms}\frac{H_{tr,ms}}{H_{tr,w}+H_{tr,ms}+H_{si}}\right)T_m=$$

$$=\Phi_m+H_{tr,em}T_e+H_{tr,ms}\frac{\Phi_{si}+H_{tr,w}T_e+H_{si}T_{air}}{H_{tr,w}+H_{tr,ms}+H_{si}}$$

For the net flow is we have:

$$\Phi_{HC,nd}=H_{ve}\left(T_{air}-T_{sup}\right)+H_{si}\left(T_{air}-T_{si}\right)-\Phi_{air}$$

The recursive solution based on Heun method is:

$$T_m\left(t_{n+1}\right)=\left(1-\lambda\frac{T}{2}\right)T_m\left(t_n\right)+\frac{T}{2}\left(-\lambda T_m\left(t_n\right)+g\left(t_n\right)\right)+\frac{T}{2}g\left(t_{n+1}\right)$$

where is:

$$\lambda=\frac{H_{tr,em}+H_{tr,ms}-H_{tr,ms}\dfrac{H_{tr,ms}}{H_{t,w}+H_{tr,ms}+H_{si}}}{C}$$

$$g=\frac{\Phi_m+H_{tr,em}T_e+H_{tr,ms}\dfrac{\Phi_{si}+H_{tr,w}T_e+H_{si}T_{air}}{H_{tr,w}+H_{tr,ms}+H_{si}}}{C}$$

The calculation thus prepared is sufficient and can be quickly implemented on Excel spreadsheet.

The input data required for the model are:

- thermal transmittance of the component, W / (m².K).
- participation factor (required by UN EN 13790)
- total surface of each element m².
- solar absorption factor for opaque walls and global solar transmittance for transparent surfaces;
- shading factor (as per UNI EN 13790).
- total building height, m;
- number of air changes per hour in the absence of VMC;
- air flow temperature of ventilation in the case of controlled mechanical ventilation;
- ambient temperature that you want to have during the night attenuation.
- specific flow to the sky;
- reference temperature for plant regulation (set equal to 20° C in winter and 26° C in summer);
- total atmospheric pressure for the town considered;
- humidity of the ventilation;
- latent heat intensity for internal sources.

An important feature of the method is the ability to customize the input vectors as a function of weather data, the real profiles for plants and internal gains.

As output, the model provides for each day (representative of the month) a time profile of the latent load, the total load required, the attenuation coefficient, the indoor air temperature and the inner surface of the walls..

5. ESTIMATION OF THE ENERGY PRODUCT CONSUMPTION

The consumption of primary energy from the thermal energy demand is determined according to the following parameters:

- number of hours of daily usage of the plant for each dwelling-type, calculated as the average of the answers and divided into climatic zones;
- reduction factor, $a_{H,red}$,for intermittent heating;
- average overall efficiency of the heating plant.

The $a_{H,red}$ coefficient takes into account that the plants don't run for all day, the solar and inner gains and the building time constant and is calculated according to the formula proposed in the UNI TS 11300-1 / 2014 [5]:

$$a_{H,red} = 1 - b_{H,red}\left(\frac{\tau_{H,O}}{t}\right)\eta_H(1 - f_{H,hr})$$

The overall performance of thermal plants is calculated as the product of the efficiencies of the subsystems in which is divided, namely the generation, distribution, control and emission.

The efficiency of each subsystem is determined as a weighted average for the plant surface of each type of dwelling inferred from the survey responses, to which a value as indicated in the UNI TS 11300-2 / 2014 [6] was assigned.

The efficiency of the generation subsystem is dependent on the primary source used, while other subsystems are independent. In the case of single or portable heating systems it was assigned to each type a single overall efficiency.

The types of considered subsystems, are:

- emission: radiators, fan coils and radiant panels;
- control: on-off and thermostatic valves;
- distribution: before and after 1990 with different efficiency values for single and multi-family house, ground floor autonomous apartments, middle and top floor autonomous apartments last and centralized apartments.

For the generation subsystem supplied by natural gas, was considered the boiler for centralized and autonomous systems and stoves for those individuals.

Table 7 shows the values of the overall efficiency calculated:

Table 7 - Global efficiency of natural gas heating systems, for each dwelling-type class [-].

	Before 1950	1950-1969	1970-1989	From 1990
S. F. House	0.767	0.765	0.767	0.768
Multi-f. House	0.766	0.767	0.769	0.761
Gr. Fl. Apt.	0.794	0.788	0.792	0.771
Mid. Fl. Apt.	0.788	0.795	0.797	0.773
Top Fl. Apt	-	0.794	0.798	0.785

6. RESULTS, DISCUSSION AND FUTURE WORK

The first result, which is also the most important for the many activities in which it can be used, is the classification of the whole Italian residential housing stock in 20 classes of dwelling-types, determined as previously described.

6.1 Thermal load

For each dwelling-type, the profiles of the indoor air temperature, of the thermal energy demand (assuming a continuous heating mode) and of the thermal load (that is the dwelling energy demand with a power profile for a total number of hours equal to the maximum allowed), were obtained.

Figure 3, Figure 4 and Figure 5 show an example of the availablehourly profiles for the dwelling-type class “top floor apartment”, period of build “before 1950”, in the case of controlled mechanical ventilation.

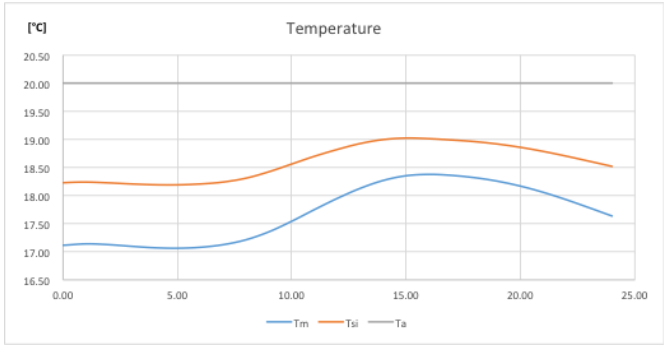

Figure 3 – Indoor temperature hourly profile, continuous heating mode [°C].

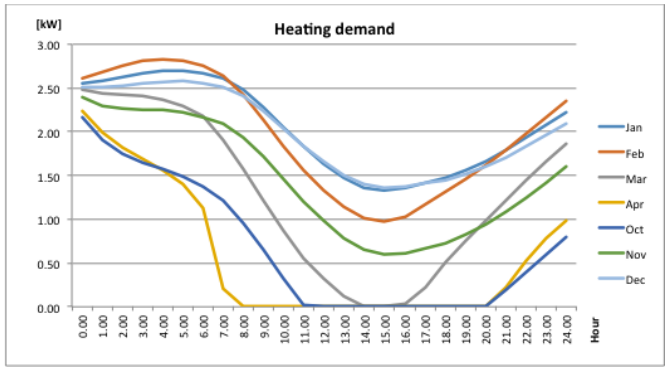

Figure 4 - Heating demand hourly profile of the average day for each month, continuous heating mode [kW].

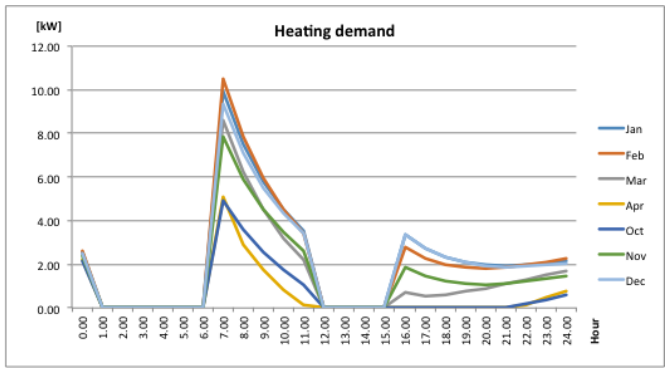

Figure 5 – Thermal load hourly profile of the average day for each month, intermittent heating mode [kW].

Figure 5 clearly shows how the presence of a power profile highlight a different distribution of the thermal output required to the heating system, providing much more detailed information and close to a real trend.

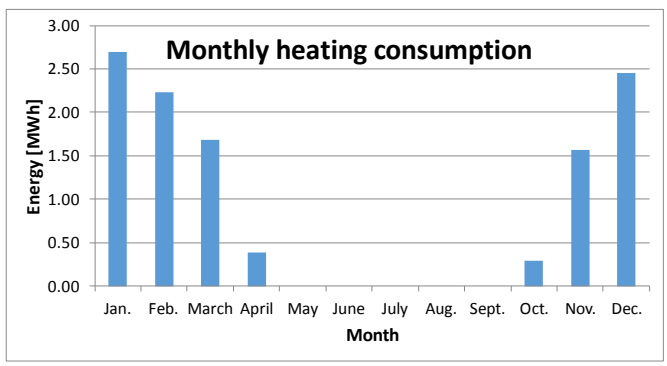

Figure 6 – Monthly heating consumption profile [MWh].

In Figure 6 an example of a monthly consumption of thermal energy for heating profile is plotted: it is referred to a

single simulation run of the 34 possible for each period of build and for each climatic zone.

6.2 Energy product consumption

Starting from the results of the 34 simulations performed for each period of build (Table 5), it is possible to obtain the thermal energy consumption of each dwelling-type, as the average weighted on the table of weights (Table 6) multiplied by its corresponding reduction factor for intermittent heating, $a_{H,red}$ (Table 8).

Table 8 – Reduction factor for intermittent heating ($a_{H,red}$) corresponding to each simulation, period of build "before 1950", climatic zone E [-].

	S1	S2	S3	S4	S5	S6	S7	S8	S9	S10
SFH	0.70	-	-	-	-	-	-	-	-	-
MFH	0.83	0.81	0.82	-	-	-	-	-	-	-
GFApt	0.80	0.74	0.77	0.78	0.77	0.73	0.75	0.77	0.73	0.75
MFApt	0.71	0.62	0.66	0.67	0.72	0.68	0.70	0.73	0.67	0.70
TFApt	0.73	0.64	0.68	0.69	0.70	0.66	0.68	0.71	0.66	0.69

Since four periods of build have been identified, for each climatic zone 136 simulations are performed, and their results, weighted on Table 6 and multiplied by their corresponding reduction factors for intermittent heating, allow the calculation of the thermal energy consumption of the 20 identified dwelling-types, as shown in Table 9.

Table 9 - Heating consumption for each dwelling-type, climatic zone E [kWhy].

	Before 1950	1950-1969	1970-1989	From 1990
S. F. House	19342	18232	17957	18500
Multi-f. House	24138	21245	22979	23325
Gr. Fl. Apt.	9947	11287	9802	9704
Mid. Fl. Apt.	5832	5678	5966	6018
Top Fl. Apt	11154	9669	10774	10174

Dividing the heating consumption table of the dwelling-types (Table 9) by the table of the dwelling-types' heated floor surfaces (Table 4), the heating consumption per area for each dwelling-type class, for the considered climatic zone, is obtained (Table 10).

Table 10 - Heating consumption per area for each dwelling-type class, climatic zone E [kWh/m^{2}y].

	Before 1950	1950-1969	1970-1989	From 1990
S. F. House	159.20	158.54	149.77	141.99
Multi-f. House	197.85	204.88	198.27	190.26
Gr. Fl. Apt.	115.27	122.16	119.39	116.78
Mid. Fl. Apt.	64.24	67.93	66.96	64.86
Top Fl. Apt	113.24	107.92	115.35	112.05

The procedure described above is then applied for all climatic zones, and a table similar to Table 10 is obtained for each climatic zone.

For each dwelling-type class, is then possible to calculate the weight of each climatic zone by considering the share of floor surface of the class, falling in each zone: in the case of the Veneto Region, for instance, the single family house class is distributed between zone E (91.5% of the heated floor surface) and zone F (8.5% of the heated floor surface).

This distribution is then summarized for each climatic zone, as shown in Table 11 for the climatic zone E.

Table 11 – % of floor surfaces of the building-type classes falling in the climatic zone E [-].

	Before 1950	1950-1969	1970-1989	From 1990
S. F. House	91.5%	95.6%	94.7%	96.6%
Multi-f. House	94.6%	93.4%	95.6%	97.2%
Gr. Fl. Apt.	100.0%	97.2%	94.5%	94.3%
Mid. Fl. Apt.	96.6%	95.6%	98.6%	100.0%
Top Fl. Apt	100.0%	95.9%	76.4%	75.8%

Weighting the simulation results of each climatic zone by the percentage of floor falling in the zone itself, the heating consumption per area for each dwelling-type class is calculated. The results for the Veneto Region are summarized in Table 12.

Table 12 - Heating consumption per area for each dwelling-type class [kWh/m^{2}y].

	Before 1950	1950-1969	1970-1989	From 1990
S. F. House	145.69	151.58	141.69	137.22
Multif. House	187.27	191.28	189.62	184.93
Gr. Fl. Apt.	115.27	118.75	112.82	110.14
Mid. Fl. Apt.	62.03	64.92	66.01	64.86
Top Fl. Apt	113.24	103.47	88.18	84.99

Multiplying the heating consumption per area by the total area of the dwellings, that use a specific energy product for heating (in the present example: natural gas), that fall in each dwelling-type class (Table 13) and dividing by the respective system's global efficiency (Table 7), it is possible to assess the total energy product consumption for heating of each dwelling-type class for the specific energy product, as shown in Table 14.

Table 13 - Total floor surface of each dwelling-type class, using Natural gas as energy product for heating [m^2].

	Before 1950	1950-1969	1970-1989	From 1990
S. F. House	5135	7785	11520	5665
Multi-f. House	1915	4950	6370	7865
Gr. Fl. Apt.	3340	7330	7375	3960
Mid. Fl. Apt.	720	3135	3400	2500
Top Fl. Apt	0	225	525	690

The sum of the elements of the table of the total annual consumption of the dwelling-type classes for the considered energy product (Table 14), provides the overall annual energy product consumption for heating of the residential building stock for the considered energy product which, in the case of the Veneto Region and of natural gas, is approx. 15.014 MWh.

Table 14 - Total annual energy product consumption for heating of each dwelling-type class, natural gas [MWhy].

	Before 1950	1950-1969	1970-1989	From 1990
S. F. House	975.3	1542.9	2129.3	1011.5
Multi-f. House	468.3	1234.0	1570.6	1910.9
Gr. Fl. Apt.	484.9	1105.2	1050.0	565.4
Mid. Fl. Apt.	56.7	255.9	281.5	209.8
Top Fl. Apt	0.00	29.31	58.03	74.69

The project activity is still in progress. The present step, in progress, is the comparison between the consumption data calculated with the presented methodology and those estimated by the ISTAT survey, the final results of the comparison will be published later.

7. CONCLUSIONS

The above presented methodology has enabled, by means of processing the data on energy consumption of Italian families provided by the ISTAT survey and with the aid of a dynamic simulation model, the realization of a tool able to estimate the energy consumption and to create the thermal load profiles of the representative dwellings of the Italian residential sector.

In particular the methodology allowed to group the entire national sample in 20 cluster of type dwellings, as a function of building (dimensions, equipment, energy characteristics, etc.), family (number of occupants, consumption habits, etc.) and environmental (region, climatic zone, etc.) characteristics.

The methodology is able to estimate energy consumptions distinguished for end use (heating, cooling and domestic hot water) and energy product.

The aim of the work is to increase knowledge of consumer habits of end users to outline a real scenery of the buildings consumption useful to address the choice of the most efficient technological solutions and to provide guidance on the policy actions of support for the dissemination of the most promising technologies.

REFERENCES

[1] Istat, “I consumi energetici delle famiglie”, Statistiche Report, 15 dicembre 2014, 2014. (In Italian). [Online]. Available: http://www.istat.it/it/archivio/142173.

[2] P. Ungaro, I. Bertini, "I modelli per la stima dei consumi energetici per finalità d'uso e fonte", 2014. [Online]. Available: http://www.istat.it/it/archivio/141193.

[3] *Abaco delle strutture costituenti l'involucro opaco degli edifici - Parametri termo fisici*, UNI/TR 11552:2014 Standard, 2014.

[4] *Energy performance of buildings - Calculation of energy use for space heating and cooling*, EN ISO 13790:2008 Standard, 2008.

[5] *Prestazioni energetiche degli edifici. Parte 1: Determinazione del fabbisogno di energia termica dell’edificio per la climatizzazione estiva ed invernale*. UNI/TS 11300-1:2014

[6] *Prestazioni energetiche degli edifici. Parte 2: Determinazione del fabbisogno di energia primaria e dei rendimenti per la climatizzazione invernale, per la produzione di acqua calda sanitaria, per la ventilazione e per l'illuminazione in edifici non residenziali*. UNI/TS 11300-2:2014